

Pilkington Library

Author/Filing Title Jefferson, B

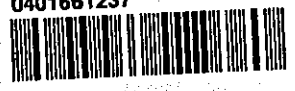
Accession/Copy No. **FOR REFERENCE ONLY**

| | |
|---------------|------------------|
| Vol. No. | Class Mark |
|---------------|------------------|

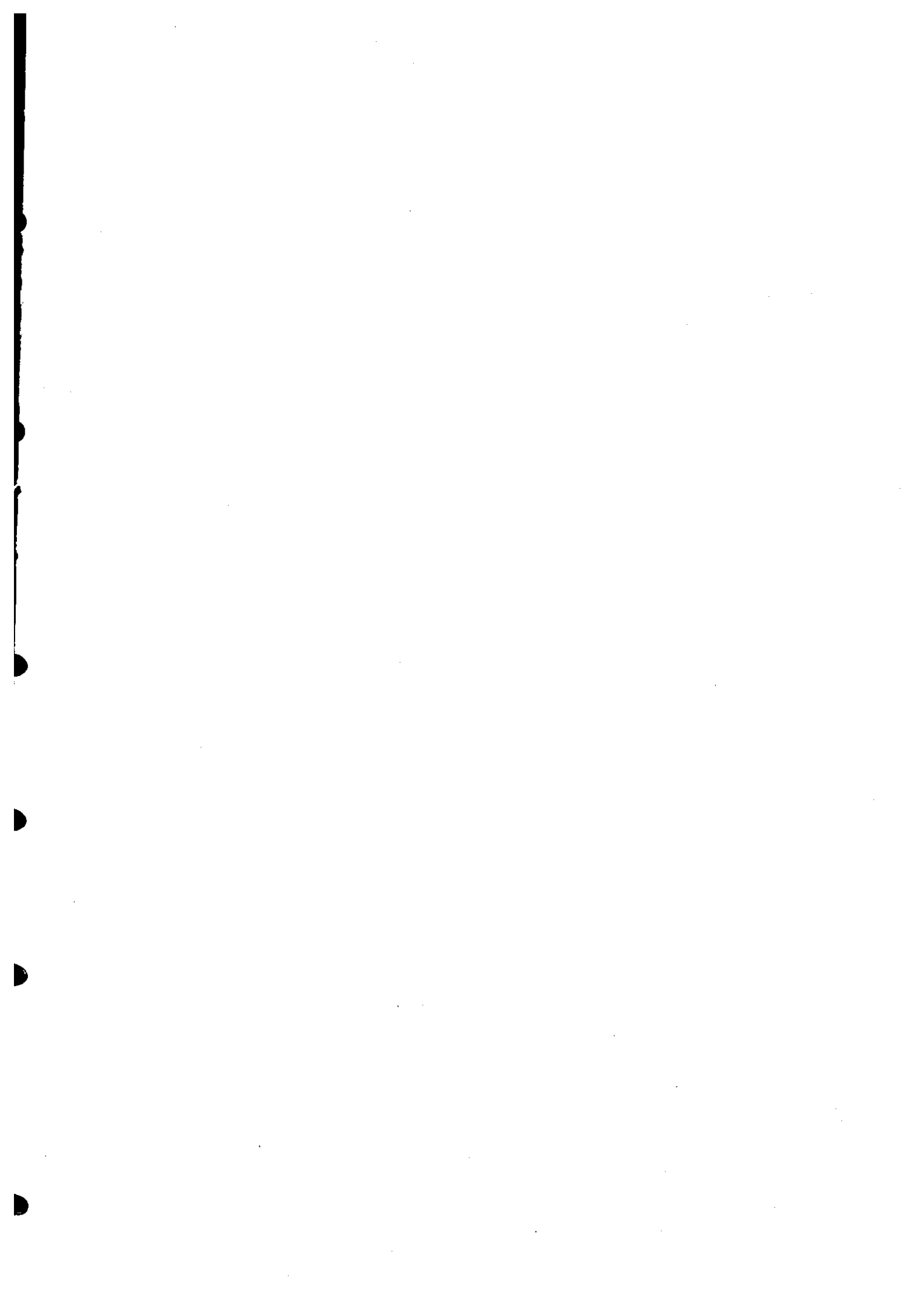
100000

90

0401661237



BADMINTON PRESS
UNIT 1 BROOK ST
SYSTON
LEICESTER, LE7 1GD
ENGLAND
TEL: 0116 260 2917

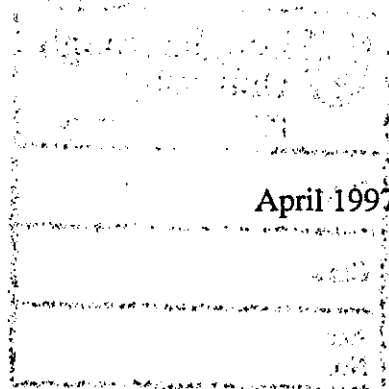



**MECHANISMS OF PARTICLE CAPTURE IN DISSOLVED AIR
FLOTATION**

by

BRUCE JEFFERSON, BEng, DIS

A Doctoral Thesis submitted in partial fulfillment of the requirements
for the award of the Degree of Doctor of Philosophy
of Loughborough University



| |
|---|
|  Loughborough University Pitt Rivers Library |
| Date <i>Oct 98</i> |
| Class |
| Acc No. <i>040166123</i> |

K0629005

ABSTRACT

The dissolved air flotation process experiences process stability problems that are attributed to a poor understanding of the fundamental mechanisms. A detailed review of the literature revealed that the mechanisms of flotation are fairly well understood in mineral flotation application but that the transfer of knowledge to water treatment application is poor, particularly regarding the differences between particle and floc flotation.

A detailed surface characterisation of kaolin and Wyoming bentonite particles was performed in terms of their zeta potential. This showed that small changes in the system's conditions could have large effects on the particle's zeta potential. Simple models can be applied to adequately describe the effects of surface conditioners for engineering application. This was particularly evident with surfactants which represented an effective method of zeta potential manipulation. Coagulants were seen to be more complex and less stable in their ability to control the zeta potential of particles.

The investigation continued by comparing the particle removal efficiency in terms of turbidity and size distribution to the zeta potentials of the interacting surfaces. The results showed that charge neutralisation is necessary with an equivalent zeta potential of 10mV on both surfaces being required for the process to be effective. No strong relationship could be found between floc size and efficiency, negating grade efficiency concepts which are often discussed. The degree of hydrophobicity increases the robustness with which the process can float particles which are charged without effecting the peak efficiency obtained. A theoretical analysis showed that upon collision the particles are swept to the underside of the bubble where they remain or are dislodged depending on the balance of forces.

The mechanisms of bubble production were examined in terms of a three staged model. This showed the critical stages in the process to be the detachment of bubbles from their nucleation sites and the degree of localised coalescence at the nozzle's exit. An experimental investigation into nozzle design by photographic bubble size measurements revealed that maximum benefit could be obtained by the use of a 45° diverging nozzle chamber or an impingement plate close to the nozzle's exit.

ACKNOWLEDGEMENTS

The author wishes to express his sincere gratitude to the following individuals.

Dr Tony Ward and Dr Ian Stenhouse for their supervision and encouragement throughout.

Dr R J Akers and Prof B.W.Brooks, my Directors of Research and Prof M.Streat, the Head of Department.

Jeff Boyden, who sadly passed on during the time of this project and whose photographic skills and insights into life will be missed.

Graham Moody for the suffering that he endured during the last three years and his excellent analytical assistance.

Pip and Barry, whose magic in the workshop enabled the smooth running of the rigs from the day they were commissioned.

Steve Graver, who took over from Jeff and enabled the photographic experiments to continue to run smoothly.

Mr A Petiraksakul for his experimental assistance

EPSRC for financial support of the project

Mel, whose support and assistance has greatly helped me through the difficult times and enabled some tricky discussion to be made.

All the administration staff, whose nagging reminded me that writing the thesis did have some advantages after all.

All the undergraduates involved in projects associated with this work, allowing some interesting avenues to be explored.

My fellow researchers within the department, especially in the office where I wrote this thesis, eranu indeed, the happy times are now upon you.

My family, whose support, encouragement, assistance and gags have made this journey of enlightenment considerably brighter than it may have been.

TABLE OF CONTENTS

| | Page |
|-------------------|---|
| Synopsis | i |
| Acknowledgements | ii |
| Table of contents | iv |
| List of figures | ix |
| List of plates | xiv |
| List of tables | xv |
| Notation | xvi |
| | |
| CHAPTER 1 | INTRODUCTION |
| | 1.1 |
| | |
| CHAPTER 2 | LITERATURE REVIEW : |
| | Removal Mechanisms |
| | 2.1 |
| 2.1 | Introduction |
| | 2.1 |
| 2.2 | Theoretical predictions of the collision efficiency |
| | 2.5 |
| 2.2.1 | Results of the collision model |
| | 2.9 |
| 2.2.2 | Inclusion of electrical forces |
| | 2.11 |
| 2.3 | Attachment |
| | 2.12 |
| 2.3.1 | Hydrophobicity |
| | 2.12 |
| 2.3.2 | Electrical neutrality |
| | 2.16 |
| 2.3.2.1 | The electrical double layer |
| | 2.16 |
| 2.3.2.2 | Total energy of interaction |
| | 2.18 |
| 2.3.3 | Experimental investigation |
| | 2.23 |
| 2.4 | Conclusions |
| | 2.24 |
| | |
| CHAPTER 3 | LITERATURE REVIEW : |
| | Bubble Production |
| | 3.1 |
| 3.1 | Introduction |
| | 3.1 |
| 3.2 | Existence of nucleation sites |
| | 3.2 |
| 3.3 | Stability of nucleation sites |
| | 3.3 |
| 3.4 | Location of the nucleation sites |
| | 3.5 |

| | | |
|------------------|--|------------|
| 3.5 | Detachment | 3.7 |
| 3.6 | Nozzle design | 3.8 |
| 3.7 | Experimental investigations into nozzle design | 3.12 |
| 3.8 | Types of saturators | 3.21 |
| 3.9 | Conclusions | 3.26 |
| | | |
| CHAPTER 4 | EXPERIMENTAL METHOD : Flotation tests | 4.1 |
| 4.1 | Introduction | 4.1 |
| 4.2 | Literature review | 4.1 |
| 4.3 | Experimental procedures | 4.2 |
| 4.3.1 | Aims and Objectives | 4.2 |
| 4.3.2 | Materials used | 4.3 |
| 4.3.2.1 | Clays | 4.3 |
| 4.3.2.2 | Surfactants | 4.3 |
| 4.3.2.3 | Coagulants | 4.4 |
| 4.3.3 | Sample preparation | 4.4 |
| 4.3.4 | Sample analysis | 4.4 |
| 4.3.5 | Flotation rig | 4.6 |
| 4.3.6 | Flocculation Bench | 4.7 |
| 4.3.7 | Analytical equipment | 4.7 |
| 4.3.7.1 | Zeta Potential | 4.7 |
| 4.3.7.2 | Turbidity | 4.8 |
| 4.3.7.3 | Surface tension | 4.8 |
| 4.3.7.4 | Particle size analysis | 4.8 |
| 4.3.7.5 | Bubble Zeta Potential | 4.9 |
| 4.4 | Experimental errors | 4.10 |
| | | |
| CHAPTER 5 | BUBBLE SIZE MEASUREMENTS: | |
| | Experimental method | 5.1 |
| 5.1 | Introduction | 5.1 |

| | | |
|-----|-----------------------------------|------|
| 5.2 | Literature review | 5.1 |
| | 5.2.1 Introduction | 5.1 |
| | 5.2.2 Recording the bubble images | 5.1 |
| | 5.2.3 Magnification | 5.2 |
| | 5.2.4 Measuring the bubbles size | 5.3 |
| | 5.2.5 Discussion | 5.4 |
| 5.3 | Experimental procedures | 5.5 |
| | 5.3.1 Aims and objectives | 5.5 |
| | 5.3.4 Experiment procedure | 5.7 |
| | 5.3.3 Bubble column: | 5.7 |
| | 5.3.3 Photographic system | 5.8 |
| | 5.3.4 Nozzle | 5.9 |
| | 5.3.5: Image analysis | 5.10 |
| | 5.3.5.1 ~Fully automatic solution | 5.11 |
| | 5.3.5.2 Semi-automatic | 5.12 |
| 5.5 | Experimental errors | 5.12 |

CHAPTER 6**RESULTS :**

| | | |
|-----|--|------|
| | Zeta potential measurements | 6.1 |
| 6.1 | Introduction | 6.1 |
| 6.2 | Evaluation of the zeta potential of clay particles | 6.2 |
| | 6.2.1 Clay composition | 6.2 |
| | 6.2.2 Theoretical predictions | 6.5 |
| | 6.2.3 Reproducibility | 6.5 |
| 6.3 | pH effects | 6.7 |
| | 6.3.1 Kaolin | 6.7 |
| | 6.3.2 Wyoming bentonite | 6.9 |
| 6.4 | Surfactant effects | 6.11 |
| | 6.4.1 Kaolin | 6.11 |
| | 6.4.2 Kaolin and ph changes | 6.14 |
| | 6.4.3 Wyoming bentonite | 6.16 |
| | 6.4.4 Wyoming bentonite and ph changes | 6.18 |

| | | |
|-------|---|------|
| 6.5 | Coagulant effects | 6.20 |
| 6.5.1 | Kaolin | 6.21 |
| 6.5.2 | Kaolin, coagulant and ph effects | 6.23 |
| 6.5.3 | Wyoming bentonite | 6.25 |
| 6.5.4 | Wyoming bentonite, coagulant and ph effects | 6.27 |
| 6.6 | Temperature effects | 6.28 |
| 6.6.1 | Agglomeration | 6.30 |
| 6.6.2 | Shear plane | 6.31 |
| 6.7 | Bubble zeta potential | 6.33 |
| 6.8 | Conclusions | 6.35 |

CHAPTER 7**RESULTS :**

| | | |
|-------|--|------|
| | Flotation tests | 7.1 |
| 7.1 | Introduction | 7.1 |
| 7.2 | Discrete particle flotation | 7.1 |
| 7.2.1 | Flotation response | 7.2 |
| 7.2.2 | Comparison of flotation and sedimentation. | 7.5 |
| 7.2.3 | Effect of recycle ratio | 7.7 |
| 7.2.4 | Hydrophobic effects | 7.9 |
| 7.3 | Floc flotation | 7.10 |
| 7.3.1 | Flotation response | 7.11 |
| 7.3.2 | Comparison of floc and particle flotation | 7.14 |
| 7.3.3 | Effect of recycle ratio | 7.15 |
| 7.3.4 | Effect of hydrophobicity | 7.17 |
| 7.4 | Coagulant flotation | 7.19 |
| 7.4.1 | Flotation response | 7.20 |
| 7.4.2 | Comparison between flotation and sedimentation | 7.22 |
| 7.5 | Theoretical analysis of the capture process | 7.23 |
| 7.5.1 | Target efficiency | 7.24 |
| 7.5.2 | Inclusion of short range forces | 7.28 |
| 7.5.3 | Results | 7.29 |
| 7.5.4 | Flotability criteria | 7.31 |

| | | |
|------------------------------------|---|------------|
| 7.6 | Conclusions | 7.34 |
| CHAPTER 8 | RESULTS : Bubble size measurements | 8.1 |
| 8.1 | Introduction | 8.1 |
| 8.2 | Model of bubble production | 8.1 |
| 8.3 | Results | 8.6 |
| | 8.3.1 Effect of saturator pressure | 8.6 |
| | 8.3.2 Effect of orifice size | 8.8 |
| | 8.3.3 Effect of nozzle length. | 8.9 |
| | 8.3.4 Effect of impingement plates | 8.11 |
| | 8.3.5 Effect of diverging cones | 8.12 |
| | 8.3.6 Effect of surfactant | 8.13 |
| 8.4 | Nozzle design | 8.14 |
| 8.5 | Conclusions | 8.15 |
| CHAPTER 9 | CONCLUSIONS AND SUGGESTIONS FOR FURTHER WORK | 9.1 |
| | 9.1 Conclusions | |
| | 9.2 Suggestions for future work | |
| REFERENCES AND BIBLIOGRAPHY | | |
| APPENDICES | Appendix A | |
| | Appendix B | |
| | Appendix C | |
| | Appendix D | |
| | Appendix E | |
| | Appendix F | |
| | Appendix G | |
| | Appendix H | |
| | Appendix I | |

LIST OF FIGURES

| | | |
|------------|---|------|
| Figure 2.1 | Three mechanisms of dissolved air flotation. A, Adhesion of a gas bubble to a suspended solid; B, Trapping gas bubbles in a floc structure as the gas bubbles rise; C, adsorption of gas bubbles in a floc structure as the floc structure is formed (after Lipták, 1974) | 2.3 |
| Figure 2.2 | Model particle-bubble collision system showing the limiting trajectory | 2.6 |
| Figure 2.3 | Single collector collision efficiency against particle size for the individual mechanisms : I (inertial), S (sedimentational)D (diffusional) | 2.10 |
| Figure 2.4 | Hydrophobicity and contact angle for (a) hydrophobic surface (b) hydrophilic surface | 2.13 |
| Figure 2.5 | Schematic of the electric double layer and the resulting potential decay curve | 2.17 |
| Figure 2.6 | Schematic energy versus distance profile of DLVO interaction | 2.21 |
| Figure 3.1 | Generalised view of the bubble formation process (after de Rijk, 1993) | 3.1 |
| Figure 3.2 | Stabilised crevice configuration for (a) hydrophobic crevice, (b) hydrophilic crevice. (after Urban, 1979) | 3.4 |
| Figure 3.3 | Visualisation of the one stage model for bubble production with a direct gas flow.(after Repanas, 1992) | 3.7 |
| Figure 3.4 | Nozzle configurations | 3.9 |
| Figure 3.5 | Development of the flow patterns within a idealised nozzle (after Urban 1979). | 3.12 |
| Figure 3.6 | Details of Takahashi nozzles (after Tkahashi, 1979) | 3.16 |
| Figure 3.7 | Various configurations of saturation systems. | 3.22 |
| Figure 4.1 | Process flow diagram of the flotation rig | 4.11 |
| Figure 4.2 | Diagrammatic sketch of the bubble zeta potential measurement cell | 4.12 |

| Figure(x) | | |
|---------------|--|------|
| Figure 5.1 | Exploded view of modular nozzle assembly | 5.14 |
| Figure 5.1b1 | Impingment plate | 5.15 |
| Figure 5.1b2 | Socket head cap screw | 5.16 |
| Figure 5.1b3 | Nozzle housing nut | 5.17 |
| Figure 5.1b4 | Orifice plate | 5.18 |
| Figure 5.1b5 | Sealing nut | 5.19 |
| Figure 5.1b6 | Diverging cone | 5.20 |
| Figure 5.1b6a | Nozzle chamber | 5.21 |
| Figure 5.1b7 | Nozzle housing adapter | 5.22 |
| Figure 5.2 | Process flow diagram of the bubble photography rig | 5.23 |
| Figure 5.3 | Schematic diagram of the observation cells tested | 5.24 |
| Figure 5.4 | Flowchart of automatic image processing routine | 5.25 |
| Figure 5.5 | Example pictureboard of automatic image processing routine | 5.26 |
| Figure 6.1 | Diagrammatic sketch of a Kaolin particle's structure | 6.2 |
| Figure 6.2 | Sketch of a typical Kaolin crystal | 6.3 |
| Figure 6.3 | Diagrammatic sketch of a Wyoming Bentonite's structure | 6.4 |
| Figure 6.4 | Zeta potential frequency plot for dispersed Kaolin particles | 6.6 |
| Figure 6.5 | Reproducibility of zeta potential measurement for dispersed Kaolin particles | 6.7 |
| Figure 6.6 | Zeta potential vs pH for dispersed Kaolin particles in tap and distilled water | 6.8 |
| Figure 6.7 | Zeta potential vs pH for dispersed Wyoming Bentonite particles in tap and distilled water. | 6.11 |
| Figure 6.8 | Zeta potential vs concentration of n-aklytrimethylammoniumbromide for dispersed Kaolin particles | 6.11 |
| Figure 6.9 | Zeta potential vs pH for various surfactant concentrations with : (a)do; (b)tetra; (c)hexa alkyltrimethylammoniumbromide on dispersed Kaolin particles | 6.14 |
| Figure 6.10 | Zeta potential vs concentration of n-aklytrimethylammonium bromide for dispersed Wyoming Bentonite particles | 6.17 |

| | | |
|-------------|---|------|
| Figure 6.11 | Zeta potential vs pH for various surfactant concentrations with : (a)do; (b)tetra; (c)hexa alkyltrimethylammoniumbromide on dispersed Wyoming Bentonite particles | 6.18 |
| Figure 6.12 | Stability diagram for Al(III) coagulation (after Johnson 1983) | 6.20 |
| Figure 6.13 | Stability diagram for Fe(III) coagulation (after Johnson 1983) | 6.21 |
| Figure 6.14 | Zeta Potential vs coagulant dose for dispersed Kaolin Particles | 6.22 |
| Figure 6.15 | Zeta potential vs pH for dispersed Kaolin particles in set solutions of Alum | 6.24 |
| Figure 6.16 | Zeta potential vs pH for dispersed Kaolin particles in set solutions of Ferric chloride | 6.25 |
| Figure 6.17 | Zeta Potential vs coagulant dose for dispersed Wyoming Bentonite Particles | 6.26 |
| Figure 6.18 | Zeta potential vs pH for dispersed Wyoming Bentonite particles in set solutions of Alum | 6.27 |
| Figure 6.19 | Zeta potential vs pH for dispersed Wyoming Bentonite particles in set solutions of Ferric Chloride | 6.28 |
| Figure 6.20 | Zeta potential vs temperature for dispersed Kaolin and Wyoming Bentonite particles. | 6.29 |
| Figure 6.21 | Mean particle size vs temperature for dispersed Wyoming Bentonite particles. | 6.30 |
| Figure 6.22 | Diagram of a potential decay curve | 6.31 |
| Figure 6.23 | Comparison of normalised viscosity and zeta potential against temperature for dispersed Wyoming bentonite particles in distilled water | 6.32 |
| Figure 6.24 | Zeta potential vs temperature for Wyoming Bentonite | 6.33 |
| Figure 6.25 | Zeta Potential vs concentration of n- aklydecyltrimethylammoniumbromide on air bubbles | 6.34 |
| Figure 7.1 | Mean particle size against surfactant dose. | 7.2 |
| Figure 7.2 | Typical flotation response for discrete particle flotation | 7.3 |

| | | |
|-------------|--|------|
| Figure 7.3 | Normalised removal efficiency against post flotation zeta potential for discrete Kaolin particles conditioned with Hexadecyltrimethylammoniumbromide, with changing recycle ratio. | 7.5 |
| Figure 7.4 | Comparison of Flotation and Sedimentation response for discrete particles conditioned with HTAB. | 7.6 |
| Figure 7.5 | Comparison of Flotation and Sedimentation response for discrete particles conditioned with TTAB | 7.6 |
| Figure 7.6 | Best fit efficiency curves for set recycle ratios. | 7.8 |
| Figure 7.7 | Maximum removal efficiency and injected bubble number against recycle ratio. | 7.8 |
| Figure 7.8 | Efficiency against zeta potential for dispersed Kaolin particles conditioned with aklydecyltrimethylammoniumbromide. | 7.10 |
| Figure 7.9 | Mean particle size against surfactant dose for Wyoming Bentonite particles | 7.11 |
| Figure 7.10 | Typical flotation response for Wyoming Bentonite conditioned with HTAB and TTAB | 7.12 |
| Figure 7.11 | Grade efficiency curves for the flotation of Wyoming Bentonite particles with HTAB | 7.13 |
| Figure 7.12 | Comparison between particle and floc flotation | 7.15 |
| Figure 7.13 | Effect of recycle ratio on the efficiency against flotation curve for Wyoming Bentonite flocs | 7.16 |
| Figure 7.14 | Grade efficiency curves for Wyoming Bentonite conditioned with HTAB at different recycle ratios | 7.16 |
| Figure 7.15 | Effect of surfactant type on the efficiency against zeta potential curves for Wyoming Bentonite flocs | 7.18 |
| Figure 7.16 | Floc size distribution for Wyoming Bentonite particles conditioned with surfactant | 7.18 |
| Figure 7.17 | Floc size distribution generated using coagulants with dispersed clay particles | 7.19 |

| | | |
|-------------|--|------|
| Figure 7.18 | Removal efficiency against zeta potential for Wyoming Bentonite and Kaolin particles conditioned with Alum and ferric chloride | 7.21 |
| Figure 7.19 | Removal efficiency against zeta potential for sedimentation and flotation of clay particles conditioned with coagulants. | 7.22 |
| Figure 7.20 | Co-ordinate system for particle trajectories | 7.28 |
| Figure 7.21 | Single collector efficiency against particle size for different bubble volume fractions. | 7.30 |
| Figure 7.22 | Single collector efficiency against particle size for different particle densities. | 7.31 |
| Figure 7.23 | Removal efficiency against the product of particle and bubble zeta potentials. | 7.33 |
| Figure 7.24 | Comparison of the flotability criteria between discrete particle and floc flotation | 7.34 |
| Figure 8.1 | Diagrammatic sketch of the 3 stage bubble production model. | 8.2 |
| Figure 8.2 | Scanning electron micrograph of side elevation of the inner orifice of two cavitation plates of different diameters. | 8.3 |
| Figure 8.3 | Video still of an injected bubble flow. | 8.4 |
| Figure 8.4 | Typical bubble size distribution. | 8.6 |
| Figure 8.5 | Effect of saturator pressure on the mean bubble size | 8.7 |
| Figure 8.6 | Effect of orifice diameter on the mean bubble size | 8.8 |
| Figure 8.7 | Effect of nozzle length on the mean bubble size | 8.10 |
| Figure 8.8 | Typical bubble photograph for different nozzle chamber lengths | 8.10 |
| Figure 8.9 | Effect of impingement plate on the mean bubble size | 8.12 |
| Figure 8.10 | Effect of diverging nozzle cone on the mean bubble size. | 8.13 |
| Figure 8.11 | Effect of surfactant concentration on the mean bubble size. | 8.14 |

LIST OF PLATES

| | | Page |
|-----------|--|------|
| Plate 4.1 | Flotation equipment | 4.13 |
| Plate 4.2 | Flocculation bench | 4.13 |
| Plate 4.3 | Laser doppler electrophoresis equipment (Malvern Zetamaster ®) | 4.14 |
| Plate 4.4 | Bubble electrophoresis measurement equipment (Rank Brothers) | 4.14 |
| Plate 4.5 | Scanning laser microscopy equipment (Lasentec ®) | 4.15 |
| Plate 5.1 | Bubble photography experimental apparatus | 5.28 |
| Plate 5.2 | Modular nozzle assembly | 5.28 |
| Plate 5.3 | Typical bubble photograph | 5.29 |
| Plate 5.4 | Lens system | 5.29 |
| Palte 6.1 | S.E.M. of a typical kaolin and Wyoming bentonite particle | 6.5 |

LIST OF TABLES

| | | Page |
|-----------|--|------|
| Table 3.1 | Configuration of nozzles (after Takahashi, 1979) | 3.17 |
| Table 5.1 | Description of nozzle component ranges | 5.10 |
| Table 6.1 | Concentration required to obtain surface saturation for each surfactant with kaolin particles | 6.13 |
| Table 6.2 | Concentration required to obtain surface saturation for each surfactant with Wyoming bentonite particles | 6.17 |
| Table 8.1 | Summary of bubble production model | 8.5 |

NOTATION

| | |
|--------------------------|--|
| A | Hamaker constant |
| c | Concentration of ions |
| d_p | Particle diameter |
| d_b | Bubble diameter |
| E_{Total} | Total energy of interaction |
| $E_{electrical}$ | Energy of interaction due to electrical repulsion |
| $E_{dispersion}$ | Energy of interaction due to dispersion forces |
| $E_{structural}$ | Energy of interaction due to structural forces |
| F_T | Total force of interaction between a bubble and a particle |
| F'_{elr} | Dimensionless force due to electrical repulsion |
| F'_{vdwr} | Dimensionless force due to dispersion force |
| F'_H | Dimensionless force due to hydrodynamic force |
| g | Acceleration due to gravity |
| ΔG | Change in free energy |
| ΔG°_{abs} | Change in free energy due to the adsorption of a CH ₂ group |
| h | Distance between bubble and particle |
| k | Boltzmann constant |
| l | Radius of envelope surrounding bubble in trajectory analysis |
| m | Flotability criteria |
| N_b | Number of bubbles |
| N_p | Number of particles |
| P | Pressure |
| P_L | Pressure of liquid phase |
| P_G | Pressure of gas phase |
| P_A | Pressure in saturator |
| Q | Saturator flowrate |
| r_c | Radius of critical trajectory |
| r_b | Radius of bubble |
| r_p | Radius of particle |

| | |
|---------------|---|
| Stk | Stokes number |
| S | Dimensionless approach distance |
| t | Nozzle thickness |
| U_0 | Terminal velocity of rising bubble |
| U_{py} | Particle velocity component in y direction |
| U_y | Fluid velocity component in y direction |
| U_{px} | Particle velocity component in x direction |
| U_x | Fluid velocity component in x direction |
| U_y' | Dimensionless velocity in y direction |
| U_x' | Dimensionless velocity in x direction |
| $x'_{0,1,2}$ | x-coordinate of predicted position of particle in streamline |
| $y'_{0,1,2}$ | y-coordinate of predicted position of particle in streamline |
| z | Valency of ions |
| ϵ | Permeability |
| κ | Debye-Hückel parameter |
| μ | Viscosity |
| θ | Contact angle |
| ρ_f | Fluid density |
| ρ_{ST} | Stokes density |
| ρ_p | Particle density |
| ρ | Density |
| σ_{AW} | Interfacial tension at air-water interface |
| σ_{AS} | Interfacial tension at air-solid interface |
| σ_{WS} | Interfacial tension at water-solid interface |
| τ | Dimensionless time |
| ψ_0 | Electrical potential at surface of a particle |
| ψ_h | Electrical potential at a distance h from the surface of a particle |
| ψ | Stream function for trajectory analysis |
| ζ_p | Particle zeta potential |
| ζ_b | Bubble zeta potential |

CHAPTER ONE

CHAPTER ONE

INTRODUCTION

Flotation processes separating aqueous mixtures of heterogeneous particulates have been a feature of the mineral processing industry for decades, but the application to water and wastewater treatment is a more recent development. The processes have many similarities but some fundamental differences. In mineral flotation, the aim is to separate a specific particle type from the bulk and it is common to use chemicals to enhance the collection and stabilise the foam. The bubbles are supplied to the process by beating air into the liquid with mechanical rotors. In water treatment the aim is clarification by non selective removal of all particles within the fluid. In these cases the air is usually supplied by dissolving air into liquid under pressure, allowing the gas to expand out of solution under the lower pressure of the separation chamber.

Process stability is a key component to any water treatment application and DAF suffers from occasional erratic periods, resulting in poor clarification. The standard practice is to alter the coagulant dose and the recycle ratio until the plant starts to operate effectively. The problems are attributed to the empirical nature of the design and operation rather than based on an understanding of the fundamental mechanisms that occur. In particular, the requirements of charge neutralisation and hydrophobicity, which are established in mineral flotation, have not been transferred clearly to the flotation of flocs.

The purpose of this investigation is to improve the understanding of the fundamental mechanisms that operate in the dissolved air flotation process. In particular it examines the role of surface forces on the process of attachment of particles to bubbles.

CHAPTER TWO

CHAPTER TWO

LITERATURE REVIEW : REMOVAL MECHANISMS

2.1 INTRODUCTION

The process of removal in dissolved air flotation can be subdivided into three key steps. The three steps are the approach and collision of a bubble with a particle, the thinning of the intervening water film between the two surfaces resulting in the eventual rupture and the attachment of the bubble to the particle. The analysis of the process usually examines each step individually. An example of this is found in the work of Kitchener (1981) who subdivided the process from a micro-kinetic view to identify three individual probability terms. The overall probability of capture is the product of the three such that:

$$\text{Chance of Flotation} = \text{Probability of Particle - bubble contact.} \times \text{Probability of Attachment.} \times \text{Probability of Retention.} \quad (2.1)$$

The first two events are responsible for the capture of the particles and much work has been completed in a search for a fundamental treatment from the mineral processing point of view; a good review of these studies can be found in Trahar (1976). The situation differs from that of mineral flotation as flocculated particles rather than discrete ones are being processed. The differences mean that a range of mechanisms can operate and these can be summarised as:

- (A) Adhesion of a gas bubble to the suspended phase as a result of collision between the bubbles and the suspended phase
- (B) The trapping of rising gas bubbles in a floc structure.
- (C) The adsorption of gas bubbles into a floc structure as it is formed

Figure 2.1 show a diagrammatic view of the different mechanisms. The first mechanism has received much attention due its extensive basis in the theories of filtration and classical mineral flotation (Bogdanov, 1980). The mechanism has two stages, firstly, transport of the particles to the gas bubble's surface and once there, adhesion between the two surfaces. The transport step is a question of hydrodynamics and is described in detail by hydrodynamic collision models. The adhesion step is a question of thermodynamics and requires the formation of a finite contact angle between bubble and particle. These ideas will be developed in more detail at a later stage.

The second mechanism, enmeshment, can occur at three stages: during floc formation, during floc breakage and subsequent reformation and as a result of the filtering out of rising air bubbles by sedimenting flocs.

Stevenson (1970) considered that, as the process is floc dependant, enmeshment would be the main capture mechanism and that the formation of a finite contact was not necessary. Although this idea was supported by Neis (1980), clearly only the third possible enmeshment mechanism is likely, i.e. that of sedimenting flocs enclosing rising bubbles. The justification of this is that the flocs are formed prior to the flotation stage and are unlikely to break up and re-form. Nevertheless, the enmeshment mechanism would be dominant when a high rate of coagulation and a rich floc concentration exists, which does not occur in the sparse systems in question.

The mechanism still has merit as it is the only explanation of the flotation of hydrophilic materials. In this case bubbles are seen to be enclosed by the floc's structure without contact, rather than becoming adhered to it. However, it is likely that a majority of the unadhered bubbles would be lost even with the slight agitation that occurs. The light open floc structures only require a few bubbles for flotation but the flocs are unlikely to trap sufficient bubbles to promote this mechanism of flotation.

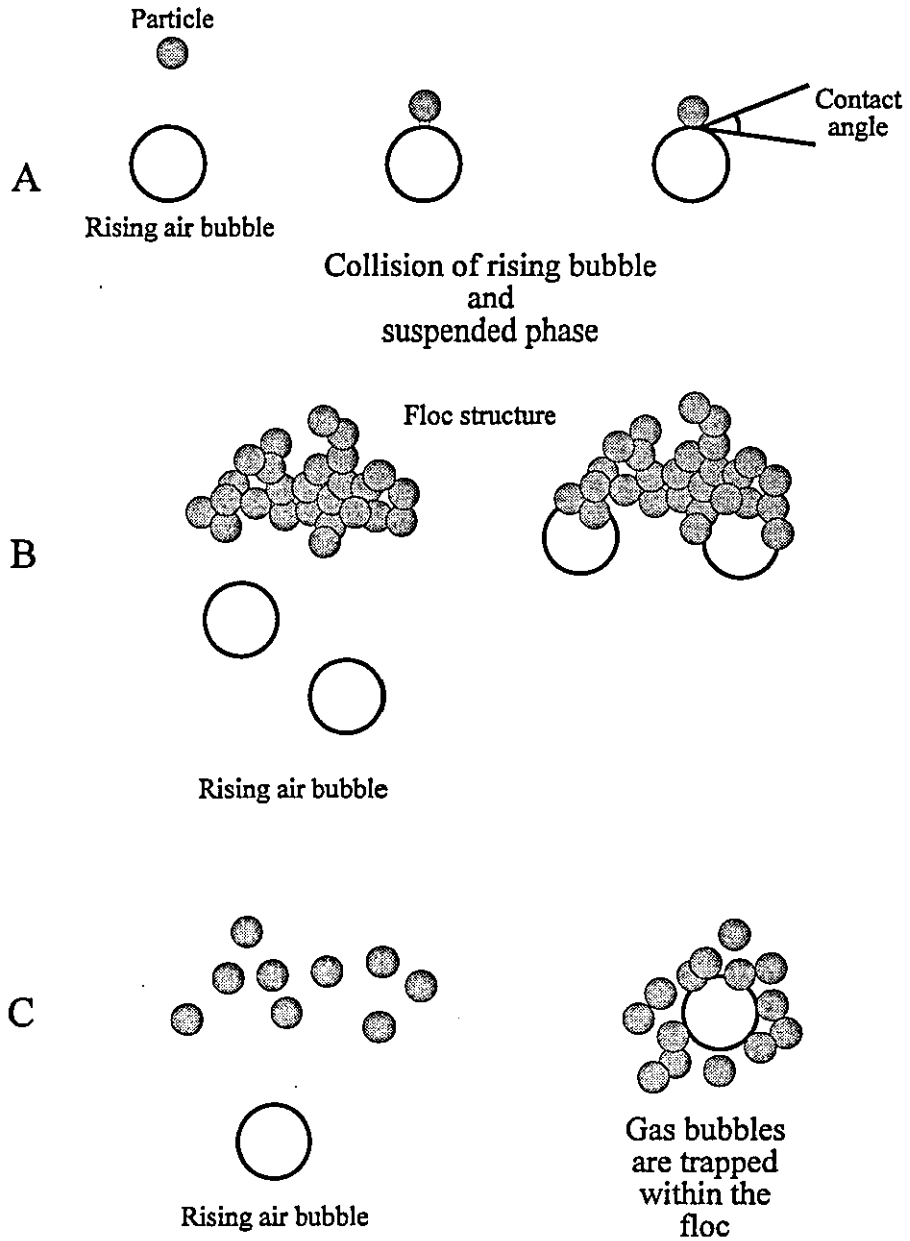


Figure 2.1 : Three mechanisms of dissolved air flotation. (A) Adhesion of a gas bubble to a suspended solid; (B), Trapping gas bubbles in a floc structure as the gas bubbles rise; (C), Adsorption of gas bubbles in a floc structure as the floc structure is formed

(after Lipták, 1974)

More likely is the existence of a few hydrophobic sites within the generally hydrophilic floc which the bubbles can adhere to after enmeshment had captured them. Neis (1980) examined the difference between particle and floc formation, stating that the adherence mechanism was not dominant as bubble size did not appear to effect the flotation rate as the classical collision theory would suggest. He accounts for this in that both his clay particles and bubbles were negatively charged creating a mutual repulsive force. When the bubble size exceeded the floc size he observed a decrease in the flotation rate and ascribed this to the flocs not being able to enclose the bubbles.

The final mechanism is one of precipitation and is thought to occur at the Harvey nucleation sites that exist on all particles as small gas cavities contained within the particles' natural surface imperfections. These sites are concave in nature and never completely dissolve in normal circumstances due to the equilibrium that forms between the water and gas phases.

Reay and Ratcliff (1973) suggest that this is an important mechanism in dissolved air flotation and offer evidence to support the idea. Although there is no doubt that the mechanism can operate, within the general scope of the systems considered here it is unlikely to operate. The reason for this is that the formation of free bubbles prior to injection into the tank is an efficient process such that only residual supersaturation remains. This is the driving force for the precipitation mechanism limiting its effect in this case. Kitchener (1981) concurs with this, dismissing this mechanism in normal situations suggesting a mode of operation where it would dominate. This involves the pressurising the whole flow such that the bubble formation occurs throughout the water volume, which of course needs to be a batch operation and is of limited practical significance.

The overall view is that the first two mechanisms are unlikely to be dominant enough to produce the observed effects. Thus the remaining alternative of adhesion of bubbles onto

the flocs upon collision is the mechanism that operates. This means that the situation is similar to that encountered in mineral flotation which can be used as a guide to modelling the system. However, the way in which bubble and floc collide will still differ as they are not discrete particles. Instead it would seem likely that a combination of multiple effects occur in conjunction with one another. The actual process is likely to be attachment of a few bubbles to specific particles within the floc, brought about by either classical collision or enmeshment followed by bubble rolling to appropriate sites. The two mechanisms differ in that bubbles will collide with the edges of the floc with classical collision and with the actual floc structure with enmeshment.

The remainder of this chapter will focus on the mechanism of collision followed by attachment. The theoretical descriptions of both processes will be reviewed and discussed in terms of the flotation of treated raw waters.

2.2 THEORETICAL PREDICTIONS OF THE COLLISION EFFICIENCY

The collision of particles and bubbles is controlled by the hydrodynamics. A number of authors have analysed the process in terms of the single collision collector efficiency. This calculates the efficiency with which particles collect on a single bubble due to deviations of the particle's motion in the fluid streamlines as they approach a bubble. To demonstrate the approach the work of Reay and Ratcliff (1973, 1975) and Flint and Howarth (1971) will be described in detail. These represent the most cited examples of the approach in the mineral flotation field. The review will then discuss some of the advances made to the model and the results that are generated.

Reay and Ratcliff (1973) based the model on calculating the trajectory of a particle relative to an approaching bubble. In particular, they considered the case of a limiting trajectory beyond which the particle would not graze the bubble and hence no collision would take place as shown in figure 2.2. The collision efficiency is described as the

fraction of particles in the volume swept out by the bubble which actually collide with it, compared to the number of particles that lie vertically above the bubble, such that:

$$E_c = \left(\frac{r_c}{R_b} \right)^2 \quad (2.2)$$

where:

E_c = collision efficiency

r_c = distance of particle from limiting trajectory (m)

R_b = bubble radius (m)

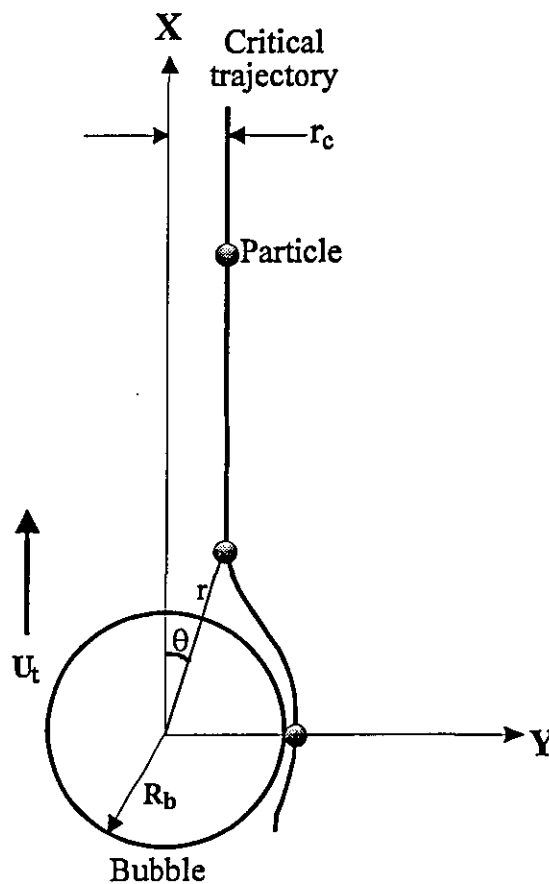


Figure 2.2 : Model particle-bubble collision system showing the limiting trajectory

It should be noted that in this the velocity is a composite of the settling velocity and bubble rise velocity and hence the relative velocity of one with the other, not just the rise velocity as sometimes reported. To solve the above equation trajectories for the fluid streamlines and the particles within them must be calculated. This represents a complex task where no analytical solutions are possible, instead numerical step by step and trial and error solutions for the respective trajectories are necessary. Reay and Ratcliff (1973) described a special case of small particles and small slow rising bubbles where an analytical solution becomes possible. The application suggested was for effluent treatment but is as equally valid for the present case of water treatment where a similar situation exists. In fact this is the exact situation encountered for dissolved air flotation and so should be most applicable to the present investigation. To create the necessary analytical equations they made a few simplifying assumptions:

1. The flow pattern around the bubble is governed by Stokes equation for a rigid sphere.
2. Electrical interactions between bubble and particle have a negligible effect on the flow trajectories.
3. Particles are swept to the back of the bubble such that the front half of the bubble is always clear.
4. The motion of the bubble is unaffected by the presence of the collected particles
5. The fluid velocity employed on the drag calculations is that which exists at the particles centre if the particle were absent.
6. Brownian motion is a negligible effect.

Jameson (1978) showed that the first assumption is valid when the bubble size is less than $100\mu\text{m}$. The bubble sizes that occur in the process will be distributed around a mean of $40\text{-}50\mu\text{m}$ and so this is valid in the present case. Okada (1990) demonstrated particles

being swept to the back of the bubble once collected supporting assumption two. This was shown to occur over the time taken for the bubble to travel one diameter and suggests that the bubble should always have a clean surface for collision. Once the particles are captured it is assumed that the flow field around the bubble is unaffected. This seems unlikely to be valid, especially when the bubble becomes more laden. It has been reported by Reay and Ratcliff (1975) that the model starts to deviate from experimental data when the particles become greater than 15 microns. This is attributed to the change in the flow field that occurs as the bubble begins to become laden with these bigger particles.

The other obvious difference is that flotation systems are far from single particle or bubble operations. Bubbles exist in highly concentrated swarms which will alter the bubble hydrodynamics. Flint and Howarth (1970) describes three ways in which a bubble swarm will affect the model

1. The bubble rise velocity will be reduced due to the hindering effect of the other bubbles.
2. The presence of other bubbles will tend to straighten the flow streamlines around a bubble.
3. The motion of particles above the target bubble will no longer be parallel to the direction of bubble motion at great distances above the bubble as the bubble layers above the target one will take effect.

Unfortunately, these factors can not be taken into account when developing the model as the problem becomes too complex again. However, the model does represent a useful first attempt in modelling the system and should always be pessimistic in its predictions. The most important assumption is that the electrical interactions between the bubble and particle are not important. This is not the case and this will be discussed in detail in section 2.4. The trajectory of a particle as it approaches a bubble is calculated by

formulating a differential equation based on a force balance for a particle. This approach is investigated in the present work and the details of the procedure can be found in section 7.5.1.

2.2.1 RESULTS OF THE COLLISION MODEL

The first important deduction that Reay and Ratcliff (1973) discussed was that within the particle sizes dealt with here only gravity played an important role in deviating particles from their streamlines. This is because small particles will be able to adjust to changes in the flow path almost immediately and so will not be affected by inertial effects. This idea concurs with the study of Flint and Howarth (1970) who conducted a similar investigation but over a wider range of particle sizes. They also found that inertial effects only become apparent with large particles, considerably larger than those encountered in the treatment of raw waters. From their investigation Reay and Ratcliff (1973) showed that the collision efficiency could be related to the ratio of the particle and bubble sizes, raised to a constant which was dependant on the density ratio.

$$E_1 = \alpha \left(\frac{r_p}{R_b} \right)^\beta \quad (2.3)$$

where the coefficients are:

$$\frac{\rho_p}{\rho_f} = 1.0 \Rightarrow \alpha = 1.25, \beta = 1.9$$

$$\frac{\rho_p}{\rho_f} = 2.5 \Rightarrow \alpha = 3.6, \beta = 2.05$$

Generally the collection efficiency is seen to be proportional to the square of the ratio of radii of the particle to bubble. This gives clear evidence for the benefits of small bubbles as the bubble radius is related to the efficiency by an inverse square relationship. They

showed later (1975) that this is only true for bubbles whose size is less than 100 μm as the Stokes flow field breaks down and the model no longer adequately describes the system. A similar approach has been directly applied to dissolved air flotation by Edzwald (1991) and Malley (1988) to examine how specific process variables would effect the process. They plotted the single collision collector efficiency for each individual mechanism of particle deviation. An example of the curve is shown in figure 2.3.

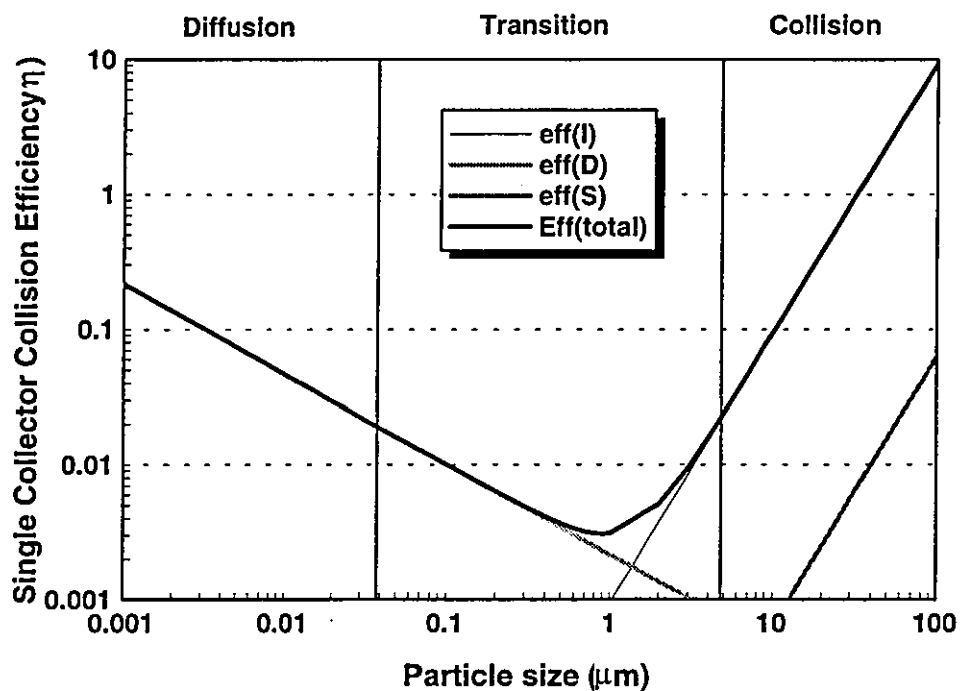


Figure 2.3 : Single collector collision efficiency against particle size for the individual mechanisms: I (interception), S (sedimentational), D (diffusional), (after Malley 1988)

The curve shows three different regions where differing mechanisms dominant; these regions are diffusion, transition, and collision respectively. The calculated efficiency is about an order of magnitude greater in the collision regime than in the diffusion regime showing a clear preference for large particles. Particle sizes that lie in between the two size bands exist in the transition regime where a combination of effects occur. The

efficiency in this regime is at its lowest value with the actual minima occurring at about $1\mu\text{m}$. The efficiency curves demonstrate the advantages of flocculating particles such that they are collected in the collision regime where the efficiency is at its greatest. However, if sub micron particles are to be flocculated it must be ensured they become sufficiently large enough to enter the collision regime, otherwise they would enter the transition regime where the efficiency would decrease, not increase as desired. The benefits of this was observed by Fukui (1979) in the flotation of ferric oxide which as a sub micron particle floated very poorly, but once the pH had been adjusted to the isoelectric point flotation became effective which was due to the natural flocculation that would occur at this point transforming the size of particles in the system.

2.2.3 INCLUSION OF ELECTRICAL FORCES

Reay and Ratcliff (1975) tested their model experimentally and showed discrepancies with particle size. They attributed these to the effects of the particles' electric charge on the attachment efficiency. Improvements in the model have been made to include terms for the electrical interactions. The early work on this was conducted by Collins and Jameson (1976, 1977) and focused on incorporating the electrophoretic mobilities of the particle into the rate equations. A more direct attempt has been conducted recently by Okada (1990) who included short range forces into his model.

Malley (1988) demonstrated that the attachment efficiency and hence the electrical properties of the system had a marked effect on the removal efficiency. He showed that unless the attachment efficiency was high, very poor overall removal efficiencies resulted. He concluded that charge neutralisation was one of the key factors in effective flotation.

2.3 ATTACHMENT

The second stage in the collection process is the attachment step and represents whether or not a particle will stick to a bubble once it has collided with it. This stage is governed by the thermodynamics of the systems which determines whether or not the particle can attach to the bubble. Gochin (1983) and Edzwalds (1995) stated that the fundamental requirements for effective flotation are charge neutralisation and hydrophobicity, without which particles will not attach. The theory concerning both of these requirements is central to general colloid science. The basic concepts for both of these effects will be reviewed below from the collective works of Shaw (1992), Hunter (1981, 1992), Israelachvili (1986), Gregory (1993) and Davies (1961) amongst others. The reader is referred to the references listed for more detailed information about the subjects covered below.

2.3.1 Hydrophobicity

When a particle attaches to a bubble, the water film that originally surrounded both must be displaced. The relative tendency of the water to be displaced is described by the hydrophobicity of the surfaces.

The central concept to hydrophobicity is in the comparison of the bond that forms between a water molecule and the surface compared to the bond that forms between two water molecules. When the bond between the two water molecules is stronger than between the water molecule and the surface, the water molecules preferentially bond with themselves. In these cases the water is easily displaced and the surface is termed hydrophobic. When the water bonds more strongly to the surface than it does to itself the water's tendency is to remain on the surface. In these cases the water is difficult to displace and the surface is termed hydrophilic.

The hydrophobicity of particles can be determined by the types of bonds that they can form with water. Hydrophobic materials are ones that present non-polar groups to the exterior surface, such that the water can only bond through relatively weak dispersion forces. Hydrophilic materials on the other hand contain 'broken bonds' or polar groups on their surface with which water can bond to with strong cohesive forces. The classical way of rendering particles hydrophobic is to condition the surface with surfactants. These work by replacing charged sites on the surface of particles with long non polar chains which bond very poorly with water and produce high levels of hydrophobicity.

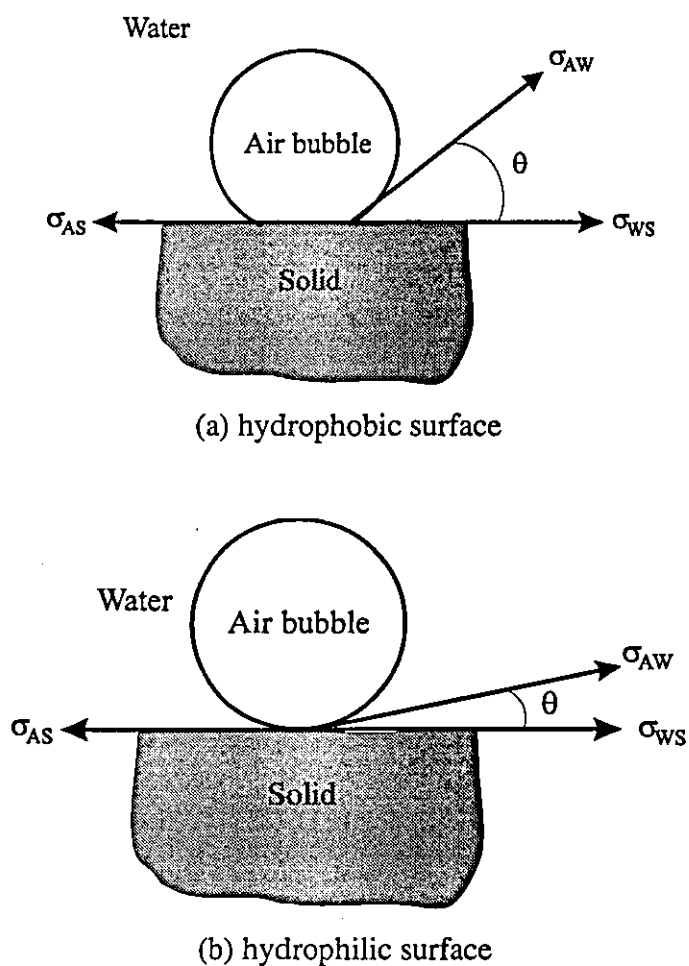


Figure 2.4 Hydrophobicity and contact angle for (a) hydrophobic surface (b) hydrophilic surface

The thermodynamic assessment of flotability is quantified by the contact angle which is formed at the three phase contact point. This is the angle that forms where the gas/liquid interface meets the solid and is shown in figure 2.4. The angle depends on the interfacial tensions of the three interfaces and at equilibrium is defined by Young's equation:

$$\sigma_{AS} = \sigma_{WS} + \sigma_{AW} \cos \phi \quad (2.4)$$

where:

- σ_{AS} = interfacial tension of the gas/solid interface (Nm^{-1})
- σ_{WS} = interfacial tension of the water/solid interface (Nm^{-1})
- σ_{AW} = interfacial tension of the gas/water interface (Nm^{-1})
- ϕ = contact angle ($^{\circ}$)

A contact angle forms when the work of adhesion (W_{AD}) between the surface and the water is less than the work of cohesion of the water (W_{CO}). The work of adhesion, defined as the work required to separate liquid water from the solid surface is given by the Dupré relationship

$$W_{AD} = \sigma_{SA} + \sigma_{AW} - \sigma_{WS} \quad (2.5)$$

combining (2.5) and (2.4) we obtain the Dupre-Young equation for the thermodynamic requirement for flotation:

$$\Delta G = \sigma_{AW} (1 + \cos \phi) \quad (2.6)$$

This equation relates to a flat surface and represents the maximum free energy change available. This means that although any angle greater than zero is theoretically required a

practical limit is set. Gochin (1982) quoted a value of 25° although significantly greater angles than this are preferable as they would represent stronger contact and so less chance of dislodgement.

The quoting of contact angles is complicated by contact angle hysteresis which occurs due to surface imperfections. The angle will be larger when the liquid advances over the solid than when it recedes. Obviously, the latter situation is more applicable to the systems under discussion in this present work. However, the former is often quoted as it is more reproducible experimentally and thus suggests that materials are more effectively floatable than seen in practice.

The application of contact angle ideas towards water treatment is complicated due to the fact that flocs are involved rather than discrete particles. The bubble to floc contact may occur at more than one point such that smaller individual contact angles are required than when only one contact point exists. A discrepancy exists with the idea that hydrophobicity is required as highlighted by Edzwald (1995) in that the flocs are formed by coagulation with metal salts which have large amounts of associated water attached there surface. This will make the flocs hydrophilic and will prevent the formation of a finite contact angle. Kitchener (1980) reported that surfactants were required to make hydrophilic flocs floatable. He suggests this as evidence that the flotation of water requires trace organics to be present to ensure that the surfaces have at least patches of hydrophobicity. Gochin (1982) tested this notion experimentally and concurred with Kitchener's belief. He suggested that when not present a small quantity of soap or humic acid should be added to enable the process to operate. The overall requirement for hydrophobicity is clear but this may only require patches on the floc's surface to be hydrophobic rather than the whole surface.

2.3.2 Electrical neutrality

When a particle approaches a bubble closer than 100nm, short range forces begin to become important. There are several types of interactions which may be critical, the best known of which are van der Waals attraction and electrical repulsion. Together these make the basis of the classical DLVO theory of colloid stability, which calculates the total interaction force between two surfaces as they approach one another.

The following section will review the basic theory and highlight some recent advances that are pertinent to bubble particle interactions. The review begins with a description of the electrical double layer that forms when a charged surface exists in an aqueous medium.

2.3.2.1 The electrical double layer

Naturally occurring particles carry a negative charge due to a number of charging mechanisms. The most significant of these for the clays investigated in this work are lattice imperfections and broken hydroxyl bonds. The charge on the surface of the particles influences the ions in the surrounding aqueous phase, attracting ions of an opposite charge (counter ions) and repelling ions of a like charge (co ions). The distribution of these ions together with the effects of thermal motion produces an electrical double layer such that overall electroneutrality is maintained. Figure 2.5 shows a schematic of the idealised system consisting of two regions. An inner region where the ions are bound to the surface within one hydrated radius. The other is an outer region made up of loosely bound ions whose concentration is distributed according to the Maxwell-Boltzmann distribution such that it decays in an exponential manner with distance.

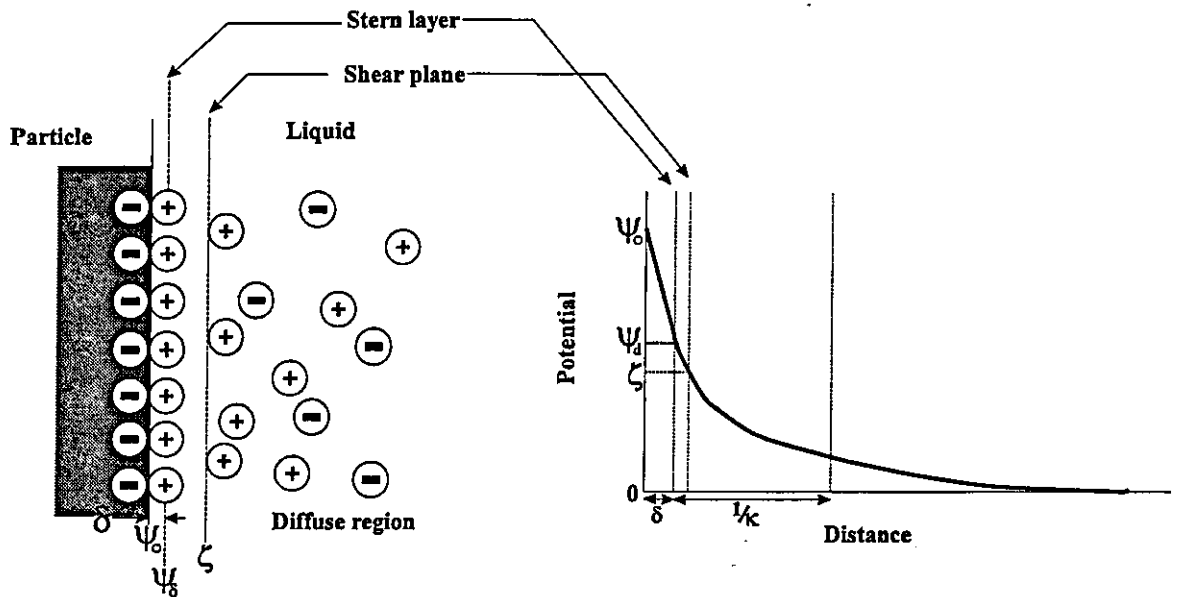


Figure 2.5 : Schematic of the electric double layer and the resulting potential decay curve

The analysis of the exact solution of the double layer is complex, but when the potential is low the expression for the diffuse region becomes:

$$\psi_h = \psi_o \exp(-\kappa h) \quad (2.7)$$

where

ψ_h = potential at distance h from the surface (mV)

ψ_o = potential at surface (mV)

h = distance from surface (m)

κ = Debye-Hückel parameter (m^{-1})

The Debye-Hückel parameter is a measure of the range of influence of the double layer. At a distance $h=1/\kappa$ the potential decays to $1/e$ of its original value and as such this position is referred as the double layer thickness. This is strongly dependant on the

electrolyte concentration in the system and for an aqueous solution at 25 °C is determined by:

$$\kappa = 0.328 \times 10^8 (cz^2) \quad (\text{cm}^{-1}) \quad (2.8)$$

where

c = concentration of ions (moll^{-1})

z = valency of ions

More complete treatments of the theory are available and the reader is directed towards the references listed at the start of this section for the detailed treatment. Difficulties exist in that the potential at the particle's surface and Stern layers cannot be measured. These problems are generally overcome by relating them back to a measurable quantity. This is the zeta potential which is a measure of the potential at a position which approximately relates to the start of the diffuse region of the double layer. The zeta potential is determined by measuring the velocity of a particle due to an applied electric field. The position in the double layer at which the zeta potential is measured is not fixed. When a particle moves due to an electric field the part of the double layer that is strongly bound to it will remain with it as it moves. The point at which this occurs is known as the plane of shear and it is at this point that the zeta potential is measured.

2.3.2.2 Total energy of interaction

The total interaction force that is generated as a particle approaches a bubble is analysed by the combination of the van der Waals and electrical interaction forces that are generated. Other forces exist such as hydration and hydrophobic forces and these will be discussed shortly. The model will be described in terms of the case for low potentials and

equal sized spheres as this represents the simplest case and demonstrates the concepts involved. The situation is more complicated and the reader is referred to Hunter (1981) who gives a fuller analysis of the model.

When two surfaces approach one another their diffuse double layers will penetrate each other. When the particles are of the same sign this will lead to a electrostatic repulsion which can be expressed in its simplest form as

$$V_R = 4\pi d\epsilon\zeta_p\zeta_B \exp(-\kappa h) \quad (2.9)$$

where

V_R = Energy of interaction due to electrostatic repulsion (J)

ζ_p = Particle zeta potential (mV)

ζ_b = Bubble zeta potential (mV)

This force is effected strongly by the zeta potentials of both particles and bubbles and by the ionic strength of the solution and it represents the main area which allows the control of colloid processes. The classical example is in coagulation theory which shows that increasing the salt concentration reduces the effects of the electrical repulsion allowing the particles to agglomerate. This effect of the electrolyte is mainly in the reduction of the size of the double layer thickness which allows the particles to approach one another more closely before the repulsion begins.

The electrostatic repulsion is counteracted by the van der Waals attractive force. In the disperse systems of interest here this is determined by the London dispersion interaction that is generated by charge fluctuations in the electron cloud. This is determined for the case of equal spheres as

$$V_A = -\frac{Ad}{12h} \quad (2.10)$$

where:

- V_A = Energy of interaction due to van der Waals attraction (J)
 A = Hamaker constant (J)
 d = particle size (m)

The negative sign of the expression denotes by convention that the force is an attractive one. The term A is the Hamaker constant of the interacting surfaces. This is the critical part of the expression as its value is difficult to determine. Gregory (1986) states the value of the Hamaker constant for a wide range of materials and shows that they lie typically between 1×10^{-19} and 1×10^{-20} J. The analysis of the van der Waals interaction tends to overestimate the magnitude of the force generated with large particles and this is usually corrected for by a retardation factor. This problem only becomes apparent for distances over 50 nm

The total energy of the interaction between two surfaces is obtained by the summation of the electrical double layer and van der Waals energies. An example of the curve that results is shown in figure 2.5.

When the zeta potentials of the particle and bubble and the ionic strength of the solution are such that repulsion outweighs attraction, an energy barrier to attachment is created and the particle will not be collected. This is seen in the total interaction curve extending into the positive region. As the zeta potential is reduced and/or the ionic strength is increased the energy barrier is reduced upto a point when the curve never crosses into the positive side and at this point no barrier to collection exists.

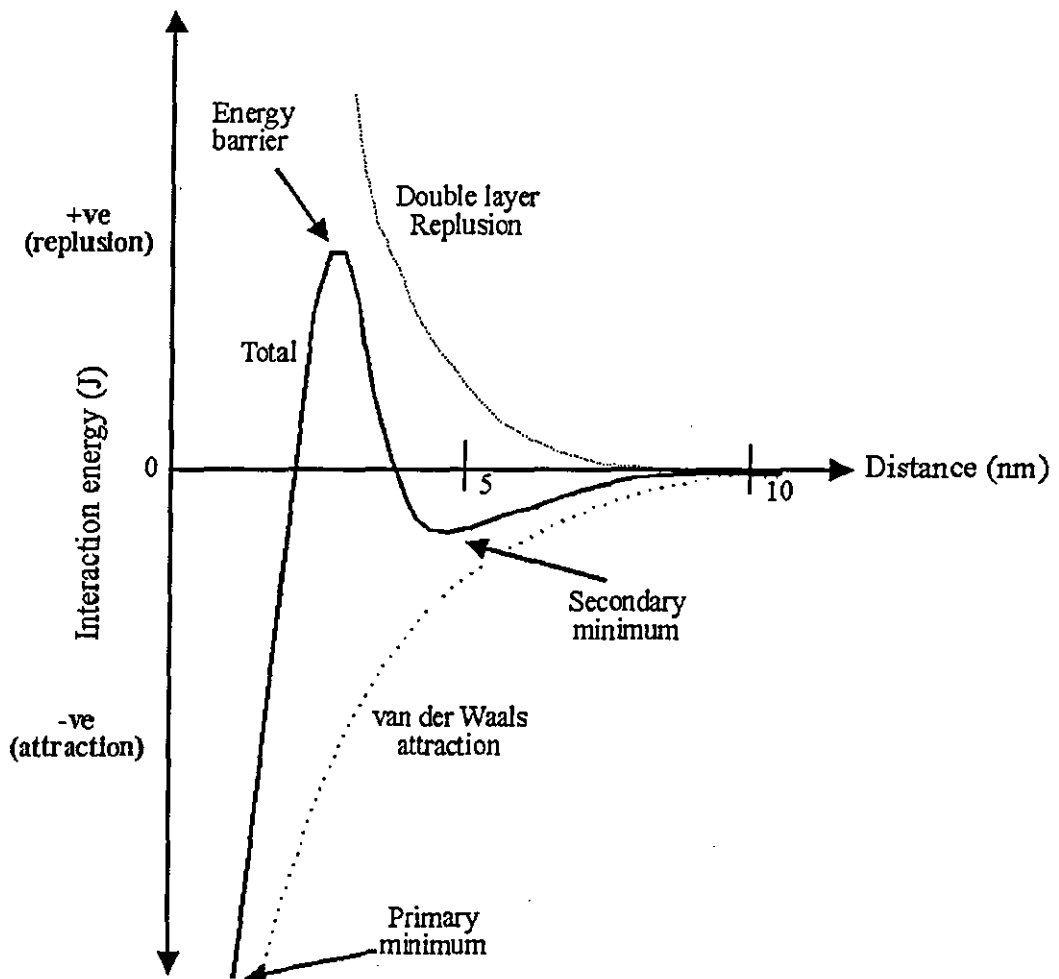


Figure 2.5 : Schematic energy versus distance profile of DLVO interaction

A number of important features are worth highlighting. When a barrier exists the colliding surfaces must overcome it in order to contact. Gregory (1995) quoted a value of 20 kT as an energy barrier that should always prevent contact. Once the barrier is overcome the primary attraction minima should always hold the surfaces together and so no detachment should occur. The other important feature is that because of the difference in the range of operation of the two forces a secondary minimum can exist which will

(1991) investigated its effect on the flotation of minerals and concluded that it was of critical importance.

2.3.3 Experimental investigation

A number of authors have examined the flotation process in terms of short range forces described above to generate a model of hetero-coagulation of a particle attaching to a bubble. The idea was most notably described by Deryaguin (1960) and also by Rao (1974) in terms of mineral flotation. The same idea was developed for fine particle flotation by Okada (1988, 1990) and by Sato (1979) for oil flotation. Other work also exists but the same idea is always developed. The curve of the total interaction force is analysed to determine the point at which the energy barrier just disappears. This generates a floatability criteria such as

$$m = \frac{4\pi\zeta_p\zeta_b}{\kappa A} \quad (2.11)$$

The exact value of m quoted by authors varies due to the slightly different forms of the model that they use; however, the value usually lies between 3 and 3.5. The model has been tested by relating the zeta potential to the removal efficiency, which involves measuring the particle zeta potential as that is relatively easy to do. In all cases the efficiency was high when the magnitude of the zeta potential was low. However, no greater link between the variables has been established, which is due probably to the complexities of the analysis and numerous variables that affect it. Okada (1988) tested the model with oil droplets and showed good agreement with the floatability criteria showing a clear cut off at about $m=3$ when he used high valency electrolytes. He extended this idea to include the bubble zeta potential in his analysis and improved the correlation between the experimental data and his model as a result.

Edzwald (1991, 1995) and Roberts (1980) have conducted similar investigations but directly to raw water treatment applications. A strong relationship was found between zeta potential and removal efficiency but no real cut off could be determined. The results were presented as demonstrating the need to reduce the charge of the flocculated particles such that no energy barrier to attachment exists. However, no direct analysis of this was conducted in terms of the short range forces described above. Edzwald (1995) concluded with the view that charge neutralisation and hydrophobicity are the key requirements to successful flotation of flocculated raw waters.

2.4 CONCLUSIONS

The literature reviewed within this chapter has led to the following conclusions. The process is made up of two fundamental steps: collision between a bubble and an approaching particle followed by attachment between the approaching surfaces. The collision stage of the process has been analysed in terms of the single collision collector efficiency which calculates the limiting trajectories of particles as they flow around bubbles. The theory has been shown to describe the situation adequately and collision efficiency can be easily calculated for systems.

The attachment stage of the process is governed by the thermodynamics of the process and can be split into two requirements. The requirements are that the surface charge of both particles and bubbles must be so low as to offer no energy barrier to attachment. This is usually determined by measurement of the zeta potential of the surfaces involved. The second requirement is that the particle must have at least some degree of hydrophobicity to allow a three phase contact between the bubble and the particle to develop.

Although the general criteria for successful flotation have been developed, little work has been conducted on how these criteria are affected by the differences that exist between particle and floc flotation. This represents the area that most requires investigation at present. In particular the application of zeta potential in terms of both particles and bubbles requires a more detailed investigation, especially in connection with flocs.



CHAPTER THREE

CHAPTER THREE

LITERATURE REVIEW : BUBBLE PRODUCTION

3.1 INTRODUCTION

The bubble cloud required in the dissolved air flotation process is generated by the saturation of air into water under pressure and its subsequent release into an atmospheric environment. The production of the bubbles represents about 10-12% of the capital costs and 50% of the operating costs of a standard plants. Thus optimisation of the system is essential, especially in terms of operating costs. The process can be split into two separate stages, the first concerns the saturation of air into water, which determines the total amount of air that is released and will be discussed later in section 3.11 and the second is about the creation of the appropriate size and number of bubbles.

The efficiency with which the supplied air is used within the process is determined by the size of the bubbles formed. This is determined by the geometrical design and operating conditions of the injection system.

The usual process operates by releasing the supersaturated water to the atmosphere via a sudden pressure drop. This is normally created by a constriction in the flow in the form of a nozzle or a valve, shown diagrammatically in figure 3.1. The effect of such an operation is for the water to 'cavitate' where the excess gas is released from within the solution

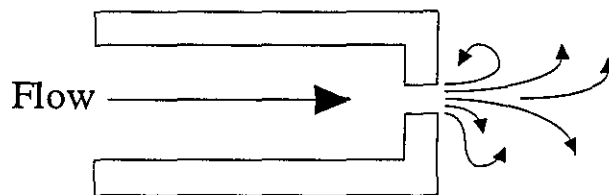


Figure 3.1 Generalised view of the bubble formation process (after de Rijk 1994)

The present chapter will review the literature that relates to the design of injection nozzles and the methods of saturation. The focus of the work is on the design of the injection nozzles as this is the least understood part of the process. The review initially examines the process at a fundamental level to ascertain the mechanisms that operate. This is then followed by a review into practical nozzle design followed by a section on the advances achieved through experiment investigations that have attempted to determine design equations.

3.2 EXISTENCE OF NUCLEATION SITES

The air that is used to generate the gas bubbles comes from the cavitation of a supersaturated water flow. The flow is cavitates by forcing it through a restriction which leads to a region of atmospheric pressure. A sudden pressure drop is created which forces the excess air out of solution. At this stage an important distinction is necessary in defining cavitation. Urban (1980) reviewed the complex work of Knapps (1970) on the subject of cavitation and highlighted two distinct types. The first involves the idea of the pulling apart of groups of water molecules to form cavity spaces in which vapour can exist. This type of nucleation is referred to as *de novo* nucleation and involves the creation of nucleation sites from within a homogeneous fluid. This process requires considerable forces to achieve stable cavities and Urban (1980) demonstrated that these are never generated within the dissolved air flotation process.

The second type of cavitation is based on the idea that as the nucleation sites already exist such a process becomes one of activation rather than creation. These sites are named after the work of Harvey (1946) who first established their existence. They exist within the natural crevices at the fluid solid boundary or as very small bubbles in solution whose size is sufficiently small as to avoid creaming, such that the bubbles remain in solution (Wedlock, 1994). When the supersaturated flow cavitates the excess air feeds these sites which then grow into free flowing bubbles.

Urban (1980) found evidence of these sites by discussing some of the anomalous properties of water. The two most significant of these are that water boils at 100 °C instead of the 300 °C that is theoretically predicted and that only ambient pressure is possible in the suction head of a liquid pump.

The existence of such nucleation sites has been demonstrated experimentally by a number of authors and Urban (1980) offers a good review of their findings. The basic approach is consistent throughout in that the experiments involve removing the nucleation sites from the water and then measuring the force required to cavitate it. The most notable of these experiments used pre-pressurisation where the system experiences pressure magnitudes greater than those normally experienced within the process. This has the effect of dissolving all the gas even in the stable nucleation sites. Knapp (1958) showed this effect with a glass venturi tube which required an increased pressure drop to achieve cavitation of the water once the tube had been pre-pressurised. Hayward (1970) showed a similar effect by improving the suction head of a pump from 10m to 17m after the pump had undergone a pre-pressurisation cycle.

3.3 STABILITY OF NUCLEATION SITES

Harvey (1947) described two possible configurations of crevice in an attempt to explain how such crevices can support stable gas pockets at equilibrium. Figure 3.2 shows the different manner in which a meniscus between air and water can exist within a crevice on the surface of a solid. The stability of such interfaces is described by Laplace's equation for mechanical equilibrium of a meniscus to a system:

$$P_L - P_g = \frac{2s}{r} \quad (3.1)$$

Where:

P_L = pressure in the liquid. (Pa)

P_g = pressure in the gas (the sum of the vapour pressure of the liquid and the partial pressure of any gas present). (Pa)

s = surface tension of the liquid. (Nm^{-1})

r = radius of curvature of the interface. (m)

Equilibrium is established when the surface tension of the meniscus resists the pressure difference between the liquid and vapour phases. The equation shows that at standard conditions the maximum radius of a stable meniscus would be $1.47 \mu\text{m}$. This is consistent with the idea that such pockets must be small otherwise they would be visible or would undergo creaming if they were free bubbles or on the surface of small particles. .

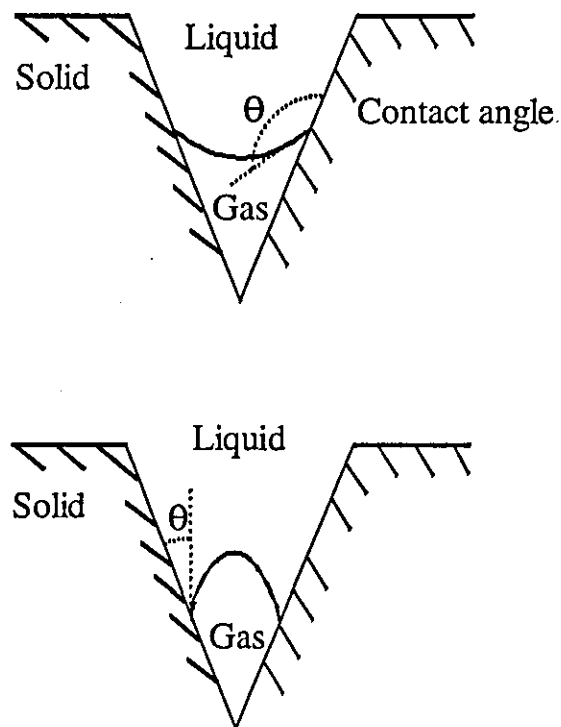


Figure 3.2: Stabilised crevice configuration for (a) hydrophobic crevice, (b) hydrophilic crevice.(after Urban 1980)

The nature of the crevices that form on the surface of a solid will mean that a range of crevice geometries exist. The stability of the meniscus that forms in these crevices is determined by the manner in which its size responds to pressure fluctuations. When the pressure goes up the radius of the meniscus needs to be decreased to maintain the balance between the two phases. Otherwise the equilibrium is no longer established and the meniscus disappears.

Figure 3.2a represents the general criteria required to produce a stable gas pocket. In this case the meniscus is convex to the gas phase with the angle of contact between the crevice wall and the meniscus being large and as such is deemed hydrophobic. This is a loosely defined term as it may be crevice geometry rather than true hydrophobicity that creates the large angle of contact. This results in the necessary alteration in the meniscus radius as the system responds to produce a stable interface and so the nucleation site is stable.

Figure 3.2b shows an alternative configuration, where the meniscus is concave to the gas phase. A pressure increase in this case would increase the radius of the meniscus which in turn increases the driving force of the radius change. Thus the meniscus is caught in a negative loop which makes it unstable and results in the nucleation site being dissolved back into solution. Such crevices are seen to have only small angles of contact and are thus referred to as hydrophilic in the present context.

3.4 LOCATION OF THE NUCLEATION SITES

The location of the nucleation sites within the systems has been an issue of concern for a number of authors. The work is split into two arguments; one for fixed sites and the other for free flowing ones.

The first idea is that the nucleation sites are not fixed but exist in the free flowing liquid. A number of possible sources have been reported but the most viable is that of Fox and Herzfeld (1954) who described the possibility of tiny gas bubbles which are

protected by *organic skins*. No exact definition of what these represent is given but presumably they refer to the adsorption of the naturally occurring organics in the system. These bubbles constantly remain in the water due to their very small size and are protected from dissolving back into solution by their organic skin. Fox and Herzfeld (1954) support this idea by explaining the results of pre-pressurisation as destroying the skins and thus allowing the gas to dissolve. Urban (1980) tested this theory by using progressively cleaner sources of water ranging from tap water to double distilled. The double distilled water would significantly decrease the number of nucleation sites available but no effect was seen in the bubble clouds produced. This shows that the sites do not exist within the flow but are fixed.

The alternative location refers to nucleation sites situated in the material of the nozzle or the container wall and are due to the surface roughness of the material which is either naturally occurring or the result of the manufacturing process. Urban (1980) simplified this by assuming that all the fixed nucleation sites were within the nozzle. This allowed for the nozzle to be conditioned externally to the rest thus effecting only the fixed sites in the system. He found that both pre-pressurisation and surfactant addition had a marked effect on the bubble cloud produced.

The position of the nucleation sites was further investigated by varying the orifice thickness and the number of holes in the orifice plate. The results demonstrated variations only with hole number indicating that the nucleation occurred at the top edge of the orifice rather than throughout its depth. Confirmation was obtained from the visual observation that two cloudy streams appeared either side of the nozzle rather than in the middle of the discharge stream.

Dean (1944) postulated an alternative theory which suggests activation in the bulk flow within the low pressure core of turbulent vortices. Calculations on such vortices by Urban (1980) showed that they could not produce the necessary pressure drop. However, the idea of these vortices has application as they will exist at the nozzle exit and will assist in the activation process. This will provide a low pressure

environment for the freshly formed bubble to grow initially, which provides a more stable environment at a point when the bubble might dissolve back into solution.

3.5 DETACHMENT

Bubbles grow on their nucleation sites by the uptake of the precipitated air. The growth continues until the buoyancy force and the fluid drag is sufficient to overcome the influence of the nucleation site as seen by the effects of the surface tension. Figure 3.3 shows a diagram of the situation:

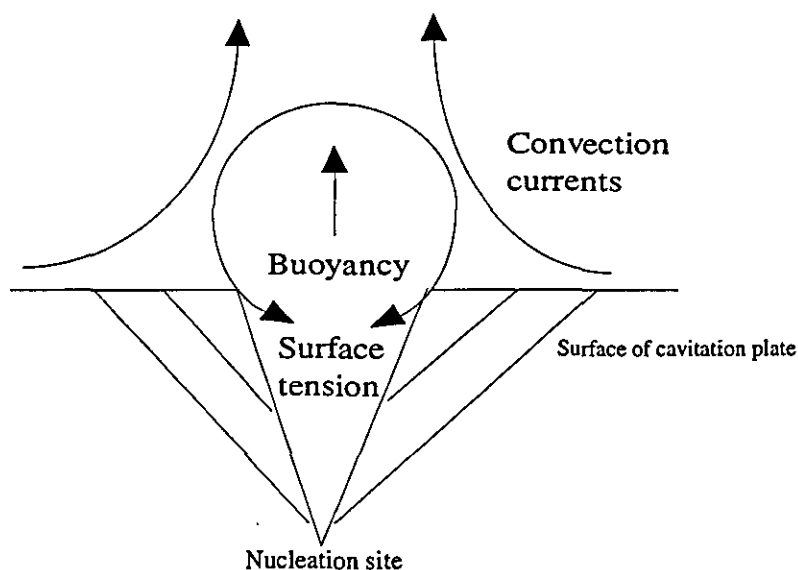


Figure 3.3 Visualisation of the one stage model for bubble production with a direct gas flow. (after Repanas 1992)

The exact nature of the detachment process does not appear to have been discussed in the literature to any significant degree. However, the work of Repanas (1992) offers a good review of the theory of bubble detachment in sparging and this can be adapted. Detachment is said to have occurred when the bubble has travelled one bubble radius from its nucleation site. The exact size produced is determined by a force balance around the bubble instantly before detachment takes place:

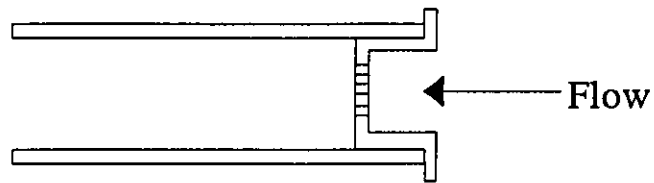
$$\text{Force}_{\text{surface tension}} = \text{Force}_{\text{drag}} + \text{Force}_{\text{buoyancy}} \quad (3.2)$$

The bubbles will detach when the combination of buoyancy and drag is greater than the surface tension force. A detailed description of this can be found in Repanas (1993) but has been excluded here as the ultimate analysis is flawed. The surface tension force presents a difficulty as this will be very dependant on the geometry of the nucleation sites. This is an unknown parameter which means that it is not possible to calculate the size of the bubbles upon dislodgement. However, it is possible to make some qualitative conclusions as pointed out by Urban (1979). Within a system it is reasonable to assume that the sites exist with a range of sizes and geometries such that a bubble size distribution will be generated at the point of dislodgement. The general concept holds that larger nucleation sites produce larger bubbles and the more open the crevice the larger the bubble will be upon dislodgement as the effects of the surface tension will be reduced.

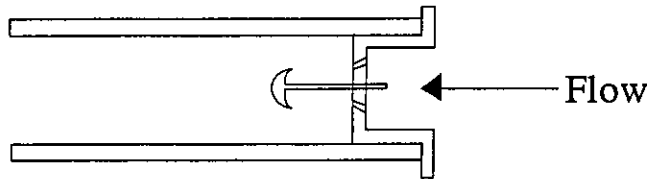
The detachment process remains a problem for any model of the process as it would have to take into account the configuration of the nucleation sites to determine the size at which they were dislodged. This is not possible at the present time and this has great implications for the ability of any model as the starting point at which the remaining process operates from is an unknown.

3.6 NOZZLE DESIGN

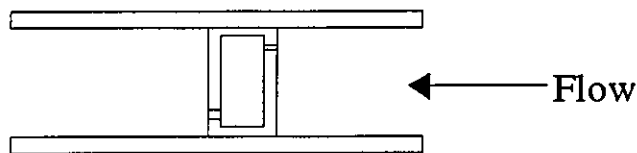
In practical situations, nozzles are designed on an empirical basis using established rules or criteria. This is because of the complexity of the system as described above preventing any rational design based on fundamentals. This section will describe the design approach used industrially to produce nozzles. The Guinness brewery company presented the initial investigations into nozzle design in their collective patents (Ash 1957, 1959, 1958, Carnaghan 1962, Painter 1966 and Hildebrand 1970) and this was followed by the Carnaghan (1962).



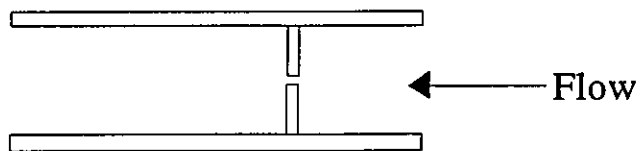
Guinness patent 1961



Guinness patent 1972



Water Research Centre 1976



Idealised 1980

Figure 3.4 : Nozzle configurations

Figure 3.4 presents a series of cited nozzle designs from industrial applications. A common feature of all the designs is the existence of a short constriction where the sudden pressure drop occurs, followed by a device to generate strong turbulence within the freshly cavitating liquid. The nozzles differ mainly in the degree of

intricacy with which this turbulence is created. The Guinness brewery company states that such turbulence homogenises the foam on a beer to produce a good foam size with a reduced standard deviation in the bubble size distribution. However, the patents do not state any figures on the mean sizes produced or on the specific effects of turbulence upon this. They also state that the reduction of pressure below atmospheric is the cause of bubble formation and not the turbulence. The Guinness brewery company conducted a series of experiments to deduce empirical design criterion for what they stated as good 'head' and these are summarised below:

1. Hole size: 0.15-0.08" {3.81-2.03 mm} (1958).
2. Thickness or depth of constriction:< 0.015" {0.381 mm}.
3. Distance between baffle and constriction:< internal diameter of tube.
4. Hole size: 0.025-0.05" {0.635-1.27 mm}, preferably 0.035" {0.889 mm} (1962).

It is believed that the size of the holes and the position of the baffle control the size of the bubble produced. The target bubble size was 0.01" {250 μ m}, somewhat larger than the present case. To achieve this size they altered the original design in two ways: Firstly, they decreased the orifice diameter and secondly increased the turbulence by introducing a concave baffle and impinging jets, maximising the disturbance of the fluid. The patents also include the composition of the gas as a factor, preferring a mixture of carbon dioxide and nitrogen to that of air, avoiding any problems with acetification. They found that varying the partial pressure of each component effected the size and endurance of the 'head', a factor rarely discussed.

Although this work represents a significant first step, no attempt is made to link design variables to bubble parameters except by qualitatively keeping nozzle design as much an art as it is a science. The Water Research Centre offers similar information in their patent for a purpose designed nozzle for dissolved air flotation operations. The actual design is very similar to that of the Guinness brewery company except in the manner with which the turbulence is created. In this case a chamber type arrangement is employed where two circular plates are positioned within a tube to generate a

confined space, see figure 3.5. The turbulence is generated as the in and outlet holes are geometrically offset, thus forcing the fluid to impinge on the second plate and alter direction in order to exit. The dimensions of the chamber are such as to provide strong turbulence; no rules are described for this or a definition of strong turbulence, however, an example is cited:

1. Diameter of tube: 1" {25.4 mm}.
2. Diameter of cavitation hole: 1/8" {3.17 mm}.
3. Diameter of exit hole: 1/4" {6.35 mm}.
4. Length of chamber: 1/4" {6.35 mm}.

These represent significantly larger sizes than those of Guinness and no mention is made of a temperature dependant critical orifice size as in one of the Guinness patents (Carnaghan 1964). Alternative devices exist; however all are based on the principle of a short constriction to evoke cavitation followed by turbulence to homogenise the swarm's characteristics. They differ only in the varying complexity of the design, especially in the feature intended to create turbulence..

Urban (1980) investigated the design of nozzles and concluded that the intricate designs employed could not produce significantly greater turbulence than a more simple open device. Apart from that, the dissipation of the excess kinetic energy does occur in a small volume and he noted that this may be beneficial to the results. Examination of the fluid dynamics indicates that the high velocity core generated by the decompression will lose its identity in 5-6 hole diameters. A boundary is established between the spreading jet and the slow moving fluid with an apex angle of 14°. The slow moving fluid circulates as eddies until the expanding jet contacts the wall in about 4 pipe diameters. The flow pattern is shown in figure 3.5 and indicates that the most appropriate design to investigate nozzle parameters would be a simple idealised configuration as no significant advantage appears apparent for the more intricate designs.

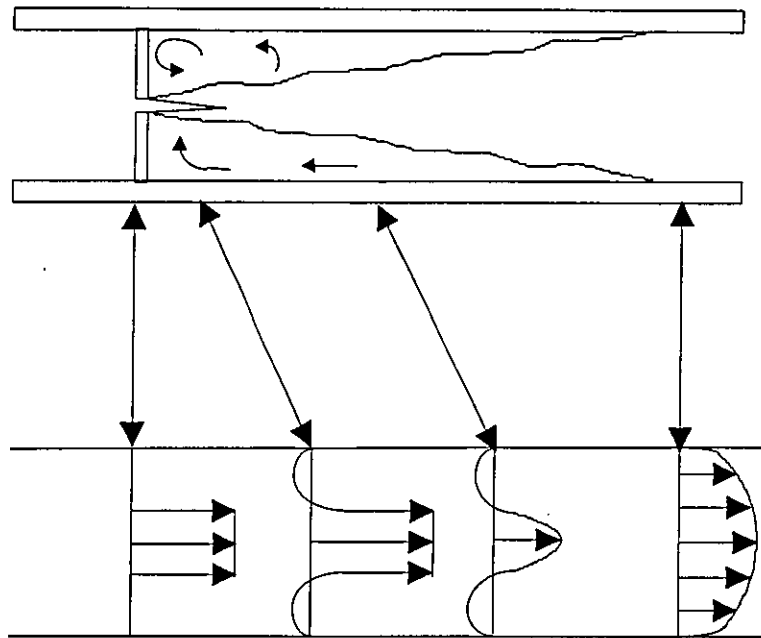


Figure 3.5 Development of the flow patterns within an idealised nozzle (after Urban 1980).

3.7 EXPERIMENTAL INVESTIGATIONS INTO NOZZLE DESIGN

Although the qualitative descriptions of the previous section are beneficial to the engineer, the overwhelming aim remains that of quantification so that consistently reliable design equations can be developed. This section describes the experimental work of the major investigations into nozzle design in a chronological order to demonstrate the development of the understanding of bubble production.

Urban (1980) acknowledged the complexity of the process and attempted to evaluate the problem in a more systematic way by setting up a fractional factorial design scheme. This approach enabled Urban to examine all the possibilities in the minimum number of tests and resulted in a set of regressed design equations being developed. In these equations, variables are assigned values of either ± 1 to represent certain prescribed values of the actual variables. An example result of this is shown for the variables of pressure, orifice diameter and percentage injection.

D Orifice diameter,

D = 0.75 mm Coefficient = -1.5

D = 1.01 mm Coefficient = -0.5

D = 1.43 mm Coefficient = 0.5

D = 2.03 Coefficient = 1.5

P Saturation pressure

P = 20 Psig Coefficient = -1.5

P = 40 Psig Coefficient = -0.5

P = 60 Psig Coefficient = 0.5

P = 80 Psig Coefficient = 1.5

G Percentage injection

G = 5 % Coefficient = -1

G = 10 % Coefficient = +1

The coefficients are then entered into the regressed equations rather than the actual values. To illustrate this the example for the calculation of mean bubble size and bubble number concentration is shown. The regressed equations are:

$$\text{Mean bubble diameter} = 57.7 + 0.5D + 3.7(D^2 - 1.25) - 5.7P + 0.7DP \quad (3.3)$$

$$\text{Bubble number/mm}^3 = 50.3 + 24.5P + G(29.1 + 11.8P) - 1.9DP \quad (3.4)$$

Thus when D = 0.75 mm, P = 80 Psig, G = 5 %. The coefficients to be entered into the regressed equations become: D = -1.5, P = 1.5, G = -1 which yields:

Mean bubble diameter = 50.53

Bubble number/ mm³ = 44.53

The above procedure has the advantages that the effect of individual variables can be determined from the estimation of the means from a series of tests due to the symmetrical nature of the experiments. More importantly, such an approach permits effects due to the interaction of combinations of variables to be examined. However, limitations exist, the application of any derived equation is constricted in a nodal manner such that any variable must relate to a pre-supposed value. The other concern relates to the confidence with which the coefficients of the regressed equations can be assigned. Increasing the number of variables results in fewer data points contributing to each individual coefficient, reducing its reliability.

The usefulness of such an approach is qualitative, enabling examination of the possible trends rather than direct correlations to be established. This more conservative approach would seem appropriate as the problem appears to be too complex for simple design equations. Urban (1980) discussed the effects of individual variables in this way, preferring to describe the observed results in terms of the concepts discussed above to try to understand the mechanisms of bubble production. The work concentrated on the two most accessible variables: orifice diameter and saturation pressure.

The results for orifice diameter showed a curve with a minimum in mean bubble size at an orifice diameter just over 1 mm. Urban discusses this in terms of the factors that alter with orifice diameter. Principally this is the perimeter of the orifice which will provide more possible nucleation sites. The degree of cavitation occurring also increases with diameter and thus increases the excess pressure available enabling a greater proportion of available sites to be activated. Counteracting this will be a reduction in the residence time within the nozzle as the average velocity of the liquid will remain constant (thus increasing the throughput). A combination of the above effects is offered tentatively to describe the processes which result in the minima observed.

The effects of pressure show a linear relationship between mean bubble size and pressure, indicating as believed, the possible advantages of increased pressure. Again a series of effects can be discussed tentatively within the suggested model. An increase in pressure would release a greater proportion of air per unit of water and generate a stronger cavitation force across the nozzle orifice. The result of this will be that smaller nucleation sites will be able to be activated. The size of the bubbles at the point of detachment will also decrease as the velocity and therefore turbulence of the fluid will have increased. This will release bubbles with a smaller size into the free flowing liquid within the nozzle at an earlier stage in their growth. The overall result will be in that a greater number of bubbles exist. The available air will have to be shared out over that greater number, decreasing the size of individual bubbles.

Urban's investigation then considered the effects of surfactant concentration in both the flotation tank and the saturator. In this way surfactant is seen as a second string variable due to its independent nature. This is observed in the regressed equations as surfactant only enters within the grouped components although such a factor may have a marked effect. The observed results did indeed demonstrate some interesting trends indicating the significance with which surface chemistry effects the process

Urban's first observation is that the application of surfactant suppresses the influence of the principal variables to almost negligible degree. A shift in magnitude is also observed showing a considerable decrease in bubble size. This is most notable with the effects of pressure, where increasing the saturation pressure no longer reduces the mean bubble size produced. This indicates that the minimum acceptable pressure for decompression would be optimal if surfactants were present. Over the pressure range investigated of 20-80 psig, the mean bubble size changed from 62-50 μm without surfactant to 46-43 μm with surfactant. The role of surfactant in achieving these results is not discussed

The work of Urban (1980) demonstrates the complex nature of the process and highlights the importance of the earlier stages of the process which lead to bubble dislodgement from the nucleation site. The work, however, did not offer any possible design equations that could be applied in general situations.

The subsequent investigations, as shown below, focus on the role of the cavitation plate and the nozzle chamber and try to link these to the bubble distributions produced. Takahashi (1979) considered the effects of dissolved pressure, liquid flowrate and nozzle configuration. He concluded that the bubbles form rapidly near the nozzle and then grow a little. The process is considered in terms of the free energy change required to establish a critical radius. However, no attempt is made to explain where or how these nuclei exist or to provide proof of his conclusion. This idea is based on the concept of *de novo* nucleation as discussed in section 3.2. It relates to the creation of nucleation sites and this has been dismissed as a possible mechanism by Urban (1980).

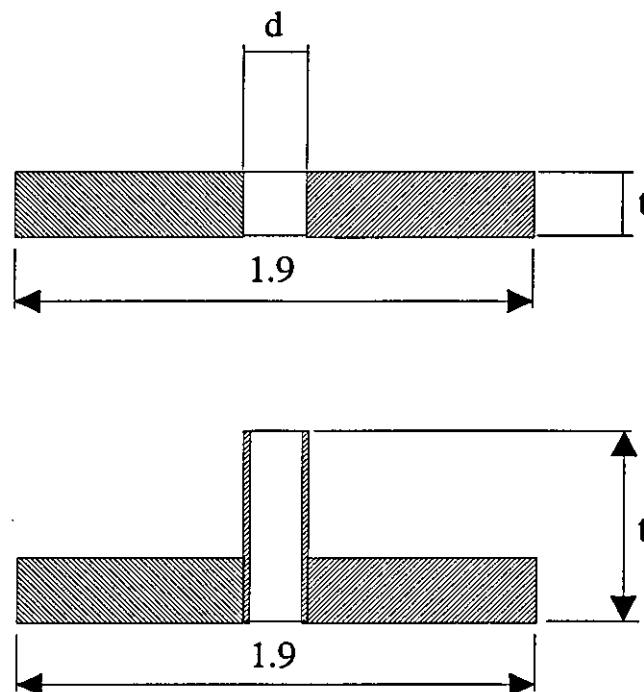


Figure 3.6 Details of Takahashi nozzles (after Takahashi 1979)

| Nozzle No. | Diameter (cm) | Thickness (cm) | t/d |
|------------|---------------|----------------|-----|
| 1-1 | 0.02 | 0.2 | 10 |
| 1-2 | 0.04 | 0.2 | 5 |
| 1-3 | 0.04 | 0.4 | 10 |
| 1-4 | 0.02 | 0.4 | 20 |
| | | | |
| 2-1 | 0.025 | 1.25 | 50 |
| 2-2 | 0.025 | 2.5 | 100 |
| 2-3 | 0.025 | 3.75 | 150 |
| 2-4 | 0.025 | 5.0 | 200 |

Table 3.1 Configuration of nozzles (after Takahashi 1979)

The results regarding pressure and liquid flowrate are as expected. Generated bubble concentration increased with increasing pressure and liquid flowrate (from the saturator). The actual measurements are low and in certain cases considerably lower than the theoretical values. This occurred most pronouncedly with a nozzle designed with a large orifice depth, attributing the results to a slow decompression. Figure 3.6 shows the nozzle configurations examined and table 3.3 shows the range of nozzles investigated.

Each nozzle is described by a single parameter, the thickness to diameter ratio, which indicates the combination of the effects of orifice size and sharpness of cavitation in a single term although no explanation is offered. The actual diameters employed appear low compared to previous work. Urban suggested that small orifice sizes would have a detrimental effect on the air release as fewer sites would exist and that an optimum of about 1mm was observed. Clearly this is in excess of the sizes in Takahashi's investigation and may explain the results. The configuration of the nozzles used means that the diameter of the cavitation plate and the nozzle chamber are always the same. This means that the nozzle chamber acts as an elongated cavitation plate, altering the hydrodynamics and not allowing for sufficient dissipation of the kinetic

energy of the injected flow. The result of this is ineffective cavitation and is the more likely reason for the poor results observed.

The results are generally erratic although a trend of decreased output with increased nozzle length was shown. Takahashi (1979) also studied these effects in relation to the system parameters and showed that increasing the nozzle length increased the average diameter although this effect decreased with pressure and liquid throughput. No explanation is offered but the effect may be due to increased coalescence. His work concluded in a series of dimensional correlations connecting bubble number with concentration of air (pressure), degree of disturbance of the liquid (liquid throughput) and nozzle configuration:

$$N_b = 0.45 \times 10^4 \left(\frac{t}{d} \right)^{\frac{1}{2}} \left(\frac{P_A - P_O}{P_O} \right)^{\frac{3}{2}} Q^{\frac{1}{2}} \quad (3.5)$$

$$5 \leq t/d \leq 20$$

$$N_b = 4.5 \times 10^4 \left(\frac{t}{d} \right)^{-\frac{1}{2}} \left(\frac{P_A - P_O}{P_O} \right)^2 Q \quad (3.6)$$

$$50 \leq t/d \leq 200$$

where:

- N_b = Number of bubbles (cm^{-3})
- t = Nozzle length (cm)
- d = Nozzle diameter (cm)
- P_A = Dissolved pressure (dynecm^2)
- P_O = Atmospheric pressure (dynecm^{-2})
- Q = Volumetric flow rate of liquid ($\text{cm}^3 \text{s}^{-1}$)

Only limited support for these equations is provided and is restricted as no mention is given of the other pertinent variables such as nozzle materials and solution.

characteristics. Takahashi (1979) suggests a trend with nozzle geometry offering a cut off point of a $t/d > 50$ to represent long nozzles where the sudden decrease in pressure no longer occurs.

Repanas (1992) investigated bubble production and discussed the type of saturation system used. The model suggested was similar to Takahashi's in that the change in free energy was considered without discussing the exact position at which the bubble first begins to grow. The idea suggests molecular fluctuations; however Urban (1980) showed this to be on too small a scale to be relevant here. The investigation examined pressure and liquid flowrate as factors. The major effect was seen with pressure and was described as the result of the nuclei's size being reduced. The effect of liquid flowrate was less influential on the bubble size, especially at the higher pressures as expected. In both cases increasing the variable decreased the bubble size and this is consistent with the work of Urban (1980) and Takashai (1979). The work was further developed by presenting an empirical formula to predict the bubble number with pressure:

$$N_b = 175P^{1.64} \quad (3.7)$$

where:

N_b = Number of bubbles per cm^3

P = Pressure (psi).

The work concluded with an examination of the uniformity of the bubble size distribution in terms of a uniformity index, which represented the standard deviation of the bubble distribution divided by its mean size. The smaller the index, the narrower the distribution is, and hence the desired result of any tests. This index was plotted against pressure and liquid flowrate and showed a decrease as both were increased, indicating advantages at higher operating conditions. The range of pressures investigated 10-60 psi (0.68-4.14 bar) should be noted as these were much lower pressures than before. The upper limit representing the approximate

conventional lower pressure threshold for operation. Below this it would be expected that incomplete release would result and the spread would be large, as seen. Again the simplification of the concept seems a little excessive and is presumably why calculated results differed from the actual measurements.

De Rijk (1994) also considered nozzle properties. He described the bubble formation process as being probably due to the cavitation formed from the sudden pressure drop through the nozzle in combination with the turbulence behind it, thus delivering the negative pressures required but only to weak spots such as pollutants and irregularities in the wall. The bubbles are then suggested to grow due to uptake of air from residual supersaturation or by coalescence. The work then notes the need for a good nozzle construction to avoid inefficient release of air and excessive coalescence. He suggested that a minimum bubble diameter exists of about 40-50 μm for the normal system arrangements.

The experiments conducted were of a similar nature to those of Takahashi (1979) showing a similar trend with pressure and liquid flowrate although the effects of liquid flowrate become small at higher pressures (6 bar). The effects of having a tube after the valve were also examined; this is equivalent to the nozzle tube after the orifice plate. However, the work was based on a pilot plant scale test and the tubes were very long compared to the length of standard nozzle chambers. The overall effect was detrimental with larger exit tubes producing a flatter distribution, representing a shift to larger bubble sizes. He concluded that using a tube removed the usual connection between pressure, liquid flowrate and bubble concentration.

Different valve types were tested and showed no significant difference indicating that orifice shape does not appear to be a pertinent variable. Although the exit pipe showed noticeable effects no trend was discovered and when tests were compared identically with a full-scale unit the laboratory rig produced larger bubbles. The full scale unit produced bubbles around the natural limit and thus Rijk concluded that no further improvements were possible. This can be seen as a problem of scale and

further supports the idea that empirical equations are of only limited application when based on laboratory experiments. He also reported an error with the experimental setup. As the photographic sampling tube had a small size certain larger bubbles were less likely to enter, influencing the results.

Rykaart (1995) attributed the poor correlation of design equations to a poor understanding of the fundamentals of the mechanisms of bubble production. He considered the bubble production process to involve two stages. The first was the bubbles growth on fixed nucleation sites and the second, their coalescence. He examined the effects of diverging cones and impingement plates as ways to improve the bubble size distributions produced, especially in terms of the fraction of macro bubbles that are detrimental to the process.

He showed that tapering outlets produce significant decreases in the mean bubble size produced but that impingement plates offer no real advantage. He discussed his finding in terms of his model and was able to adequately describe the results. He concluded that a rational nozzle design is still required and that this can only be developed through a fundamental examination of the bubble production process.

3.8 TYPES OF SATURATORS

The amount of available air to generate bubbles is controlled by the saturation systems which determines the level of air saturation in the water. In designing a saturation system the aim is to achieve efficient dissolution of air into water at an elevated pressure. Complete saturation is desired so that the total bubble volume upon release is at a maximum. Numerous configurations are possible although three main groups are classified, see figure 3.7

Vrablik (1959) describes the application of pump suction air injection systems as a common method of air dissolution. In this technique air is injected into the suction side of a centrifugal pump where the air and water is intimately mixed by the shearing

action of the impeller, creating a large contact area for the mass transfer operation. The major disadvantage of such systems is that air binding limits the possible volume percentage of air to be injected. Bratby (1975) has quantified this and has shown a range of 2-11% by volume is possible depending upon the pressure of the system (1-1.7 bar).

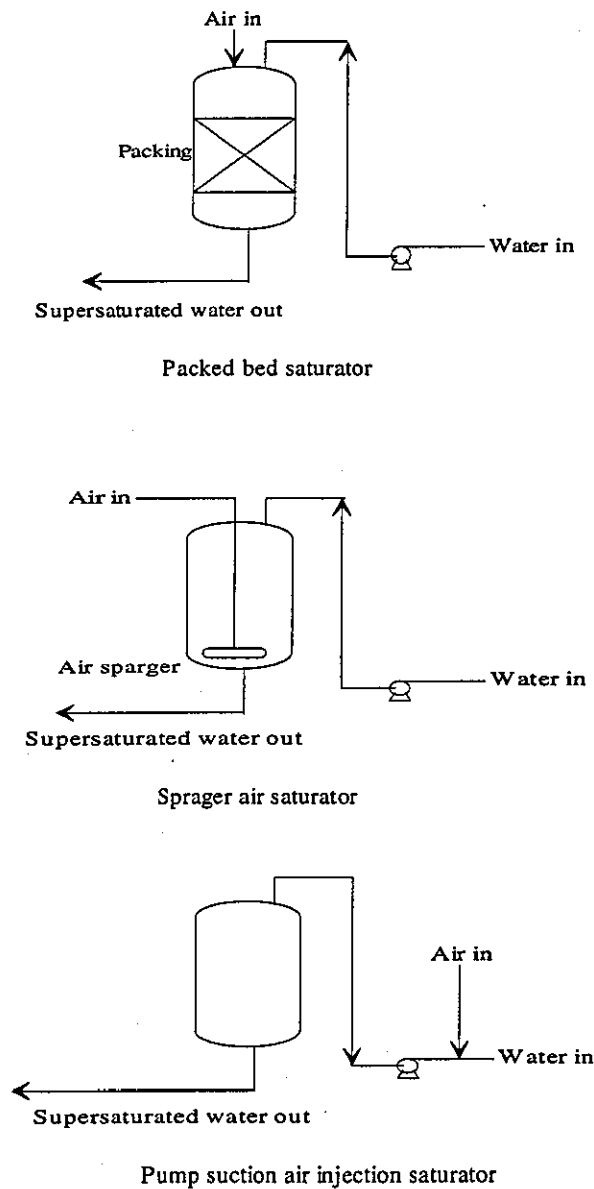


Figure 3.7 Various configurations of saturation systems.

The overall effect is that only a fraction of the maximum possible dissolution is achieved even with the aid of retention tanks. This is shown in the work of Bratby

(1975) who managed only 23 % saturation with his system. The early work of Vrablik (1959) was far more favourable claiming upto 80 % although no details are presented concerning his experimental rig. The inefficiencies of such systems have made their application extremely limited in practical situations.

The simplest of these is the sparged air system where either gas is bubbled through a reservoir of water (Bratby, 1975) or water is sprayed over a compressed air space (WRC, 1980). The efficiencies of such systems have been studied and it was found that two factors were of principal importance, namely, the air flow rate and the retention time in the saturator vessel. Bratby (1975) showed that the following factors have negligible effect:

- (1) Shape and roughness of the valve.
- (2) Degree of turbulence downstream of the valve.
- (3) Dilution of the saturator feed downstream of the valve.
- (4) Concentration of particulate matter.

Although the findings allow considerable freedom in the design of systems, the tests were performed at 826 kPa and at this pressure possible effects of other variables are likely to be diminished. The above factors may prove to be more influential when the saturator pressure is lower, perhaps near its minimum permissible value, which would be likely in practice although no investigation seems available. The effects of both air flow rate and saturator retention time were examined in more depth and it was found that a limiting condition existed. To obtain equilibrium conditions a retention time of 40 minutes was required with all air flow rates. However, under 70 l/min the equilibrium value was not its saturation level. Increasing the air flowrate above this level did not decrease retention time criteria, probably due to a limiting gas transfer rate in the conditions employed. Unfortunately this investigation was conducted at the high pressure of the previous work and the effect of lowering the pressure is not reported. Such action would decrease the driving force by which the process operates and so an increase in retention time is likely.

The effects of bubble size and tank geometry must also be important as they will effect the mass transfer operation but these were not considered. The WRC (1980) in their alternative layout altered the height of the distribution pipe and employed nozzles to observe how efficiency was affected. They found that a maximum of 60% saturation was possible when the distribution plate was a metre away from the saturated reservoir. This was found to be increased to 100% by employing nozzles to increase the transfer area. This change however produced a problem in that a pressure drop of 400 kPa was required across the nozzle making their application economically undesirable. In practice Bratby's system is generally the preferred one of the two as control of the air bubble size is seen to be easier than that of water droplet size. However, the process is still seen to be inefficient and costly on compressed air. The application of such systems is towards applications where inexpensive and uncomplicated saturators are required. This represents batch experimental work where packed bed saturators become too expensive. In such cases the scale of equipment is much smaller and so optimum transfer can be more easily achieved and operating times are not so crucial.

In industrial situations where large continuous saturation systems are required the third option becomes favourable. Packed bed saturators overcome the difficulties encountered by sparged air systems because the packing material provides a large transfer area in a small volume. In such systems it is conventional not to pass the air counter-currently but to merely introduce the air at the top of the column. This acts to maintain the pressure in the saturator and to replace any air that is dissolved and has the benefit of increasing the maximum possible water throughput of the unit. The important variable is the surface loading rate not the retention time and this is closely linked to the packing material adopted. A large packing size is preferred for throughput and a small size for contact area and so a compromise is required. Experimentation by Rees (1980) has shown greatest efficiency is achieved with either 25 mm Raschig or Pall rings. The need to avoid short circuiting is of great importance and is generally achieved by employing a good nozzle to provide a fine droplet spray.

Directed flow into the centre of the packing can also be effective as the flow pattern of the liquid tends naturally towards the walls. Bratby (1975) also presents a criterion to reduce such effects by suggesting that the nominal packing size: column diameter should be less than 1:8.

The effects of packing depth and surface loading rate are in some question as Bratby (1975) and the WRC (1980) offer differing opinions. Concerning surface loading rate, Bratby states that full saturation occurs above pressures of 250 kPa (36 psi) throughout the range of surface loading rates (1000-2500 m³/m²/d). Below 1000 m³/m²/d saturation is not quite complete although only a slight drop is noticed. It is also stated that a maximum of 2500 m³/m²/d exists as above this ponding would occur. The W.R.C. differ on this point as they suggest 5000 m³/m²/d is the limiting rate. Considering the packing is of a similar type in both investigations this would seem strange. However, the acceptable surface loading range is similar from both sources and seems a useful start. The disagreement is more substantial on the height of packing required. Bratby (1975) suggests a minimum of 0.3 metres whereas the WRC (1980) suggest 0.8 metres. No explanations are provided although both produce evidence. In this the WRC do not make clear the conditions under which the experiments are undertaken and so comparison is difficult. The overall conclusions to be taken from the work are that saturator design and study is sufficiently advanced to enable effective design to occur. The work seems to suggest the following criteria should be embraced when designing a saturation system so that complete saturation can be assumed considerably likely:

1. A packed bed saturator is employed.
2. The saturation pressure exceeds 3 atm.
3. The packing bed depth exceeds 0.3m and is preferably greater than 0.5m.
4. The nominal packing size: column diameter does not exceed 1:8.
5. The surface loading rate is within the range 300-2500 m³/m²/d.
6. A good distribution system is employed such as a ring distributor or a series of nozzles depending on the saturator dimensions.

With the current position in saturator design, no further work appears to be required particularly although the need to reduce capital and operating costs will always exist. This also means that any decreased response in terms of mass of air precipitated can be assumed to be due to problems post saturator. Therefore the pipework between the saturator and the nozzle should be designed carefully to avoid the creation of sites where precipitation of air might occur.

3.9 CONCLUSIONS

The literature reviewed within this chapter has led to the following conclusions. The bubble production process operates by the cavitation of a supersaturated water flow. The bubbles form at pre existing fixed nucleation sites in the surface roughness of the top edge of the orifice in the cavitation plate. These bubbles grow until the buoyancy force and fluid drag are sufficient to dislodge them from their nucleation sites. The point of dislodgement is controlled by the geometry of the sites and this remains an unknown to the process. It limits any model used to predict the performance of injection nozzles as the size of the bubble upon dislodgement into the flow can not be determined.

The experimental investigations have focused on examining the effects of pressure and flowrate on the bubble distributions produced. Some advancements have been made by including nozzle configuration into the equations. All the models have failed to predict adequately the performance of injection nozzles, which is attributed to a poor understanding of the fundamental mechanisms that occur within the process. In particular the oversimplification of ignoring the initial dislodgement stage seems critical as this will control the bubble size distribution produced.

This highlights the need for a conceptual model that can be used to understand the process such that design criteria can be developed on a fundamental basis. This

objective is clearly indicated as the main requirement in the investigation of bubble production at present.

The design of saturators has been reviewed and shows that the present design approach is adequate with a clear set of design rules having already been established. The state of knowledge is considerably more advanced than for nozzle design which represents the area that needs to be researched the most.

CHAPTER FOUR

CHAPTER FOUR

EXPERIMENTAL METHOD : FLOTATION TESTS

4.1 INTRODUCTION

This chapter describes and discusses the methods employed to measure the process response of a batch flotation column, treating clay suspensions conditioned with surfactants and coagulants. Below is a brief review of the pertinent literature together with a description of the equipment and methodology used.

4.2 LITERATURE REVIEW

Experimental investigations of the fundamental mechanisms can be split into two sections representing the collection and attachment stages of the process. Collection experiments focus on the hydrodynamics in an attempt to predict the kinetic behaviour of the process. These involve tracking streamlines by photographic techniques (Collins and Jameson 1976, Flint and Howarth 1971, Okada 1990) or counting the number of particles collected on individual bubbles (Anfruns 1976, Kitchener 1981).

Investigations into attachment mechanisms involves batch flotation tests, relating bulk properties such as the overall removal efficiency or the outlet turbidity to the surface variables such as zeta potential, surface tension and critical rupture thickness (Roberts 1980, Malley 1988, Yordan 1989). A limiting factor in the past has been the unavailability of the required analytical equipment or established techniques necessary to achieve these measurements. Emphasis is now being placed on these tests to improve the understanding of the process (Edzwald, 1995). A number of important issues relating to these tests will now be discussed.

The physical limitations imposed by batch testing greatly influence the credence of the results and these have been examined by Stevenson (1986, 1994) and Bratby (1983). The major concern relates to wall effects, offering a path of lesser resistance for the flow (Vesilind 1965). The majority of studies into size effects has been conducted in sludge

thickening applications (Wood and Dick 1973, Gehr 1978, Leininger 1979) where scale was seen to be most important for dilute systems. This effect is counteracted by the need for tall vessels to maximum bubble contacting (Stevenson 1986) while minimising the flow rate into the column (Bratby and Marais 1977) which both require smaller diameter columns. Thus a compromise is required and has led to optimum sizes of around 80mm being used (Malley 1989).

The majority of investigations reported used a simple injection pipe to input the supersaturated water into the flotation columns. Zabel (1975) reports that proper nozzles should be used as injection tubes produce very different bubble size distributions. Typically, these are broader spreads thus incorporating greater numbers of larger bubbles that are known to be detrimental to the process (Edzwald 1995).

4.3 EXPERIMENTAL PROCEDURES

4.3.1 Aims and Objectives

The specific aims and objectives of the experimentation were as follows:

1. The characterisation of the zeta potential of the clay particles and air bubbles conditioned with a range of surfactants and coagulants
2. To investigate the relationship between zeta potential and particle removal efficiency for the clay systems characterised in (1).

The principal aim of the work was to investigate the mechanisms of removal within the dissolved air flotation process. This focused on the role of the attachment mechanism and involved a comparison of the zeta potential of the particles and bubbles to the removal efficiency obtained. Clay particles were used as the pollutant to be removed and their zeta potential was characterised over a wide range of conditions, prior to the flotation experiments.

The experimental procedure involved the preparation of a sample to a desired concentration of clay and conditioning chemicals, which was then poured into the flotation column. The sample was then injected with a known volume of supersaturated water, which produced a bubble cloud. The sample was left while the bubble cloud rose up through it and removed the particles. Samples were analysed before and after flotation to determine the removal efficiency.

4.3.2 Materials used

4.3.2.1 Clays

The clay minerals used for the investigation were kaolin and montmorillite in the form of Wyoming bentonite. The clay mineralogy of the samples was analysed by the Natural History Museum and the results can be seen in appendix I and these are discussed in detail in section 6.2.1.

Clays were used in this investigation because they represent a simple simulant of natural waters; examples of their use in this way can be found in the literature (Roberts 1980, Malley 1988). Both types of clay were used to offer a range of surface properties; kaolin particles are relatively large and have a relatively low charge compared to the smaller, more highly charged bentonite particles. The clays were kept in sealed plastic containers to prevent moisture or chemical contamination which could alter their surface properties.

4.3.2.2 Surfactants

Since the clays carry an overall negative charge, the surfactants need to be cationic. Alkyl-trimethylammonium bromides were selected with three different chain lengths, dodecyl, tetradecyl and hexadecyl. Powder forms of the surfactants were obtained from Sigma-Aldrich Company Ltd, Dorset, England.

4.3.2.3 Coagulants

The coagulants used were Alum (Aluminium sulphate) and Ferric chloride as these represent the two most common surfactants employed in practical situations. The chemistry of these chemicals is complicated as they undergo a hydrolysis reaction in water to form a variety of hydrolysis products; section 6.5 discusses this in detail. The chemicals were analytical grade and were obtained from Sigma-Aldrich Company Ltd, Dorset, England.

4.3.3 Sample preparation

Clay suspensions were prepared by dispersing 200 mg of dry powder into 300ml of distilled water. The suspensions were dispersed using an ultrasonic probe, which was set to an output rating of 80 watts. The samples were initially hand stirred to break down any lumps that formed. Bulk solutions of dissolved surfactant and coagulant were made up with distilled water to a level 10 times that of the highest concentration used in the experiments. The final samples were made by mixing the relevant bulk solutions in the required ratios to ensure the clay concentration was always 100 mg l^{-1} .

4.3.4 Sample analysis

The investigation focused on zeta potential measurements, examining the effects of surfactant and coagulant variations in terms of dose and in conjunction with pH. The procedure involved injecting a 20 ml sample into the Zetamaster ® by syringe and then initiating the computer controlled measurement routine. The samples were prepared as described above except in the case of the post process zeta potential measurements. In these circumstances a sample was withdrawn from the flotation column after the batch experiments was completed. The temperature of each sample was measured prior to injecting the sample.

The pH experiments were conducted using an automatic pH titrator connected to the Zetamaster ®. In these cases the clay suspension was poured into the titrator's sample compartment and the measurement initiated. This procedure allowed the zeta potential to be measured as a function of either alkaline or acid addition, which meant that to produce a complete series of pH measurements two cycles of the routine were required. Once the measurement was initiated the machine controlled the procedure, injecting a volume of the pH adjusted sample into the electrophoresis cell.

A water bath was connected to the Zetamaster ® to investigate the effects of temperature. The bath comprised of an heating and cooling element, producing a temperature range of 5°C to 60°C. The samples were injected manually once the temperature had stabilised to the desired value. In conjunction to the zeta potential measurements the size distribution was measured as a function of temperature, by connecting the water bath to the Lasentec ®.

The performance of the flotation and sedimentation experiments was analysed in terms of turbidity, size distribution and surface tension. The measurements were made before and after each experiment was conducted, except that the surface tension which was only measured afterwards.

4.3.5 Flotation rig

The flotation tests were conducted with a extended batch column consistent with the semi continuous rig of Bratby and Marais (1977). The flotation rig is illustrated in figure 4.1 and plate 4.1, consisting of a flotation column connected to an air saturator through a timer controlled ball valve.

The flotation column was a 80mm diameter, 700mm tall cast acrylic tube, with two sampling taps connected 250mm and 450mm up the column. The sampling points were glued acrylic blocks drilled for a screw thread, into which 7mm internal diameter ball valves were inserted. The column was connected to the rig by placing it on a base plate

which protruded 5mm up the column; the join was made leak proof with an o-ring seal fixed into the base plate.

A 100 mm internal diameter stainless steel sparged air saturator was used to feed the flotation column with bubbles. The sparger was constructed out of stainless steel with a sintered metal top plate to allow air flow. The sparger was centrally fed with compressed air through a regulator valve to maintain the pressure throughout at 4 bar. The sparger was operated on a 2 litre batch basis, with each batch being left to equilibrate for 40 minutes, which is in excess of the Water Research Centre's guidelines for effective saturator design (Rees, 1980).

All the pipework was constructed in stainless steel to avoid any possible problems with contamination. The line from the saturator to the column was set at a slight angle to improve drainage, avoiding any water slugs remaining in the line. The saturator pipeline connected to the flotation column through a nozzle in the centre of the base plate.

4.3.6 Flocculation Bench

A flocculation bench based on the design of the WRC (Hyde 1977) was employed for the flocculation of the dispersed clay particles, see plate 4.2. The bench consisted of six tall one litre beakers simultaneously stirred by small bladed rotors, connected to a communal drive shaft. The rotational speed of the stirrers was controlled by a variable potentiometer power source.

The experimental procedure followed the standard jar test methods described by Ives (1978). The samples were coagulated in a two stage sequence of rapid mix (200 rpm, 1 min) followed by the coagulation stage (40 rpm, 20 mins). The sequence was initiated just after the coagulant solution was added and was automatically controlled. Once the sequence was completed the sample were either left to settle for 20 minutes and then analysed, or transferred to the flotation column.

4.3.7 Analytical equipment

4.3.7.1 Zeta Potential

The zeta potential of the particles was measured using a Malvern Zetamaster ®, Malvern Instruments Ltd, England. The measurements were based on the laser doppler electrophoresis technique as described in Hunter (1981). The technique operates by measuring the interference fringes of two laser beams at the point where the beams cross. Any particles that enter the crossed beams will cause the interference fringes to shift and this can be related back to the particle's velocity and hence to the electrophoretic mobility.

This technique offers several advantages over the traditional microscope methods. It averages its measurement over thousands of readings, generating an intensity distribution, greatly reducing statistical errors. Very low or zero zeta potentials can also be measured accurately by virtue of an optical modulator which causes a doppler shift in one of the beams. This means even very low charged particles will cause a shift change and so can be measured.

4.3.7.2 Turbidity

The turbidity of the samples was measured on a Hach model 16800, (Camlab, Cambridge). The technique measures the light scattered at right angles to an incident light beam that is passed up through the sample. The measurements are calibrated against a universal formazine standard set in Nephelometric Turbidity Units (NTU). The standards are made by diluting a stable 4000 NTU bulk with distilled water. The lens of the light source required cleaning occasionally to remove any built up dirt. Removal efficiency was determined as the change in turbidity of the sample due to flotation divided by the influent turbidity.

4.3.7.3 Surface tension

The surface tensions were measured by the DuNouy method where a known diameter platinum ring is pulled through the liquid until it breaks the liquid film. The force required at this point is measured. The ring was cleaned in alcohol and passed through a flame before each test to prevent contamination. To remove any particles from the samples, they were filtered through a cellulose nitrate Whatman filter rated at 0.8 μ m, prior to measurement.

4.3.7.4 Particle size analysis

The size distributions were measured by scanning laser microscopy, with the Lasentec ®, (Lasentec Inc. Redmond USA), see plate 4.5. The technique measures the back scattered light pulse produced when a particles passes through the beam. The particle size is related directly to the length of the back scattered pulse and is independent of its intensity. A filter blocks out any pulses with a long rise time thus ensuring that only particles within the focal volume are measured.

Scanning laser microscopy has several advantages for the present situation. The analysis is independent of concentration and can be made *insitu*, avoiding any requirements for special preparation to be required. The Lasentec ® is ideally suited to the measurement of the floc encountered within this investigation as it does not break or damage the flocs as a result of the analysis.

The initial settings of the machine had to be altered to optimise the measurements for the dilute systems investigated. The most important feature was the update time which needed to be set to its maximum of 3s to generate a sufficient count. The measurement of flocs was initially complicated as the Lasentec ® was able to measure both the flocs and the individual particles within the floc. To correct for this the focus point of the laser beam was set in front of the observation window, desensitising the measurement.

It was important to clean the observation window between readings and this was checked each time and continued until the count was below 300.

4.3.7.5 Bubble Zeta Potential

The zeta potential of air bubbles was measured using the adapted electrophoresis technique described by Collins (1977), which uses a modified rectangular cell with platinum electrodes inserted into the top and bottom of the cell, enabling the production of small gas bubbles by electrolysis, see figure 4.2 and plate 4.4. The technique measures the zeta potential in a single bubble system rather than the swarms encountered in the process. This has been shown by Jameson (1978) to be the preferential method as techniques that measure the zeta potential of bubbles within a swarm are affected by the interactions of the bubbles upon one another.

The charge on the bubbles is determined by measuring the horizontal displacement caused by applying an electric field across the cell as the bubble rises, in a set time interval. This is then converted into zeta potentials according to the Smoluchowski equation. A more detailed description of the process and the method of calculation can be found in Jameson (1978).

The bubble's motion was recorded with a video camera and played back frame by frame to measure the bubble's position. A horizontal diameter was taken and the co-ordinates of the two end points and the centre were recorded. The velocity was calculated by measuring the displacement within a set time interval; this varied between 4-6 seconds depending on the degree of displacement measured. The time interval was limited to a 40th of a second which represents a single frame of the video.

A major concern with these measurements is whether the bubbles have reached equilibrium with the surrounding liquid. Collins (1977) analysed this situation for the case of a 30 μm bubble in a solution of CTAB in distilled water and calculated that a

time of 0.137 seconds was required for equilibrium. This represents only a few bubble diameters of movement once the bubbles have been formed.

4.4 EXPERIMENTAL ERRORS

The main sources of error in the experimental program has already been discussed in sections 4.2. An additional problem is associated with the natural variations in the clay properties. The reproducibility was tested in terms of zeta potential and removal efficiency and these were found to have error bands of $\pm 5\text{mV}$ and $\pm 5\%$ respectively.

The size distributions measured using the Lasentec® all had a common problem, the size distribution showed a slight oversize. This was because the system analysed was dilute, allowing particles beyond the principal focus point to reflect light back to the probe. As the size is related to the time of the back pulse these particles will be oversized. These problems are overcome as all the size distributions measured were used for comparison and so only relative changes in the distribution were important rather than the actual size distributions measured.

A similar situation exists with the turbidity measurements; the light source in the meter got progressively dirty, reducing the turbidity reading. The problem was overcome by regular cleaning of the lens, which occurred once the turbidity had dropped by 5 NTU. The effect of the reduce turbidity readings is negligible as the efficiency of the process was measured in terms of the comparative change between before and after flotation; cancelling out any errors that occurred.

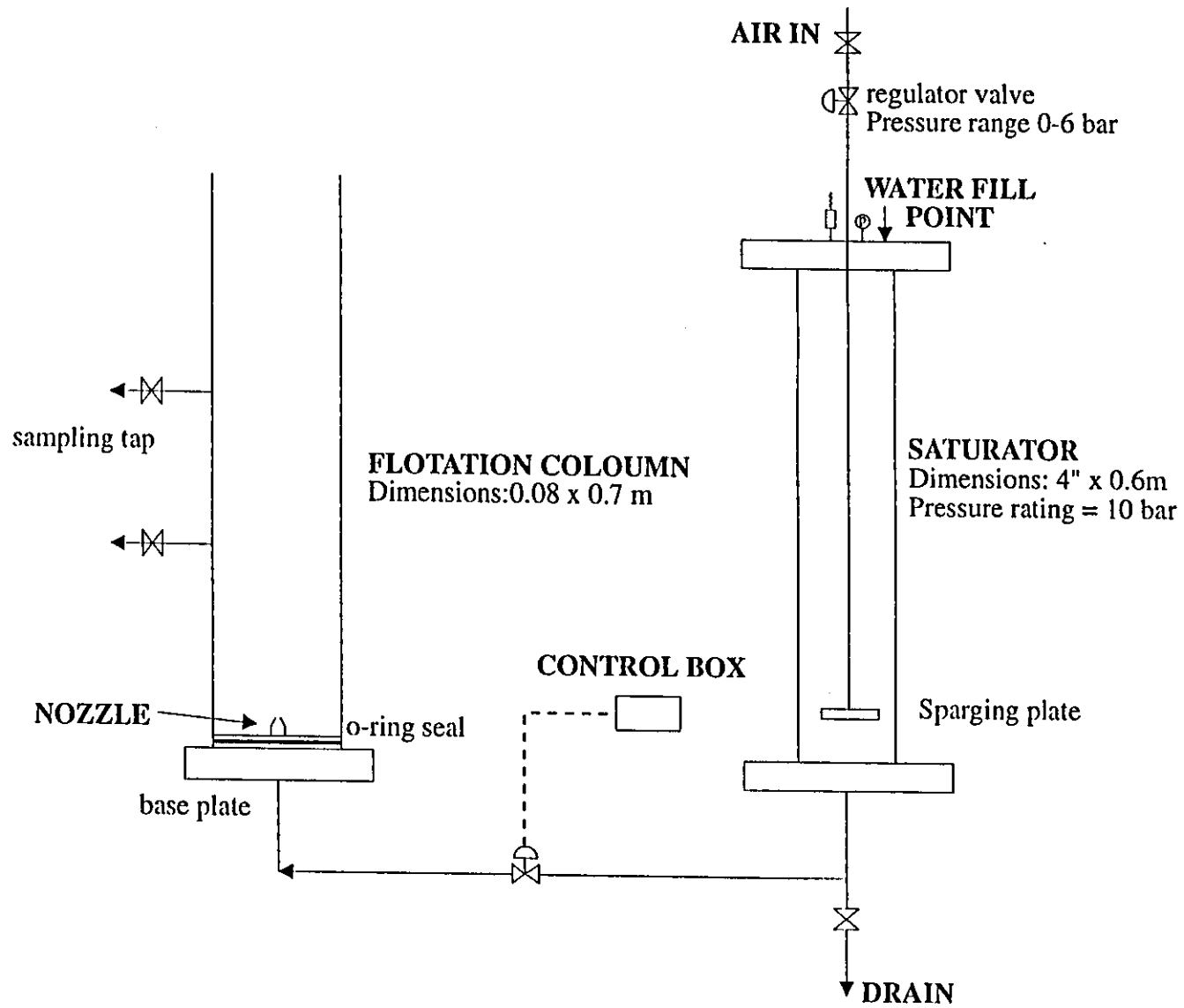


Figure 4.1 : Process flow diagram of the Flotation rig

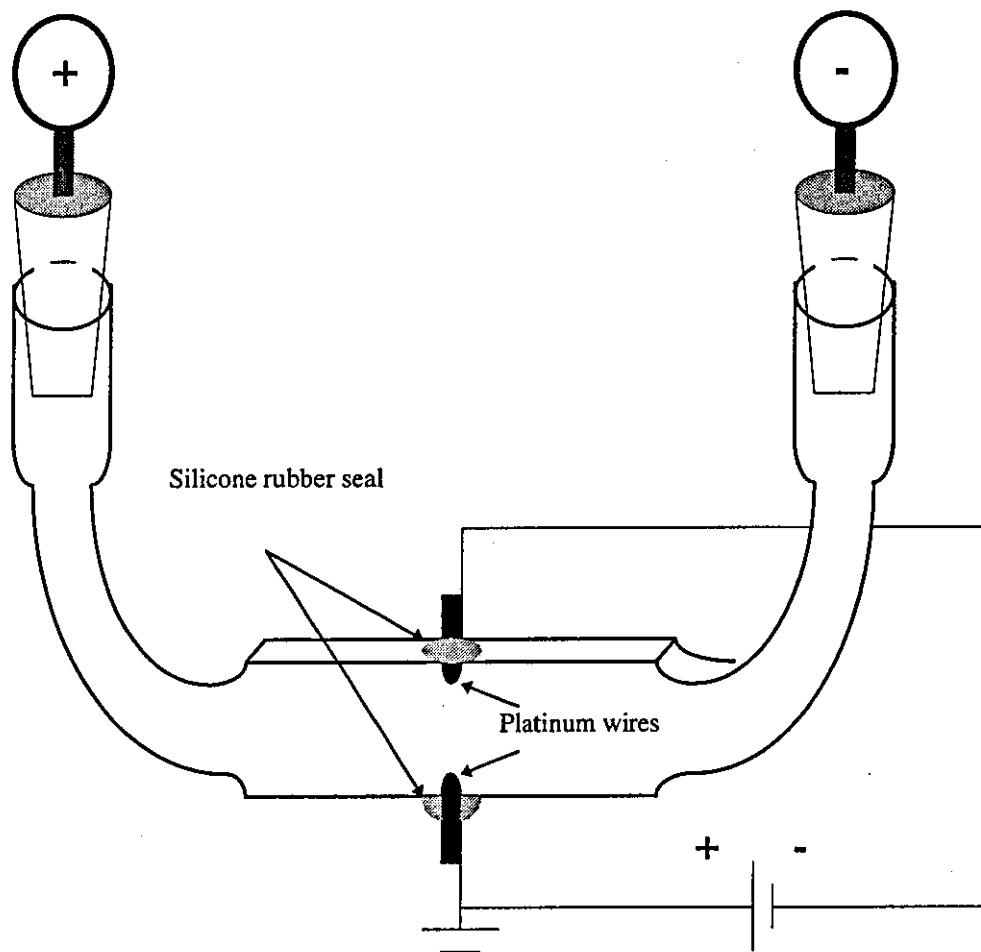
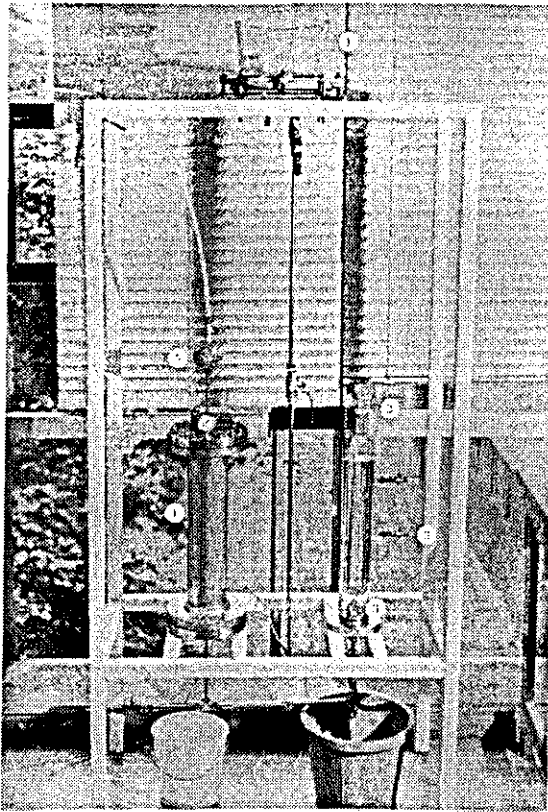
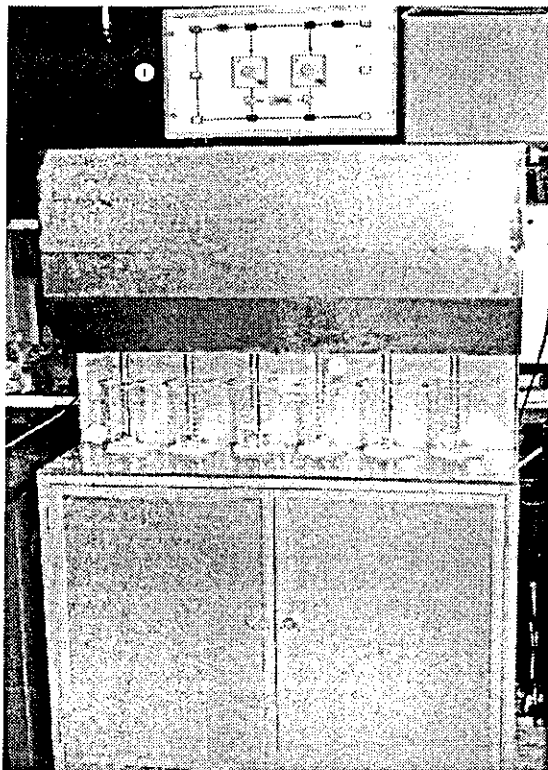


Figure 4.2 : Modified zeta cell for bubble zeta measurements



| Key | Description |
|-----|--------------------|
| 1 | Saturator |
| 2 | Flotation column |
| 3 | Sampling tap |
| 4 | Header tank |
| 5 | Pressure regulator |
| 6 | Nozzle |

Plate 4.1: Flotation equipment



| Key | Description |
|-----|----------------------|
| 1 | Flocculator controls |
| 2 | Beaker |
| 3 | Mixer |

Plate 4.2: Flocculation Bench

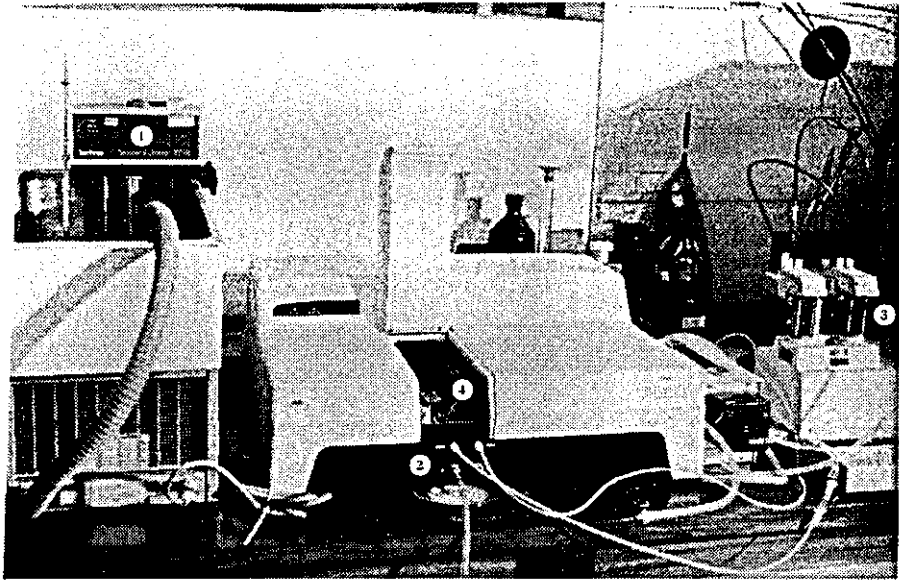


Plate 4.3: Laser doppler electrophoresis equipment (Malvern Zetamaster ®)

| Key | Description |
|-----|----------------------|
| 1 | Water bath |
| 2 | Injection point |
| 3 | Autotitrator |
| 4 | Electrophoresis cell |

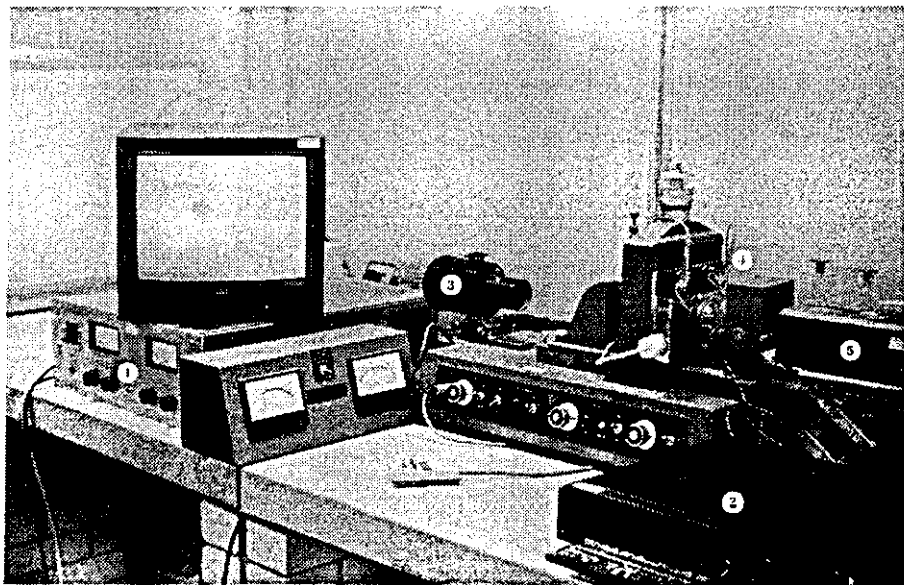
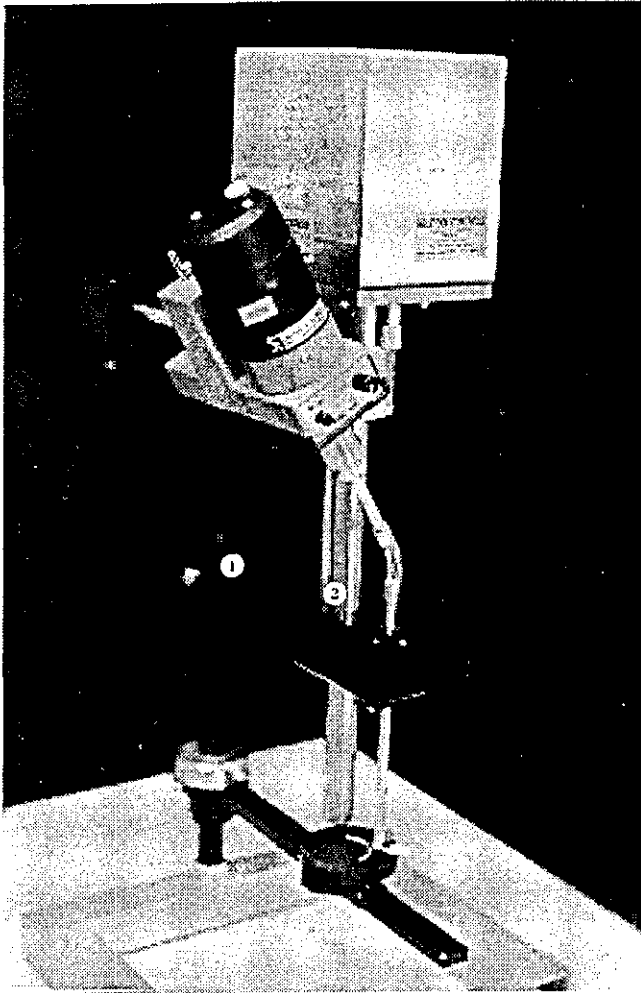


Plate 4.4: Bubble electrophoresis measurement equipment (Rank Brothers)

| Key | Description |
|-----|----------------------|
| 1 | Voltage supply |
| 2 | Video recorder |
| 3 | Light source |
| 4 | Electrophoresis cell |
| 5 | Camera |



| Key | Description |
|-----|-------------|
| 1 | Mixer |
| 2 | Probe |

Plate 4.5: Scanning laser microscopy equipment (Lasentec®)

CHAPTER FIVE

CHAPTER FIVE

BUBBLE SIZE MEASUREMENTS: EXPERIMENTAL METHOD

5.1 INTRODUCTION

This chapter describes and discusses the methods used to measure the bubble size distribution produced when a solution of supersaturated water is released through a nozzle device. The literature on the subject is discussed briefly and the equipment and methodology used in this work are then described.

5.2 LITERATURE REVIEW

5.2.1 Introduction

The measurement of bubble size distributions has remained basically unchanged from the original methods employed. The work of Urban (1980) and Rykaart (1995) represent good examples and illustrate the simplicity of the technique. Firstly, images of the bubbles are recorded, usually by taking a series of photographs. The size of individual bubbles is then measured with reference to a known scale (graticule). Development of the technique has focused on improvements made in photographic equipment and the use of image analysis techniques to facilitate rapid collection and more reproducible data analysis. The major areas of variation between the techniques currently used are in the level of magnification and the method of analysis (Urban 1980, Cassell 1974, Repanas 1992, De Rijk 1994, Takahashi 1979, Zhu 1993, etc.)

5.2.1 Recording the bubble images

The nature of the dissolved air flotation process means that the bubbles form in a free flowing highly concentrated swarm and that the bubble's surface is not stabilised as found in other processes (Jameson, 1978). The result of this is that the flotation

column turns opaque, preventing direct photography into the column as lighting becomes a problem. This is solved by creating an observation cell where the concentration of bubbles is greatly reduced. This can be achieved in one of two ways. The first is with a side stream that is taken off the main column so that only a small percentage of the total flow passes through it (de Rijk 1994, Zhu 1993, Jefferson 1995). Alternatively, a transparent block is placed in the column near the front wall to produce a thinned water layer (Urban 1980, Repanas 1992, Rykaart 1995). Both methods have similar disadvantages as they must alter the flow path to achieve their goal. This will increase the chance of coalescence and offers a path of greater resistance than the bulk flow. This results in a partial selection of smaller bubbles as they are less able to deviate from the flow streamlines and will have a greater chance of being carried along the fluid path (Urban, 1980)

5.2.3 Magnification

The problems of lighting are very closely linked to the degree of magnification used. The greater the magnification, the greater the light intensity required. A short exposure time is needed to freeze the bubbles which are in motion and this necessitates a further increase in light intensity. The degree of magnification used is a compromise between accuracy and ease. A high degree of magnification produces a more accurate measure of the bubble's size but reduces the number of bubbles that are recorded per photograph.

The degree of magnification controls the depth of field of the image. This can be thought of in terms of a three dimensional volume, any object within this volume will appear in focus on the photograph. The depth of field represents the depth of the volume element. The greater the magnification, the smaller the depth of field will be and hence the volume element that makes up the photograph. A problem occurs when the depth of field is greater than one bubble diameter as the position of each bubble will affect the size of its image. Bubbles will appear in focus even if they are some distance from the central focusing point. This will lead to errors as the effects of

perspective are not taken into account. As the graticule is a two dimensional scale any bubbles that are in focus and not in the same spacial position as the graticule will be over or under sized depending if they are in front or behind the position of the graticule respectively. When possible it is preferable for the depth of field to be one bubble diameter deep such that any bubbles in focus will automatically be in the correct plane and thus sized at the right scale.

5.2.4 Measurement of bubble size

The second stage is to analyse the photographs such that sufficient bubbles are measured to represent a characteristic bubble size distribution. The British Standard on microscope counting suggests 625 individual readings are necessary (BS 3406,1963). However, this has not been common practice due to the time taken to undertake such an approach, (Repanas 1992, Takahashi 1979) leading to questions of reliability on the results.

Both focused and unfocused images of bubbles will appear on each photograph. This means that a selection protocol is required to ensure only focused bubbles are measured. Manual selection approaches are the most common and many examples exist within the literature (Cassell 1974, De Rijk 1994). The advent of computers has now allowed the introduction of involved computational methods for automatic selection. These are gaining greater application as they represent a more reliable and sensitive technique (Rykaart 1995, Zhu 1993).

The actual measurements are made by comparing an individual bubble's image to an image of a known size or scale. This represents either using a wire of known diameter (Rykaart 1995, Repanas 1992) or a microscope graticule (Cassell 1974, Jefferson 1996). In all these problems the magnification of the photograph is critical. This determines the accuracy with which the measurements can be made. The method of the actual measurement is determined by whether a computer is used or not. When the measurements are made manually they are conducted in accordance with BS 3625

(1963). This means that the bubbles are classified by a set of known diameter circles and the number that fall into each band counted. If an automatic method is employed, each bubble is sized individually in terms of its pixel dimensions (Area, Feret's diameter) and so is not limited to the size of the band widths of the manual approach.

5.2.5 Discussion

The fundamental approach required to make bubble size distribution measurements are clearly defined in the literature (Rykaart 1996). The merits of the different options is based upon sensitivity and complexity, which are inversely linked. The relative changes in the bubble size distributions that are expected to be observed require an accurate approach to be used. This dictates that the magnification of the photographs should be relatively high and the analysis be carried out using an image processing package.

The use of a high level of magnification can solve an important problem usually associated with these measurements. When the level of magnification is low the depth of field of the photograph is large and the effects of perspective become important. The size of a bubble then becomes dependent on its relative spatial position when compared to the graticule. Higher levels of magnification resolve this by reducing the depth of field to one bubble diameter; thus any bubbles that are in focus will be measured at the correct scale. The problem then becomes one of selection of focused rather than unfocused bubbles with the contrast between focused and unfocused decreasing with magnification. To solve this requires clear definition of the rules that will need to be applied to establish whether a bubble is in focus or not.

5.3 EXPERIMENTAL PROCEDURES

5.3.1 Aims and Objectives

The specific aims and objectives of the experimentation were as follows

1. To investigate the relationship between the design and operating characteristics of the system and the bubble size distribution of a free moving bubble cloud.
2. To develop an automatic image processing system for the analysis of bubble photographs

The principal aim of the work was to investigate the effects of various parameters on the bubble size distribution produced in a flotation column. The simplest method of changing the bubble size distribution available to the designer is to alter the nozzle's physical configuration. To reflect this, the experimental program concentrated on mechanical variations to the nozzle's configuration. This was made possible by the use of a modular nozzle design so that a range of nozzle configurations could be attached to a basic nozzle housing (see figure 5.1). In particular, the effect of diverging nozzle cones and impingement plates were investigated as the literature suggests these will produce the maximum reduction in the mean bubble size and number of large bubbles that are formed (Rykaart 1995).

Chemical conditioning of the system is an uncontrolled variable in practical situations and results from the raw water quality and the chemical conditioning required to optimize the coagulation stage of the process. However, evidence suggests that chemical conditioners may have significant influence on the bubble size distributions produced (Prince 1990a and 1990b). The investigation examined the effects of surfactants; the concentration range was set to coincide with the flotation experiments conducted in Chapter 4.

To complement the photographic measurements a series of experiments were conducted in which video footage was recorded of the early stages of bubble formation in the column. The series of experiments covered the same range of tests as the still photographic measurements but concentrated more on the mechanical changes as these were more likely to be noticeable on video. The video footage enabled measurement of the spray angle of the injected supersaturated jet from the nozzle and this was incorporated in the design of the diverging cone experiments, this is discussed in a later chapter.

As highlighted in the literature review a sensitive measurement technique was required as some of the anticipated changes in the size distributions were relatively small. This dictated that a high level of magnification be used. Subsequent decisions on the experimental setup were based on optimizing the high level magnification approach. Principally, this represented using a side arm to reduce the fluid width through which the photographs were taken as this enabled less complicated designs of the lens and lighting systems to be used.

Previously, a major difficulty with bubble size measurements has been in the analysis of the photographs. The main source of concern is encountered in the selection procedure adopted to identify which bubbles are in focus. This is overcome by the application of image processing software that can be programmed with rigid selection protocols, offering high levels of consistency. Two image processing solutions have been developed within this investigation, a semi-automatic and a totally automatic system. The first measures the bubbles once they have been manually selected by means of a light pen on the screen. The second system includes the selection of which bubbles are to be measured, selecting focused and rejecting unfocused. The difficulty in developing such a solution is in ensuring that the size of the bubble remains unaltered by the processing functions selected.

5.3.4 Experiment procedure

The experimental procedure involved the photography of a side stream that flowed off the main column. Preparation for the experimentation involved the charging of the saturator to produce the supersaturated water that was to be injected. Once the saturated water was ready it was injected into the column through a nozzle device. The injection volume was fed through a ball valve controlled by a timer, situated in the injection line immediately prior to the nozzle, resulting in the deadline's volume being negligibly small. Once the bubble cloud reached the level of the side arm a set of 36 photographs was taken. A new film was loaded into the camera and the process repeated with a fresh injection such that approximately 70 bubble photographs were taken per test. The remaining photographs on the films were used to take photographs of the graticule and an identification label.

5.3.5 Bubble column:

The bubble size distribution measurements were conducted using the batch flotation rig as described in section 4.3.3. A process flow diagram of the system can be seen in figure 5.2 with a photograph of the rig shown in plate 5.1. The major difference between the rig used in the flotation study and present setup was in the saturator used. In the present case a tall packed bed saturator was used, designed in accordance with WRC guide lines (Rees 1980). Water is added to the column which is then pressurized by exposure to compressed air, from a gas cylinder. Water is recycled from the base of the column through a spray nozzle to trickle over the packing. The level of saturation was tested by the inverted cylinder technique described by Roberts (1980); the measurements showed it to be at its equilibrium.

The flotation column was an 80 mm diameter, 1.5m tall cast acrylic tube. A side arm was connected 1m up the column's height that fed a small fraction of the flow to an observation cell. The side arm was a 7 mm diameter acrylic tube connected to the

observation cell via some rubber tubing. It was found that the flowrate through the side arm was insufficient to produce an adequate bubble density in the flow. This was solved by connecting a peristaltic pump to the end of the flow arm. A photographic system was connected to the observation cell to record the bubble photographs

The development of the observation cell was centered on minimizing the problems associated with lighting the cell and flow deviation, see figure 5.3. The initial design was a rectangular box constructed out of microscope slides. It was found that this dissipated the bubbles over the whole cell making the bubble density very low. This cell also had dead spots in it that influenced the flow patterns. The solution to the problem was to make the cell width thinner and so progressive cells were constructed decreasing the channel depth. Once the optimum cell width was established a final cell was constructed out of an acrylic block with a channel machined into it. The final side of the cell consisted of a microscope slide, which could easily be cleaned or replaced. The dimensions of the channel were 47 x 10 x 1.5 mm deep. The horizontal and vertical positions of the cell relative to the lens could be moved via a traveling vernier, allowing the point of observation in the cell to be optimized between experiments. The distance between the cell and the lens could be controlled by a screw thread along the lens system. This enabled a graticule to be measured without moving the lens, such that the magnification ratio was unaltered.

5.3.6 Photographic system

The bubble cloud was photographed through a microscope lens attached to an adjustable bellows, see plate 5.4. The end of the lens was aligned to the central point of the observation channel. The magnification factor of the lens was 10 with the total magnification being set by the position of the bellows. The photographs were taken with a 35 mm Camera attached to the bellows unit through a standard mount connector. The camera was loaded with 200 ASA black and white film and a shutter speed of $1/250^{\text{th}}$ of a second was used.

The level of magnification produced a depth of field of approximately 60 microns and an image area of 1728 x 1135 microns. This meant that focusing was very important and the optimal focus point had to be determined by trial and error, this was found to be when the microscope lens was 5 mm from the end of observation cell. This represented a starting point for each set of tests. Fine focusing was made by adjustment after bubbles had been injected into the cell to ensure sufficient numbers were likely to be included in an individual photograph.

The graticule was photographed during each test by clamping it to the front of the observation cell and then moving the whole cell unit backwards until the graticule was in focus. This meant that the lens system was not moved and ensured that the degree of magnification was the same as in the bubble photographs.

A standard flash gun was used as the lighting source set at its automatic rating. The position of the flash was set so the camera, cell and light source were all in central alignment. A condenser lens was placed in front of the observation cell to focus the light onto the cell. This produced excessive illumination so two neutral density filters rated at a total of 0.8, were placed behind the cell, preventing overexposure.

5.3.7 Nozzle

To enable the investigation of a series of different nozzle assemblies, a modular nozzle unit was designed, see figure 5.1.a-f and plate 5.2. The nozzle assembly comprised of a communal housing unit into which various configurations of cavitation plate and nozzle chamber could be attached. The unit was constructed out of brass and connected to the flotation column via a screw thread on the flotation base plate.

The design of the nozzle was scaled down from the patents of Guinness (Ash 1958,1959) and the W.R.C. (Hyde 1976). It was designed to resemble the basic structure of actual nozzles used in industry. To this end the ratio of the orifice to nozzle chamber diameter was kept within the range shown in the patents. Although

the basic structure of the nozzle resembled actual units in operation a simplified nozzle was required to allow investigation of the effects of the individual components. Table 5.1 shows the list of modular components available and the range over which they were tested, see figure 5.1.a1-7.:

| Nozzle component | Range |
|--|----------------------------|
| Orifice plate : size of hole (mm) | 0.5, 1, 2, 3, 4, 5 |
| Nozzle chamber : diameter and length (mm) | 0-0, 1-10, 5-5, 5-10, 5-20 |
| Nozzle chamber : diverging cone angle(°) | 30, 45, 60 |
| Impingement plate : distance between plate and exit of nozzle chamber (mm) | 0.5-20 |

Table 5.1: Description of nozzle component ranges.

5.3.5: Image analysis

Once the photographs had been taken, the negatives were processed and printed. This was carried out externally by a Kodak Ltd. As previously discussed, image analysis software was used to make the size measurements. The bubble size was based on a mean Feret's diameter which was found to be the most consistent measure. Feret's diameter is a measure of the distance between two parallel vertical lines that enclose an image. Area measurements are suggested in the literature as the most robust but cannot be used here as focused bubbles appear doughnut in shape and so are undersized. The major difficulty with the measurement of the bubbles was the selection procedure that needed to ensure that only focused ones were measured. Two approaches to this problem were developed, semi-automatic and fully-automatic solution.

5.3.5.1 Fully automatic solution

A fully automatic image processing routine was developed to enable the selection and sizing of a set of photographs without the need for human input. The routine was developed using Visilog, the image processing software distributed through Data Cell Ltd., Maidenhead. The approach was based on eliminating unfocused bubbles rather than selecting focused ones and is made possible by the unique qualities of focused bubbles. Plate 5.3 is representative of the photographs developed. In terms of the image, focused bubbles are sharper, darker and more circular in nature than unfocused bubbles. This means that the bubble's edge is more clearly identifiable. However, standard thresholding techniques are not subtle enough to enable selection. Similar problems were encountered with standard image processing functions such as edge detection and image sharpening. This means that standard analysis methods are unable to process the image successfully.

The actual processing routine that was used was based on the shape of the focused bubbles as they appeared doughnut shaped on the photographs. Each bubble had a white slit in its center produced by the flash gun and was unique to bubbles that were in focus. Figure 5.4 illustrates the flowchart of the processing routine required to manipulate this property to allow selection. Figure 5.5 shows a typical photograph through each stage of the process listing its name and describing its effect on the image.

The key function in the routine is the skeleton function. This reduces the thickness of the image down to its minimum size while still keeping the structure of the object intact. This makes the focused bubbles appear as circles and all unfocused bubbles are dendritic lines. All non circle shapes can then be removed relatively easily leaving only focused bubbles. The images that remain act as marker points for comparison with the original. Any image on the original that corresponds to a marker point is retained and the rest removed. This means that the focused bubbles are selected but at their original size such that the processing does not affect the final measurement of

each bubble's size. The rest of the routine is involved in cleaning up the image to make the running time of the process quicker. Once this process is complete the image can be straightforwardly analysed using standard functions in order to determine the diameter of each individual focused bubble.

The running time of the routine is approximately two hours per photograph, generating on average eight bubble measurements. In view of the quantity of data required this was too time consuming so an alternative procedure was developed on a semi-automatic basis.

5.3.5.2 Semi-automatic

A semiautomatic image processing routine was developed which measured the size of individual bubbles once they had been selected manually. This was developed on the image processing system 'Magiscan' manufactured by Joyce-Loebl. The initial step was to digitize the image using a video camera connected to a grabber board on the computer. Individual bubbles could then be sized by selecting them with a light pen connected to the monitor.

The measurements were made on a Feret's diameter basis as before. The graticule was analysed by measuring the distance between individual lines on the scale such that a microns per pixel scale factor could be determined. Once the data had been measured the distribution was calculated and analysed in terms of standard statistical variables (mean, mode, standard deviation).

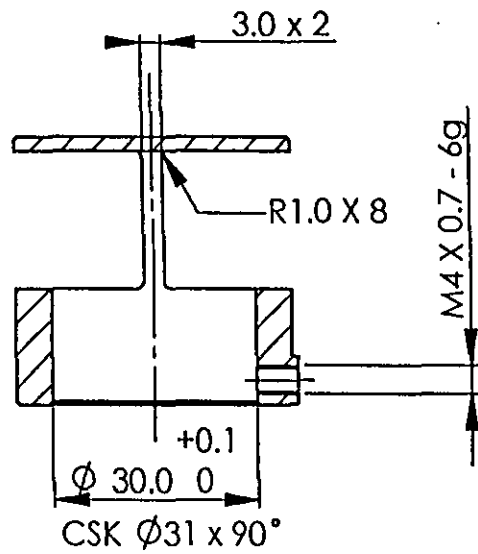
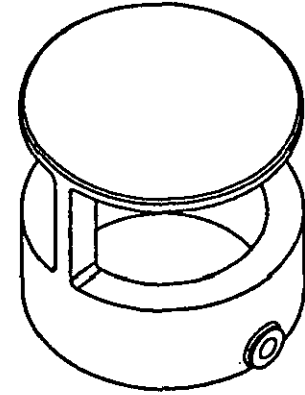
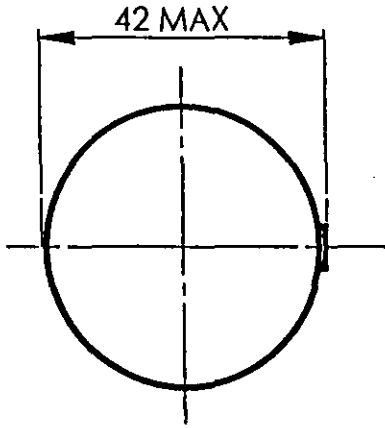
5.5 EXPERIMENTAL ERRORS

The main errors with the photographic measurement of bubble size distributions are associated with the selection of which bubbles should be measured. To achieve the level of sensitivity necessary for investigation in this field of research a high level of magnification is required. The result of this is to reduce the depth of field to

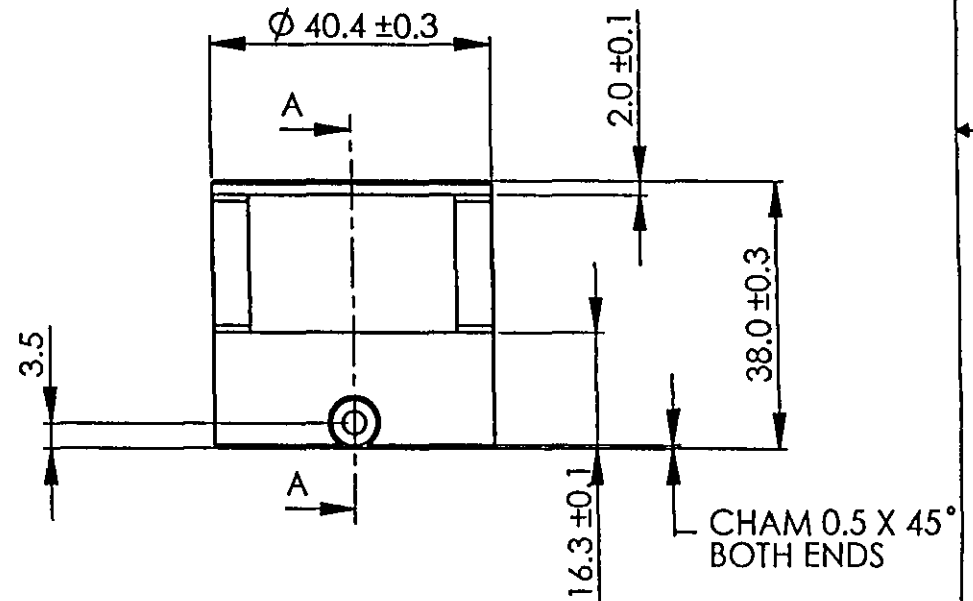
approximately one bubble diameter. This has the benefit of removing the problems of perspective but increasing the difficulty with which focused bubbles are selected. The problem is solved by choosing strict selection protocols that will eliminate all unfocused bubbles.

The major source of experimental difficulty was in photographing the graticule. The high levels of magnification employed meant that focusing the graticule was very sensitive such that a slight knock of the lens system meant that the image was out of focus.

5.1b.1

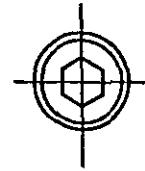
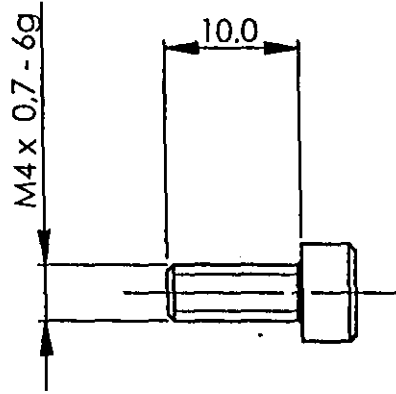


Section -AA

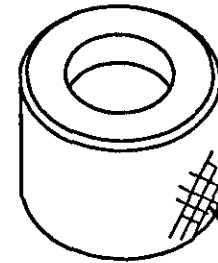
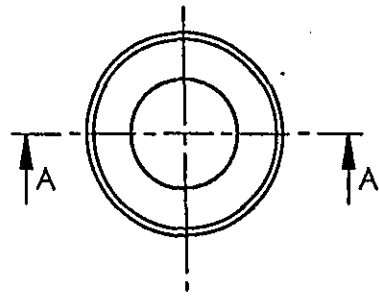


| | | | | |
|---|----------------------|--|-------------------|--------------|
| DIMENSIONS IN MILLIMETERS (mm) REMOVE SHARP EDGES UNLESS OTHERWISE STATED - TOLERANCES LINEAR ± 0.2 SURFACE ROUGHNESS $\sqrt{3.2}$ ANGULAR $\pm 5^\circ$ | DO NOT SCALE DRAWING | | TITLE | |
| | PROJECTION | | IMPINGEMENT PLATE | |
| MATERIAL -- BRASS | SCALE 1 : 1 | | DWG. NO. 5.1b.1 | SHEET OF 1/1 |
| FINISH -- CHROMIUM | | | | |

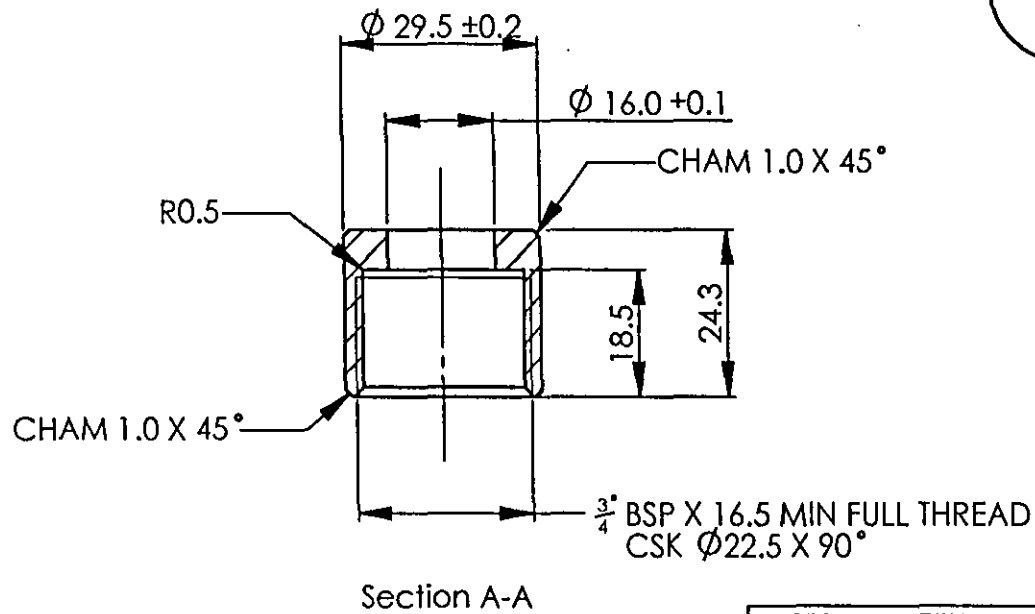
5.1b.2



| | | | |
|---|----------------------|--------------------------|-------|
| DIMENSIONS IN MILLIMETERS (mm) REMOVE SHARP EDGES UNLESS OTHERWISE STATED - TOLERANCES | DO NOT SCALE DRAWING | TITLE | |
| | | SOCKET HEAD CAP SCREW | |
| LINEAR ± 0.3 SURFACE ROUGHNESS $\nabla 3.2$ | PROJECTION | DWG. NO. | SHEET |
| ANGULAR | SCALE | 5.1b.2 | 1/1 |
| MATERIAL | | | |
| FINISH | | | |

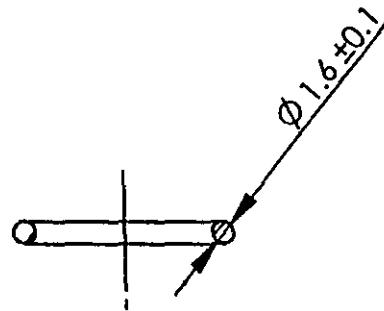
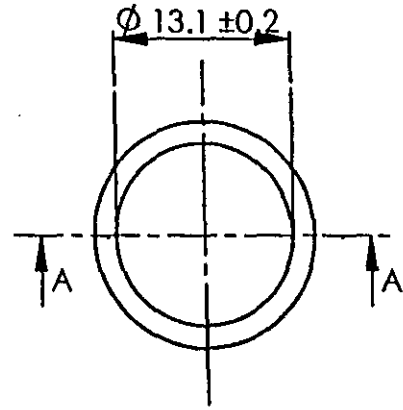


DIAMOND KNURL
1.5 PITCH



| | | | | | |
|---|-----------|----------------------|-----|--------------------|-------|
| DIMENSIONS IN MILLIMETERS (mm) REMOVE SHARP EDGES UNLESS OTHERWISE STATED - TOLERANCES | | DO NOT SCALE DRAWING | | TITLE | |
| LINEAR | ±0.2 | SURFACE ROUGHNESS | 1.6 | NOZZLE HOUSING NUT | |
| ANGULAR | ±5° | PROJECTION | | DWG. NO. | |
| MATERIAL | — BRASS | SCALE | | 5.1b.3 | SHEET |
| FINISH | — NATURAL | 1:1 | | | 1/1 |

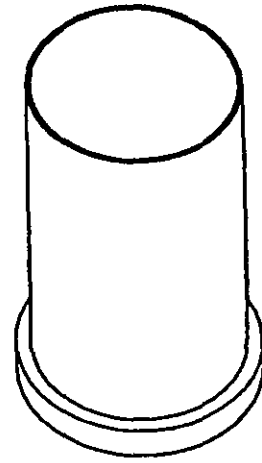
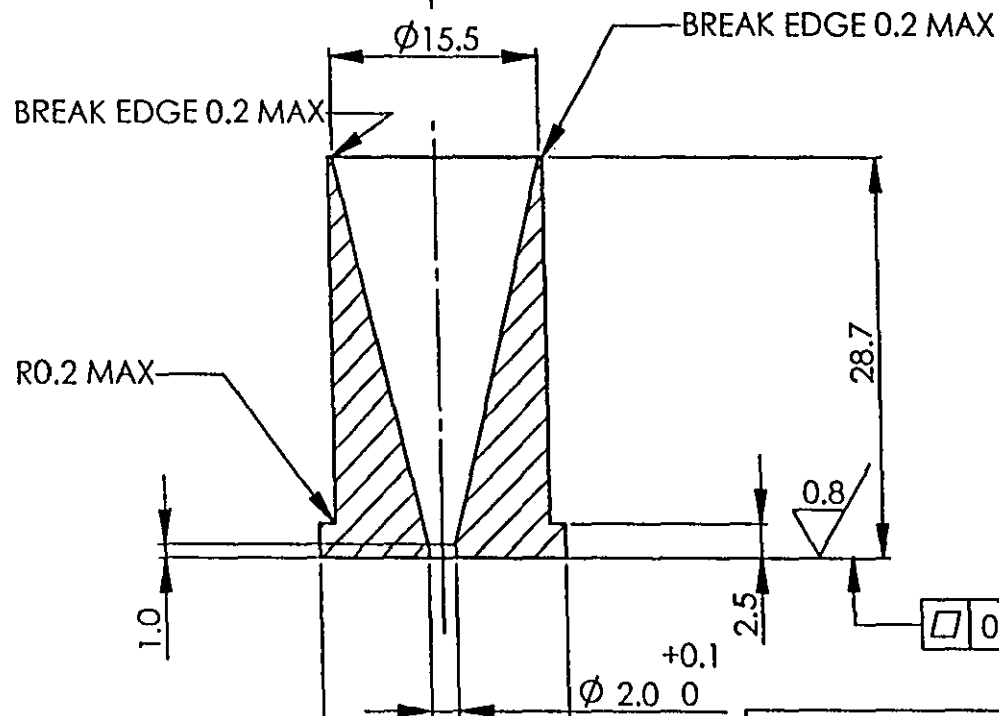
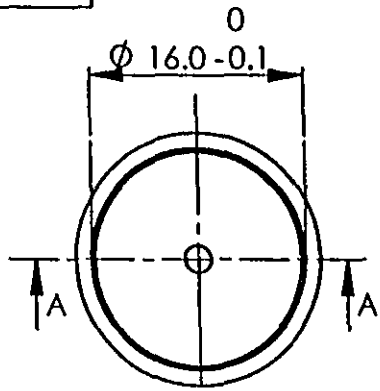
5.1b.5



Section A-A

| | | | | | |
|---|-------------------|----------------------|-----|--------------|--------|
| DIMENSIONS IN MILLIMETERS (mm) REMOVE SHARP EDGES UNLESS OTHERWISE STATED - TOLERANCES | | DO NOT SCALE DRAWING | | TITLE | |
| LINEAR | SURFACE ROUGHNESS | PROJECTION | | SEALING RING | |
| ANGULAR | | SCALE | 2:1 | DWG. NO. | 5.1b.5 |
| MATERIAL | - NITRILE | | | SHEET | 1/1 |
| FINISH | - BLACK | | | | |

5.1b.6



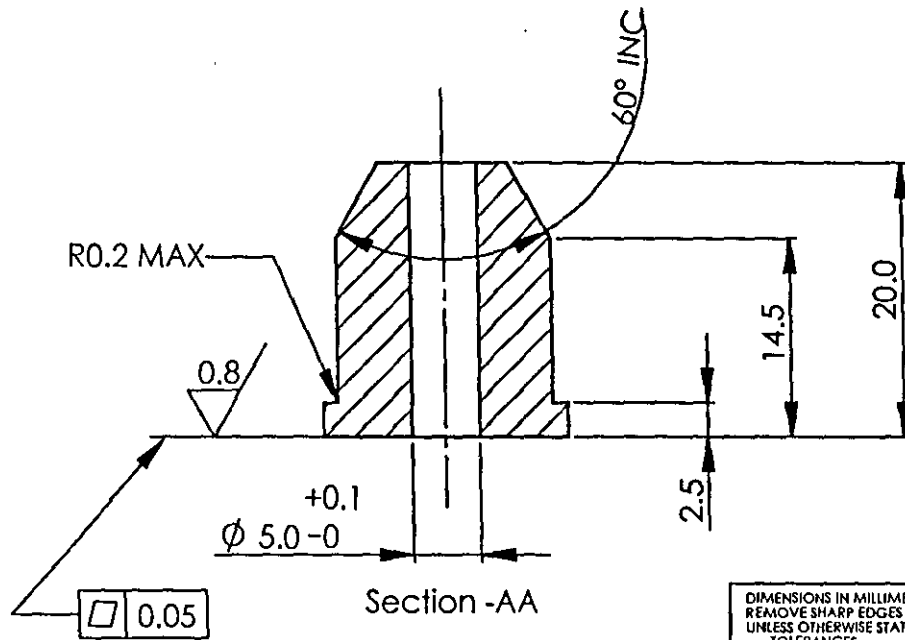
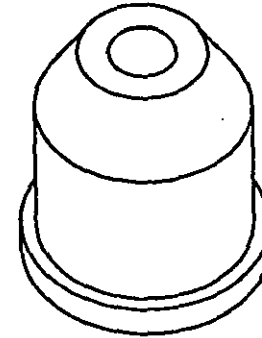
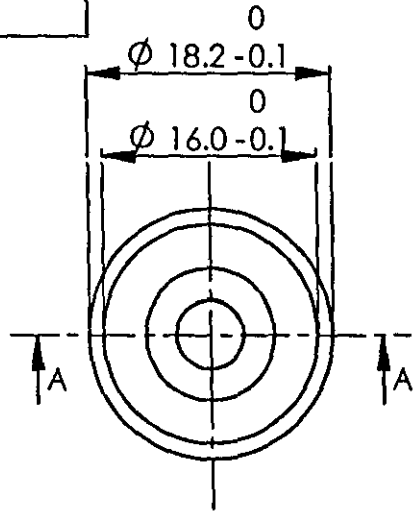
Section A-A

| | | |
|---|---------|-----|
| DIMENSIONS IN MILLIMETERS (mm) REMOVE SHARP EDGES UNLESS OTHERWISE STATED - TOLERANCES | | 1.6 |
| LINEAR | ±0.2 | |
| ANGULAR | ±5° | |
| MATERIAL | BRASS | |
| FINISH | NATURAL | |

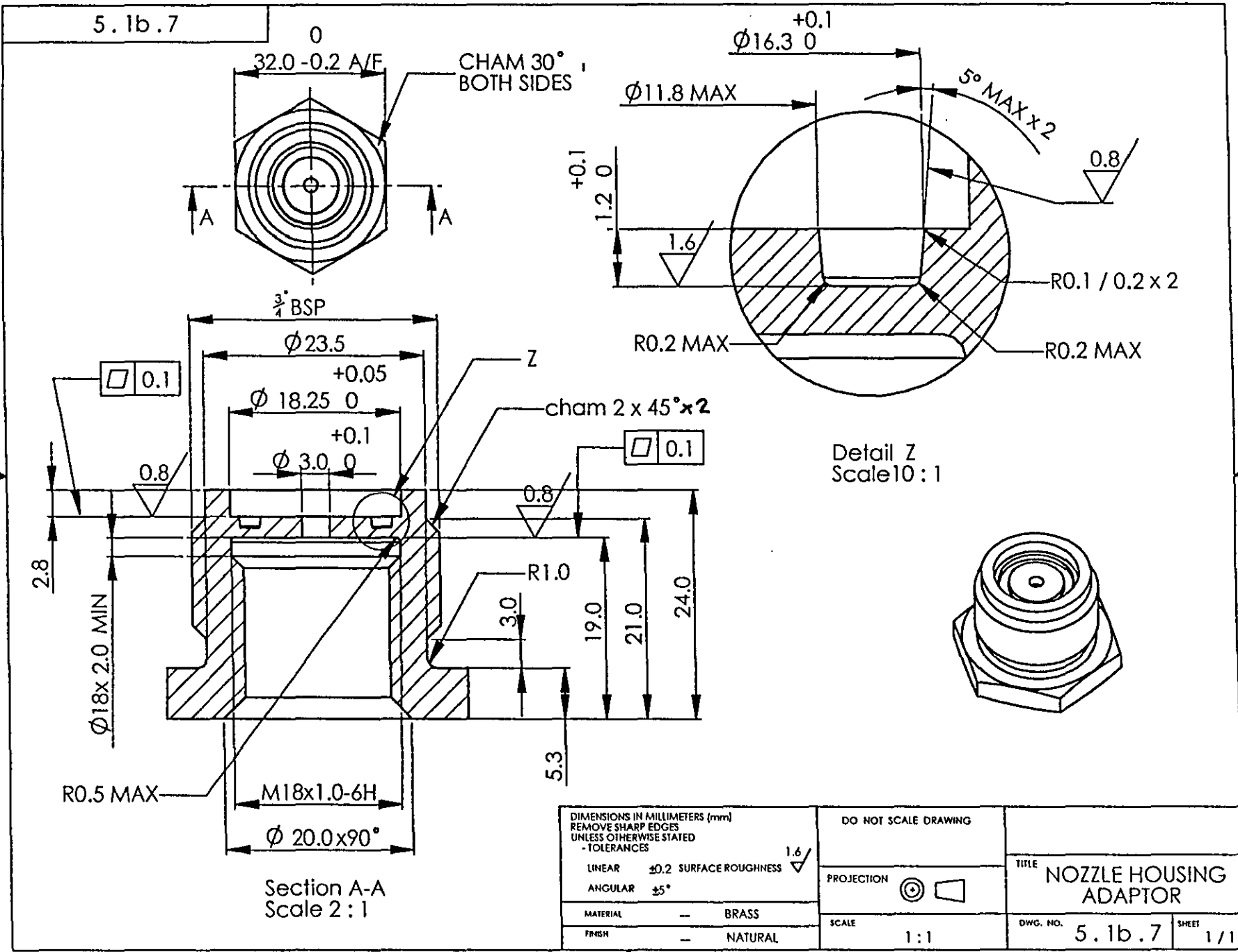
| | |
|----------------------|-----|
| DO NOT SCALE DRAWING | |
| PROJECTION | |
| SCALE | 2:1 |

| | |
|----------------|--------|
| TITLE | |
| DIVERGING CONE | |
| DWG. NO. | 5.1b.6 |
| SHEET | 1/1 |

5.1b.6A



| | | | |
|---|---|----------------------|--|
| DIMENSIONS IN MILLIMETERS (mm) REMOVE SHARP EDGES UNLESS OTHERWISE STATED - TOLERANCES | | DO NOT SCALE DRAWING | |
| LINEAR ± 0.2 ANGULAR $\pm 5^\circ$ | SURFACE ROUGHNESS $1.6 \sqrt{\text{ }}$ | PROJECTION | TITLE NOZZLE CHAMBER |
| MATERIAL — BRASS | FINISH — NATURAL | SCALE 2:1 | DWG. NO. 5.1b.6A SHEET 1/1 |



5.1b.7

0

32.0 -0.2 A/F

CHAM 30°
BOTH SIDES

$\phi 16.3 \begin{smallmatrix} +0.1 \\ 0 \end{smallmatrix}$

$\phi 11.8 \text{ MAX}$

5° MAX x 2

0.8

R0.1 / 0.2 x 2

R0.2 MAX

R0.2 MAX

$\frac{3}{4}$ BSP

$\phi 23.5$

Z

cham 2 x 45° x 2

Detail Z
Scale 10:1

0.1

$\phi 18.25 \text{ } 0$

$\phi 3.0 \text{ } 0$

0.1

2.8

$\phi 18 \times 2.0 \text{ MIN}$

0.8

R1.0

3.0

19.0

21.0

24.0

R0.5 MAX

M18x1.0-6H

$\phi 20.0 \times 90^\circ$

Section A-A
Scale 2:1

| | | | | |
|---|---------------|----------------------|--|-----------------|
| DIMENSIONS IN MILLIMETERS (mm) REMOVE SHARP EDGES UNLESS OTHERWISE STATED - TOLERANCES | | DO NOT SCALE DRAWING | TITLE NOZZLE HOUSING ADAPTOR | |
| LINEAR | ± 0.2 | | | |
| ANGULAR | $\pm 5^\circ$ | SCALE | 1:1 | DWG. NO. 5.1b.7 |
| MATERIAL | BRASS | | | SHEET 1/1 |
| FINISH | NATURAL | | | |

| | |
|----------------------|-----|
| DO NOT SCALE DRAWING | |
| PROJECTION | |
| SCALE | 1:1 |

| | |
|--|--------|
| TITLE NOZZLE HOUSING ADAPTOR | |
| DWG. NO. | 5.1b.7 |
| SHEET | 1/1 |

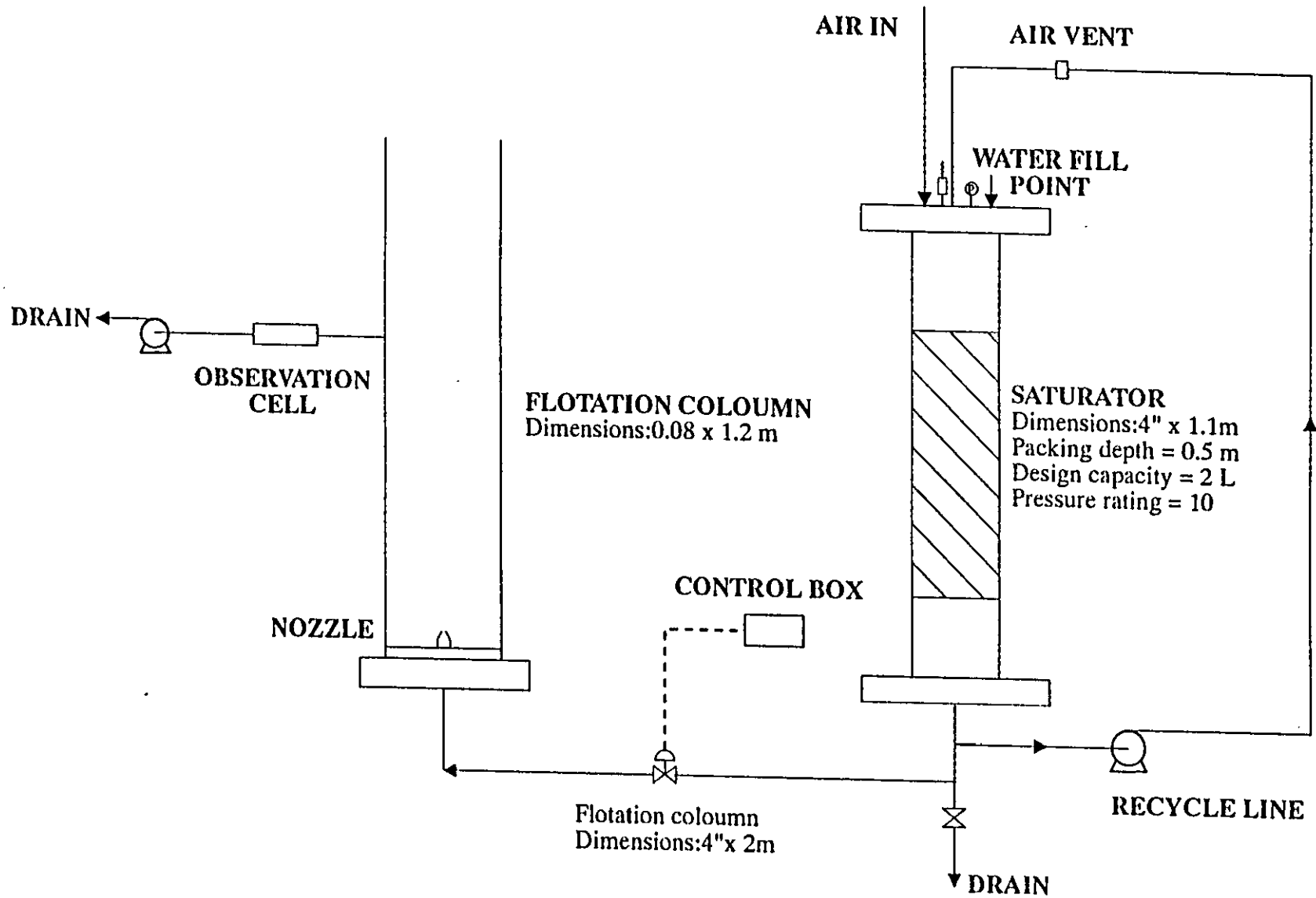
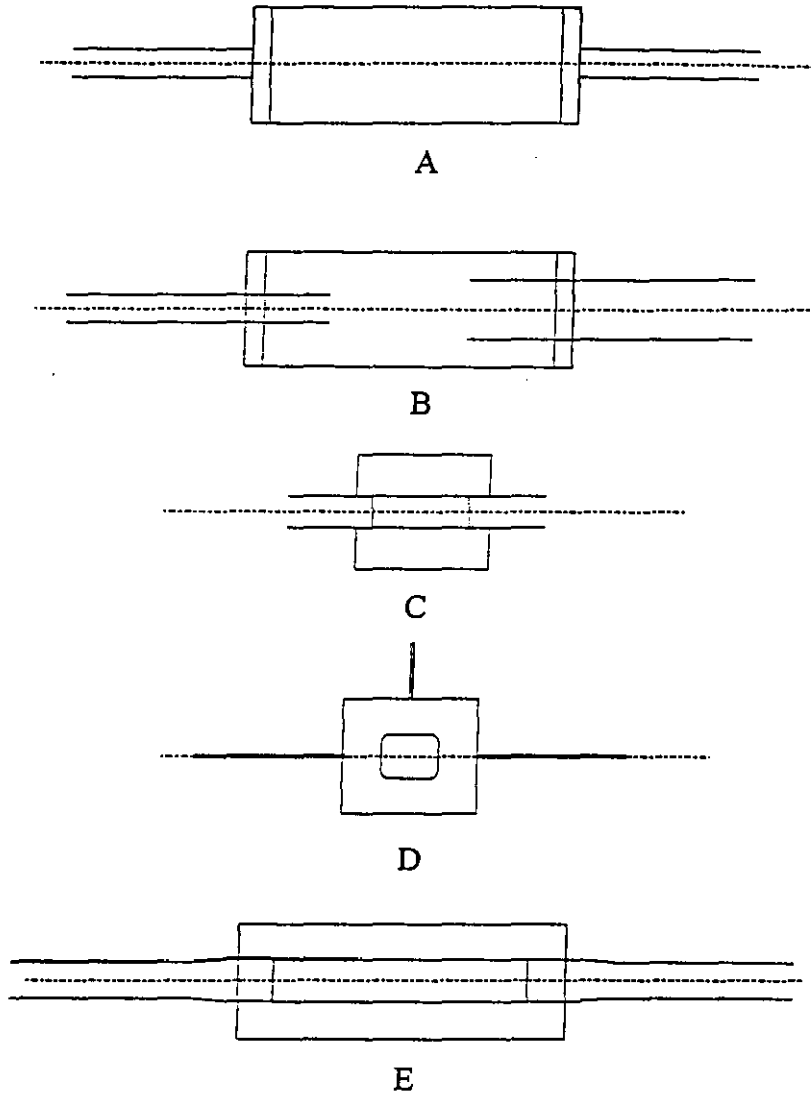


Figure 5.2 : Process flow diagram of the bubble photography rig



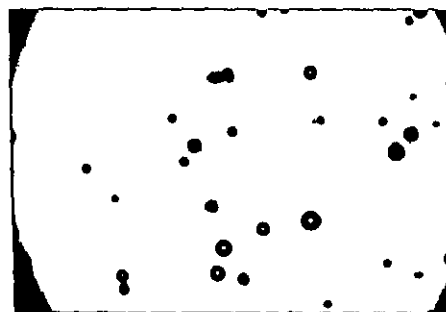
| | Height | Length | Width | Inlet Pipe diameter | Outlet Pipe diameter |
|---|--------|--------|-------|---------------------|----------------------|
| A | 27 | 77 | 27 | 10 | 10 |
| B | 27 | 77 | 27 | 10 | 15 |
| C | 26 | 26 | 7 | 7 | 7 |
| D | 26 | 26 | 3 | 3 | 3 |
| E | 27 | 77 | 7 | 7 | 7 |

Dimensions of observation cells (mm)

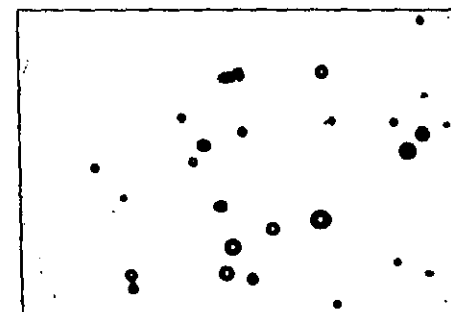
Figure 5.3 : Schematic diagram of the observation cells tested



(1) Read : Input photograph as grey scale image



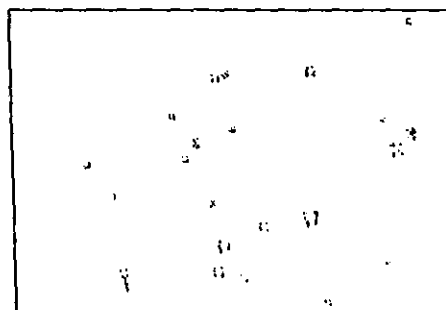
(2) Threshold : Convert grey scale image into binary form.
Range 0-140



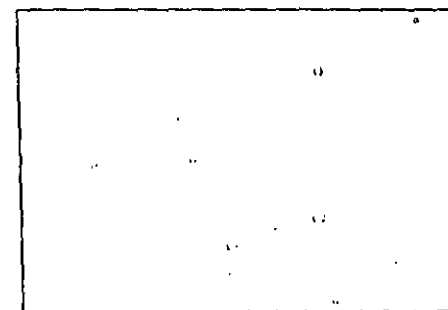
(3) Borderkill : Removes all pixels connected to the edge of the image frame (required 8 iterations)



(4) Open : Removes noise on image.
This function is a combination of Erode then Dilate (Set-3 iterations)



(5) Skeleton : Thins down image to its smallest representative form
(required 237 iterations)



(6) Prune : Erodes skeleton to remove dendritic structures
(required 206 iterations)

Figure 5.5 : Example pictureboard of automatic image processing routine

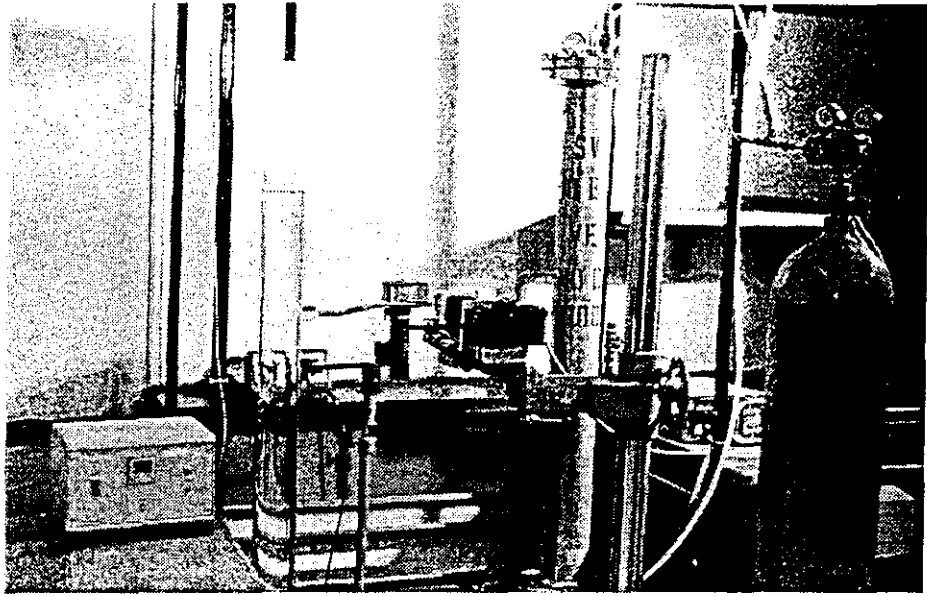


Plate 5.1 : Bubble photography experimental apparatus

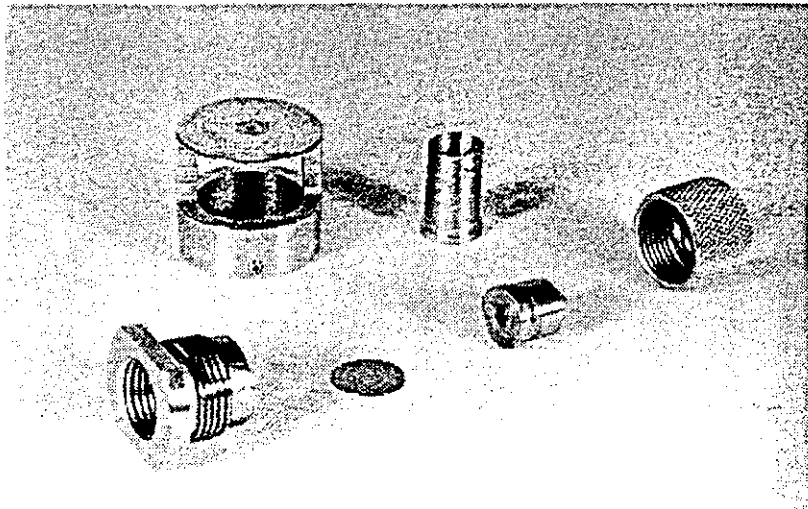


Plate 5.2 : Modular nozzle assembly

CHAPTER SIX

CHAPTER SIX

RESULTS : ZETA POTENTIAL MEASUREMENTS

6.1 INTRODUCTION

This chapter discusses the results obtained from the zeta potential characterisation measurements, the methodologies of which have been described in chapter 4. To aid clarity of the discussion the bulk of the results are contained within appendices A and D, although certain results have been highlighted within this chapter (see figure 6.1 to 6.25).

The discussion focuses on the evaluation of zeta potential measurements as a tool to describe the electrical response of clay particles. In accordance with Hunter (1981) detailed theoretical examination of the data will not be conducted as present theory poorly describes clay systems. Clay particles carry a high surface charge but a relatively low corresponding zeta potential. James (1982) attributed this to the porous nature of clays and corroborated Hunter's (1987) belief that both zeta potential and ion titration measurements were necessary for a complete description of the electrical nature of a clay particle. In this investigation the potential that is involved in the interaction of a bubble and a particle is the most important. This is best represented by the zeta potential as it is a measure of the potential closest to the diffuse double layer where the interactions will occur.

The following sections will discuss the response of the clays to a range of surface conditioning variables. In each case a simple model will be developed to describe how the zeta potential changes. The models have been tested extensively to assess the viability of zeta potential to act as a marker of the surface properties of the clay.

6.2 EVALUATION OF THE ZETA POTENTIAL OF CLAY PARTICLES

6.2.1 Clay composition

Before the discussion on zeta potential of clay particles can begin it is necessary to examine the clay composition. Clays are aluminosilicates made up of flat sheets of silicates (tetrahedral) and aluminium oxide (octahedral) layers. The individual layers bond together to form the basic units that make up each clay type.

Figure 6.1 is a schematic diagram of a basic kaolin particle in which a tetrahedral and an octahedral layer are bonded together, such particles are referred to as 1:1 layer silicates. These units stack together forming a hydrogen bond between individual units and combine to up to 100 layers in an individual particle. Figure 6.2 shows a simplified view of a kaolin particle, the particle carries a net negative charge caused by isomorphous substitution of Aluminium ions (Al^{3+}) for Silicon ions (Si^{4+}) in the tetrahedral sheet and Iron ions (Fe^{2+}) for Aluminium ions (Al^{3+}) in the octahedral sheet. This gives the face of the particle a large negative charge, which is said to be fixed (James 1982) as it is unaffected by changes in pH. The charge is partially counteracted by broken bonds on the particle's edges together with hydroxyls which undergo dissociation reactions and so are pH dependant.

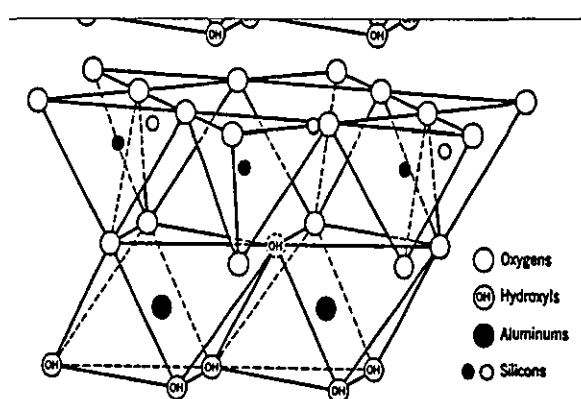




Figure 6.2 : Sketch of a typical kaolin crystal

A sample of the kaolin used in these experiments was analysed by the Natural History Museum and the results can be seen in Appendix I. These show the sample to be very pure (90% kaolin) with a cation exchange capacity (CEC) of 12.5 meq/100g which is relatively high when compared to the quoted figures (Jefferson 1993). This would suggest that a greater relative percentage of the total charge is derived from fixed site substitution. The morphology of kaolin is a flat hexagonal platelet crystal, but the high CEC suggests large amounts of substitution which tend to result in smaller less regular crystal shapes.

The other type of clay particle investigated was Wyoming bentonite which is a 2:1 layer silicate, see figure 6.3. In this arrangement an octahedral sheet is sandwiched between two tetrahedral sheets with successive layers being bonded by van der Waals forces only. This makes the particle smaller with typically only 2-5 layers stacked together in a single particle. Water molecules can associate between the triple layers expanding the clay. This increases the surface area making the clay more active. Extensive substitution occurs principally in the octahedral sheets that causes the CEC to be considerably higher than for kaolin. A sample of the bentonite used was found to be very pure (93%) with a CEC of 63.1 meq/100g. This is low when compared to quoted values (Jefferson 1993) indicating a low level of substitution which may cause the bentonite to be more active to changes in pH. The total charge of the particle is typically split as 80% to substitution and 20% to edge effects indicating that dissociation reactions are considerably less important for Wyoming bentonite particles. The high specific surface area of the particles means the double layer is

small with most of the counterbalancing charge being situated in the Stern layer of the particles. The morphology of the particles are equidimensional flakes that appear as plate.

Plate 6.1 shows scanning electron micrographs of a kaolin and a Wyoming bentonite particle, demonstrating the fundamental differences in their morphologies. The kaolin particles tend to be large stacks which offer a much smaller specific surface area than the smaller more porous Wyoming bentonite particles. The comparison of the clay's CECs indicate that the Wyoming bentonite is likely to have a greater proportion of fixed site charge and hence will be more stable to changes in pH.

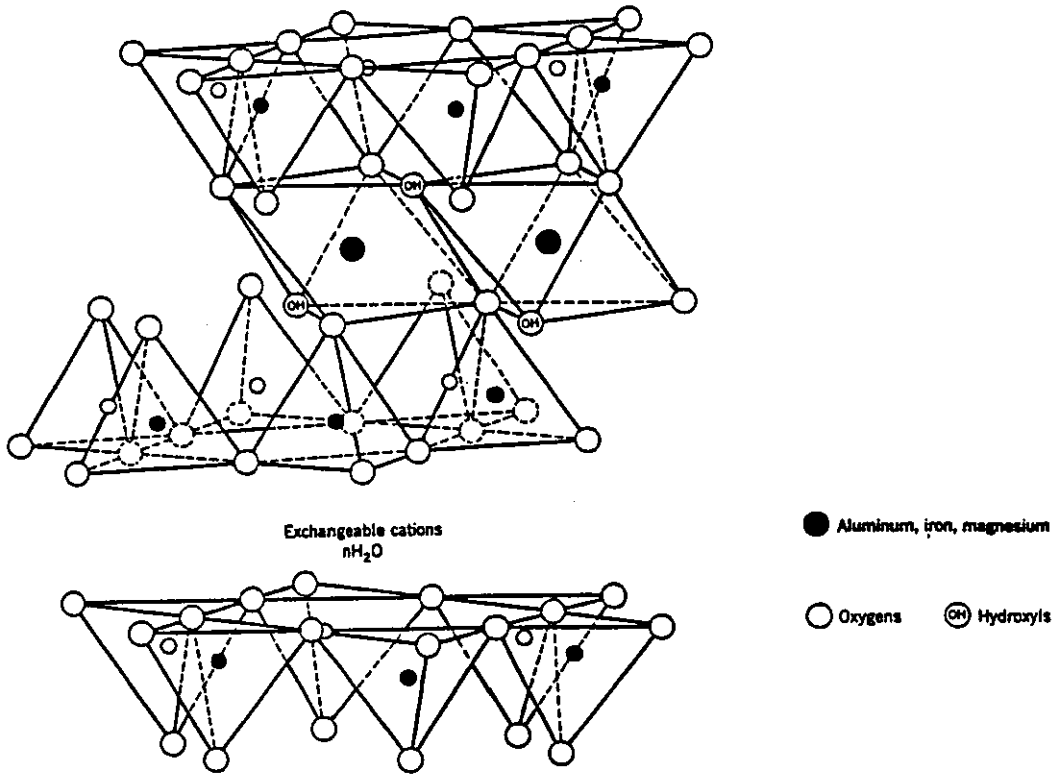
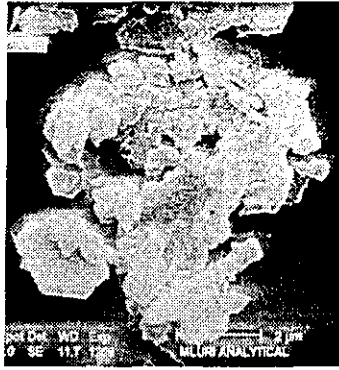
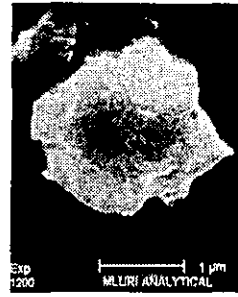


Figure 6.3 : Diagrammatic sketch of a Wyoming bentonite's structure



Kaolin



Wyoming Bentonite

Plate 6.1 : SEM of a typical kaolin and Wyoming bentonite particle

6.1.2 Theoretical predictions

Theoretical prediction of the electrical double layer of clay particles has been described by James (1980) in his site-dissociation-site-binding-model. The model is based on the surface of the clay containing a fixed number of dissociation sites, some of which become neutralised by specific adsorption. The result is a function relating potential at the Stern layer with pH and electrolyte concentration. To solve this the number of dissociation sites and the dissociation constants need to be determined. This is a complex procedure which has not been proved to work effectively for clays such that James (1982) admits that this model is best suited to qualitative description. The subsequent discussion in this chapter will be based on the ideas of James (1982) and in accordance with Hunter (1981) no attempt will be made to compare experimental data with theoretical predictions.

6.2.2 Reproducibility

The measurement of zeta potentials by the laser Doppler technique, described in section 4.3.7.1, produces a mobility distribution rather than a single value allowing an accurate determination of the individual error of each measurement. A typical distribution is shown in figure 6.4 and is described in terms of a mean zeta potential

and a standard deviation. The measurement of zeta potential also has variations due to the complex nature of the clays and the possible impurities coated on them. Figure 6.5 shows the reproducibility of the measurement on a dispersed sample of kaolin particles without any conditioners being used. It is likely that this variation will represent the maximum that will be encountered as any conditioning should buffer the zeta potential measurement. The plot indicates that changes of ± 5 mV should be attributed to natural variations in the clay. A similar result was found for the Wyoming bentonite particles. This represents a limit on the sensitivity of the measurements such that only variations in zeta potential greater than ± 5 mV should be considered as significant.

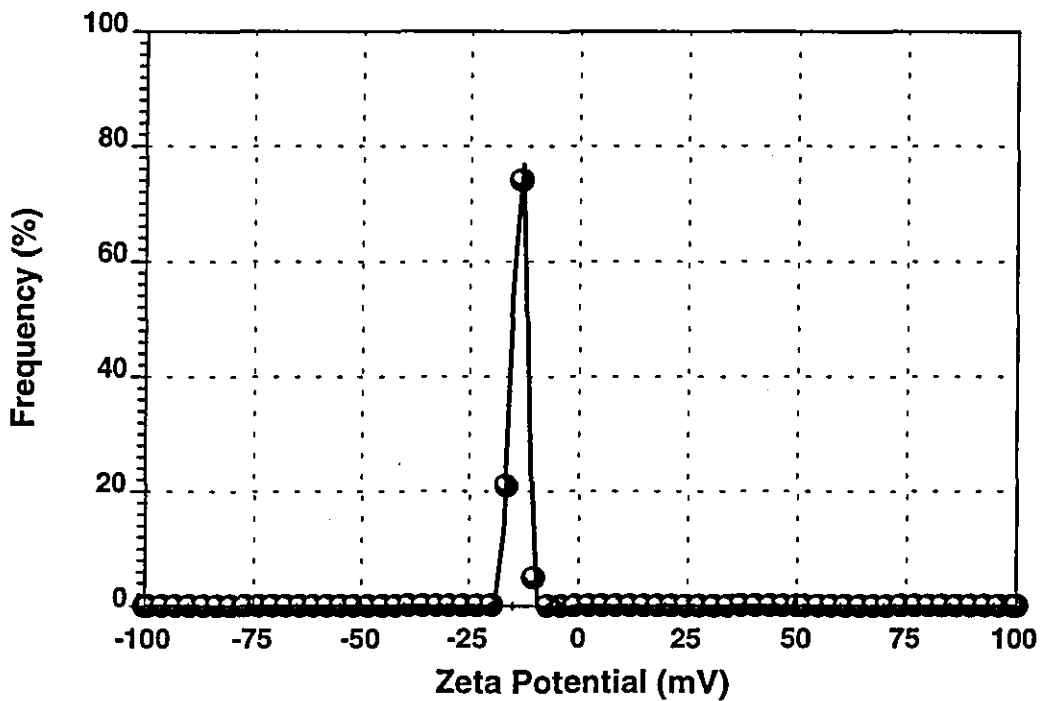


Figure 6.4 : Zeta Potential frequency plot for dispersed kaolin particles

Other factors that have been considered as possibly contributing to these effects were the method of dispersion and length of time the Wyoming bentonite particles had been dispersed. Investigation into both factors failed to show any appreciable change in the zeta potential so that any change was within the 5 mV error band of the

measurements. In particular, the difference between using the sonic probe and mechanically stirring the sample was very small, -21.59 mV and -22.34 mV respectively. The problem associated with dispersion became less complicated with Wyoming bentonite as it is very difficult to disperse and the sonic probe was required to achieve effective dispersion. The small difference in the dispersion techniques is due to the low concentrations tested within this investigation.

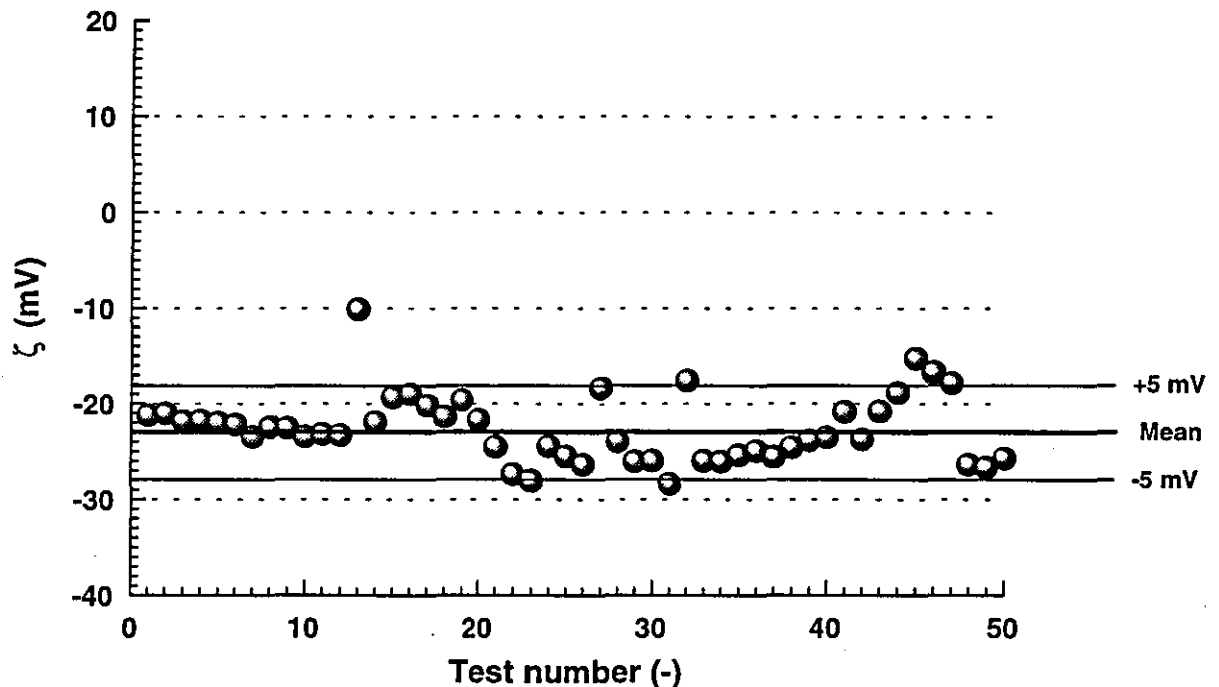


Figure 6.5 : Reproducibility of zeta potential measurement for dispersed kaolin particles

6.3 pH EFFECTS

6.3.1 Kaolin

The effect of pH on the zeta potential of dispersed kaolin particles in both distilled and tap water can be seen in figure 6.6. The distilled water result is in agreement with previous studies (Ferris 1975, Packham 1965, Williams 1978) in that there appears to be a gradual decrease in zeta potential with pH. This change is due to the presence of

ionizable surface groups on the edge of the particles. These sites are amphoteric such that they become either positively or negatively charged depending on the pH:

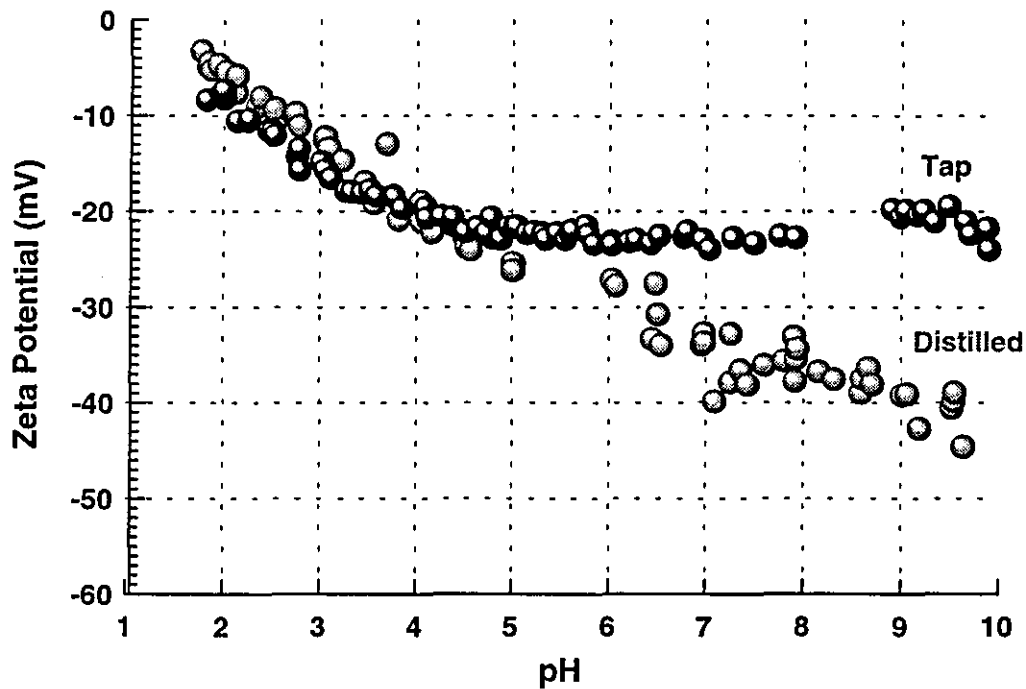
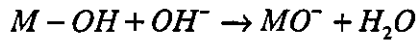


Figure 6.6 : Zeta Potential vs pH for dispersed kaolin particles in tap and distilled water

James (1982) states that the degree of charge due to the edge dissociation reactions is of a similar magnitude to that of the fixed sites. This accounts for the shape of the graph with the value at the neutral pH being approximately the mid point in the zeta potential curve. The zeta potential remained negative for all pHs and this contradicts the results of Packham (1965) who showed the zeta potential to be positive below pHs of 3. The difference seen in this investigation is due to the relatively high CEC of the kaolin sample used. This suggests the clay has a relatively large amount

of fixed negative charge which in turn requires a greater degree of proton accepted dissociation on the edges to counteract it.

The measurements made using tap water agree with the results of Roberts (1980) in that they show no appreciable change when the pH is greater than 4, which is due to the increased ionic concentration in the tap water compressing the double layer and acting as a buffer. This compression can be seen in the change in the double layer thickness, which according to Hughes (1981) changes from 900 to 40nm for distilled and tap water respectively. The range of pH that is of practical interest is from pH greater than 4 and so the results show that kaolin is stable in high ionic solutions over the range of interest.

6.2.2 Wyoming bentonite

The equivalent result for Wyoming bentonite can be seen in figure 6.7. The most important feature of this data is the plateau response to a wide range of the pH scale for both tap and distilled water. This is in agreement with the site-dissociation-site-binding model as Wyoming bentonite has a much greater percentage of fixed site charge, buffering any changes due to dissociation.

The data is made up of results from a series of tests conducted on freshly dispersed and samples left for a day. No difference between the two can be seen over acidic regions but the general trend is surprising. The magnitude of the zeta potential increases once the pH is lower than pH 3. The explanation of this is that the strong acidic conditions are breaking down the structure of the clay. Jefferson (1993) reports that silicon ions dissolve at extreme pH's increasing the charge deficit on the particles' faces.

The overall trend of the zeta potential becoming more negative with increasing pH in alkaline conditions is seen in both sets of tap water data. However, the one day sample has a lower initial value and changes at a greater rate with pH such that the

two samples converge at the very high pHs. This is explained in terms of Wyoming bentonite's known tendency to destabilise. The one day sample is likely to have agglomerated into card house structures as discussed by van Olphen (1987) such that negative edges would contact positive faces reducing the overall charge. This would also tend to increase the relative amount of edges exposed thus increasing its pH sensitivity and thus the increased slope of the curve.

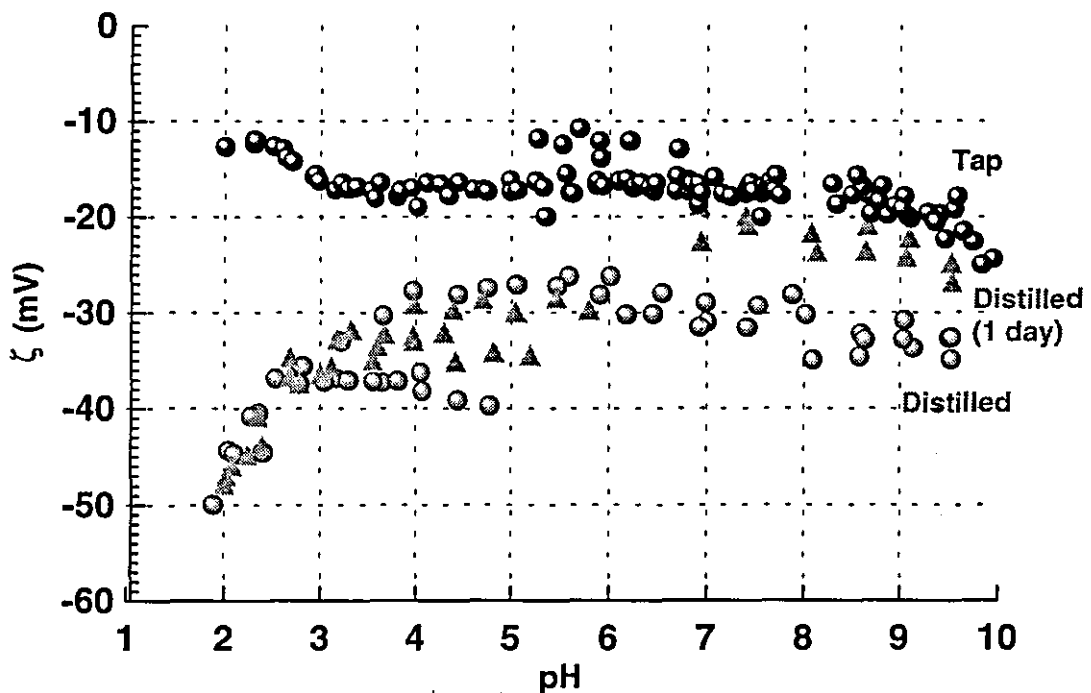


Figure 6.7 : Zeta Potential vs pH for dispersed Wyoming bentonite particles in tap and distilled water.

When the test is run with tap water a similar result to that obtained with kaolin is observed. The increased ionic concentration of the sample buffers the particles. This makes the particles very stable to changes in pH and over the particular range of interest the zeta potential remains unchanged.

6.4 SURFACTANT EFFECTS

6.4.1 Kaolin

The effect of concentration of the surfactants n-alkyldecyltrimethylammonium bromide on the zeta potential of dispersed kaolin particles is shown in figure 6.8. The general shape of the curves is consistent with the belief of Roberts (1980) and Rosen (1989) that cationic surfactants adsorbing onto charged surfaces follow a S type adsorption isotherm.

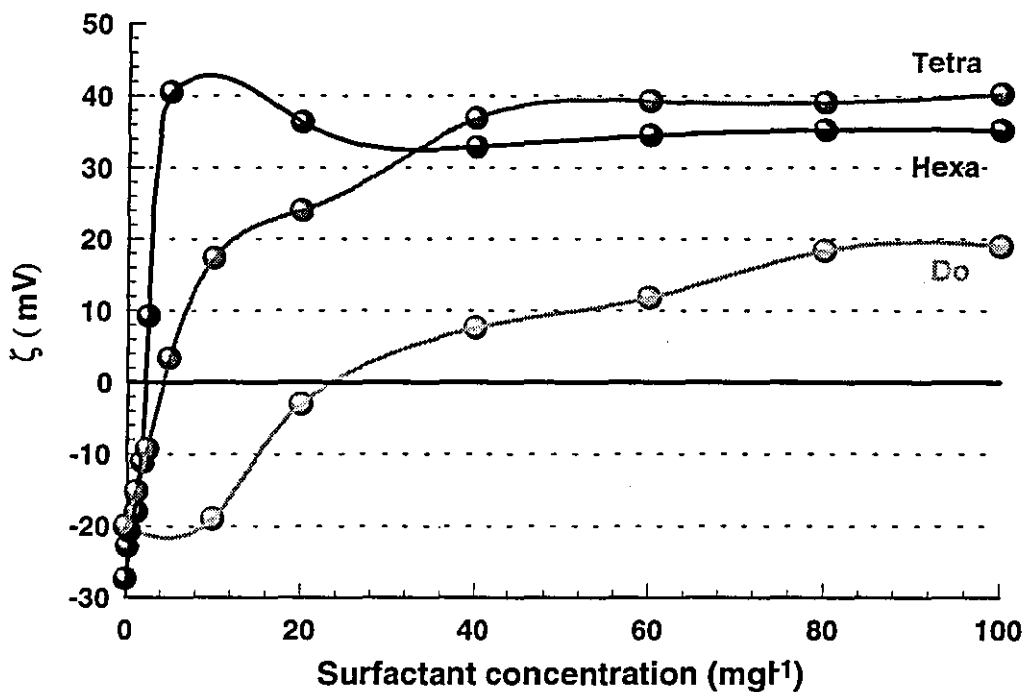


Figure 6.8 : Zeta potential vs concentration of n-alkyltrimethylammonium bromide for dispersed kaolin particles, at natural pH

The most important feature is the efficiency of adsorption which is defined by Rosen (1989) as rate of change of zeta potential with surfactant concentration. The results show that an increase in hydrocarbon chain length improves the efficiency of adsorption as less surfactant is required to achieve a point of zero potential. The rate increases dramatically with increasing chain length and this is seen with a total change

A more quantitative analysis was performed following the calculations detailed in Hunter (1981). The first of these calculates the free energy of adsorption (θ') per CH_2 group on a hydrophilic surface, relative to that for micelle formation in the bulk. A value of $1.331kT$ was obtained which is higher than the value for micelle formation, quoted by Hunter (1981) of $1.1kT$, agreeing with the result obtained by Lin (1971). The other calculation determines the specific free energy of adsorption ($\Delta G^\circ_{\text{ads}}$), a value of $0.98kT$ was calculated which is close to the value of $1kT$ that represents complete removal of a CH_2 group from water. This support the idea of hemi-micelle formation and thus perpendicular adsorption.

The evidence presented above indicates that the adsorption of surfactant onto kaolin particles occurs in a perpendicular orientation with the formation of surfactant clusters. This is in agreement with the work of Roberts (1980) and Smith (1993). The role of surfactants in this case can be reasonably well described even if quantitative predictions are not possible. One possible calculation is that of adsorption density which was found to be 6.07×10^6 molecules/ m^2 .

A specific area of interest in terms of the dissolved air flotation investigation is the point at which surfactant concentration no longer affects the zeta potential. This would represent a point of surface saturation such that the remaining surfactant would be free to adsorb onto the surface of the bubbles in the process. Table 6.1 shows the concentration at which saturation begins for each of the surfactants.

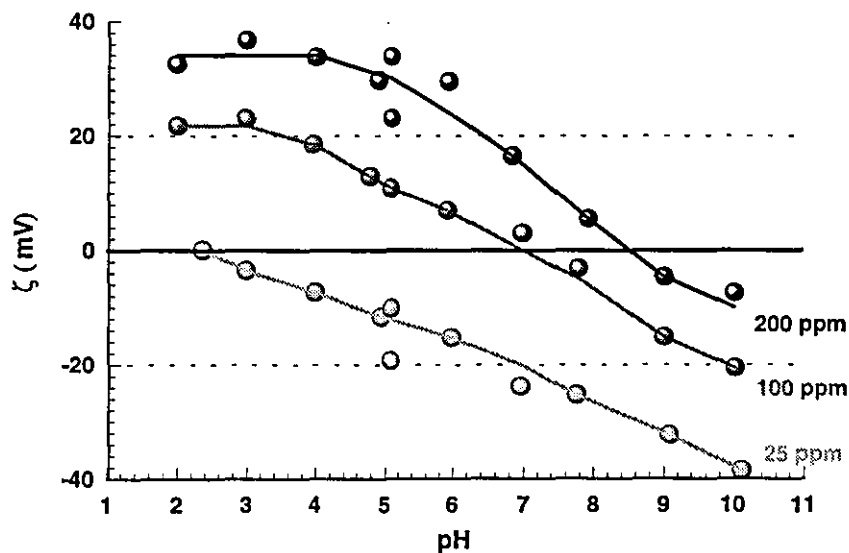
| Surfactant | Concentration at saturation (ppm) |
|------------|-----------------------------------|
| HTAB | 4 |
| TTAB | 40 |
| DTAB | 80 |

Table 6.1 : Concentration required to obtain surface saturation for each surfactant

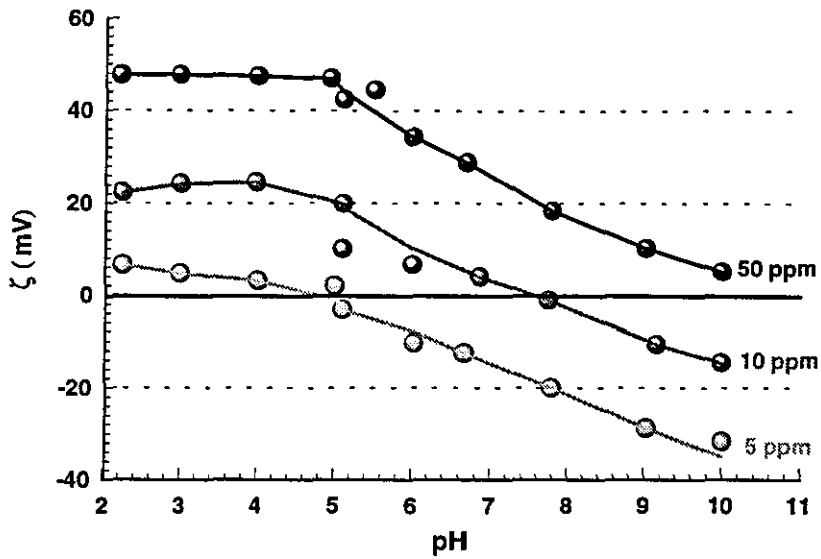
6.4.2 Kaolin and pH changes

The effect of pH on the adsorption process can be seen in the series of graphs, figure 6.9a-c. These show the zeta potential with changing pH at set surfactant concentrations for each of the three surfactants investigated. The results agree well with the study of Smith (1993) with the majority showing no change in zeta potential with acid and a gradual decrease with addition of base. Rosen (1989) states that quaternary ammonium cationic surfactants are unaffected by pH; this means that any alteration in the zeta potentials of the kaolin particles is a result of changes to the surface of the particles. This notion is demonstrated by the approximate parallel nature of the curves for the different concentrations and the different chain lengths.

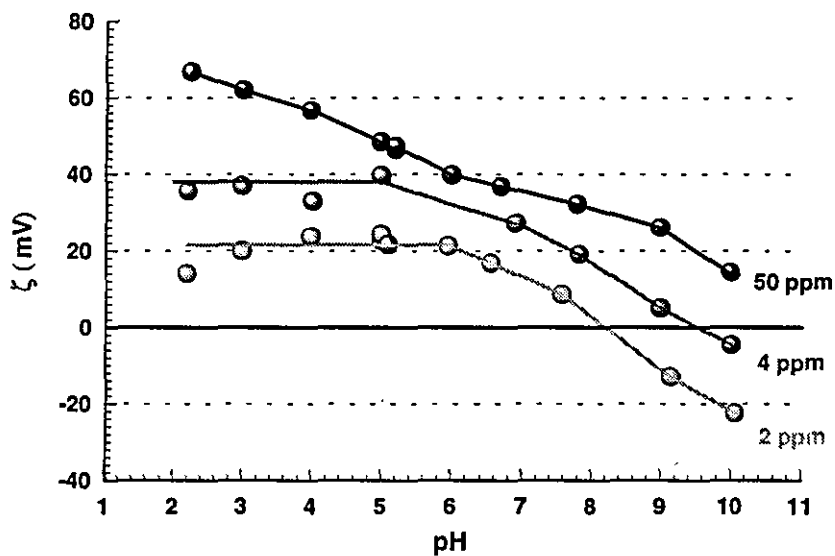
The natural pH of the samples was between pH 4.5-5 which corresponds to the position where pH starts to show an affect. This means that addition of acid has no effect on the zeta potential and addition of alkaline does. The slope of the curves with increasing pH is similar to the case of surfactant free kaolin, this means that the adsorption is taking place on faces of the clay, not interfering with the pH reactive edges



(a) Dodecyltrimethylammoniumbromide



(b) Tetradecyltrimethylammoniumbromide



(c) Hexadecyltrimethylammoniumbromide

Figure 6.9 : Zeta potential vs pH for various surfactant concentrations with : (a)Do; (b)Tetra; (c)Hexa alkyltrimethylammoniumbromide on dispersed kaolin particles

The reason for the stable response to addition of acid is less clear. It is likely that it is due to competition between the acid and the surfactant at the clay's edges. This reduces the amount of surfactant adsorbed as the pH decreases, reducing the zeta

potential and this is counteracted by the normal dissociation reaction that occurs with pH, producing no net effect.

The curves for DTAB at 25 ppm and HTAB at 50 ppm deviate from the general trend showing a continued change with pH into the acidic region. These represent the upper and lower limits of the investigation and result from a change in the adsorption of the surfactant, presumably at the edges. The DTAB case is due to the low concentration which often relates to a low level of adsorption but this will not be true in the case of HTAB. The implications in terms of the investigated presented here are negligible as the anomalous behaviour occurs outside the range of interest to the flotation experiments discussed in chapter 8.

6.4.3 Wyoming bentonite

Figure 6.10 shows the results of Wyoming bentonite conditioned with the three surfactants. The shape of the curves are similar to those of kaolin which suggests the mechanism of adsorption is the same. This is confirmed by quantitative analysis of the adsorption, which reveals values for the change in the specific free energy of $0.92kT$. This value is lower than for kaolin ($0.98kT$) and is in agreement with Hunter (1981) who attributes it to Wyoming bentonite's lower hydrophobicity.

The major difference between the two sets of curves is in the concentration range. The Wyoming bentonite particles require approximately double the amount of surfactant to bring the zeta potential to an equivalent value. This is consistent with the ratio of the specific surface areas of the two clays, if we assume that the surfactant only adsorbs onto the outer surface of the Wyoming bentonite particles.

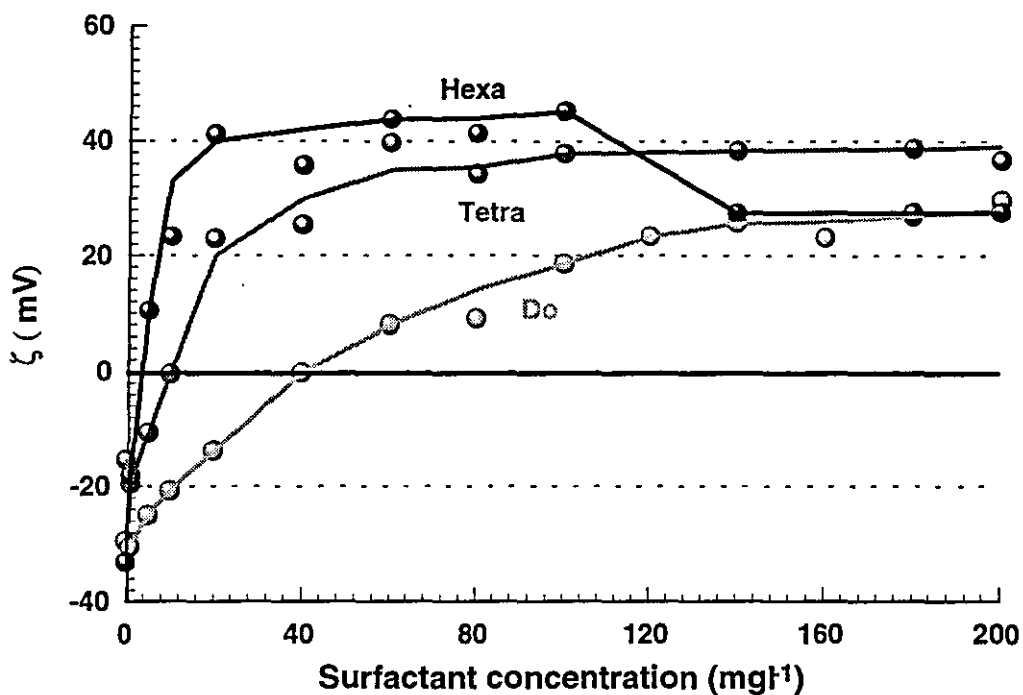


Figure 6.10 : Zeta potential vs concentration of n-alkyltrimethylammonium bromide for dispersed Wyoming bentonite particles

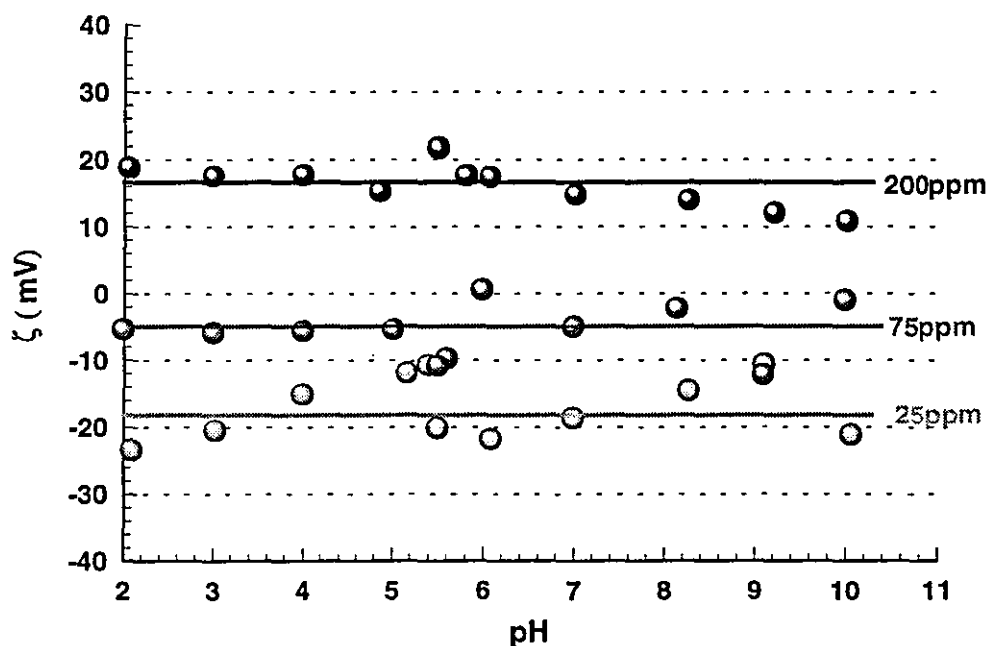
The concentration that gives surface saturation is shown in table 6.2. The results are compared to those of kaolin to show the much greater concentrations required. A similar trend in scale is seen with the surface saturation concentration with values being approximately double the concentrations needed for kaolin.

| Surfactant | Wyoming bentonite (ppm) | kaolin (ppm) |
|------------|-------------------------|--------------|
| HTAB | 12 | 5 |
| TTAB | 80 | 40 |
| DTAB | 160 | 80 |

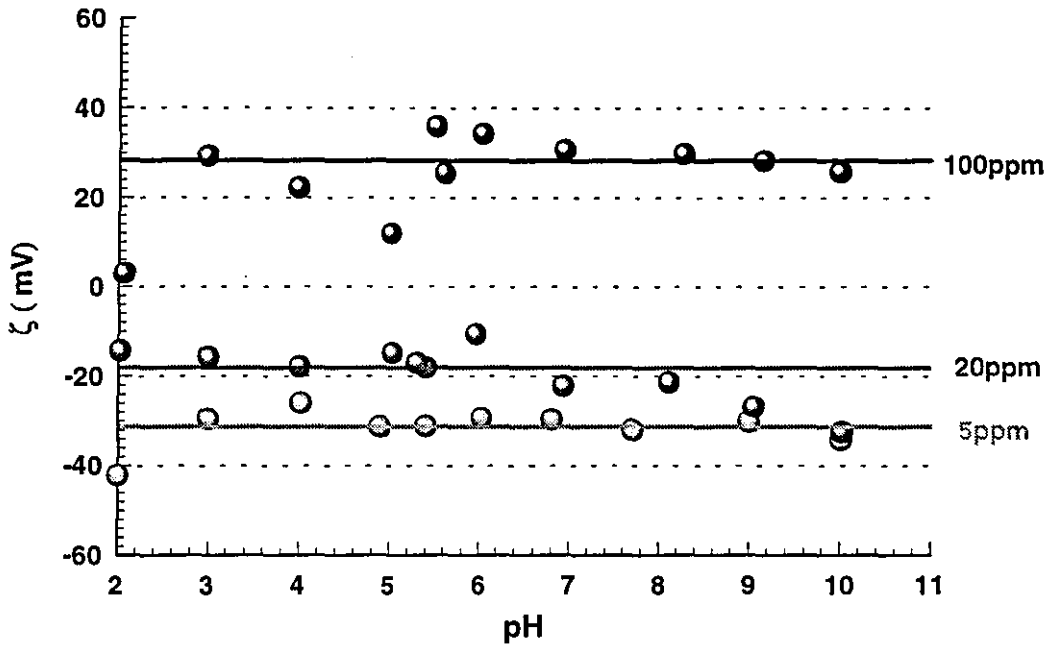
Table 6.2 : Concentration required to obtain surface saturation for each surfactant

6.4.4 Wyoming bentonite and pH changes

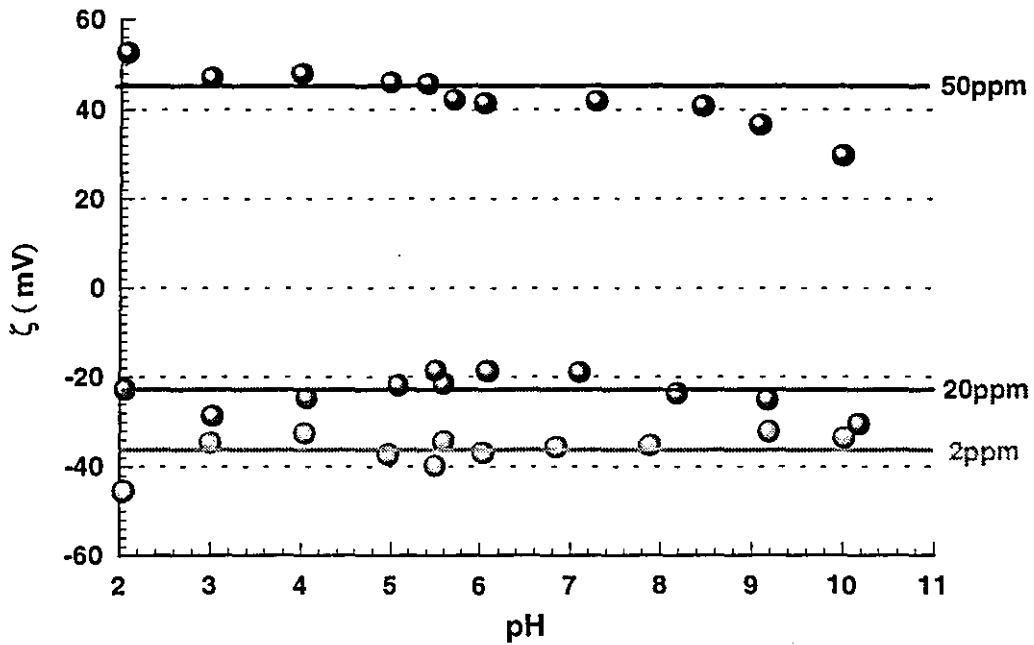
The effect of changes in pH at a range of set surfactant concentrations can be seen in figure 6.11a-c. The most striking feature of the curves is that they are essentially flat showing little change with pH. This is expected as the charge on Wyoming bentonite particles is made up almost entirely of fixed site substitution, which is unaffected by pH. The high degree of charge on the faces on the particles will mean that virtually all the adsorption will occur on the faces, restricting competitive adsorption on the edges as seen with the kaolin particles. The high degree of scatter which is observed is similar to those found when no surfactant was present, see figure 6.7. It is possible that a small pH effect can be seen but the level of change is small and occurs at the extreme values of pH which represent the areas of least interest.



(a) Dodecyltrimethylammoniumbromide



(b) Tetradecyltrimethylammoniumbromide



(c) Hexadecyltrimethylammoniumbromide

Figure 6.11 : Zeta potential vs pH for various surfactant concentrations with : (a)Do; (b)Tetra; (c)Hexa alklytrimethylammoniumbromide on dispersed Wyoming bentonite particles

6.5 COAGULANT EFFECTS

The discussion below looks at the effect of coagulant dose on the zeta potential of the two clays investigated. The situation is more complicated than with surfactants due to the fact that the coagulant undergoes hydrolysis reactions in water. This process represents a hydroxyl group replacing a water molecule that has associated with the metal ion. The process is shown by equation 6.2 and results in a range of hydrolysis products being formed, ranging from monomeric to polymeric ions and precipitated hydroxide.



The exact proportion of each species is dependant on the coagulant dose and the pH of the system. Johnson (1983) shows these changes on stability diagrams and examples for the coagulants used in this investigation are presented in figures 6.12 and 6.13

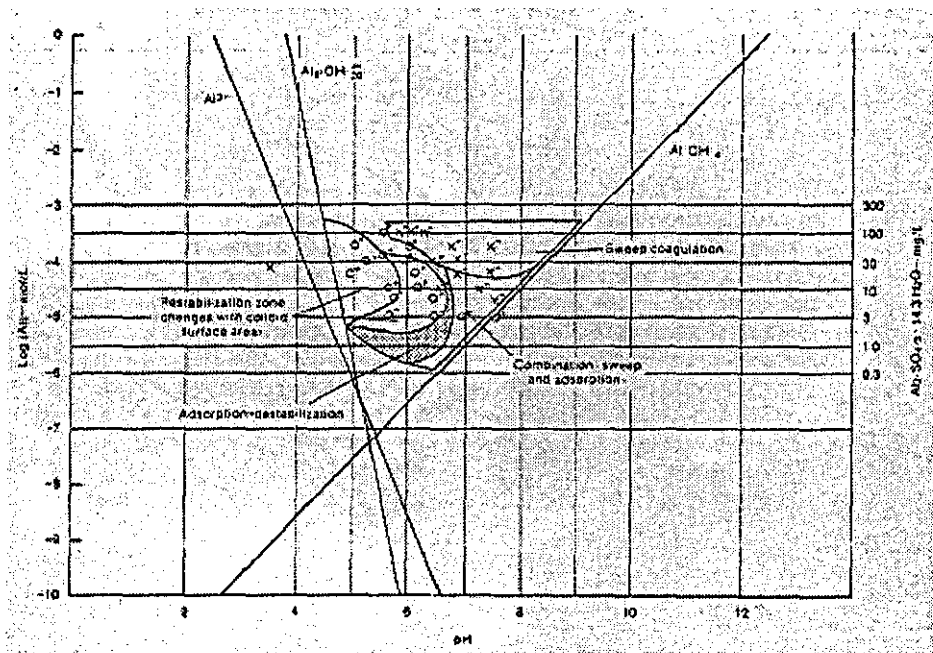


Figure 6.12 : Stability diagram for Al(III) coagulation (after Johnson 1983)

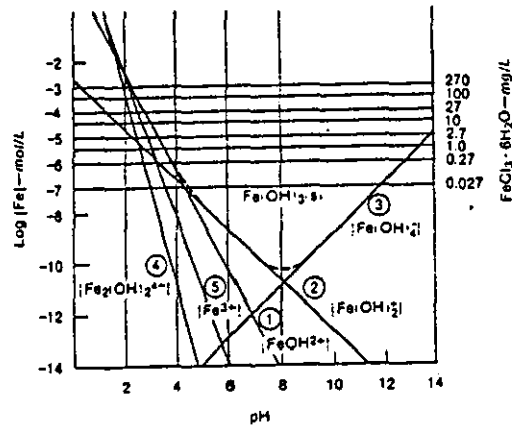


Figure 6.13 : Stability diagram for Fe(III) coagulation (after Johnson 1983)

The complications that this generates are common to both types of clay and so a simplified view of the situation will be presented here and then applied to both clays. When the stability diagrams are examined two predominant hydrolysis species become apparent. In acidic conditions positive ions are formed and come in either monomeric (Al^{3+}) or polymeric ($\text{Al}_8(\text{OH})_{20}^{4+}$) forms. As the pH is raised the metal ion precipitates out in a hydroxide form which then coats the particles. As the concentration is raised the hydroxide species become the dominant form over a wider range of pH.

The two species will affect the clay's zeta potential in different ways. The charged ionic species will act as potential determining ions adsorbing onto the clay's surface. Whereas, the hydroxide precipitate will coat the surface of the clay, which will then dominate the zeta potential properties of the surface. The results presented below will be examined in terms of this two species model.

6.5.1 Kaolin

The effect of the two coagulants on the zeta potential of kaolin particles can be seen in figure 6.14. The data is taken from the jar tests presented in appendix D, which measures the post settlement zeta potential. The graph shows that the two coagulants

behave very differently. The Alum curve shows a progressively reducing slope of zeta potential with concentration such that the final zeta potential is reached asymptotically. Whereas, the Ferric chloride shows an almost linear change with concentration.

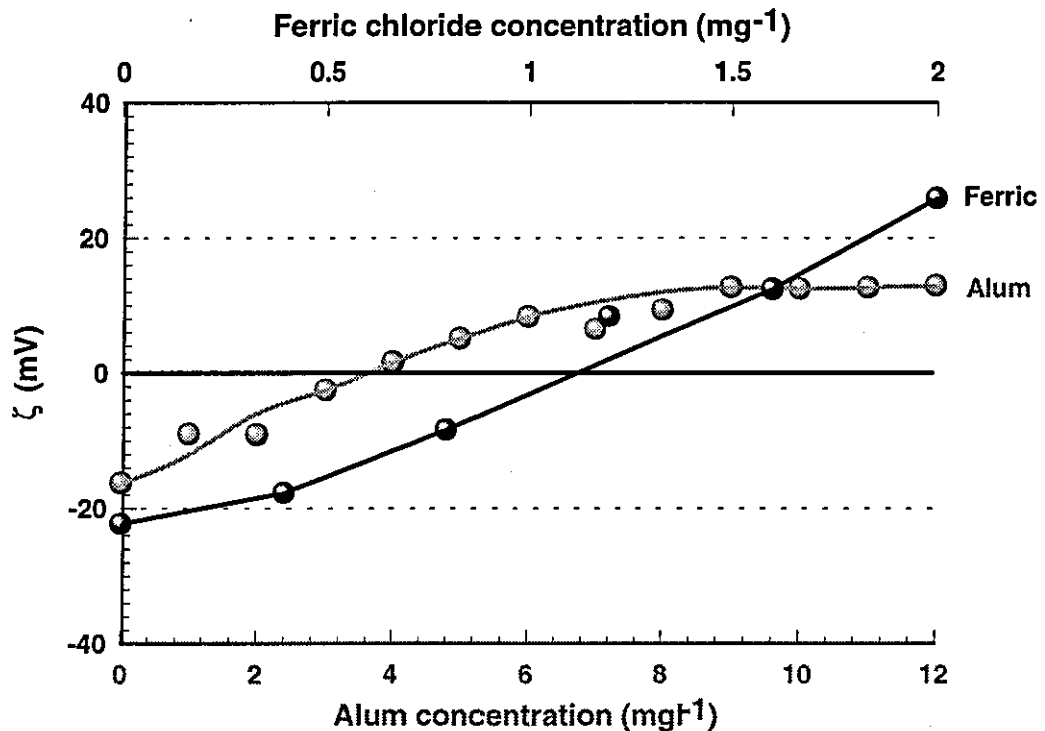


Figure 6.14 : Zeta Potential vs coagulant dose for dispersed kaolin Particles

The shape of the Alum curve is consistent with electrolytes that do not specifically adsorb onto the surface of the particles; Hunter (1981) refers to these as indifferent electrolytes. Clearly, Alum does not act as an indifferent electrolyte with the reversal of the charge giving a clear indication that specific adsorption is occurring. The situation under which the experiments were performed was an uncontrolled pH environment. Amirtharajah (1982) pointed out that addition of Alum would decrease the pH as a result of the progressive hydrolysis of the aquometal ion, shown in equation 6.2.

The initial pH was 5.5 and decreased to 4.5 over the concentrations tested; the stability diagram shows that metal ions are the predominate hydrolysis species. Rubin

(1979) confirmed this and showed that they consisted of two monomeric and one polymeric species. Initially, the monomeric ions are the predominate species and these are able to adsorb specifically, changing the sign of the zeta potential of the particles. As the pH drops the equilibrium will shift towards the polymeric species. The size of these ions together with the high levels of water that associates to them will prevent specific adsorption, such that they act as indifferent electrolytes. This has the effect of compressing the double layer which, Hunter (1983), showed makes the curve tend asymptotically.

The effect of Ferric chloride dosing is very different. The slope of the curve is almost linear with charge reversal resulting in the zeta potential changing from -22mV to +24mV. The broadness of the stability diagram for Ferric chloride will mean that the predominant hydrolysis species will be the metal hydroxide. James (1982) showed the zeta potential of hydroxides to be very pH dependant and this is seen in the curve which shows the effects of the dissociation reaction of the hydroxide in the acidic conditions. This makes the zeta potential of the hydroxide coating progressively more positive. Increasing the dose has two effects, the solution becomes more acidic and more hydroxide precipitates out of solution. The combination of these effects will make the zeta potential progressively more positive.

6.5.2 Kaolin, coagulant and pH effects

Figure 6.15 shows the effect of pH for specific concentrations of Alum. The general shape is consistent with the work of Packham (1965) and Mangravite (1975). The stability diagram for Alum shows that over the concentration ranges investigated here, the equilibrium will shift from hydroxide precipitate to negative metal ion complexes, as the pH becomes progressively more acidic.. The steep decrease in zeta potential for kaolin when Alum is included shows that precipitate coating is strongly influencing the surface properties. This confirms the predictions of greater dissociation constants for hydroxides compared to clays made by James (1982).

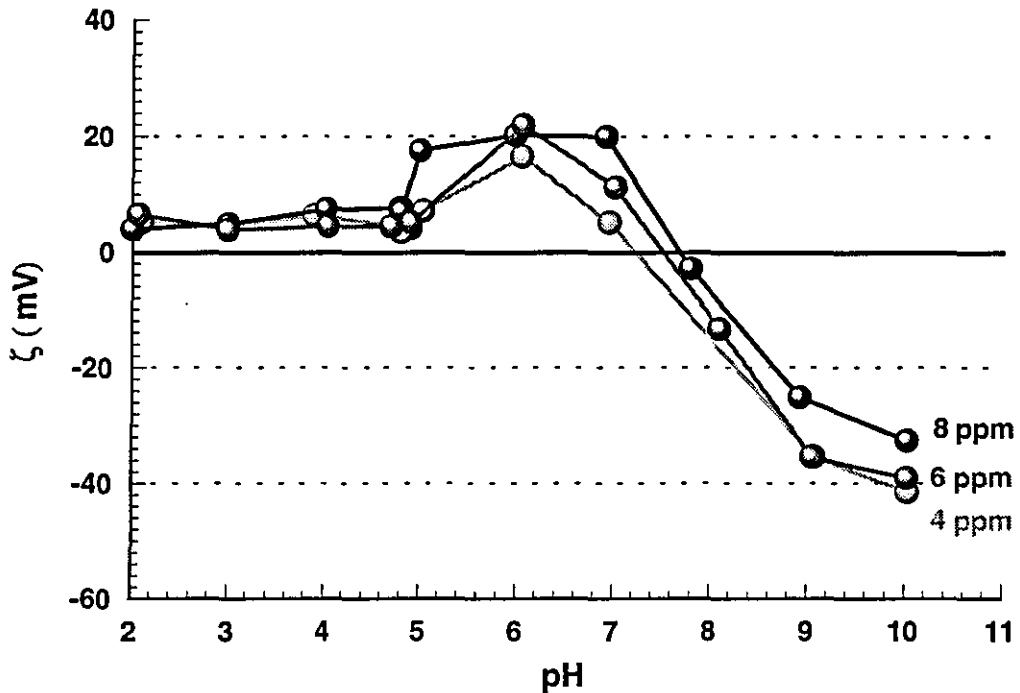


Figure 6.15: Zeta potential vs pH for dispersed kaolin particles in set solutions of Alum

The effect of acid addition is anomalous with the most interesting feature being the decrease in zeta potential as the pH drops from 6 to 4. The equilibrium of the hydrolysis products shifts towards polymeric species and these cannot adsorb onto the surface. As the total concentration of Alum is fixed this means that less ions are able to adsorb, reducing the value of the zeta potential. The curves then flatten at a stable zeta potential representing the counteracting effects of dissociation to the decreased adsorption that occurs. However, a difference between the plateau regions would be expected and is not seen.

Changes in pH with Ferric chloride can be seen in Figure 6.16. The results are similar in shape to those encountered with surfactants. The curves decrease steadily as the pH is raised, with the different doses tending to converge at higher pHs. Increasing the dose shifts the curves up increasing the pH at the isoelectric point. The shift in the curves with dose indicates some degree of specific adsorption is occurring along with the precipitate coating. The fact that the curves are almost linear suggests dissociation is the key reaction and so the surface properties are controlled by the precipitate.

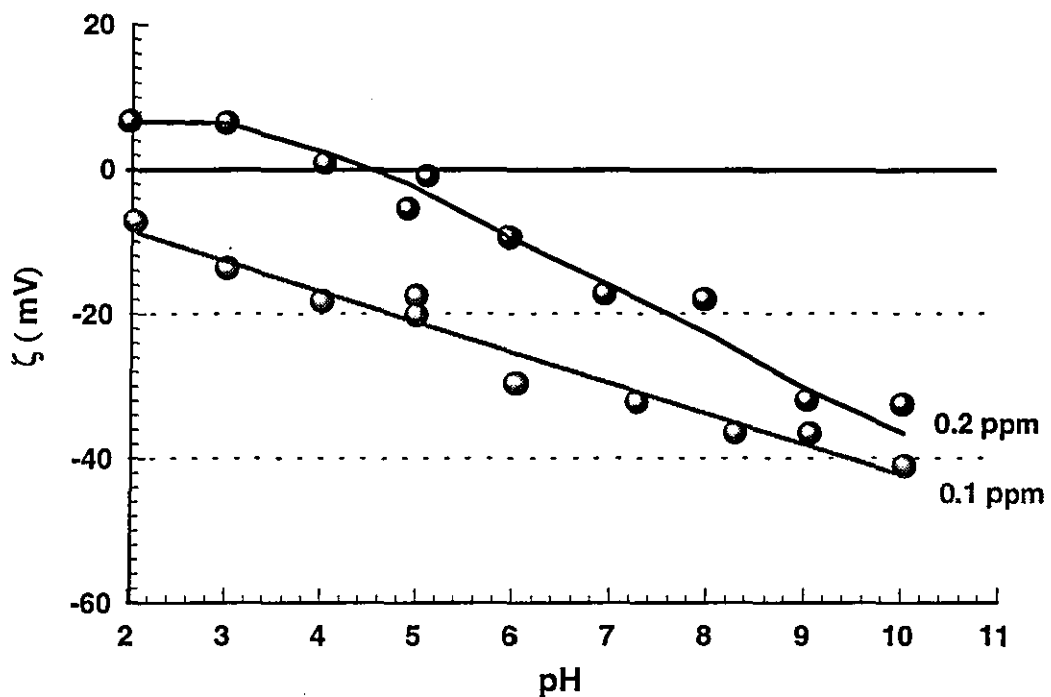


Figure 6.16 : Zeta potential vs pH for dispersed kaolin particles in set solutions of Ferric chloride

6.5.3 Wyoming bentonite

A similar investigation was performed with Wyoming bentonite and the results of altering the coagulant dose can be seen in Figure 6.17. These are similar to those for kaolin except for one important point. In the case of Alum, the curve does not cross the isoelectric point, suggesting that little or no specific adsorption is taking place. This can be explained in terms of the mono and polymeric ions as in the case for kaolin. The greater concentration range shifts the equilibrium of the hydrolysis products towards polymeric species, which do not specifically adsorb and so no charge reversal is possible.

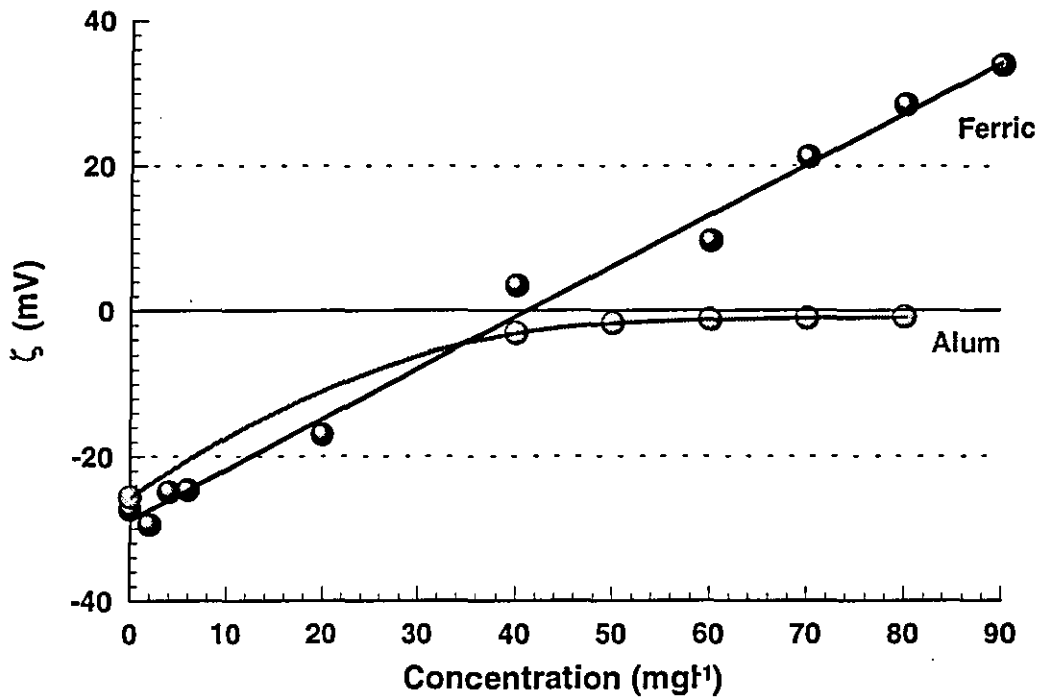


Figure 6.17 : Zeta Potential vs coagulant dose for dispersed Wyoming bentonite Particles

The Ferric chloride curve is similar in shape to the kaolin results; the major difference is in the range of dose required. The same is true of Alum and is due to the increased surface area generated with Wyoming bentonite particles. A similar result was seen for the surfactant investigation but on a smaller scale. The maximum difference is seen with the Ferric Chloride experiments where the concentration ranged from 2 ppm for kaolin to 90 ppm for Wyoming bentonite. The difference in surface area for the two particles is at first glance not sufficient to explain the differences. However, the Wyoming bentonite particles are expanded by the coagulant ions penetrating into the triple layers, forcing them apart, vastly increasing their surface area. Jefferson (1993) reports that specific surface area ranges from 40-120 m^2g^{-1} externally to 800 m^2g^{-1} total. This means that when expanded the specific area of the Wyoming bentonite particles can be up to 80 times that of kaolin. This would be sufficient a change to explain the differences in scale between the two.

6.5.4 Wyoming bentonite, coagulant and pH effects

The effects of pH in conjunction with coagulant can be seen in figures 6.18 and 6.19. The response of the Wyoming bentonite is different from that of kaolin, this is due to the unreactive nature of Wyoming bentonite particles to changes in pH. Any changes that occur here are solely due to changes in the hydrolysis products. The curves for Alum compare well with the work of Rubin (1979); both zeta potential curves showing peaks around pH 5, which then converge at a pH of 9 to a value of -34 mV. Only at the highest dose does the pH curve cross the isoelectric point.

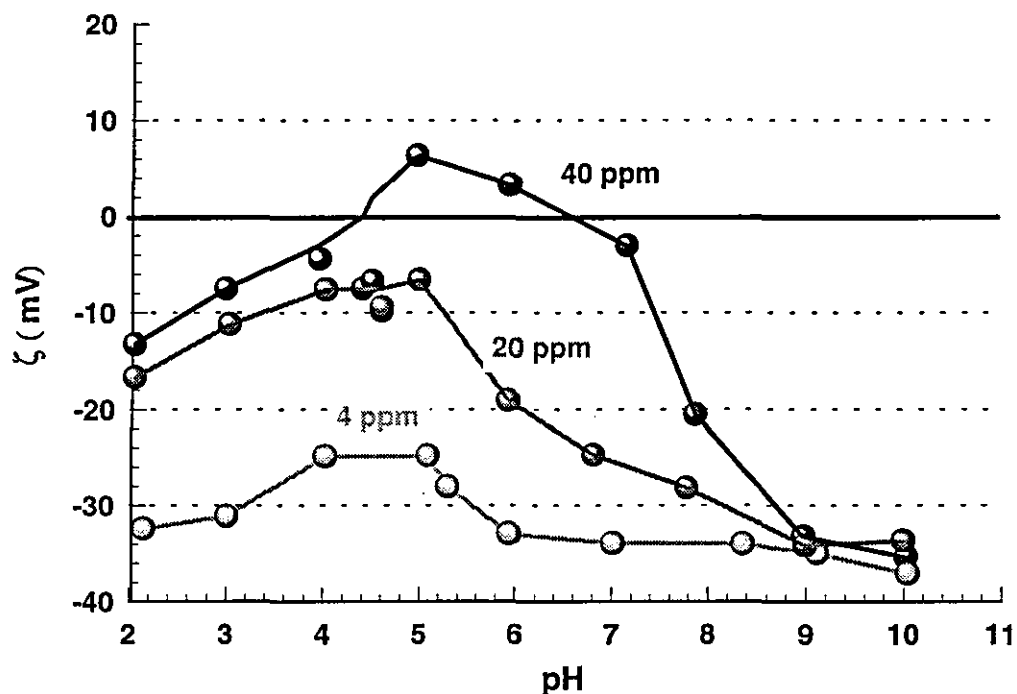


Figure 6.18 : Zeta potential vs pH for dispersed Wyoming bentonite particles in set solutions of Alum

As the dose is increased the proportion of hydroxide precipitate increases and this can be seen in the increased slope of the zeta potential curve with increasing dose. The convergence represents a point where coagulant dose does not affect the zeta potential

of the clay. This means that the clay's surface is saturated and is likely to represent the limit of the negative hydrolysis products adsorbing on the edges of the clay.

The results with Ferric chloride can be seen in figure 6.19. The curves converge at around pH 9 showing the same point of saturation as above. The concentration of the curves are all at the lower end of the stability diagram. This demonstrates the effects of small changes in concentration at the onset of the coagulation regimes. The curves changed from a relatively flat line at 2 ppm to a more linear decrease at 8 ppm.

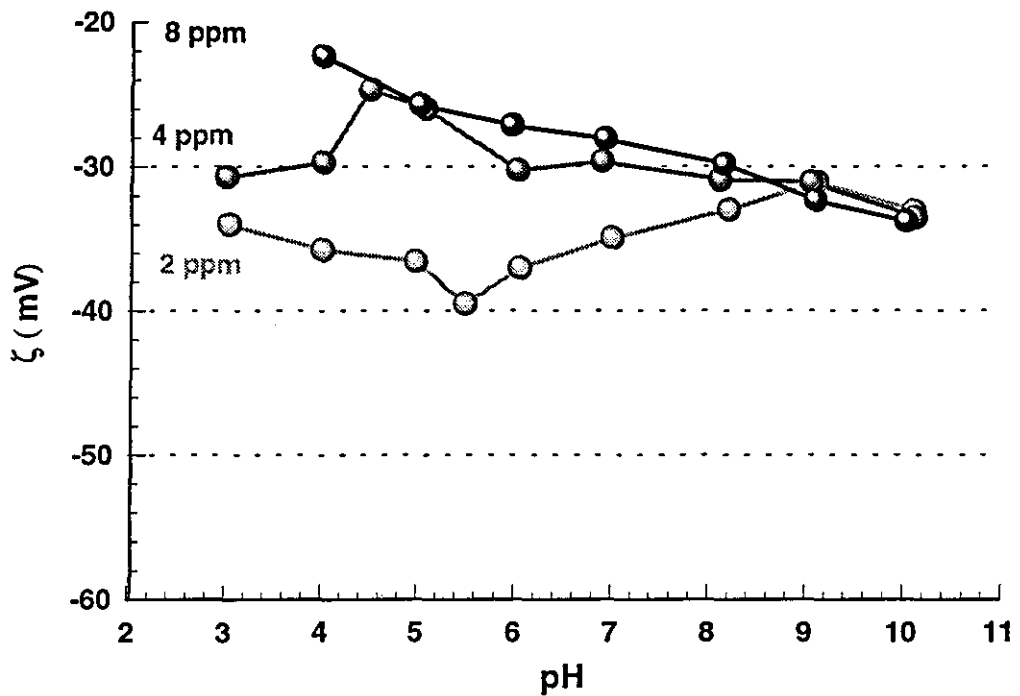


Figure 6.19 : Zeta potential vs pH for dispersed Wyoming bentonite particles in set solutions of Ferric Chloride

6.6 TEMPERATURE EFFECTS

The effect of temperature was investigated over the range 4 to 60°C and the results can be seen in figure 6.20. The two clays responded very differently with kaolin showing no significant change throughout the range, remaining constant at -29 mV. The degree of scatter did increase with temperature but always remained within the limits of accuracy set in section 6.2.2.

The magnitude of zeta potential of the Wyoming bentonite particles decreased in an approximately linear fashion with temperature. The values were found to range from -38 mV to -15 mV over the temperatures investigated. The data was extrapolated to find the temperature that would be required to reach the isoelectric point. This was found to occur at a temperature of 85 °C.

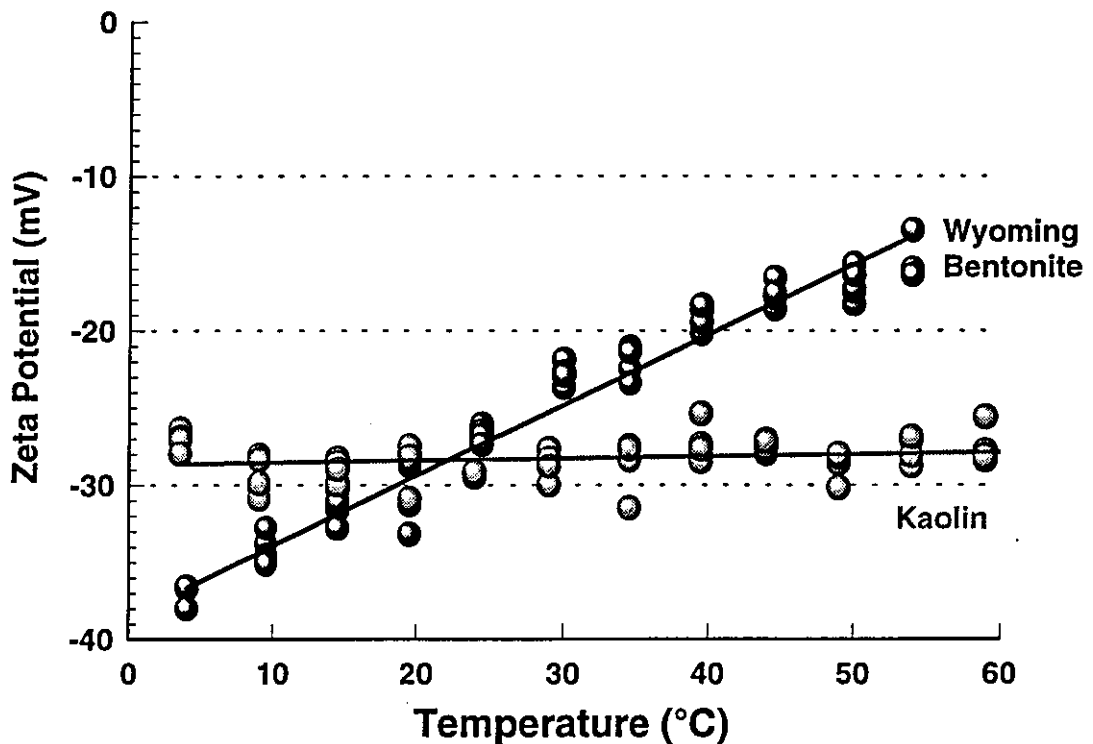


Figure 6.20 : Zeta potential vs temperature for dispersed kaolin and Wyoming bentonite particles.

Theoretical analysis of the effects of temperature confirm the kaolin result but offer no explanation for the Wyoming bentonite. Classical double theory as described in section 2.3.2.1 shows only viscosity and dielectric constant are affected by temperature. The effect of each of these variables opposes the other and so the net result is negligible. To explain the Wyoming bentonite data two different mechanisms of charge reduction are postulated.

6.6.1 Agglomeration

The first possible mechanism is based on the principle that temperature driven particle coagulation occurs. This coagulation would result from positive edges combining with negative faces, reducing the potential of the overall agglomerate. The linear reduction in the zeta potential with temperature means that the coagulation process would need to follow a similar trend. The type of coagulation encountered here is diffusion controlled and so a strong link to temperature would be expected. The floc produced would be of the card house structure as described by van Olphen (1963) and so is likely to be weak and easily dispersed.

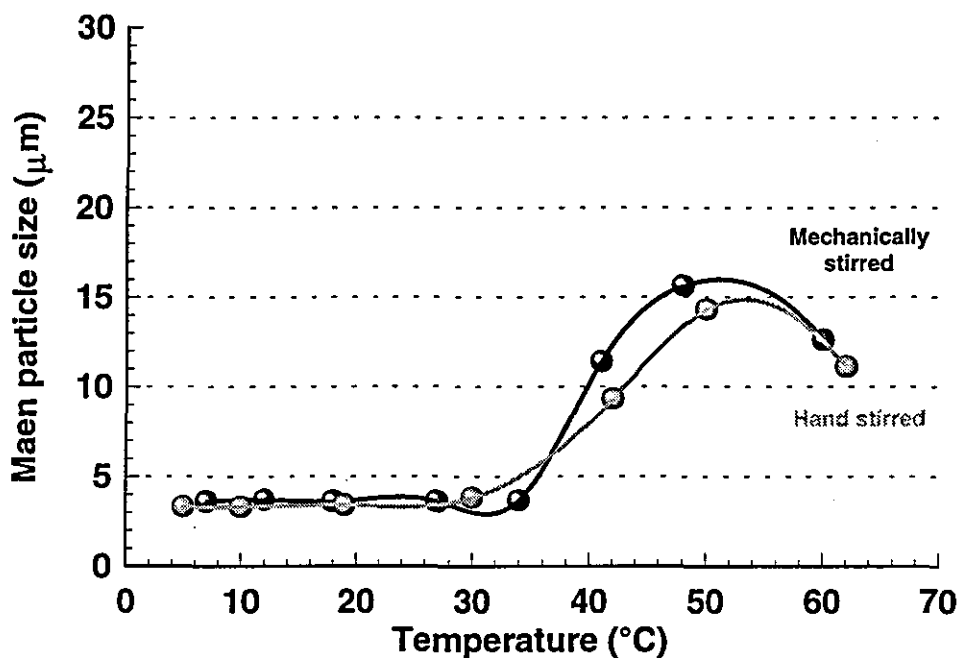


Figure 6.21 : Zeta potential vs temperature for dispersed Wyoming bentonite particles.

The mechanism was tested by measuring the size distribution with temperature and the results can be seen in figure 6.21. The size distribution of the suspension remains constant up to a temperature of about 35 °C. After 35 °C the mean size of the distribution significantly changed showing a maximum at about 50 °C. The sizing equipment had a stirrer attached that rotated at a speed of 150 rpm. It is possible that

the speed of the impeller was breaking up the agglomerate and affecting the results. This was tested by repeating the experiment without the stirrer. A similar result was obtained with the onset of coagulation starting marginally early at 30 °C.

The result suggests that this mechanism is not causing the reduction in zeta potential. The shape of the curves indicates that coagulation is occurring when the zeta potential has been sufficiently reduced. This would mean that agglomeration is the result of the zeta potential reduction rather than the cause of it.

6.6.2 Shear plane

The alternative mechanism is based on the position at which the zeta potential is measured. This position is called the plane of shear and has been described in section 2.3.2.1.. It represents a position equivalent to the point at which the diffuse region of the double layer begins. In this mechanism it is postulated that the position of the shear plane is shifting down the potential decay curve, see figure 6.22.

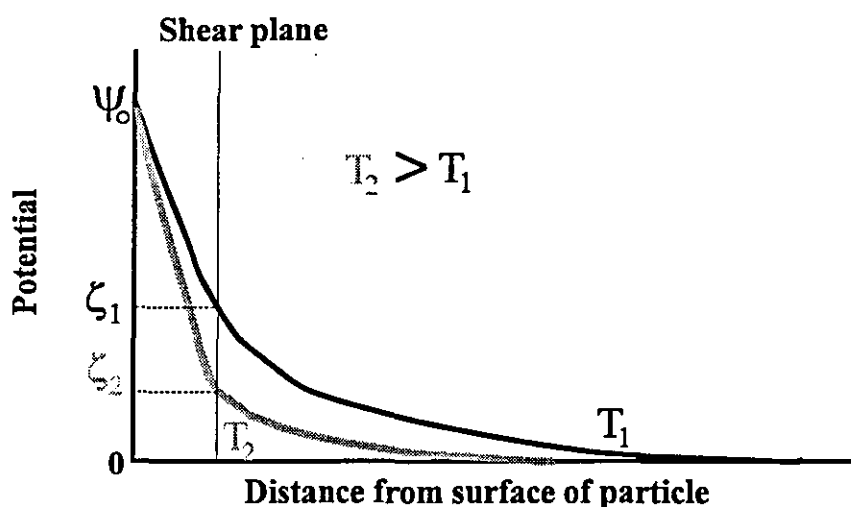


Figure 6.22 : Diagram of a potential decay curve

To test this mechanism the position of the plane of shear would need to be measured as a function of temperature. This is not possible so as an alternative the viscosity was measured and the results can be seen in figure 6.23. Although the viscosity is not a

measure of the plane of shear it is in nature similar and so should react in an equivalent way to temperature. The comparison shows good agreement at temperatures above 20 °C. This suggests that a similar effect is occurring and so supports the idea of this mechanism.

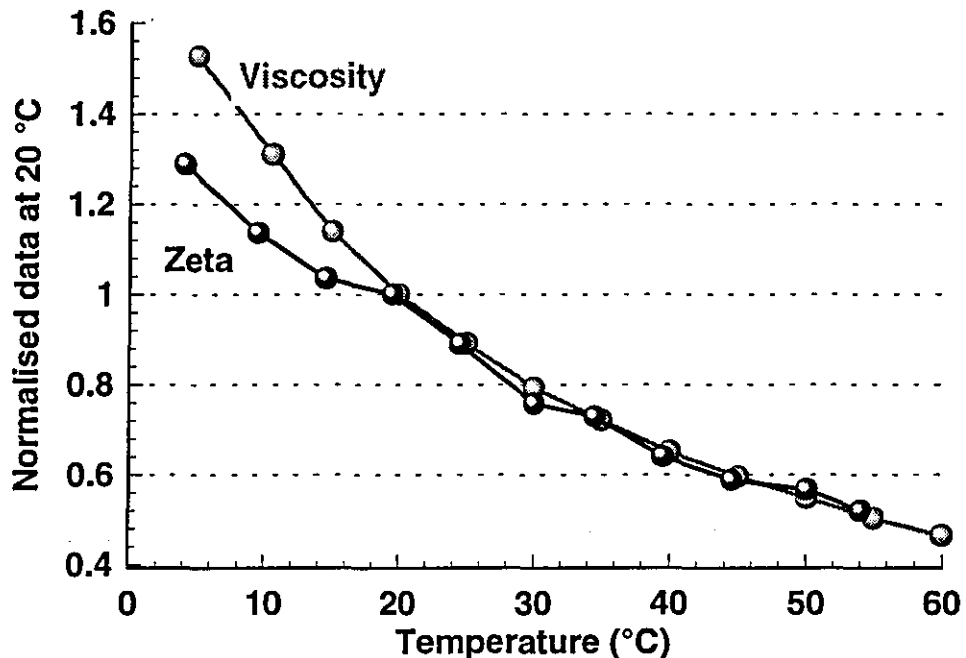


Figure 6.23 : Comparison of normalised viscosity and zeta potential against temperature for dispersed Wyoming bentonite particles in distilled water

Further support can be seen in figure 6.24 which shows the effect of increasing then decreasing the temperature. The curves show a hysteresis effect that is due to the particles having agglomerated. However, the overall trend is for the zeta potential to decrease again as the temperature is reduced. The effects of the temperature in this case is postulated to reduce the hydrated radius of the ions in the system. This would allow them to pack more closely into the Stern layer and so reduce the potential by a greater amount, see figure 6.22.

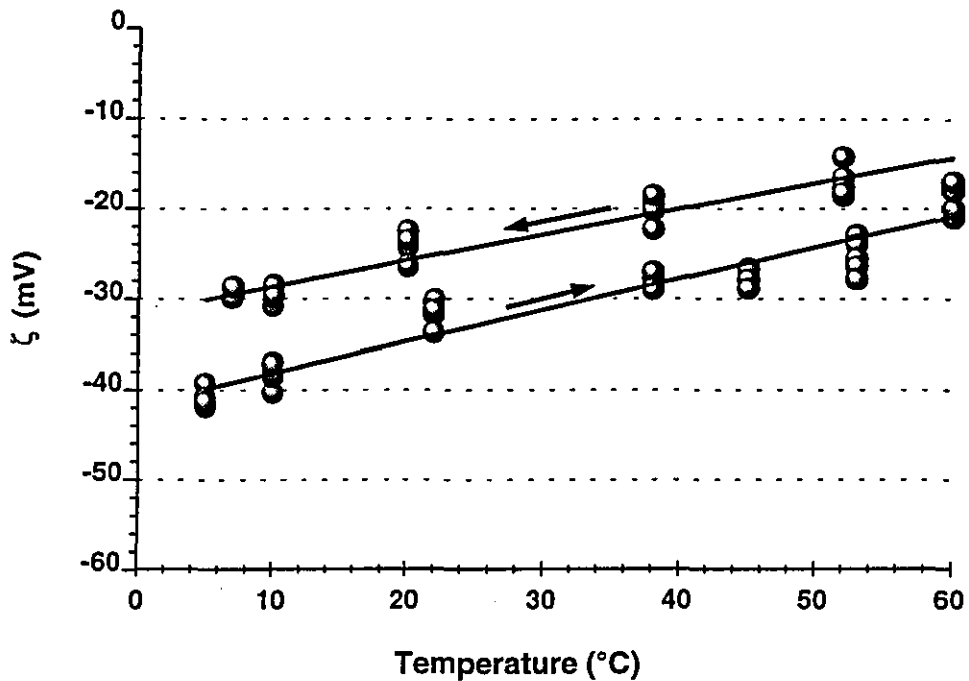


Figure 6.24 : Zeta potential vs temperature for Wyoming bentonite

The above discussion is valid for all particle systems and so does not explain the difference between the kaolin and the Wyoming bentonite. This is explained by the relative influence that the double layer has on the two particles. Wyoming bentonite is smaller with a higher CEC and so is relatively more electrically active than kaolin. Jefferson (1993) shows that kaolin has a more pronounced double layer and so can buffer any changes that occur, whereas small changes in the double layer of Wyoming bentonite can have a much greater influence on the properties of the clay.

6.7 BUBBLE ZETA POTENTIAL

Figure 6.25 shows the effect of surfactant dose on the zeta potential of gas bubbles. In these experiments the bubbles were formed by electrolysis and as such the gas in the bubbles was oxygen rather than air. The shapes of the curves are all similar showing a relatively stable region over low surfactant concentrations followed by a period of more rapid change. The effect of decreasing the chain length has a similar effect as before. This is seen in the rate of change of zeta potential with surfactant

concentration which is greatest for HTAB and least for DTAB. The three curves converge together but do not show a stable region.

The procedure of measuring bubble zeta potentials is difficult and prone to greater errors than in the case of particles. This can be seen in the scatter of the data which is most pronounced for TTAB. No curves have been drawn with the data for this reason although a clear indication of the shape can be seen. The data compares well with the study of Kubota (1993) which represents the most detailed investigation into bubble zeta potentials prior to the work presented here. However, the size of the bubble measured in the case of Kubota was 4 μm which is not representative of the process. This problem was overcome in the present investigation with the bubbles sizes being in the range of 20 to 40 μm .

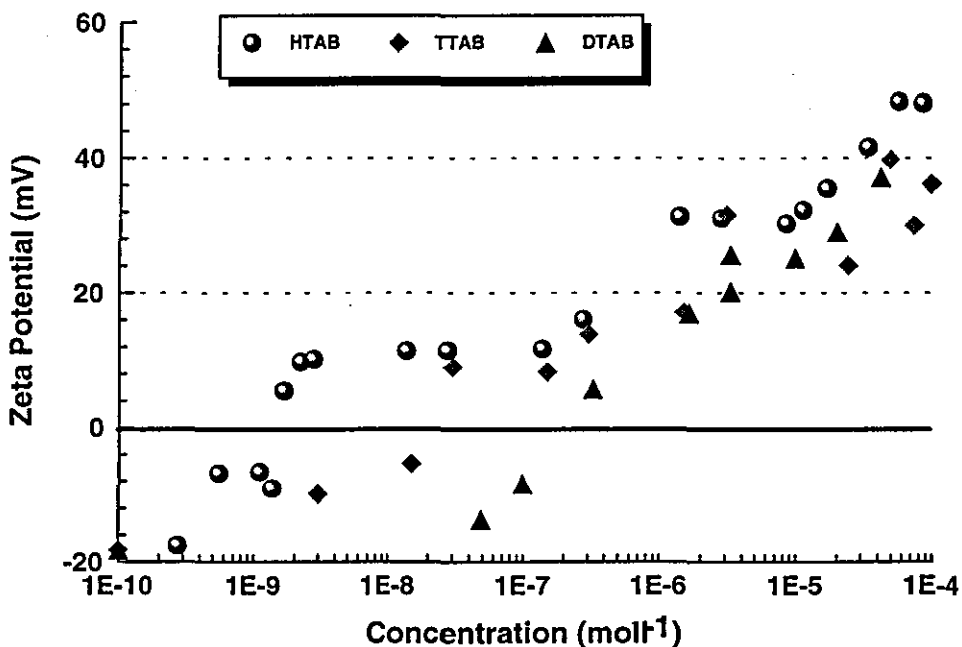


Figure 6.25 : Zeta Potential vs concentration of n-alkyldecyltrimethylammoniumbromide on air bubbles

The shapes of the curves show that the zeta potential constantly increases with surfactant concentration. This means that the surface never becomes saturated with

surfactant. The adsorption isotherm encountered here is of the s-type as encountered with the clays. Hemimicelle formation is likely to be very important in these cases and this can be seen by the value for the free energy of adsorption of a CH_2 group. This was calculated as in the case of the clays and was found to be $1.25kT$. Once again this agrees with the notion of cluster formation and indicates a perpendicular adsorption pattern.

The data above gives a relationship between surfactant concentration and zeta potential for a single bubble. This data needs to be scaled up to use in the flotation analysis. Only the low concentration regions of the graph are likely to be important. The differences between the surfactants greatest over the early regions with DTAB showing very little change

6.8 CONCLUSIONS

The analysis of the two clays' composition has generated a simple model where the structure is considered as a crystal. On the faces of the crystal ion substitution generates a large negative charge which is unaffected by changes in pH. On the edges of the crystal, the charge is generated by broken bonds and hydroxyls which undergo dissociation reactions and can be controlled by pH.

The zeta potential of kaolin particles is more sensitive to pH changes than is the zeta potential of Wyoming bentonite particles. Buffering the particles with tap water stabilises the charge on the clay's surface, causing the zeta potential to be constant over a wide range of pH values. Alkaline conditions produce more scattered results than acidic conditions, due to the increased radius of the hydroxyl groups that are adsorbing.

The zeta potential of the clay particles can be controlled by the addition of surfactant. The adsorption mechanism follows a simple model which describes the results qualitatively. The kaolin particles can be controlled by the combination of surfactant

dose and pH to offer a wide range of zeta potentials to be used in subsequent investigations. Surfactants represent an ideal conditioner to control the zeta potential of particles for the investigation of the effects of zeta potential on any process.

Coagulants are less effective at controlling the zeta potential of clay particles than surfactants. This is because the coagulants undergo a hydrolysis reaction in water which produces a range of hydrolysis products. The proportion of each type of hydrolysis product is dependent on the dose and pH of the system. A model based on the effects of the two main species of hydrolysis products that form describes the results adequately. The results indicate that coagulant use is an ineffective method for manipulating the zeta potential of particles. However, coagulants are used to flocculate the raw waters encountered in industrial applications and so offer an important test of the use of zeta potential.

The effect of temperature was seen to be significant for Wyoming bentonite particles but not for kaolin particles. The Wyoming bentonite particles showed a constant decrease in zeta potential as the temperature rose. This was attributed to a reduction in the hydrated radius of the ions of the systems, allowing them to pack more closely in the Stern layer. The difference between the two clays was attributed to the relative importance that the double layer has on each system. Wyoming bentonite particles are much smaller than kaolin particles and so are more affected by changes in the double layer. This would be true of any particle system and so this may play an important role in any process that is controlled by zeta potential.

CHAPTER SEVEN

CHAPTER SEVEN

RESULTS : FLOTATION TESTS

7.1 INTRODUCTION

This chapter discusses the results obtained from the investigation into the effects of zeta potential on the dissolved air flotation process, the methodologies of which have been discussed in chapter 4. To improve the clarity of the discussion the bulk of the results are contained within appendices B-F. Certain results will be presented within this chapter to highlight specific points in the discussion, see figures 7.1 to 7.24.

The discussion focuses on the role of zeta potential on the dissolved air flotation process, examining the link between zeta potential and removal efficiency. The investigation concentrates on the difference between discrete particle and floc flotation together with changes in the recycle ratio. The investigation concludes with an examination of flotability criteria and modelling for the system.

7.2 DISCRETE PARTICLE FLOTATION

In the experiments conducted on Kaolin particles conditioned with surfactant the particles did not coagulate and so remained discrete. This is seen in figure 7.1 which shows the mean particle size as a function of surfactant dose for all the surfactants used. The concentration is plotted as a normalised value relative to the maximum concentration tested, which allows all three surfactants to be more easily compared. The important aspect of the graphs is that they remain essentially flat showing no change in size. The DTAB data does show a marginal change and this corresponds to the doses that bring the zeta potential close to zero. In these cases some coagulation appears to have occurred but the majority of particles still remain discrete.

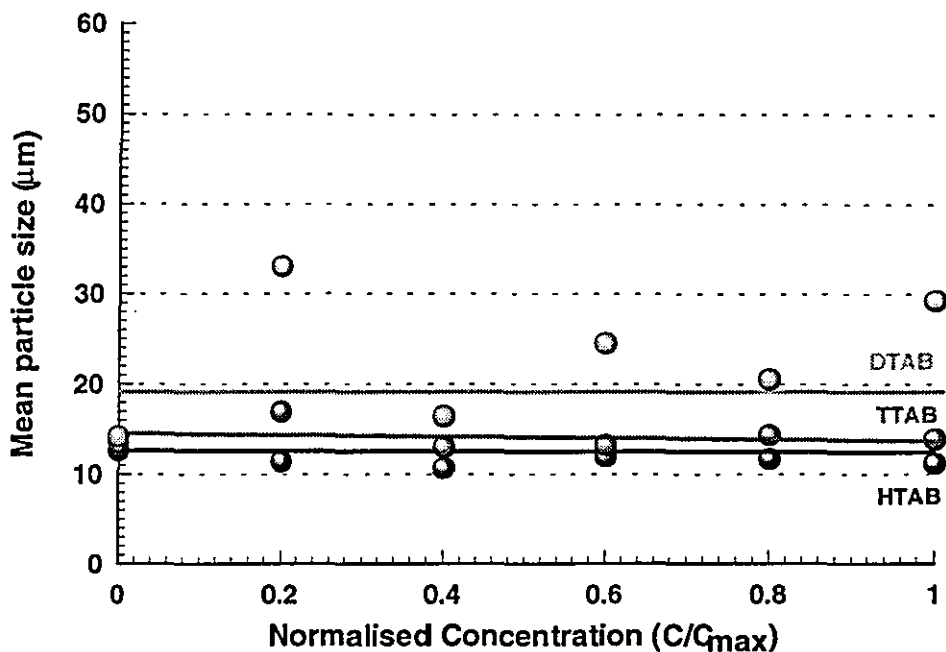


Figure 7.1 : Mean kaolin particle size against surfactant dose.

7.2.1 Flotation response

A typical flotation response can be seen in figure 7.2 which shows the change in post flotation zeta potential and removal efficiency with HTAB dose. The post flotation zeta potential graph showed two distinctive regions. An early period of rapid change followed by a plateau where increasing the concentration had no effect on the zeta potential value. The period of rapid rise corresponds to the region of hemi-micelle adsorption, as described in section 6.4. This will mean that the surface of the particles is becoming saturated with surfactant molecules, which will then determine the surface properties of the particles. The start of the plateau region indicates the point where the particle's surface is saturated with surfactant and as no more can be adsorbed the remainder of the surfactant is free in the system.

The removal efficiency rises sharply as the zeta potential reverses sign and then drops to a stable low value when the zeta potential reaches a constant high value. The peak of the efficiency curve corresponds to a point close to the isoelectric point but not exactly at it. This shows the need for charge neutralisation which is one of the two

requirements for successful flotation according to Edzwald (1995). The shape of the curves match one another demonstrating a strong link between the magnitude of zeta potential and efficiency.

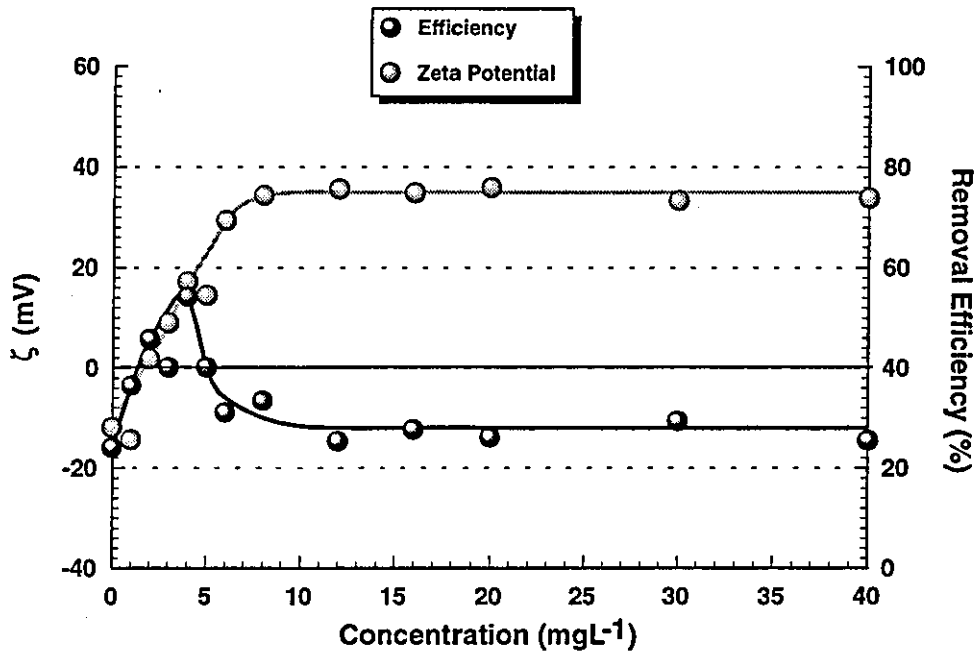


Figure 7.2 : Typical flotation response for discrete particle flotation conditioned with HTAB

A similar response is seen with all three surfactants and over all the different air injection ratios tested. The changes in the recycle ratio and surfactant type will alter the shape of the efficiency peak and this aspect will be discussed in detail later. The curves show a clear trend with high removal efficiencies corresponding to low zeta potentials and low efficiencies to high zeta potentials.

A fuller indication of the relationship between zeta potential and removal efficiency is shown in figure 7.3. The graph shown is for Kaolin particles conditioned with HTAB and shows the individual values for each recycle ratio. The efficiency results have been normalised to take into account the different degree of dilution that occurs with changing recycle ratio. The line represents the best fit relationship based on a 4th order polynomial fit and excludes the 5% data which does not follow the same trend. The reasons for this will be discussed below.

The peak of the efficiency curve occurs at a value close to the isoelectric point of the system. The region around this point would represent a situation where the repulsive energy barrier to attachment would be a minimum close to zero, which is due to the electrical double layer component of the total interaction energy being reduced. At this condition any contact between particles and bubbles would result in capture with the process having an attachment efficiency of 1. The flotation efficiency would then become dependent on other factors such as the collision efficiency.

In this way the process can be split into two regions, each of which is governed by a different removal mechanism. The difference between the two regions is controlled by the total interaction energy as a bubble approaches a particle and this is shown in equation 7.1

$$E_{\text{total}} = E_{\text{electrical}} - E_{\text{dispersion}} - E_{\text{structural}} \quad (7.1)$$

When the magnitude of the zeta potentials is large, a large repulsive force results and thus an energy barrier to film rupture. Over this region the attachment efficiency will control the process by limiting the amount of successful collisions. However, when the zeta potential is low no barrier will exist as explained above and the removal will be controlled by the amount of collisions that occur.

The region of high removal efficiency is independent of zeta potential once the energy barrier has been eliminated. This is seen in the data with the efficiency between -4mV and +16mV showing no change. The majority of the data lies within the 5% error bands for the best fit line although some data does extend outside these limits. The suggestion is that the zeta potential can act as a guide to good flotation, not to completely describe the mechanisms that operate and the data supports this notion.

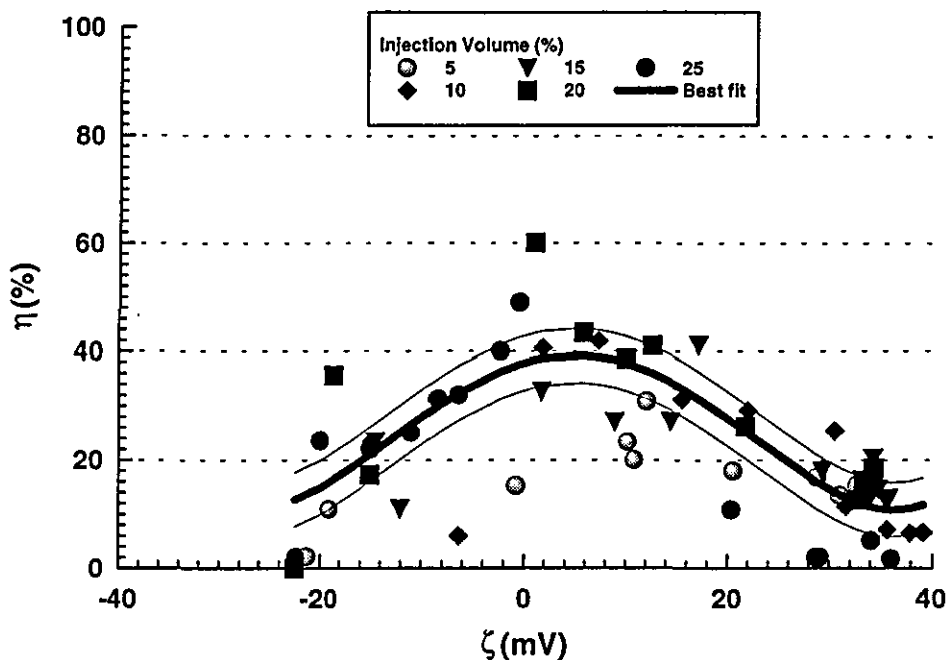


Figure 7.3 : Normalised removal efficiency against post flotation zeta potential for discrete Kaolin particles conditioned with Hexadecyltrimethylammoniumbromide, with changing recycle ratio.

7.2.2 Comparison of flotation and sedimentation.

Figure 7.4 shows the comparison between flotation and sedimentation of discrete particles. The results for the sedimentation are shown with triangles and those for flotation with spheres. The post process zeta potential is similar for both processes but the efficiency curves are very different. The sedimentation efficiency is very low which is to be expected as the particles are small and would settle at a very slow rate according to Stoke's law, which calculates a terminal settling velocity of $1.57 \times 10^{-5} \text{ ms}^{-1}$. The sedimentation tests showed no efficiency peak; this can be expected to occur at a similar concentration to that found in the flotation experiments.

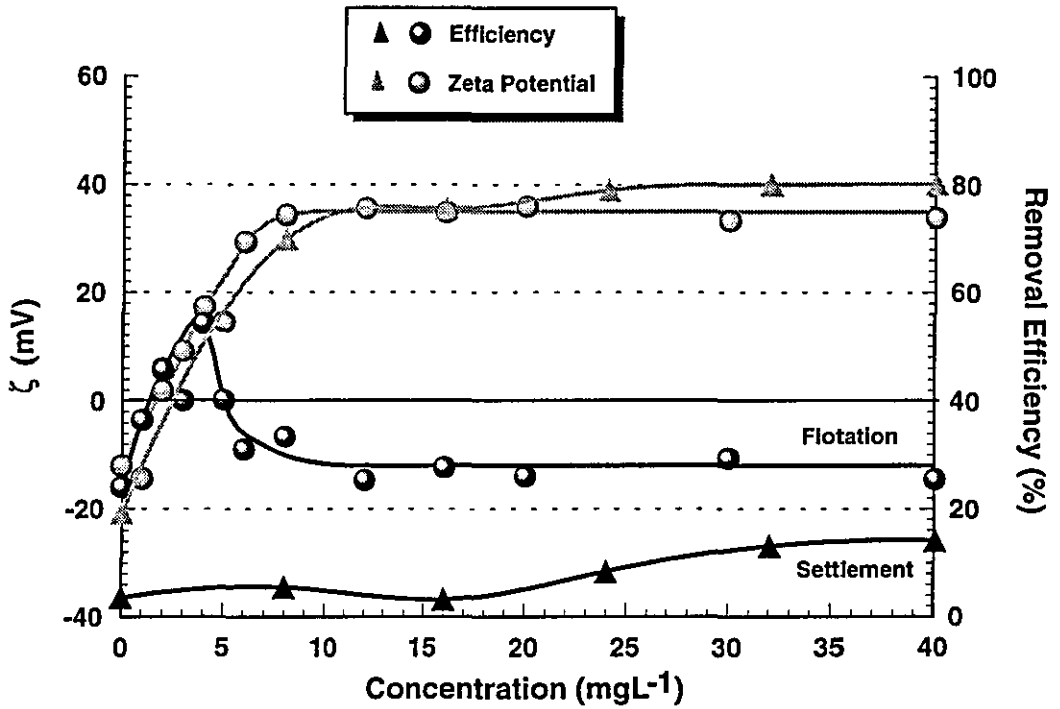


Figure 7.4: Comparison of Flotation and Sedimentation response for discrete particles conditioned with HTAB.

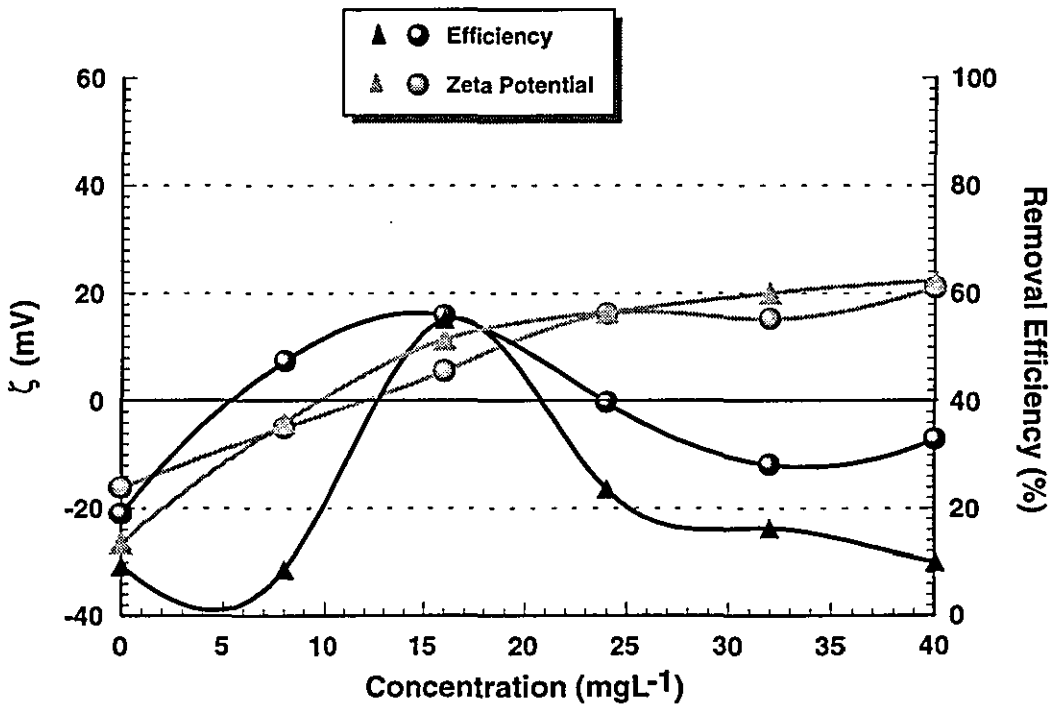


Figure 7.5: Comparison of Flotation and Sedimentation response for discrete particles conditioned with TTAB

Better results are shown in comparable experiments with TTAB, where some of the surfactant concentrations correspond to low zeta potentials at which point the efficiency rises. The efficiencies for both processes peak when the zeta potential is close to zero, reaching approximately the same maximum removal efficiency. However, the efficiency peak for the flotation process is much wider than the sedimentation equivalent resulting in high removal efficiency over a wider range of zeta potentials. The post process zeta potentials' curves were very similar for both processes and indicate that the bubbles do not strip any surfactant off the particles, which means that changes in recycle ratio will only affect the bubble side of the process.

7.2.3 Effect of recycle ratio

The recycle ratio is the main control variable in industrial operations and the effect it has on the efficiency curves can be seen in figure 7.6. Increasing the recycle ratio and hence the bubble number concentration improves the removal efficiency. The shape of the curves remains constant with the height of the peak progressively increasing as the ratio rises from 5% to 20%. The 10, 15 and 20% curves all converge at the higher positive zeta potentials and follow the same curve once the zeta potential has exceeded 12 mV.

The curves show a number of anomalous features which lead to some interesting observations. The most important of these is that the change in peak efficiency does not show a regular trend with recycle ratio. This is shown in figure 7.7 which relates peak removal efficiency to recycle ratio and shows the corresponding effect on the bubble number concentration. The difference between the peak efficiencies for the recycle ratios 10, 15 and 25 % is marginal showing only slight benefit in injecting more air. As pointed out by Jefferson (1995) 50% of the operating costs are derived from the air injection system. The implication of this is that the minimum air injection that achieves this stable efficiency should be used.

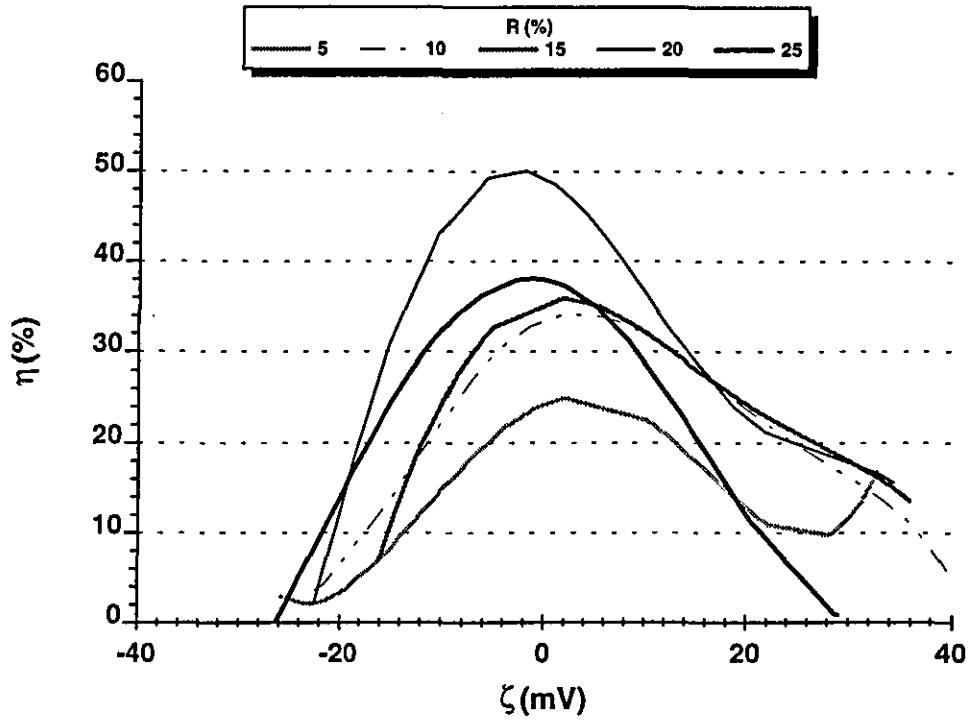


Figure 7.6 : Best fit efficiency curves for set recycle ratios.

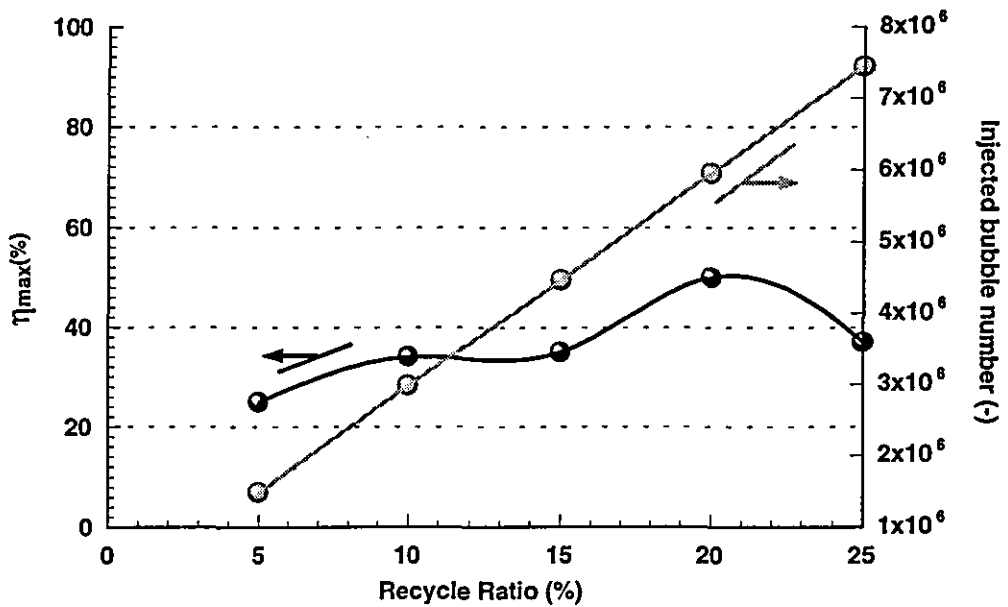


Figure 7.7 : Maximum removal efficiency and injected bubble number against recycle ratio.

The results in figure 7.6 show that in this case the optimum recycle ratio lies between 5 and 10%. The 5% curve shows a reduced peak efficiency although the same trend with zeta potential is shown. This confirms the point that once there are enough bubbles present to carry the particles, the efficiency is determined by other factors

7.2.4 Hydrophobic effects

The effect of changing the hydrophobicity of the particles can be seen in figure 7.8. The imposed hydrophobicity due to adsorbed surfactant will increase with chain length such that the hydrophobicity varies as HTAB>TTAB>DTAB. The peak efficiency obtained is the same with all three surfactants. However, the HTAB curve shows a slower decline in efficiency with zeta potential with the sharpest decline being seen with DTAB. The point where the peak efficiency occurs shifts from a low negative zeta potential for DTAB to a low positive zeta potential for HTAB.

The results agree with the suggestions of Israelachvili (1982, 1984) in his work on the hydrophobic interaction, see section 2.3.2.2. The force is generated by the hydrophobic surface of a particle inhibiting the formation of structured units in the surrounding liquid. This increases the free energy of the water near the particle's surface relative to that in the bulk and creates a driving force for water to migrate to the bulk, resulting in a force of attraction between hydrophobic surfaces.

The wider spread of the HTAB results when compared to those for the other surfactants are due to the increased hydrophobicity created. This will generate a larger hydrophobic interaction force which will be able to neutralise a greater repulsive force, see equation 7.1. Thus the zeta potential has a reduced effect as the hydrophobicity of the particles is increased.

The understanding of this force is still relatively incomplete so that it is not yet possible to calculate the force for the complex systems under investigation here. It

should also be noted that, as the range of the force is up to 20 nm, zeta potentials will still play an important role as their influence extends over a greater range.

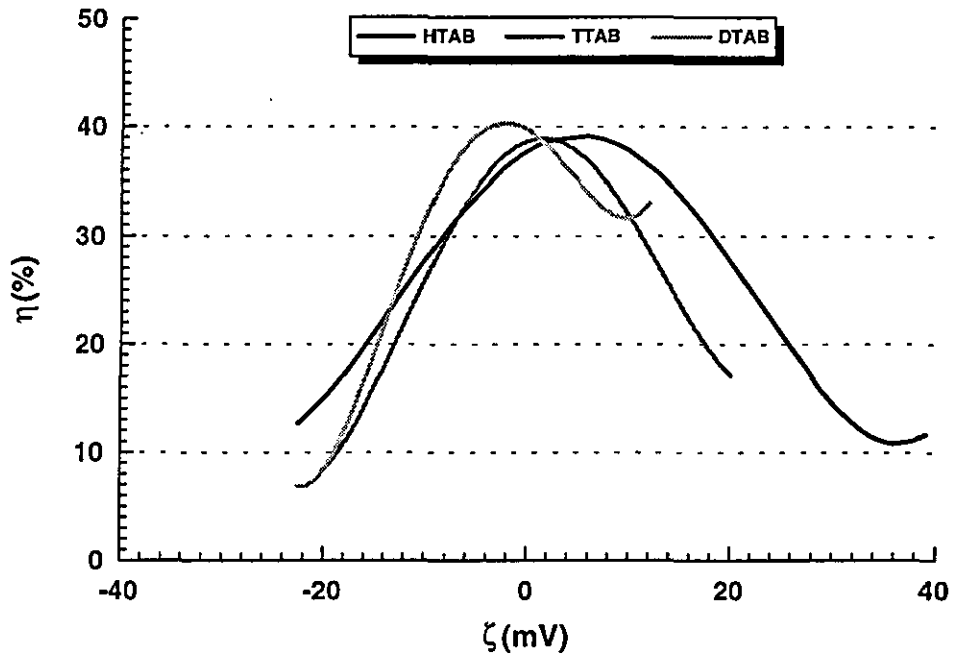


Figure 7.8 : Efficiency against zeta potential for dispersed Kaolin particles conditioned with alkyldecyltrimethylammoniumbromides.

7.3 FLOC FLOTATION

A similar investigation to the one reported in section 7.2 was performed with Wyoming Bentonite. Figure 7.9 shows the change in mean particle size with increasing surfactant dose during the sedimentation experiments. The curves show that the mean particle size remained unchanged with low doses of HTAB and TTAB. The shape of the three curves are very different but in each case the change in size occurred when the zeta potential had become positive. The zeta potential remained at a lower value throughout the experiment compared to Kaolin. This has been explained in terms of the relative surface areas of the two particles in section 6.4.3.

The overall observation is that the addition of surfactant to suspensions of Wyoming Bentonite produces flocculated particles. This enables the effects discussed in section 7.2 to be examined for flocs rather than discrete particles.

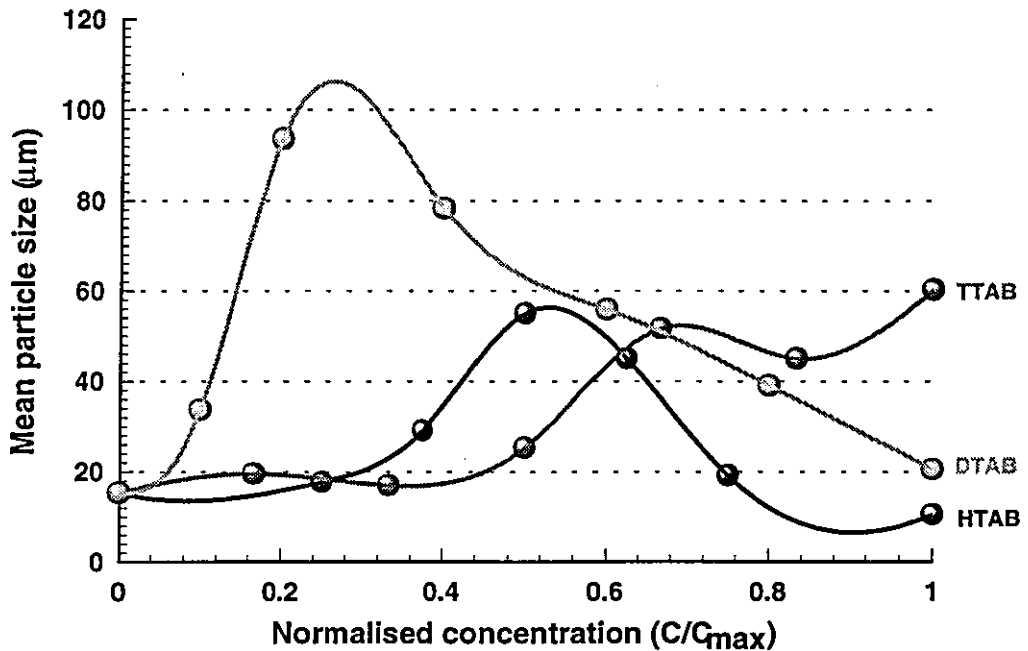


Figure 7.9 : Mean particle size against surfactant dose for Wyoming Bentonite particles

7.3.1 Flotation response

A typical flotation response can be seen in figure 7.10 which shows the removal efficiency and post flotation zeta potential of Wyoming Bentonite particles conditioned with HTAB and DTAB. The HTAB curves show that once again the removal efficiency is good when the zeta potential is low and poor when the zeta potential is high. The removal efficiency at high zeta potentials is the same as the effects due to dilution thus showing that no flotation is occurring. The DTAB data are plotted with the broken lines and shows a constant high efficiency once the zeta potential has decreased to a low value. The zeta potential curve remained close to the isoelectric point even with increasing dose and so agrees well with the other findings.

The investigation above agrees well with the studies of Roberts (1980), who showed a relationship between zeta potential and flotation efficiency, although the link is more vague than seen here and does not involve a direct analysis of efficiency and zeta potential. Another aspect that is seldom examined in dissolved air flotation is the idea of grade efficiency curves. In the industrial process a range of floc sizes are expected but are seldom measured due to the extensive difficulties involved. The Lasentec particle counter offers an opportunity to examine these effects as its operation does not destroy or damage the flocs.

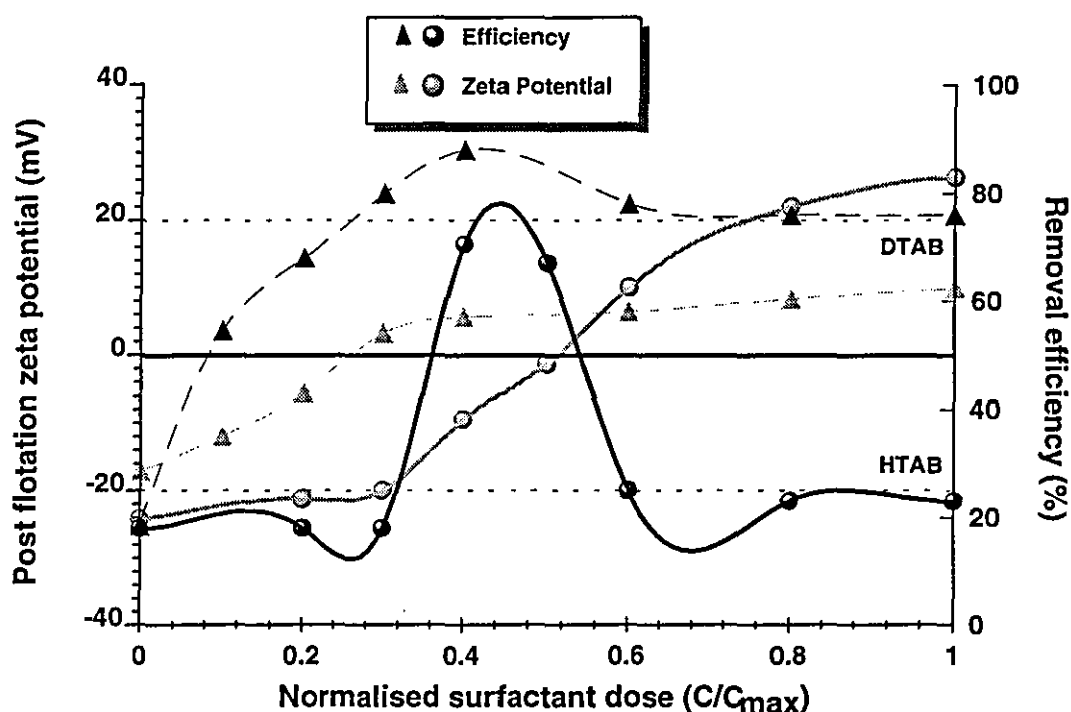


Figure 7.10 : Typical flotation response for Wyoming Bentonite conditioned with HTAB and DTAB.

The floc size distributions measured were very scattered as the particle counts were very low in certain size ranges. To reduce the sensitivity of the measurements only size ranges that had at least 50 particles in the initial sample were analysed. Figure 7.11 shows a characteristic set of curves for Wyoming Bentonite conditioned with HTAB. It appears that separation efficiency is not related strongly to floc size. This is seen in figure 7.11 and these plots are referred to as grade efficiency curves.

A major limitation of the concept of grade efficiency curves is because irregular shaped flocs are being measured, rather than discrete particles which have a homogeneous surface. The measurements do not take into account the shape or structure of the flocs which will be important. Flocculated particles will provide a very inhomogeneous surface to the bubble. This allows the flotation process to proceed on patches of the floc and this is independent of size and so negates grade efficiency concepts.

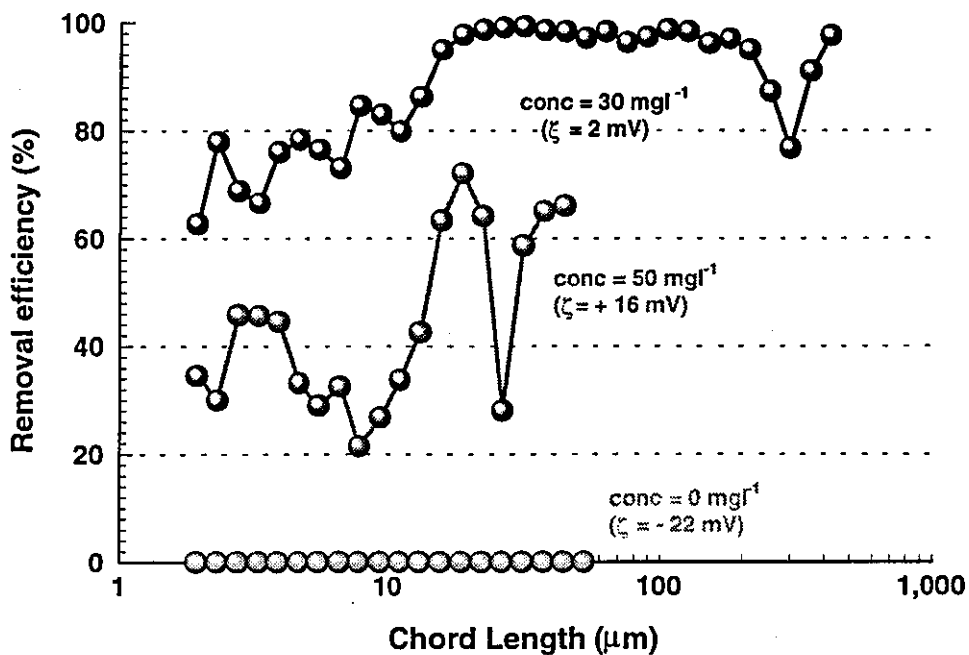


Figure 7.11 : Grade efficiency curves for the flotation of Wyoming Bentonite particles conditioned with HTAB.

Although grade efficiency curves do not show much of an effect of size they do allow a more detailed look into the process and so can yield interesting information. Figure 7.11 shows three such curves each covering a specific region of zeta potential. As expected the curve for a low zeta potential shows very good flotation over the whole size range. The middle curve shows the case for a high positive zeta potential generated by a high surfactant dose. This shows that increasing the zeta potential decreases the removal at all floc sizes. The results also show a much better response

than for the high negative which shows no removal at all. This is due to the increased hydrophobicity that the higher dose creates. As explained in the previous section, this generates a larger hydrophobic force which can counteract the repulsive force that the zeta potential generates.

7.3.2 Comparison of floc and particle flotation

Figure 7.12 shows a comparison of the relationship between zeta potential and removal efficiency for discrete particles and flocs. The two curves show the same response, demonstrating the need for charge neutralisation for effective flotation. The flocculated particles show a much higher peak efficiency compared to the discrete particles, with the value being almost twice as much. This can be explained in terms of the open floc structures that are formed. These will result in a much higher collision efficiency as the projected area of the floc will be very large. Kitchener (1981) also suggests that these should increase the attachment efficiency. He postulates that once bubbles collide with a floc they can roll over the underside of the floc's surface until they find an acceptable site to attach. This patchwork idea of flotation is likely as discussed above; however, the hydrodynamic forces of the process would seem sufficiently great as to prevent much bubble rolling and so this seems unlikely.

The shape of the curve for the flocs has a narrower base line than for the discrete particles. This means that at the higher values of zeta potential the flotation efficiency is better for discrete particles. However, at these higher values the particles are less flocculated, especially at the high negative values which correspond to either very low doses or none at all. This would mean that the Wyoming Bentonite particles remain discrete, especially at the negative end where the surfactant dose is low or non-existent. Wyoming Bentonite particles are smaller than Kaolin particles and so would have a much lower collision efficiency. At higher zeta potentials the collision efficiency will dominate and so results in lower overall removal efficiency.

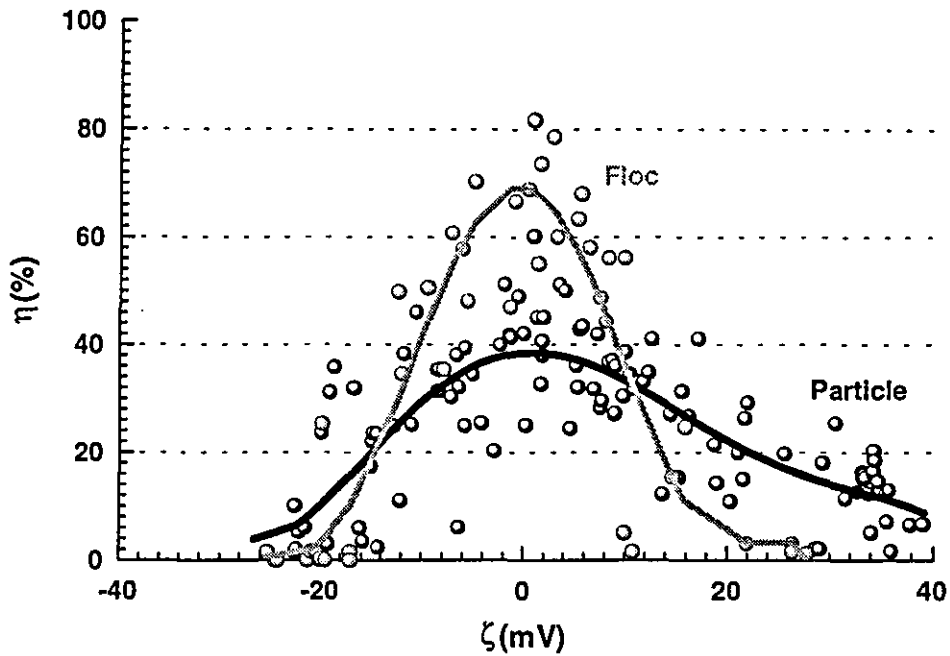


Figure 7.12 : comparison between particle and floc flotation

7.3.3 Effect of recycle ratio

Figure 7.13 shows the effect of recycle ratio on the flotation efficiency of flocculated particles. The two curves show the extremes of the recycle ratio previously tested. The 25% curve shows more effective flotation over negative zeta potentials but no difference over positive region. The peak efficiency is shown to be 10% better for the higher recycle ratio. The difference between the two curves over negative values of zeta potential is seen when the efficiency is measured at both -10 and +10mV. At +10mV no difference is seen but at -10mV an increase of 11% can be seen as the recycle ratio is increased from 5% to 25%.

A more detailed picture is provided by examining the grade efficiency curves. Once again the data is very scattered but a trend can be seen. Figure 7.14 shows the grade efficiency curve for a set dose of surfactant at both recycle ratios. Increasing the recycle ratio flattens out the grade efficiency curve such that the process becomes more robust to size. This is seen particularly at the smaller sizes as would be expected as these are the most difficult to float. This explains the differences between the two

recycle ratios above as the negative zeta potential region corresponds to smaller flocs sizes and a greater proportion of particles that remain discrete.

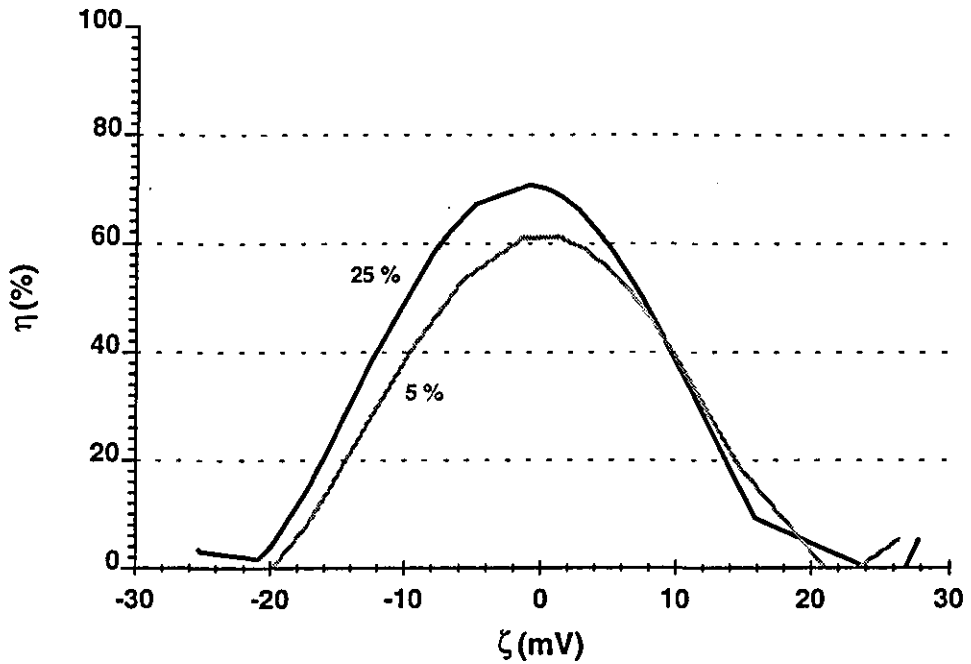


Figure 7.13 : Effect of recycle ratio on the efficiency against zeta potential curve for Wyoming Bentonite flocs.

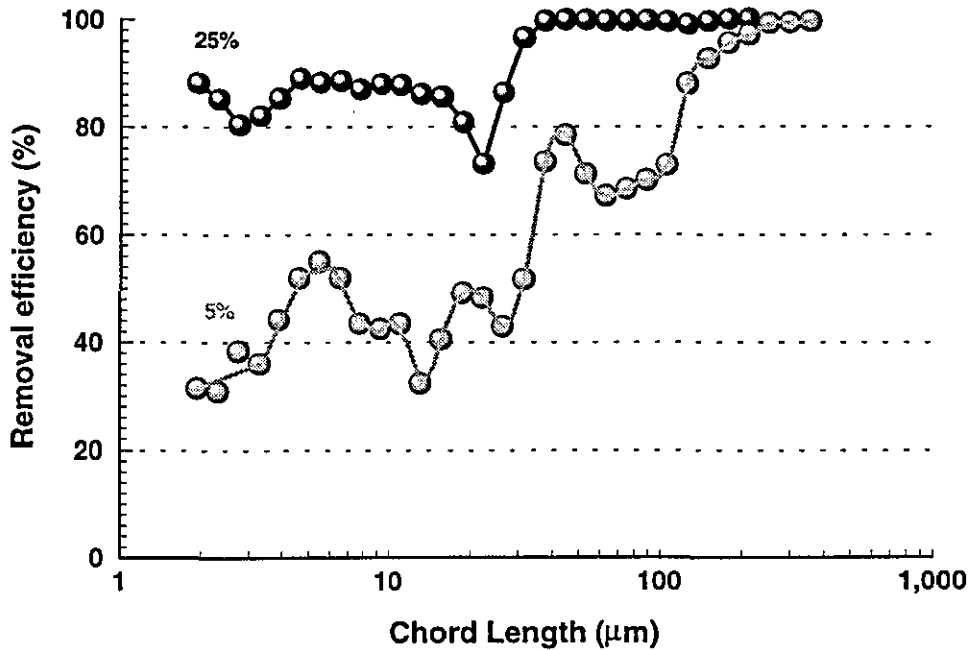


Figure 7.14 : Grade efficiency curves for Wyoming Bentonite conditioned with HTAB at different recycle ratios.

7.3.4 Effect of Hydrophobicity

The effect of changing the hydrophobicity of the flocs is shown in figure 7.15. The curves all show similar behaviour over negative zeta potentials but show a large difference over the positive values. This is to be expected as the greatest effect is seen when the doses are at their highest levels and hence the hydrophobicity. However, the trend is surprising with HTAB showing the least effect. This is the opposite of that seen with discrete particles where HTAB showed the widest response. The difference between the peak efficiencies is also greater with flocs. The change occurs over a zeta potential range of 10mV and results in an improvement in efficiency of 8% when the surfactant is changed from HTAB to DTAB.

The degree of hydrophobicity does not significantly alter the peak efficiency that can be achieved but affects the range over which the attachment efficiency will be high. The reason why the shortest chain length produces the widest response cannot be explained in terms of the indirect effect of the surfactant. Figure 7.16 shows the pre flotation size distributions for each surfactant when the zeta potential is slightly positive. This should offer the clearest indication of the effects of hydrophobicity on the size distributions produced. Examining the size distributions shows that the DTAB produces the most open floc structure. This would result in the improved response seen even though the hydrophobicity is decreased.

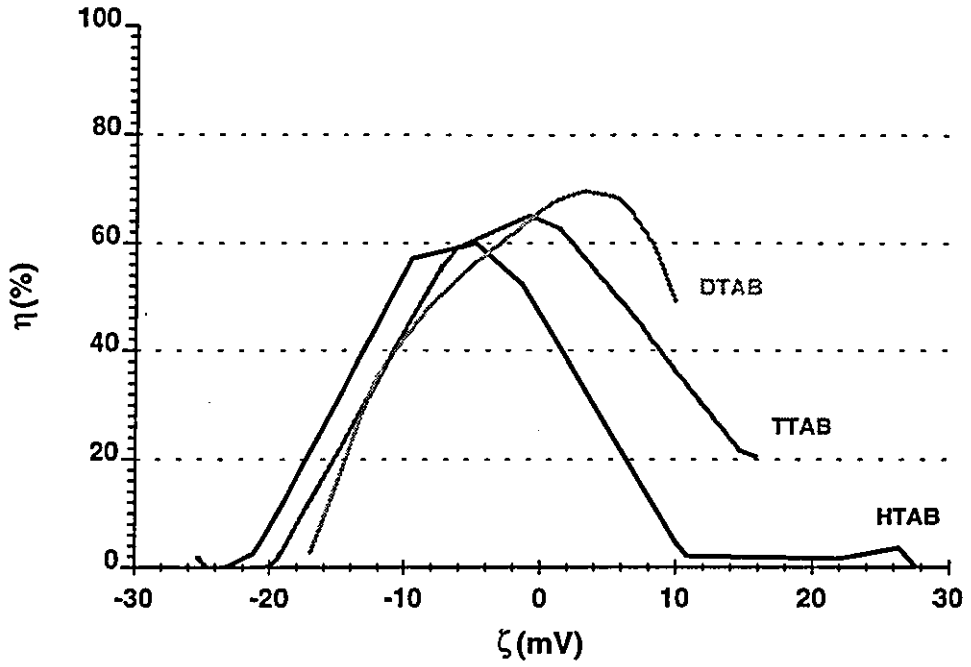


Figure 7.15 : Effect of surfactant type on the efficiency against zeta potential curves for Wyoming Bentonite floccs.

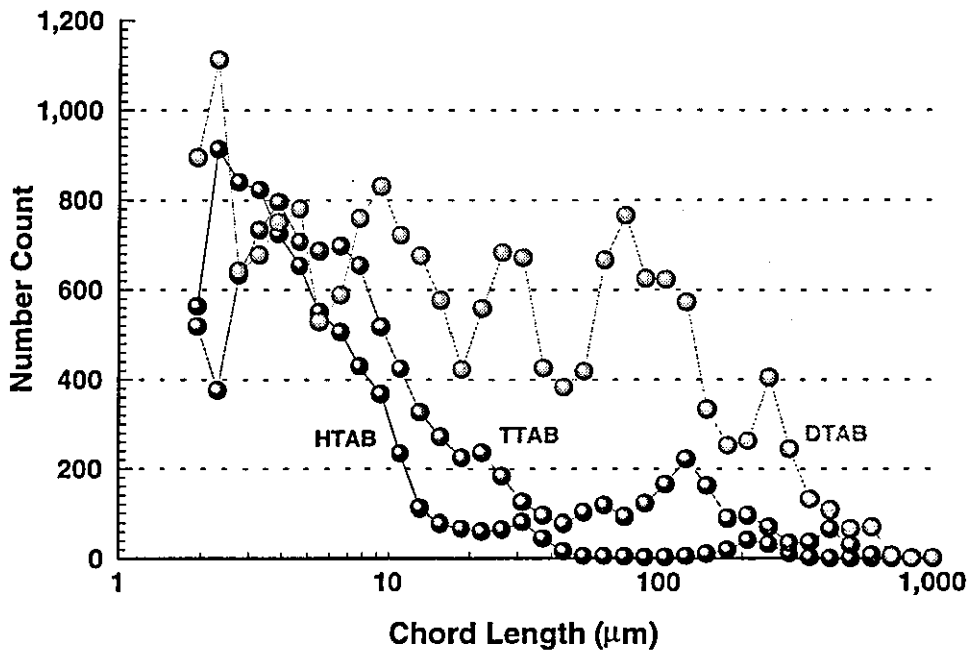


Figure 7.16 : Floc size distribution for Wyoming Bentonite conditioned with surfactant

7.4 COAGULANT FLOTATION

A detailed investigation into the effects of coagulants on the surface properties of clay particles has been discussed in chapter 6. The results demonstrated the complex way in which the coagulants worked due the numerous hydrolysis products that are formed. The experiments reported here were all conducted in the acidic pH range and so the coagulation would primarily result from ion adsorption onto the surface of the clay particles.

The effect of each type of coagulant on the floc size produced can be seen in figure 7.17. The black lines show the data for Wyoming Bentonite and the grey lines for kaolin. The Wyoming Bentonite curves show a much greater proportions of large flocs than do the kaolin curves. This is consistent with the work of Bennett (1973) who examined the flocculation of clay particles. He showed that Wyoming Bentonite particles form gel networks which are open and porous, compared to tighter structures for kaolin particles.

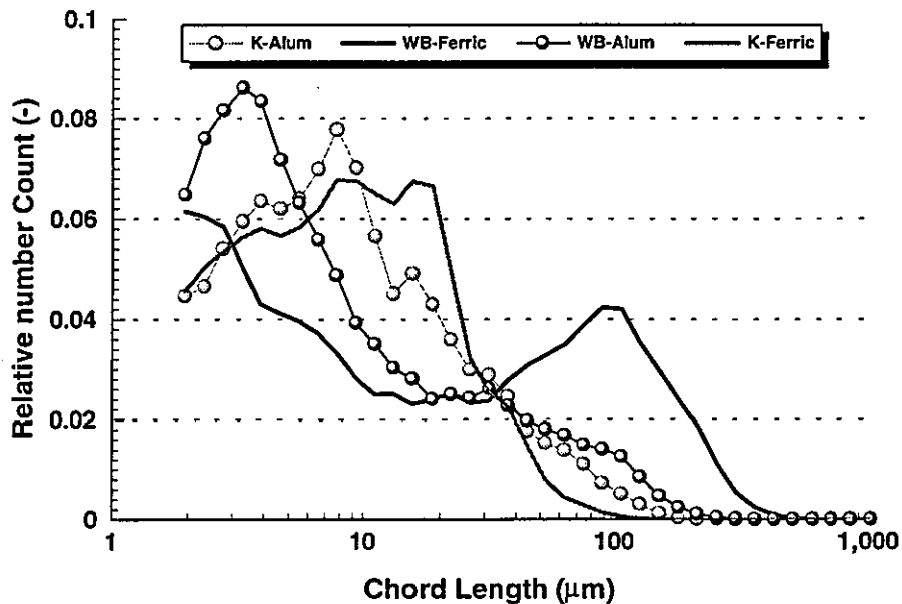


Figure 7.17 : Floc size distribution generated using coagulants with dispersed clay particles

All the curves converge at a size of 30 μm which according to Edzwalds (1995) is the optimum size for the flotation of raw waters. The larger Ferric Chloride flocs allow investigation into a greater size range than before. However, the size of these flocs is more suited to a sedimentation process and so some settlement to the bottom of the flotation column is likely.

7.4.1 Flotation response

The flotation response of the clays conditioned with coagulant showed no effective difference between the type of coagulant. The result for Wyoming Bentonite particles showed high removal efficiency with both Alum and Ferric Chloride. The major difference was seen between the type of clay used and this can be seen in figure 7.18 which shows the removal efficiency against zeta potential curves for both clays conditioned with both coagulants. The Wyoming Bentonite curve shows high removal efficiency once the post flotation zeta potential has extended past the isoelectric point and remains high for all positive zeta potentials. The kaolin curve shows low removal efficiency over the entire test range with the curve peaking at an efficiency of 40% when the zeta potential is +14mV. Once the zeta potential reached +22mV the curve shows a vertical decline which extends down to zero efficiency.

The curves show some interesting anomalies which require further discussion. The Wyoming Bentonite curve contradicts the results seen with surfactants in that high removal efficiencies are obtained even with high zeta potentials. The reason for this is that a significant portion of the flocs settled to the bottom of the column as previously predicted. Visual observation showed that approximately 20% of the total floc volume settled to the bottom of the column. This means that the efficiency shown in figure 7.18 is not solely due to flotation. Further analysis reveals that the high zeta potential data points all referred to Ferric chloride and the larger floc sizes.

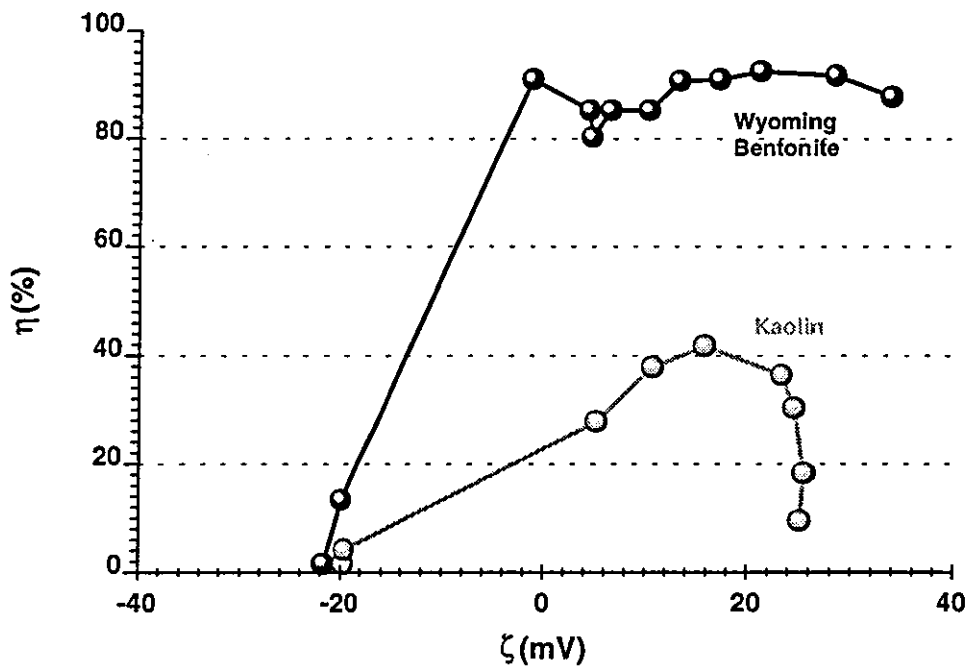


Figure 7.18 : Removal efficiency against zeta potential for Wyoming Bentonite and Kaolin particles conditioned with Alum and Ferric chloride

The poor response measured for Kaolin flocs was due to floc breakage. Visual observation showed that the flocs broke up when the sample was transferred into the flotation column and during sampling. This was most apparent with the kaolin Alum experiments and these relate to the worst flotation efficiencies. The relative weakness of kaolin flocs has been discussed by Jefferson (1994) in which he compared the electrical and mechanical forces that operate on each type of clay. He showed that the smaller Wyoming Bentonite particles are strengthened by the electrical forces that interact between them, whereas, the larger kaolin particles are more affected by mechanical forces which makes them more prone to breakage.

A more detailed investigation into floc flotation is seen by examining the grade efficiency curves in appendix C. The majority of the graphs are essentially horizontal lines offering no change in efficiency with size. This is a similar result to the one found for surfactants and is due to the inhomogeneity of the floc's surface, which allows patch flotation mechanisms to operate as described in section 7.3.1.

7.4.2 Comparison between flotation and sedimentation

The sedimentation experiments all showed good removal efficiency as would be expected with flocculated particles. Figure 7.19 shows the comparison between the removal efficiency against zeta potential curves for Kaolin particles under both processes. Only one of the Wyoming Bentonite curves is shown as the response was similar under both processes with a high removal efficiency of about 95%.

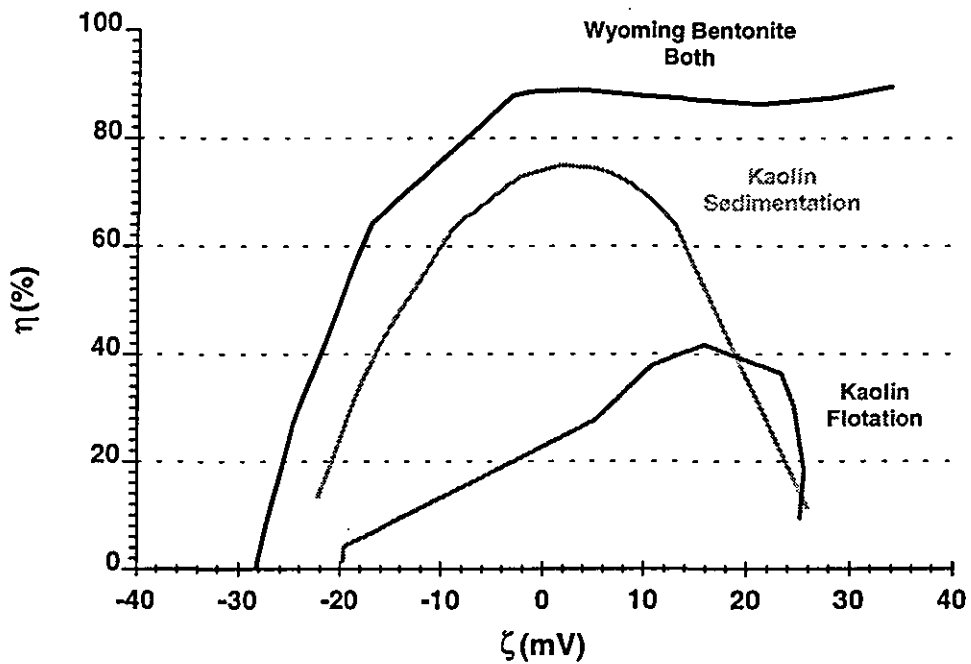


Figure 7.19 : Removal efficiency against zeta potential for sedimentation and flotation of clay particles conditioned with coagulants.

The curves for the Kaolin particles show better removal efficiencies for sedimentation than for flotation. The peak of the efficiency curve corresponds to the isoelectric point agreeing with the results from the previous sections. The peak removal efficiency is shown to be 10% lower than for Wyoming Bentonite flocs and is because of the relative size of the Kaolin flocs being smaller and thus settling more slowly.

The discussion above raises an interesting question concerning the need for hydrophobicity in flotation. The simplest form of hydrophobicity is generated by reducing the charge on the surface of the particle, which means that water can bond with the particle only by van der Waals forces. This produces an unfavourable free energy situation; so the water tends to self associate and thus the surface is hydrophobic. A problem exists in the present case as explained by Edzwald (1995) as the adsorbing coagulant ions will have associated water connected to them thus making them hydrophilic. The answer to this problem is again related to the idea of the inhomogeneity of the floc's surface. The clay particles are naturally hydrophobic and this can be seen in their reluctance to disperse. Areas of the floc will be made up of clay without adsorbed coagulant and these will offer the necessary contact points for the bubble to adhere to the floc. Evidence for this can be seen in the flotation response curves which show a slight decrease in removal efficiency with increasing dose. This will relate to the floc becoming coated progressively with more coagulant and thus becoming less hydrophobic.

7.5 THEORETICAL ANALYSIS OF THE CAPTURE PROCESS

The capture of small particles by small bubbles may be modelled theoretically by calculating the single collision collector efficiency for a bubble. The model described calculates the trajectories of small particles in a hydrodynamic field as they approach a bubble. The trajectory equations and the forces acting on the particles are first described. The effect of particle inertia, as quantified by the Stokes number, the particle size relative to that of the bubble (interception parameter), the gravity force and the air to liquid ratio in the system are included in the description of target efficiency. Close range forces including hydrodynamic, electric double layer and Van der Waal adhesion forces are taken into account in determining the probability of particle retention. These forces are included in the trajectory equations and the behaviour of particles as they approach the bubble is shown.

7.5.1 Target Efficiency

The trajectory equation for particle motion in the Stokes regime is as follows and is shown schematically by figure 7.21.

$$\frac{\pi d^3}{6} \rho_p \frac{du_{py}}{dt} = 3\pi\mu d(u_{py} - u_y) \quad (7.2)$$

$$\frac{\pi d^3}{6} \rho_p \frac{du_{px}}{dt} = 3\pi\mu d(u_{px} - u_x) + \frac{\pi d^3}{6} (\rho_p - \rho)g$$

where

U_{py} = particle velocity component in y direction (ms^{-1})

U_y = fluid velocity component in y direction (ms^{-1})

U_{px} = particle velocity component in x direction (ms^{-1})

U_x = fluid velocity component in x direction (ms^{-1})

d = Particle size (m)

ρ_p = Particle density (kgm^{-3})

ρ = Fluid density (kgm^{-3})

The density term on the L.H.S. of 7.2 is in dispute. Derjaguin (1959) used $(\rho_p - \rho)$, the density of the particle less that of the fluid; however, Flint and Howarth (1970) claimed that this was wrong and that the density of the particle only should be used. Since the densities of the particle and the fluid are close this term is highly significant and the argument is worthy of further consideration. In appendix I it is shown that in the present case, which is a low inertia system, the term used by Derjaguin is correct.

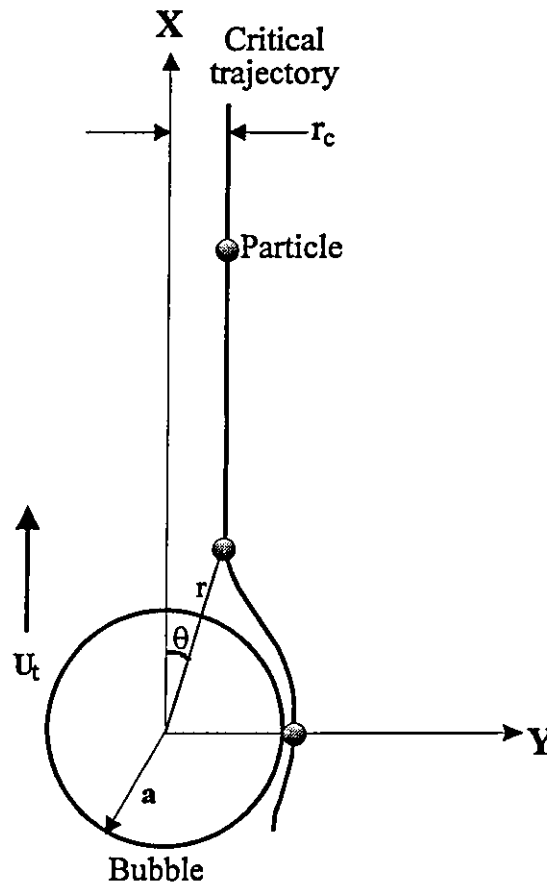


Figure 7.21 : co-ordinate system to analysis particle trajectory

The trajectory equations above can be expressed in dimensionless form as follows:

$$2Stk \frac{d^2 y'}{d\tau^2} + \frac{dy'}{d\tau} - u'_y = 0 \quad (7.3)$$

$$2Stk \frac{d^2 x'}{d\tau^2} + \frac{dx'}{d\tau} - u'_x - G = 0$$

where,

$$Stk = \frac{\rho_{st} u_o d_p^2}{9\mu d_b}$$

$$\rho_{st} = \rho_p - \rho$$

$$x' = \frac{2x}{d_b}$$

$$y' = \frac{2y}{d_b}$$

$$u'_x = \frac{u_x}{u_o}$$

$$u'_y = \frac{u_y}{u_o}$$

$$\tau = \frac{2tu_o}{d_b}$$

$$G = \frac{(\rho_p - \rho)d_p^2 g}{18\mu u_o}$$

In this case the Stokes number has been used to describe the level of particle inertia. This is a convention adopted in aerosol science. The fluid density in that case is negligible and the Stokes number reduces to the particle stop distance divided by the target radius.

Equation 7.2 can be expanded to include the short range forces which apply close to the bubble and these will be described later. For the present purposes equation 7.2 is expressed in finite difference form so the trajectories can be computed. The predicted point on the trajectory is computed using equation 7.4 and the two preceding points:

$$y'_2 = \frac{1}{(4Stk + \tau)} \{2u'_y \tau^2 + y'_o (\tau - 4Stk) + 8y'_1 Stk\} \quad (7.4)$$

$$x'_2 = \frac{1}{(4Stk + \tau)} \{2(u'_x + G)\tau^2 + x'_o (\tau - 4Stk) + 8x'_1 Stk\}$$

The dimensionless velocity was determined using the Kuwabara flow field. This is a cellular model in which the equation of creeping motion is solved for the fluid in an envelope surrounding the bubble. It is a simplified case of the Navier-Stokes equation in which the fluid inertial terms are ignored. This is valid as the particle Reynolds number does not exceed 0.2, which is the limit of the approximation. This allows the effects of neighbouring bubbles to be taken into account.

$$0 = \frac{\nabla p}{\rho} + \nu \nabla^2 u \quad (7.5)$$

The thickness of the envelope is determined by the concentration of bubbles. The ratio of the bubble volume to that of the cell is the same as the volume concentration of air in the system. The boundary condition at the inner surface of the envelope i.e. at the bubble surface, is taken as zero velocity and that at the outer surface is taken as zero velocity. The Happel (1958) model which is physically the same differs in that the outer boundary condition is taken as zero shear stress. The fields produced by the two models are very similar but experimental evidence suggests that the Kuwabara (1959) model is a closer representation of reality.

The stream function for the field is given by:

$$\psi = \left(\frac{A}{r} + Br + Cr^2 + Dr^4 \right) \sin^2 \theta \quad (7.6)$$

where

$$A = -\frac{1}{4} \frac{U_0}{k} a^3 \left(1 - \frac{2}{5} \frac{a^3}{l^3} \right)$$

$$B = \frac{3}{4} \frac{U_0}{k} a$$

$$C = -\frac{1}{2} \frac{U_0}{k} \left(1 + \frac{a^3}{2l^3} \right)$$

$$D = \frac{3}{20} \frac{U_0 a}{kl^3}$$

$$k = \frac{1}{5} \left(\frac{a}{l} \right)^6 \left\{ 5 \left(\frac{l}{a} \right)^6 - 9 \left(\frac{l}{a} \right)^5 + 5 \left(\frac{l}{a} \right)^3 - 1 \right\}$$

(a/l) is the ratio of the bubble radius to cell radius

The fluid velocity resolutives are computed from

$$u_r = -\frac{1}{r^2 \sin \theta} \frac{\partial \psi}{\partial \theta} \quad (7.7)$$

$$u_{\theta} = \frac{1}{r \sin \theta} \frac{\partial \psi}{\partial r}$$

these expressions, when resolved with 7.6 yield

$$u_r = -2 \left(\frac{A}{r^3} + \frac{B}{r} + C + Dr^2 \right) \cos \theta \quad (7.8)$$

$$u_{\theta} = - \left(\frac{A}{r^3} - \frac{B}{r} - 2C - 4Dr^2 \right) \sin \theta$$

where u_r and u_{θ} are the velocity resolutives in cylindrical polar co-ordinates. These velocities were rendered dimensionless, transformed to cartesian co-ordinates and re-entered into 7.2. It should be noted that 7.7 is for the case of a rigid sphere moving across the cell at velocity U_0 , so some manipulation is necessary to convert to the case of a stationary rigid sphere. The rigid sphere assumption is valid as the bubble diameter is about 40 μm and Jameson (1978) showed that bubble diameters exceeding 100 μm were required for internal circulation to become important. In these cases the drag term in 7.2 would need to be reduced by 2/3.

7.5.2 Inclusion of short range forces

The discussion in the present chapter has focused on the need for charge neutralisation to achieve affective flotation. To incorporate this effect into the model the short range forces that are experienced when a particle approaches a bubble are included; the details of these forces can be found in section 2.3.2.2. The forces presented below were expressed in dimensionless form for addition to the trajectory equation by dividing by:

$$6\pi\mu_r u_0$$

to yield

$$F'_{elr} = \left(\frac{2\epsilon\kappa\zeta_p\zeta_b}{3\mu u_o} \right) \frac{\exp(-\kappa h)}{[1 + \exp(-\kappa h)]} \quad (7.9)$$

$$F'_{vdw_r} = \left(\frac{A}{9\pi\mu_o d_p^2} \right) \frac{d_p^2}{h^2} \quad (7.10)$$

$$F'_{H} = -\frac{3}{2} \frac{R^2(S+1)}{(1+SR+R^2)} 3\pi\mu d_p u_r f(h) \quad (7.11)$$

where

$$S = \frac{h}{r_p} \quad R = \frac{r_p}{r_b}$$

$$f(H) = 3.23 - 2.91S + 1.56S^2$$

The same method as described before has been used to calculate the trajectories when the short range forces are included. It should be noted that very small steps in the trajectory calculations are required close to the bubble surface.

7.6.3 Results

Appendix I shows a typical trajectory plot together with a listing of the programme which was run to calculate the trajectories. The results show that particles which approach the surface of the bubble are held at a very short equilibrium distance and travel round radially to the tail of the bubble. Clearly although the particles may not touch the bubbles neither may they be dislodged from this equilibrium position. If the repulsion force is great enough the particles will not approach closely enough for this to occur and will be swept past the bubble.

An analysis of this shows that the important force balance to calculate occurs when the particle is downstream of the bubble. The particle on the critical trajectory will

enter the downstream section of the flow at an equilibrium distance from the bubble and escape when the drag force, coupled with gravity, is sufficient to remove the particle from the bubble's influence. In this respect the force balance described by Okada (1990) was wrong in that they carried out a balance on the upstream side of the bubble. He acknowledged this in this later paper (1992) in which he reverted to a balance at the back end of the bubble.

Figure 7.21 shows the effect of bubble volume fraction on the process. The results exclude short range forces and show that bubble volume fraction does have an effect but is small when compared with the influence of the other parameters which is in contradiction to the beliefs of Flint and Howarth (1971). The curves also show a significant effect with particle size. This would mean that grade efficiency curve would be expected and this is not seen. This discrepancy is due to the differences between flocs and particles as discussed in section 7.1.3.

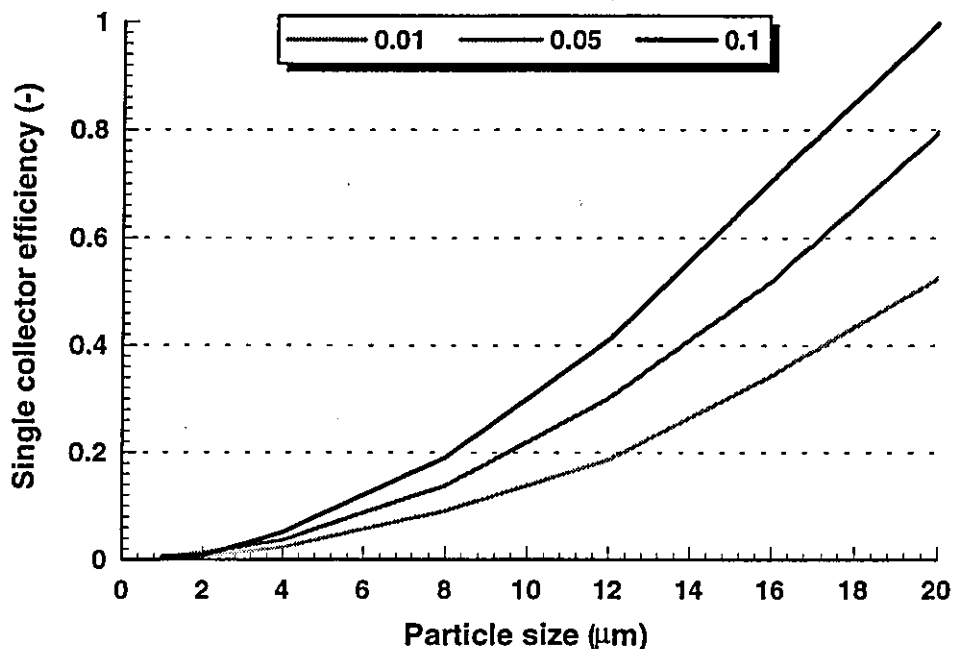


Figure 7.21 : Single collector efficiency against particle size for different bubble volume fractions.

The effect of particle inertia in the system is negligible. For a 15 μm diameter particle of density 2000 kgm^{-3} approaching a 40 μm diameter bubble the Stokes number is 0.0003. The deviation from a trajectory caused by this level of inertia was totally insignificant in this case. The most important parameter is gravitation which agrees well with the study of Okada (1990). The effects of this can be seen in figure 7.22 which plots the single collector efficiency over a range of particle densities.

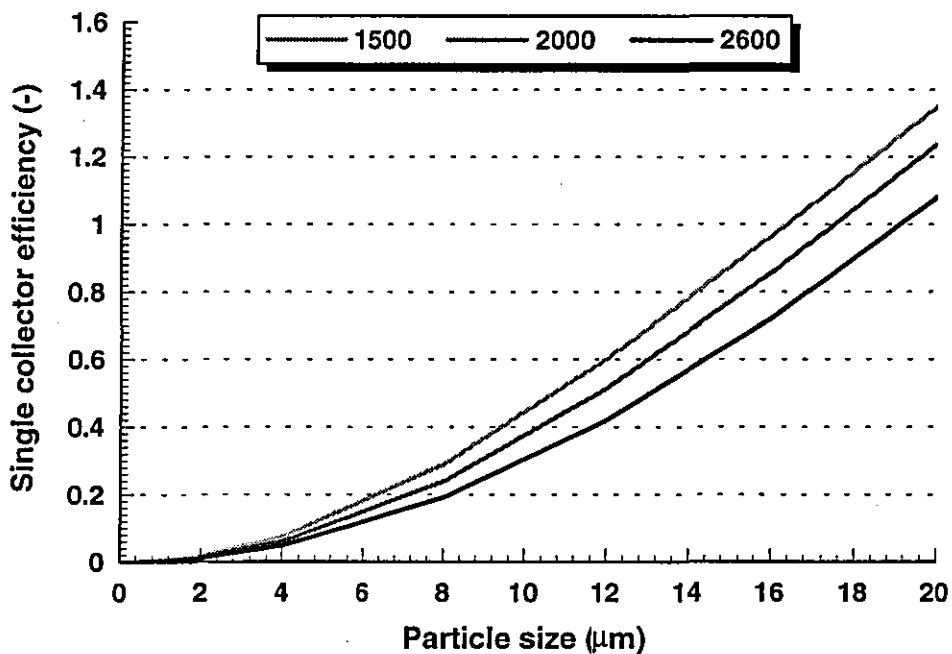


Figure 7.22 Single collector efficiency against particle size for different particle densities.

7.6.4 Flotability criteria

The critical stage of the process has been shown within this investigation to be the attachment process. This is further analysed in terms of an heterocoagulation process between a particle and a bubble. The total energy of interaction between a bubble and a particle can be expressed from double layer theory, explained in section 2.3.2.2, as:

$$F_T = 2\pi\epsilon\kappa d_p \zeta_p \zeta_b \exp(-\kappa h) - \frac{Ad_p}{12h} \quad (7.12)$$

The point when the force barrier to attachment disappears occurs when:

$$F_T = 0 \quad (7.13)$$

$$\frac{dF_T}{dh} = 0 \quad (7.14)$$

This enables the critical attachment parameter to be determined as the point when the energy barrier to attachment just disappears. In this case:

$$m = \frac{4\pi\epsilon\zeta_p\zeta_b}{\kappa A} \quad (7.15)$$

This approach has been developed by a number of authors, most notably Deryagin (1960). The resulting expression is always of the form shown in 7.15 with the product of the zeta potentials on the numerator and the Hamaker constant on the denominator. The expressions have been expanded to include more complicated forms of the double layer expressions and a term to represent the hydrophobic interaction force, see Yordan (1989). However the same basic expression is always achieved. The inclusion of the hydrophobic interaction should prove a major improvement to the analysis but its application is limited as the constants involved in the equation are only known for very pure materials. For this reason the term is usually left out as in this case but should always act to improve the situation such that any prediction from the analysis above will be pessimistic.

The results from this analysis can be seen in figure 7.23. The flotability criterion has been calculated as the product of the zeta potentials alone. This eliminates any problems associated with the reliability of Hamaker constants for clays. The bubble zeta potentials were calculated from the data in figure 6.25 and scaled up on a number

basis. The original intention was to use the surface tension data for both sedimentation and flotation tests to monitor the residual surfactant concentration. However, the measurements did not prove sensitive enough to detect the changes. A range of alternative methods were tried including carbon analysis but none prove able to provide adequate information.

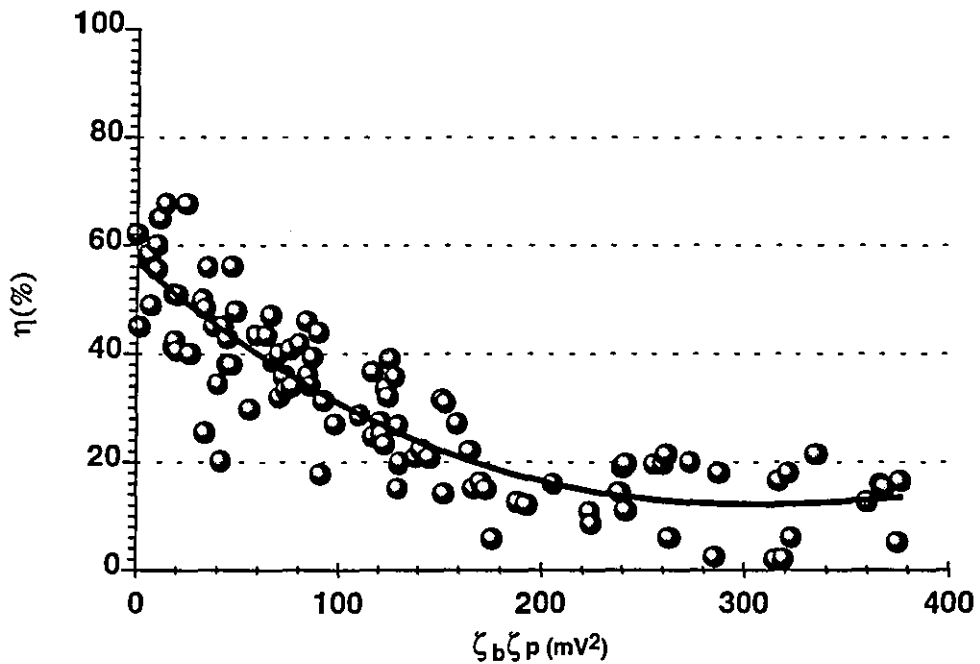


Figure 7.23 : Removal efficiency against the product of particle and bubble zeta potentials.

The results show that the removal efficiency is a clear function of zeta potential and that both zeta potentials need to be taken into account. The overall efficiency is low as is expected for discrete particle systems. The efficiency drops by 50% when the zeta potential is an equivalent 10mV for both particles and bubbles. The comparison between discrete particle and floc flotation is seen in figure 7.24. The graph shows a much greater decline in floc flotation showing that zeta potential is more important in flocculated systems. The two curves cross over at the equivalent 10 mV point as discussed above. This is a critical point which marks the onset of effective flotation.

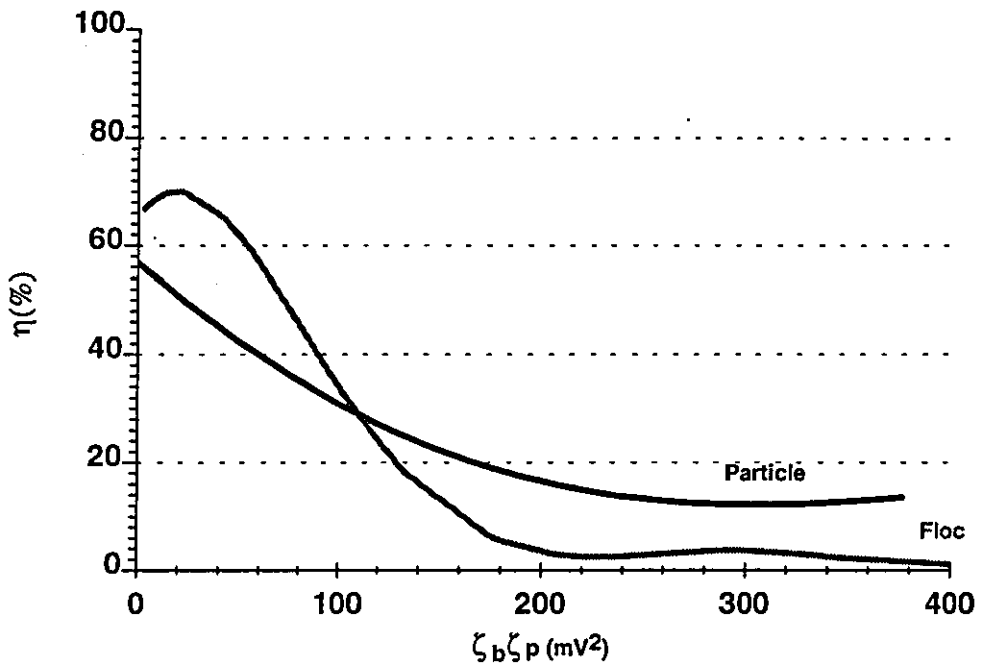


Figure 7.24 : Comparison of the flotability criteria between discrete particle and floc flotation

7.3.4 CONCLUSION

The discussion into the flotation of discrete particles showed that particles are removed most effectively when the zeta potential is low. The peak of the efficiency occurs when the zeta potential is ± 4 mV around the isoelectric point. This reduces the energy barrier to capture due to the electrical double layer repulsion between a bubble and a particle. Examining the process in terms of the bubble concentration and the degree of hydrophobicity produced two important results; which were increasing the recycle ratio above a certain optimum value produces only marginal improvements while increasing the operating costs significantly. The hydrophobicity of the particles has been shown to increase the robustness with which the process can float particles that are charged. However, it does not affect the peak efficiency that is obtainable.

Comparison between the flotation of discrete particles and flocs shows that flocs are more effectively removed than particles by flotation, but the process is governed by

the same flotation criteria as for discrete particles. The concept of grade efficiency curves has been shown not to be particularly relevant to the flotation of flocs and this is due to the inhomogeneity of their surface. Increasing the recycle rate has less effect with floc flotation although an improvement is seen and this is due to the smaller flocs being more effectively removed at the higher recycle ratios. The hydrophobicity of the flocs has been shown not to affect the peak efficiency obtained. However, reducing the hydrophobicity has been shown to improve the flotation response and this is explained in terms of the more open floc structure that corresponds to it.

A theoretical analysis of the process has shown that the effects of bubble volume fraction and particle inertia are not important to the capture of particles by rising bubbles compared with other factors. Particles approach a bubble to an equilibrium distance and then are swept round the surface of the bubble until they reach the underside at which point they are either captured or released. This depends on whether the forces of gravity and hydrodynamics are sufficient to overcome the influence of the bubble. The dependence of flotation on the zeta potential of both particles and bubbles has been demonstrated and shows the need for an equivalent zeta potential of 10mV on both particle and bubble for effective flotation.

CHAPTER EIGHT

CHAPTER EIGHT

RESULTS : BUBBLE SIZE MEASUREMENTS

8.1 INTRODUCTION

This chapter discusses the results obtained from the bubble size characterisation experiments, the methodologies of which have been discussed in chapter 5. To improve the clarity of the discussion the bulk of the results are contained within appendices F and G. Certain results will be presented within this chapter to highlight specific points in the discussion, see figures 8.1 to 8.12

The physical configuration of the nozzles was altered systematically and the bubble size distribution measured at each change. In this way the overall effect of nozzle design parameters was established. The effects of pressure used as a comparison between this investigation and those previously reported. The results are discussed in terms of a simple three stage model of bubble production. The chapter concludes with a guide towards optimising nozzle design and its implications with respect to dissolved air flotation.

8.2 MODEL OF BUBBLE PRODUCTION

The most important characteristic of the air supplied to the dissolved air flotation process is determined by the size of the bubbles produced. This is independent of the method of saturation used and so that will not be discussed here. The size and size distribution of the bubbles will be controlled by the geometrical design and operating conditions of the injection nozzle. This bubble production process is visualised in terms of a three stage model which is diagrammatically represented by figure 8.1. The model splits up the processes of bubble creation, bubble growth and bubble stability in the bulk flow; these are referred to as birth, adolescence and maturity respectively.

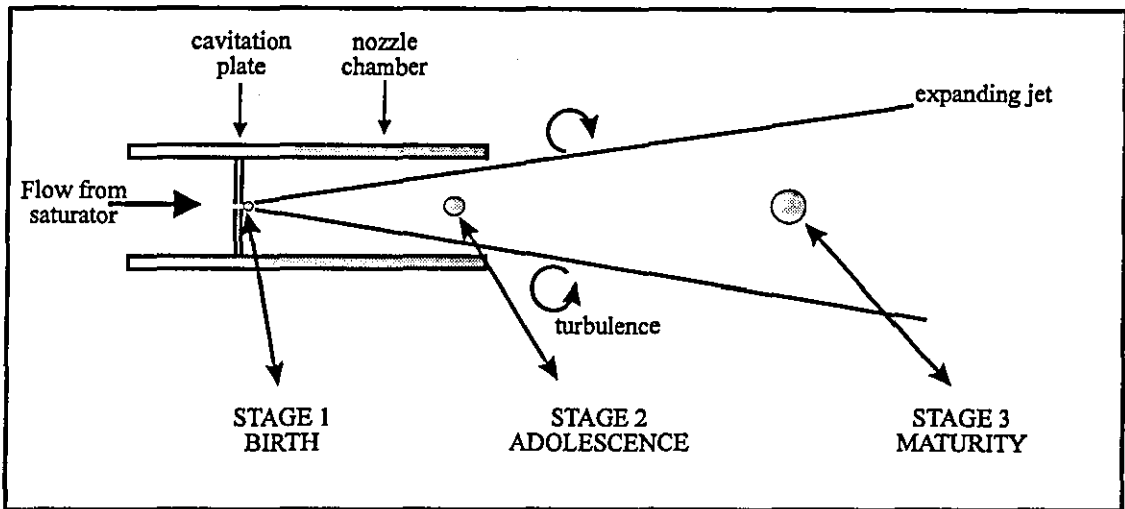
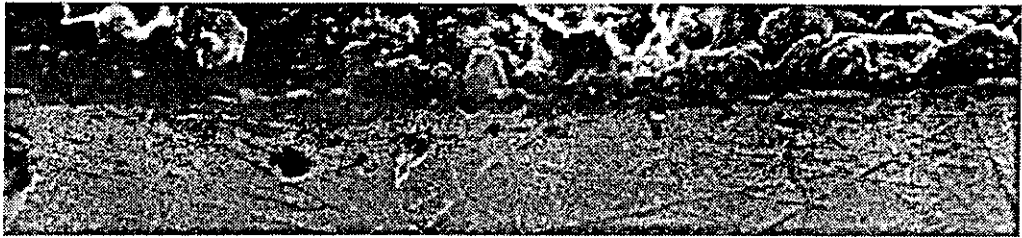


Figure 8.1 : Diagrammatic sketch of the 3 stage bubble production model.

Stage one of the process refers to the point at which the bubbles are first created. It is important to note that this does not involve the creation of a vapour space in the liquid and hence is not what is generally thought of as cavitation. In this case the nucleation sites already exist and Urban (1980) provided conclusive proof that these sites exist within the surface roughness of the cavitation plate. The sites are fed with gas until the combination of the buoyancy force and the drag created by the flowing liquid is sufficient to dislodge them. The gas that feeds the nucleation sites is produced when the supersaturated liquid is forced through a tiny orifice, which causes the liquid to cavitate rapidly, precipitating out all the excess gas from solution.

The nucleation sites are crevices around the edge of the orifice which are shaped geometrically so that a stable equilibrium forms between gas in the crevices and the surrounding liquid phase. Figures 8.2 (a) and (b) are scanning electron micrographs of the profiles of two cavitation plates, showing the surface roughness that produces the crevices for the nucleation sites. The size and geometry of the sites will control the size of the bubbles that are produced by determining the size at which the bubbles dislodge and hence enter the later stages of bubble growth. It is at this stage that the initial size and number of the bubbles is determined.



(a) 0.5 mm orifice



(b) 1.5 mm orifice

Figure 8.2 : Scanning electron micrograph of side elevation of the inner orifice of two cavitation plates of different diameters.

The second stage of the model involves the continued growth of the bubbles due to the transfer of precipitated air. This stage is distinct from stage one as it involves the growth of free moving bubbles within the flow. The rate of growth is controlled by the diffusion of air to the bubble's surface without any coalescence occurring. This part of the process operates over the volume of the nozzle chamber and a small volume just beyond. Past this point no further excess air will exist and so no bubble growth will occur. This stage of the process is typified by the size of the bubbles increasing while the total number remains constant. The controlling variable is the residence time of the bubbles in the nozzle chamber.

The final stage of bubble growth is due to coalescence and occurs when the bubbles have left the nozzle chamber. Coalescence is related to the degree of turbulence in the system and so the most important area is the boundary between the injected flow and the bulk phase. This occurs at the nozzle exit when the injected jet pushes the bulk

water out and so creates a recirculation flow around the nozzle exit, which will increase the number of bubble collisions and hence the amount of coalescence. The ultimate amount of coalescence is dependant on the surface chemistry of the bubbles and can be viewed in terms of a coagulation mechanism as discussed in section 7.6.4. Figure 8.3 illustrates bubble coalescence in this stage and shows a video still of a bubble stream being injected into the column. The larger coalesced bubbles are seen as brighter white spots in the light grey injection cloud. This stage of the process is controlled by the degree of localised turbulence at the nozzle exit and is typified by an increase in bubble size with a reduction in total bubble numbers.

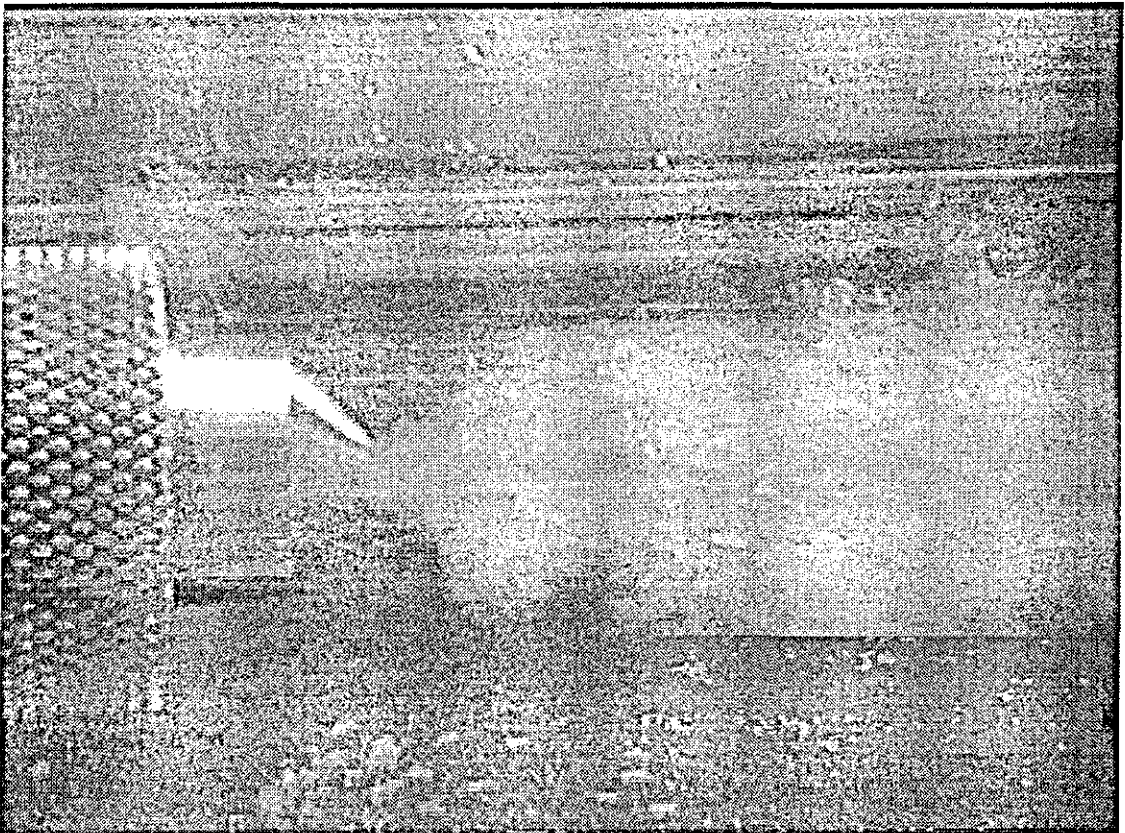


Figure 8.3 Video still of an injected bubble flow.

The model above represents a qualitative assessment of the bubble production process. The problems of quantifying the model all concern stage one of the process. The later stages have been studied in detail and proven models are available.

However, stage one of the process is poorly understood. It seems that the exact relationship between crevice configuration and the bubble size upon dislodgement is not known. This sets the starting point from which the latter stages develop and so without such a relationship no fundamental model can be evolved, which is why previous attempts have presented poor predictions. Constants are set in the equations which would represent stage one of the process and can be true only for the specific nozzle that was tested. Prediction of the performance of another nozzle would require its specific constant to be known rather.

The model presented here examines all parts of the process and so can be used as a tool to aid the understanding of the bubble production process operates and how individual variables affect the process. This will lead to useful indications towards a more systematic approach to nozzle design. The model is summarised in table 8.1 which shows the critical variables of each stage and how that stage should effect the bubble size distribution

| | Critical variables | Effect on distribution |
|---------|--|--|
| Stage 1 | Crevice configuration Flow rate of injected phase | Determines number and size of bubbles that enter stage 2 |
| Stage 2 | Time within nozzle chamber Amount of excess air | Bubble size increases Bubble number remains constant |
| Stage 3 | Degree of turbulence Surface chemistry of bubbles | Bubble size increases Bubble number decreases |

Table 8.1 : Summary of bubble production model

8.3 RESULTS

The results of the bubble size measurements can be found in appendix G and figure 8.4 shows a typical bubble size distribution. The distributions shows two main features, the bulk of the bubbles are between 20 and 60 μm in diameter and a small fraction of large bubbles greater than 100 μm are sometimes seen. The discussion of the effects of the investigated variables will focus on changes in the mean bubble size as this represents a convenient description of the distribution.

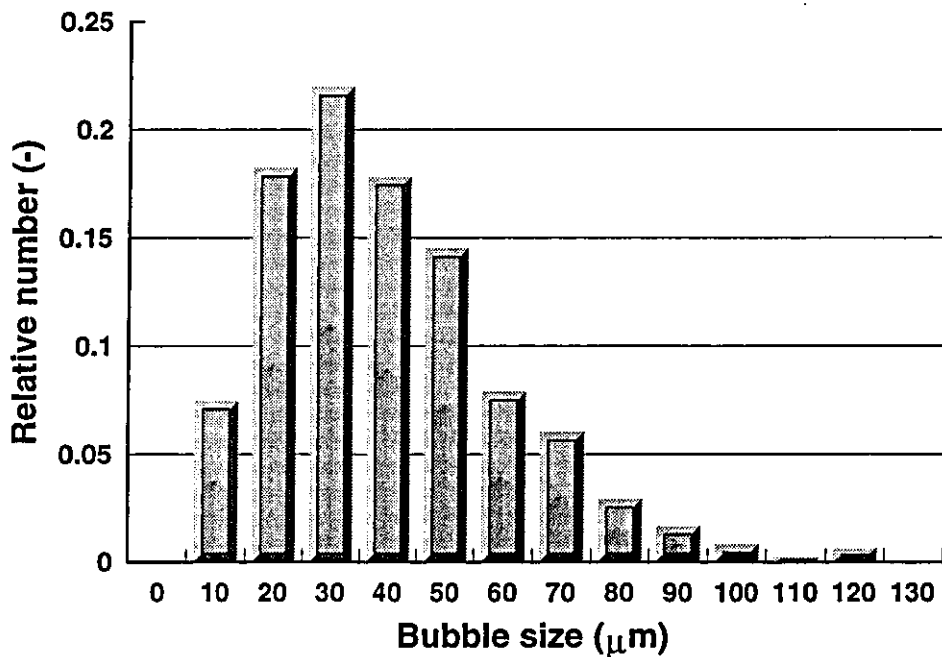


Figure 8.4 : Typical bubble size distribution.

8.3.1 Effect of saturator pressure

The effect of increasing the saturator pressure can be seen in figure 8.5. The graph shows a slight decline in mean bubble size with increasing pressure. The overall trend agrees with the majority of published results except the that overall change in mean size is less here. Examining the individual size distributions shows that the fraction of 10 and 20 μm bubbles increases slightly as the pressure is increased.

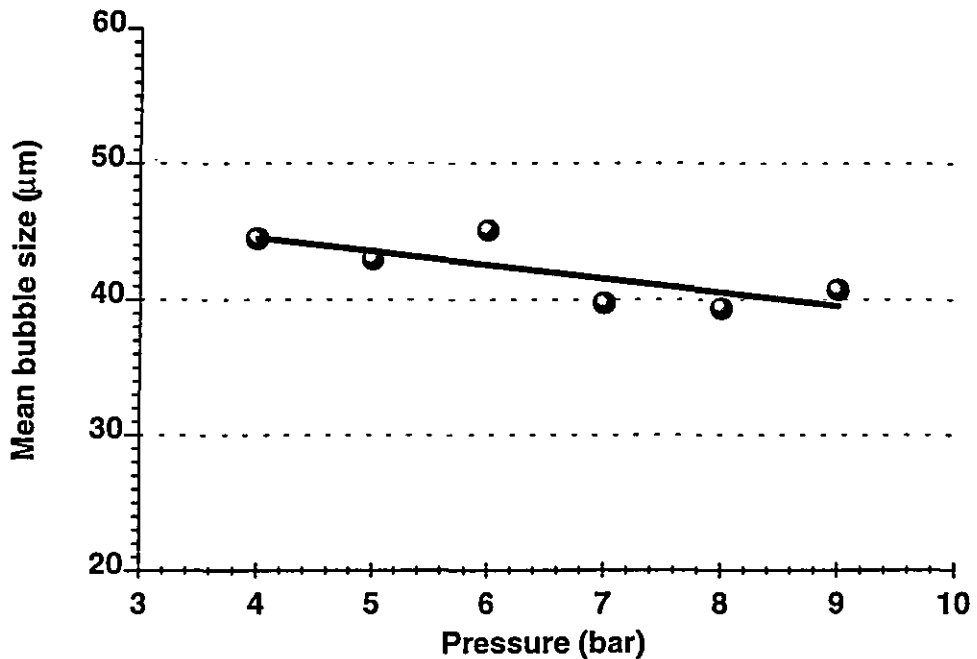


Figure 8.5 : Effect of saturator pressure on the mean bubble size

The pressure will affect all three stages of the bubble production process but in differing ways. The effect of stage one will be to increase the flow velocity of the liquid passing through the orifice. This will increase the drag force on the bubbles as they grow on the nucleation sites, dislodging them at a smaller size. The result of this is to reduce the size of the bubbles as they enter into stage two. In this stage the increased flowrate will reduce the time the bubbles remain in the nozzle chamber and hence the time available to grow by diffusion, which will also decrease the size of the bubbles as they exit stage two. The decrease in both stages due to the increased pressure will be counteracted at least partly by the increased amount of precipitated air the increased pressure generates. This will affect stage two more pronouncedly as it will produce a greater driving force and so the rate of diffusion will increase. The final stage will be adversely affected as a greater relative velocity will result and this will increase the degree of turbulence and hence the amount of coalescence.

Thus there is a situation of counterbalancing effects which result in only a minor overall change. The effect of reducing the bubble size upon dislodgement from the nucleation sites is the most important and this can be seen in the fact that the overall change is a decrease and that the proportion of very small bubbles increases. The overall change in mean size is sufficiently large to be physically significant. The decrease in mean size would result in an increase of over 30% in the number of bubbles produced based on a monosized bubble at the mean size. The increase in bubble numbers although of process benefit would be uneconomic and so this result suggests that saturators should be operated at around 4 bar. All following experiments were conducted at 4 bar.

8.3.2 Effect of orifice size

The effect of orifice diameter can be seen in figure 8.6 with the diameter being increased by a factor of four. The results show that the mean size significantly increases as the orifice diameter is increased. Examining the size distributions shows that this is due to the greater production of bubbles that are 70 μm and above.

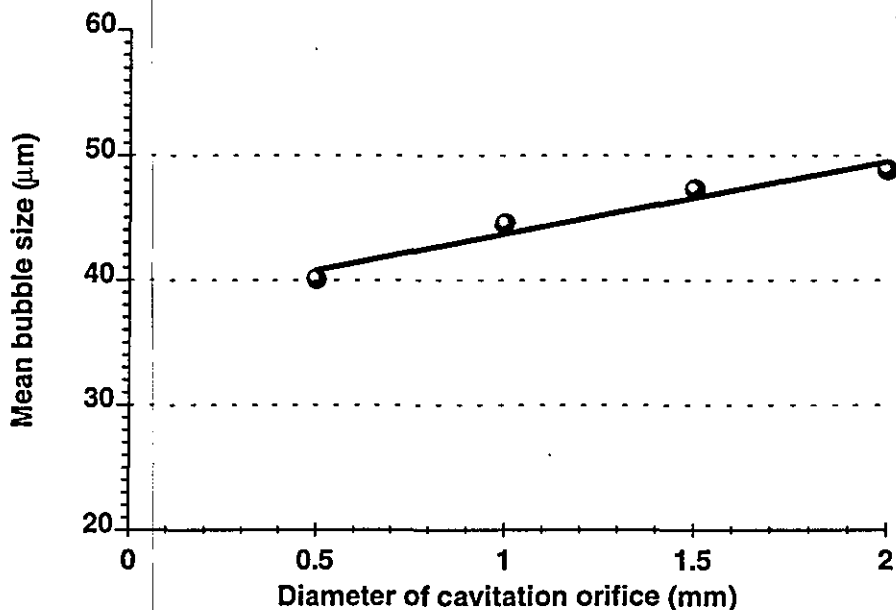


Figure 8.6 : Effect of orifice diameter on the mean bubble size

Enlarging the orifice diameter principally effects the first stage of the process because the total number of nucleation sites increases as the circumference of the orifice expands. However, this will be accompanied by a decrease in the velocity through the orifice, reducing the drag force on the bubbles allowing them to increase more in size before they are dislodged. This notion is supported by the fact the bubble numbers decreased with diameter with the 2mm, orifice barely providing enough bubbles to be measured with two rolls of film. The overall flowrate increases as the diameter widens as less resistance is given to the flow. This will affect the process by greatly reducing the time that the bubbles spend in the nozzle chamber and increasing the relative velocity between injected flow and the bulk. Both of these will increase the size of the bubble and in particular the greater coalescence in stage three will produce more macro bubbles as seen in the distributions. Thus all three stages of the process are adversely affected by an increase in the orifice diameter.

8.3.3 Effect of nozzle length.

The effect of increasing the nozzle length can be seen in figure 8.7. The mean size of the bubbles initially increased up to nozzle lengths of 10 mm then decreased with a 20 mm nozzle. The individual size distributions, presented in appendix G, show a marked rise in the amount of larger bubbles when the 5 and 10 mm nozzles are used. A peak in the mean size is seen with a nozzle length of 11 mm.

Changing the nozzle length will only affect stage two of the process with the time the bubbles are in the nozzle chamber increasing with nozzle length. This will allow the bubble to grow more by the time it reaches the bulk flow, thus increasing its size. This is seen in the rise in mean size up to 10 mm. The performance is improved with the 20 mm nozzle, showing the best performance of all with a mean size of 14 μm below the maximum.

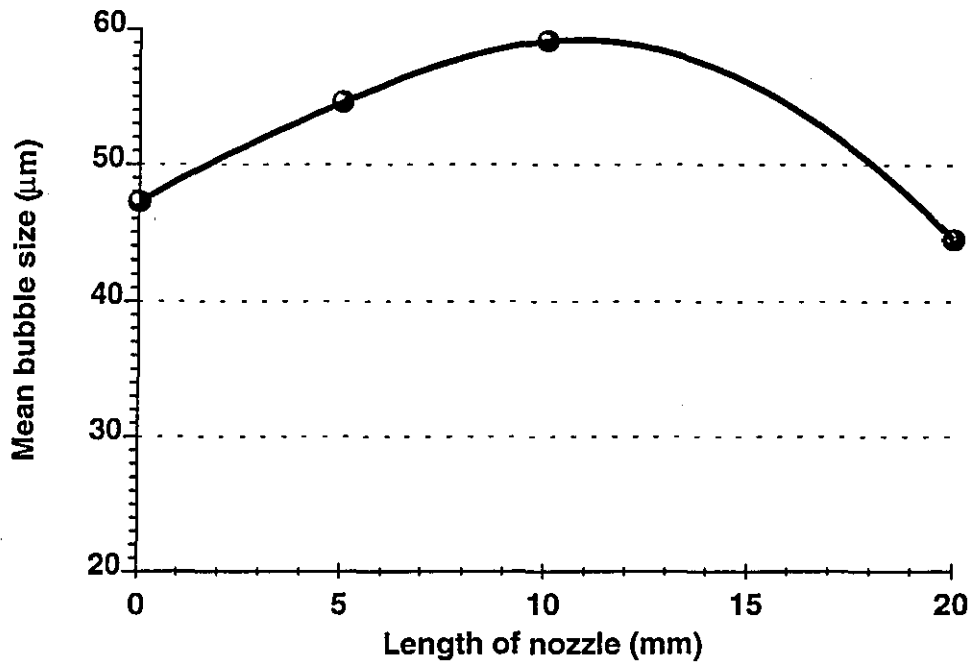


Figure 8.7 : Effect of nozzle length on the mean bubble size

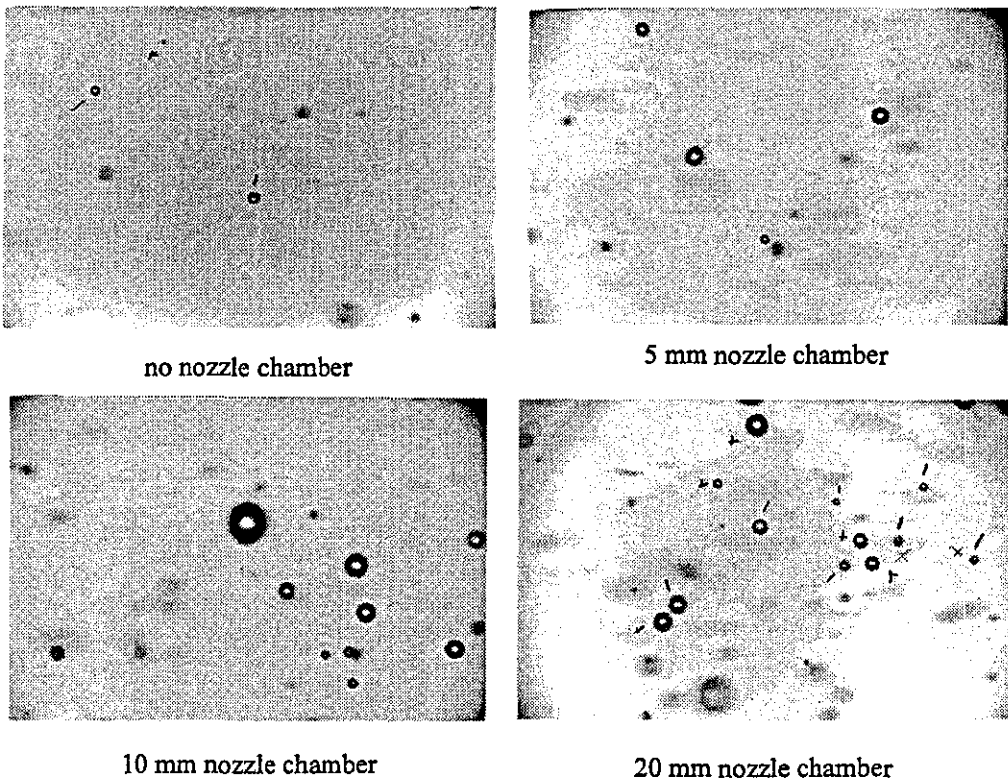


Figure 8.8 : Typical bubble photographs for different nozzle chamber lengths

The other important aspect concerned with nozzle chambers is the effective use of the available air. Any air that has not been consumed by the bubble growth in stage 2 will remain dissolved in the bulk water when it enters stage 3 and hence wasted. The shorter nozzle will offer less time for the consumption of the excess air and this results in the total bubble number decreasing. This can be seen in figure 8.8 which shows a typical photograph taken during the experiments with the different nozzle lengths. The photographs clearly show that the bubble number concentration increases with nozzle length. This means that long nozzle chambers are necessary for maximum utilisation of the dissolved air.

8.3.4 Effect of impingement plates

One of the most common methods of trying to control the bubble size distribution is by using an impingement plate with which the bubble stream collides thus breaking up the bubbles. This will have a greater effect on the larger bubbles as the surface tension will have a smaller effect on stabilising the bubble's surface. The use of such devices has been seen especially in the beer industry where they are supposed to homogenise the bubble size distribution. The results obtained in this investigation can be seen in figure 8.10 and show that the mean size is only affected when the impingement plate is between 1 and 5 mm away from the nozzle exit. The change in size is seen in the distributions by a reduction in the number of bubbles whose size is greater than 70 μm and this supports the notion of bubble break-up. The plate will also produce two counterbalancing effects on the degree of coalescence. The impingement will slow down the flow velocity and thus reduce the degree of turbulence but will create a large deviation in the flow. The results show that the peak effect occurs when the plate is very close to the nozzle exit and this will be because the flow velocity will be at its highest thus generating the greatest force which may be used to break up smaller bubbles.

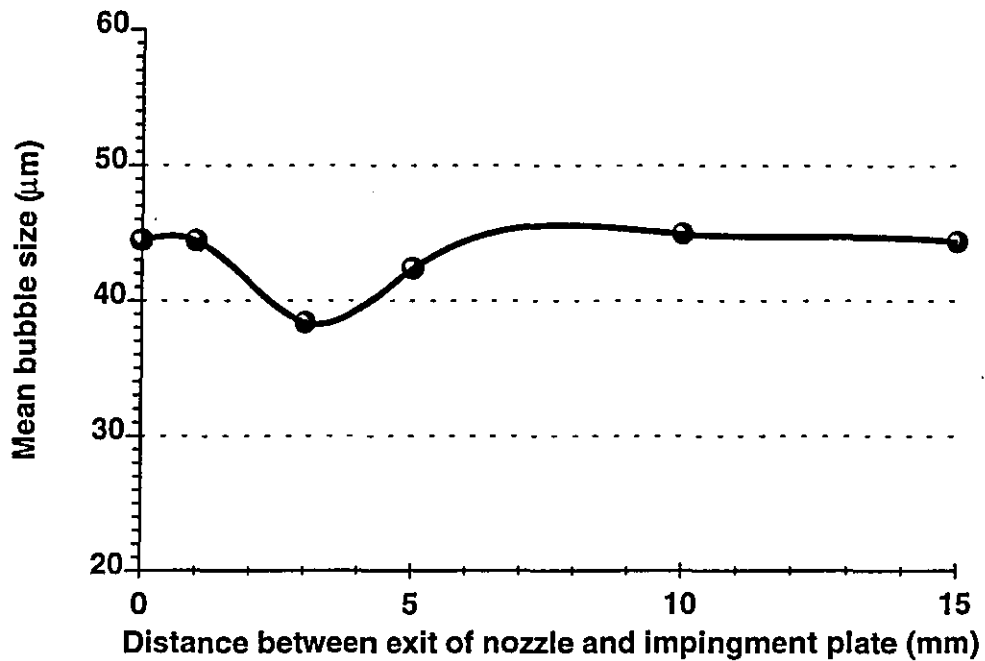


Figure 8.9 : effect of impingement plate on the mean bubble size

8.3.5 Effect of diverging cones

Another way to effect stage three of the process is to reduce the degree of turbulence that occurs where the injected flow meets the bulk without creating a large flow deviation. This can be achieved chemically but has undesirable effects on the rest of the flotation process. However, it can also be achieved mechanically by making the nozzle chamber a diverging cone at the natural angle of the expanding jet. Measurements from the video footage taken showed that the diverging flow spread outwards at an angle of approximately 45° . To test this three nozzle were made with cone angles of 30° , 45° and 60° . The results of this can be seen in figure 8.11. The diverging cones show an improvement in mean size providing the cone angle is less than the natural angle of the expanding jet. The peak reduction in size occurs with the 45° cone which produced the least number of bubbles over $70\ \mu\text{m}$ which supports the notion of turbulence reduction as this angle should not affect the flow path unlike the other two.

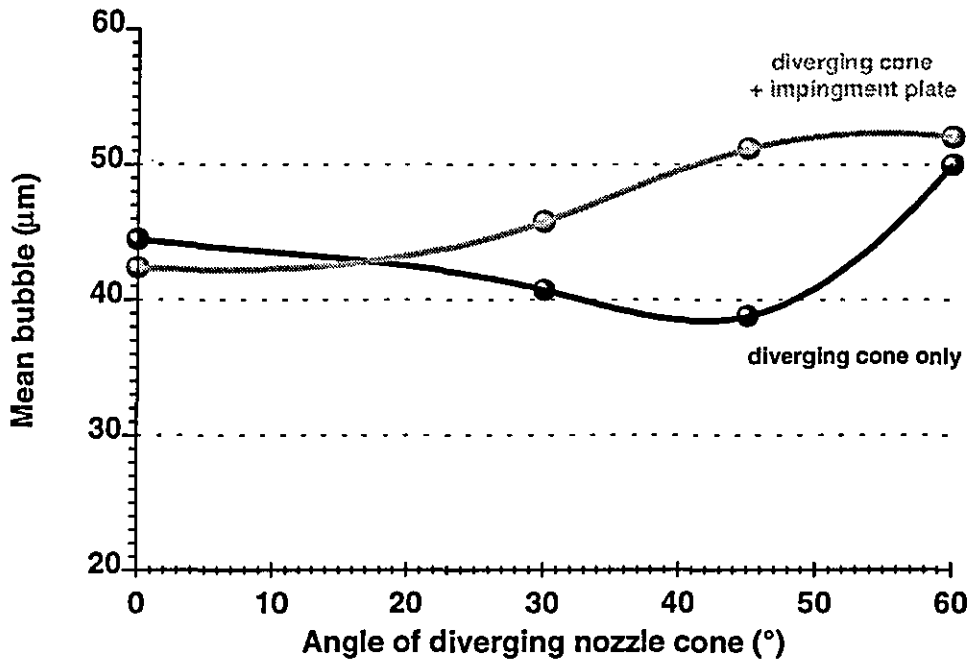


Figure 8.10 : effect of diverging nozzle cone on the mean bubble size.

The graph also shows the effect of adding an impingement plate after the diverging nozzle. In each case the plate was 5 mm from the end of the cone. The results shows that the combination of cone and impingement plate increases the mean bubble size. This difference is highlighted with the 45° cone which shows an increase in mean size of 12µm when an impingement plate is used as well. Comparing the 45° cone with the impingement plate alone showed the effects to be very similar with both producing a mean size of around 38 µm.

8.3.6 Effect of surfactant

The effect of increasing the surfactant concentration can be seen in figure 8.12. The results show a significant decrease in the mean size as the concentration is increased. The size distributions show that the number of bubbles whose size is greater than 70 µm decreases with increasing concentration. The effect of surfactant addition is

spread throughout the process. It is common to assume the decrease is purely the result of steric forces stabilising the bubble's surface thus reducing the degree of coalescence. However, the surfactant will also have a pronounced effect on stage one of the process by reducing the surface tension of the nucleation sites. This will make the dislodgement process easier and so will reduce the bubble size when they enter stage two. The effect of surfactant addition will improve the bubble size at each of the critical steps in the process, generating a large decrease overall.

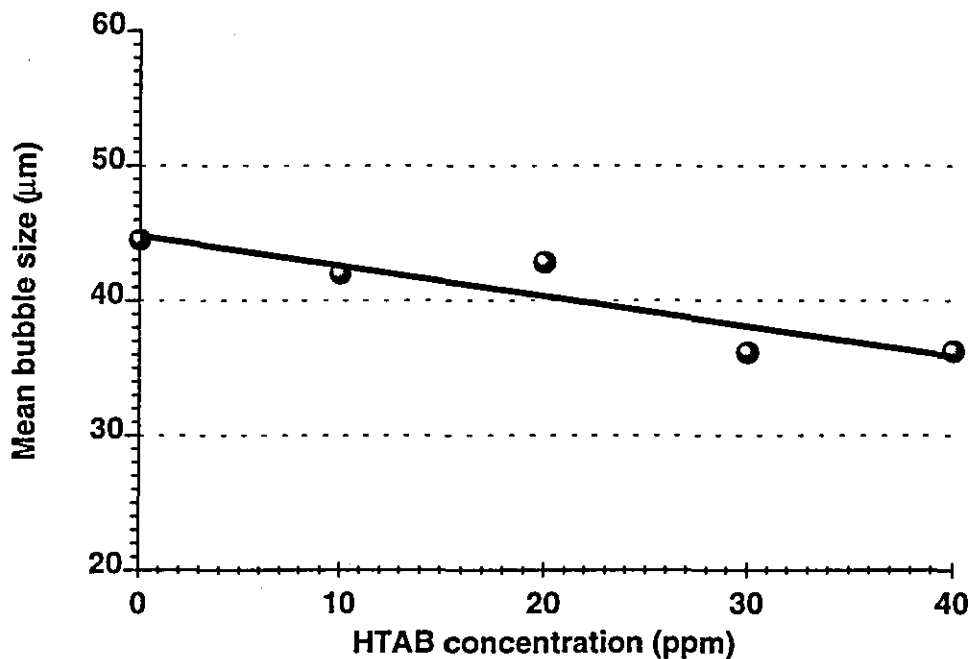


Figure 8.11 : Effect of surfactant concentration on the mean bubble size.

8.4 NOZZLE DESIGN

The aim of effective nozzle design is to produce a bubble size distribution that has a narrow spread of sizes with a mean between 40 and 50µm. Larger bubbles are particularly undesirable as they are a less effective use of the available air and create high shear rates which can break up the flocs. However, it is also undesirable to have too many very small bubbles, say less than 20 µm, as these are less effective at removing particles as the density difference produced is small.

The complexities of the process as highlighted in this chapter preclude any useful quantitative nozzle design equations from being developed. However, the model presented here can be used to generate a number of generalised rules for effective nozzle design. The cavitation plate should have as small an orifice as possible although this will decrease the flowrate and so will have a limiting condition set by the required recycle ratio. The nozzle chamber connected to this should be sufficiently long to allow all the excess air to be used. Maximum benefit is obtained when either an impingement plate or a diverging nozzle cone is used. Although the results are very similar the impingement plates offer the more complete option as it has the added benefit of reducing the velocity of the injected bubbles, increasing the bubble's residence time in the flotation column. The plate should be connected with a gap no greater than one nozzle diameter from the nozzle exit as beyond this no effects are produced. The configurational changes suggested here enable the mean bubble size to be decreased by upto 6 μm which will improve the bubble numbers produced by upto 20%. This change can also be achieved with an increase in pressure but this corresponds to an increase in operating costs which obviates its application.

8.5 CONCLUSIONS

Measurement of bubble size distributions and bubble numbers have been made for a series of nozzles with different configurations. The results of these experiments have led to the development of a simple qualitative model which describes the bubble production process. It is shown above that the model can describe the process adequately in terms of three separate stages and the model highlights the complexity of the process where a multitude of different effects act in unison. However, it clearly shows the key steps in the process are the dislodgement of bubbles from their nucleation sites and the degree of localised turbulence at the nozzle exit.

Examining the results of the experimental investigation in terms of this model shows a number of important criteria that need to be included in nozzle design in order to maximise its effect. In particular small cavitation orifices and long nozzle chambers have been shown to improve the size distribution generated. To achieve maximum benefit an impingement plate should be connected close to the nozzle exit to break up any large bubbles and reduce the flowrate of the injected jet. This enables a decrease in mean size of upto 6 μm which increases the bubble number concentration by upto 20 %.

CHAPTER NINE

CHAPTER NINE

CONCLUSIONS AND SUGGESTIONS FOR FUTURE WORK

9.1 CONCLUSIONS

The investigation into the mechanisms of dissolved air flotation showed that the surface chemistry of the particles to be removed and the air bubbles that are generated are critical to the effective operation of the process. Simple qualitative models can effectively describe the surface chemical systems for engineering applications to yield a much improved understanding of how the process operates.

A detailed surface characterisation of two clay minerals was performed in terms of their zeta potential. This showed that small changes in the system's conditions could have large effects on the zeta potential of the particles. This was most evident with the use of surfactants, where charge reversal occurred with very low surfactant concentrations. The surfactant adsorbed onto the clay particles in a perpendicular orientation, following a simple model of adsorption. This showed surfactants to be a very effective way of controlling the zeta potential of particles. Coagulants are less effective as they undergo hydrolysis reactions in water producing a range of aquometal products; the proportion of each type depends on the pH and dose of the system. In acidic environments positive aquometal complexes are predominant; this equilibrium shifts towards hydroxide precipitates when the condition becomes alkaline or the high concentrations are used. The model of how these two species interact with the particles and the resulting effect on the zeta potential adequately describes the systems, showing how sensitive the zeta potential is to changes in dose or pH when they are used. An anomalous result was found with the effects of temperature; the magnitude of the zeta potential of Wyoming bentonite particles decreased with increasing temperature. The mechanism for this potential reduction was a decrease in the hydrated radius of the adsorbing ions. This resulted in more ions being adsorbed into the Stern layer and caused the particles to coagulate as the temperature exceeded 35 °C.

The mechanisms of flotation were investigated for both discrete and flocculated particles and showed that charge neutralisation and hydrophobicity are necessary for effective flotation. The peak efficiency occurred when the zeta potentials of the particles or flocs was $\pm 4\text{mV}$, with the decrease in the efficiency being much steeper for the flotation of flocs as the magnitude of their zeta potential was increased. No strong relationship could be found between removal efficiency and particle size, negating the concepts of grade efficiency which are often discussed. This is attributed to the fact that the bubbles contact the flocs on patches where the hydrophobicity is high, due to trace organic adsorption. The degree of hydrophobicity has been shown to increase the robustness with which the process can float particles that are charged without affecting the peak efficiency that is obtained. Increasing the recycle ratio above a certain optimum is shown to have little effect on the peak efficiency that is obtained; except in the flotation of poorly coagulated particles which are small or have remained discrete. A theoretical analysis of the process has shown that particles approach a bubble to an equilibrium distance and then are swept round the surface of the bubble until they reach the underside at which point they are either captured or released, depending upon whether the forces of gravity and hydrodynamics are sufficient to overcome the influence of the bubble. The dependence of flotation on the zeta potential of both particles and bubbles has been shown to require an equivalent zeta potential of 10mV on both surfaces for effective flotation.

The mechanisms of bubble production within the process have been described in terms of a three stage model. This showed that the important stages in the process are: the dislodgement of the bubbles from their nucleation sites and the degree of localised turbulence at the nozzle exit. A number of important features have been highlighted to ensure an optimised nozzle design. In particular, small cavitation orifices followed by long nozzle chambers are required. Maximum benefit is gained by the inclusion of a 45° diverging nozzle cone or an impingement plate close to the nozzle's exit, both of which reduce the mean bubble size by $6\ \mu\text{m}$. Similar effects are produced by increasing the pressure or adding surfactants but both are undesirable due to the implications on the rest of the flotation process.

9.2 SUGGESTIONS FOR FUTURE WORK

The following are suggestions for future work aiming either to improve the current experimental techniques or to develop further the understanding of the mechanisms that operate.

The effect of floc structure is poorly understood and the concepts of grade efficiency need to be extended to include a parameter for shape as well as size. This is most effectively achieved by the measurement of the flocs fractal dimension and this should yield much greater information than size measurements alone.

The need for hydrophobicity is clearly defined and the current models should be refined to include these effects. This can be effectively achieved by including a term for the hydrophobic interaction force into the balance of the short ranged forces. The model can be verified by experimenting with combinations of coagulants and surfactants to produce manufactured flocs with known hydrophobic spots.

The requirement for charge neutralisation is clear but the investigation needs to extend to the characterisation of the bubble's zeta potential as this represents a limiting stage in the current analysis of the process. In particular the effect of the coagulants need detailed investigation as their effects are likely to be very complex due to the range of hydrolysis products that can form. This can then be extended to see if the zeta potential of both particles and bubbles can be manipulated by simple changes in the pH which then could control the flotation process.

The model of bubble production clearly shows the importance of the detachment of bubbles from their nucleation sites. However, the actual detachment process is poorly understood and this represents a fundamental limitation preventing any model from adequately describing the process. The detachment process is clearly linked to the surface roughness and the crevice geometry that it creates and this needs quantifying. One possible method of achieving this is to measure the profile of the crevices in terms

of a shape factor such as the fractal dimension. This can then be experimentally verified by recording video footage of bubble production through a high magnification lens using a glass nozzle. Alternatively, the surface roughness can be controlled by electroplating the orifice plate and subsequent etching to generate pre-determined degrees of roughness.

The need for computer controlled image analysis has been shown and a solution has been developed to analyse an individual photograph automatically. This needs to be extended to enable a series of photographs to be analysed before the technique will become feasible. This requires alteration to the core programme which is written in the computer language visual C+ and represents a complex task.

Improvements in the design of nozzles has been shown to increase dramatically the efficiency with which the supplied air is utilised. The development of nozzle design is still in its relatively early stages and much still needs to be done. In particular the application of diverging nozzle chambers requires a detailed investigation as these offer the best option for the future. This should then be extended to include the combination of diverging cones and impingement plates, which when resolved should offer the optimum design.

REFERENCES AND BIBLIOGRAPHY

Amirtharajah A. And Mills K.M. *Rapid-mix design for mechanisms of alum coagulation.* J. AWWA pp210-216 1982.

Anfruns J.F. and Kitchener J.A. *Rate of capture of small particles in flotation.* Trans Inst Min Metall Sec C. C9-C15, March, 1977.

Anfruns J.F. *The flotation of small particles.* PhD thesis, University of London, Imperial college of science and technology, London, SW7, April 1976.

Angelidou C.; Keshavarz E.; Richardson M.J. and Jameson G. J. *The Removal of Emulsified oil Particles from Water by Flotation.* Ind. Eng. Chem., Process Des. Dev. Vol. 16, No.4 1977.

Arbiter N.; Fujii Y.; Hansen B.; Raja A. *Surface properties of hydrophobic solids.* AICHE symposium series. Advanced interfacial phenomena. No.150, Vol.171, pp176-182.

Aronson M.P. and Princen H.M. *Aqueous films on silica in the presence of cationic surfactant.* Colloid and polymer science. Vol.256, pp140-149, 1978.

Ash M.E. *Improvements in a method of dispensing beverages containing gas in solution.* Patent specification no. 2314/58, index class 102(2), B3(A3C:B12). 1957.

Ash M.E. *Improvements in means for dispensing liquids containing gases in solution.* Patent specification no. 22757/59, January 1959.

Ash M.E. *Improvements in means for dispensing beverages containing gases in solution.* Patent specification no. 2314/58, January 1958.

Aveyard R. and Haydon D.A. *An introduction to the principles of surface chemistry.* Cambridge university press, Bentley House, 200 Euston Rd, London, NW1 2DB,1973.

Bargero F.; García R.M.; Vilchez M.A.C. and Hidalgo-Alvarez R. *Effect of surface charge density on the electrosurface properties of positively charged polystyrene beads.* Colloids and surfaces A. Vol.92, pp121-126, 1994.

Barbery G. *Engineering aspects of flotation in the minerals industry: flotation machines, circuits and their simulations*. In 'The scientific basis of flotation'. Nato advanced study series, Sijthoff and Noordhoff, Alphen aan den Rijn, The Netherlands 1978. (ed Ives K.J.)

Bennett R.H. *Clay fabric and geotechnical property in selected submarine sediment cores from the Mississippi Delta*. PhD Texa A& M University, college station, Texas. 1973

Bleier A.; Goddard E.D.; Kulkarni R.D. *Adsorption and critical flotation conditions*. J. Colloid and Interface Science. Vol.59, No.3, pp490-504, May, 1977.

Bogdanov O.S.; Emelyanov M.F.; Maximov I.I.; Otrozhdenova L.A. *Influence of some factors on fine particle flotation*. In "Fine particle processing volume 1". American institute of mining, metallurgical and petroleum engineers inc. New York, New York, 1980.

Botes V. and van Vuuren L.R.J. *Dissolved air flotation for the removal of algae and inorganic turbidity on a large scale*. Water supply, Vol.9, pp133-139, 1991.

Bratby J. *Coagulation and Flocculation*. Uplands press ltd. Uplands press ltd, Croydon, CR9 1LB. 1980

Bratby J. and Marais G.V.R. *Dissolved air flotation*. Filtration and separation, Nov/Dec, pp614-624, 1974.

Bratby J. and Marais G.V.R. *Saturator performance in dissolved air (pressure) flotation*. Water research, Vol.9, pp929-936, 1975.

Bratby J. *Batch flotation tests: How useful are they?* J. Water Pollut Control Fed, Vol.55, pp110-113, 1983.

Bratby J. and Marais G.V.R. *Flotation*. Chapter 5 in "Solid/liquid separation equipment scale up" edition II. ed by Bryant E.F. Uplands press ltd, 1 Katherine st, Croydon, CR91LB. 1977

Bratby J. *Treatment of raw wastewater overflows by dissolved air flotation.* J. Water Pollut Control Fed., Vol.54, No.11, pp1558-1565. 1982

Bratby J. and Marais G.V.R. *Dissolved air (pressure) flotation- an evaluation of the inter-relationships between process variables and their optimisation for design.* Water S.A. Vol.1, No.2, pp57-69, July 1975.

Bratby J. and Marais G.V.R. *A guide for the design of dissolved air (pressure) flotation systems for activated sludge processes.* Water S.A. Vol.2, No.2, pp87-100, April 1976.

Bruyn de P.L. *Some aspects of the physical chemistry of solid/water interfaces.* In 'The scientific basis of flotation'. Nato advanced study series, Sijthoff and Noordhoff, Alphen aan den Rijn, The Netherlands 1978. (ed Ives K.J.)

Buffham B.A. and Cumming I.W. *Prevention of particle deposition in crossflow microfiltration.* Trans IchemE, Vol 73, Part A, pp 445-454, May 1995.

Button D.D.; Lawrence W.G. *Effect of Temperature on the Charge on Kaolinite Particles in Water.* Journal of the American Ceramic Society, Vol.47, No.10, pp503-509, 1964.

Carrique F.; Zurita L. and Delgado A.V. *Correlation of the Dielectric and Conductivity Properties of Polystyrene Suspensions with Zeta Potential and Electrolyte Concentration.* J. Colloid and Interface Science, Vol.166, pp128-132, 1994.

Carnaghan D.W.B. *Improvements in means for dispensing liquids particularly beverages containing gases in solution.* Patent specification no. 9385/62, March 1962.

Cassell E.A., Kenneth M.F. and Matijevic E. *The effects of bubble size on microflotation.* Water Res., Vol.9, pp1017-1024, 1975.

Cassell E.A., Matijevic E., Mangravite F.J., Buzzell T.M. and Blabac S.B. *Removal of colloidal pollutants by microflotation.* AIChE journal, Vol.117, No.6, pp1486-1492. 1974

Ching H.W.; Tanaka T.S.; Elimelech M. *Dynamics of coagulation of kaolin particles with Ferric Chloride.* Wat Res. Vol 28, No. 3, pp 559-569, 1994

Ching H.W.; Tanaka T.S.; Elimelec M. *Dynamics of coagulation of kaolin particles with ferric chloride.* Water Res. Vol.28, No.3, pp559-569, 1994.

Choi I-K.; Wen W.-W.; Smith R.W. *The effect of a long chain Phosphoate on the Adsorption of Collectors on Kaolinite.* Minerals Engineering, Vol.6, No.11, pp1191-1197. 1993.

Christenson H.K.; Claesson P.M.; Parker J.L. *Hydrophobic attraction: A reexamination of electrolyte effects.* J. Phys Chem. Vol 96, No. 16, 1992.

Clift R., Grace J.R. and Weber M.E. *Bubbles, drops and particles.* Academic press inc. (London) ltd. 24/28 Oval Rd, London, NW1.

Collins, G.L. and Jameson G.J. *Experiments on the flotation of fine particles.* Chem Eng Sci, Vol. 31, pp985-991, 1976.

Collins G.L. and Jameson G.J. *Double layer effects in the flotation of fine particles.* Chem Eng Sci, Vol.32, pp239-246, 1977.

Collins G.L.; Motarjemi M.; Jameson G.J. *A method for measuring the charge on small gas bubbles.* J. Colloid and Interface Science Vol 63, No. 1, Jan 1978.

Craig V.S.J.; Ninham B.W.; Pashley R.M. Journal of physical chemistry. Vol.97, pp10192-10197, 1993.

Davidson J.F. and Schüler B.O.G. *Bubble formation at an orifice in an inviscid liquid.* Trans Instn Chem Engrs. Vol.138, pp335-342, 1960.

Davidson J.F. and Schüler B.O.G. *Bubble formation at an orifice in a viscous liquid.* Trans Instn Chem Engrs. Vol.138, pp144-154, 1960.

Davies J.T. and Rideal E.K. *Interfacial phenomena*, second edition. Academic press ltd. Berkeley square House, London, W1, 1961.

Dean R.B. *The formation of bubbles.* J. Appl. Phys. Vol.15, pp446-451, 1944

Degremont. *Water treatment handbook, fifth edition.* Halsted press book, John wiley & sons, Chichester, 1979.

Deryagin B.V.; Dukhin S.S.; Lisichenko V.A. *The kinetics of the attachment of mineral particles to bubbles during flotation I-The electric field of a moving bubble.* Russian journal of physical chemistry. Vol.33, No.10, pp389-393, October 1959.

Deryagin B.V.; Dukhin S.S. and Lisichenko V.A. *The kinetics of the attachment of mineral particles to bubbles during flotation II-The electric field of a moving bubble when the surface activity of the ionogenic substance is high.* Russian journal of physical chemistry. Vol.34, No.3, pp248-251, March 1964.

Deryagin B.V.; Dukhin S.S. and Rulyov N.N. *Kinetic theory of flotation of small particles.* Surface and Colloid Science. Vol.13, pp71-110, Plenum Press, 1984.(edited by E. Matijevic and R.J. Good)

Dibbs H.P.; Sirois L.L. and Bredin R. *Some electrical properties of bubbles and their role in the flotation of quartz.* Canadian Metallurgical Quarterly, Vol 13, No. 2 1974

Dobler F.; Affrossman S. and Holl Y. *Surface analysis of model Latex Particles.* Colloids and Surfaces, Vol.89, pp23-35, 1994.

Dukhin S.S. *The kinetics of the attachment of mineral particles to bubbles during flotation III- secondary electrical double layer in the vicinity of the moving bubble surface.* Russian journal of physical chemistry. Vol.34, No.5, pp501-504, May 1960.

Dukhin S.S.; Deryagin B.V. *The kinetics of the attachment of mineral particles to bubbles during flotation V-Motion of the bubble surface strongly retarded by surface active substances. Distribution of the surface-active material and electric field of the bubble* Russian journal of physical chemistry. Vol.35, No.7, pp715-717, July 1961.

Dukhin S.S.; Deryagin B.V. *The kinetics of the attachment of mineral particles to bubbles during flotation IV-Retardation of bubble surface movements by surface active agents.* Russian journal of physical chemistry. Vol.35, No.6, pp611-616, June 1961.

Dwight D.W. *Surface analysis and adhesive bonding (I. Fluoro polymers)*. J. Colloid Interface Science. Vol.59, No.3, pp447-455, May 1977.

Edzwald J.K., Malley J.P. and Yu C. *A conceptual model for dissolved air flotation in water treatment*. Water supply, Vol.9, pp141-150, 1991.

Edzwald J.K., Walsch J.P., Kaminski G.S. and Dunn H.J. *Flocculation and air requirements for dissolved air flotation*. J. AWWA. Vol.84, 1992.

Edzwald J.K. *Algae, bubbles, coagulants, and dissolved air flotation*. Wat. Sci. Tech. Vol 27, No. 10, pp 67-81, 1993.

Edzwald J.K. *Principles and applications of dissolved air flotation*. Wat.Sci. Tech. Vol 31, pp1-24, 1995

Ferris A.P. and Jepson W.B. J. Colloid Interface Sci. Vol. 5, pp245, 1975

Flint, L.R. and Howarth, W.J. *The collision of small particles with spherical air bubbles*. Chem Eng Sci, Vol. 26, pp 1155-1168, 1971.

Flint L.R. *A Mechanistic approach to Flotation Kinetics*. Trans. Instn. Min. Metall. (Sect.C: Mineral Process. Extr. Metall.). Vol.94, , ppC90-C95, 1974.

Fox F.E. and Herzfeld K.F. *Gas bubbles with organic skins as cavitation nuclei*. J.Acoust.Soc.Amer. Vol.26. pp984-989. 1954

Fuerstenau D.W. *Fine particle processing*. In "Fine particle processing volume 1". American institute of mining, metallurgical and petroleum engineers inc. New York, New York, 1980.

Fukui Y. and Yuu S. *Collection of submicron particles in electroflotation*. Chem Eng Sci. Vol.35, pp1097-1105, 1980.

Fukushi K., Tambo N. and Matsui Y. *A kinetic model for dissolved air flotation in water and wastewater treatment*. Wat.Sci. Tech. 31, pp37-49, 1995

Gehr R. and Henry J.G. *Measuring and predicting flotation performance*. J. Water Pollut Control Fed. Vol.50, pp203-214, 1978.

- Giese R.F.; Wu W. and van Oss C.J. *Surface and electrokinetic properties of clays and other mineral particles, untreated and treated with organic and inorganic cations.* J. Dispersion Science and Technology , 17(5), pp527-547 , 1996
- Gochin R.J. *Flotation.* Chapter 19 in "Solid/liquid separation" (third edition). ed by Svarovsky L. Butterworth & Co. (publishers) ltd, 1990.
- Gochin R.J. and Solari J. *The role of hydrophobicity in dissolved air flotation.* Water Res. Vol. 17, No.6, pp651-657, 1983.
- Gould R.F. *Contact angle, wettability and adhesion.* Advances in chemistry series 43, American chemical society publications, 1964.
- Graciaa A.; Morel G.; Saulner P.; Lachaise J. and Schechter R.S. *The ζ -potential of gas bubbles.* J. Colloid and Interface Science. Vol.172, pp131-136, 1995.
- Gregory J. *Flocculation.* in "Progress in filtration and separation" Elsevier, Oxford. 1986 (edited by Wakeman R.J.)
- Gregory J. *The role of colloid interactions in solid-liquid separation.* Wat. Sci. Tech. Vol 27, No. 10, pp1-17, 1993
- Gulas V.; Benefield L.; Lindsey R.; Randall C. *Design considerations for dissolved air flotation.* Water and sewage works. pp30-31, July 1980.
- Gulas V.; Benefield L.; Lindsey R.; Randall C. *Factors affecting the design of dissolved air flotation systems.* J. Water Pollut Control Fed. Vol.50, pp1834-1840, 1978. [G4]
- Gungor N.; Tulun T. *Studies on the Zeta Potential of Bentonite clay in a aqueous solution.* Revue Roumaine de Chimie, Vol.39, No.2, pp177-182, 1994
- Haarhoff J. and Rykaart E.M. *Rational design of packed saturators.* Wat.Sci. Tech, 31, pp179-191, 1995
- Haarhoff J. and van Vuuren L.R.J. *Design parameters for dissolved air flotation in South Africa.* Wat.Sci. Tech, 31, pp203-213, 1995

Halpern D. and Grotberg J.B. *Dynamics and transport of a localised soluble surfactant on a thin film.* Journal of fluid mechanics. Vol.237, pp1-11.

Hahn H.H. *Wastewater treatment.* In 'The scientific basis of flotation'. Nato advanced study series, Sijthoff and Noordhoff, Alphen aan den Rijn, The Netherlands 1978. (ed Ives K.J.).

Happel J. Viscous flow in multiphase systems: Slow motion of fluids relative to beds of spherical particles. A.I.ChE Journal, Vol. 4, No.2, pp197-201, 1958

Harvey E.N., Cooper K.W. and Whiteley A.H. Bubble formation from contact of surfaces. J. Am. Chem. soc., Vol.68, pp 2119-2120, 1946

Harvey E.N., McElroy W.R. and Whiteley A.H.. On cavity formation in water. J. Appl. Phys. Vo.18, pp 162-172, 1947

Hayward A.T.J. *New law for liquids: don't snap, stretch.* New scientist, Vol.45, pp196-199. 1970

Hildebrand S.H. and Yoakley F.G. *Device for use in dispensing beverages containing gas in solution.* Patent specification no. 21252/70, July 1970.

Higashitani K., Iseri H., Okuhara K., Kage A. and Hatade S. *Magnetic effects on zeta potential and diffusivity of nonmagnetic colloidal particles.* J. Colloid and Interface Science. Vol.172, pp383-388. 1995

Hornsby D. and Leja J. Selective flotation and its surface chemical characteristics. Surface and colloid science. Vol.12, chp.3, pp217-301,1982.

Hughes M.A. *Coagulation and flocculation part1.* In "Solid-liquid separation second edition". Butterworths monographs in chemistry of chemical engineering, Butterworths London 1981, (edited by L.Svarovsky)

Hunter R.J. *Zeta Potential in colloid science.* Academic Press inc. 24/28 Oval road, London NW1. 1981

Hunter R.J. *Introduction to modern colloid science*. Oxford University press, Walton street, Oxford, OX2 6DD, 1992

Hyde R.A.; Miller D.G.; Packham R.F. and Richards W.N. Water clarification by flotation. J. AWWA. Vol.69, pp369, 1977.

Hyde R.A. *Water clarification by flotation 4: Design and experimental studies on a dissolved air flotation pilot plant treating 8.2 m³/h of river Thames water*. Technical report TR13, Water research centre, Stevenage laboratory, Elderway, Stevenage, Herts., SG11TH.

Hyde R.A.; Richards W.N.; Burley M.J. *A nozzle for introducing gas into liquid*. Patent specification no.10561/76, July 1976.

Isenberg C. *The science of soap films and soap bubbles*. Tieto ltd. 5 Elton road, Clevedon, Avon, BS21 7RA.

Israelachvili J. and Ninham B.W. *Intermolecular forces- the long and short of it*. J. Colloid and Interface Science. Vol 58, No. 1, Jan 1977.

Israelachvili J. and Pashley R. *The hydrophobic interaction is long range, decaying exponentially with distance*. Nature Vol 300, Nov 1982.

Israelachvili J. and Pashley R. *Measurement of the hydrophobic interaction between two hydrophobic surfaces in aqueous electrolyte solutions*. J. Colloid and Interface Science. Vol 98, No. 2, April 1984.

Israelachvili J. *Intermolecular and Surface forces*. Academic Press inc. 24/28 Oval road, London NW1. 1986

Ives K.J. *Coagulation and flocculation part2*. In "Solid-liquid separation second edition". Butterworths monographs in chemistry of chemical engineering, Butterworths London 1981, (edited by L.Svarovsky)

Ives K.J. *The scientific Basis of Flocculation*. Sijthoff & Noordhoff International Publishers B.V., Alphen aan den Rijn, The Netherlands, 1978

James A.M. *Electrophoresis of Particles in Suspension*. Surface and Colloid Science, Volume 11 , pp 121-182, Plenum Press, 1979 (edited by R.J. Good and R.R. Stromberg)

James R.O. and Parks G.A. *Characterisation of Aqueous Colloids by Their Electrical Double Layer and Intrinsic Surface Chemical Properties*. Surface and Colloid Science, Volume 12 , pp119-208, Plenum Press, 1982 (edited by E. Matijevic)

Jameson G.J. *Bubbles in motion*. Trans Instn Chem Engrs. Vol.71, part A, pp587-594, November 1993.

Jameson G.J. *Physics and hydrodynamics of bubbles*. In 'The scientific basis of flotation'. Nato advanced study series, Sijthoff and Noordhoff, Alphen aan den Rijn, The Netherlands 1978. (ed Ives K.J.)

Janssens J.G. and Buekens A. *Assessment of process selection for particle removal in surface water treatment*. Journal of water SRT-AQUA. Vol.42, No.5, pp279-286, 1993.

Jefferson B.; Ward A.S. and Stenhouse J.I.T. *Thermo-Agglomeration of clay*. Proc. IChemE. Nottingham, 1997 (*in press*)

Jefferson B.; Ward A.S.; Stenhouse J.I.T. and Petirakasakul A. *Dissolved air flotation as an Hetro-Coagulation process*. Proc IChemE. Nottingham, 1997 (*in press*)

Jefferson B.; Ward A.S.; Stenhouse J.I.T. and Ponting J. *Size distribution and zeta potential effects in dissolved air flotation*. Proc IChemE. Leeds, pp286-288. 1996

Jeffersons B.; Ward A.S. and Stenhouse J.I.T. *The role of zeta potential in dissolved air flotation*. Third UK colloid and surface science student meeting, Hull, 1995

Jefferson I. and Smalley I. *Six definable particle types in engineering soils and their participation in collapse events: Proposals and discussions*. Civil and building engineering department, Loughborough university of Technology. (to be published)

Jefferson I. *Temperature effects on clay soils*. PhD thesis. Loughborough Univeristy, Loughborough Leics, LE11 3TU. 1993

Jepson W.B. *Kaolins: their properties and uses*. Phil. Trans. R. Soc. Lond.A. Vol.311, pp411-432, 1984.

Jiang Z.W. and Holtham P.N. *Theoretical model of collision between particles and bubbles in flotation*. Trans. Instn. Min. Metall. (Sect.C: Mineral Process. Extr. Metall.) Vol.95, December 1986, ppC187-C194.

Johnson P.N. and Amirtharajah. *Ferric Chloride and Alum as single and dual coagulants*. J. AWWA. May 1983

Jones A.D. and Hall A.C. *Removal of Metal ions from Aqueous Solution by Dissolved Air Flotation*. Filtration and Separation, pp386-388, Sep/Oct 1981.

Jowett A. *Formation and disruption of bubble-particle aggregates in flotation*. In "Fine particle processing volume 1". American institute of mining, metallurgical and petroleum engineers inc. New York, New York, 1980.

Kalman K.S. and Ratcliff G.A. *Precipitate flotation- A preliminary study of the underlying mechanisms*. The Canadian journal of Chemical Engineering. , Vol.49, October 1971.

Kitchener J.A. and Gochin R.J. *The Mechanism of dissolved air flotation for potable water: Basic analysis and a proposal*. Water Res. Vol.15, pp585-590, 1981.

Kitchener J.A. *The froth flotation process: Past, present and future in brief*. In 'The scientific basis of flotation'. Nato advanced study series, Sijthoff and Noordhoff, Alphen aan den Rijn, The Netherlands 1978. (ed Ives K.J.)

Knapp R.T. *Cavitation*. McGraw Hill inc., London, 1970

Kumar R and Kuloor N.R. *The formation of bubbles and drops*. Advances in Chemical Engineering. Vol.8, pp256-377, 1970.

Kubota K. and Jameson G.J. *A study of the Electrophoretic Mobility of a very small inert gas bubble suspended in aqueous inorganic electrolyte and cationic surfactant solutions*. Journal of Chemical Engineering of Japan, Vol26, No.1, pp7-12, 1993.

Kubota K.; Harima T. and Hayashi S. *Removal of Fine Particles from Aqueous Medium by Flotation of Sodium Dodecylbenzenesulfonate-Barium Sulfate System.* The Canadian Journal of Chemical Engineering, Vol.68, pp608-6-1, 1990

Kwabara S. The forces experienced by randomly distributed parallel circular cylinders or spheres in viscous flow at small Reynolds numbers. *Journal of the physical society*

Langerberg D.E. and Jameson G.J. *The coexistence of the froth and liquid phases in a flotation column.* Chem Eng Sci. Vol.47, No.17, pp4345-4355, 1992.

Laskowski J. *Particle-bubble attachment in flotation.* Minerals science engineering. Vol.6, No.4, pp223-235, October 1974.

Lay M., Wu M. and Huang C. *Study of the zeta potential of Fe(O)OH colloids.* J. Mat Sci. Vol.30, pp5473-5478, 1995.

Lee C.H.; Erickson L.E.; Glasgow L.A. *Bubble breakup and coalescence in turbulent gas-liquid dispersions.* Chem Engng Commun. Vol.59, pp65-84, 1987.

Leininger K.V. *Discussion on paper.* J. Water Pollut Control Fed, Vol.51, No.5, pp1068, 1979.

Lin I.J. and Somasundaran P. *Free energy changes on transfer of surface active agents between various colloidal and interfacial states.* J. Colloid and Interface Science. Vol 37, No. 4, Dec 1971.

Lipták B.G. *Flotation and foaming.* Chp5.9 in "Environmental engineers' handbook volume 1: Water pollution first edition". Chilton book company, Radnor, 1974.

Lu S. *Hydrophobic interaction in flocculation and flotation 3. Role of hydrophobic interaction in particle-bubble attachment.* Colloids and Surfaces, 57 pp73-81, 1991

Lucassen-Reynders E.H. and Lucassen J. *Thin films, contact angles, wetting.* In 'The scientific basis of flotation'. Nato advanced study series, Sijthoff and Noordhoff, Alphen aan den Rijn, The Netherlands 1978. (ed Ives K.J.)

Lundgren H. *Theory and practice of dissolved air flotation*. Filtration and separation. January/February 1976.

MacEwan D.M.C. *Short range Electrical Forces between Charged Colloid Particles*. Nature, Vol.174, No.4418, pp39-40. 1954

Malley J.P. and Edzwald J. *Laboratory comparison of DAF with conventional treatment*. Research and technology. pp56-61, September 1991.

Malley J.P. *A fundamental study of dissolved air flotation for treatment of low turbidity waters containing natural organic matter*. PhD thesis, The University of Massachusetts, Massachusetts, USA, September 1988.

Mangravite F.J.; Buzzell T.D.; Cassell A.; Matijevic E. and Saxton G.B. *Removal of humic acid by coagulation and microflotation*. J. AWWA. pp88-94, February 1975. [M4]

Matijevic E. *Interactions in mixed colloidal systems (part1)*. Pure and Applied Chemistry. Vol.53, pp2177-2178, 1981.

Mavros P.; Lazardis N.K.; Matis K.A. and Staudis G.A. *A study of flotation column performance of fine particles*. Sep. Sci. Technol. Vol.25, No.182, pp155-170, 1990.

Miller N.P.; Berg J.C. and O'Brien R.W. *The electrophoretic mobility of a porous aggregate*. J. Colloid and Interface Science. Vol.153, No.1, pp237-243, 1992.

Montgomery J.M. *Water treatment principles and design*. Wiley inter science publications. John Wiley and sons, Chichester, 1985.

Neis U. and Kiefhaber P. *Differences between particle flotation and floc flotation*. In "Fine particle processing volume 1". American institute of mining, metallurgical and petroleum engineers inc. New York, New York, 1980.

Nguyen-Van A. *The collision between fine particles and single air bubbles in flotation*. J. Colloid and Interface Science. Vol.162, pp123-128, 1994.

Niak D. *Effect of Temperature and Pore Fluid on Shear Characteristic of Clay*. International Symposium on Environmental Geotechnology, pp382-390. 1980

Nilsson U.; Jönsson B. and Wennerström H. *Cationic amphiphilic layers. A monte carlo simulation study of surface forces.* Journal of physical chemistry. Vol.97, pp5654-5600, 1993.

Nonaka M. *A wastewater treatment system applying aeration cavitation flotation mechanism.* Separation science and technology. Vol 21, No.5, pp457-474, 1986.

Okada K.; Akagi Y.; Kogure M. and Yoshioka N. *Effect on surface charges of bubbles and fine particles on the air flotation process.* The Canadian journal of Chemical Engineering., Vol. 68, pp 393-399, 1990.

Okada K. and Akagi Y. *Method and apparatus to measure the zeta potential of bubbles.* Journal of Chemical Engineering of Japan. Vol.20, No.1, pp11-15, 1987.

Okada K.; Akagi Y. and Yoshioka N. *Effect of Zeta Potentials of Oil Droplets and Bubbles on Flotation of Oil-in-Water Mixtures.* The Canadian Journal of Chemical Engineering, Vol. 66, pp276-281, 1988.

Okada K.; Akagi Y.; Kogure M. and Yoshioka N. *Analysis of particle trajectories of small particles in flotation when the particles and bubbles are both charged.* The Canadian Journal of Chemical Engineering. Vol.68, pp614-621, 1992.

van Olphen H. *An introduction to clay colloid chemistry.* Interscience publishers, John Wiley and sons. London, 1963.

van Olphen H. *Dispersion and Flocculation,* in General Principles of Colloidal Stability in 'Chemistry of Clays and Clay Minerals' Longman Scientific and Technical, Harlow, Essex, CM20 2JE. (Edited by A.C.D. Newman) 1987

Oolman T.O. and Blanch H.W. *Bubble coalescence in stagnant liquids.* Chem Engng Commun. Vol.43, pp237-261, 1986.

Packham R.F. *Some studies of the coagulation of dispersed clays with hydrolyzing salts.* Journal of Colloid Science, 20, pp81-92, 1965

Packham R.F. and Richards W.N. *Water clarification by flotation 3: Treatment of Thames water in a pilot scale flotation plant*. Technical report TR2, Water research centre, Stevenage laboratory, Elderway, Stevenage, Herts., SG1 1TH, February 1975.

Packham R.F. and Richards W.N. *Water clarification by flotation 1: A survey of the literature*. Technical report TP87, Water research association, Medmenham, Marlow, Bucks., SL7 2HD, November 1972.

Packham R.F. and Richards W.N. *Water clarification by flotation 2: A laboratory study of the feasibility of floc flotation*. Technical report TP88, Water research association, Medmenham, Marlow, Bucks., SL7 2HD, November 1972.

Packham R.F. and Richards W.N. *Water clarification by flotation 1: A multiple stirrer unit for flotation tests*. Technical memorandum TM121, Water research association, Medmenham, Marlow, Bucks., SL7 2HD, March 1976.

Painter A. and Thomasson P.G. Improvements in means for dispensing liquids particularly beverages containing gases in solution. Patent specification no.51934/66, November 1966.

Pashley R.M. and Israelachvili J.N. *DLVO and Hydration forces between Mica surfaces in Mg^{2+} , Ca^{2+} , Sr^{2+} , and Ba^{2+} Chloride solutions*. J. Colloid and Interface Science. Vol 97, No. 2. February 1984.

Pashley R.M.; Mcguiggan P.M. ; Ninham B.W. and Fennell Evans D. *Attractive forces between uncharged hydrophobic surfaces: Direct measurements in aqueous solution*. Science. September 1985.

Pietschker D.A. *Practical application of Zeta Potential*. Tappi Journal, Vol.68, No.4, pp84-86. 1985

Prince M.J. and Blanch H.W. *Transition electrolyte concentrations for bubble coalescence*. Journal of the AIChE. Vol.36, No.9, pp1425-1429, September 1990a.

Prince M.J. and Blanch H.W. *Bubble coalescence and break-up in air sparged bubble columns*. Journal of the AIChE. Vol.36, No.10, pp1485-1499, October 1990b.

Pryor E.J. *Principles of froth flotation (chp17) and Flotation practice (chp18)*. In "Minerals processing (third edition)" Elsevier publishing co. ltd., London, 1965

Pugh R.J. and Yoon R.H. *Hydrophobicity and rupture of thin aqueous films*. J. Colloid Interface Science. Vol.163, pp169-176, 1994.

Rao S.R. *Surface forces in flotation*. Minerals science engineering. Vol.6, No.1, pp45-53, January 1974.

Reay D. and Ratcliff G.A. *Removal of fine particles from water by dispersed air flotation: effects of bubble size and particle size on collection efficiency*. The Canadian journal of Chemical Engineering. Vol. 51, pp178-185, 1973.

Reay D. and Ratcliff G.A. *Experimental testing of the hydrodynamic collision model of fine particle flotation*. The Canadian journal of Chemical Engineering. Vol. 53, pp481-486, 1975.

Repanas K. *A study of bubble generation and hydrodynamics in dissolved air flotation*. PhD thesis. University of Newcastle upon Tyne. 1992

Rees A.J., Rodman D.J. and Zabel T.F. Dissolved air flotation for solid/liquid separation. J. Separ. Proc. Technol. Vol.1, pp19-23, 1980.

Richards W.N. *Dissolved air flotation-Discussion*. Filtration and separation. pp624, November/December 1974.

de Rijk S.E.; van der Graff J.H.J.M. and den Blanken J.G. *Bubble size in flotation thickening*. Water Res. Vol.28, No.2, pp465-473, 1994.

Roberts K.L. *A surface chemical model for dissolved air flotation*. PhD thesis, The university of Tennessee, Knoxville, Tennessee, USA, March 1980.

Roe L.A. *Flotation of liquids and fine particles from liquids*. In "Fine particle processing volume 1". American institute of mining, metallurgical and petroleum engineers inc. New York, New York, 1980.

Rosen M.J. *Surfactant and interfacial phenomena*, second edition, John Wiley and sons, 1989

Rubin A.J.; Cassel E.A.; Henderson O.; Johnson J.D. and Lamb J.C. *Microflotation: New low gas flow rate foam separation technique for bacteria and algae.* Biotechnology and bioengineering. Vol.8, issue1, pp135-151, August 1965.

Rubin A.J. and Erickson S.F. *Effect of coagulation and restabilisation on the microflotation of illite.* Water Res. Vol.5, pp437-444, 1971.

Rubin A.J. and Blocksidge H. *Coagulation of Montmorillonite suspensions with Aluminium Sulfate.* J. AWWA. February 1979.

Rykaart E.M. and Haarhoff J. *Behaviour of air injection nozzles in dissolved air flotation.* Wat.Sci. Tech, 31, pp25-37, 1995

Sato Y.; Murakami Y.; Hirose T.; Yamamoto H. and Uryu Y. *Removal of Emulsified oil particles by dissolved air flotation.* Journal of Chemical Engineering of Japan. Vol.12, No.6, pp454-459. 1979.

Sato Y.; Murakami Y.; Hirose T.; Yamamoto H. and Uryu Y. *Removal of Emulsified oil particles by dispersed air flotation.* Journal of Chemical Engineering of Japan. Vol.13, No.5, pp385-389. 1980.

Saville D.A. *Dielectric behavior of colloidal dispersions.* Colloids and surfaces A. Vol.92, pp29-40, 1994.

Saville P.M.; White J.M.; Hawker C.J.; Wooley K.L. and Frechet J.M.J. *Dendrimer and polystyrene surfactant structure at the air-water interface.* Journal of physical chemistry. Vol.97, pp293-294, 1993.

Shaw D.J. *Introduction to Colloid and surface chemistry,* fourth edition. Butterworth-Heinemann Ltd. Linacre house, Jordan Hill, Oxford, OX2 8DP, 1992.

Sirios L.L. and Millar G. *Method to study surface electrical characteristics on a single bubble.* Canadian Metallurgical Quarterly. Vol12, No.3, pp281-284, 1973.

Smith R.W. and Narimatsu Y. *Electrokinetic Behaviour of Kaolinite in Surfactant solutions as measured by both the Microelectrophoresis and streaming Potential Methods.* Minerals Engineering, Vol.6, No.7, pp753-763, 1993.

Somasundaran P. *Interfacial chemistry of particulate flotation*. AICHE symposium series. Advanced interfacial phenomena. No.150, Vol.171, pp176-182.

Stebe K.J. and Maldarelli C. *Remobilizing surfactant retarded fluid particle interfaces II. Controlling the surface mobility at interfaces of solutions containing surface active components*. J. Colloid Interface Science. Vol.163, pp177-189, 1994.

Stevenson D.G. *Flotation*. Chapter 3 in "Solid/liquid separation equipment scale up" edition II. ed by Bryant E.F. Uplands press ltd, 1 Katherine st, Croydon, CR91LB. 1986

Stevenson D.G. *Gravity separation equipment*. Chapter 4 in "Solid/liquid separation equipment scale up" edition II. ed by Bryant E.F. Uplands press ltd, 1 Katherine st, Croydon, CR91LB. 1994

Swartzen-Allen S.L. and Matijevic E. *Surface and Colloid Chemistry of Clays*. Chemical Reviews, Vol 75, No. 3. 1974.

Szatkowski M. and Freyberger W.L. *Model describing mechanism of the flotation process*. Trans. Instn. Min. Metall. (Sect.C: Mineral Process. Extr. Metall.). Vol.94, September 1985, ppC661-C670.

Szatkowski M. and Freyberger W.L. *Kinetics of flotation with fine bubbles*. Trans. Instn. Min. Metall. (Sect.C: Mineral Process. Extr. Metall.). Vol.94, September 1985, ppC129-C135.

Szatkowski M. *Some comments on Flotation Kinetics*. Chem Eng Sci. Vol.42, No.10, pp2475-2478, 1987.

Takahashi T.; Miyahara T. and Mochizuki H. *Fundamental study of bubble formation in dissolved air pressure flotation*. Journal of Chemical Engineering of Japan..., pp275-280 . 1979a

Takahashi T.; Miyahara T and Nishizaki Y. *Separation of Oily Water by Bubble Column*. Journal of Chemical Engineering of Japan. Vol.12, No.5, 1979.

Tewari S.N. and Biswas A.K. *Flotation kinetics for calcite in a semi batch system.* J Appl Chem. Vol.19, pp173-177, June 1969.

Trahar W.J. and Warren L.J. *The flotability of very fine particles-A review.* International journal of mineral processing. Vol.3, pp103-131, 1976.

Travis J. *Helping premature lungs breathe easier.* Science. Vol.261, pp426, July 1993

Travers S.M. and Lovett D.A. *Pressure flotation of abattoir waste waters using carbon dioxide.* Water Res. Vol.19, No.12, pp1479-1482, 1985.

Tucker A.S. and Ward C.A. *Critical state of bubbles in liquid-gas solutions.* Journal of applied physics. Vol.46, no.11, pp4801-4808, November 1975.

Urban M.R. *Aspects of bubble formation in dissolved air flotation.* PhD thesis, University of London, Imperial college of science and technology, London, SW7, April 1980

Usui S. and Sasaki H. *Zeta potential measurements of bubbles in aqueous surfactant solutions.* J. Colloid and Interface Science. Vol65, No.1, pp36-44, 1978.

Usui S.; Sasaki H. and Matsukawa H. *The dependence of zeta potential on bubble size as determined by the dorn effect.* J. Colloid and Interface Science. Vol.81, No.1, pp80-84, 1980.

Vera P.; Gallardo V.; Salcedo J. and Delgado A.V. *Colloidal stability of a pharmaceutical latex: Experimental determinations and theoretical predictions.* J. Colloid and Interface Science. 177, No. 2, pp 553-560, Feb 1996.

Vesilind P.A. *The influence of Stirring in the Thickening of biological sludge.* PhD. University of North Carolina

Vrablik E.R. *Fundamental principles of dissolved air flotation of industrial wastes.* Industrial wastes conference, Purdue university, pp743-779, 1959. [V1]

Ward A.S. *Dissolved air flotation for water and wastewater treatment*. Lecture notes, Department of chemical engineering, Loughborough University of Technology, Loughborough, Leics. LE11 3TU.

Ward A.S. *Dissolved air flotation for water and wastewater treatment*. Trans IChemE. Vol.70, part B, November 1992.

Ward A.S. *Coagulation and Flocculation*. Lecture notes, Department of chemical engineering, Loughborough University of Technology, Loughborough, Leics. LE11 3TU.

Ward C.A.; Balakarishran A; Hopper F.C. *On the thermodynamics of nucleation in weak gas-liquid solutions*. TransASME Basic. December 1970, pp695-704.

Weber M.E. and Paddock D. *Interception and Gravitational collision efficiencies for single collectors at intermediate Reynolds numbers*. J. Colloid and Interface Science. Vol.94, No.2, pp328-335, 1982.

Wedlock D.J. *Controlled particle, droplet and bubble formation*. Oxford-Butterworth, 1994

Wiersema P.H.; Loeb A.L. and Overbeek J.TH.G. *Calculation of the Electrophoretic Mobility of a spherical Colloid Particle*. J. Colloid and Interface Science, Vol.22, pp78-99, 1966.

Williams D.J.A. and Williams K.P. *Electrophoresis and Zeta Potential of Kaolinite*. J. Colloid and Interface Science. Vol 65. No. 1. June 1978

Wnek W.J. *An Analysis of the dependance of the Zeta Potential and Surface Charge on Surfactant Concentration, Ionic strength and pH*. J. Colloid and Interface Science, Vol.60, No.2, pp361-375, 1977.

Wood R.F. and Dick R.I. *Factors influencing batch flotation tests*. J. Water Pollut Control Fed, Vol.51, No.5, pp1068. 1973

Vera P.; Gallardo V.; Salcedo J. and Delgado A.V. *Colloidal stability of a pharmaceutical latex: Experimental determinations and theoretical predictions*. J. Colloid and Interface Science. Vol.177, pp553-550, 1996.

Yaminsky V.V.; Yushchenko V.S.; Amelina E.A. and Shchukin E.D. *Cavity formation due to a contact between particles in a nonwetting liquid.* J. Colloid and Interface Science. Vol 96, No. 2, December 1983.

Yordan H.J.L. *Studies on the stability of thin films in bubble particle adhesion.* PhD thesis. Virginia polytechnic institute and state university, Blacksburg, Virginia. February 1989.

Yoon⁶⁶ R. and Yordan J.L. *Zeta-potential measurements on microbubbles generated using various surfactants.* J. Colloid and Interface Science. Vol 113, No.2 pp430-438, 1986.

Zabel T. *The advantages of dissolved air flotation for water treatment.* J. AWWA. Vol.77, pp42, February 1975.

Zabel T. *Flotation in water treatment.* In 'The scientific basis of flotation'. Nato advanced study series, Sijthoff and Noordhoff, Alphen aan den Rijn, The Netherlands 1978. (ed Ives K.J.)

Zhu S.; Pelton R.H.; Ajersch M.; Towers M. and Baird H.I. *Measurement of air bubble size using densitometer.* The Canadian journal of Chemical Engineering. Vol. 71, pp269-277, April 1993.

APPENDIX A

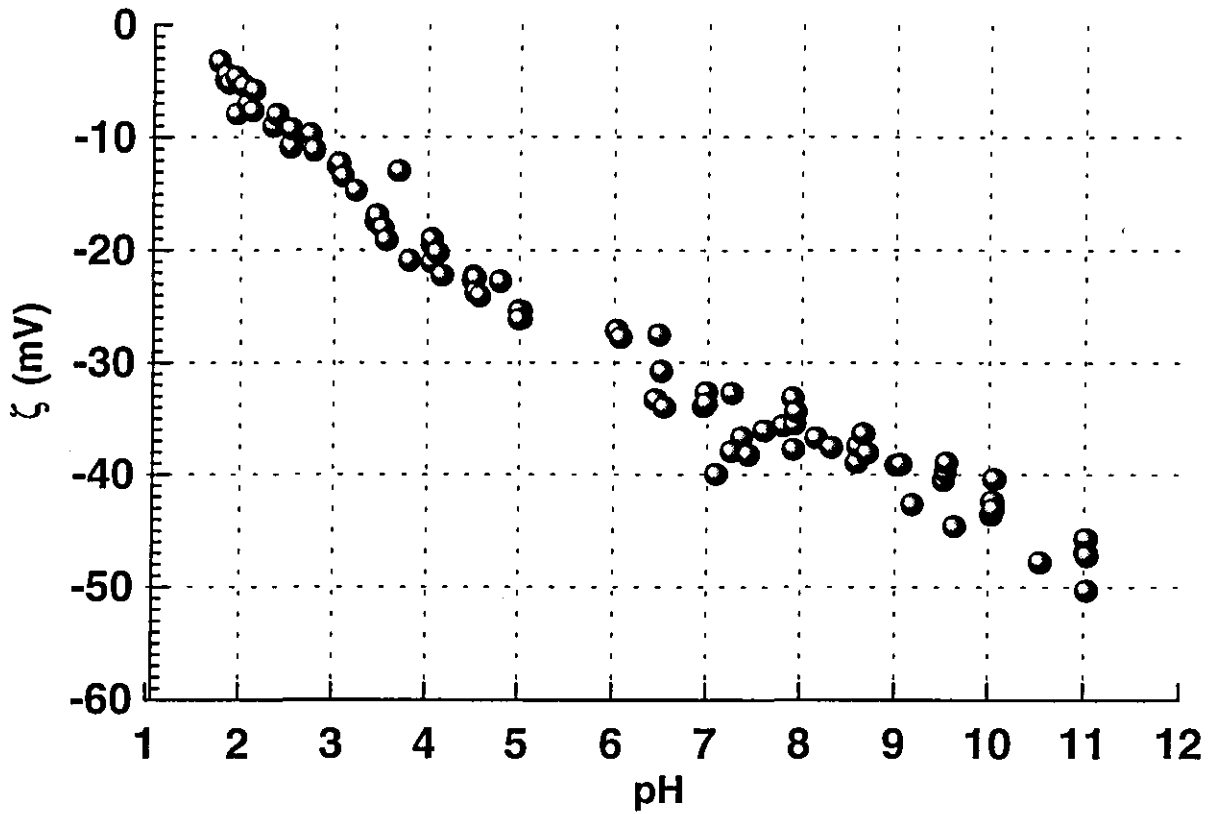


Figure A1: Zeta Potential vs pH for dispersed Kaolin particles in distilled water

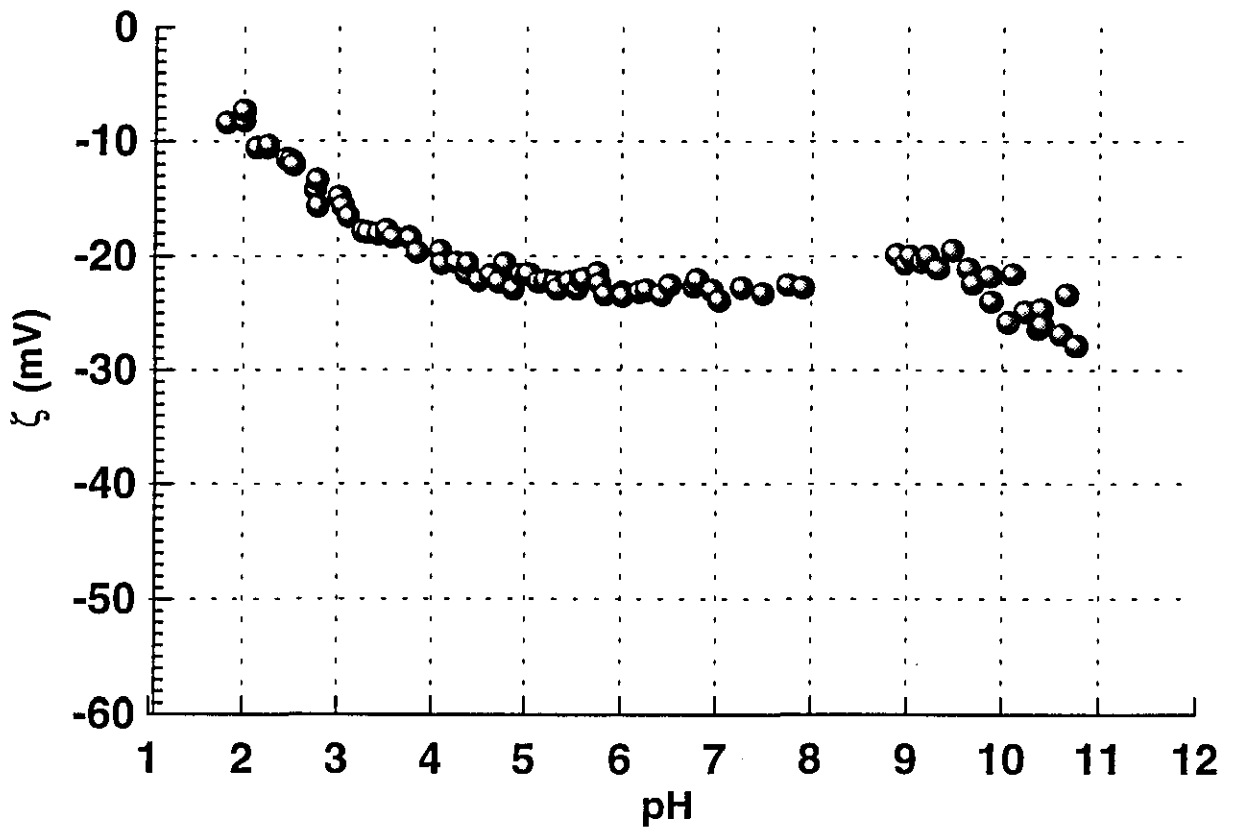


Figure A.2: Zeta Potential vs pH for dispersed Kaolin particles in tap water

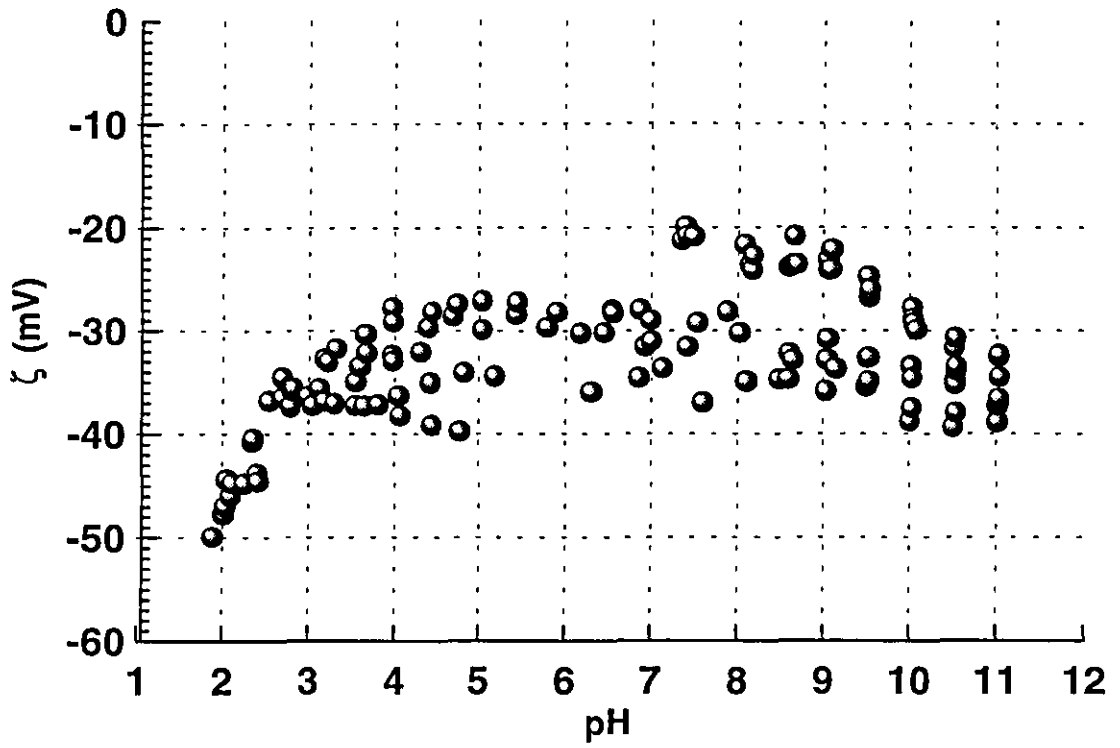


Figure A.3: Zeta potential vs pH for dispersed Wyoming Bentonite particles in distilled water

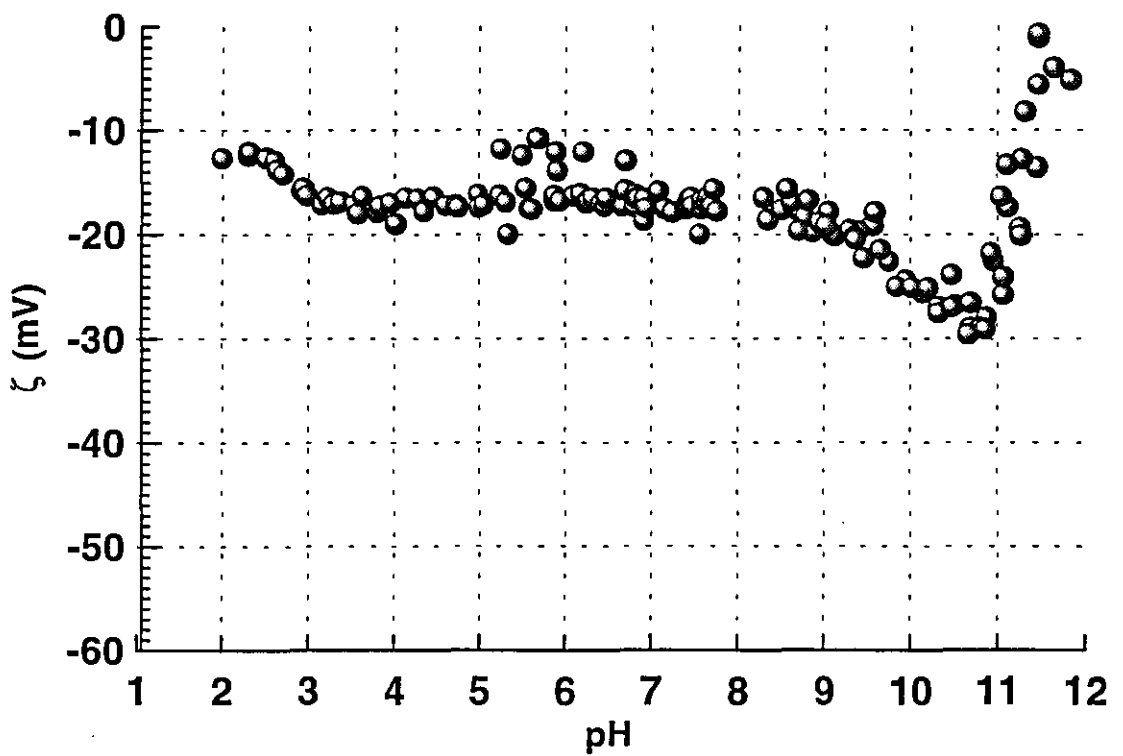


Figure A.4: Zeta Potential vs pH for dispersed Wyoming Bentonite particles in tap water

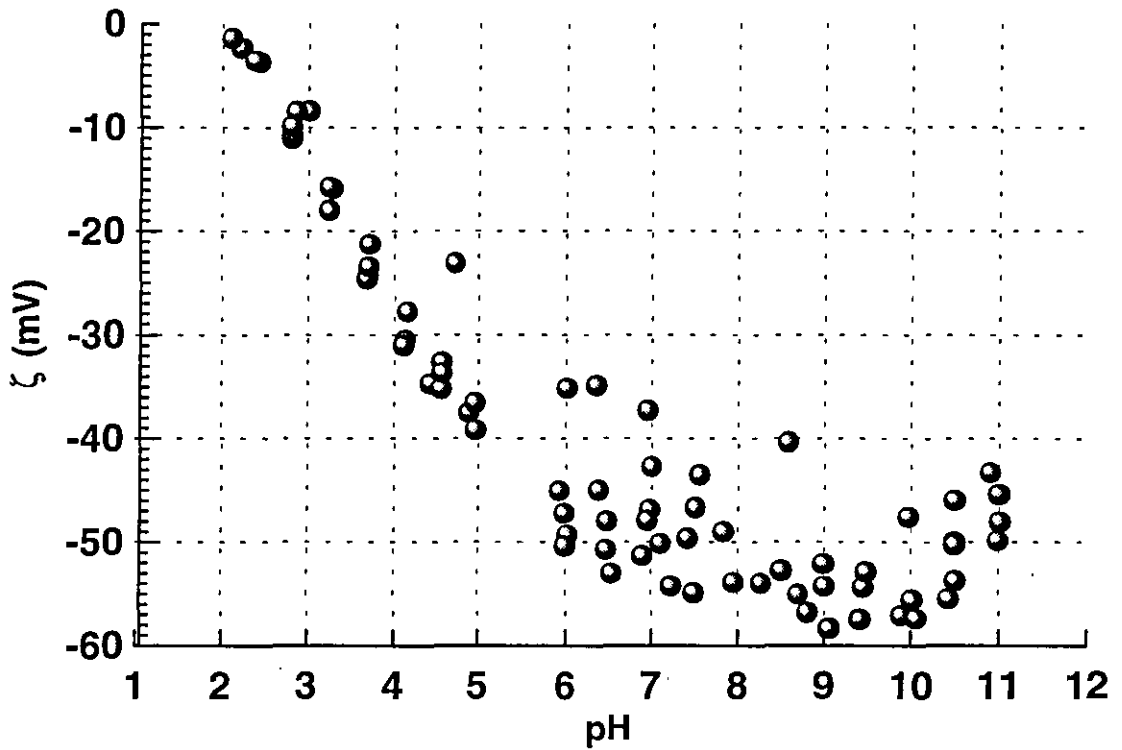


Figure A.5: Zeta potential vs pH for dispersed Latex particles in distilled water

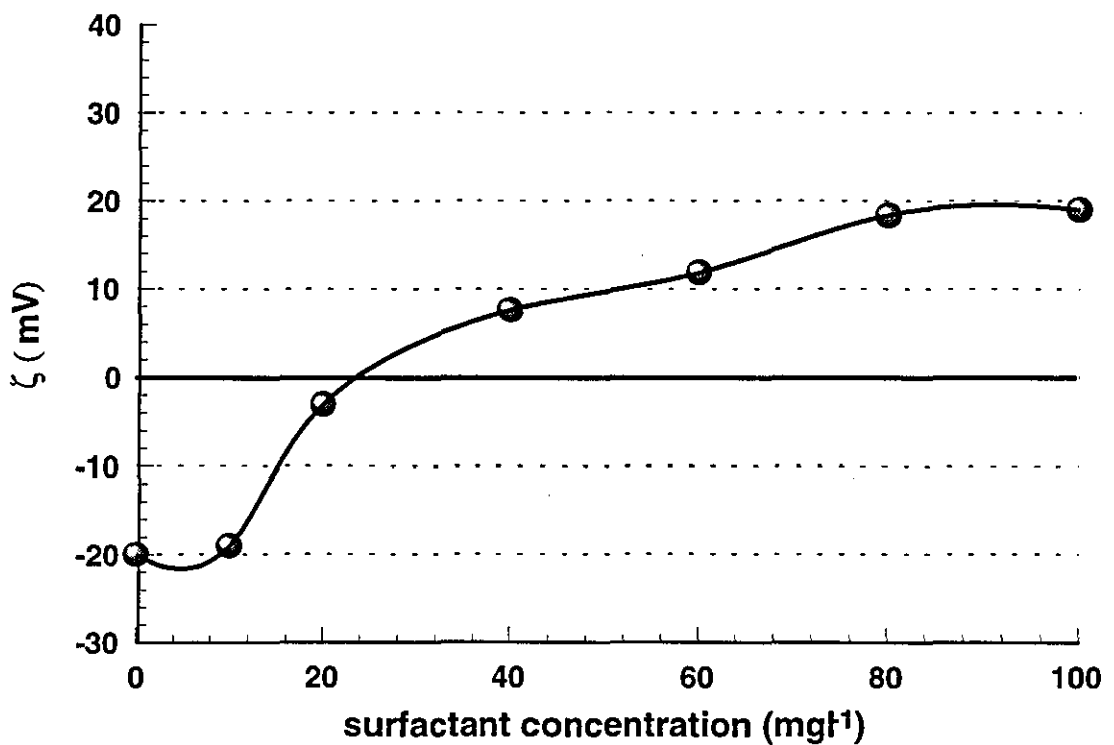


Figure A.6: Zeta Potential vs concentration of Dodecyltrimethylammoniumbromide on dispersed Kaolin particles in distilled water

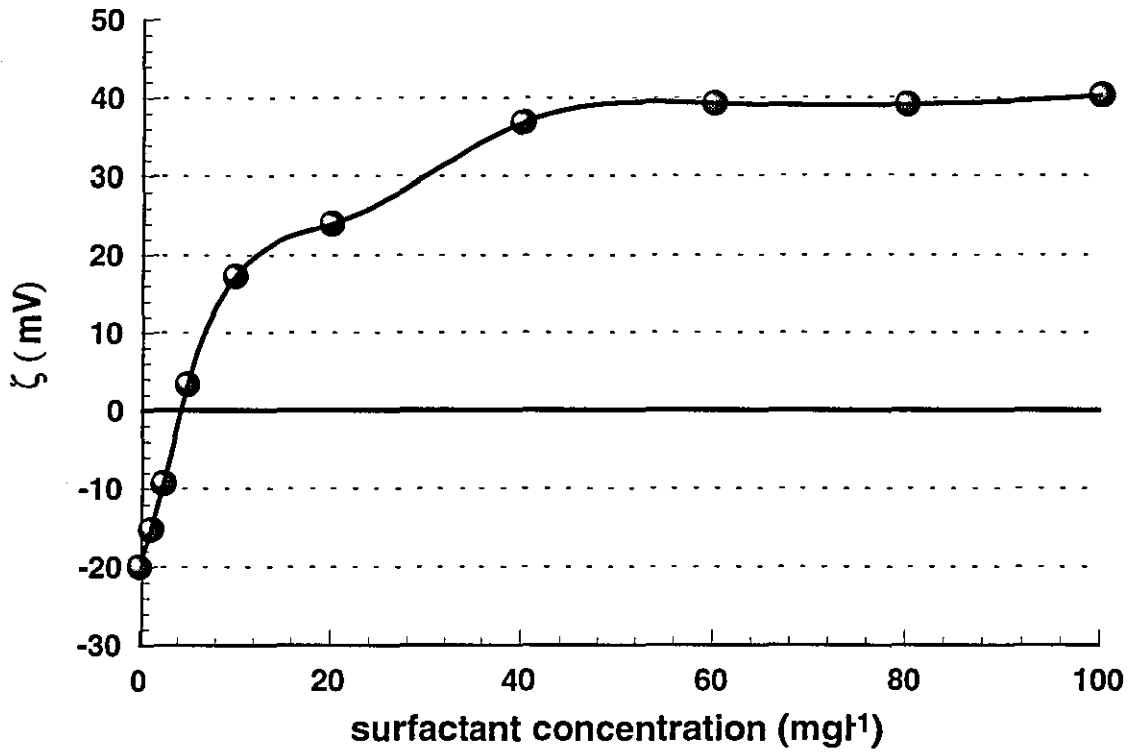


Figure A.7: Zeta Potential vs concentration of Tetradecyltrimethylammoniumbromide on dispersed Kaolin particles in distilled water

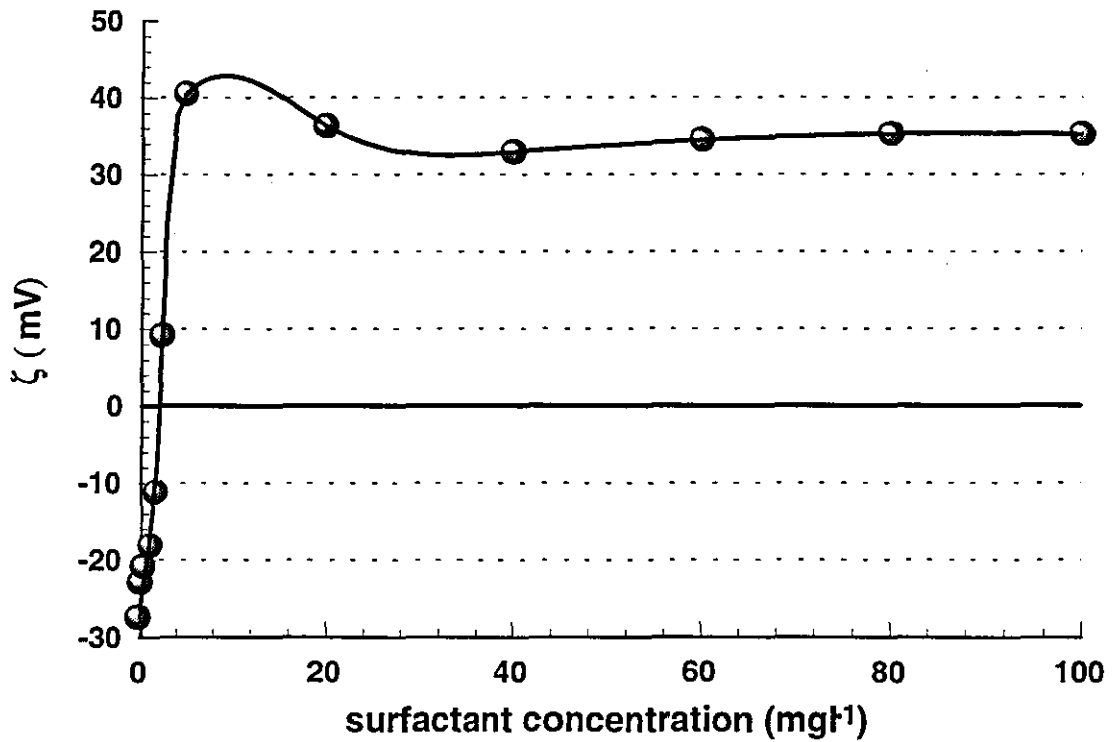


Figure A.8: Zeta Potential vs concentration of Hexadecyltrimethylammoniumbromide on dispersed Kaolin particles in distilled water

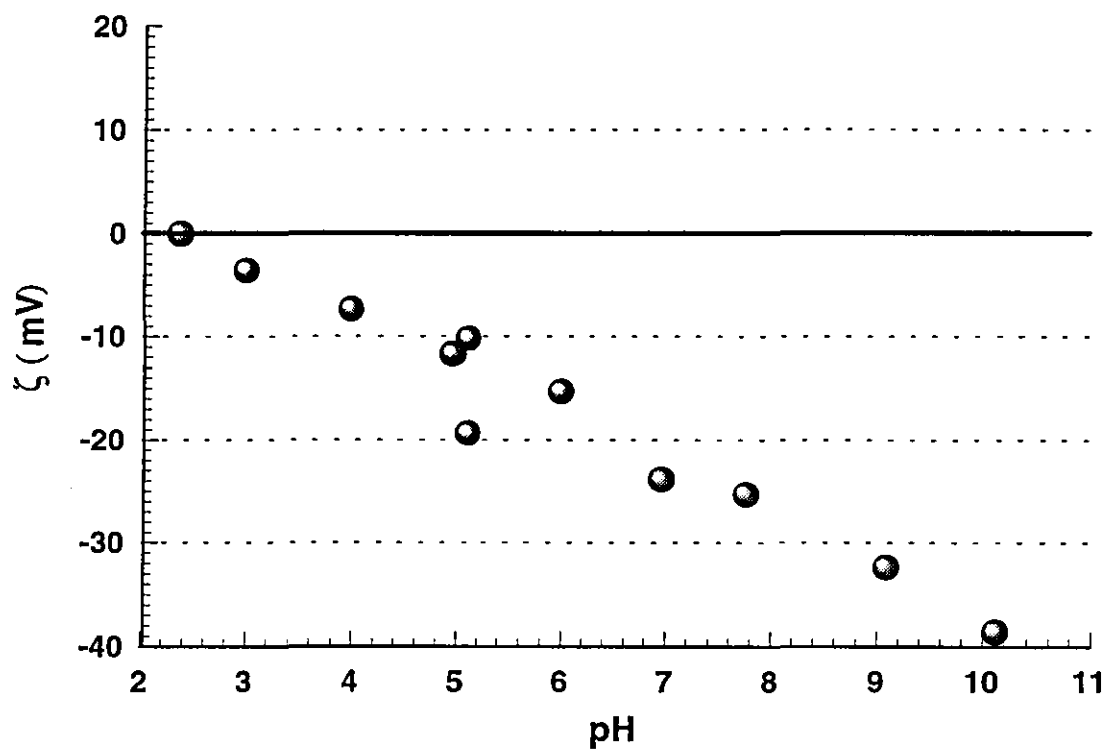


Figure A.9: Zeta Potential vs pH for dispersed Kaolin particles in 25 mgL⁻¹ solution of Dodecyltrimethylammoniumbromide

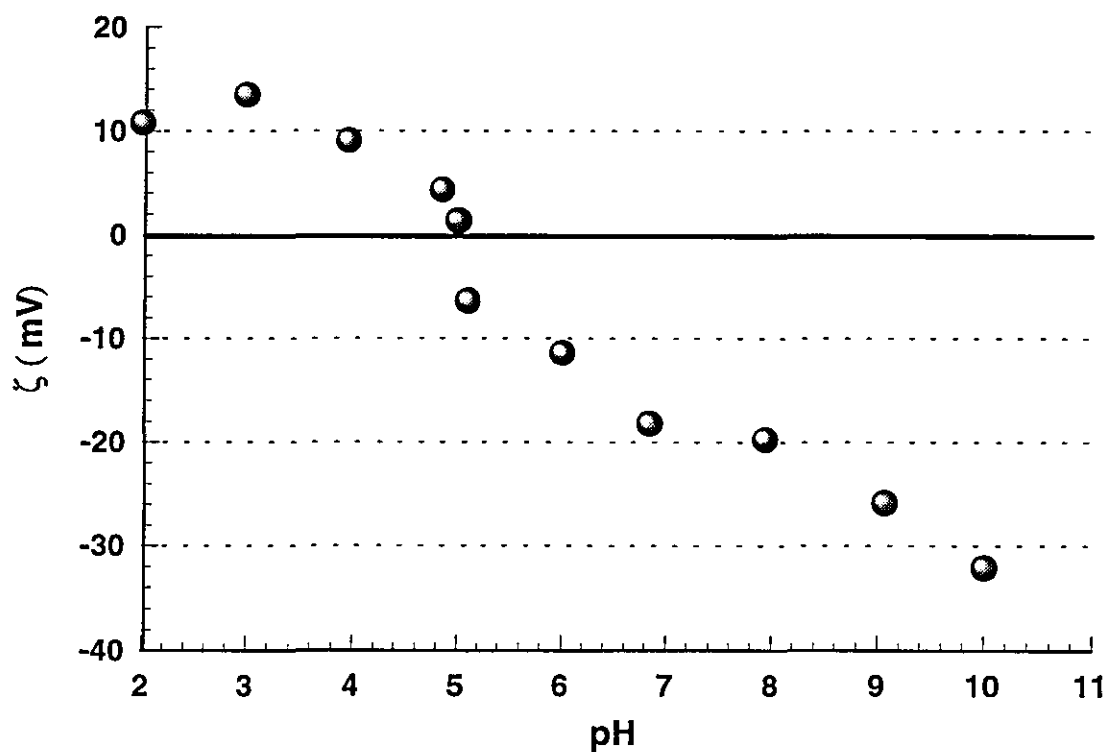


Figure A.10: Zeta Potential vs pH for dispersed Kaolin particles in 50 mgL⁻¹ solution of Dodecyltrimethylammoniumbromide

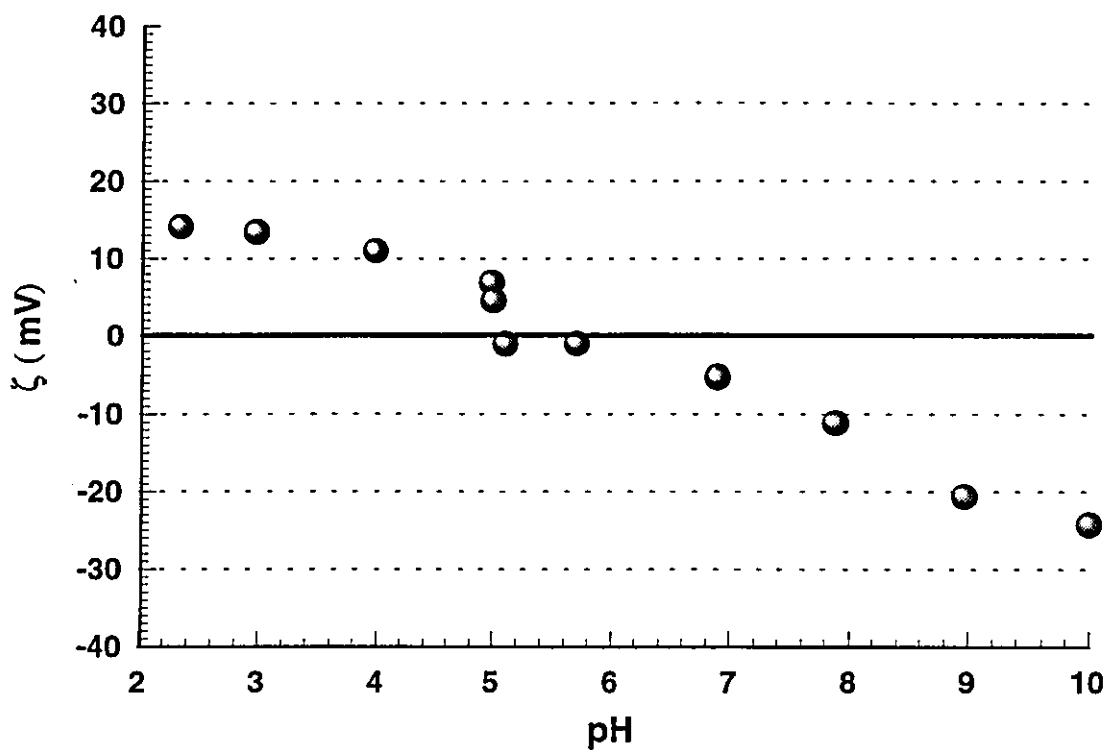


Figure A.11: Zeta Potential vs pH for dispersed Kaolin particles in 75 mgL⁻¹ solution of Dodecyltrimethylammoniumbromide

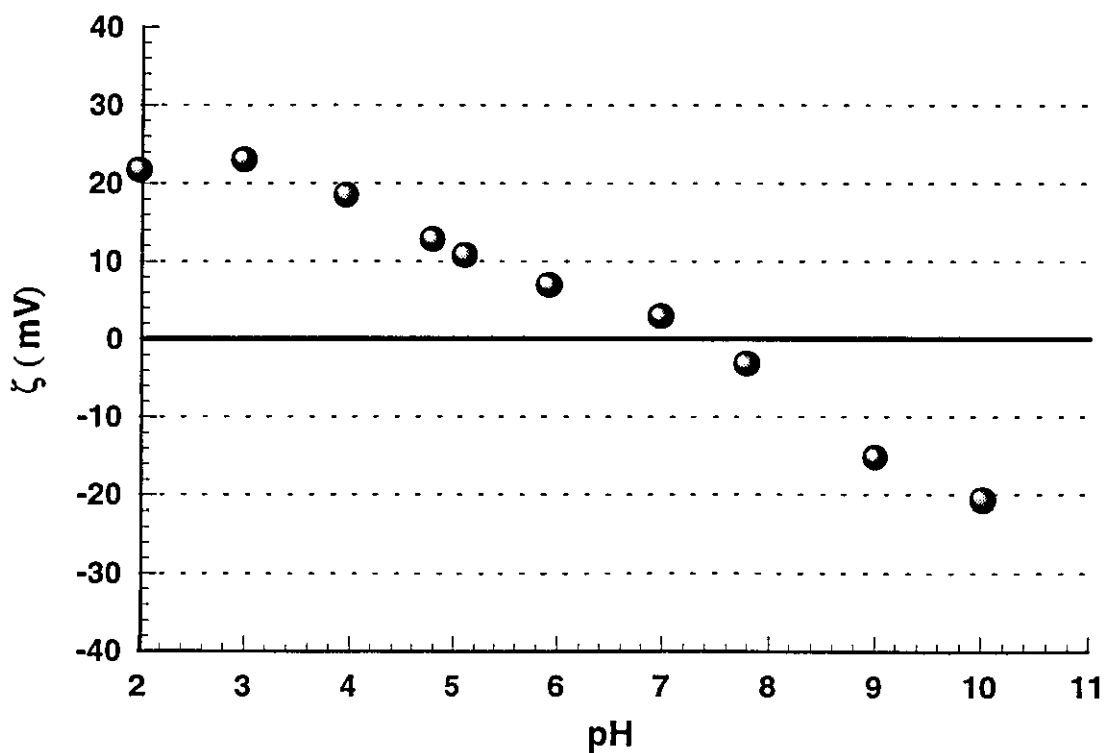


Figure A.12: Zeta Potential vs pH for dispersed Kaolin particles in 100 mgL⁻¹ solution of Dodecyltrimethylammoniumbromide

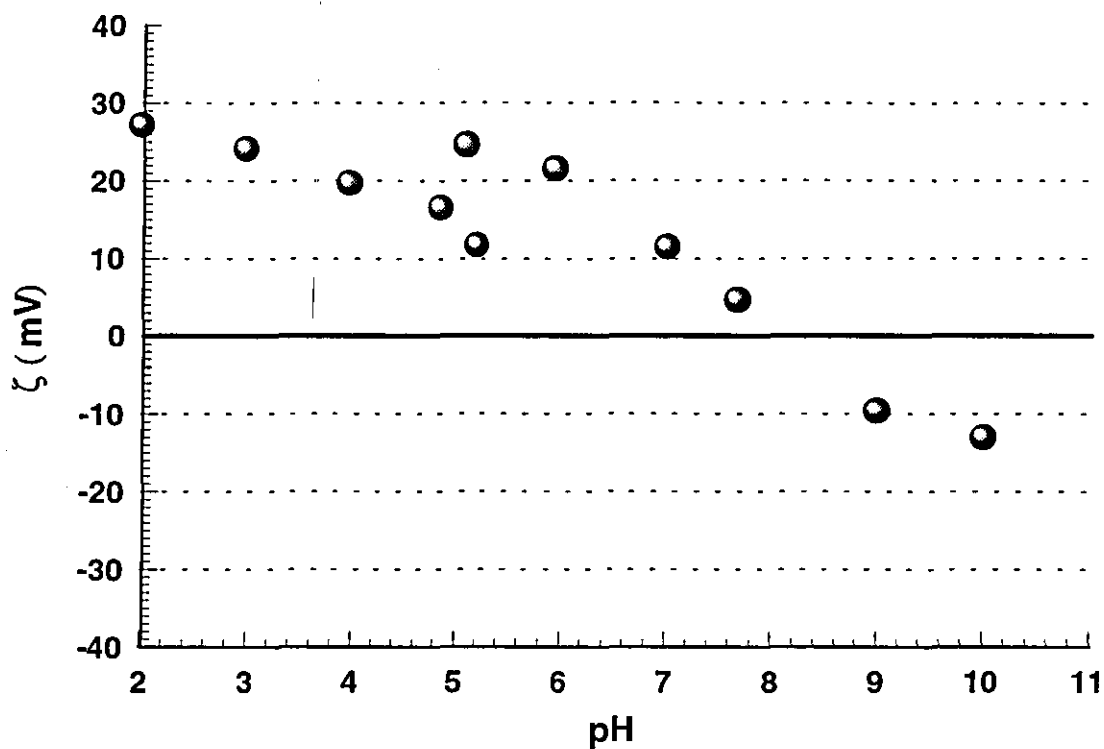


Figure A.13: Zeta Potential vs pH for dispersed Kaolin particles in 150 mgL⁻¹ solution of Dodecyltrimethylammoniumbromide

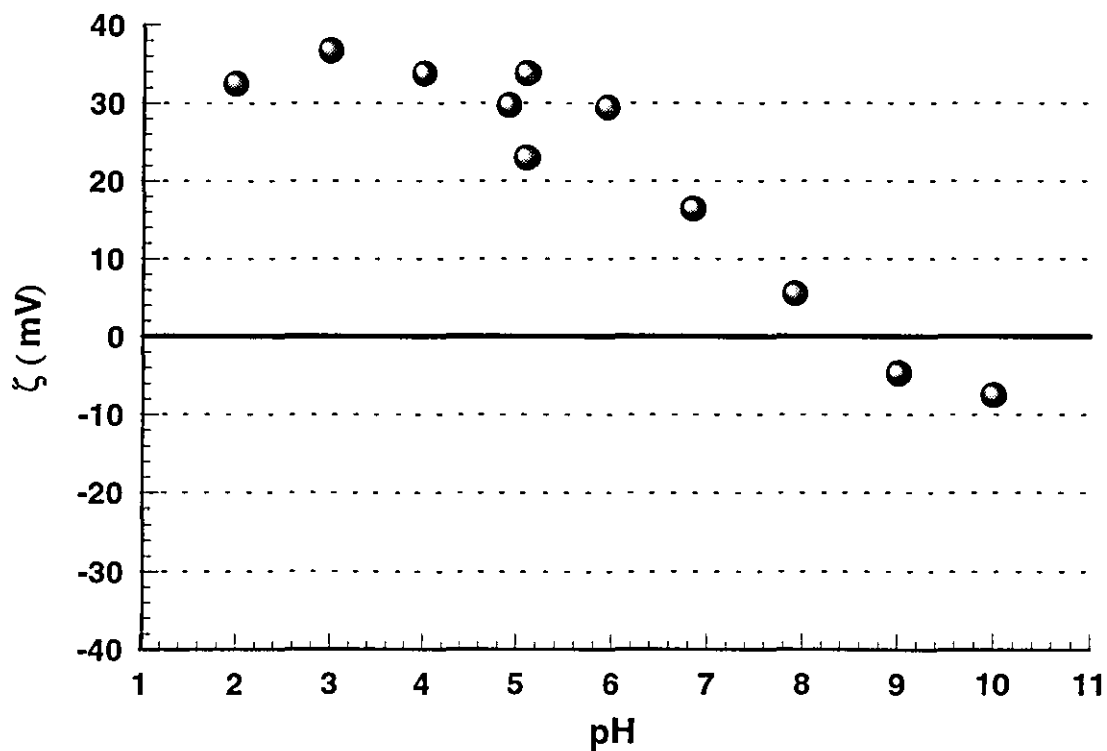


Figure A.14: Zeta Potential vs pH for dispersed Kaolin particles in 200 mgL⁻¹ solution of Dodecyltrimethylammoniumbromide

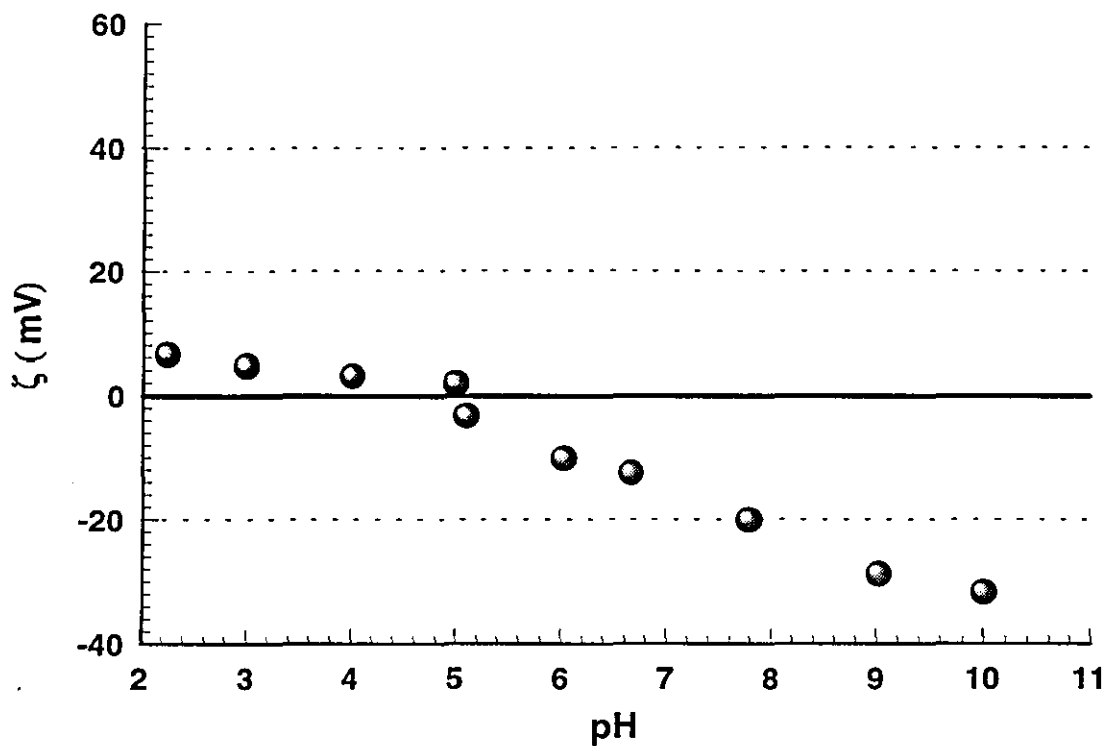


Figure A.15: Zeta Potential vs pH for dispersed Kaolin particles in 5 mgL⁻¹ solution of Tetradecyltrimethylammoniumbromide

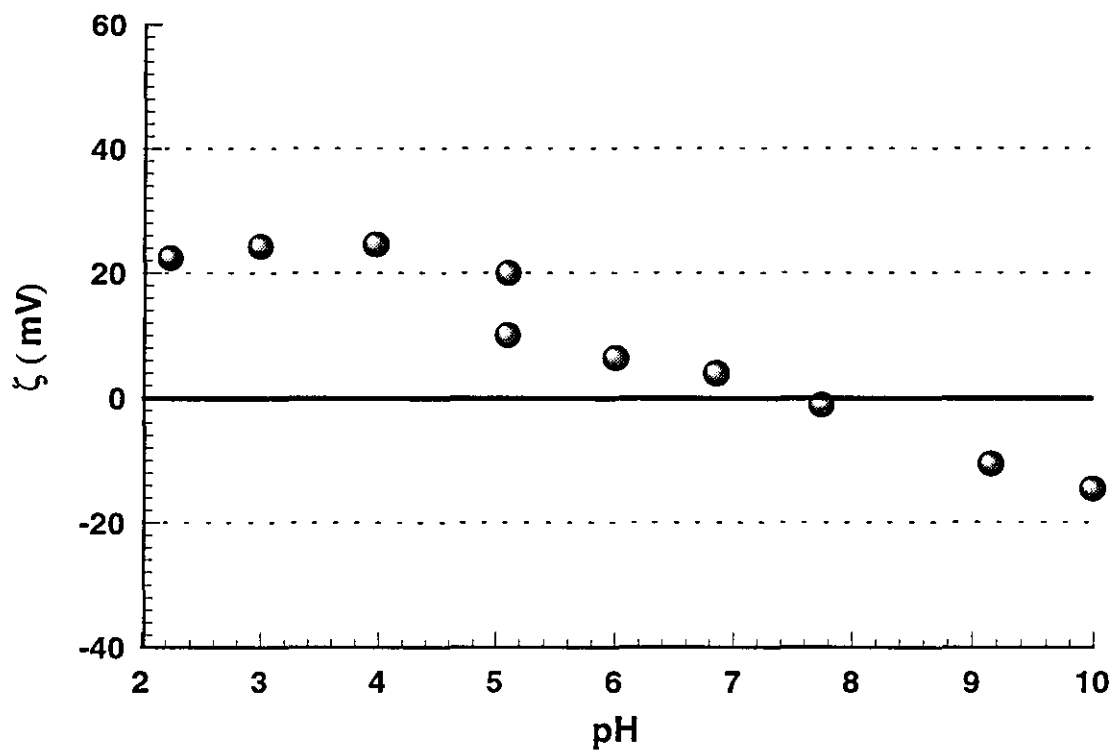


Figure A.16: Zeta Potential vs pH for dispersed Kaolin particles in 10 mgL⁻¹ solution of Tetradecyltrimethylammoniumbromide

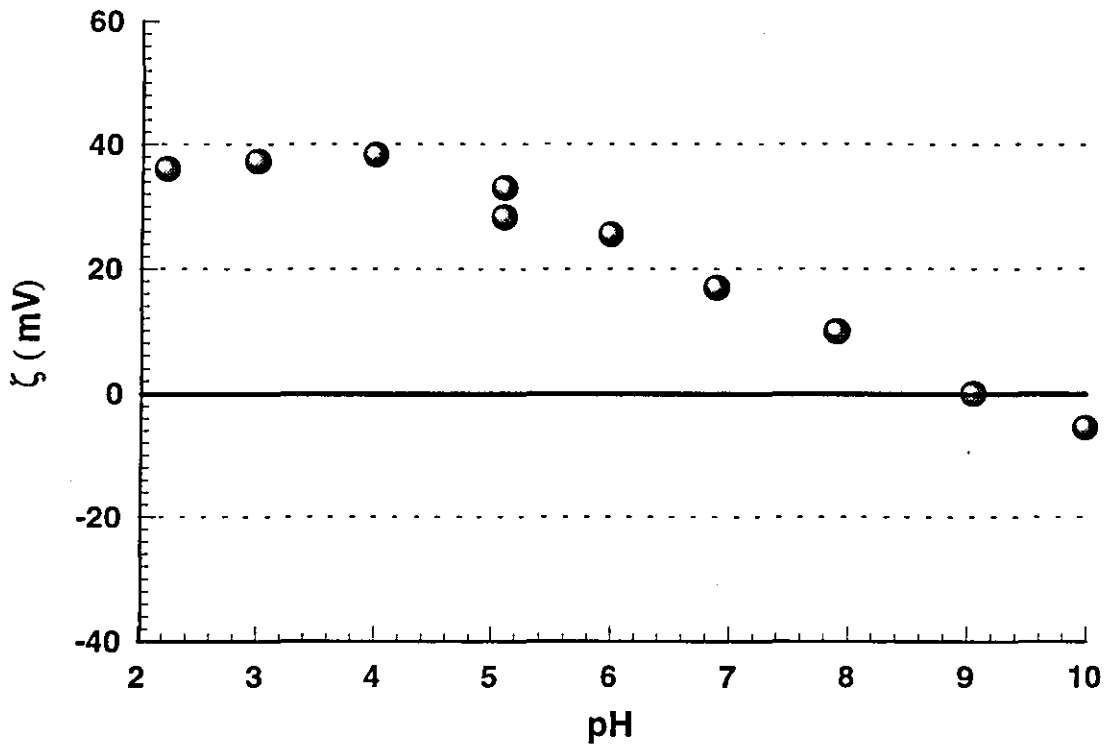


Figure A.17: Zeta Potential vs pH for dispersed Kaolin particles in 20 mgL^{-1} solution of Tetradecyltrimethylammoniumbromide

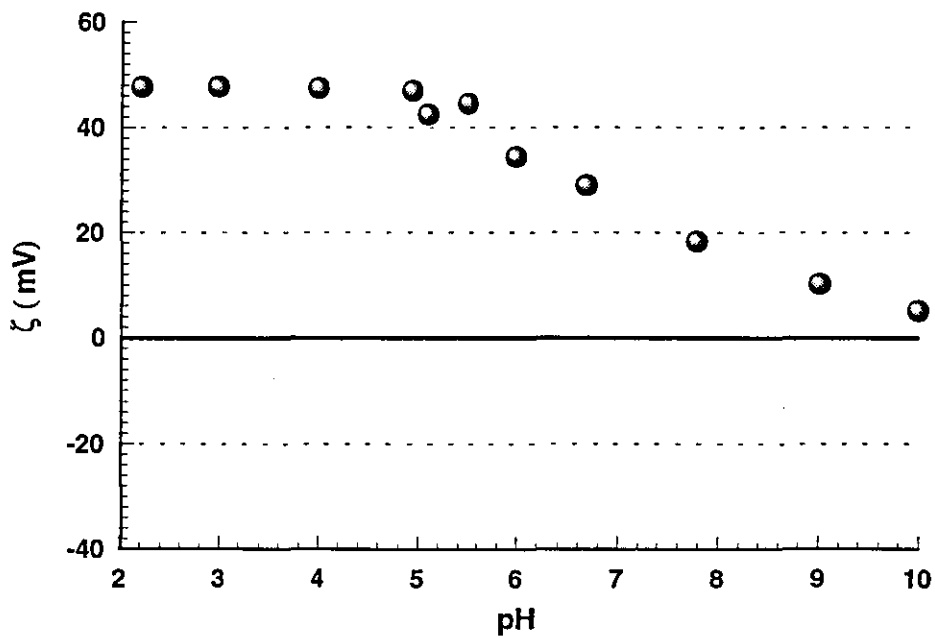


Figure A.18: Zeta Potential vs pH for dispersed Kaolin particles in 50 mgL^{-1} solution of Tetradecyltrimethylammoniumbromide

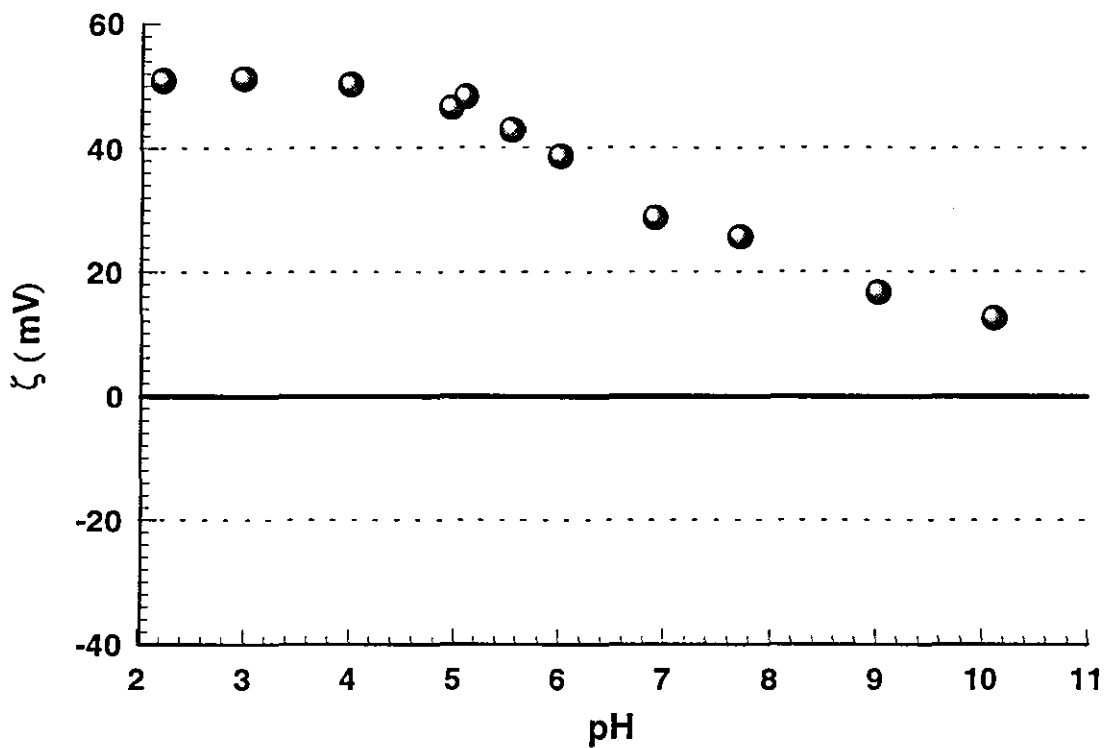


Figure A.19: Zeta Potential vs pH for dispersed Kaolin particles in 50 mgL⁻¹ solution of Tetradecyltrimethylammoniumbromide

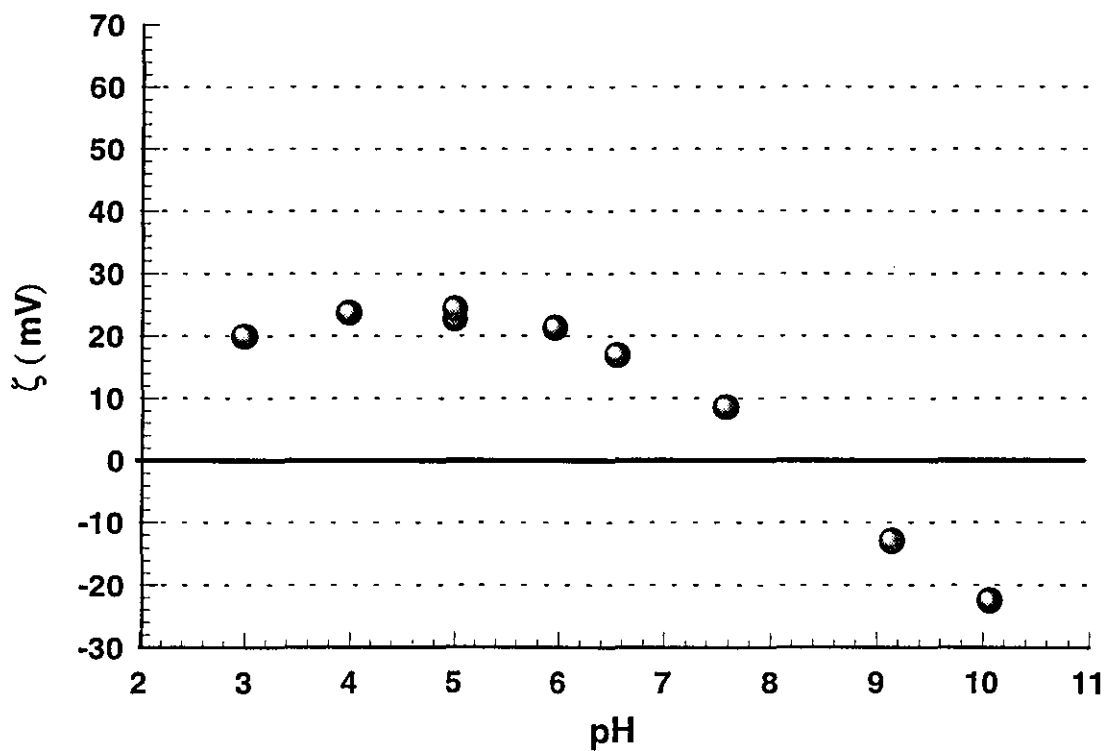


Figure A.20: Zeta Potential vs pH for dispersed Kaolin particles in 2 mgL⁻¹ solution of Hexadecyltrimethylammoniumbromide

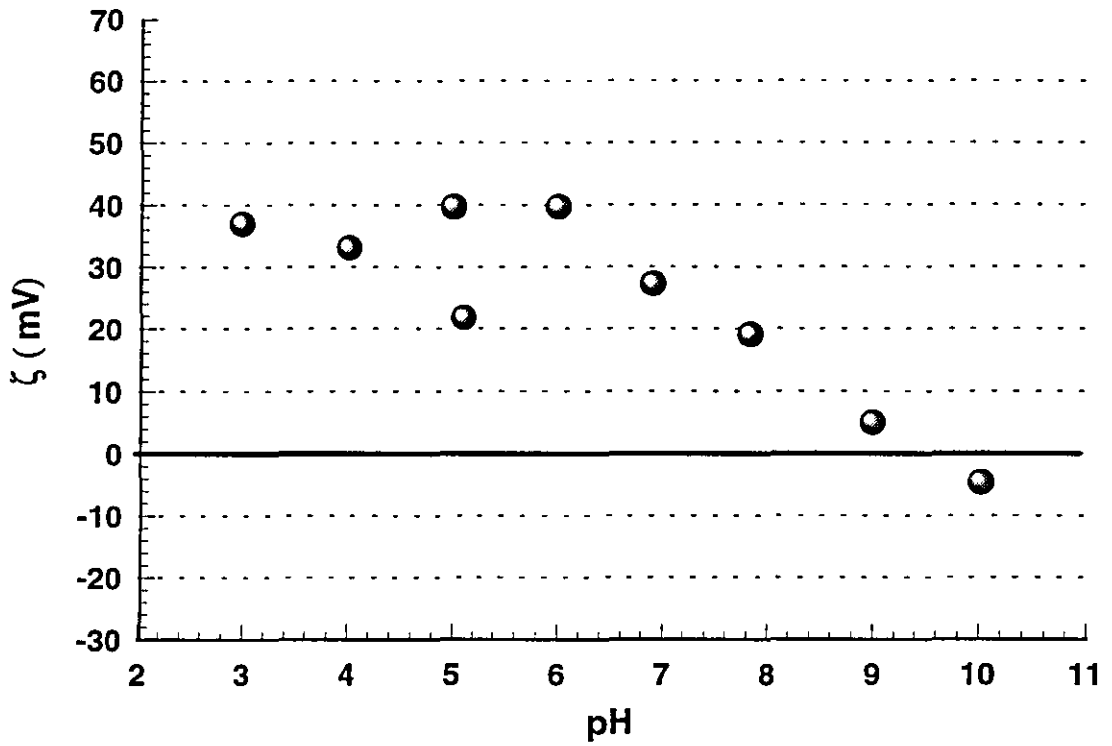


Figure A.21: Zeta Potential vs pH for dispersed Kaolin particles in 4 mgL^{-1} solution of Hexadecyltrimethylammoniumbromide

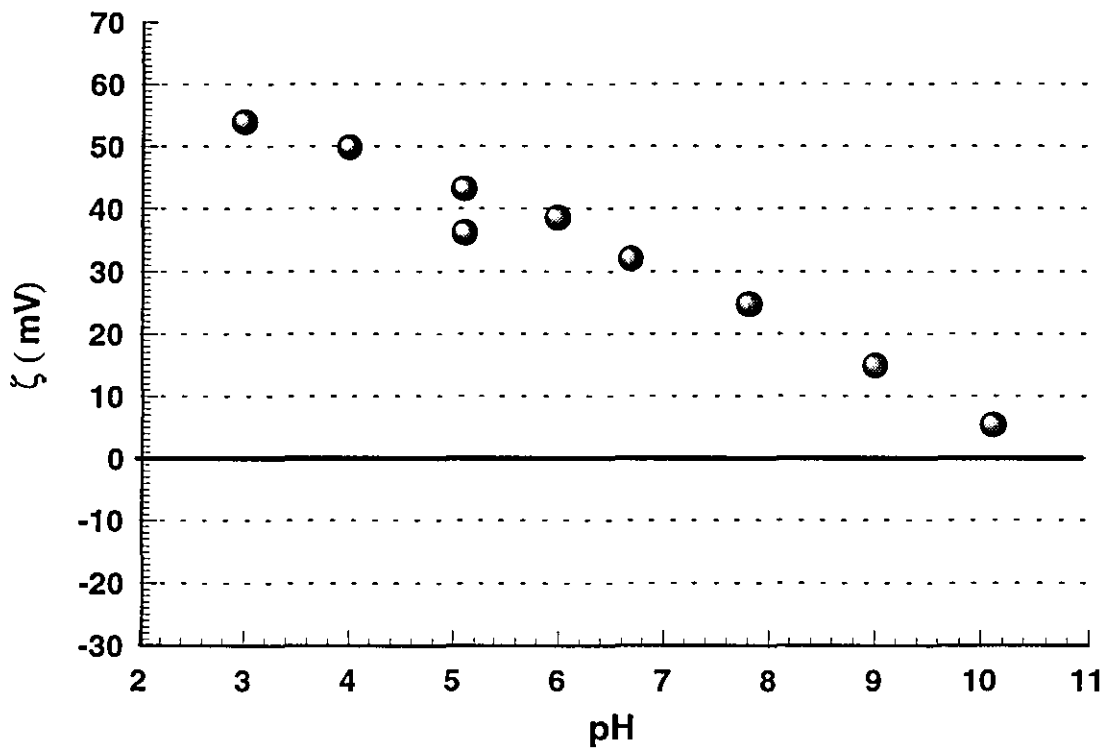


Figure A.22: Zeta Potential vs pH for dispersed Kaolin particles in 10 mgL^{-1} solution of Hexadecyltrimethylammoniumbromide

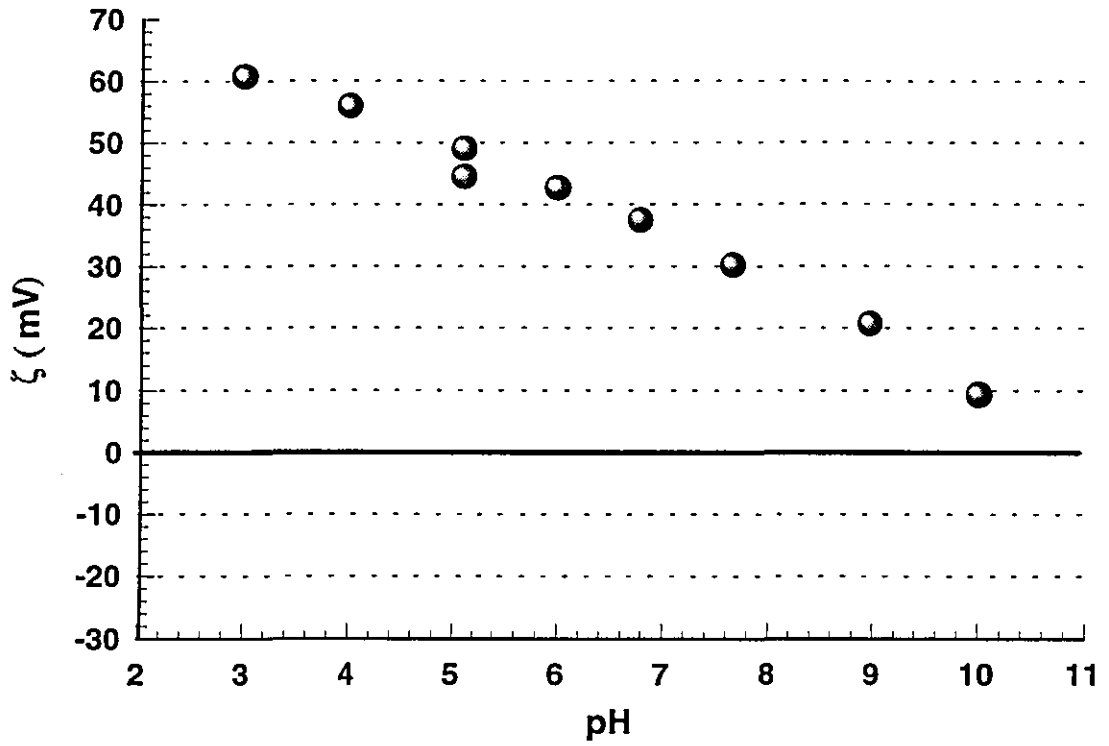


Figure A.23: Zeta Potential vs pH for dispersed Kaolin particles in 20 mgL⁻¹ solution of Hexadecyltrimethylammoniumbromide

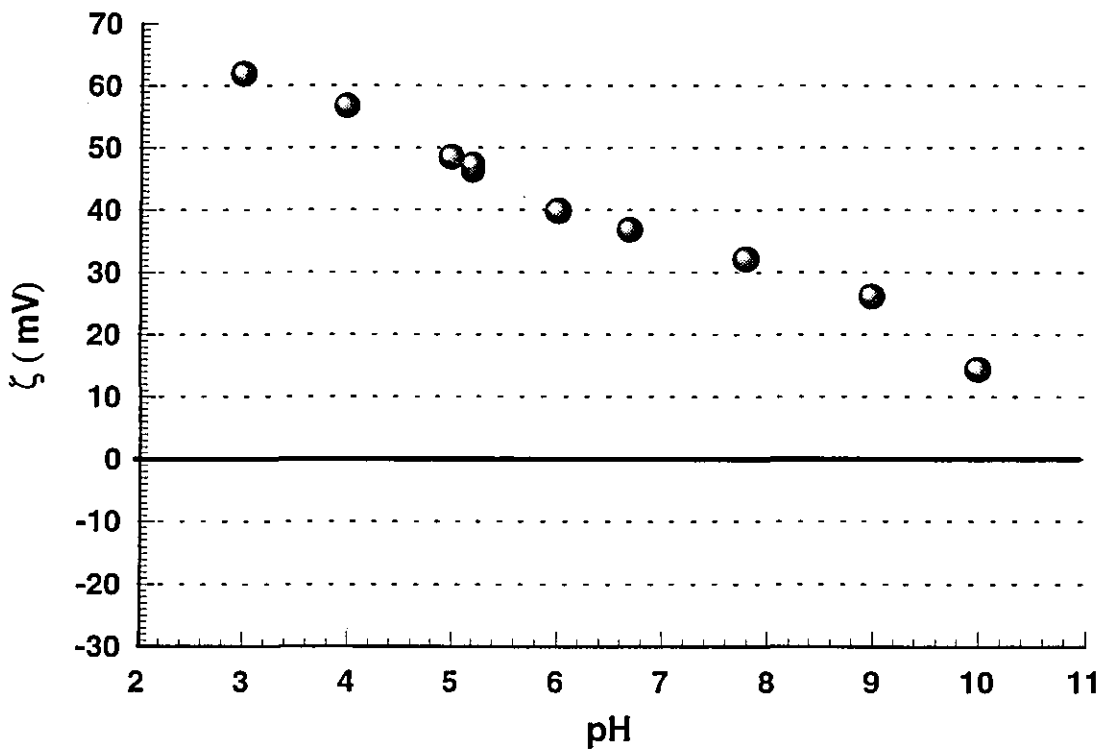


Figure A.24: Zeta Potential vs pH for dispersed Kaolin particles in 50 mgL⁻¹ solution of Hexadecyltrimethylammoniumbromide

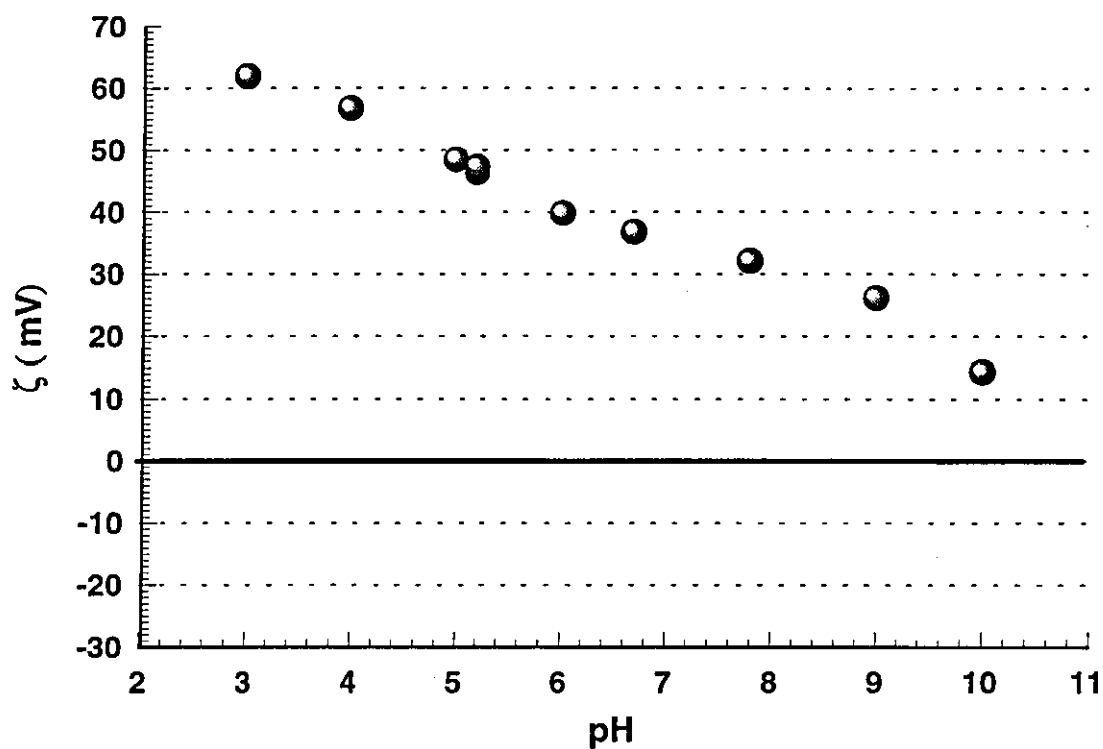


Figure A.25: Zeta Potential vs pH for dispersed Kaolin particles in 100 mgL⁻¹ solution of Hexadecyltrimethylammoniumbromide

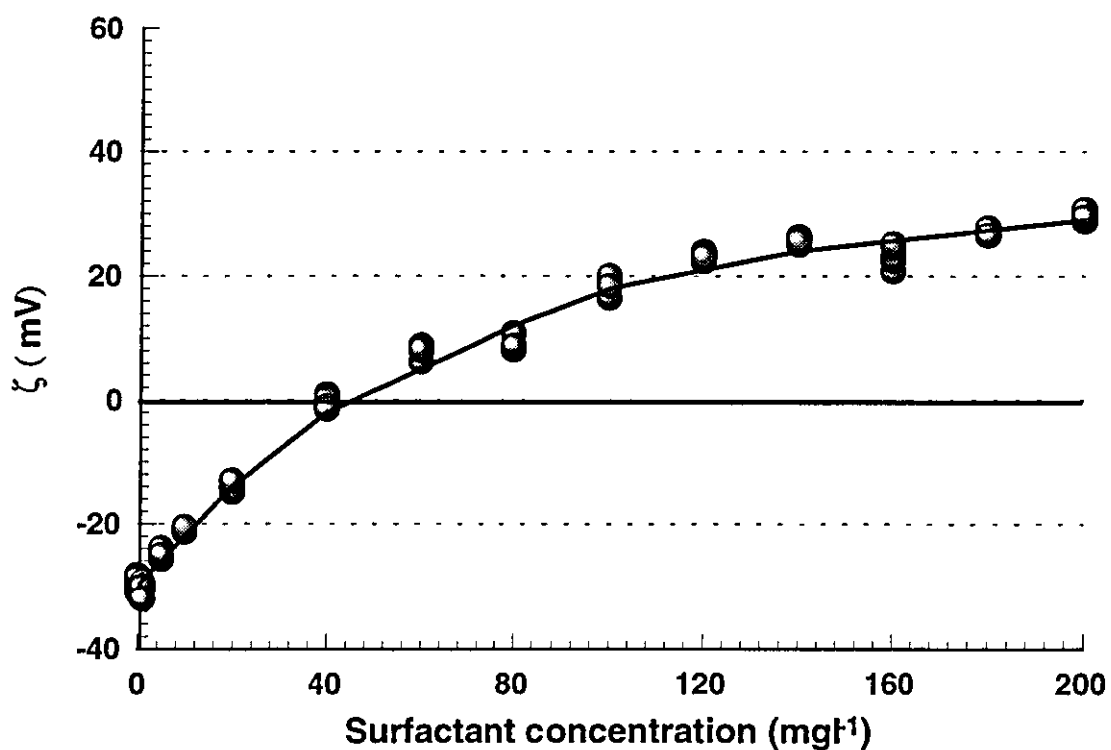


Figure A.26: Zeta Potential vs concentration of Dodecyltrimethylammoniumbromide on dispersed Wyoming Bentonite particles in distilled water

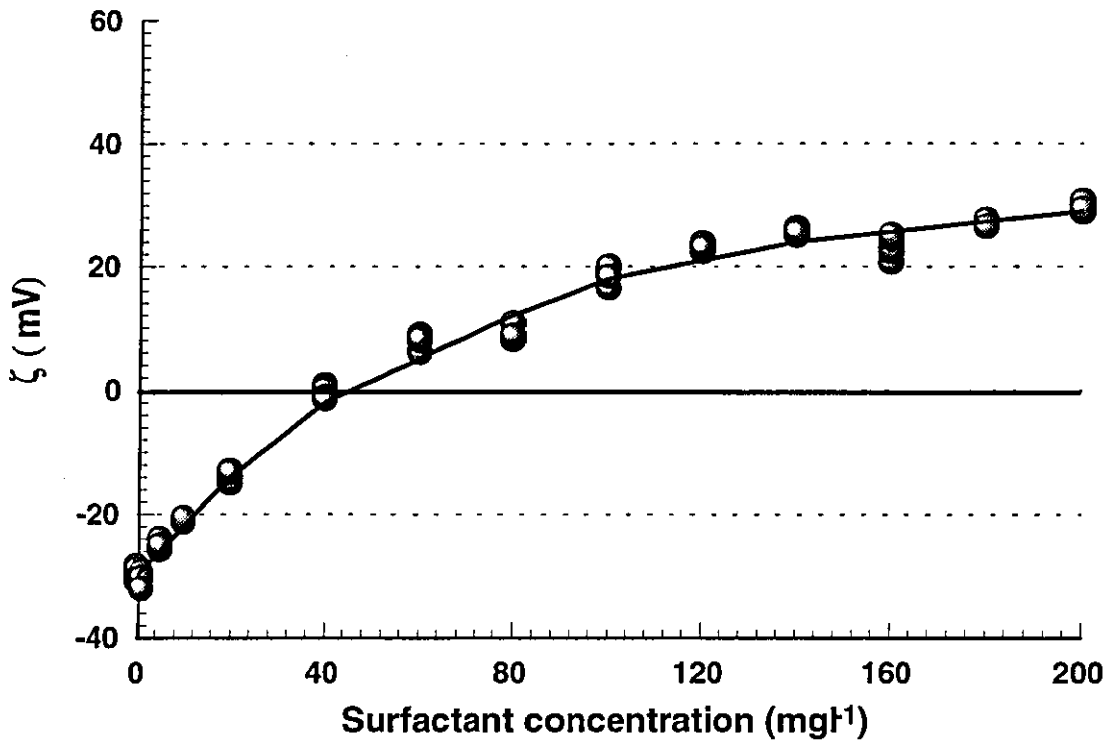


Figure A.27: Zeta Potential vs concentration of Tetradecyltrimethylammoniumbromide on dispersed Wyoming Bentonite particles in distilled water

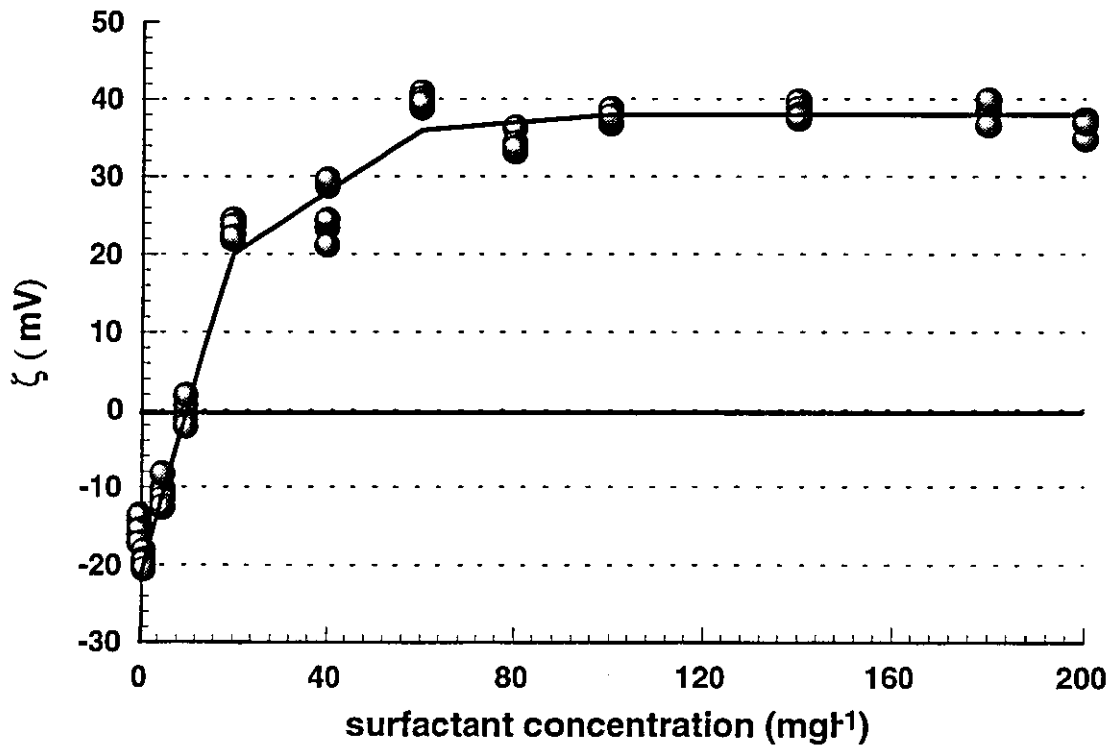


Figure A.28: Zeta Potential vs concentration of Hexadecyltrimethylammoniumbromide on dispersed Wyoming Bentonite particles in distilled water

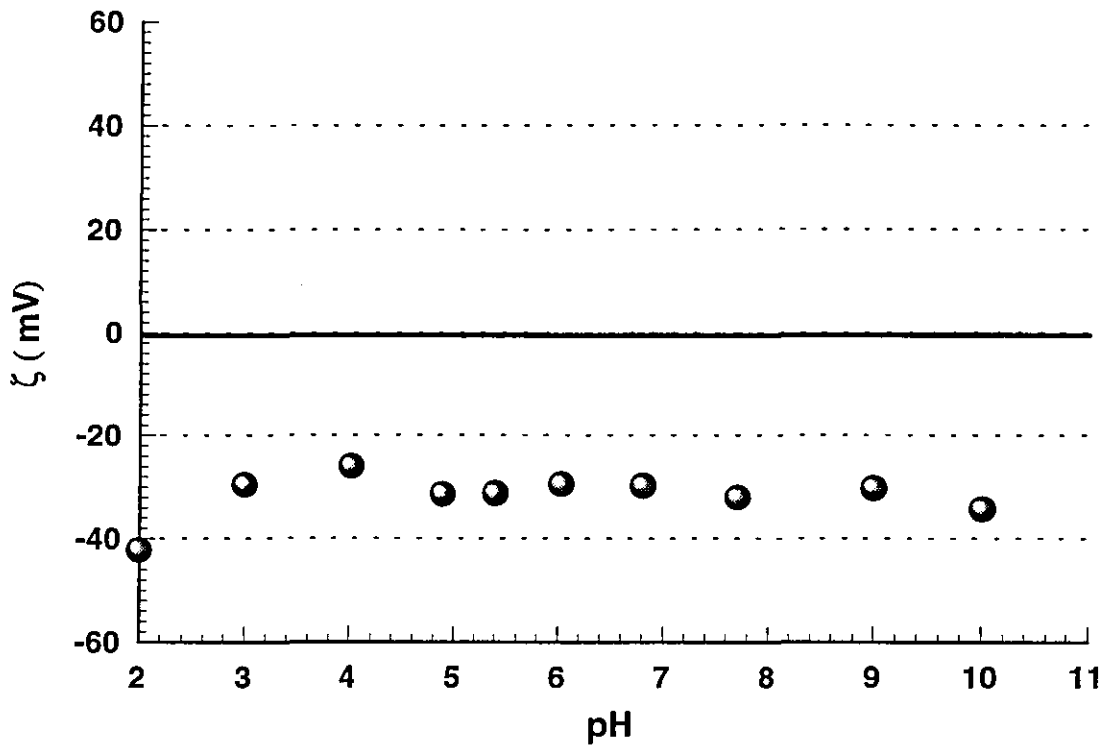


Figure A.29: Zeta Potential vs pH for dispersed Wyoming Bentonite particles in 5 mgL^{-1} solution of Tetradecyltrimethylammoniumbromide

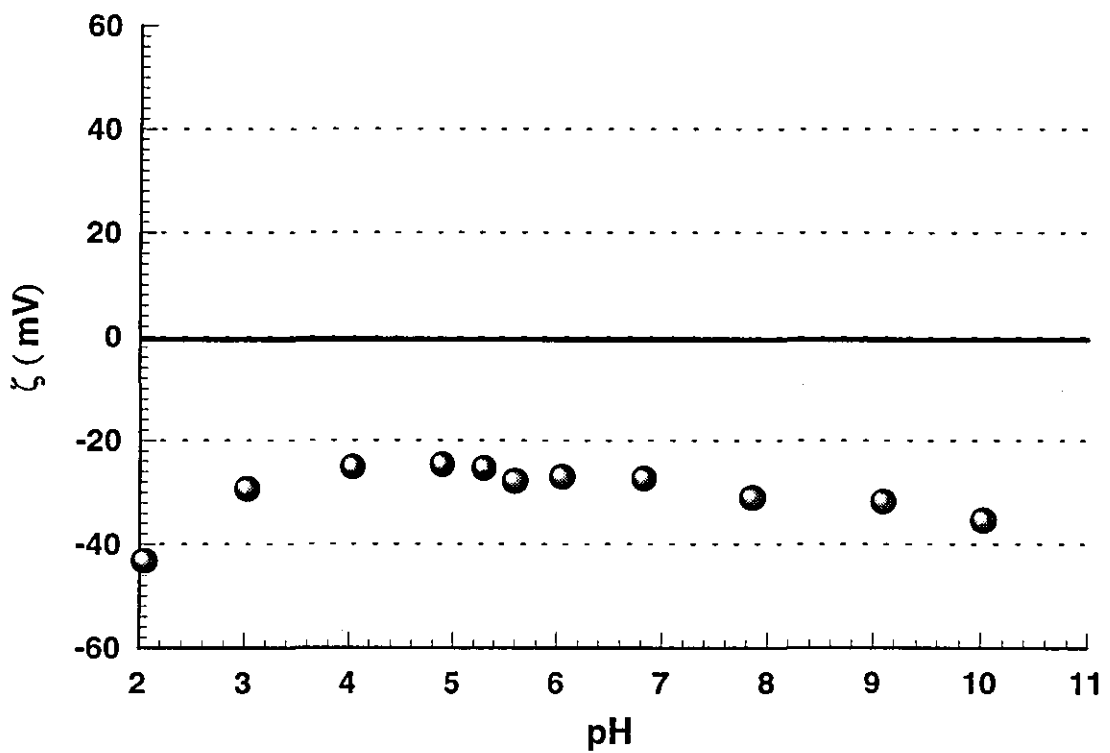


Figure A.30: Zeta Potential vs pH for dispersed Wyoming Bentonite particles in 10 mgL^{-1} solution of Tetradecyltrimethylammoniumbromide

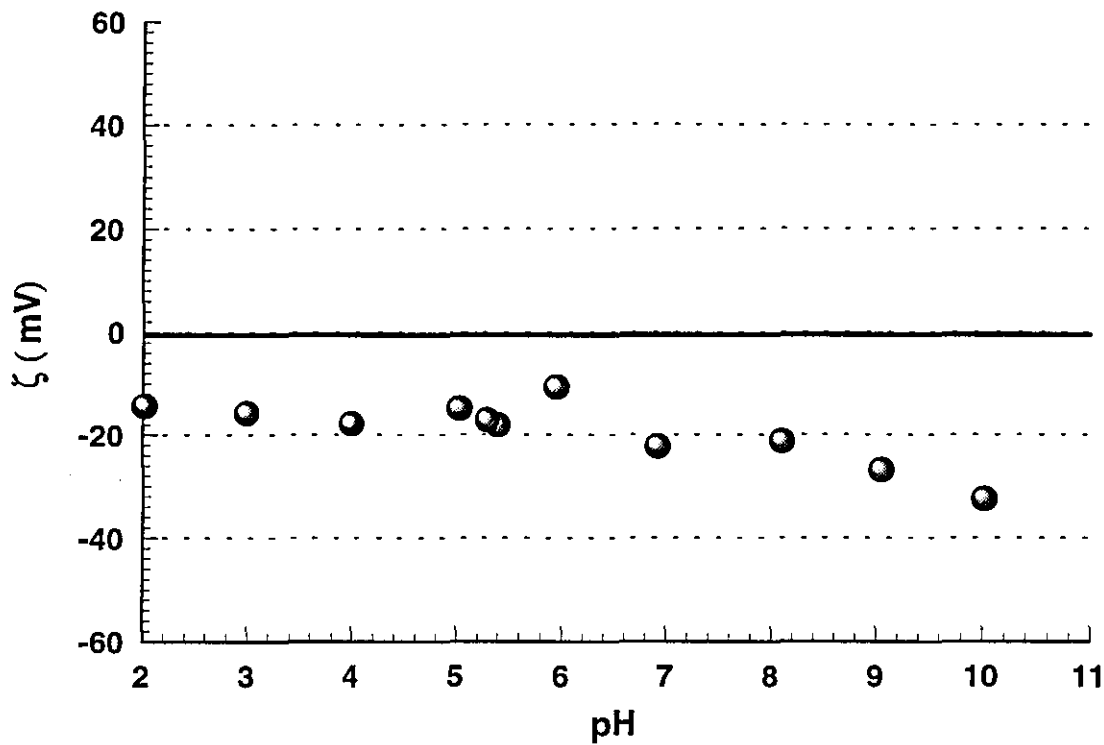


Figure A.31: Zeta Potential vs pH for dispersed Wyoming Bentonite particles in 20 mgL⁻¹ solution of Tetradecyltrimethylammoniumbromide

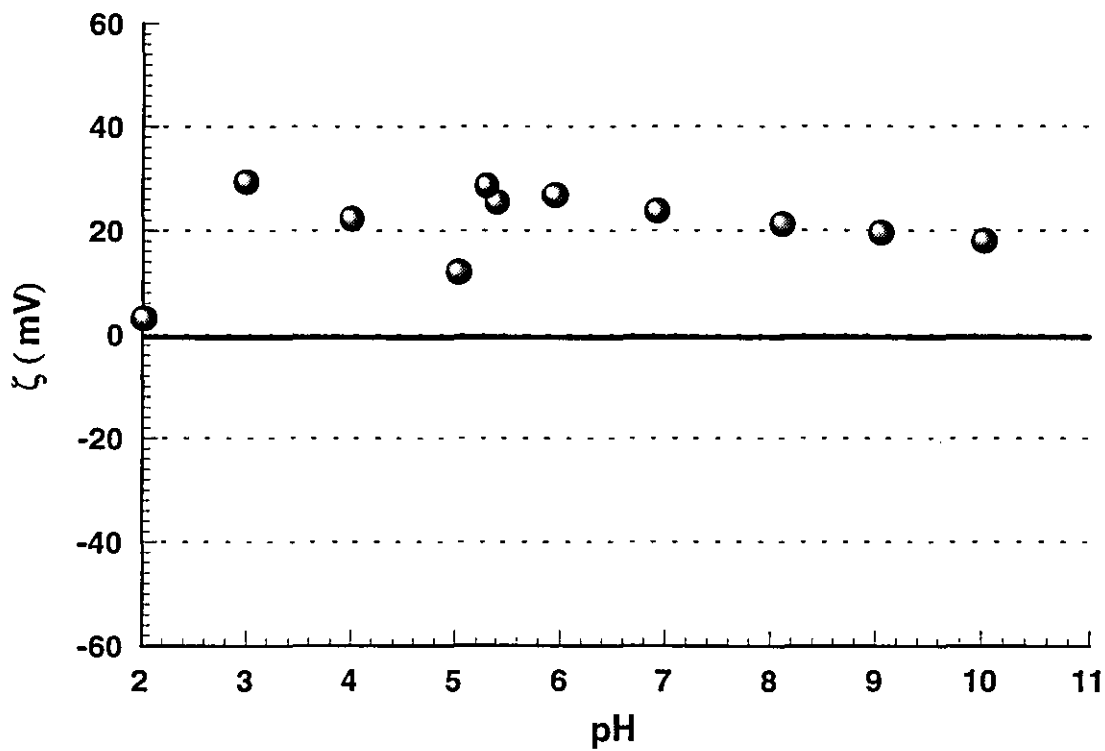


Figure A.32: Zeta Potential vs pH for dispersed Wyoming Bentonite particles in 50 mgL⁻¹ solution of Tetradecyltrimethylammoniumbromide

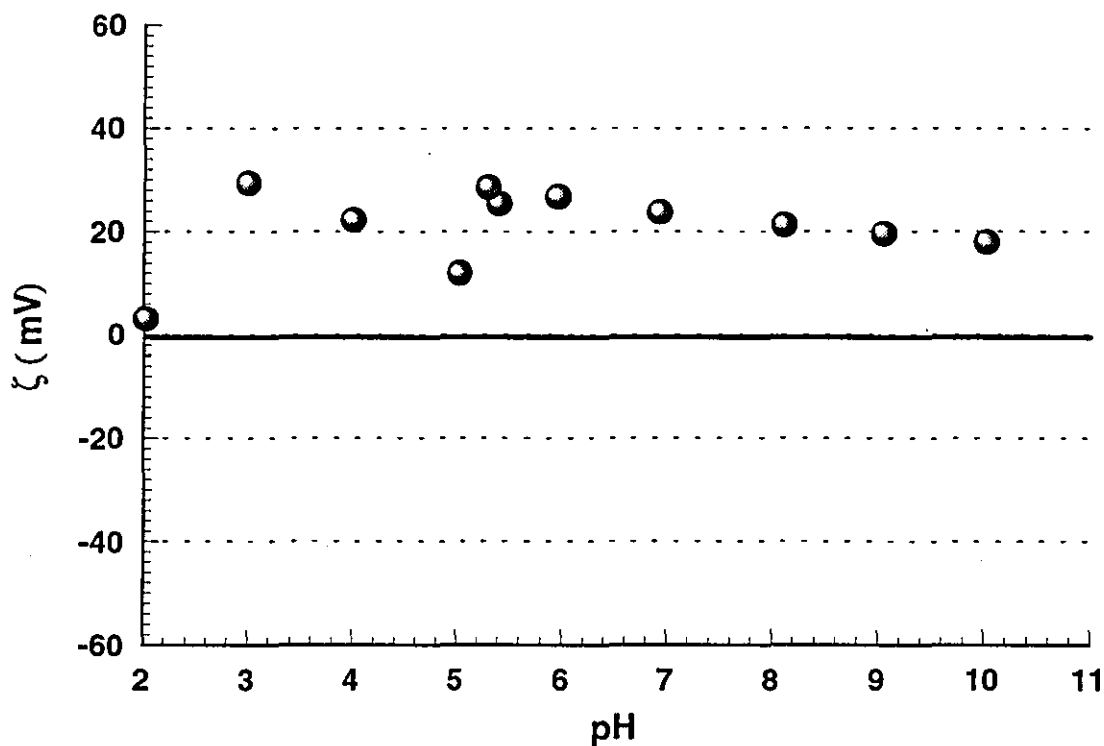


Figure A.33: Zeta Potential vs pH for dispersed Wyoming Bentonite particles in 100 mgL^{-1} solution of Tetradecyltrimethylammoniumbromide

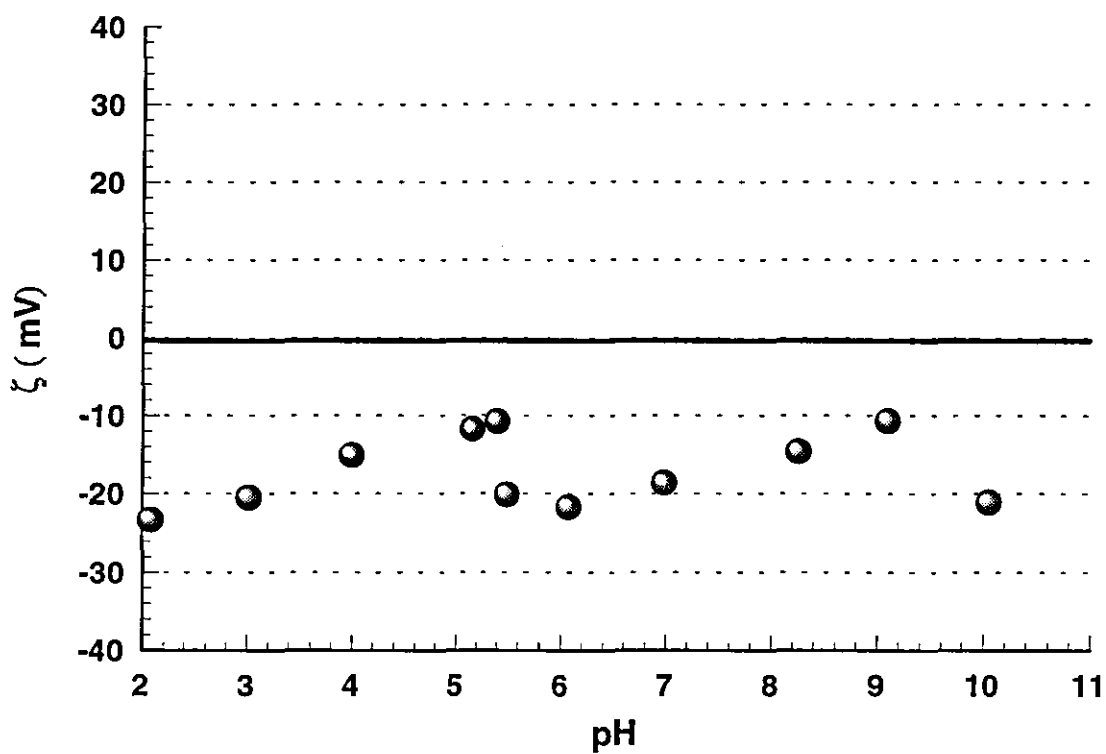


Figure A.34: Zeta Potential vs pH for dispersed Wyoming Bentonite particles in 25 mgL^{-1} solution of Dodecyltrimethylammoniumbromide

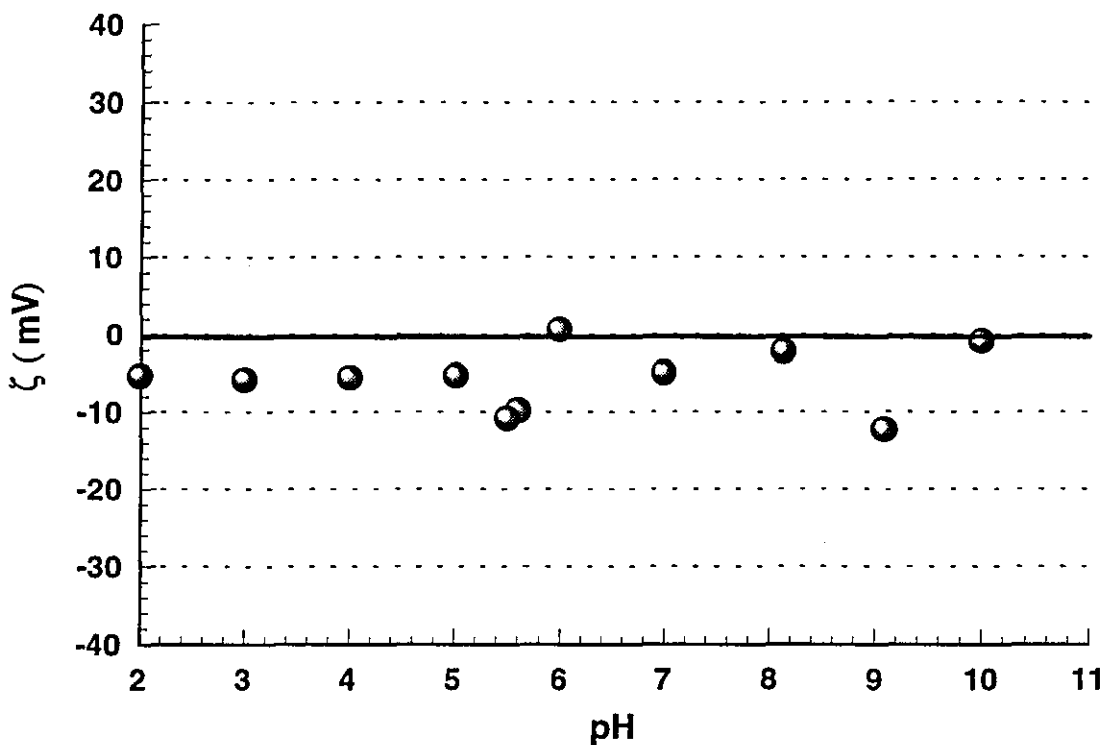


Figure A.35: Zeta Potential vs pH for dispersed Wyoming Bentonite particles in 50 mgL^{-1} solution of Dodecyltrimethylammoniumbromide

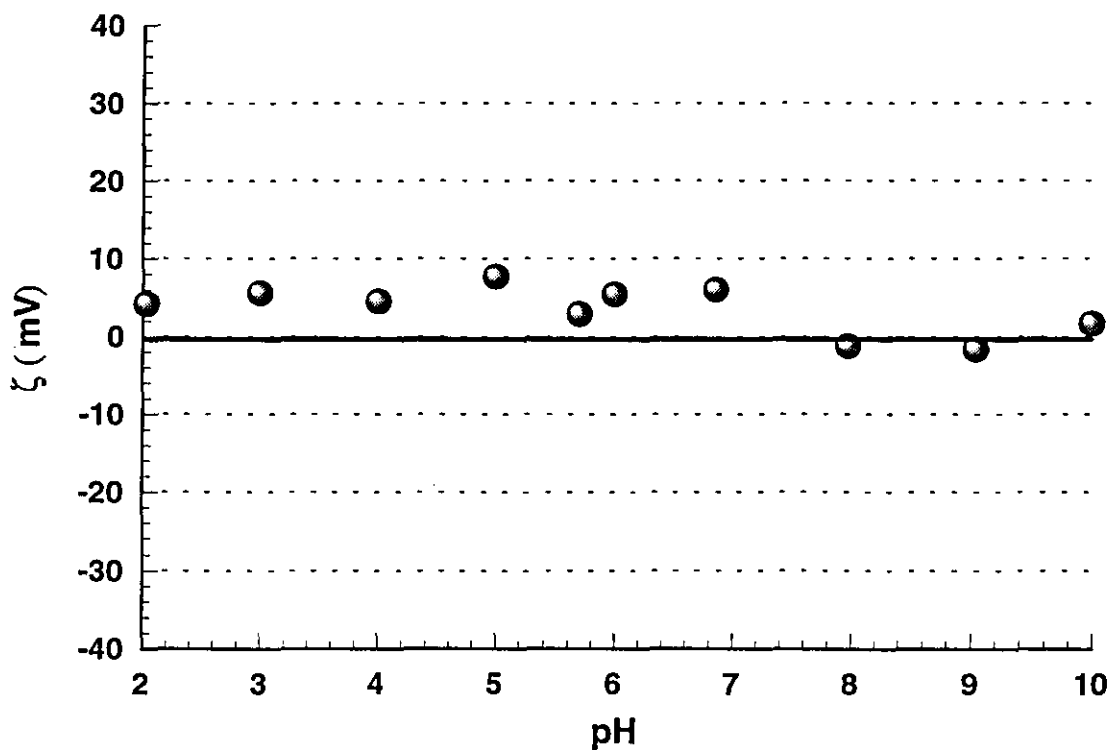


Figure A.36: Zeta Potential vs pH for dispersed Wyoming Bentonite particles in 75 mgL^{-1} solution of Dodecyltrimethylammoniumbromide

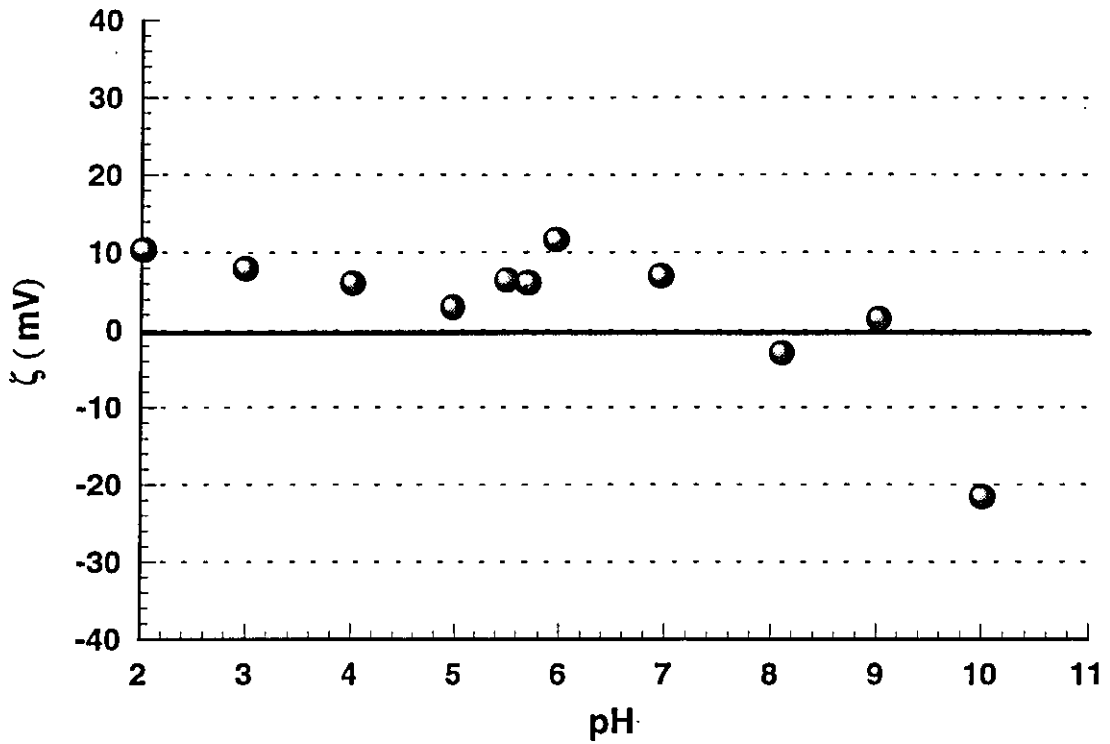


Figure A.37: Zeta Potential vs pH for dispersed Wyoming Bentonite particles in 100 mgL^{-1} solution of Dodecyltrimethylammoniumbromide

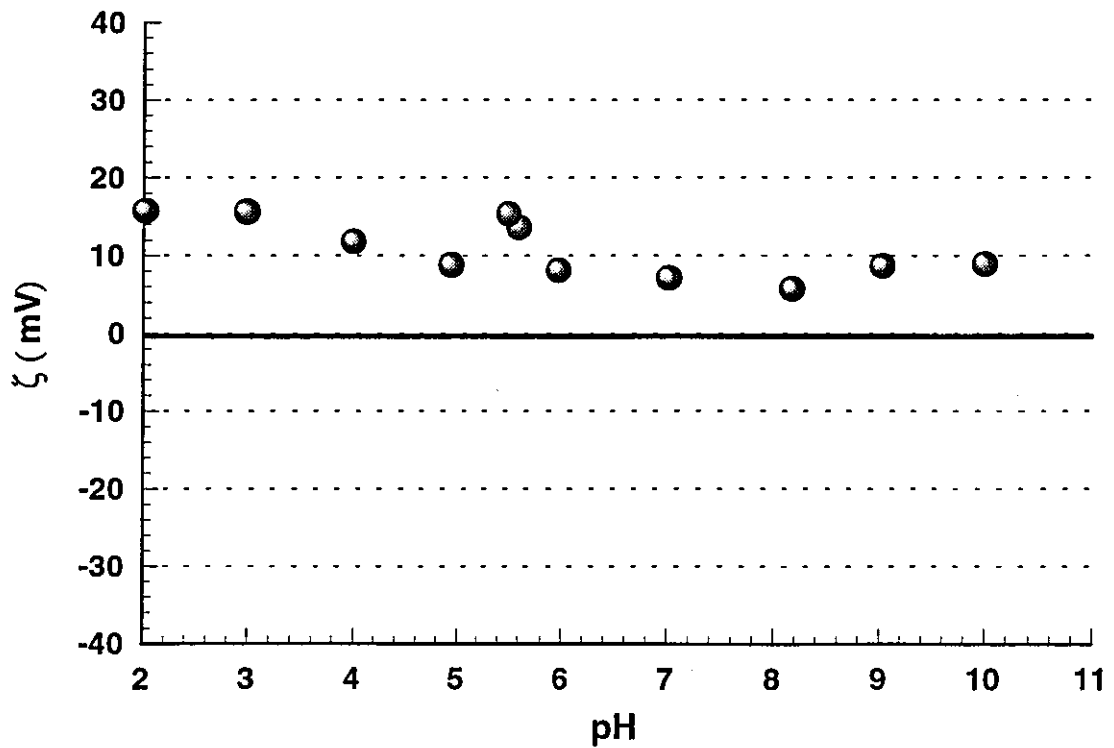


Figure A.38: Zeta Potential vs pH for dispersed Wyoming Bentonite particles in 150 mgL^{-1} solution of Dodecyltrimethylammoniumbromide

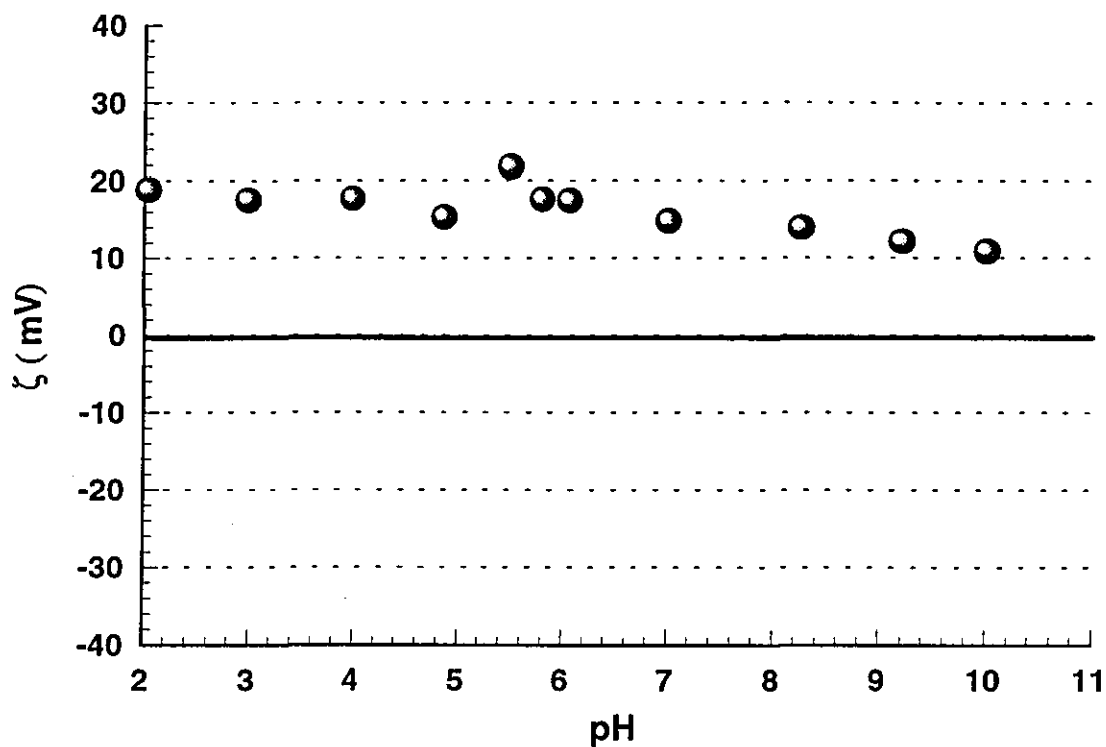


Figure A.39: Zeta Potential vs pH for dispersed Wyoming Bentonite particles in 200 mgL⁻¹ solution of Dodecyltrimethylammoniumbromide

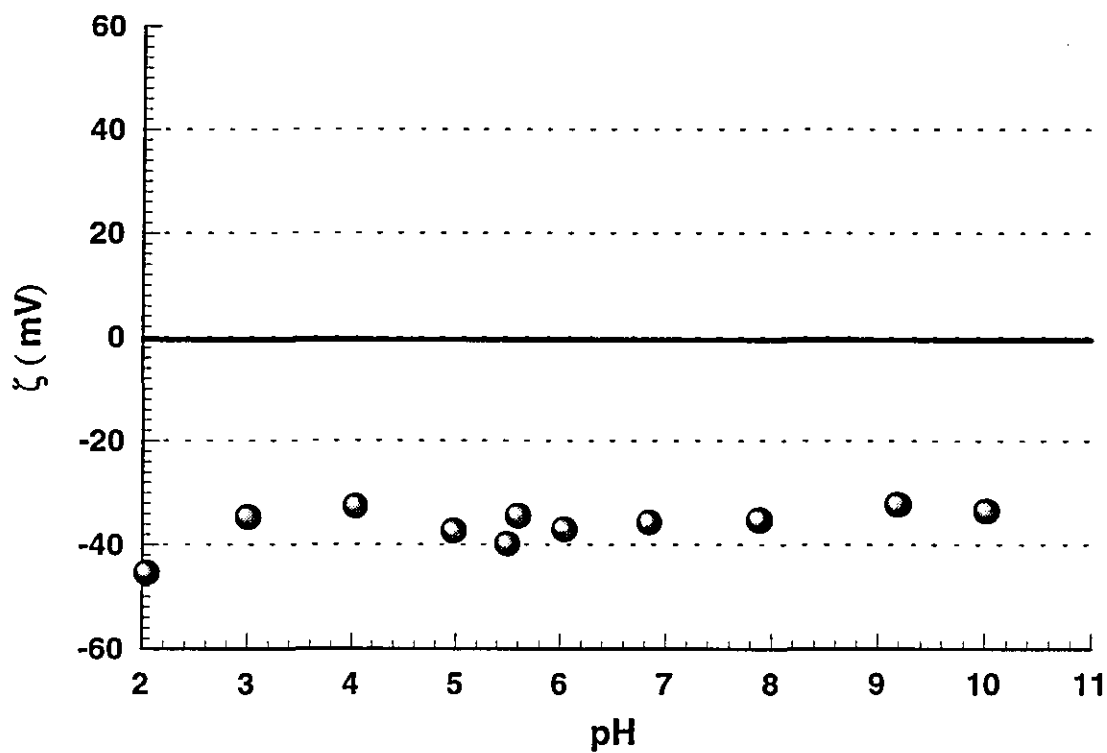


Figure A.40: Zeta Potential vs pH for dispersed Wyoming Bentonite particles in 2 mgL⁻¹ solution of Hexadecyltrimethylammoniumbromide

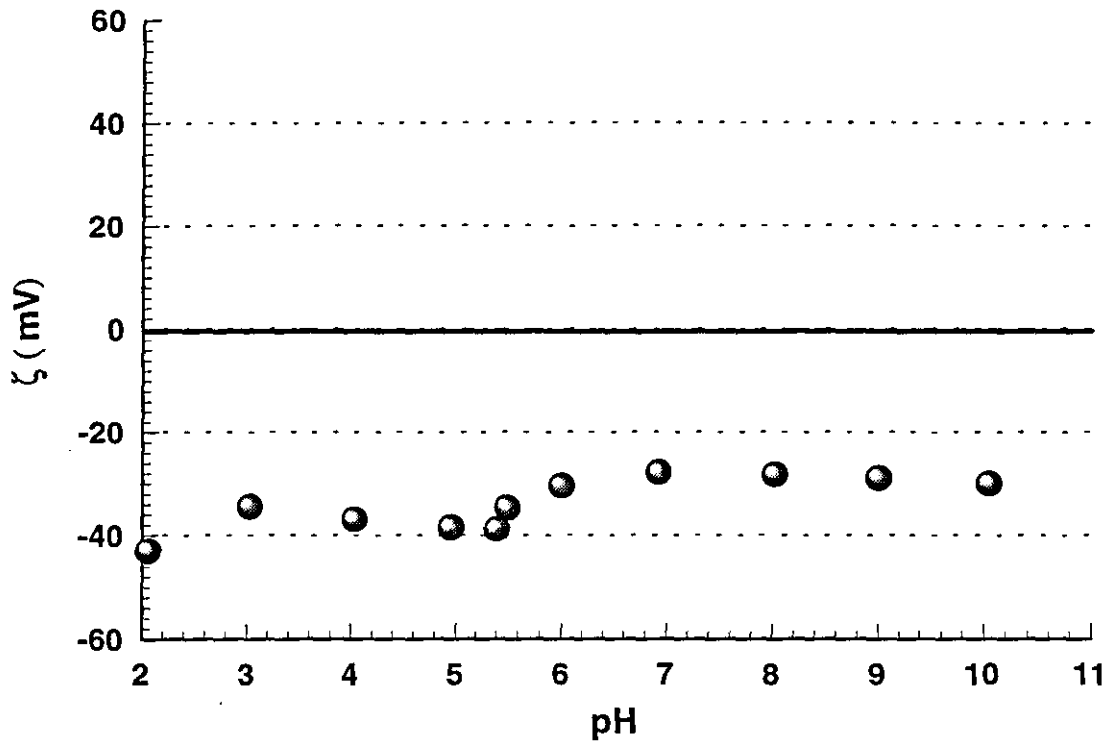


Figure A.41: Zeta Potential vs pH for dispersed Wyoming Bentonite particles in 4 mgL^{-1} solution of Hexadecyltrimethylammoniumbromide

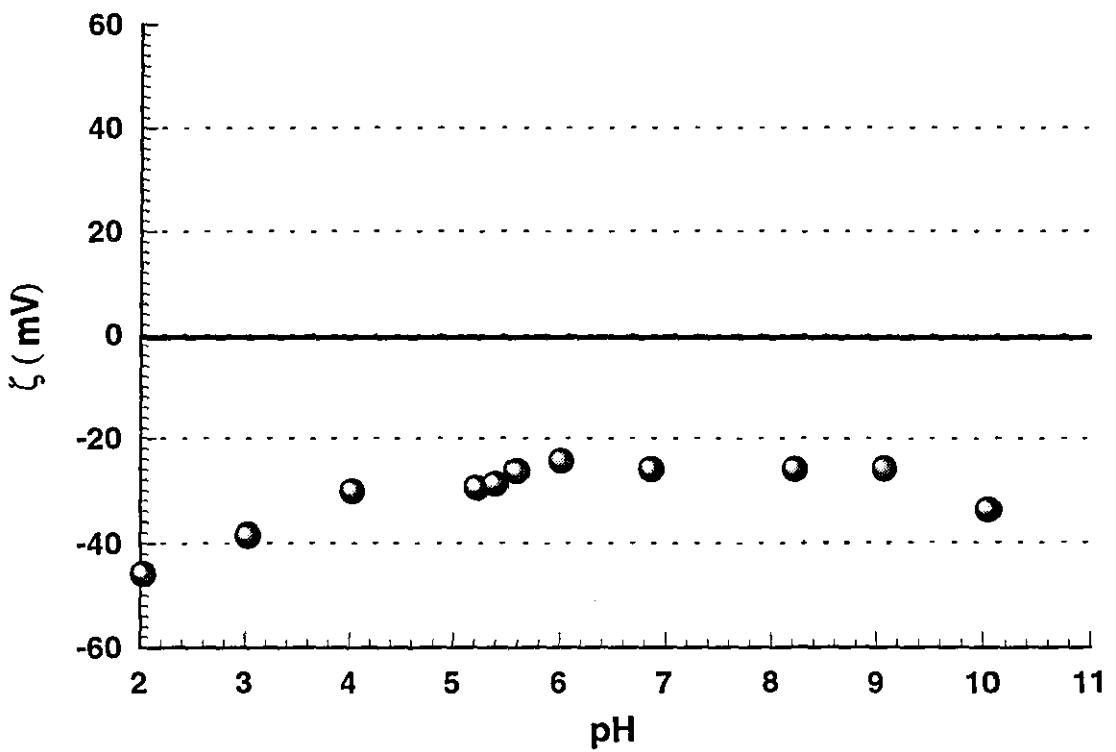


Figure A.42: Zeta Potential vs pH for dispersed Wyoming Bentonite particles in 10 mgL^{-1} solution of Hexadecyltrimethylammoniumbromide

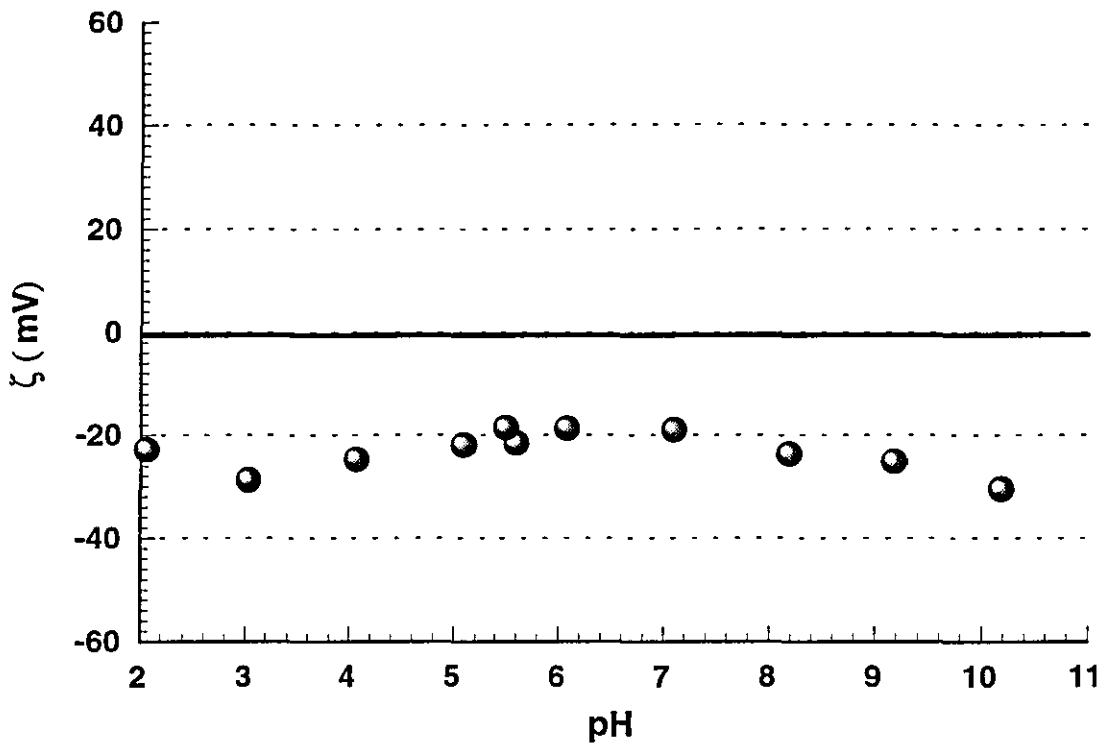


Figure A.43: Zeta Potential vs pH for dispersed Wyoming Bentonite particles in 20 mgL⁻¹ solution of Hexadecyltrimethylammoniumbromide

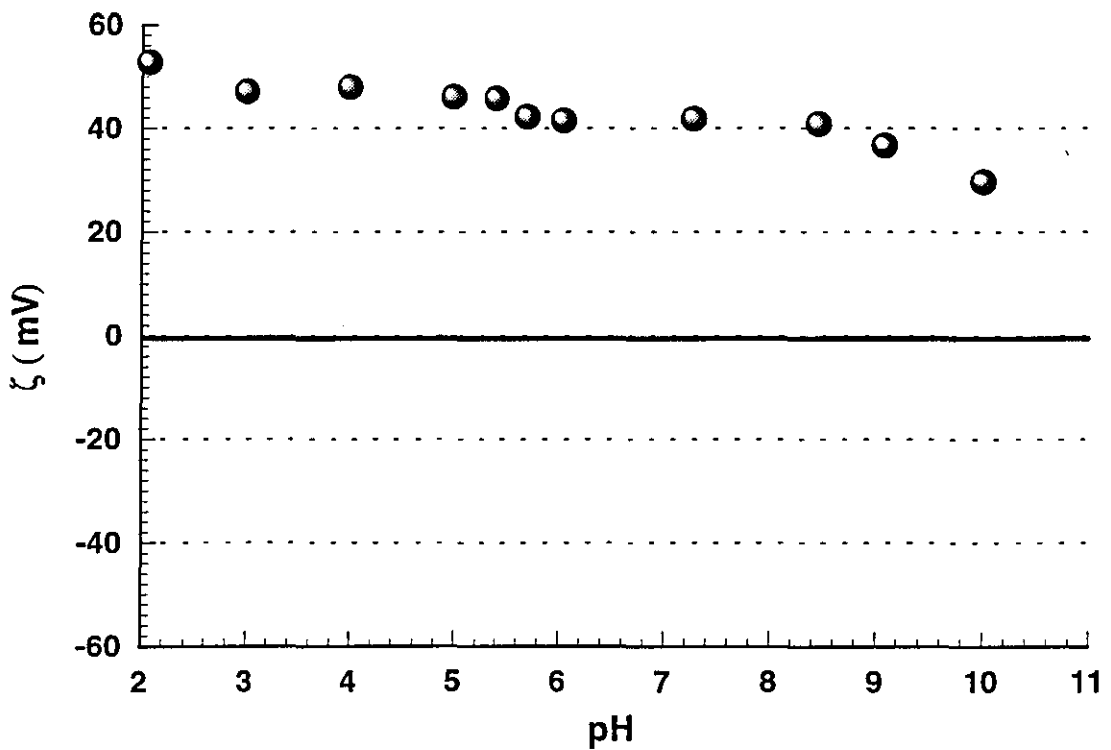


Figure A.44: Zeta Potential vs pH for dispersed Wyoming Bentonite particles in 50 mgL⁻¹ solution of Hexadecyltrimethylammoniumbromide

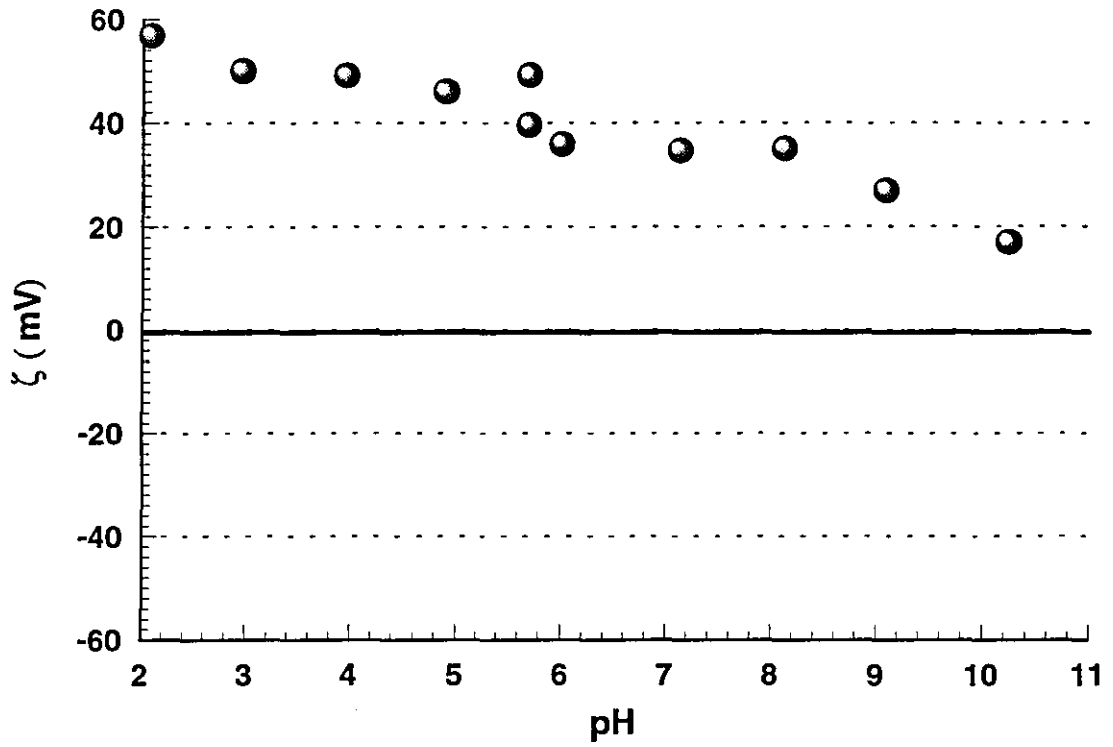


Figure A.45: Zeta Potential vs pH for dispersed Wyoming Bentonite particles in 100 mgL^{-1} solution of Hexadecyltrimethylammoniumbromide

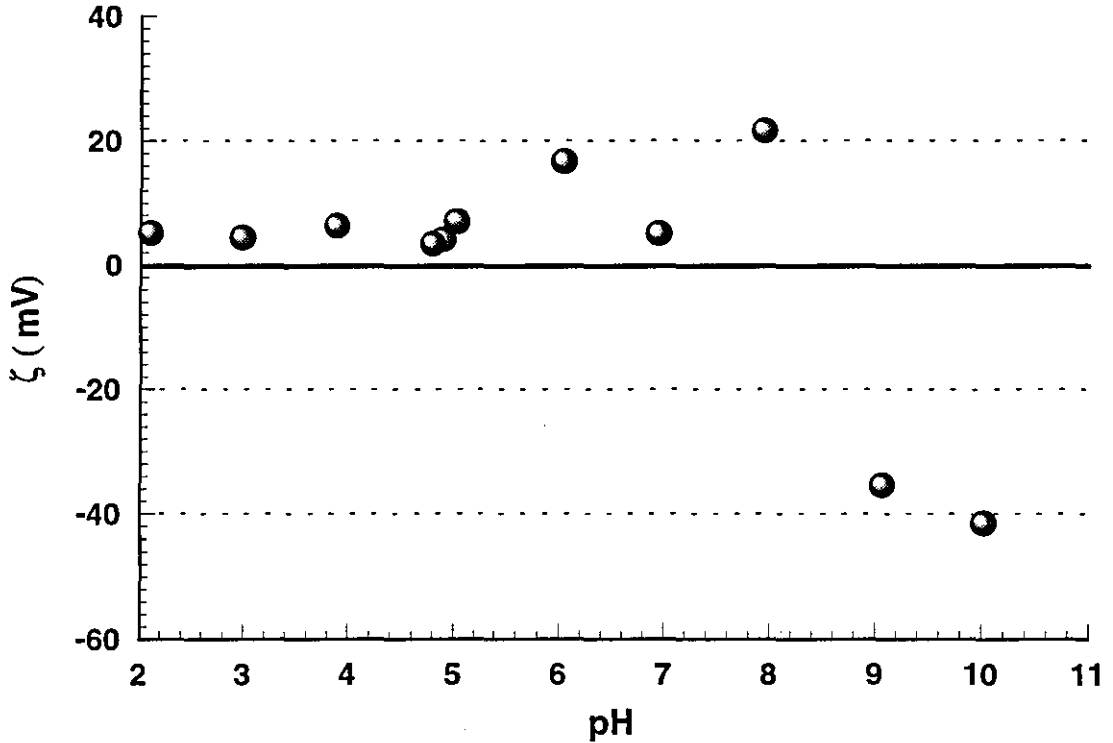


Figure A.46: Zeta Potential vs pH for dispersed Kaolin particles in 4 mgL^{-1} solution of Alum

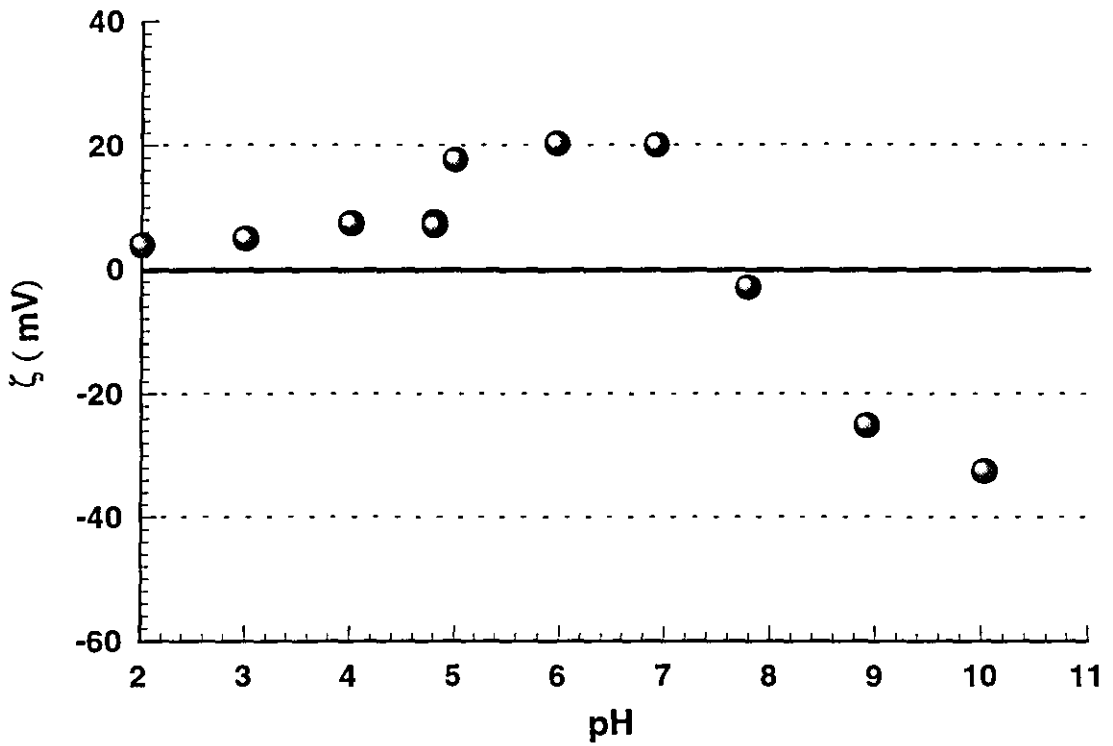


Figure A.47: Zeta Potential vs pH for dispersed Kaolin particles in 8 mgL⁻¹ solution of Alum

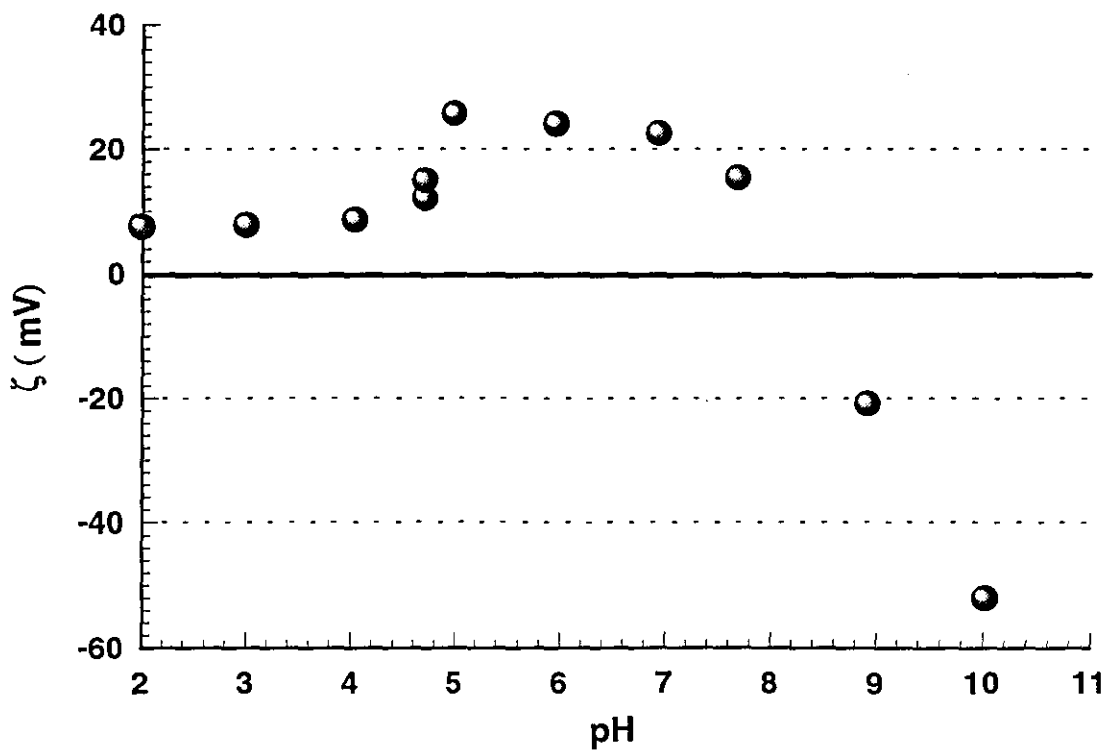


Figure A.48: Zeta Potential vs pH for dispersed Kaolin particles in 16 mgL⁻¹ solution of Alum

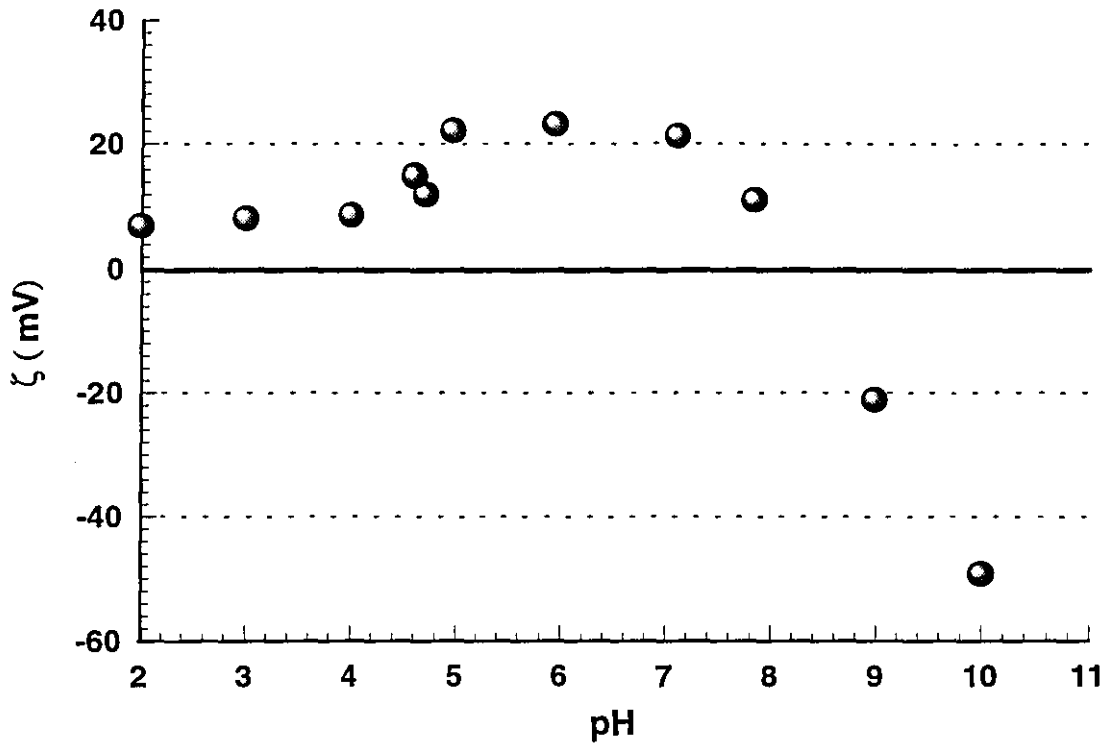


Figure A.49: Zeta Potential vs pH for dispersed Kaolin particles in 20 mgL⁻¹ solution of Alum

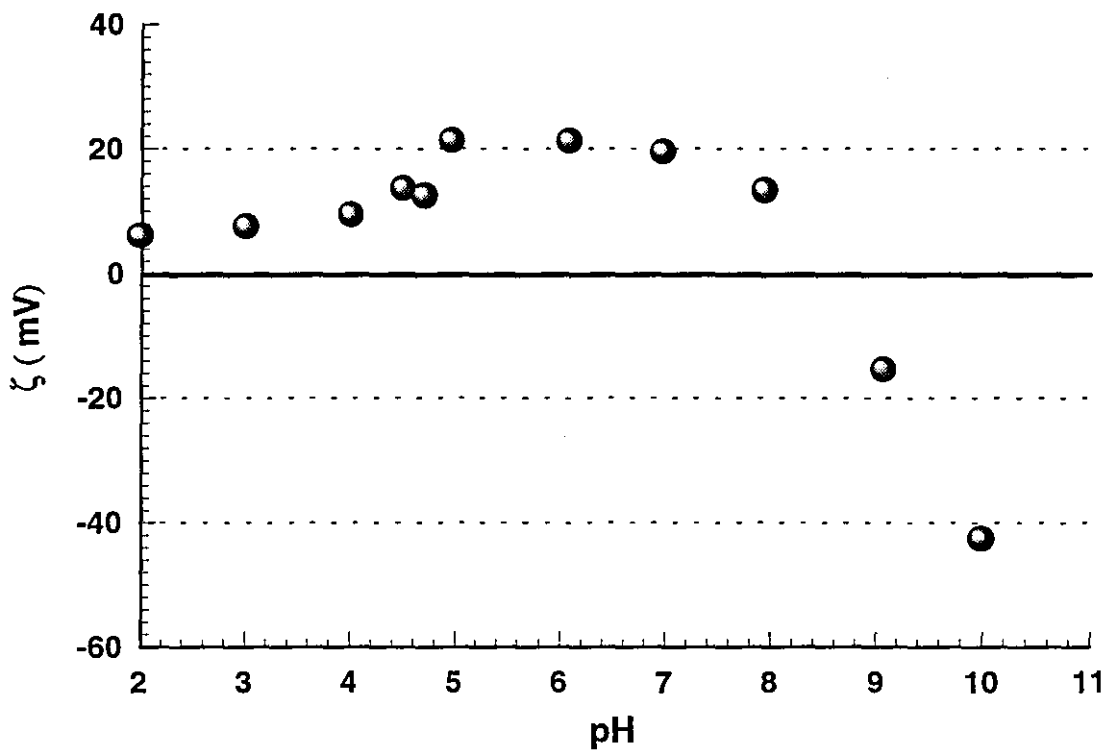


Figure A.50: Zeta Potential vs pH for dispersed Kaolin particles in 40 mgL⁻¹ solution of Alum

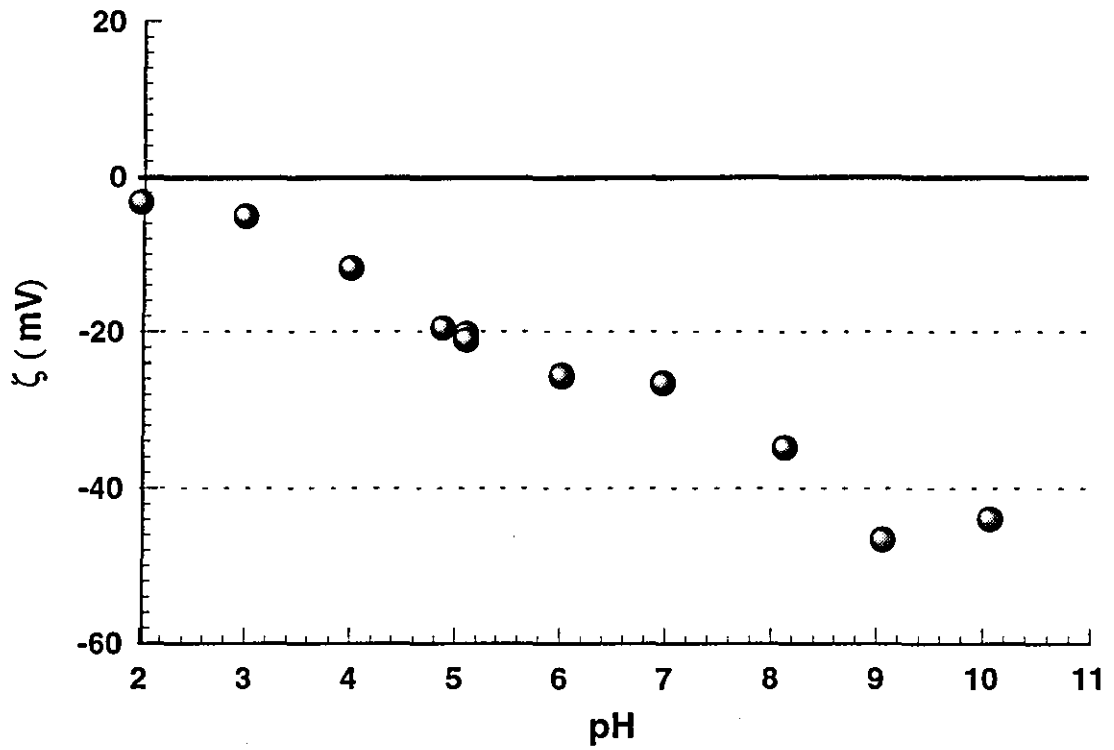


Figure A.51: Zeta Potential vs pH for dispersed Kaolin particles in 0.02 mgL⁻¹ solution of Ferric Chloride

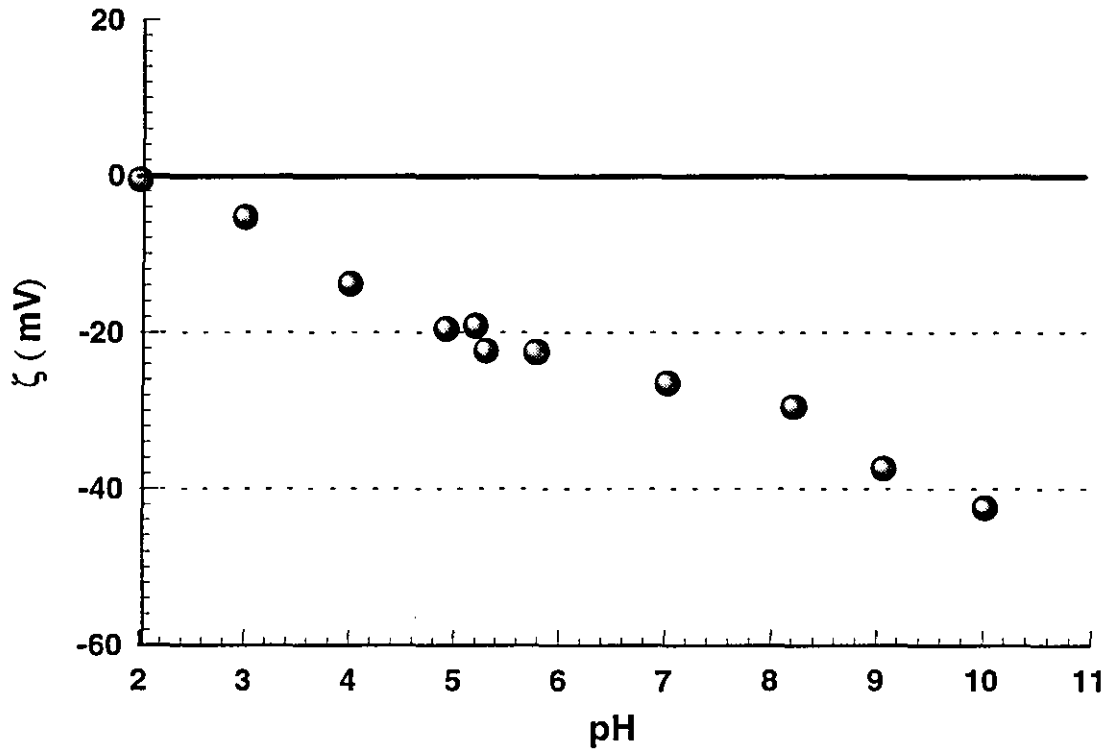


Figure A.52: Zeta Potential vs pH for dispersed Kaolin particles in 0.06 mgL⁻¹ solution of Ferric Chloride

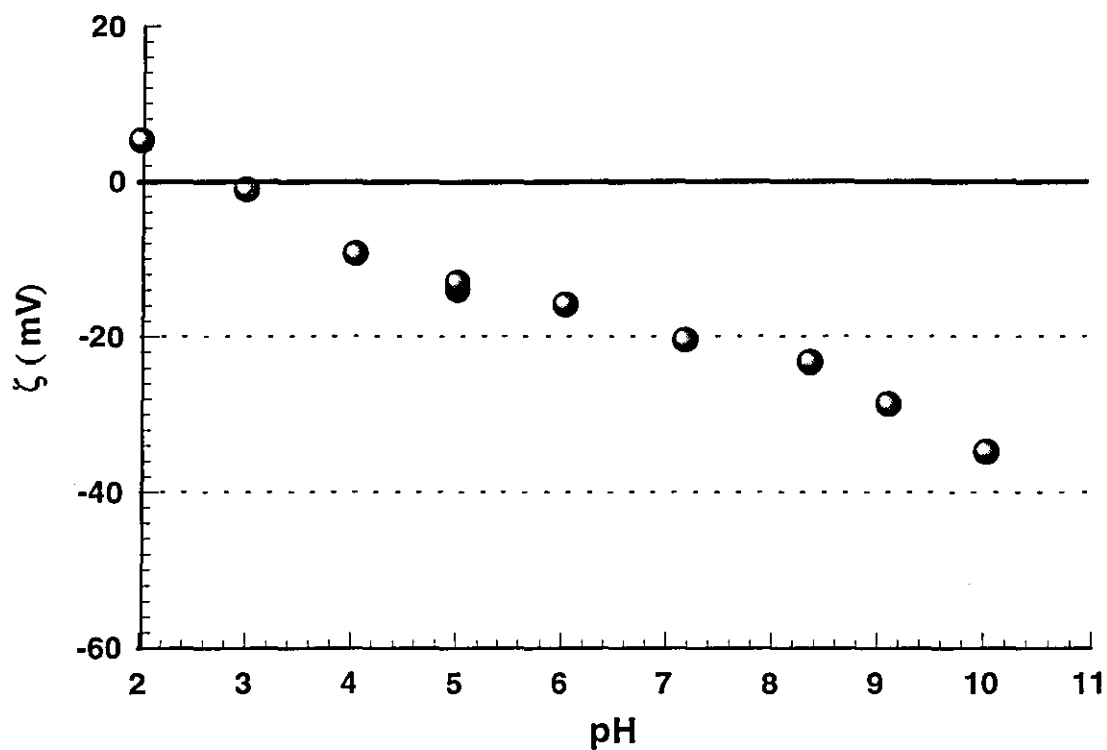


Figure A.53: Zeta Potential vs pH for dispersed Kaolin particles in 0.1 mgL^{-1} solution of Ferric Chloride

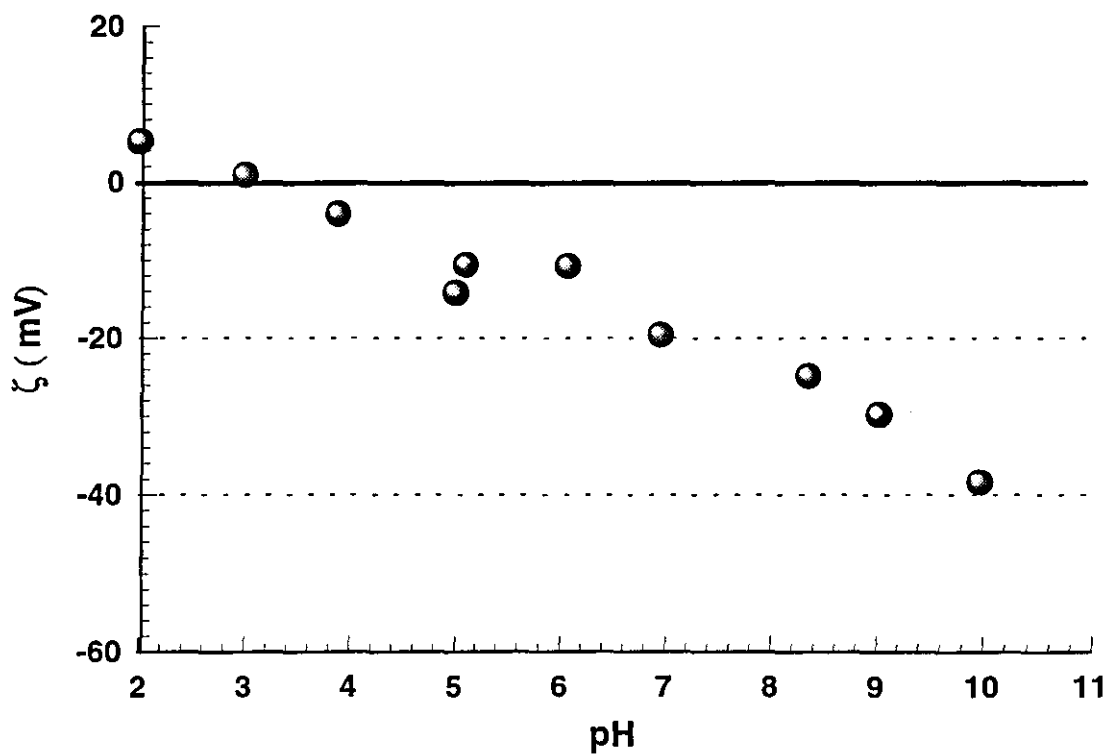


Figure A.54: Zeta Potential vs pH for dispersed Kaolin particles in 0.14 mgL^{-1} solution of Ferric Chloride

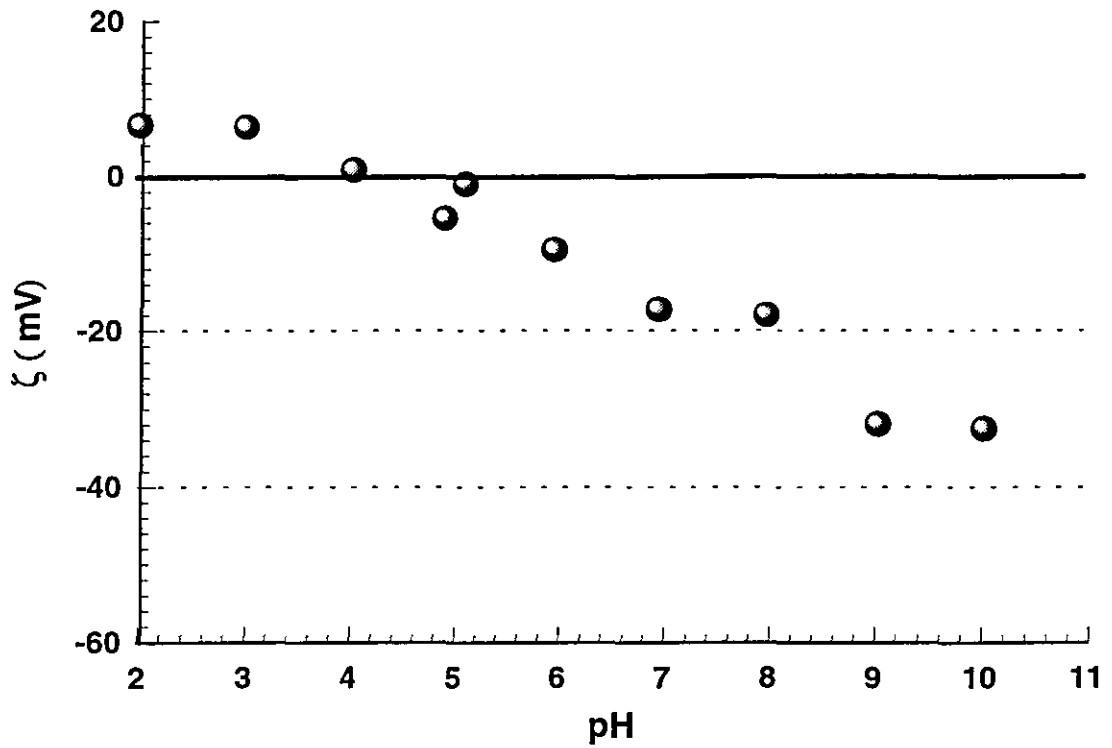


Figure A.55: Zeta Potential vs pH for dispersed Kaolin particles in 0.2 mgL⁻¹ solution of Ferric Chloride

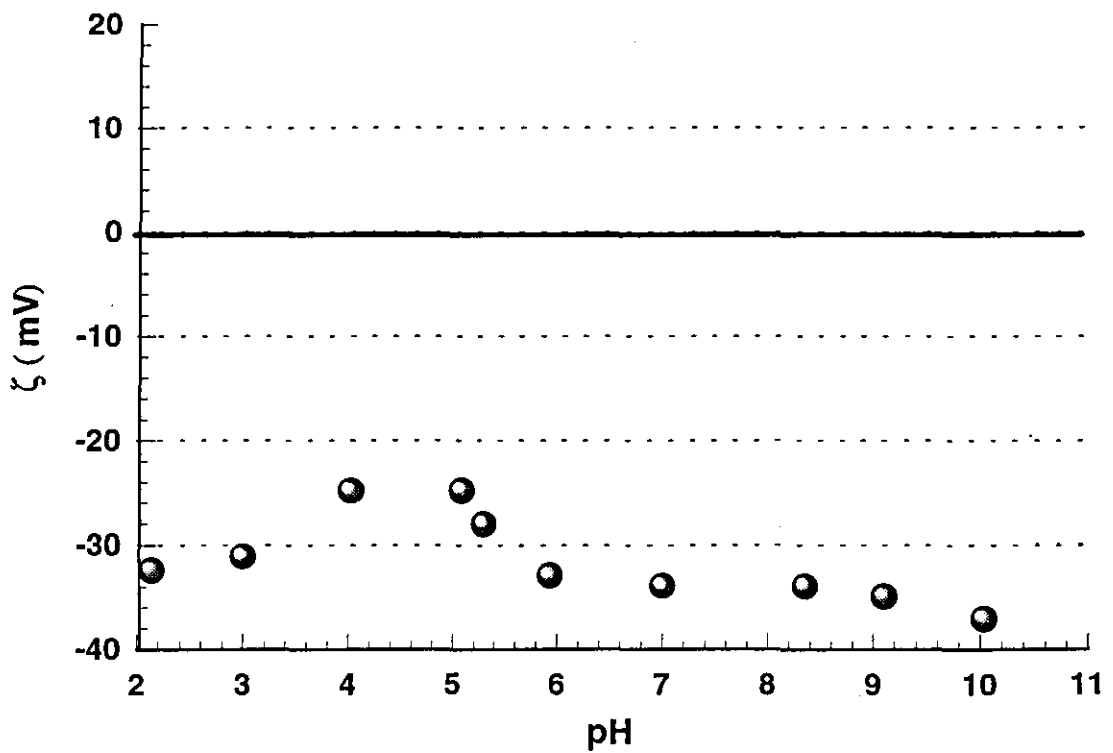


Figure A.56: Zeta Potential vs pH for dispersed Wyoming Bentonite particles in 4 mgL⁻¹ solution of Alum

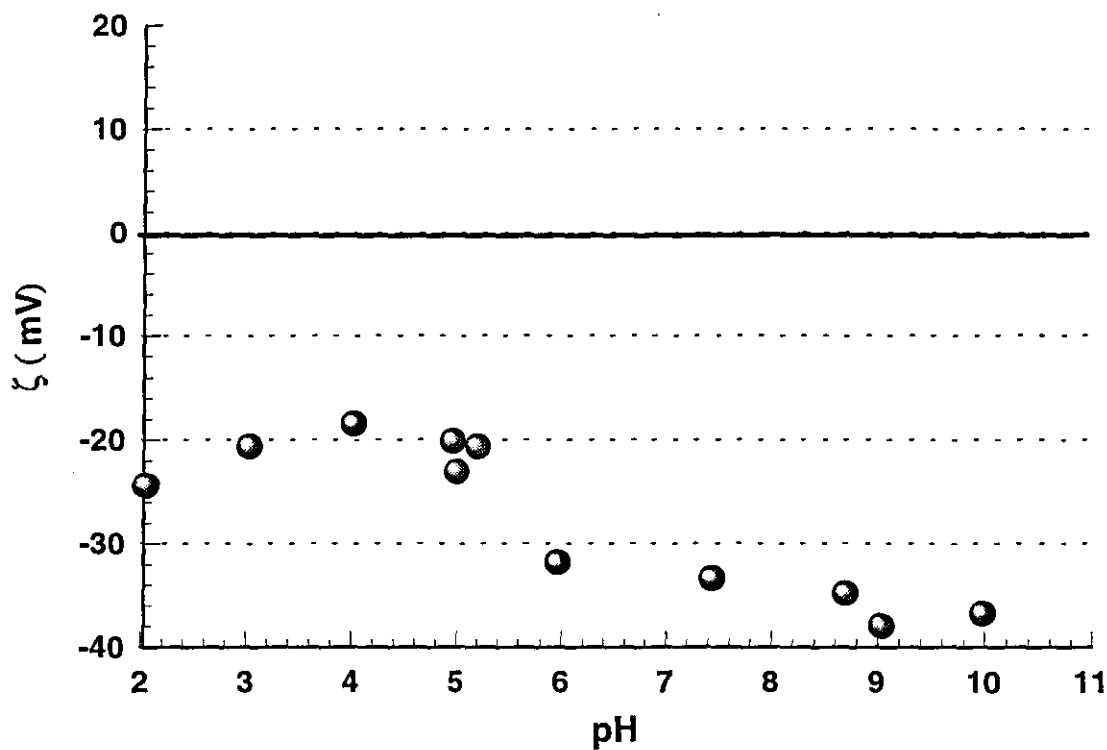


Figure A.57: Zeta Potential vs pH for dispersed Wyoming Bentonite particles in 8 mgL⁻¹ solution of Alum

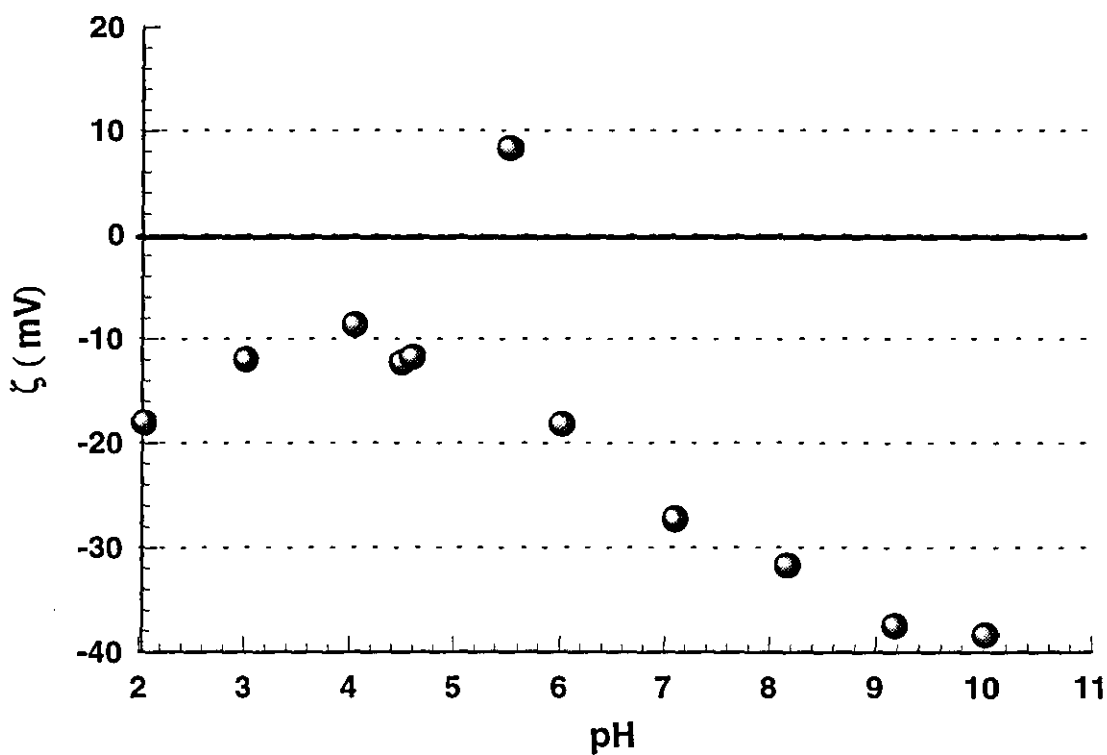


Figure A.58: Zeta Potential vs pH for dispersed Wyoming Bentonite particles in 16 mgL⁻¹ solution of Alum

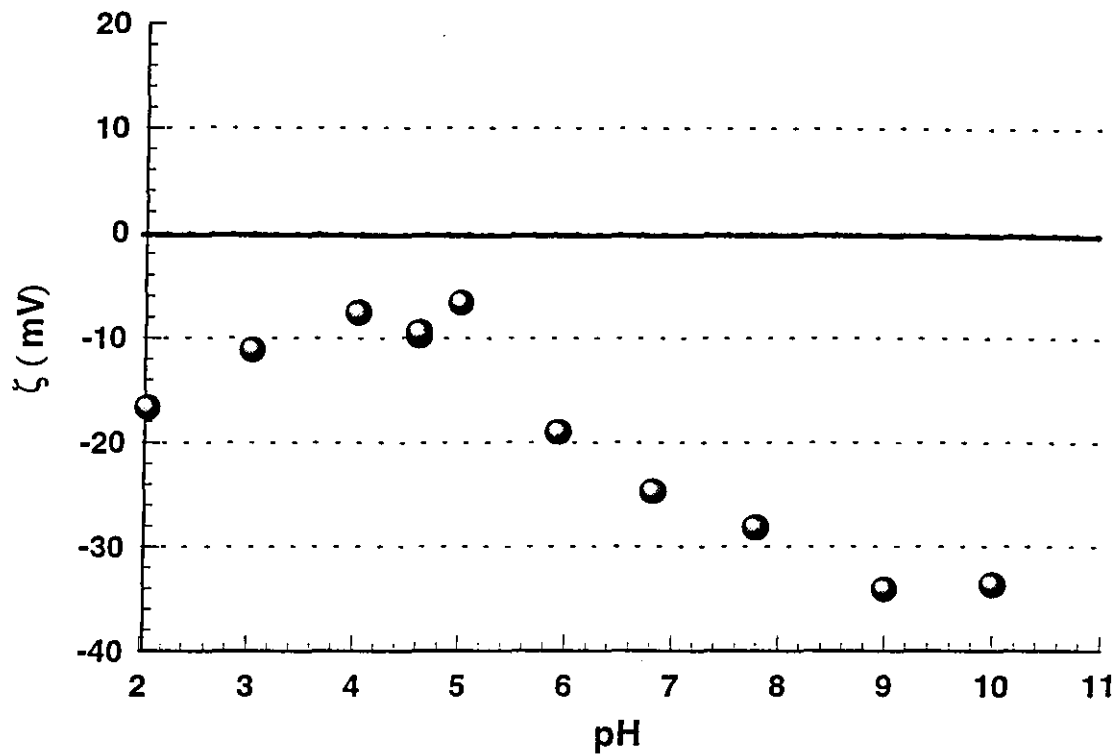


Figure A.59: Zeta Potential vs pH for dispersed Wyoming Bentonite particles in 20 mgL⁻¹ solution of Alum

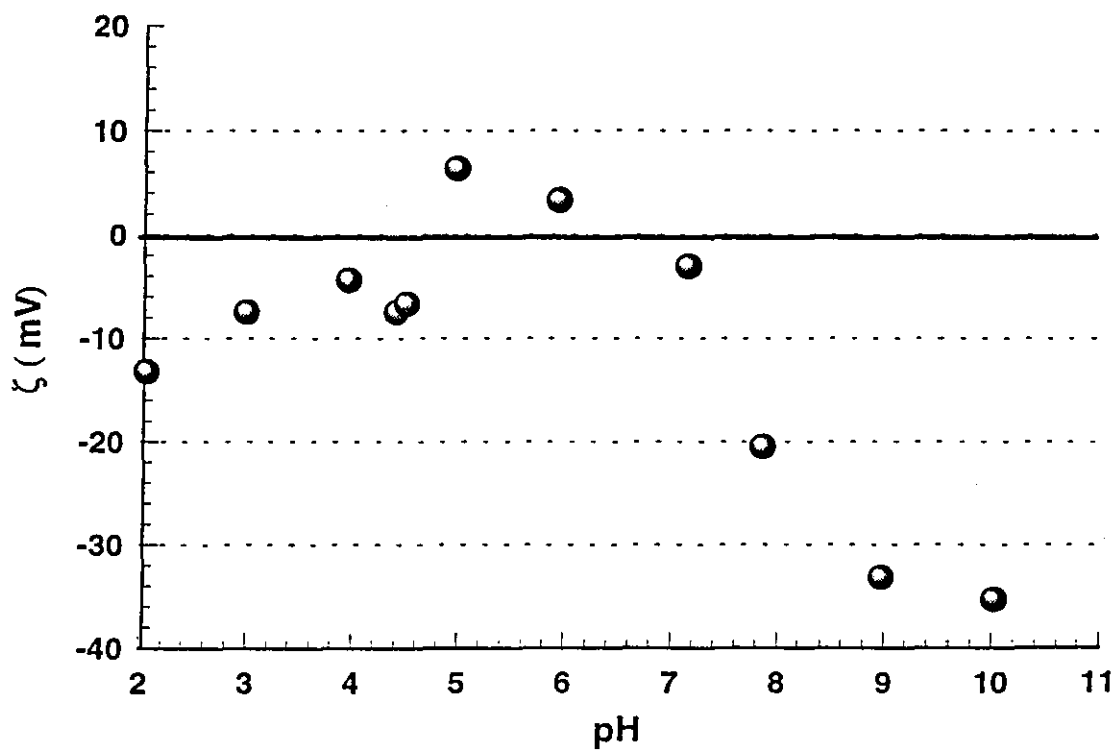


Figure A.60: Zeta Potential vs pH for dispersed Wyoming Bentonite particles in 40 mgL⁻¹ solution of Alum

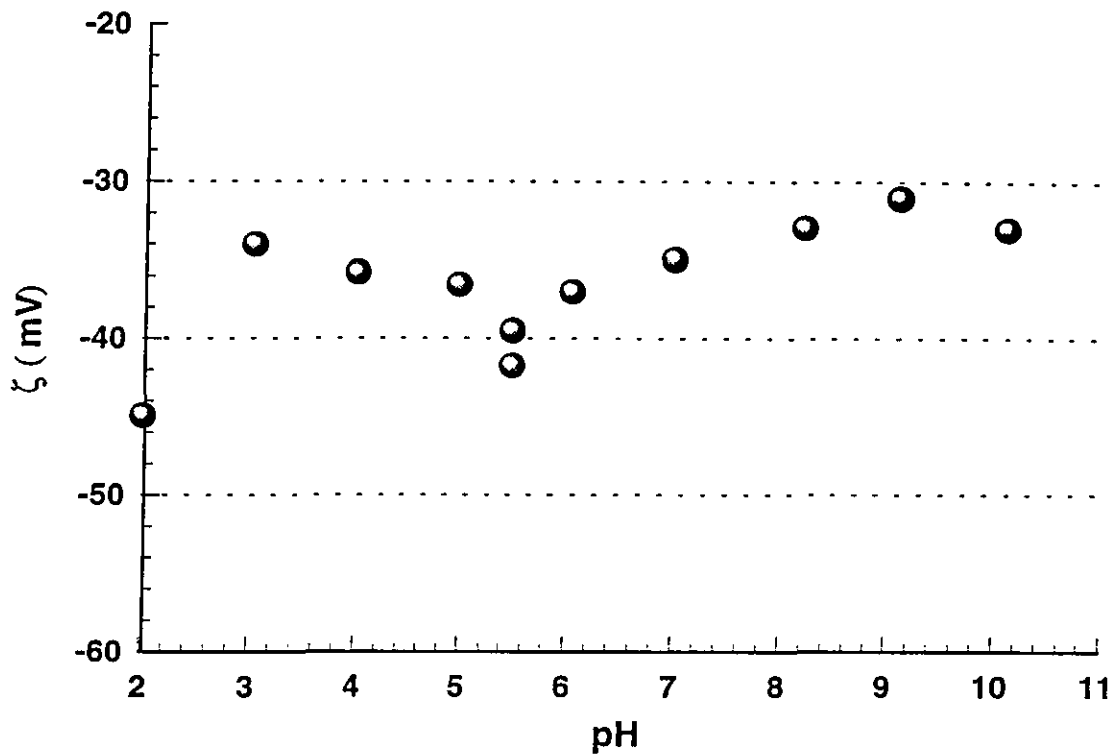


Figure A.61: Zeta Potential vs pH for dispersed Wyoming Bentonite particles in 0.02 mgL^{-1} solution of Ferric Chloride

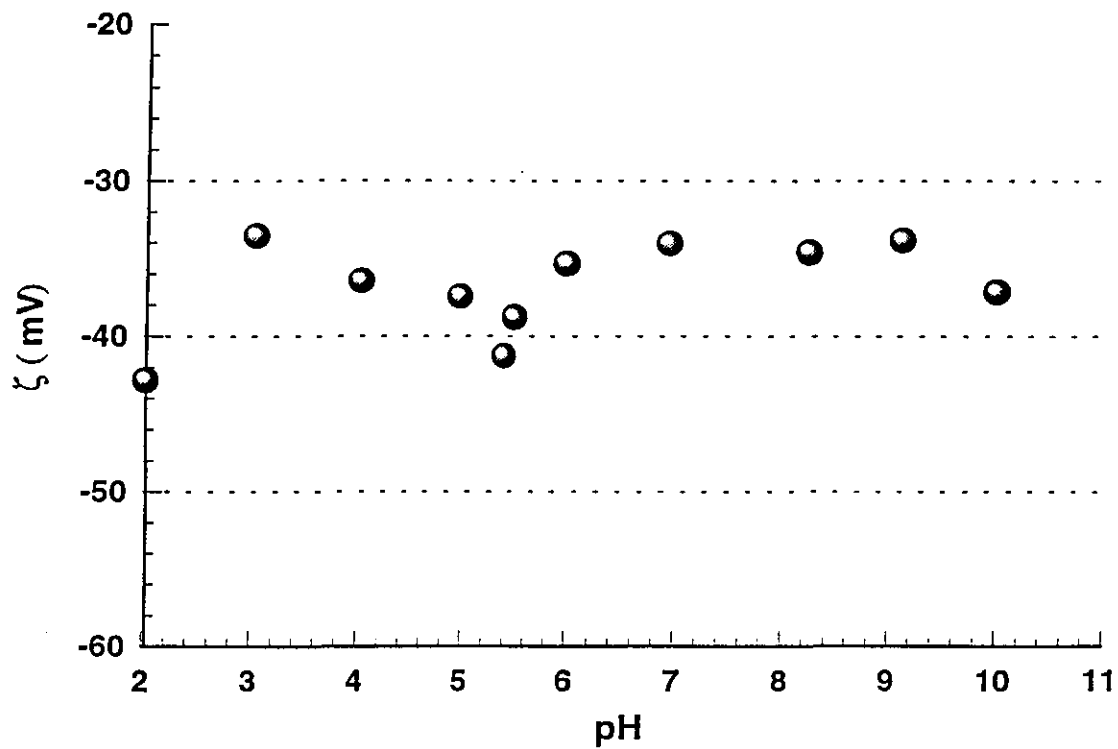


Figure A.62: Zeta Potential vs pH for dispersed Wyoming Bentonite particles in 0.06 mgL^{-1} solution of Ferric Chloride

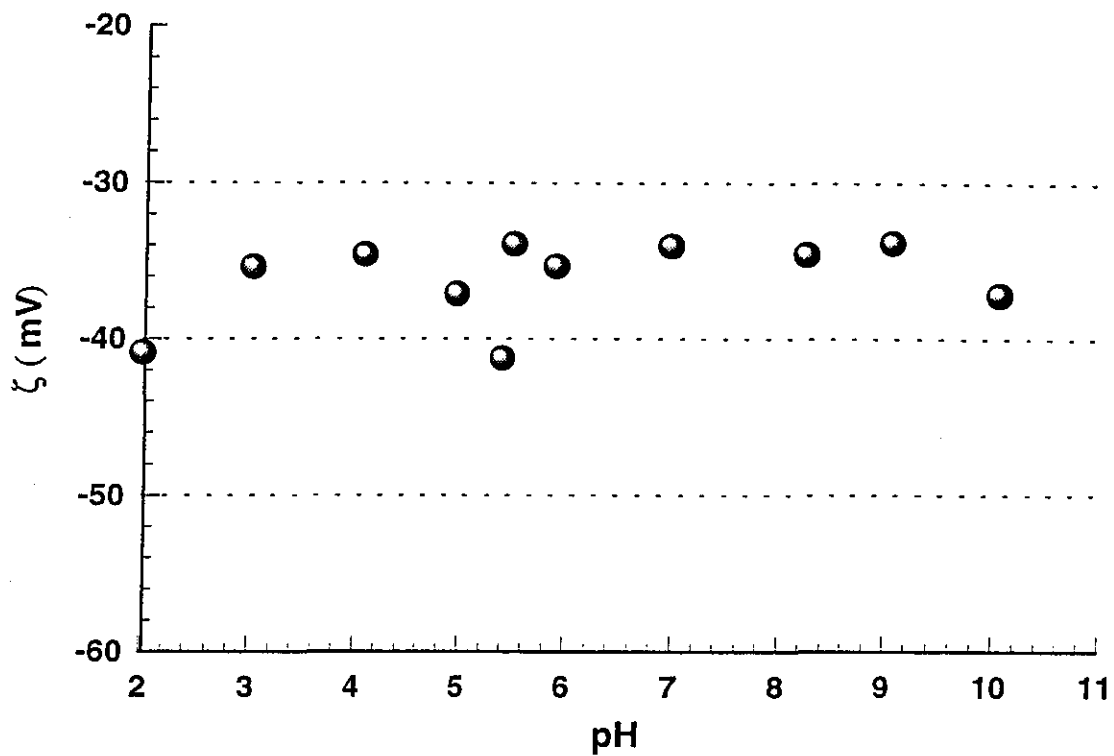


Figure A.63: Zeta Potential vs pH for dispersed Wyoming Bentonite particles in 0.1 mgL⁻¹ solution of Ferric Chloride

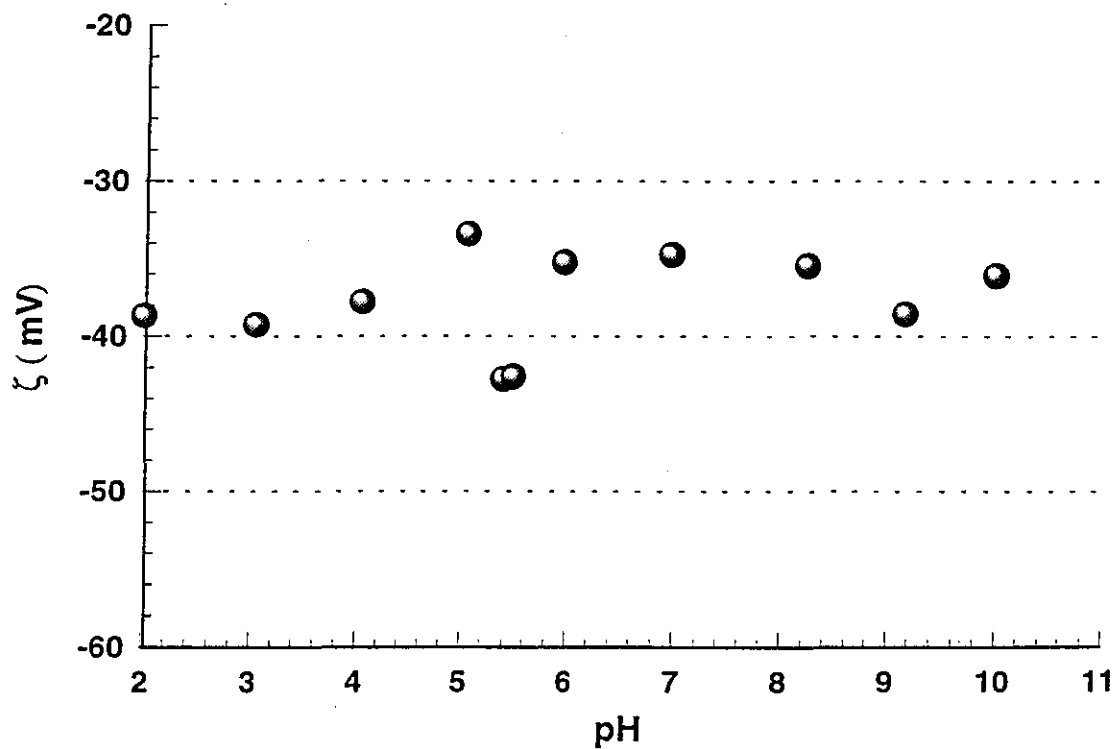


Figure A.64: Zeta Potential vs pH for dispersed Wyoming Bentonite particles in 0.14 mgL⁻¹ solution of Ferric Chloride

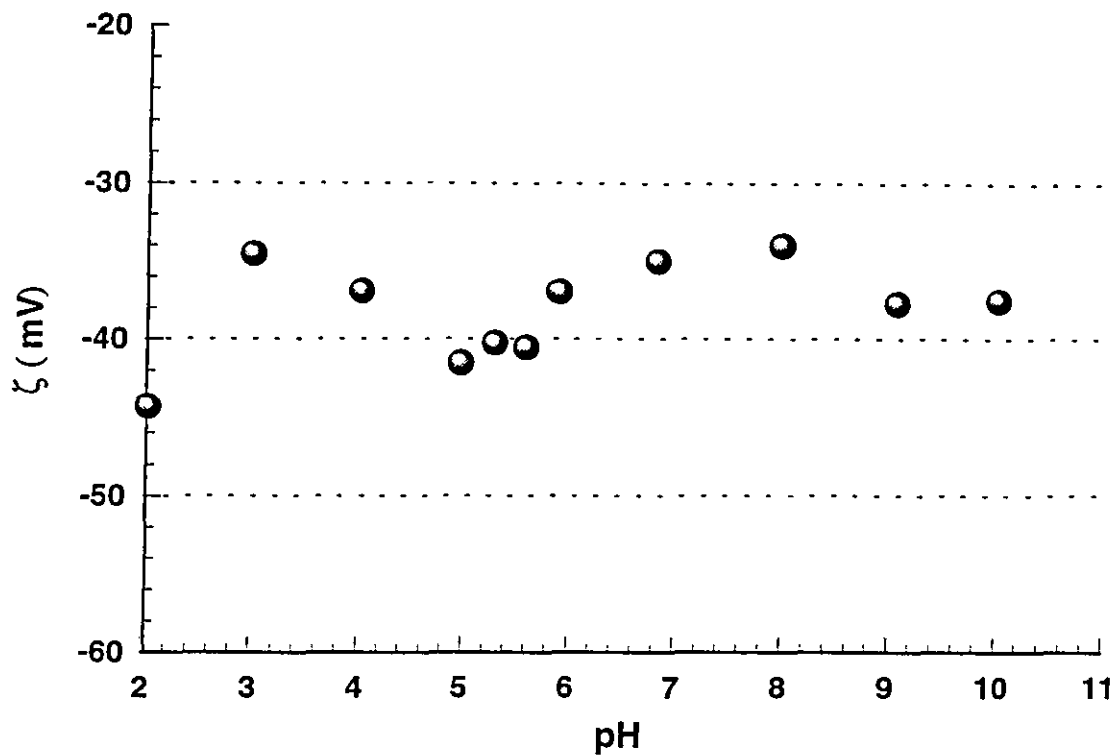


Figure A.65: Zeta Potential vs pH for dispersed Wyoming Bentonite particles in 0.2 mgL^{-1} solution of Ferric Chloride

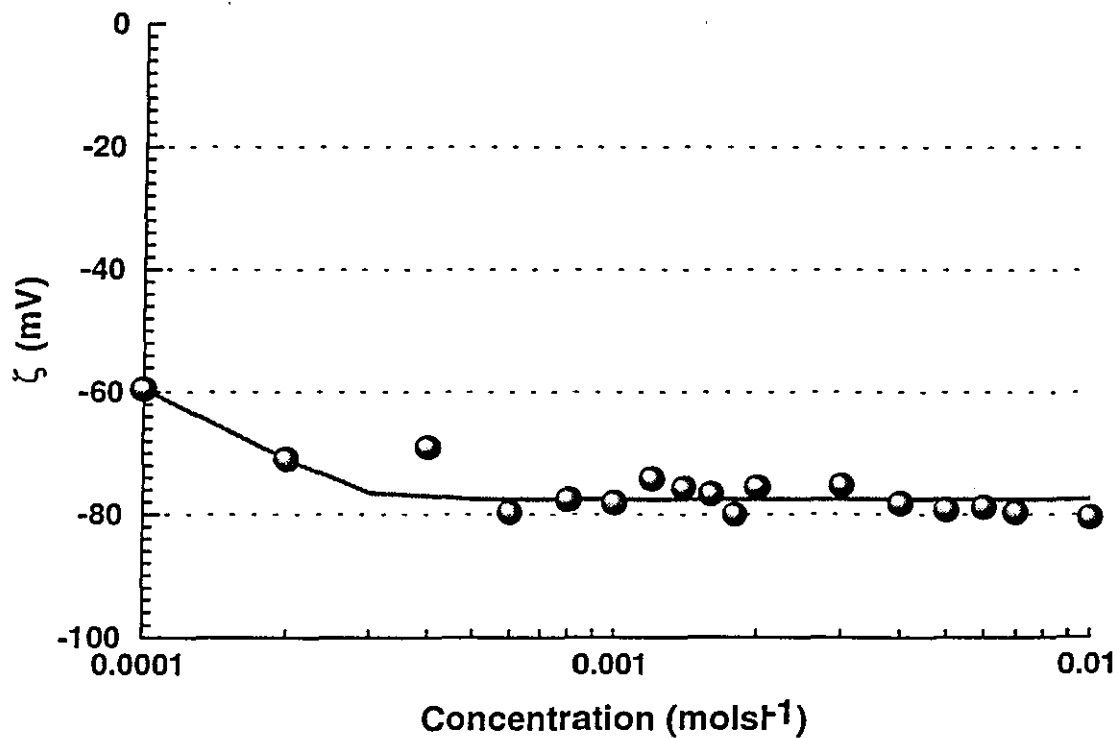


Figure A.66: Zeta Potential vs concentration of Sodium Hexametaphosphate on dispersed Kaolin particles in distilled water

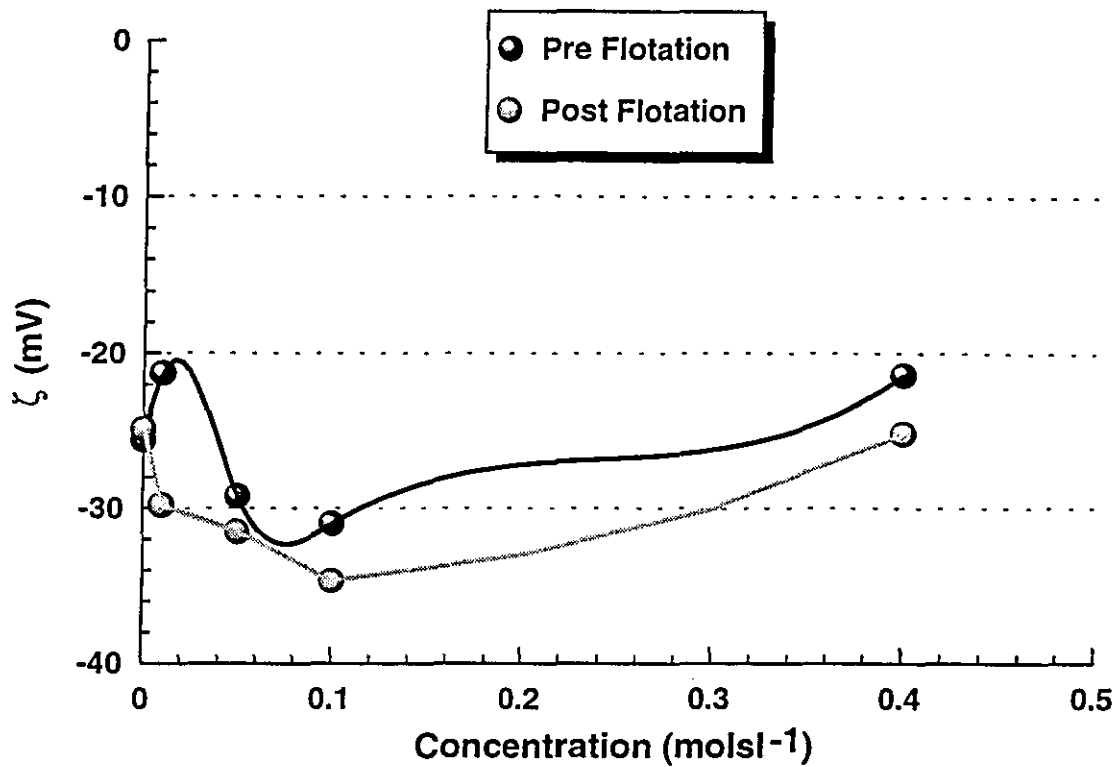


Figure A.67: Pre and Post Flotation Zeta Potential vs concentration of Sodium Chloride

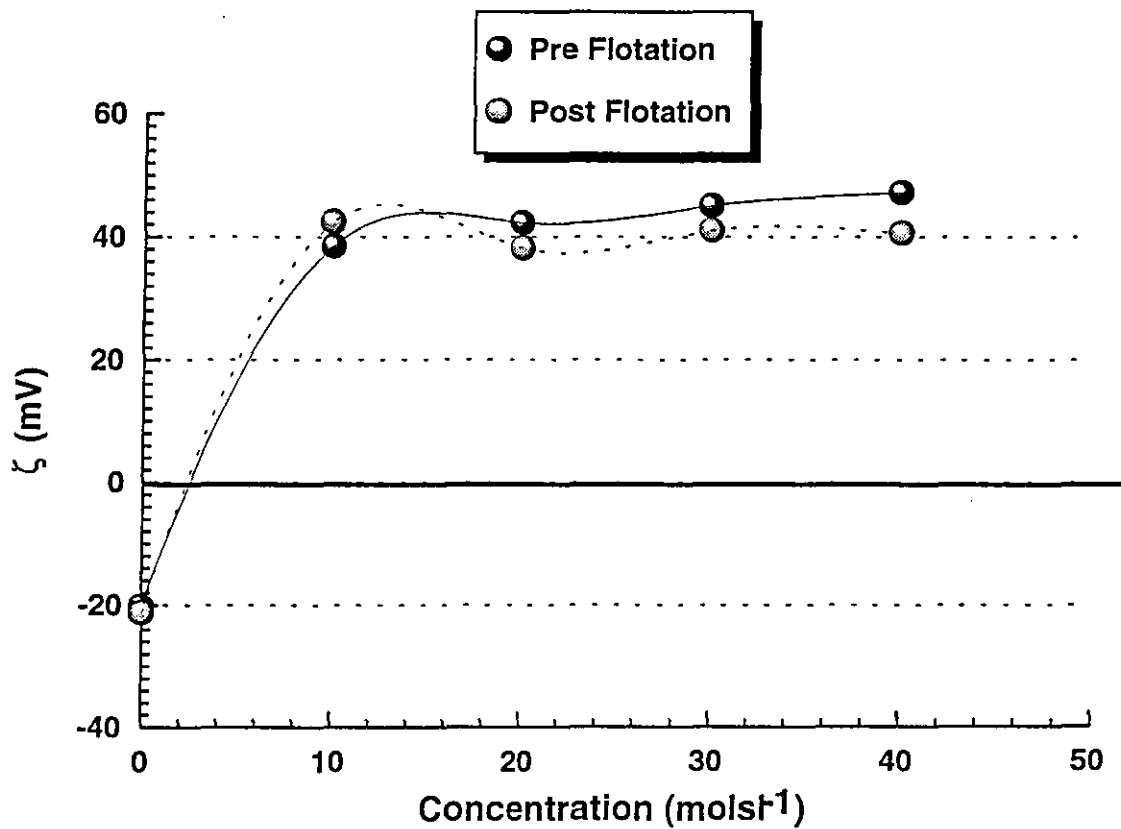


Figure A.68: Pre and Post Flotation Zeta Potential vs concentration of Ferric Chloride

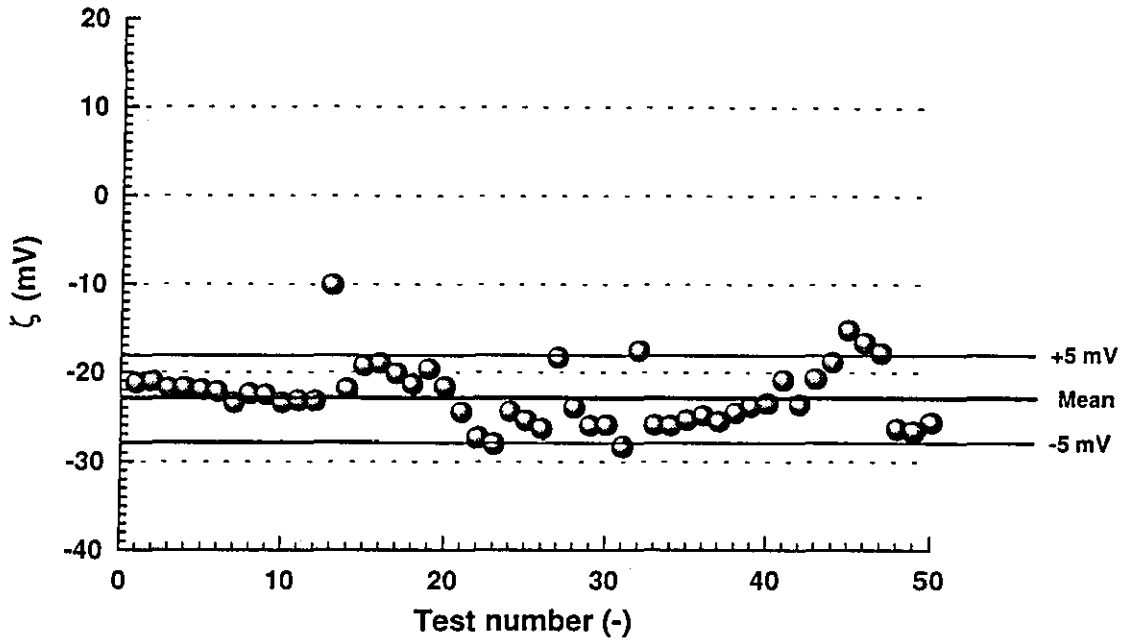


Figure A.69: The reproducibility of the Zeta Potential of Kaolin at its natural pH

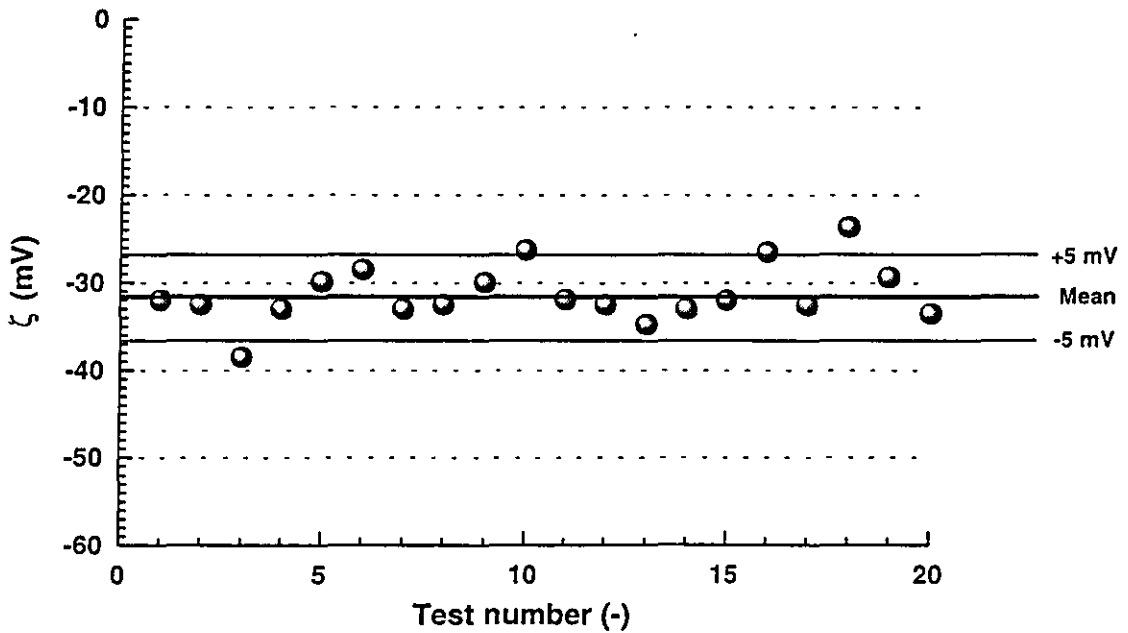


Figure A.70: The reproducibility of the Zeta Potential of Wyoming Bentonite at its natural pH

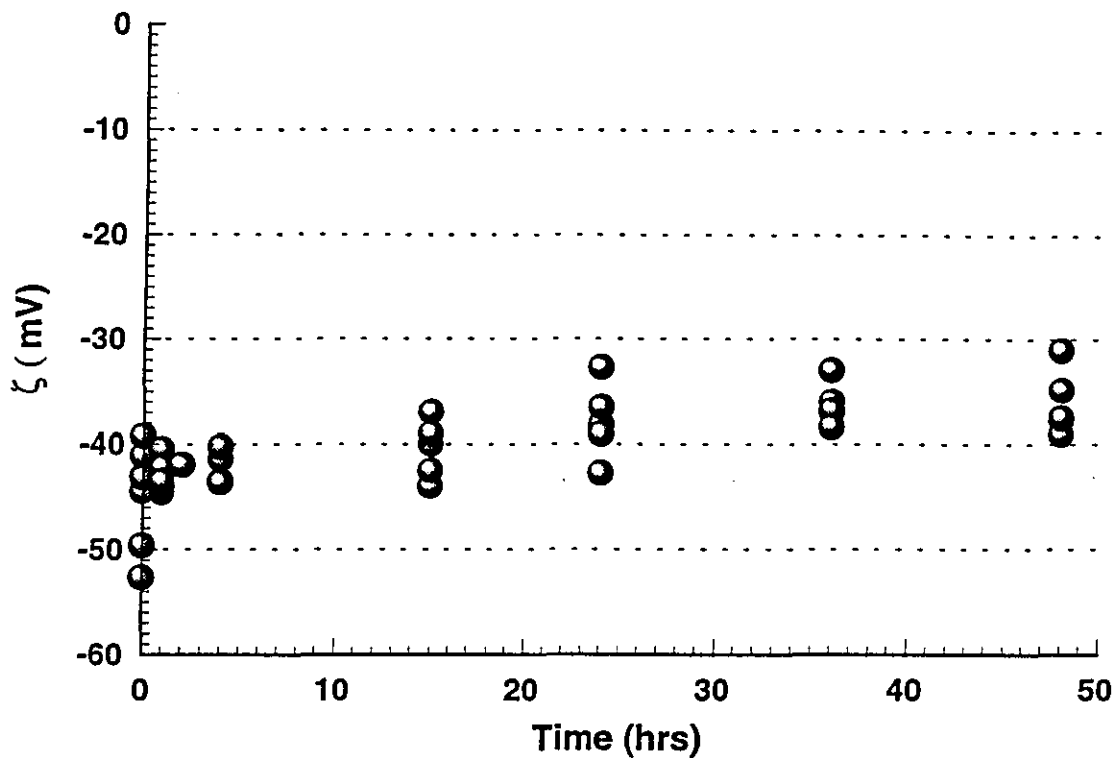


Figure A.71: Zeta Potential vs time for dispersed Wyoming Bentonite particles in distilled water

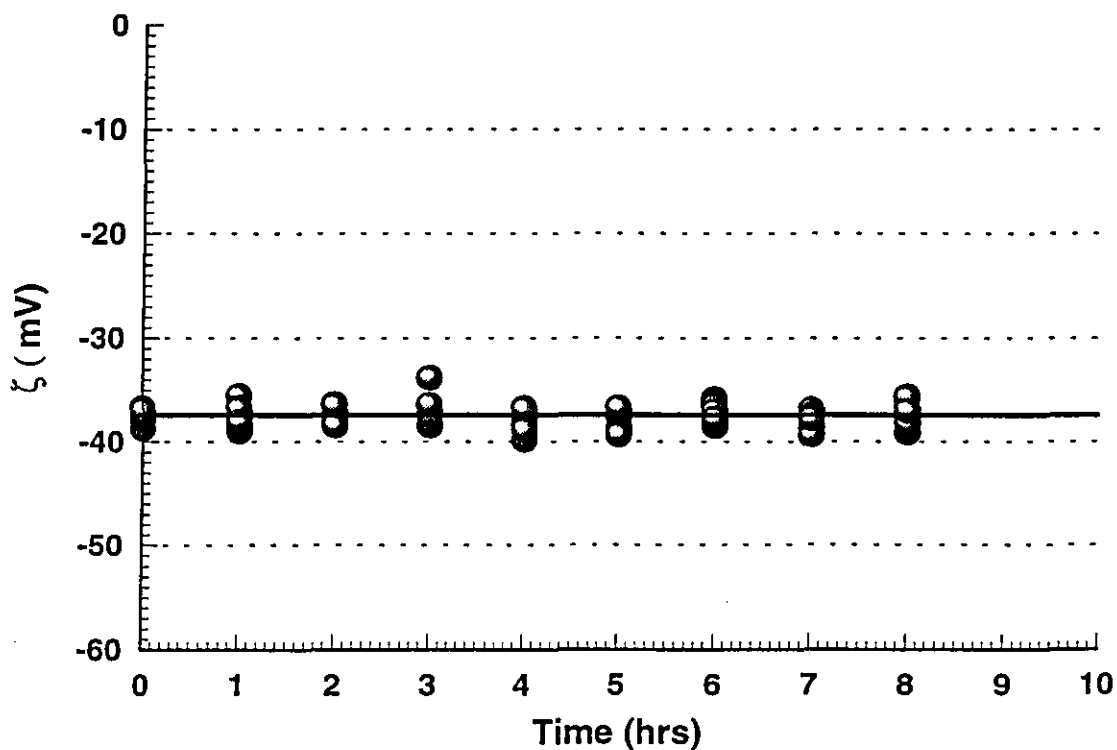


Figure A.72: Zeta Potential vs time for dispersed Wyoming Bentonite particles in distilled water at pH 2

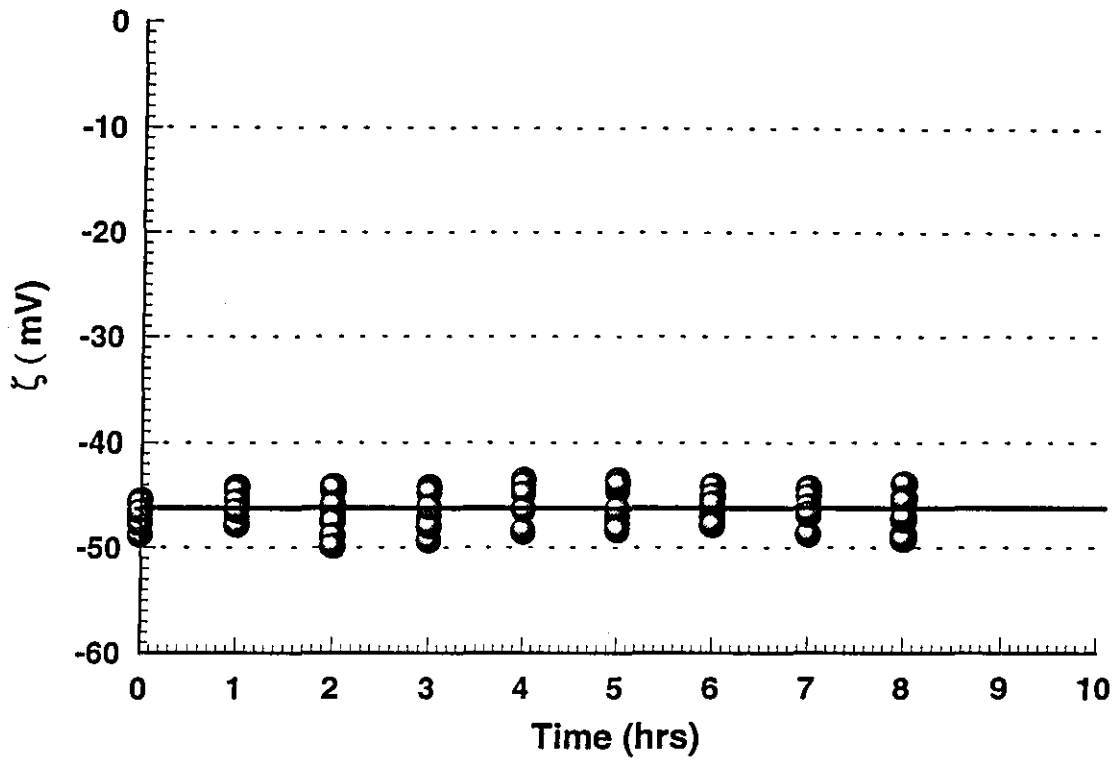


Figure A.73: Zeta Potential vs time for dispersed Wyoming Bentonite particles in distilled water at pH 11

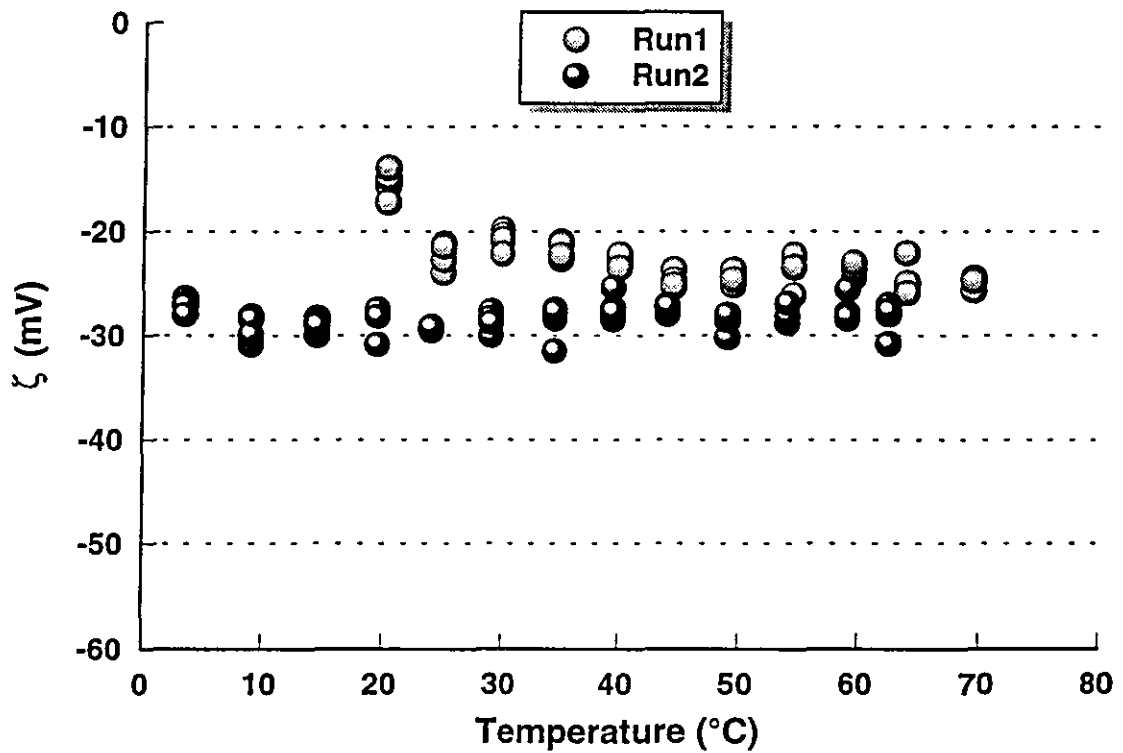


Figure A.74: Zeta Potential vs temperature for dispersed Kaolin particles in distilled water

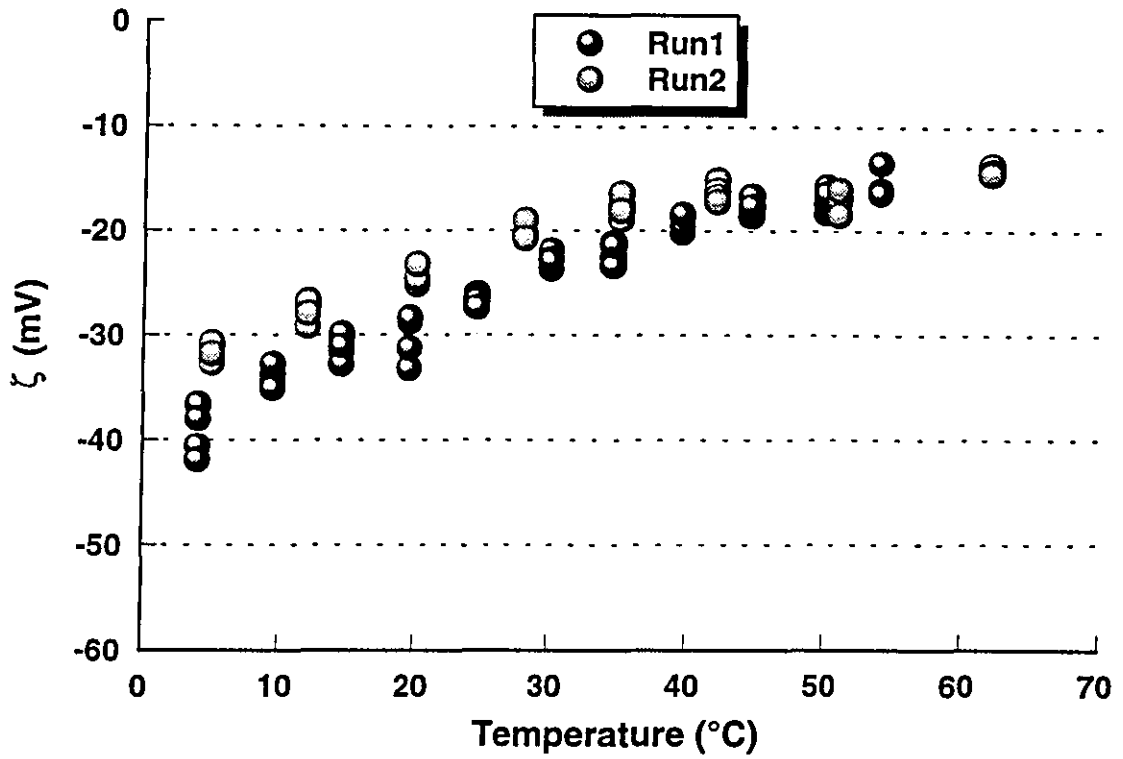


Figure A.75: Zeta Potential vs temperature for dispersed Wyoming Bentonite particles in distilled water

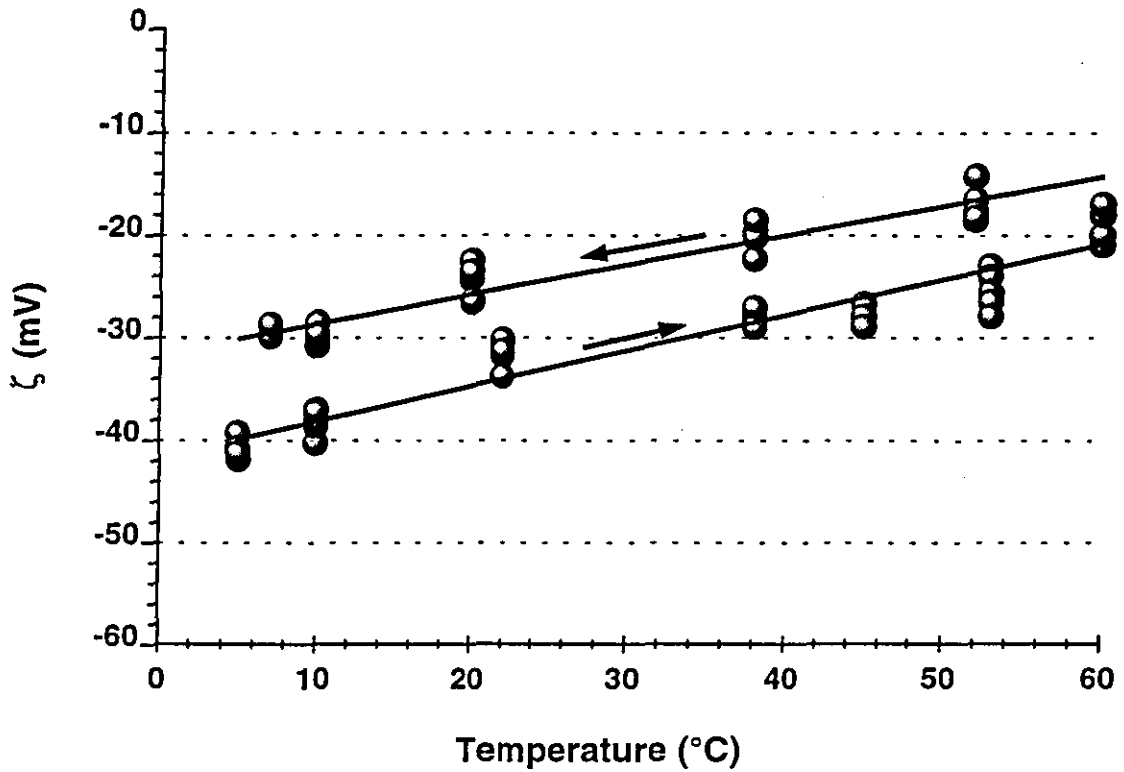


Figure A.76: Zeta Potential vs temperature for dispersed Wyoming Bentonite particles in distilled water

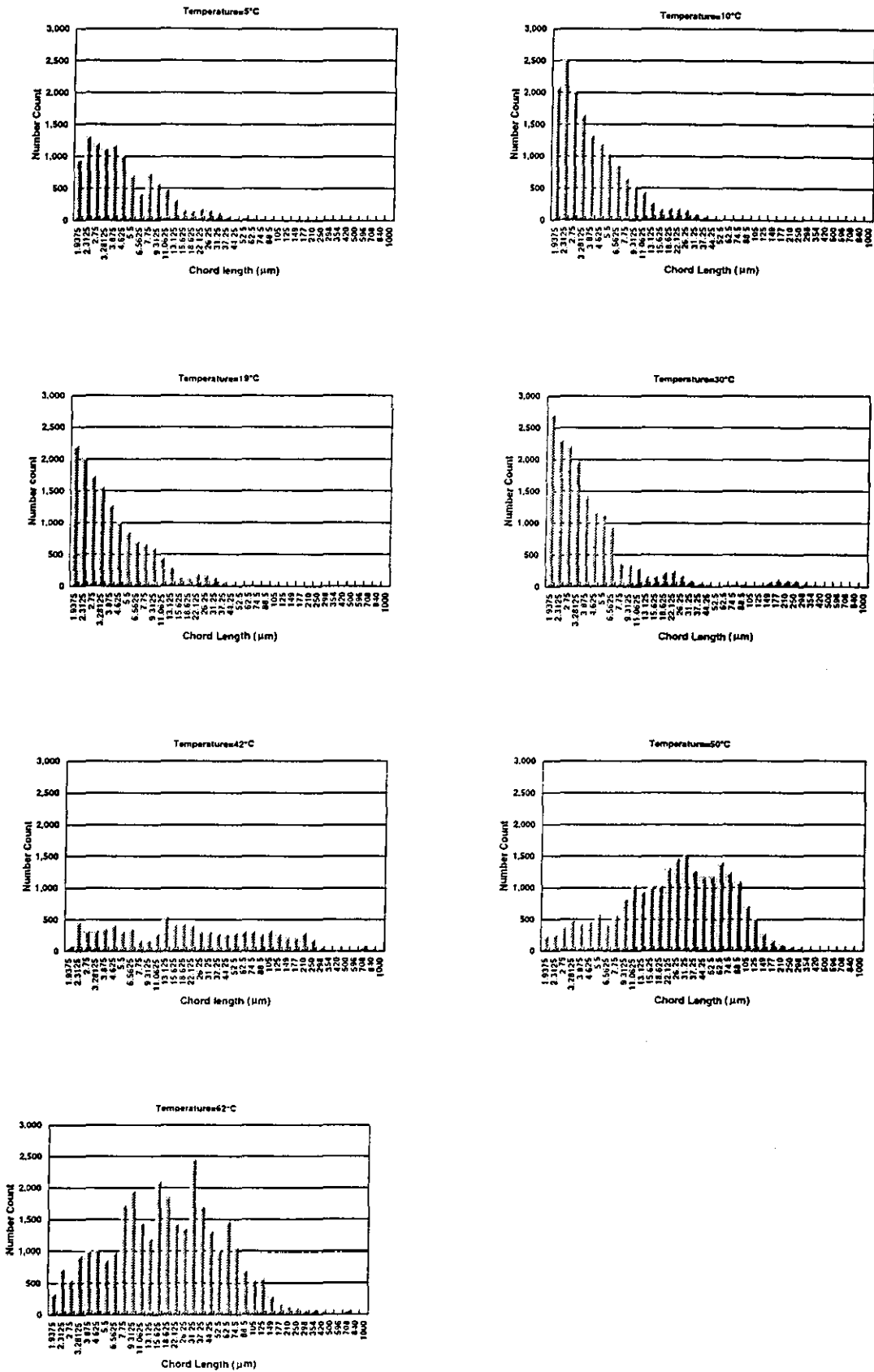


Figure A.77: Particle size distribution vs temperature for dispersed Wyoming Bentonite particles in distilled water

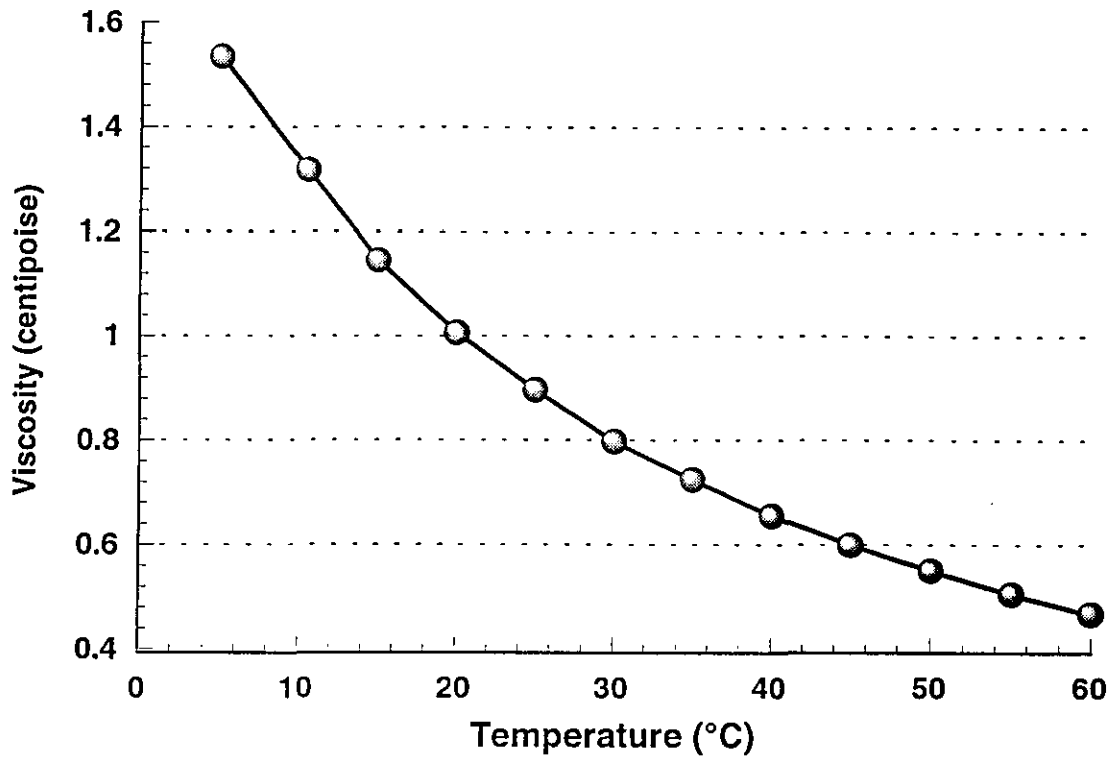


Figure A.78: Viscosity vs temperature for dispersed Wyoming Bentonite particles in distilled water

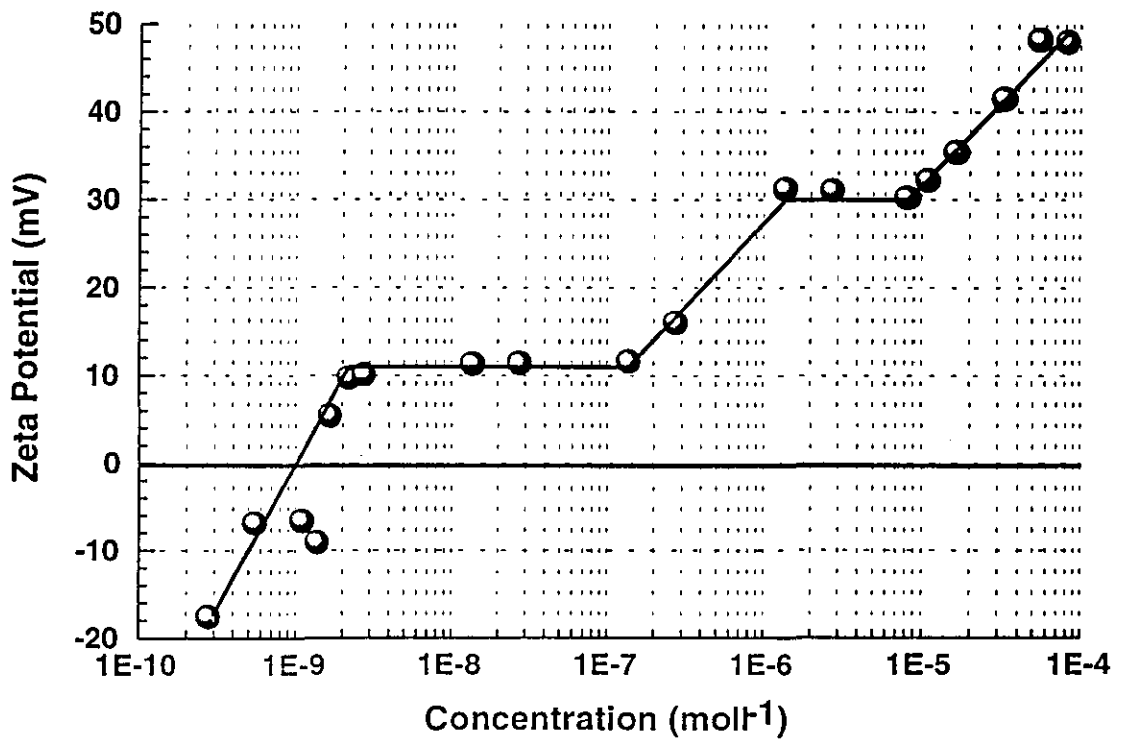


Figure A.79: Zeta Potential vs concentration of Hexadecyltrimethylammoniumbromide on single air bubbles in distilled water

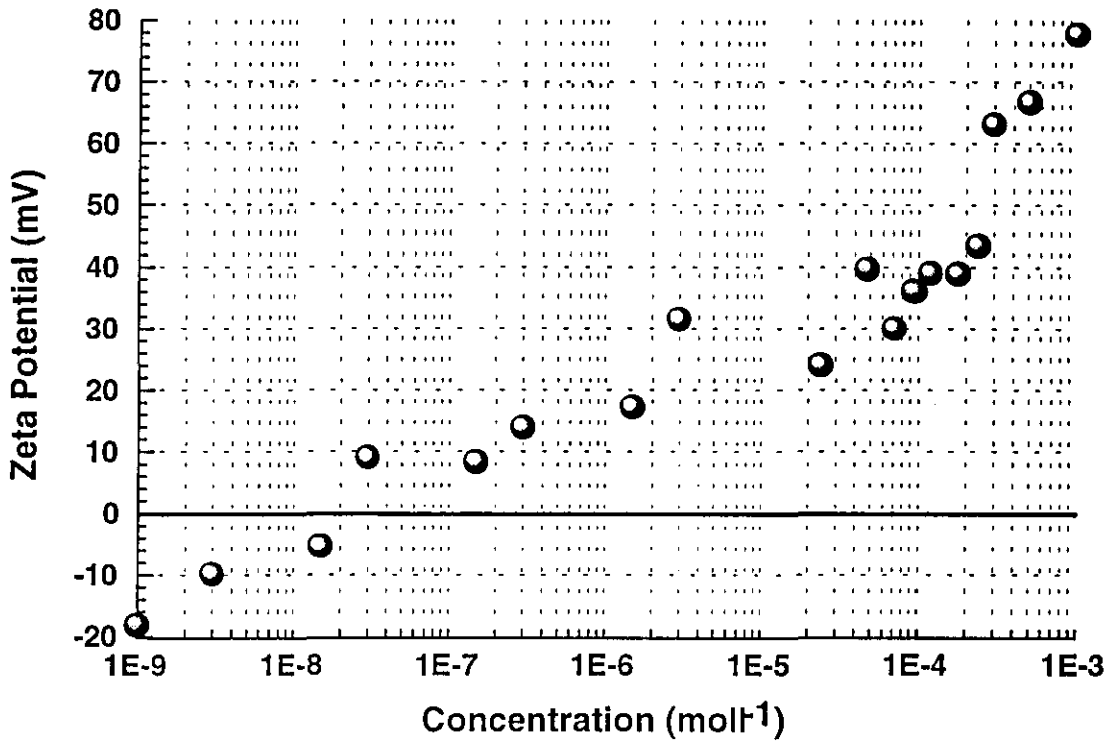


Figure A.80: Zeta Potential vs concentration of Tetradecyltrimethylammoniumbromide on single air bubbles in distilled water

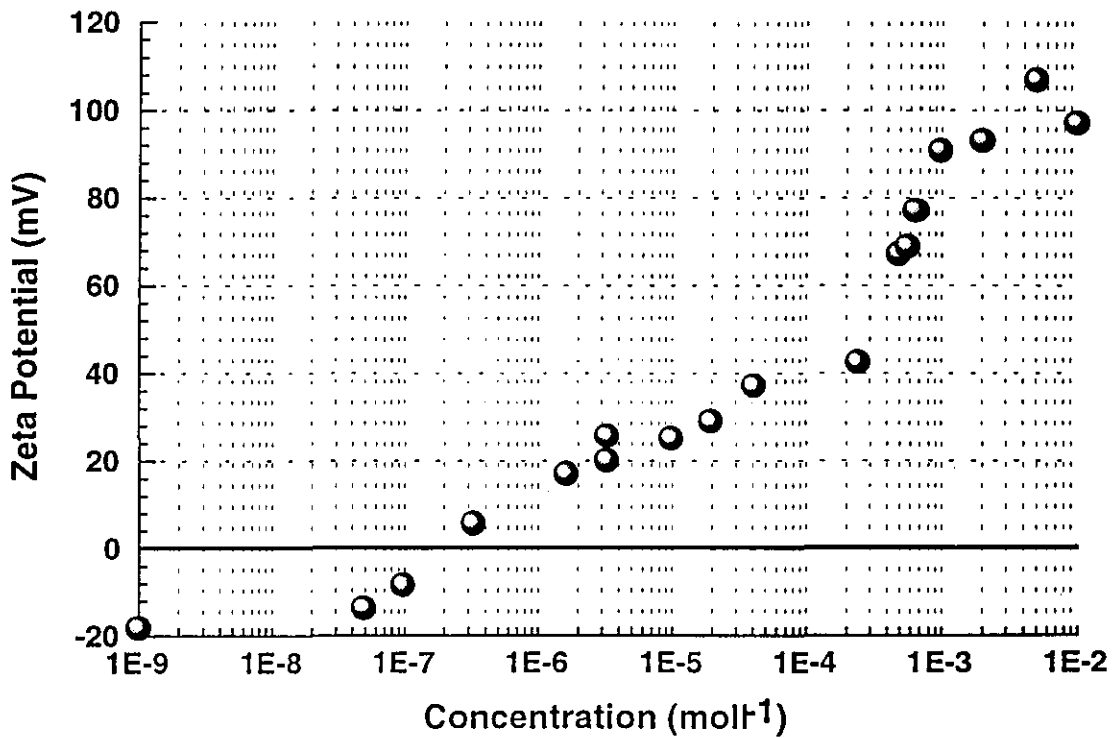


Figure A.81: Zeta Potential vs concentration of Dodecyltrimethylammoniumbromide on single air bubbles in distilled water

APPENDIX B

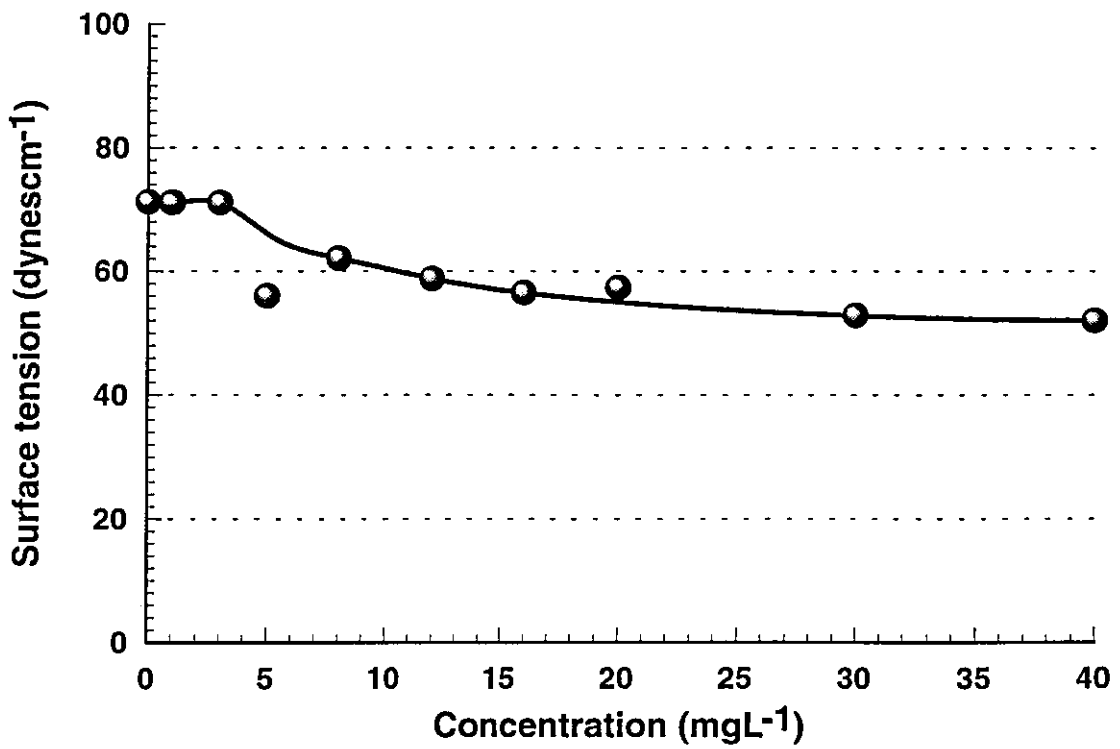
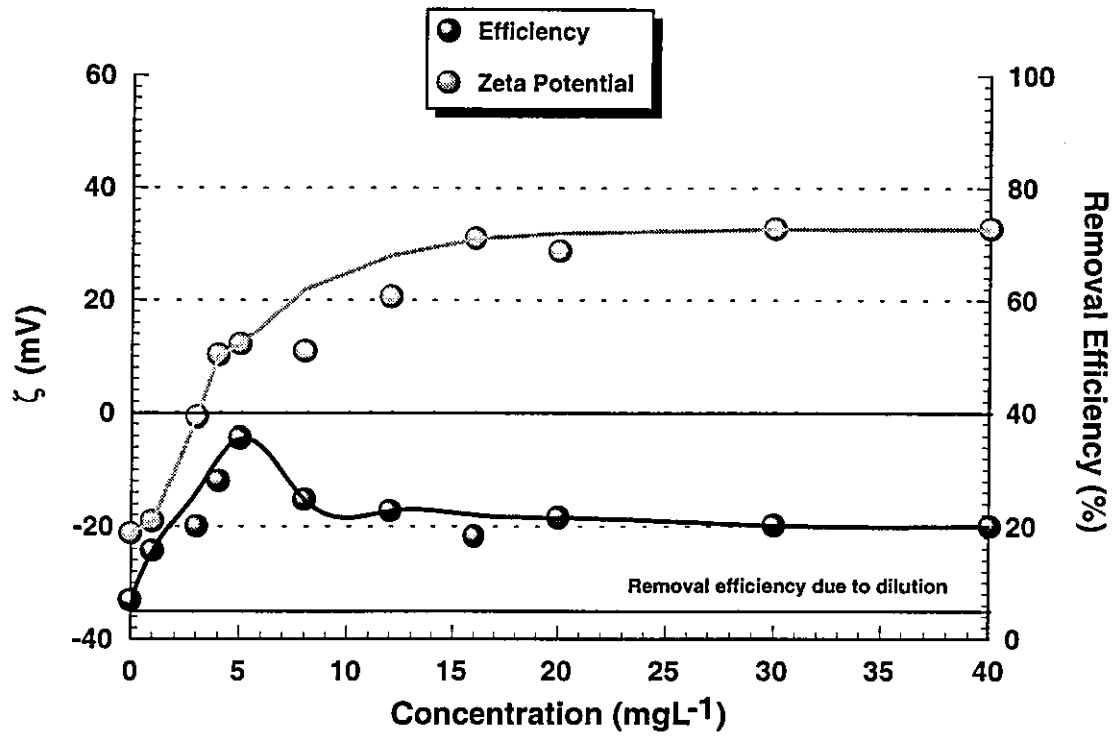


Figure B1: Flotation response vs concentration of Hexadecyltrimethylammoniumbromide for dispersed Kaolin particles, R=5%

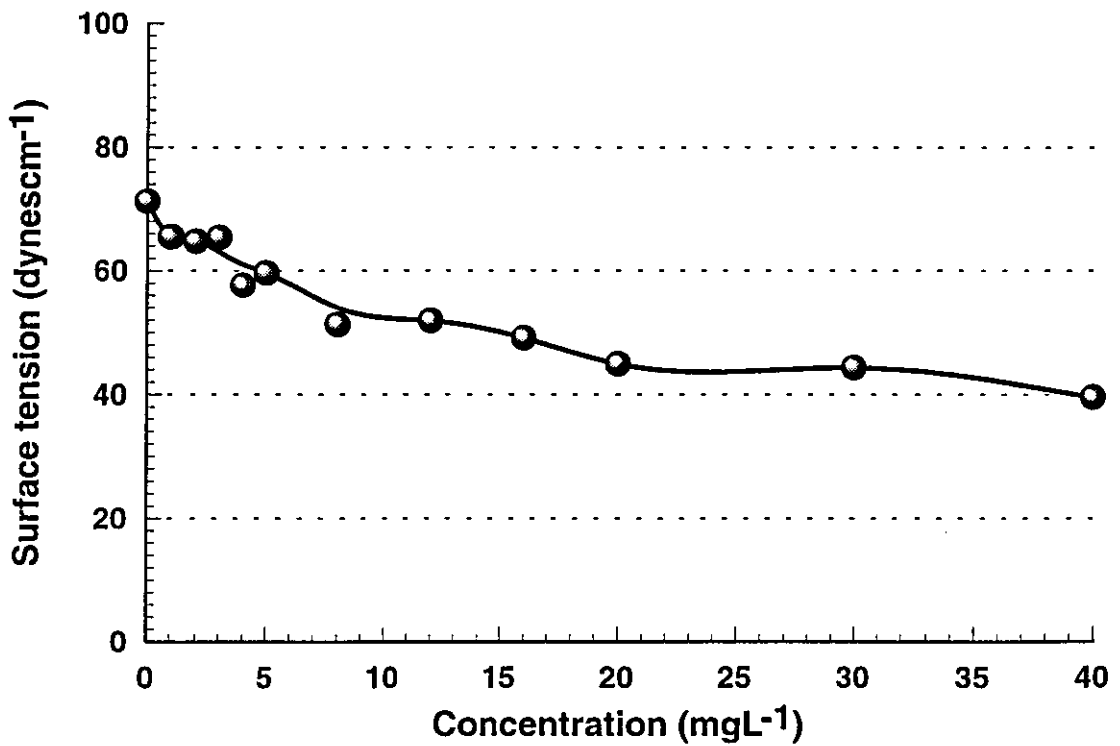
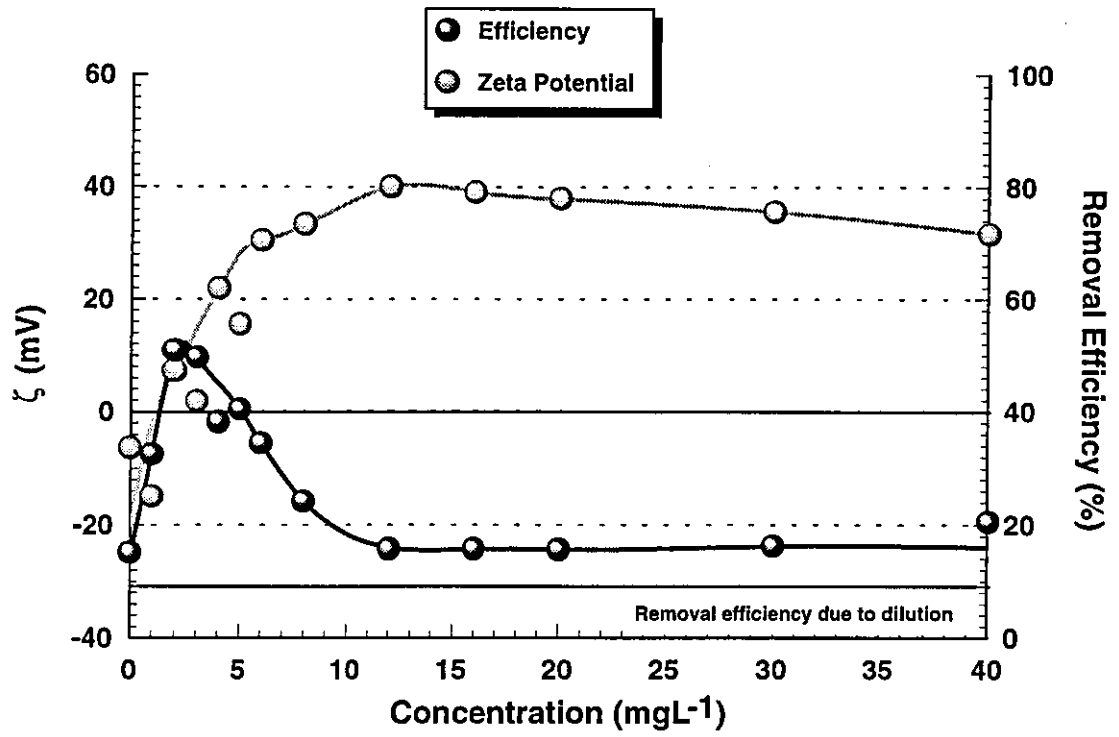


Figure B2: Flotation response vs concentration of Hexadecyltrimethylammoniumbromide for dispersed Kaolin particles, R=10%

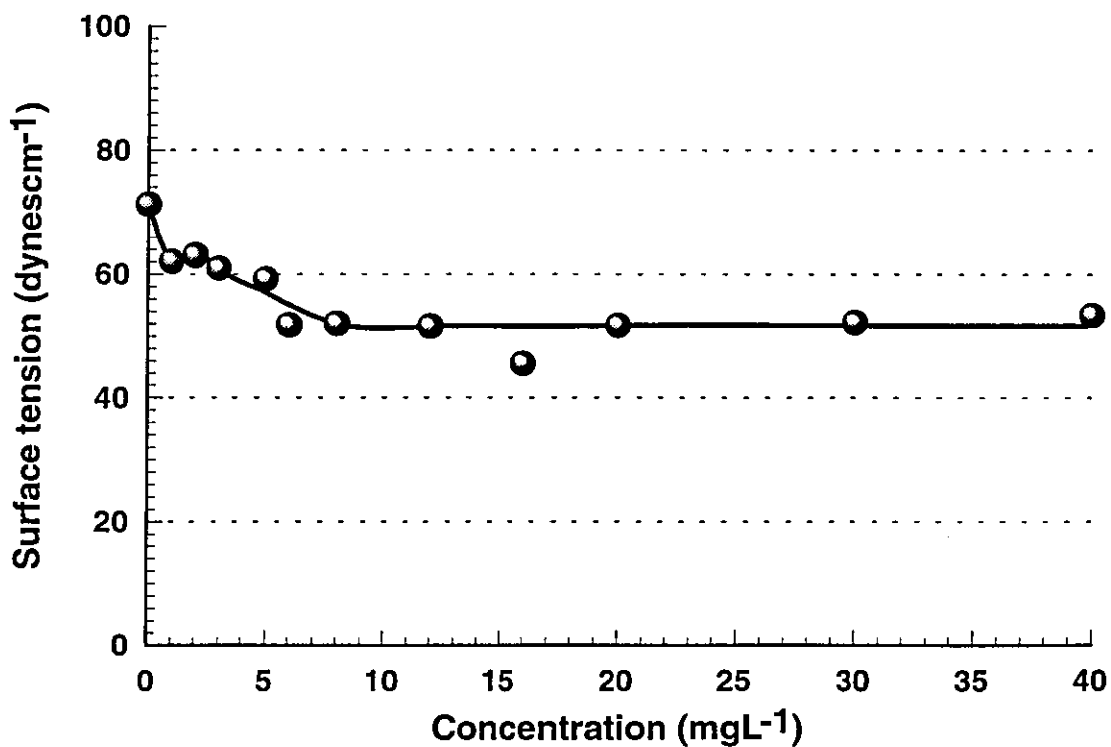
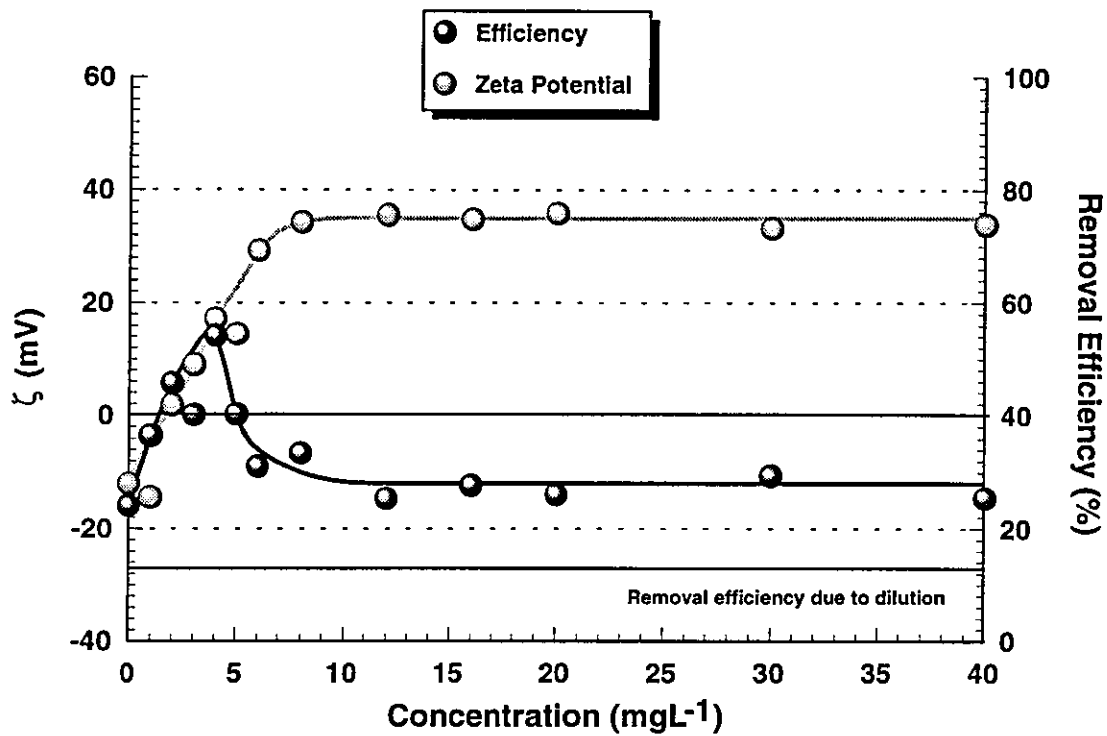


Figure B3: Flotation response vs concentration of Hexadecyltrimethylammoniumbromide for dispersed Kaolin particles, R=15%

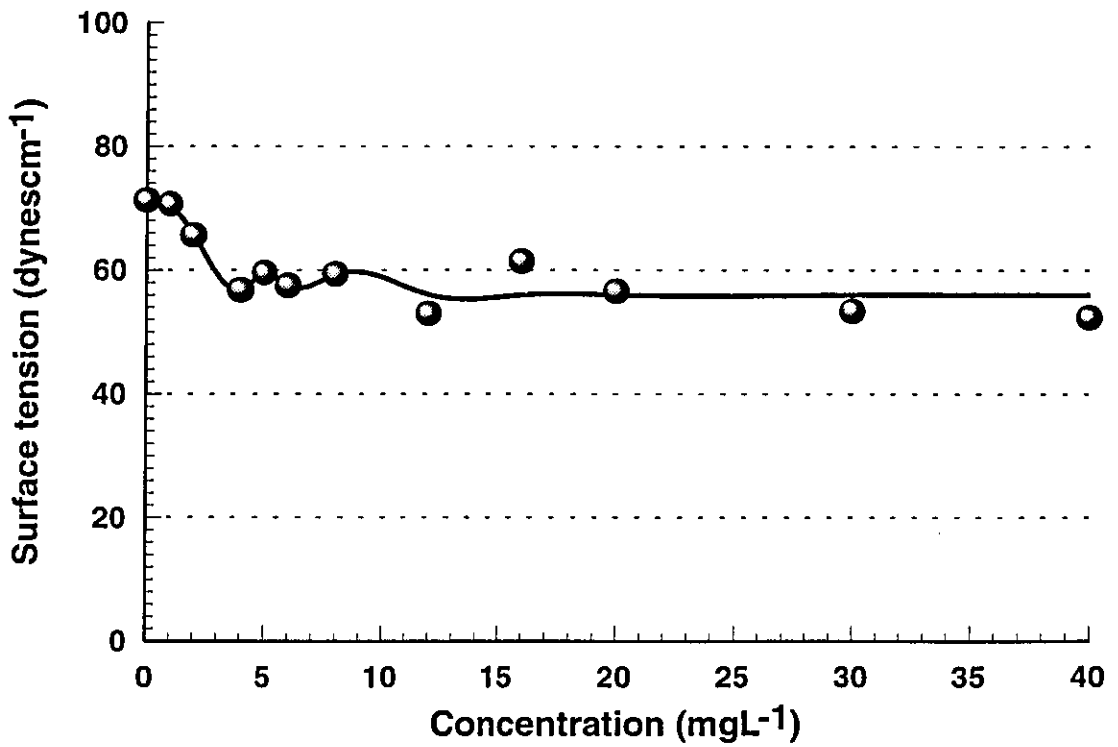
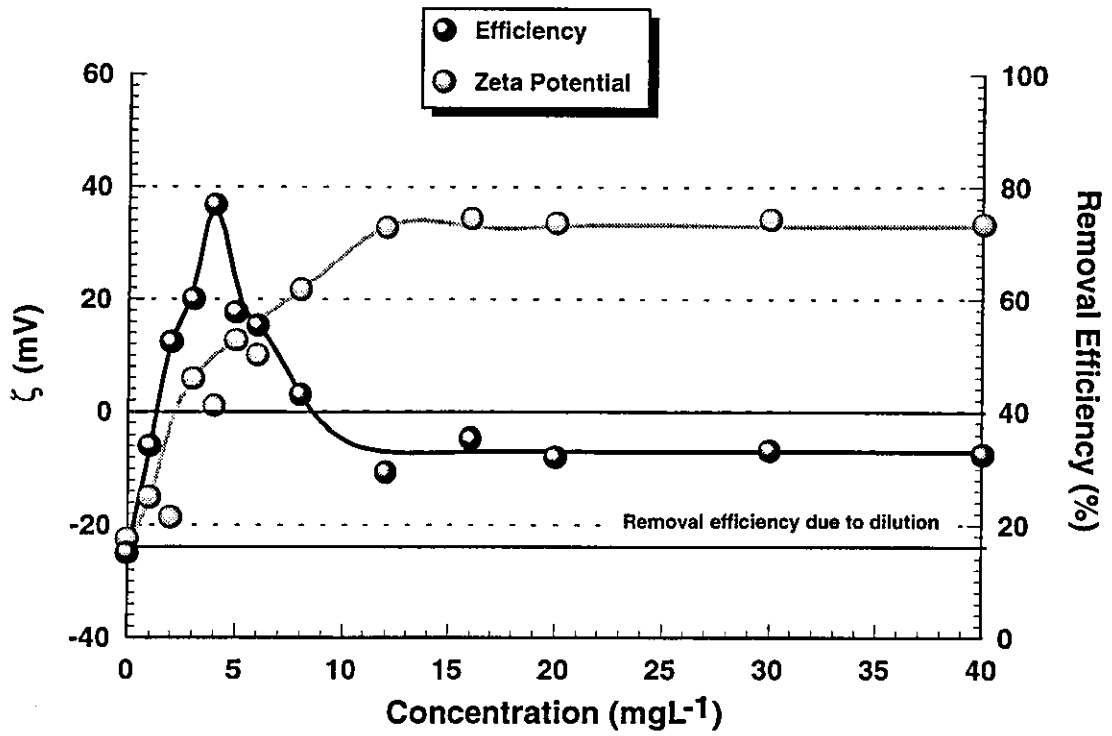


Figure B4: Flotation response vs concentration of Hexadecyltrimethylammoniumbromide for dispersed Kaolin particles, R=20%

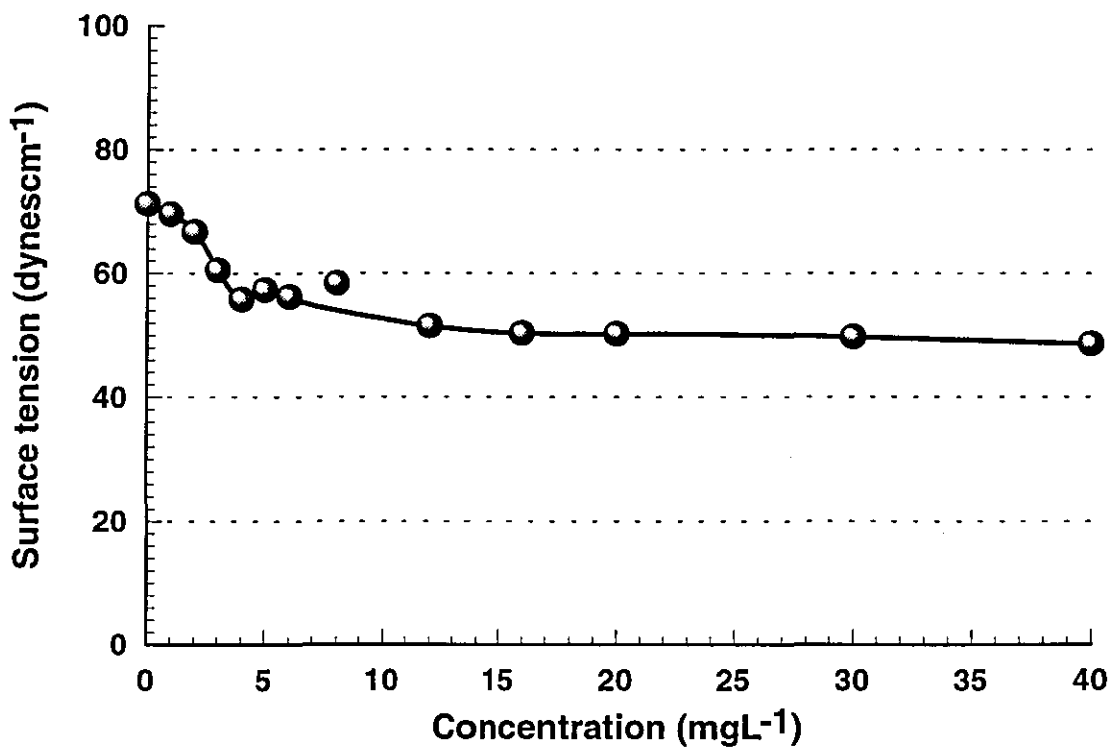
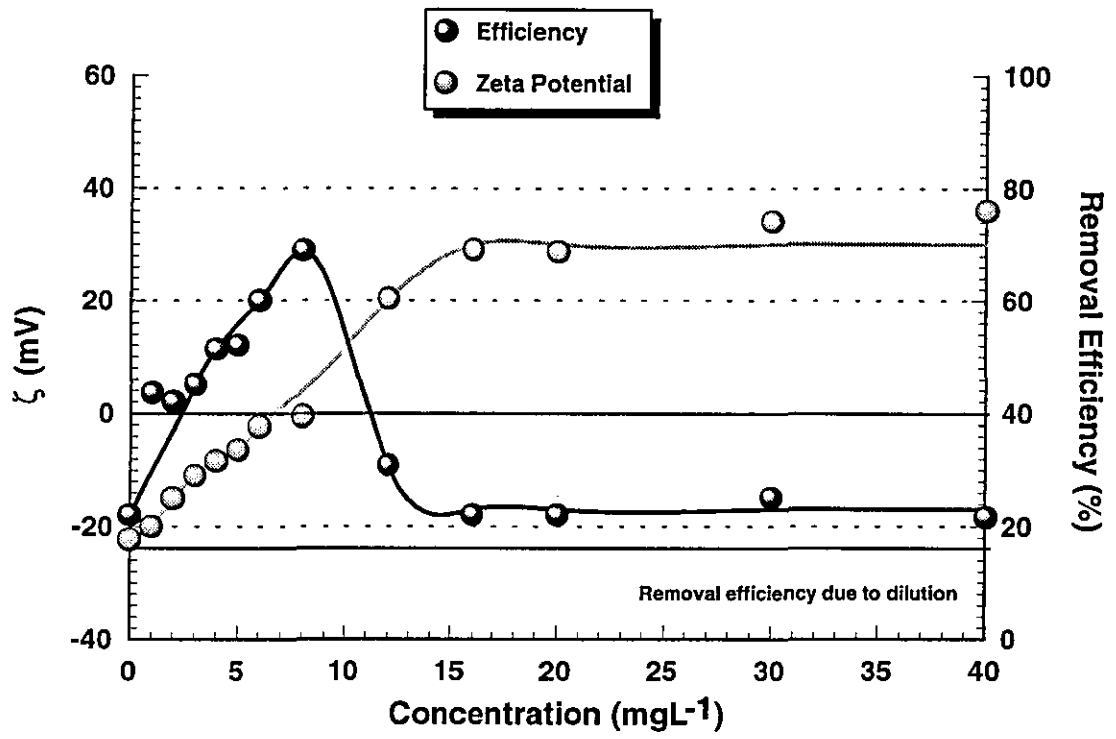


Figure B5: Flotation response vs concentration of Hexadecyltrimethylammoniumbromide for dispersed Kaolin particles, R=25%

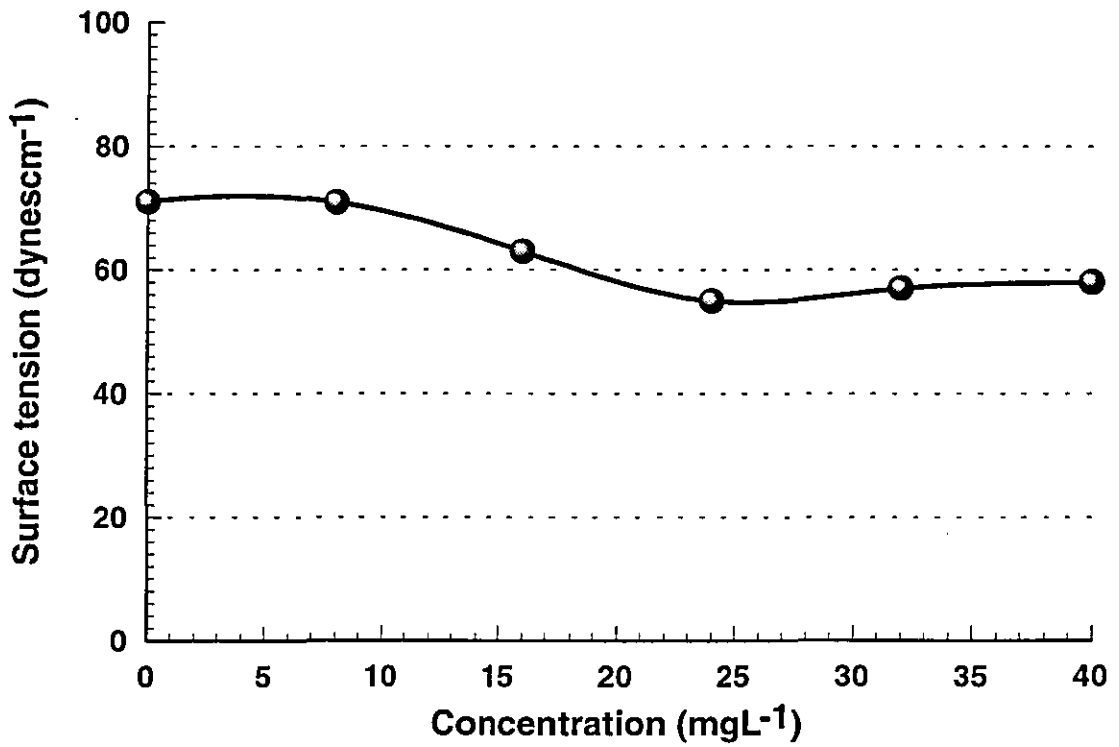
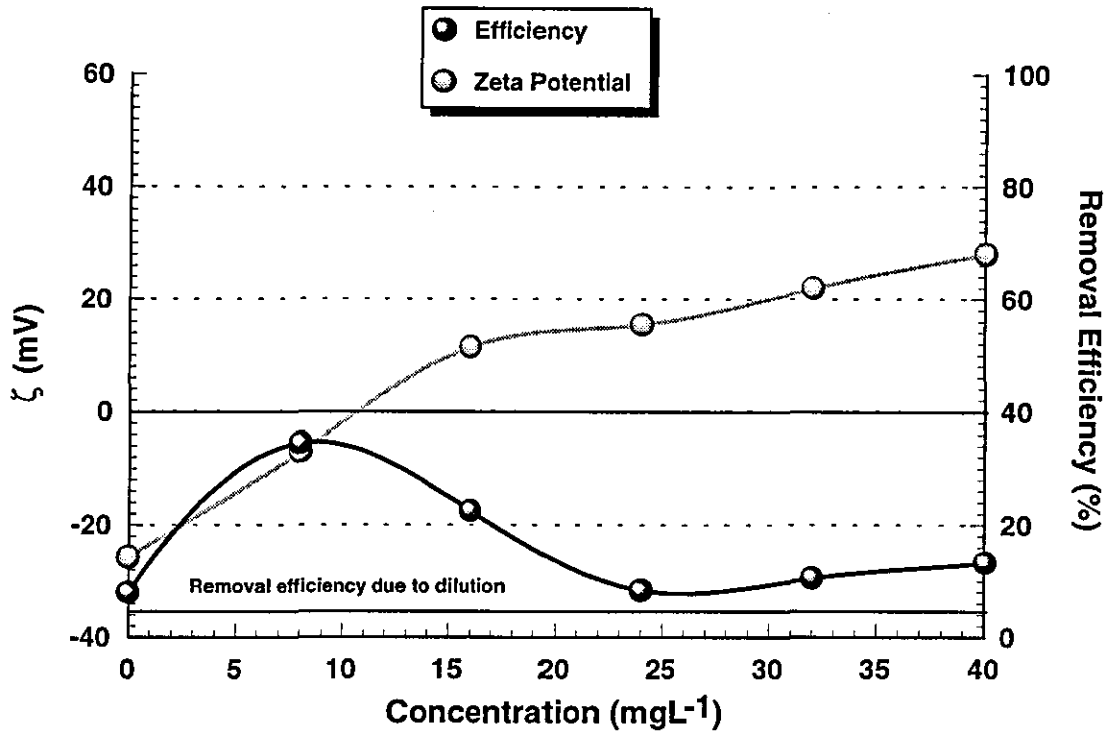


Figure B6: Flotation response vs concentration of Tetradecyltrimethylammoniumbromide for dispersed Kaolin particles, R=5%

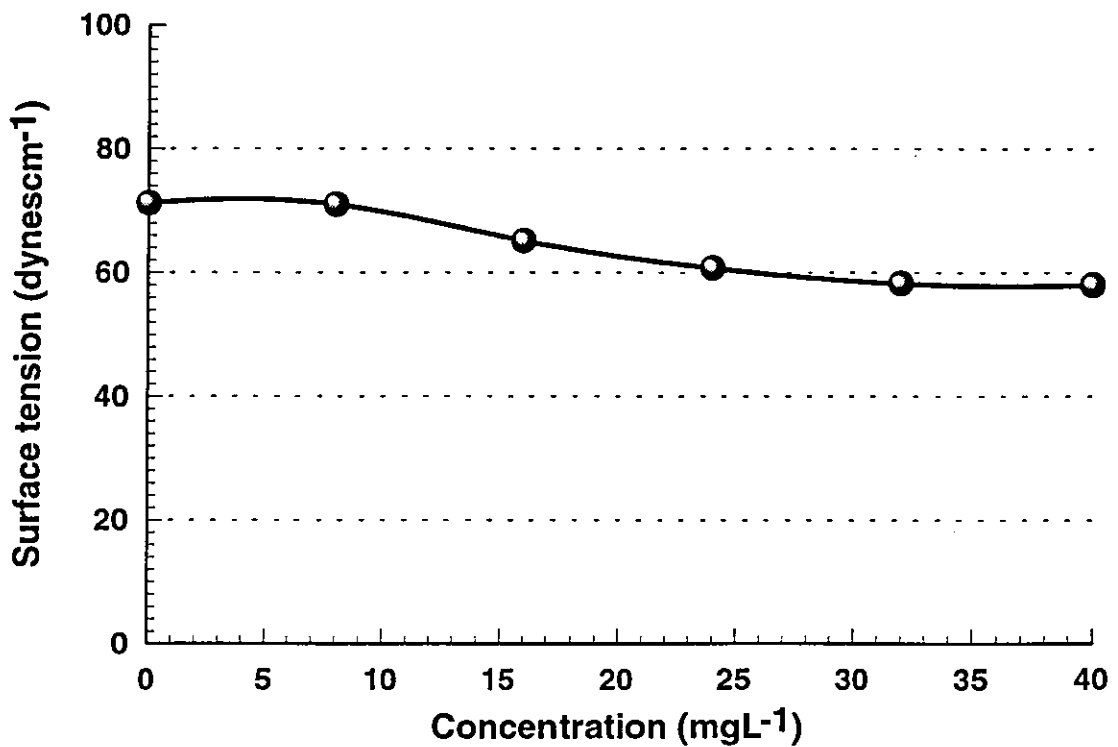
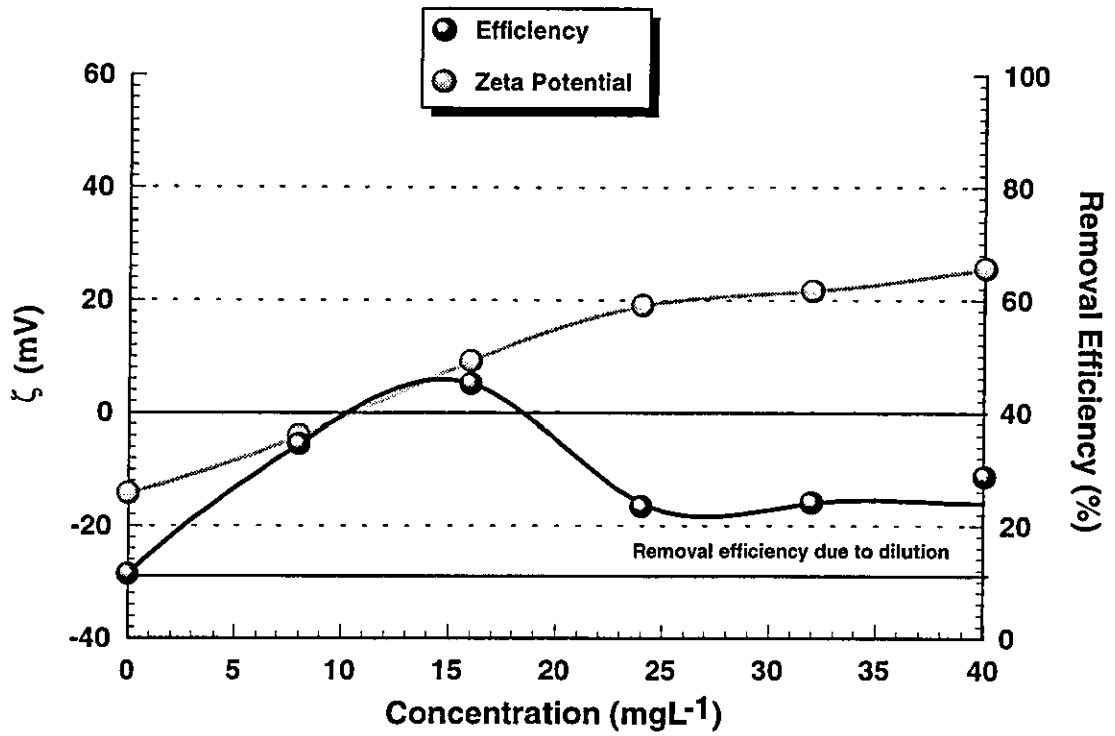


Figure B7: Flotation response vs concentration of Tetradecyltrimethylammoniumbromide for dispersed Kaolin particles, R=10%

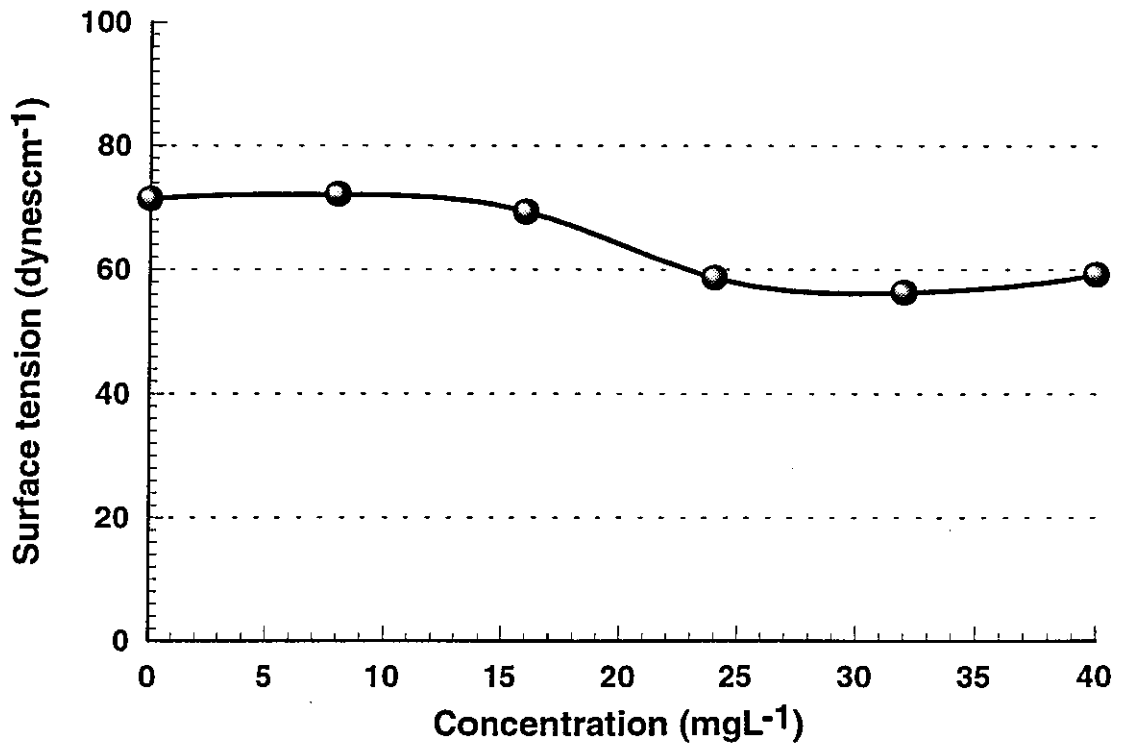
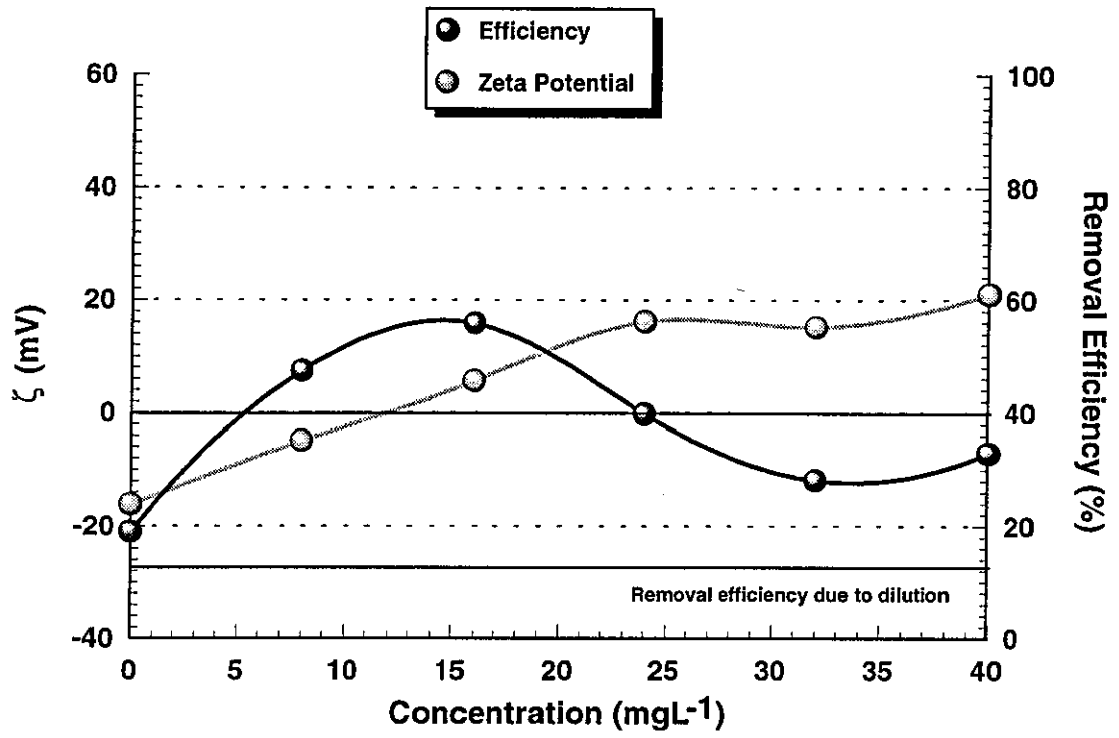


Figure B8: Flotation response vs concentration of Tetradecyltrimethylammoniumbromide for dispersed Kaolin particles, R=15%

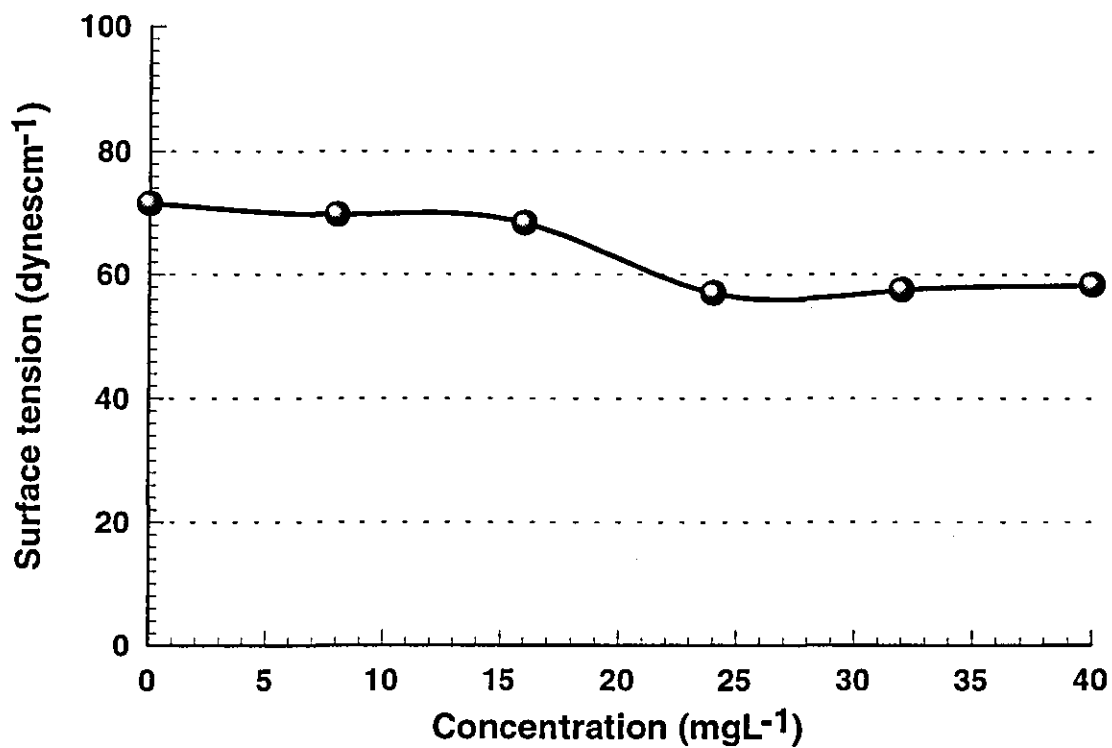
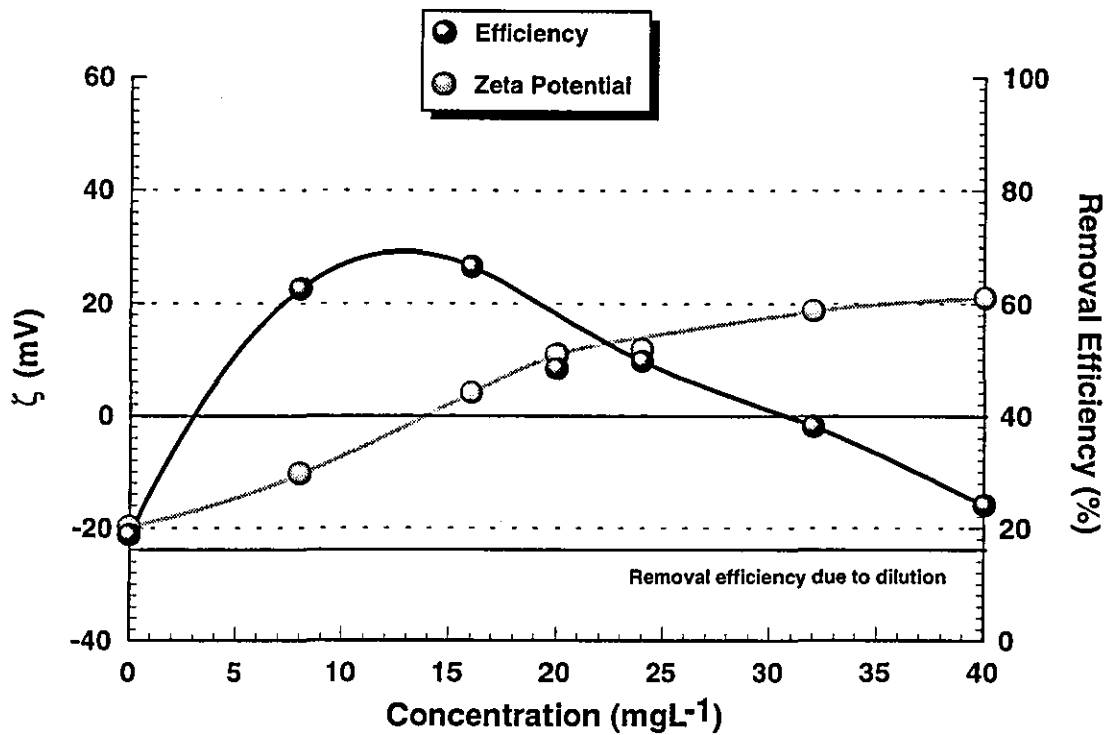


Figure B9 Flotation response vs concentration of Tetradecyltrimethylammoniumbromide for dispersed Kaolin particles, R=20%

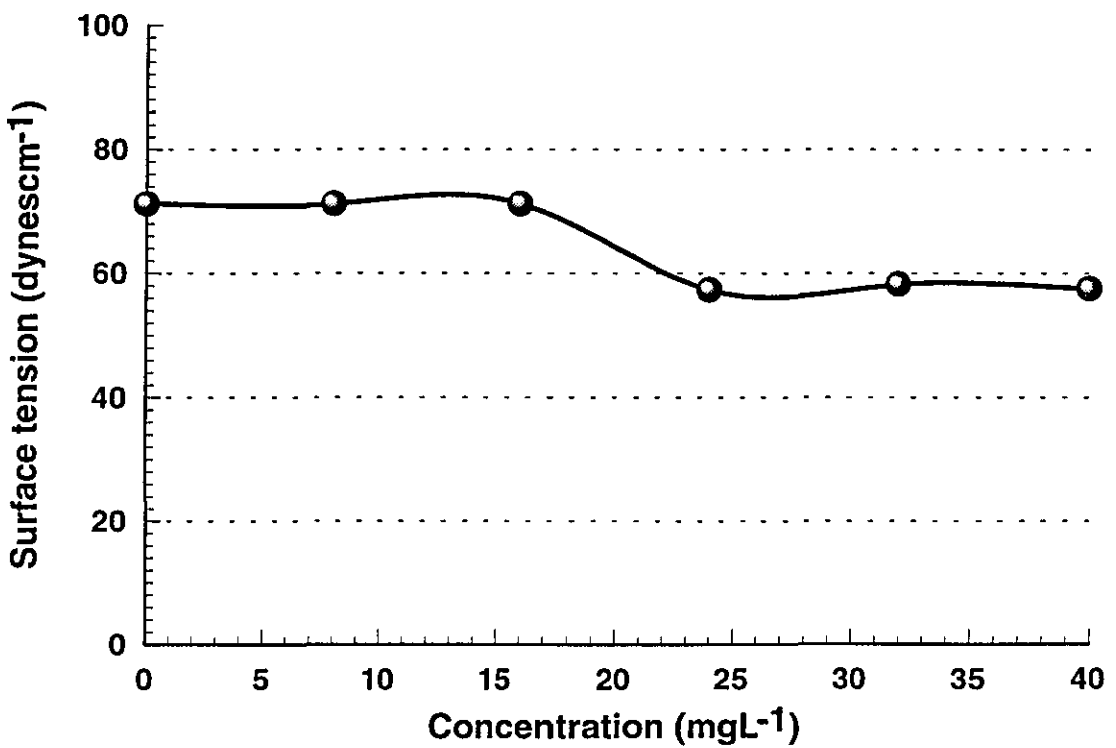
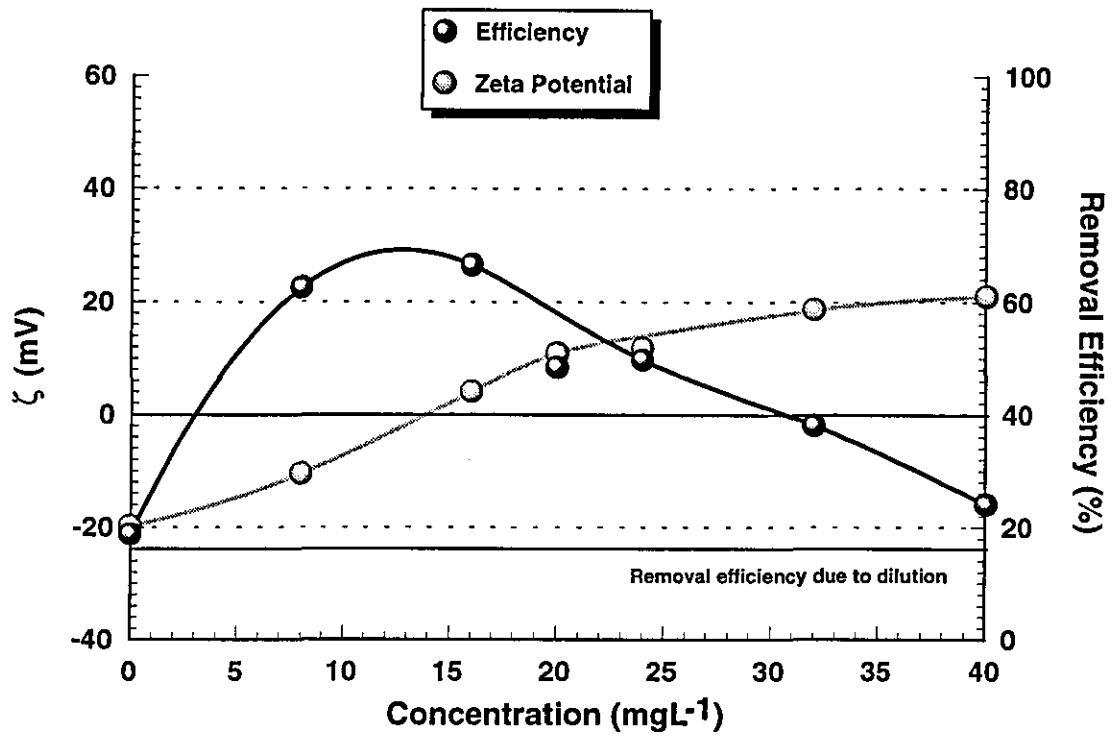


Figure B10 Flotation response vs concentration of Tetradecyltrimethylammoniumbromide for dispersed Kaolin particles, R=25%

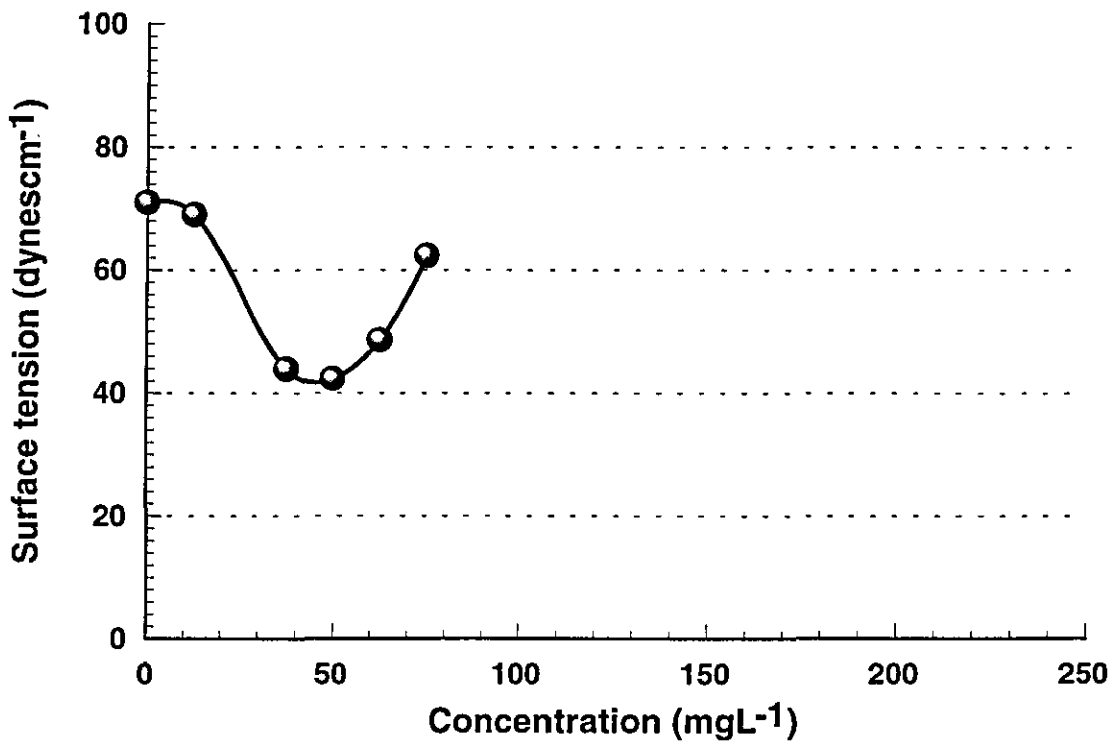
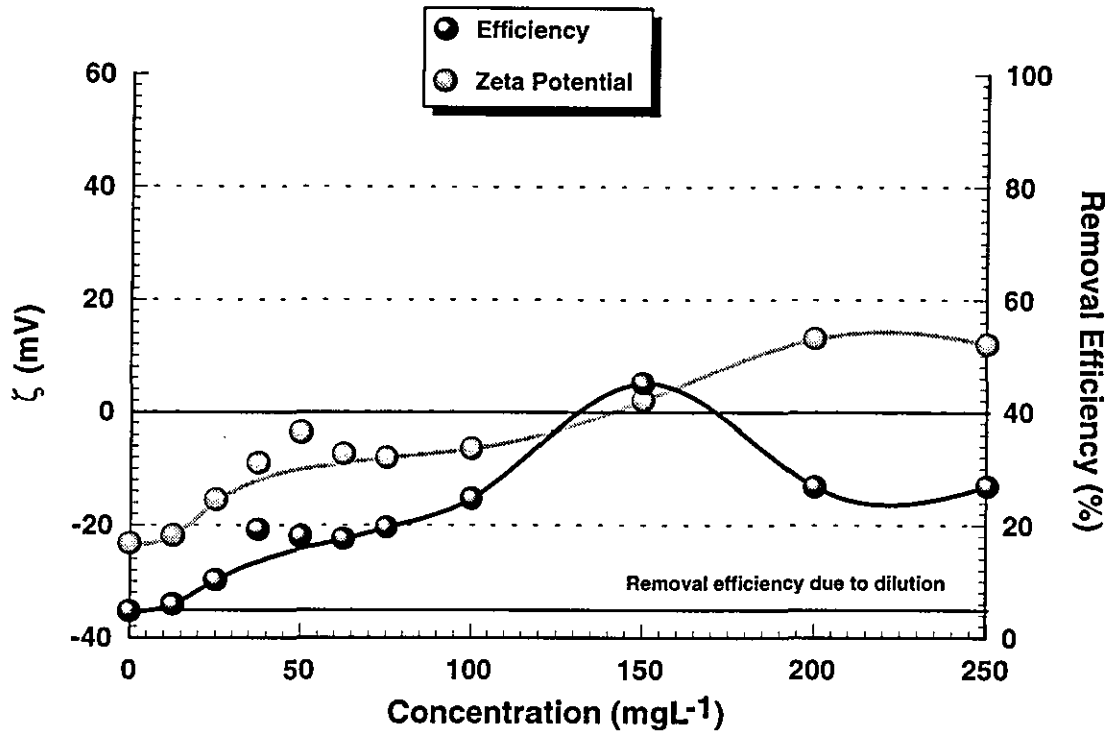


Figure B11: Flotation response vs concentration of Dodecyltrimethylammoniumbromide for dispersed Kaolin particles, R=5%

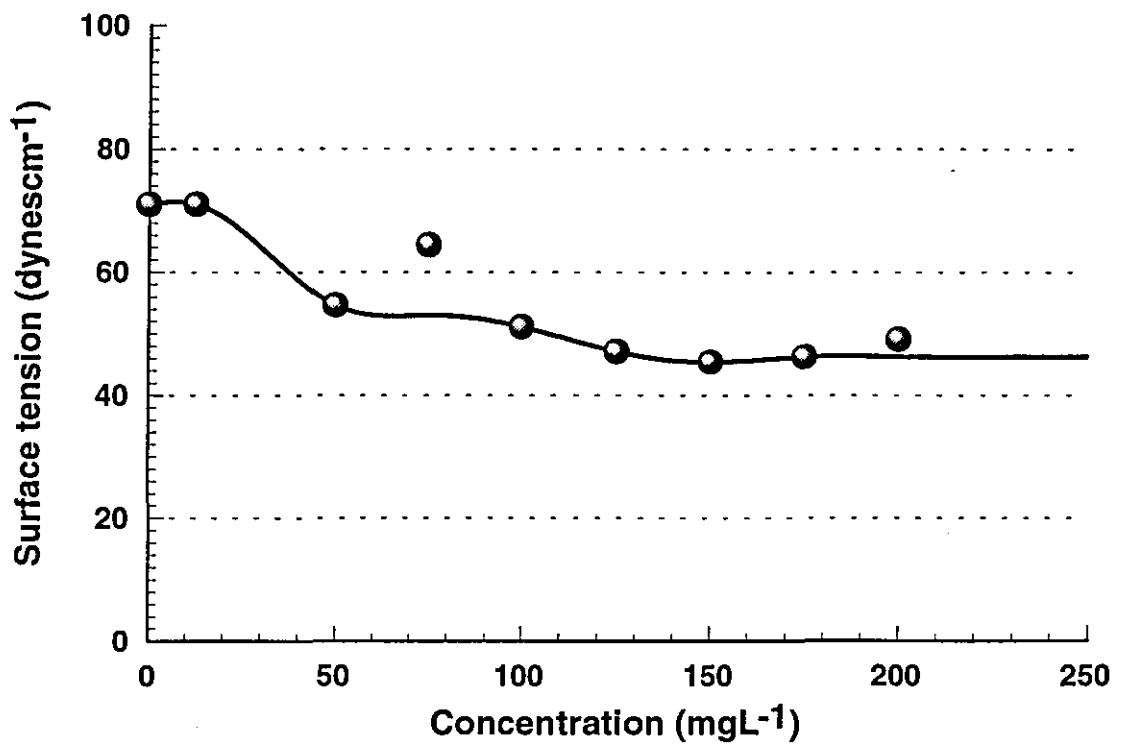
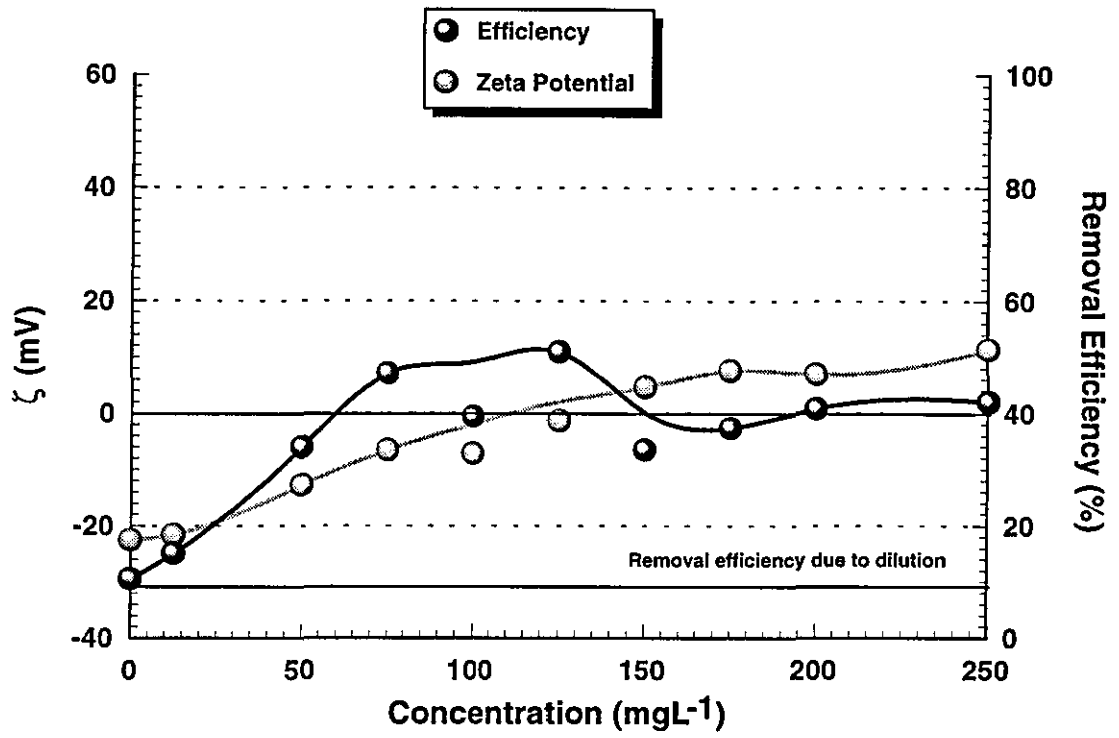


Figure B12: Flotation response vs concentration of Dodecyltrimethylammoniumbromide for dispersed Kaolin particles, R=10%

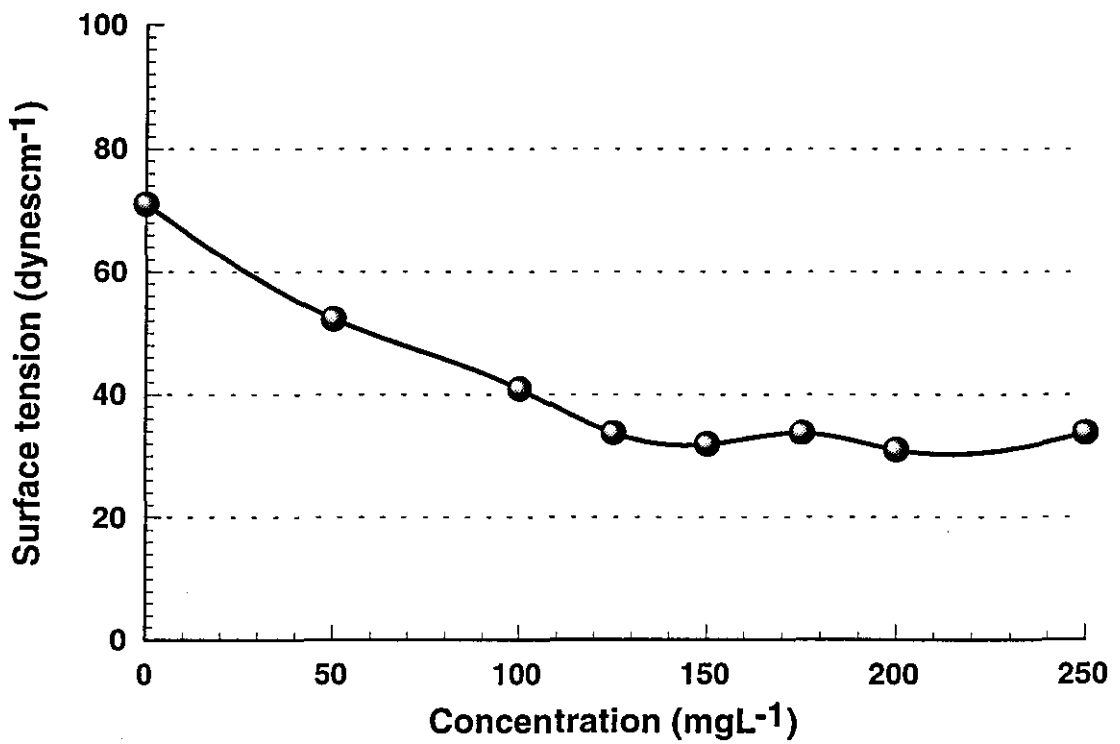
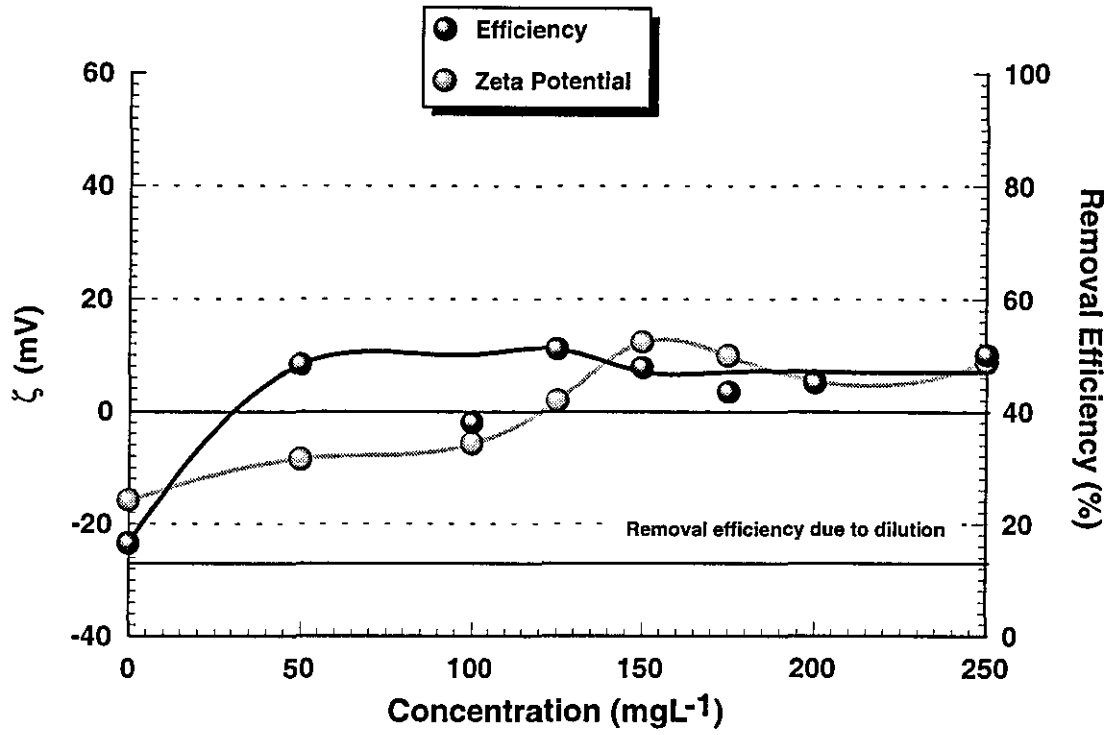


Figure B13: Flotation response vs concentration of Dodecyltrimethylammoniumbromide for dispersed Kaolin particles, R=15%

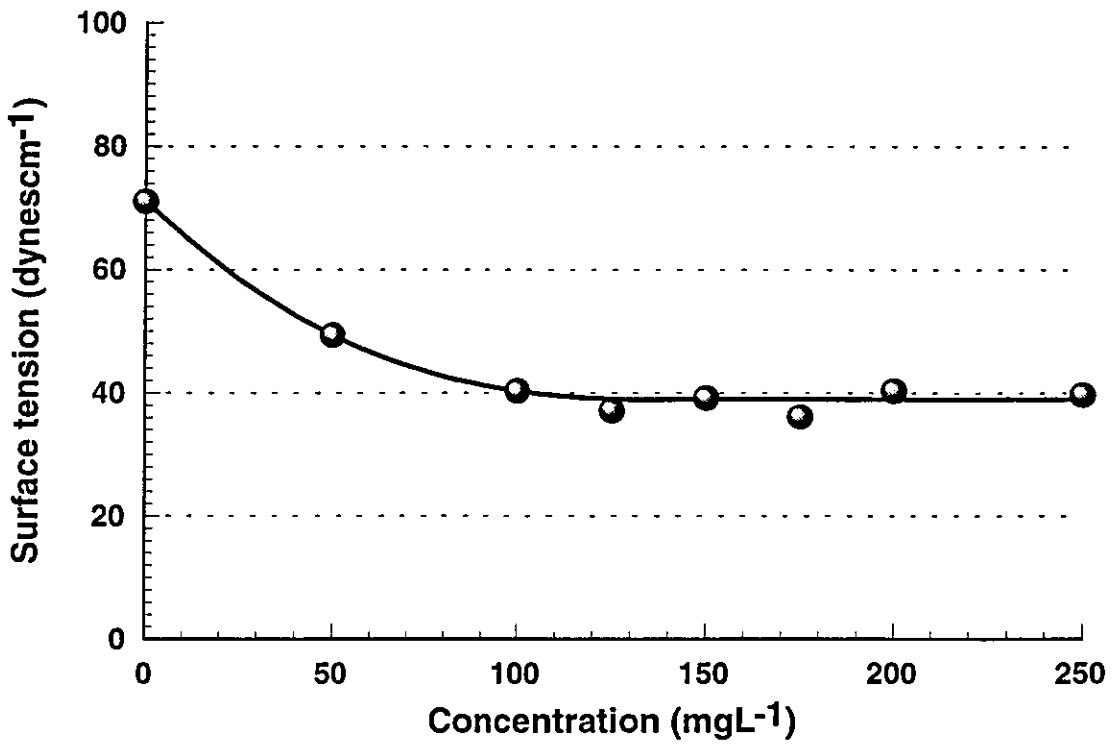
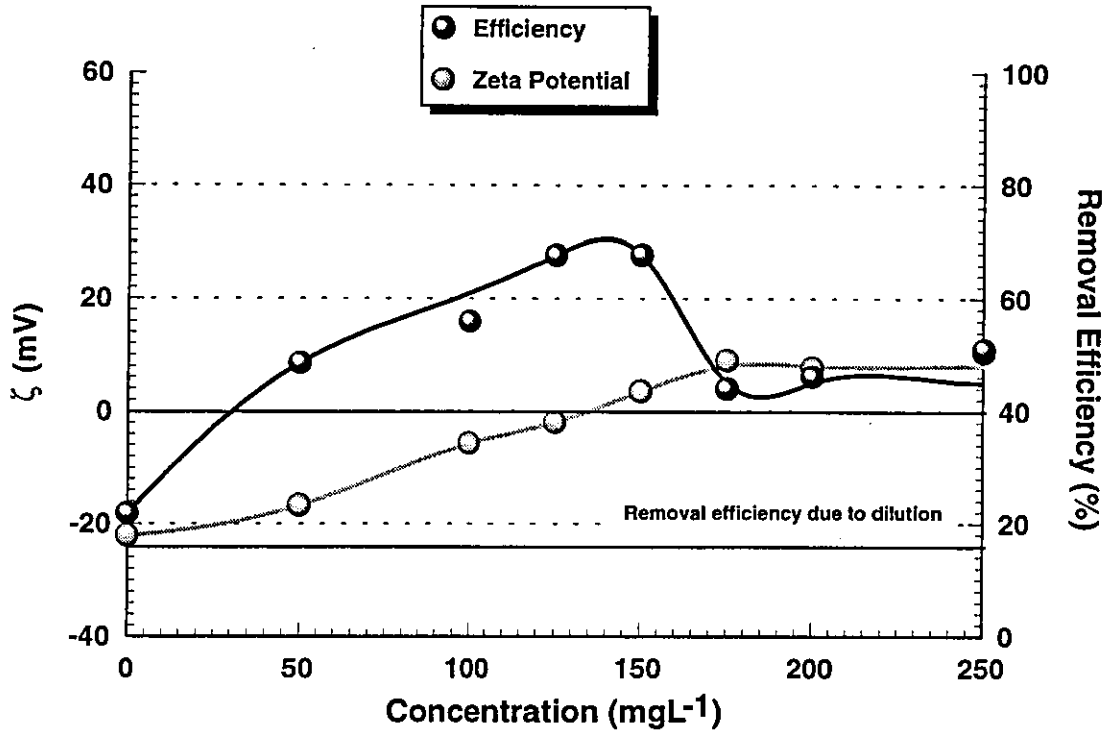


Figure B14: Flotation response vs concentration of Dodecyltrimethylammoniumbromide for dispersed Kaolin particles, R=20%

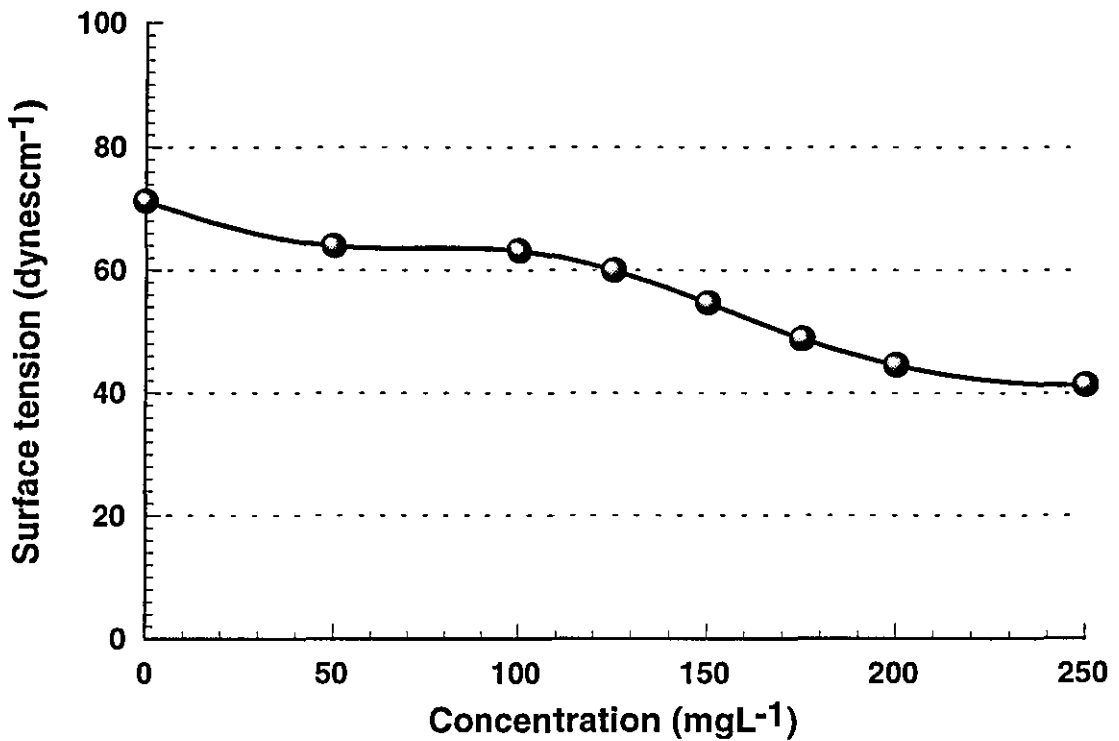
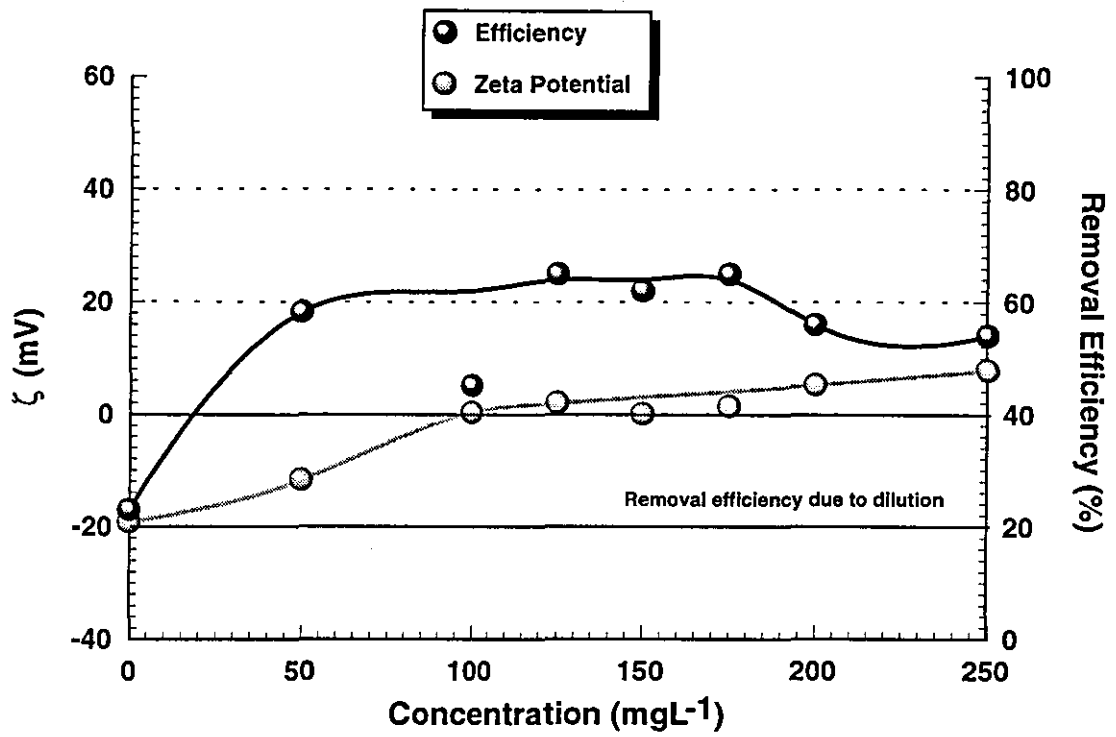


Figure B15: Flotation response vs concentration of Dodecyltrimethylammoniumbromide for dispersed Kaolin particles, R=25%

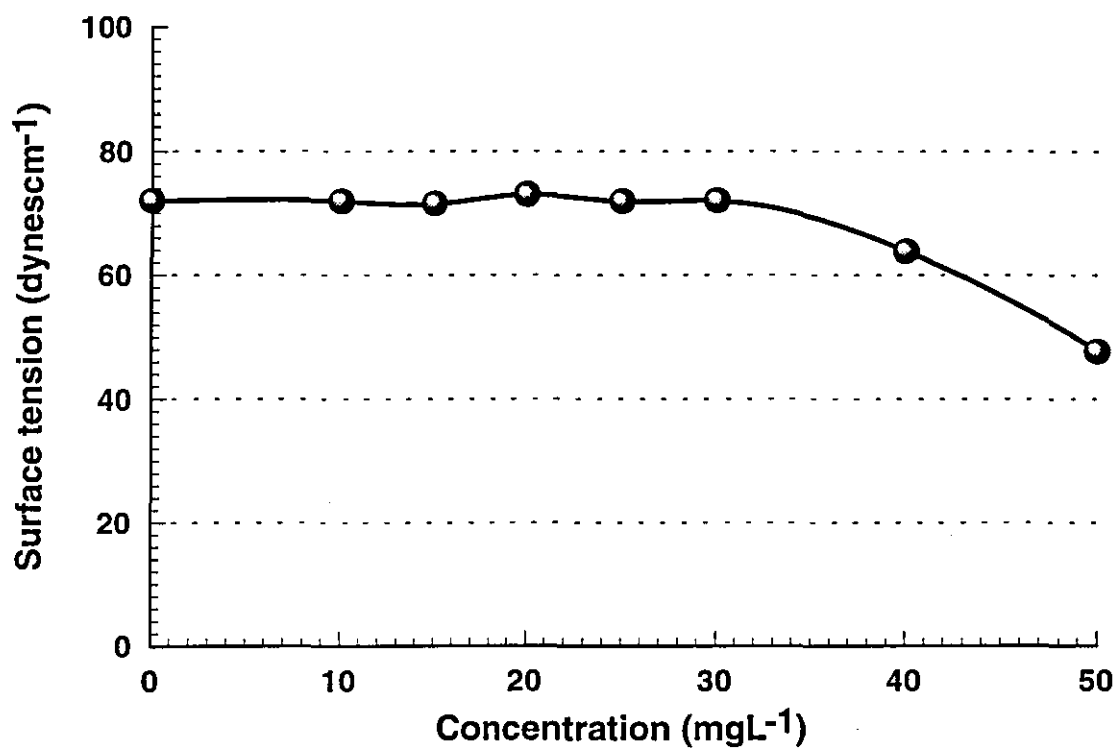
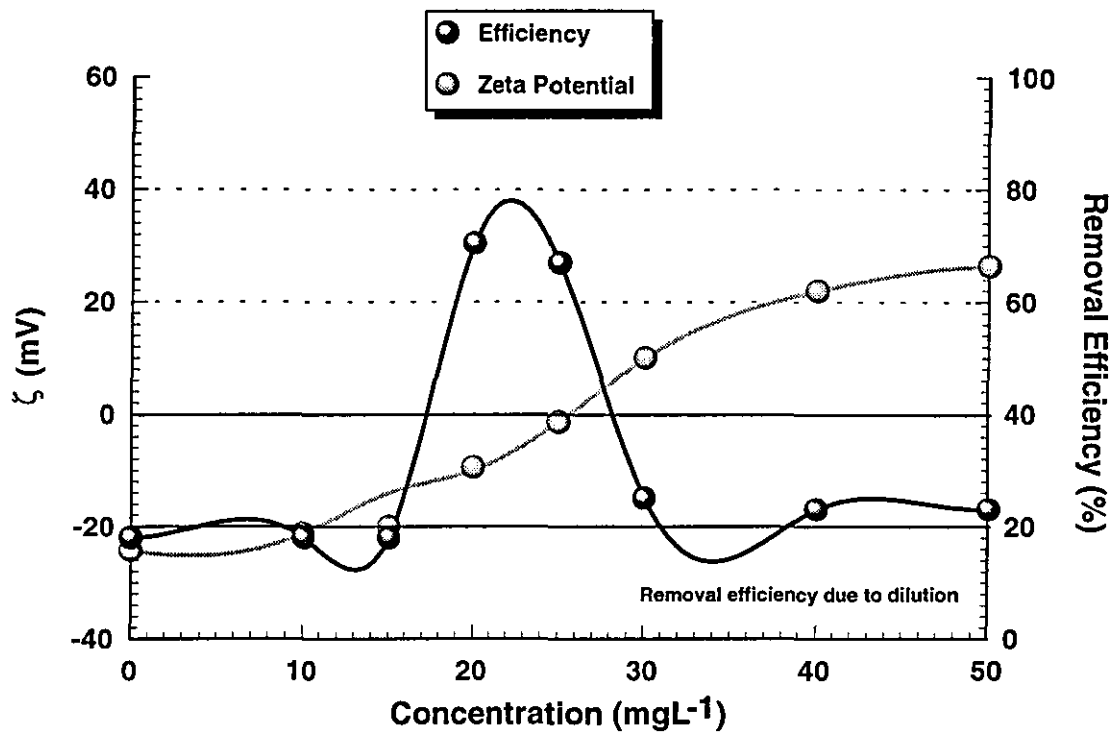


Figure B16: Flotation response vs concentration of Hexadecyltrimethylammoniumbromide for dispersed Wyoming Bentonite particles, R=25%

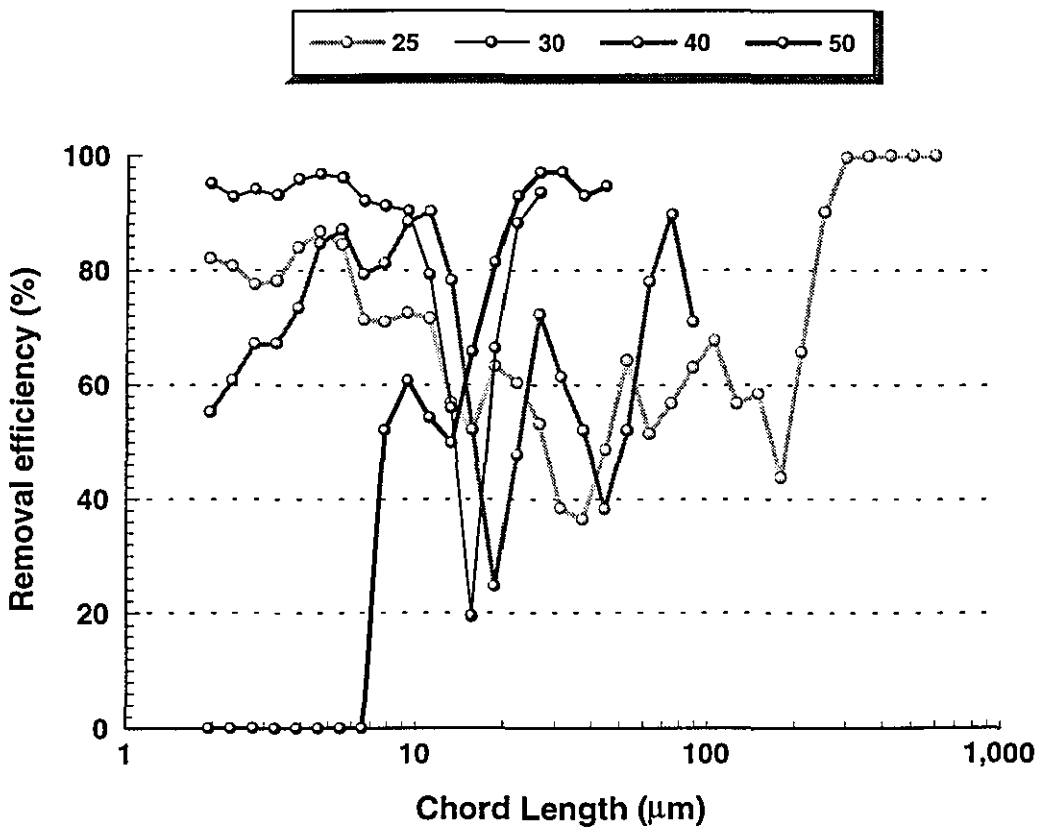
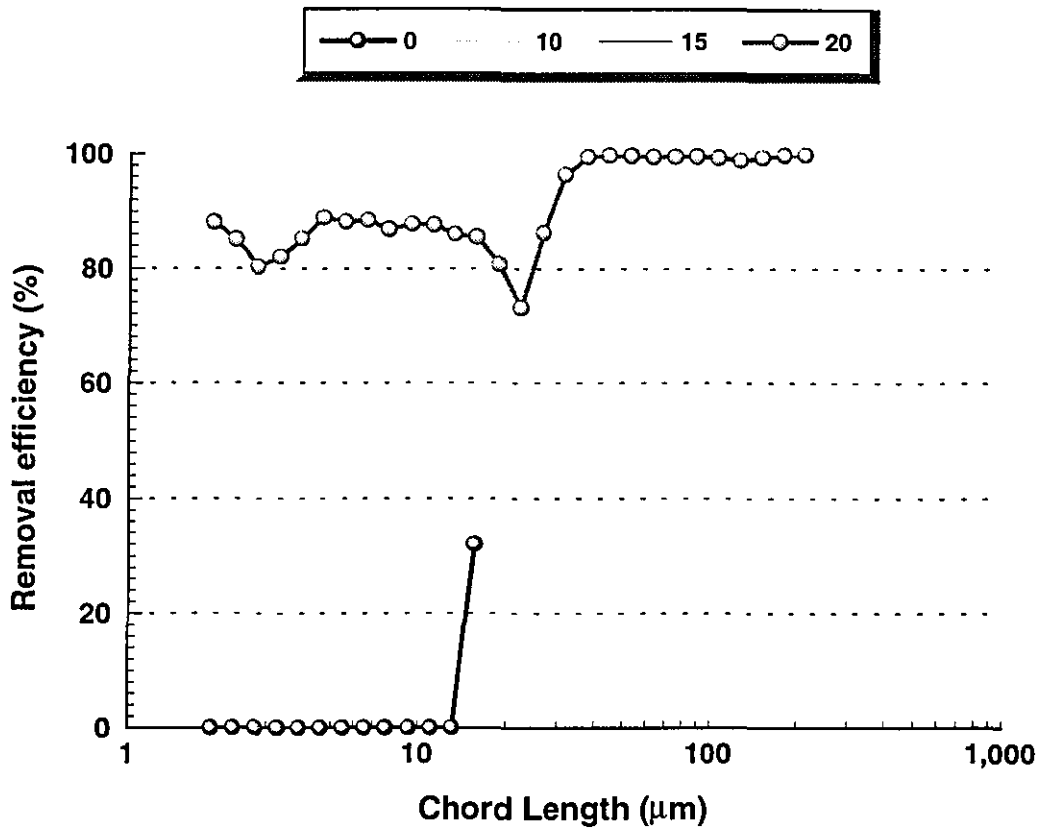


Figure B17: Grade efficiency curves vs Hexadecyltrimethylammoniumbromide concentration for dispersed Wyoming Bentonite particles, R=25%

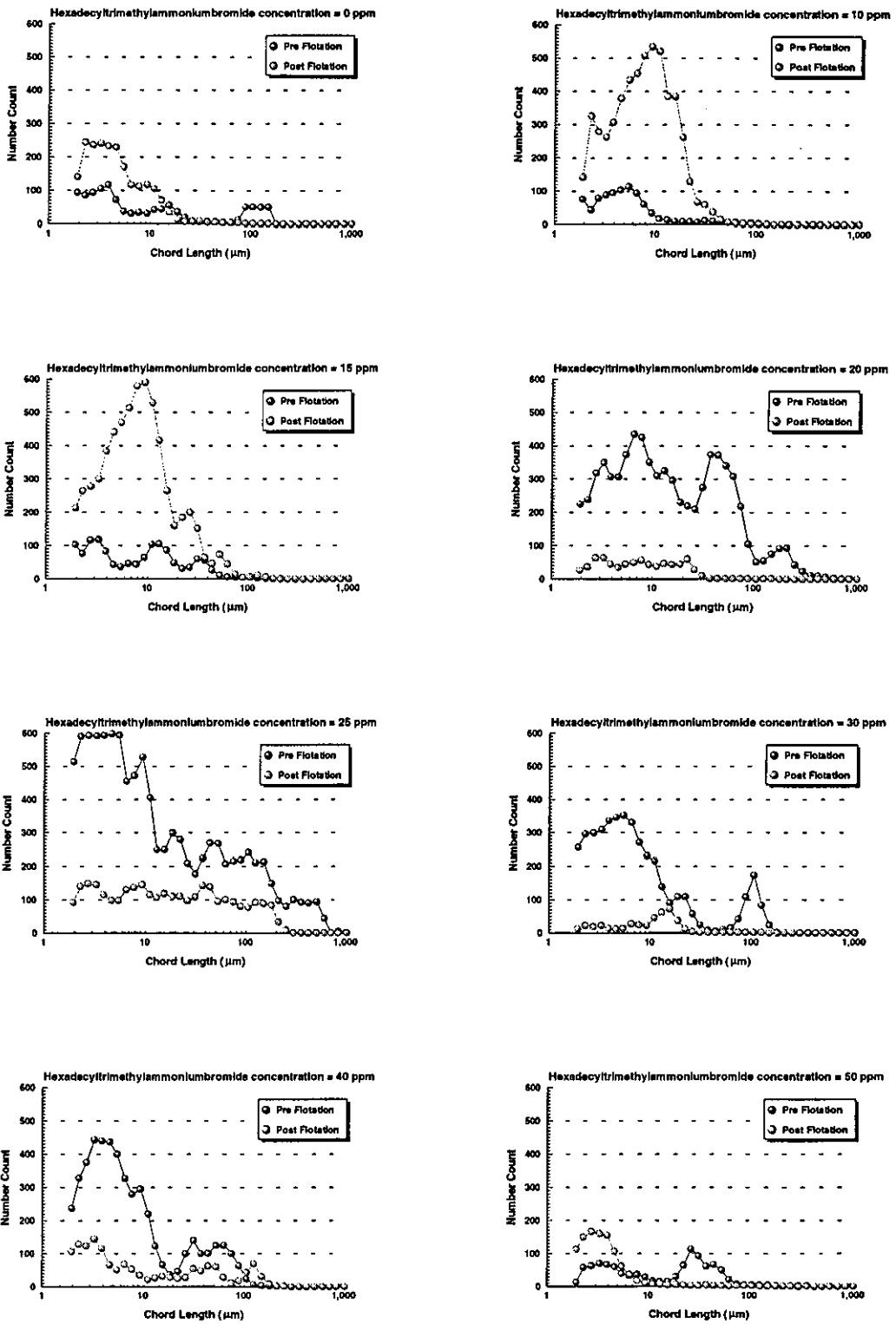


Figure B18: Pre and Post flotation particle size distributions for dispersed Wyoming Bentonite particles conditioned with Hexadecyltrimethylammoniumbromide, R=25%

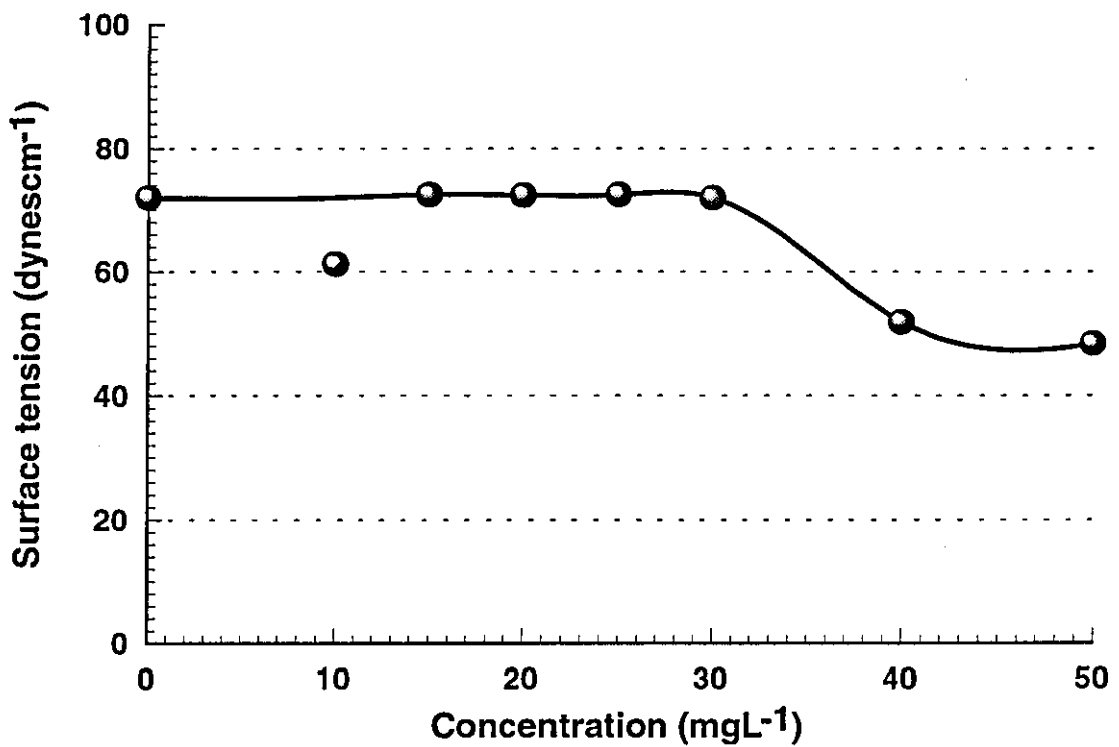
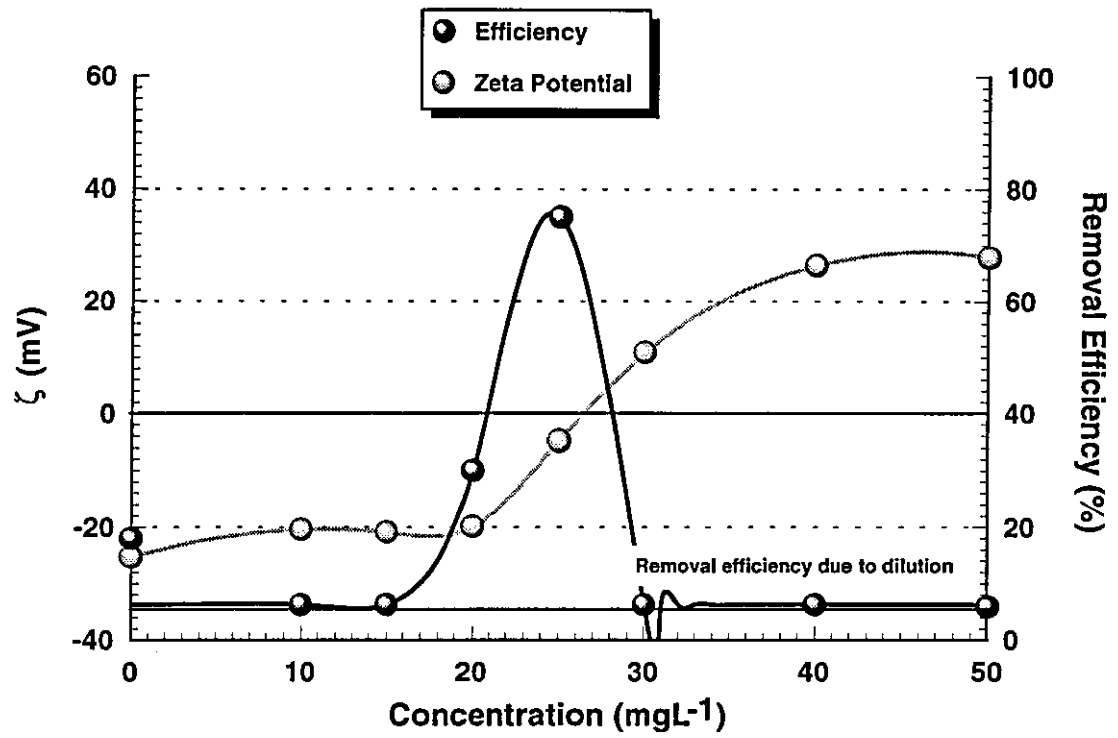


Figure B19: Flotation response vs concentration of Hexadecyltrimethylammoniumbromide for dispersed Wyoming Bentonite particles, R=5%

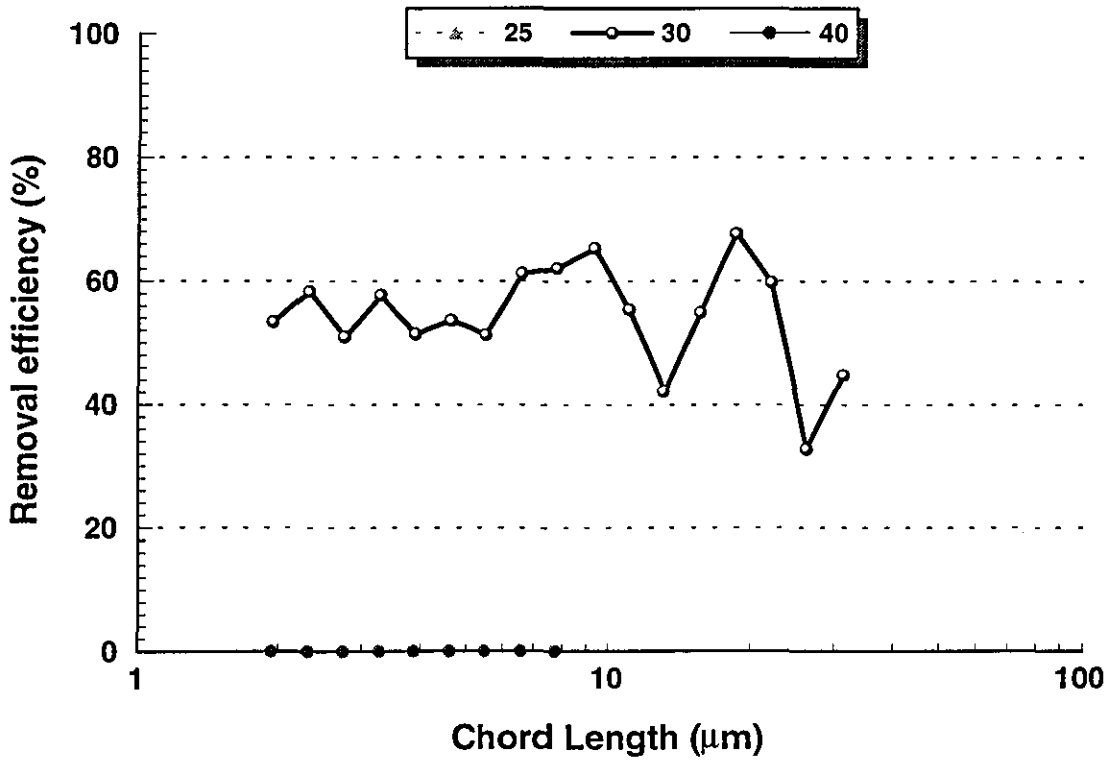
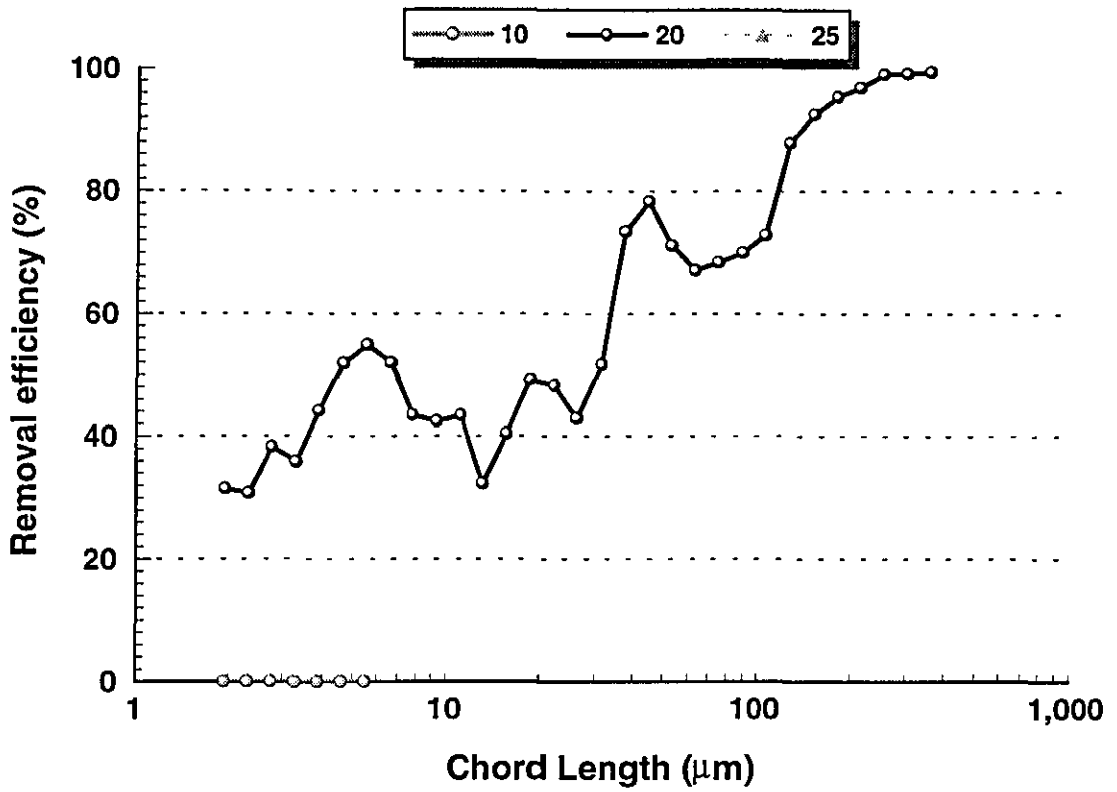


Figure B20: Grade efficiency curves vs Hexadecyltrimethylammoniumbromide concentration for dispersed Wyoming Bentonite particles, R=5%

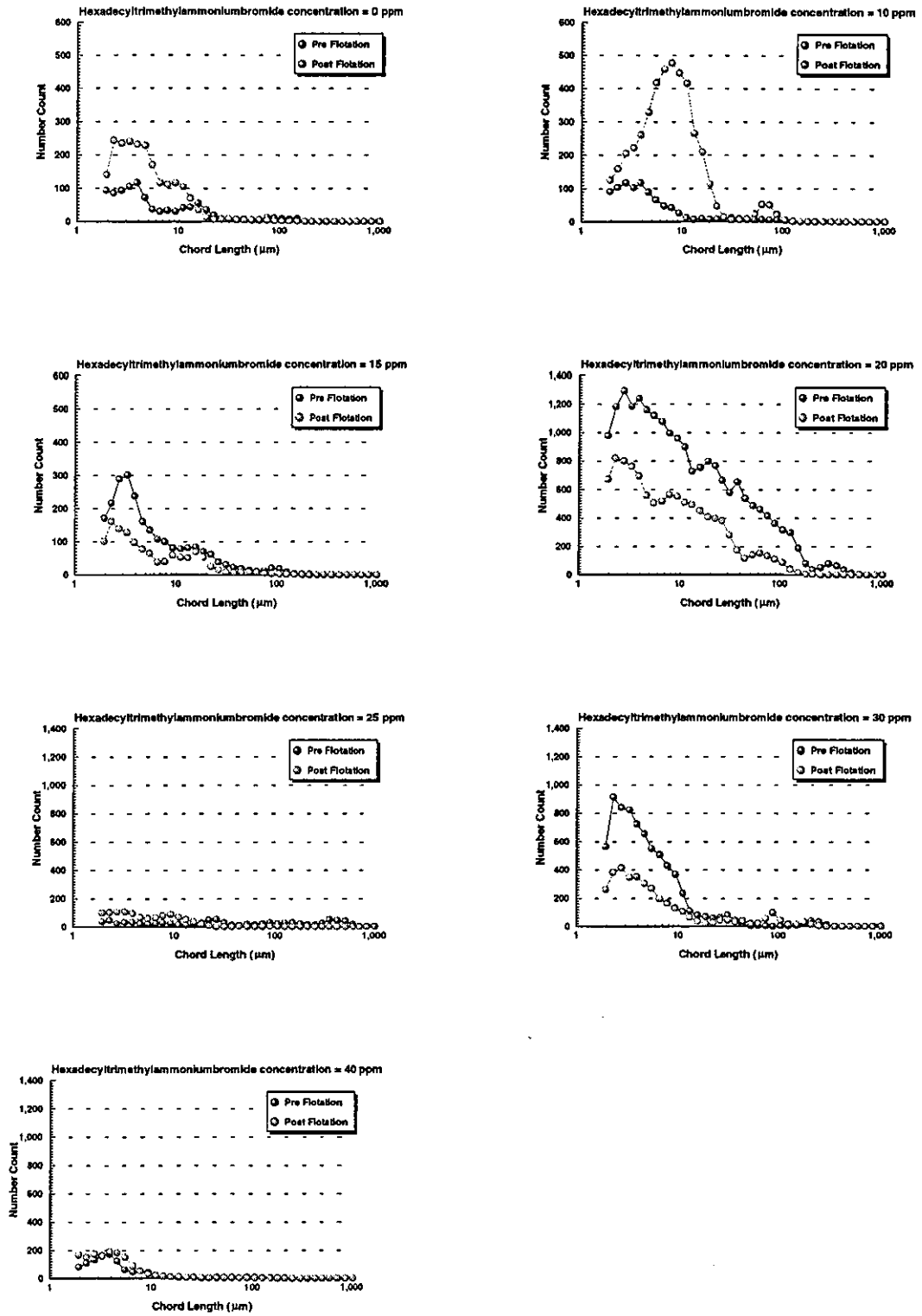


Figure B21: Pre and Post flotation particle size distributions for dispersed Wyoming Bentonite particles conditioned with Hexadecyltrimethylammoniumbromide, R=5%

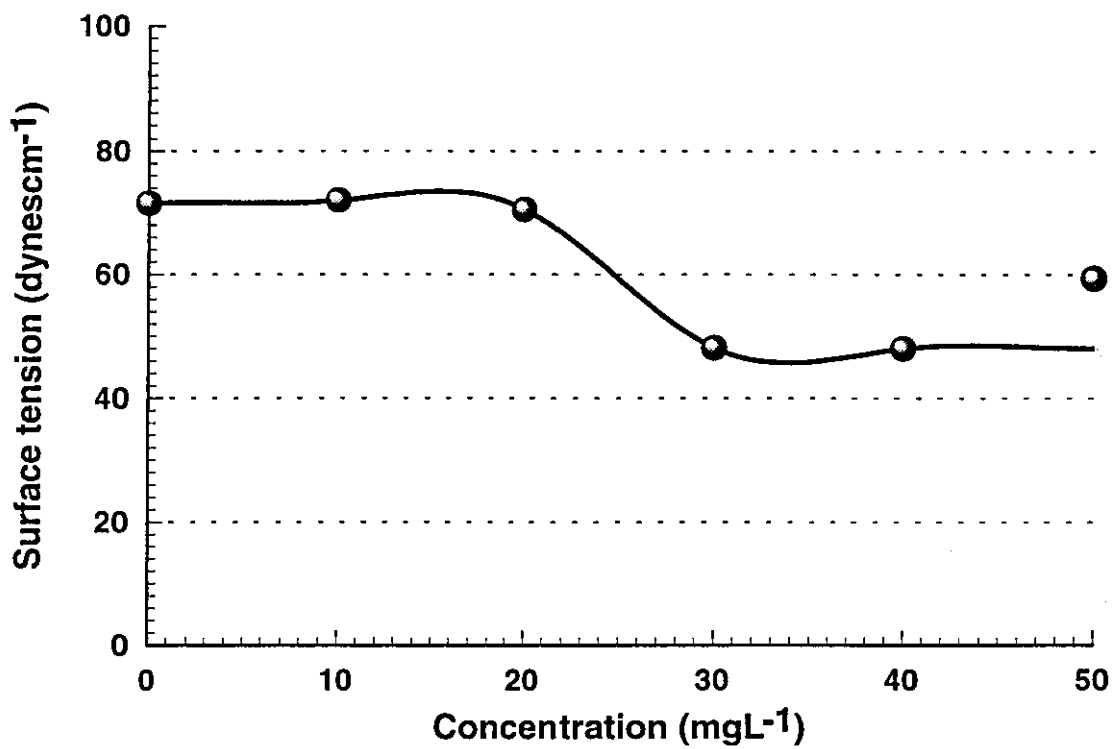
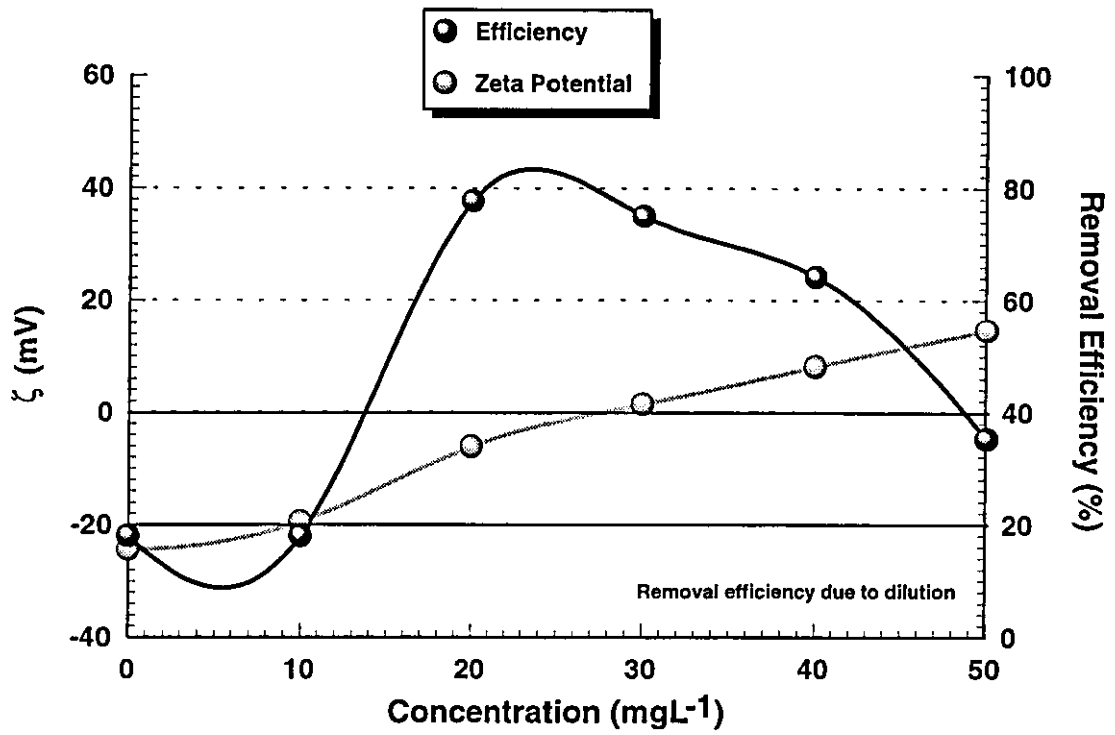


Figure B22: Flotation response vs concentration of Tetradecyltrimethylammoniumbromide for dispersed Wyoming Bentonite particles, R=25%

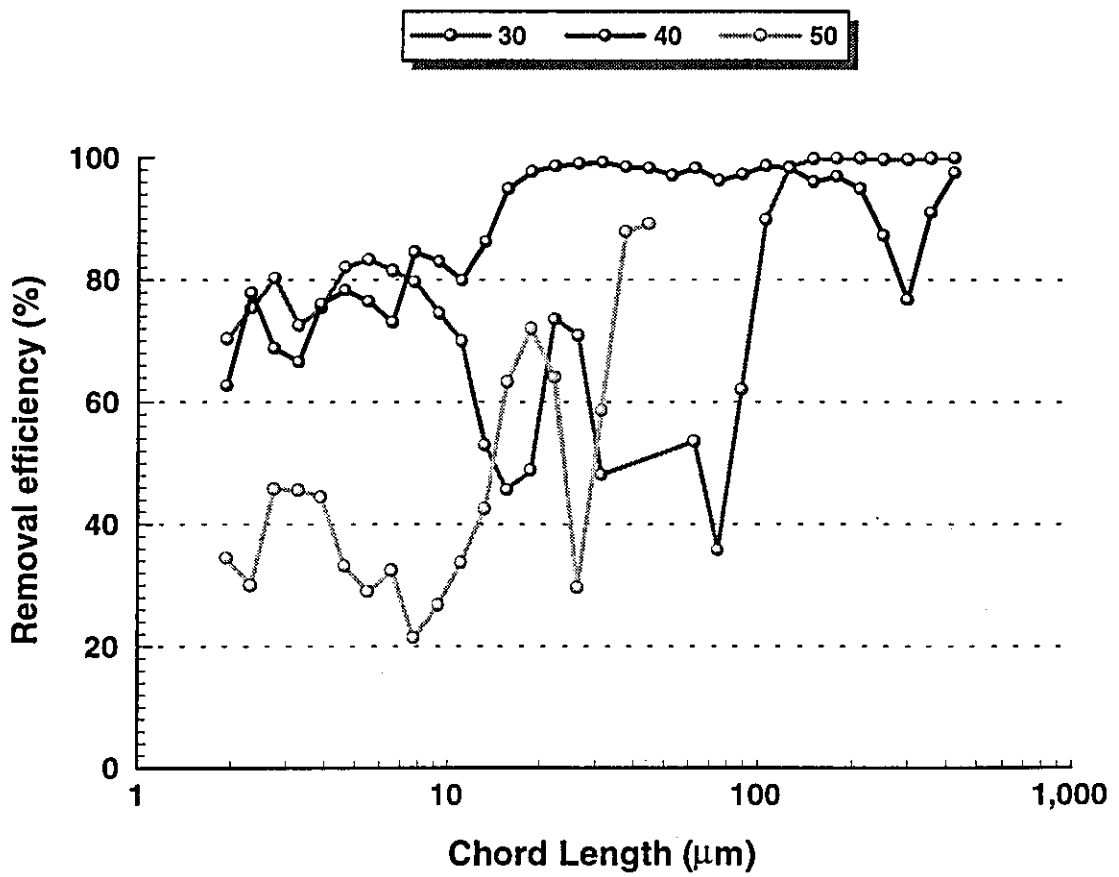
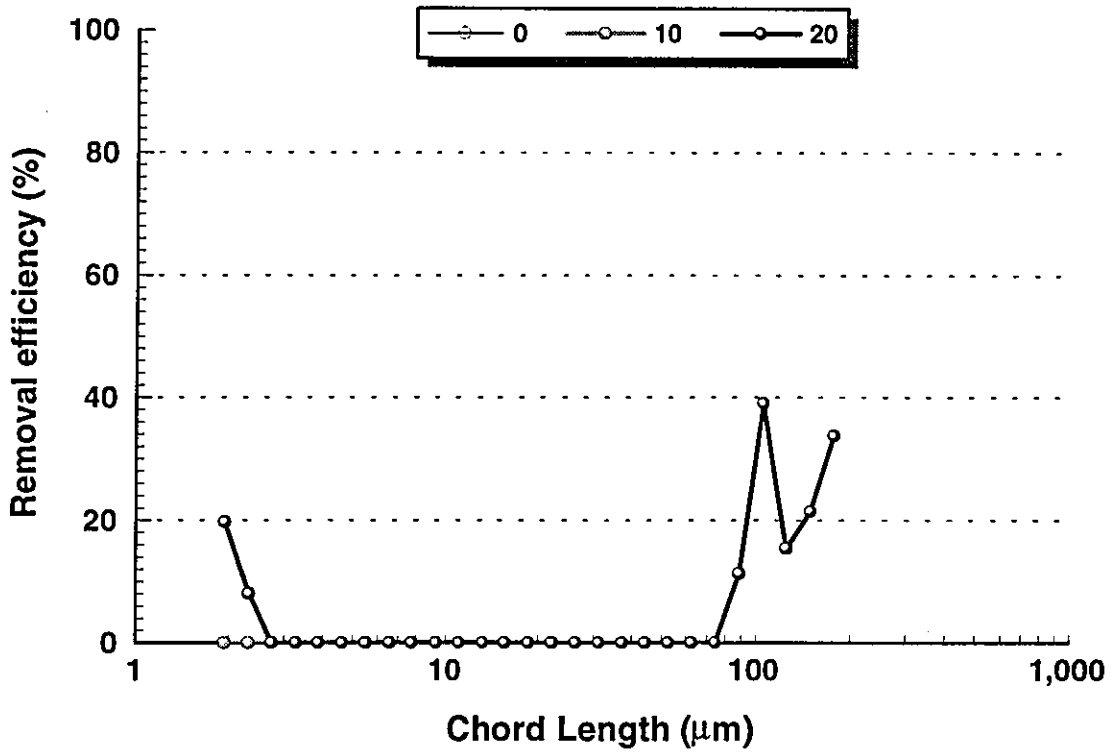


Figure B23: Grade efficiency curves vs Tetradecyltrimethylammoniumbromide concentration for dispersed Wyoming Bentonite particles, R=5%

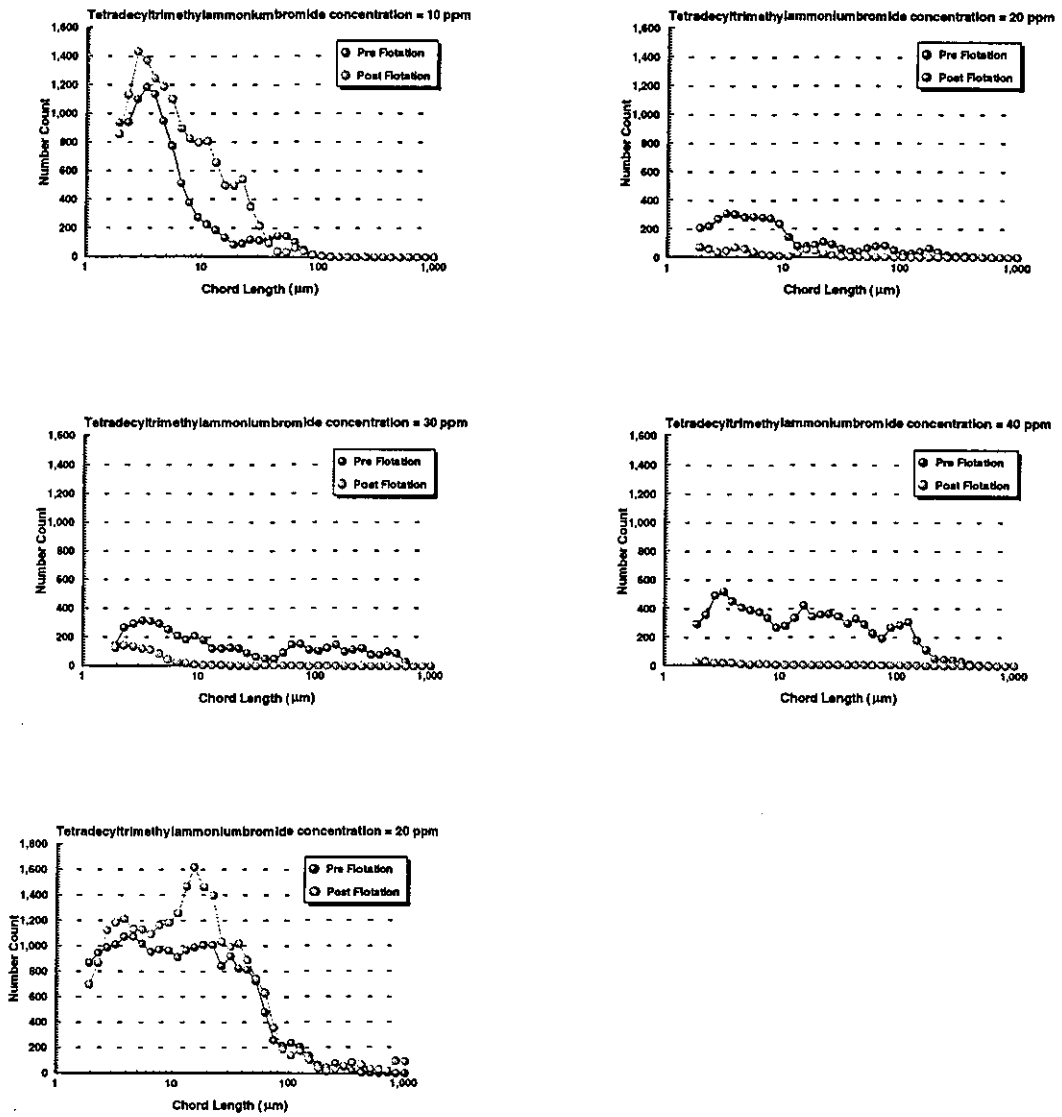


Figure B24: Pre and Post flotation particle size distributions for dispersed Wyoming Bentonite particles conditioned with Tetracycltrimethylammoniumbromide, R=25%

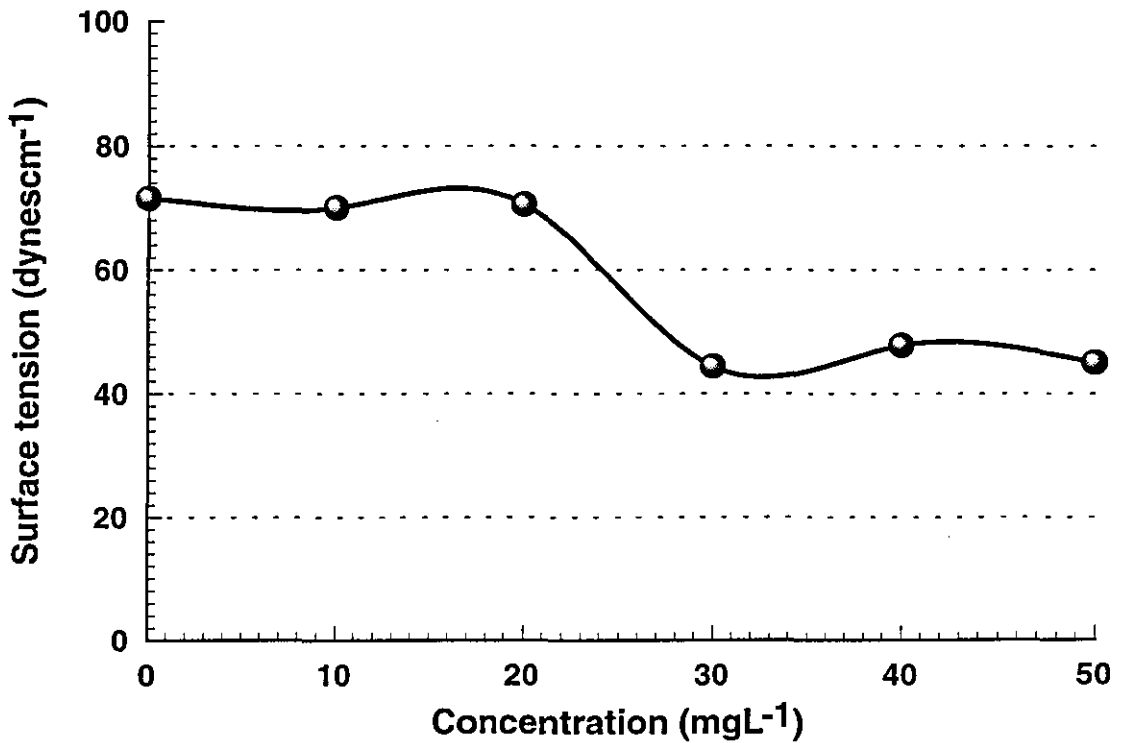
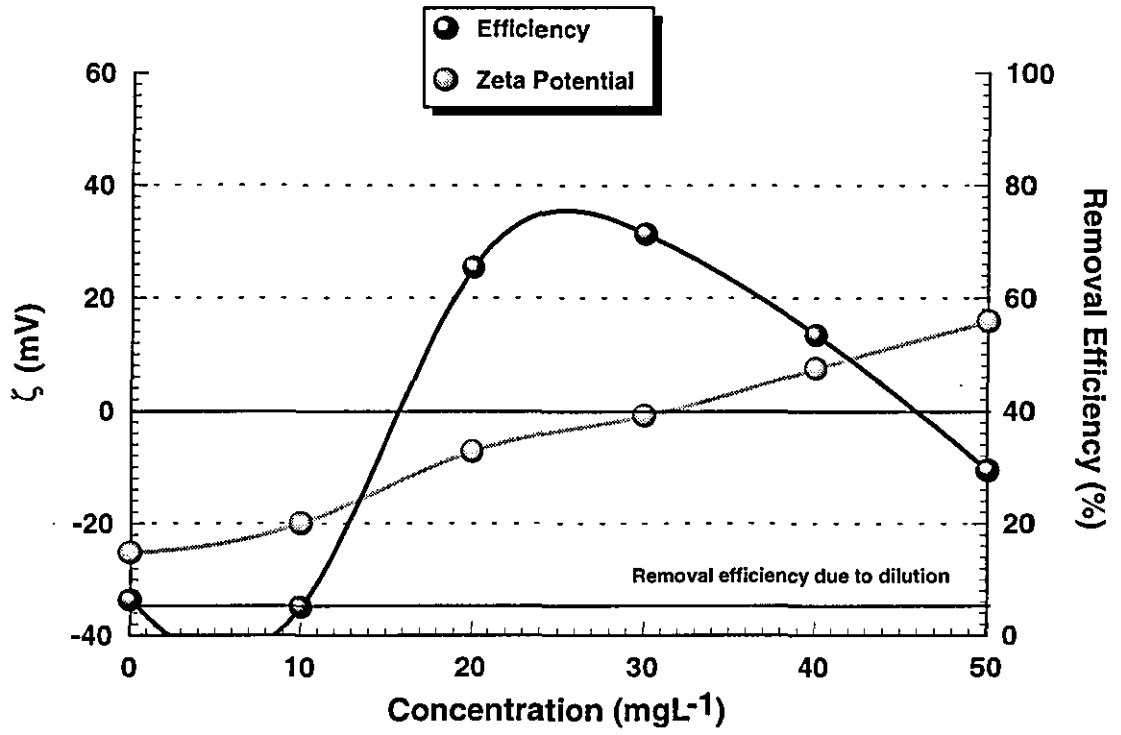


Figure B25: Flotation response vs concentration of Tetradecyltrimethylammoniumbromide for dispersed Wyoming Bentonite particles, R=5%

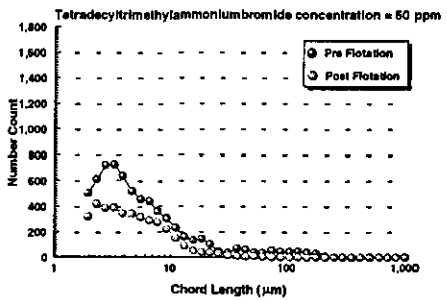
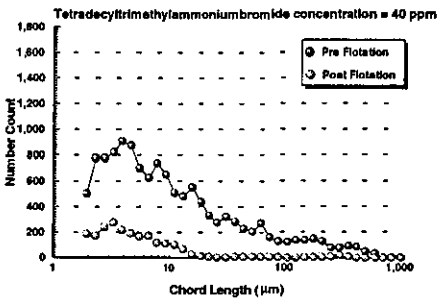
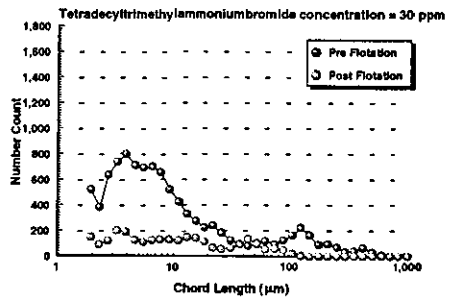
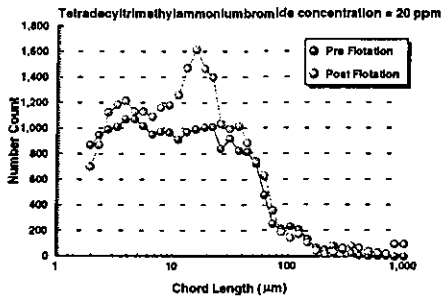
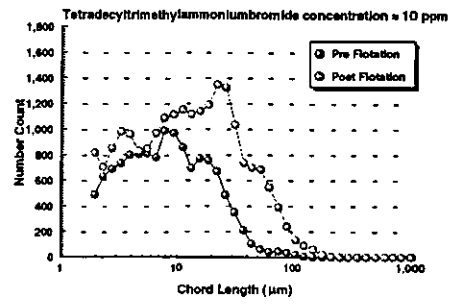
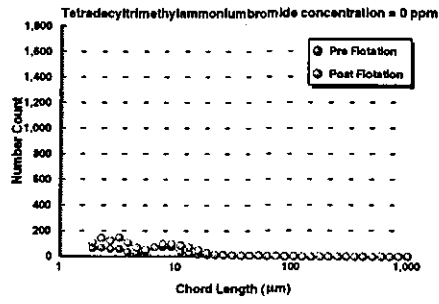


Figure B27: Pre and Post flotation particle size distributions for dispersed Wyoming Bentonite particles conditioned with Tetradecyltrimethylammoniumbromide, R=5%

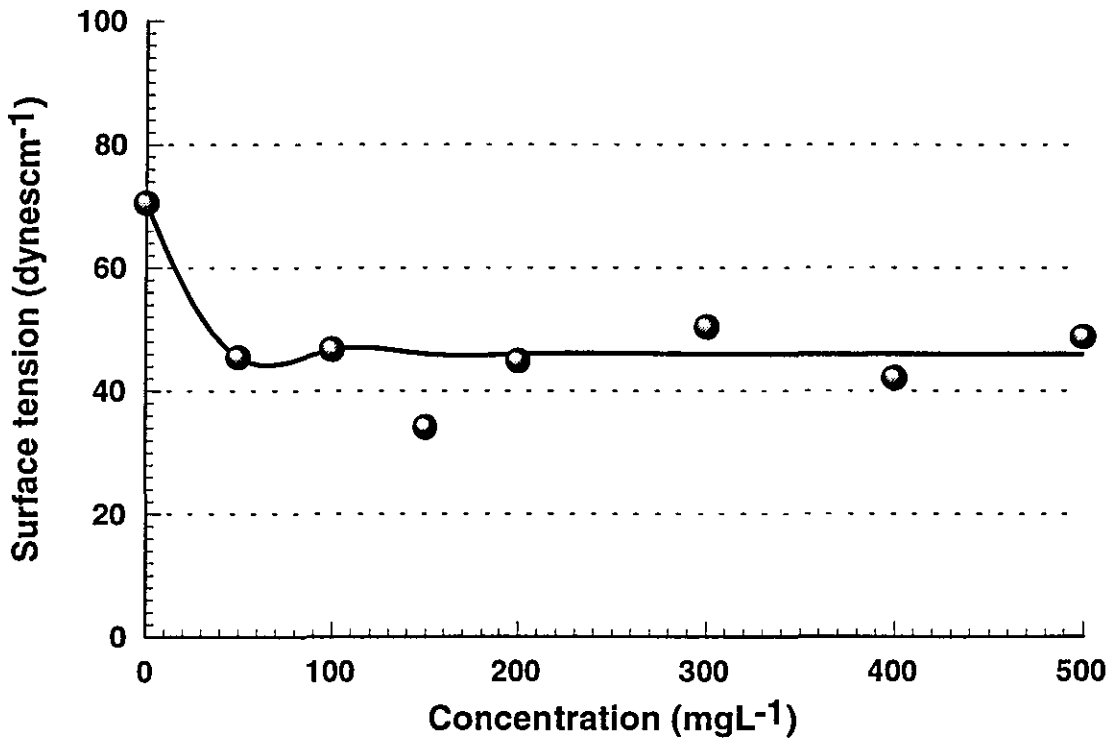
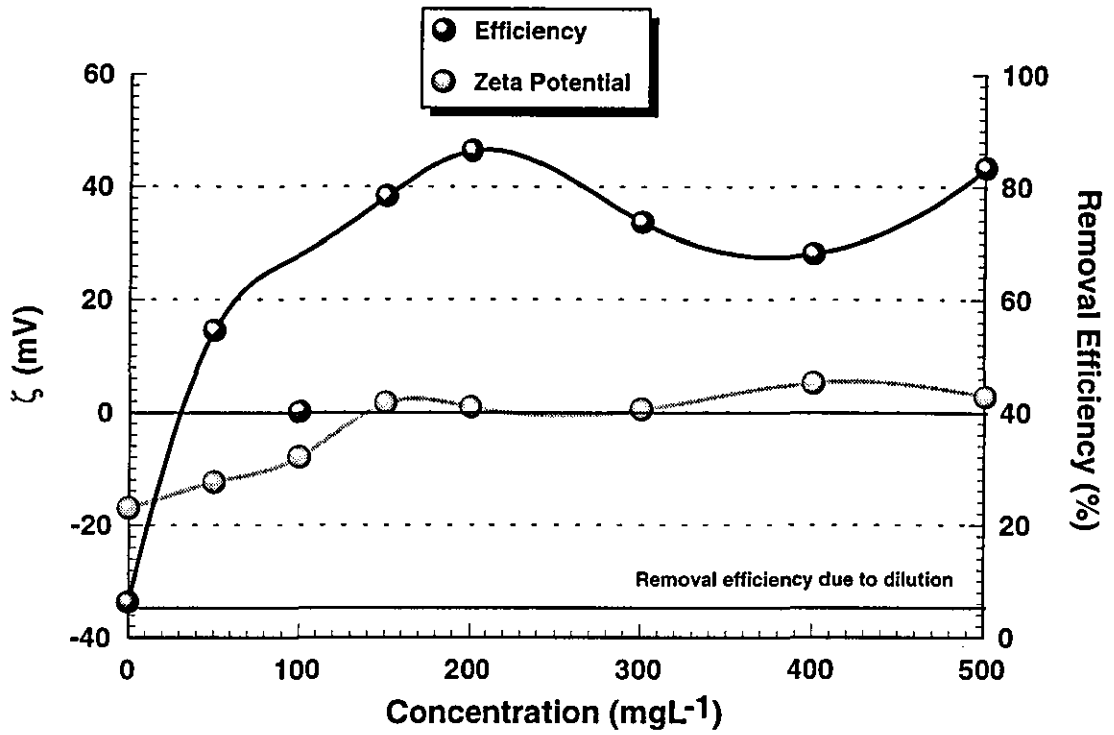


Figure B28: Flotation response vs concentration of Dodecyltrimethylammoniumbromide for dispersed Wyoming Bentonite particles, R=5%

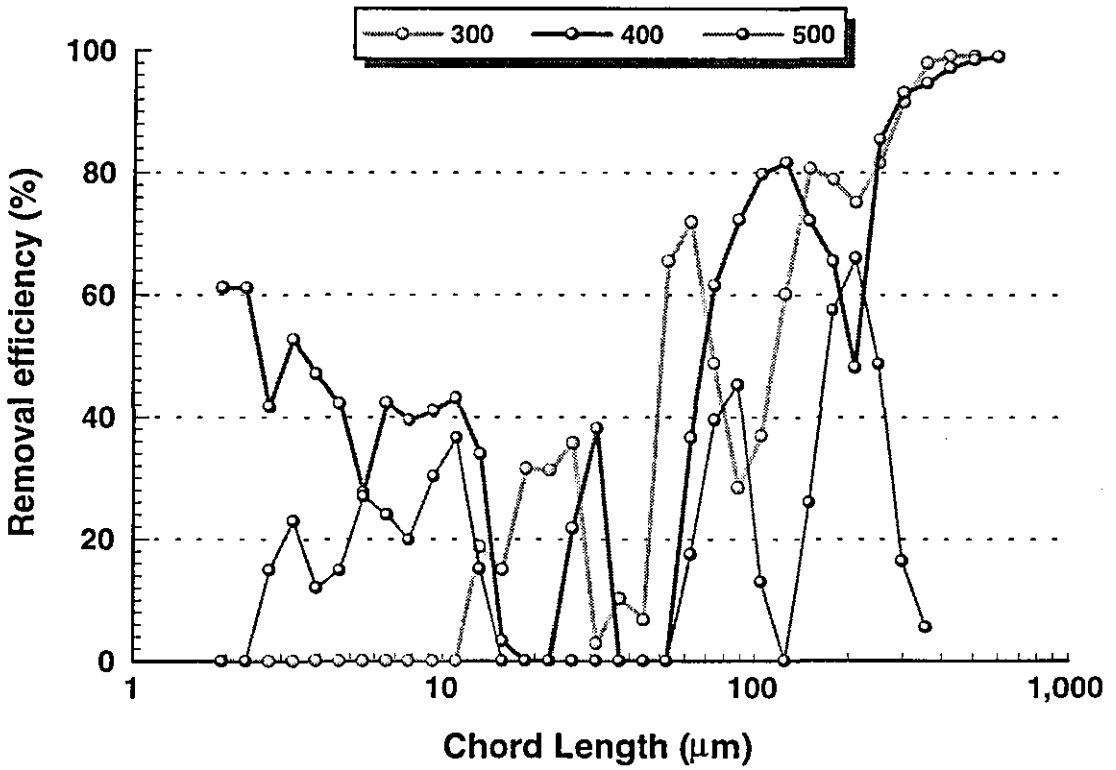
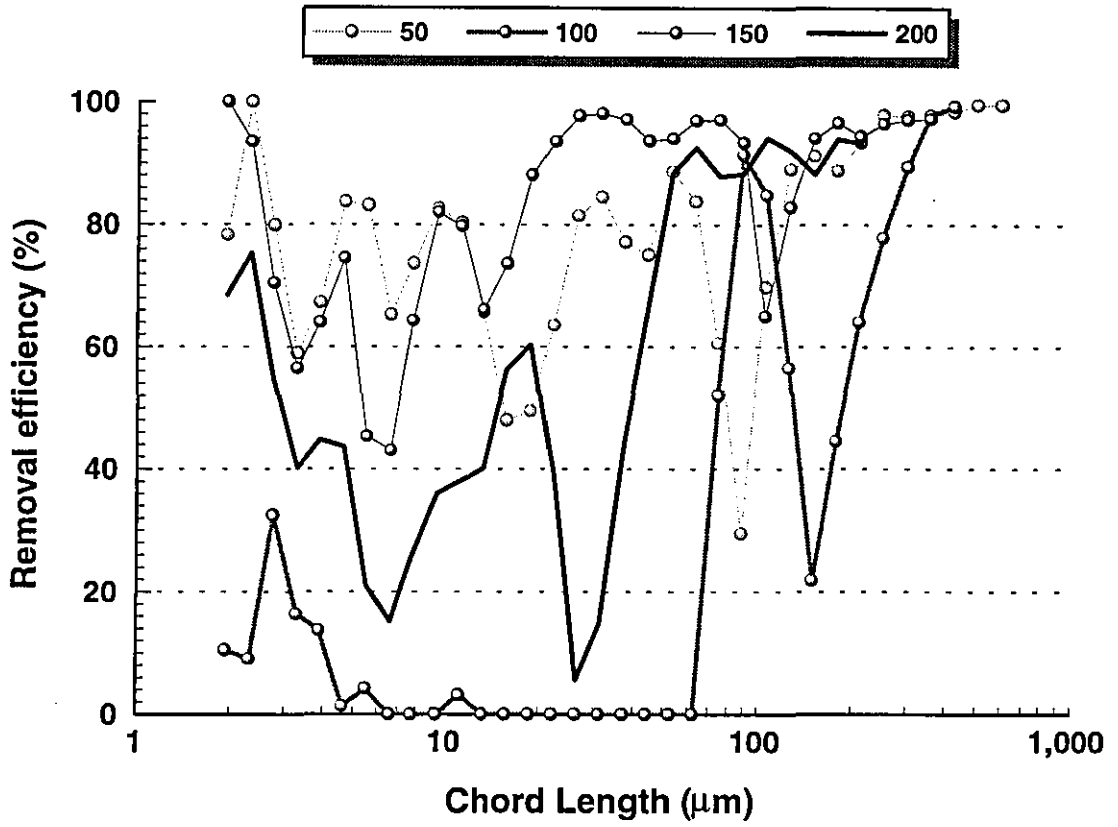


Figure B29: Grade efficiency curves vs Dodecyltrimethylammoniumbromide concentration for dispersed Wyoming Bentonite particles, R=5%

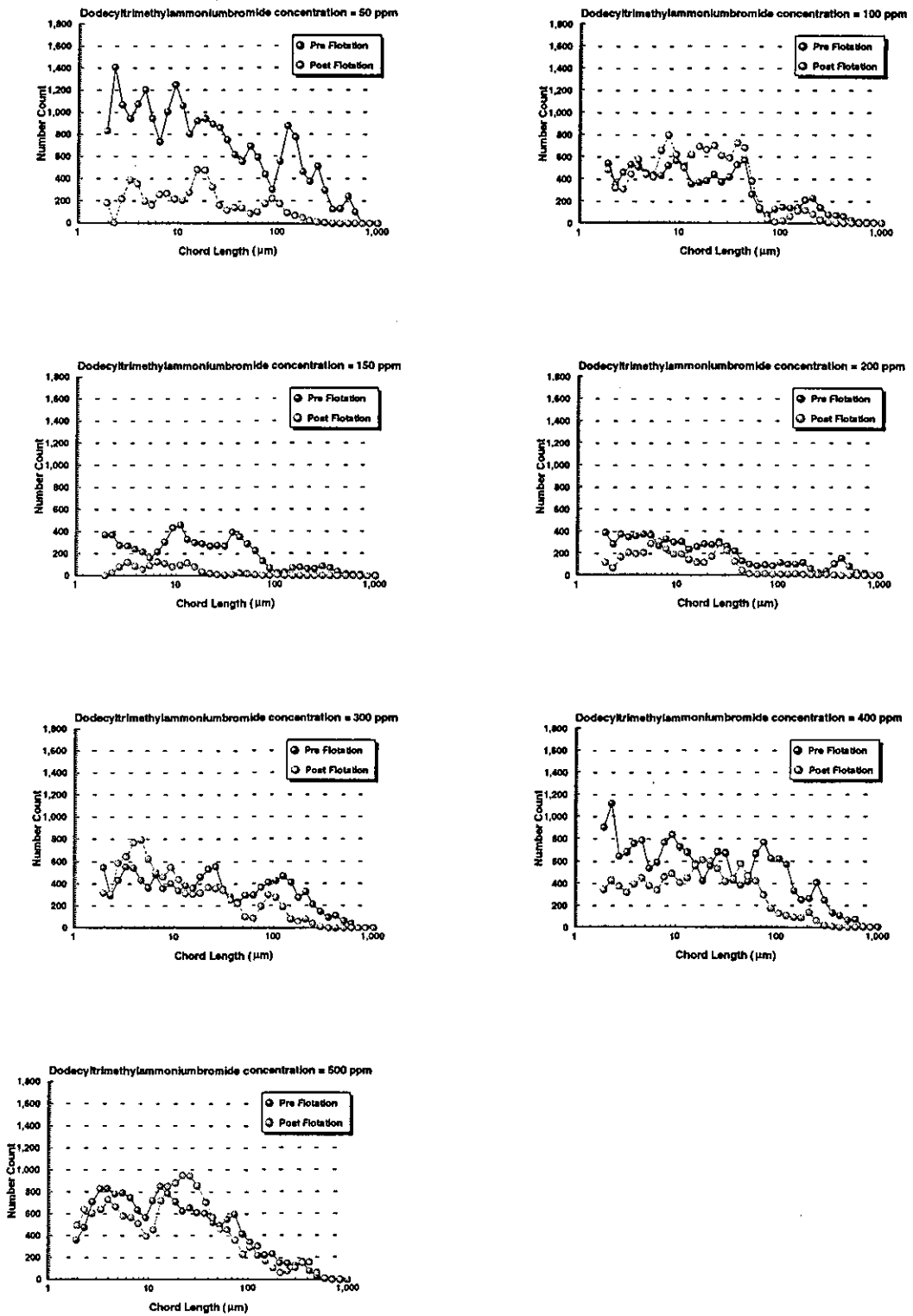


Figure B30: Pre and Post flotation particle size distributions for dispersed Wyoming Bentonite particles conditioned with Dodecyltrimethylammoniumbromide, R=5%

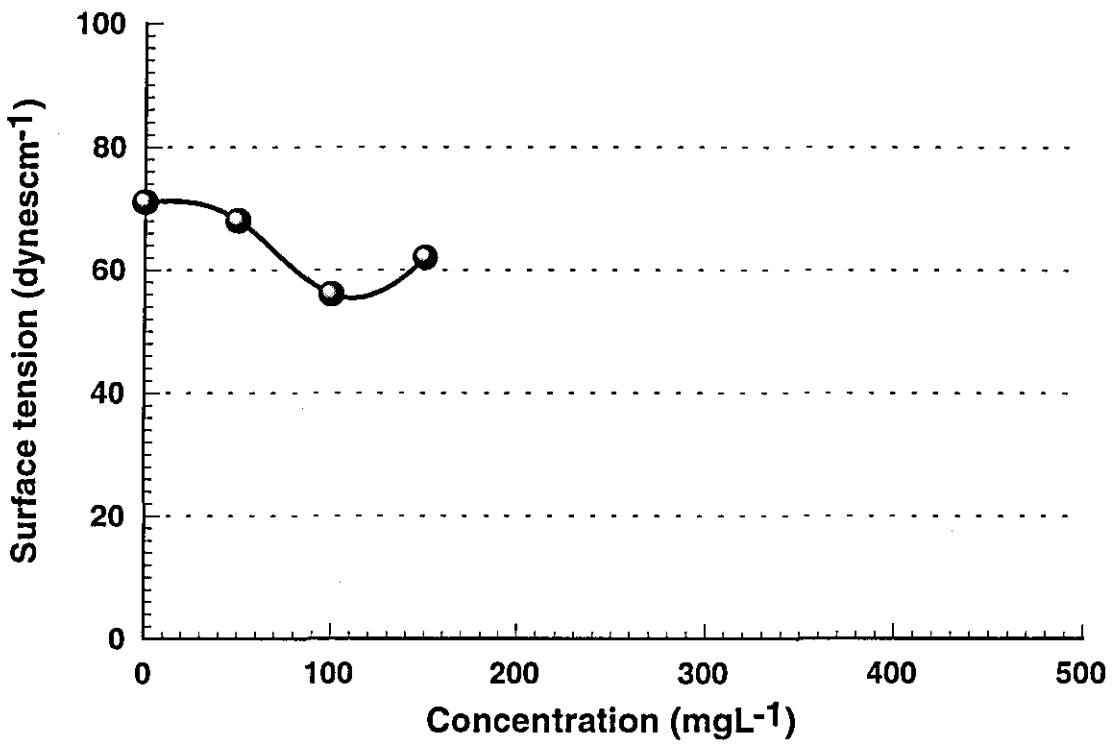
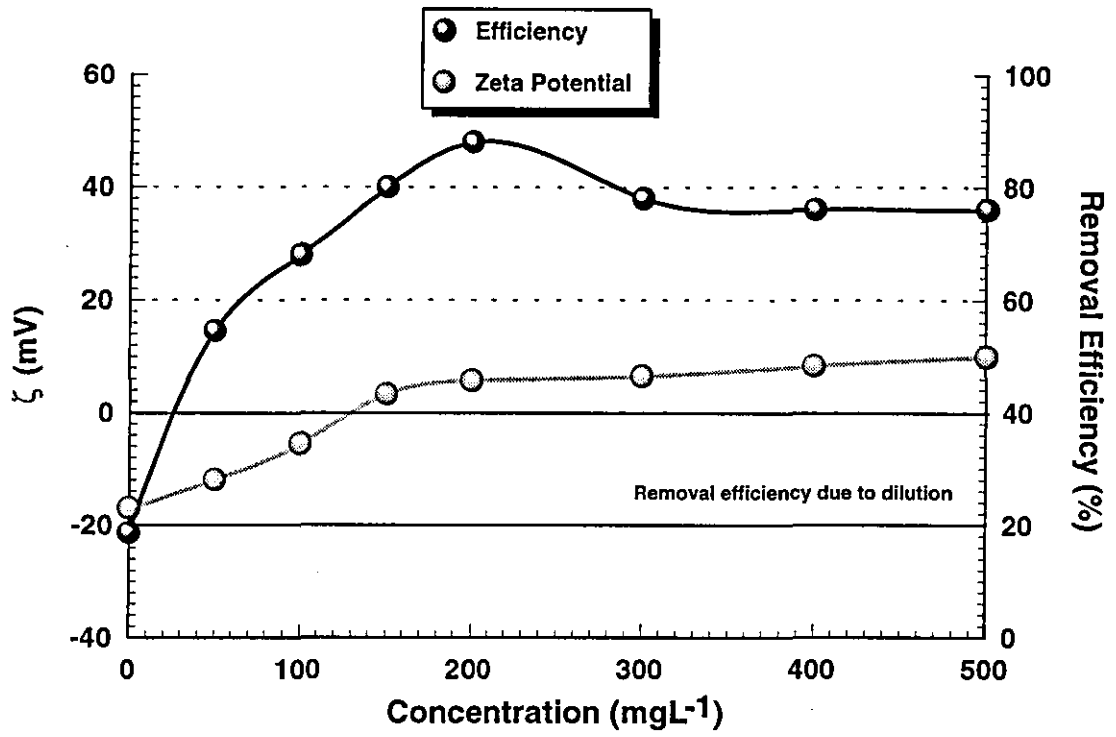


Figure B31: Flotation response vs concentration of Dodecyltrimethylammoniumbromide for dispersed Wyoming Bentonite particles, R=25%

APPENDIX C

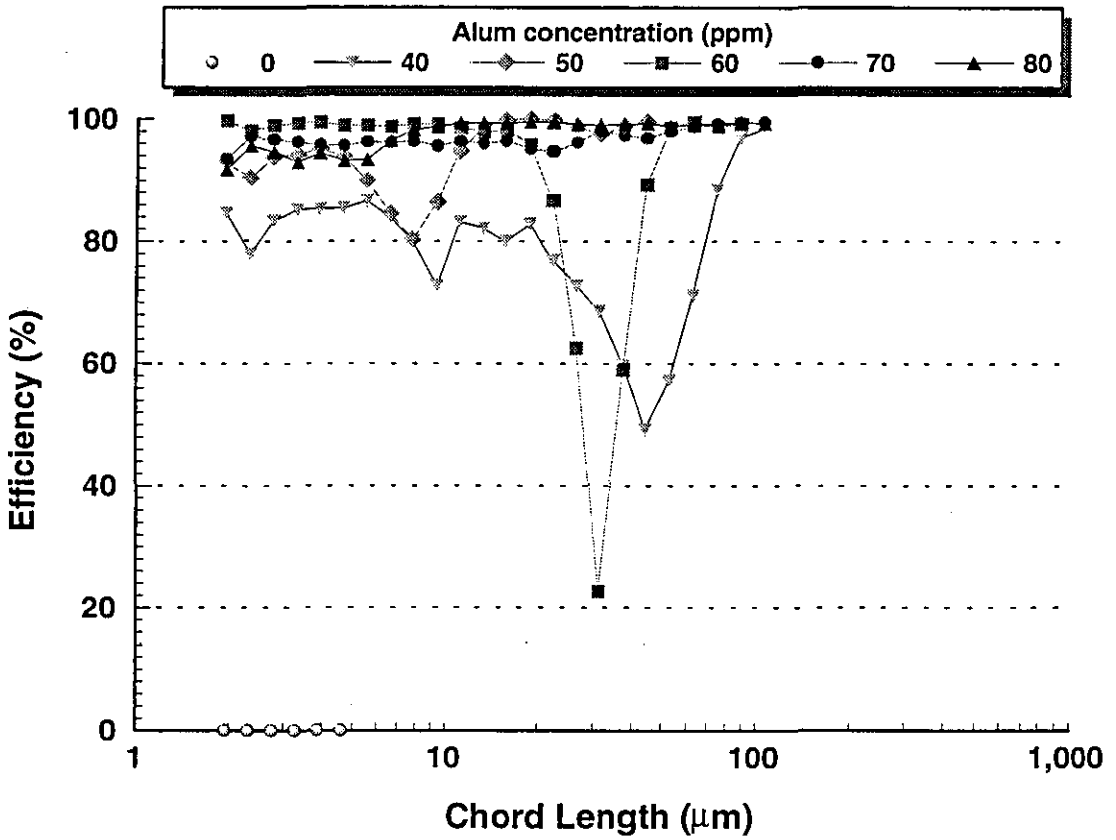
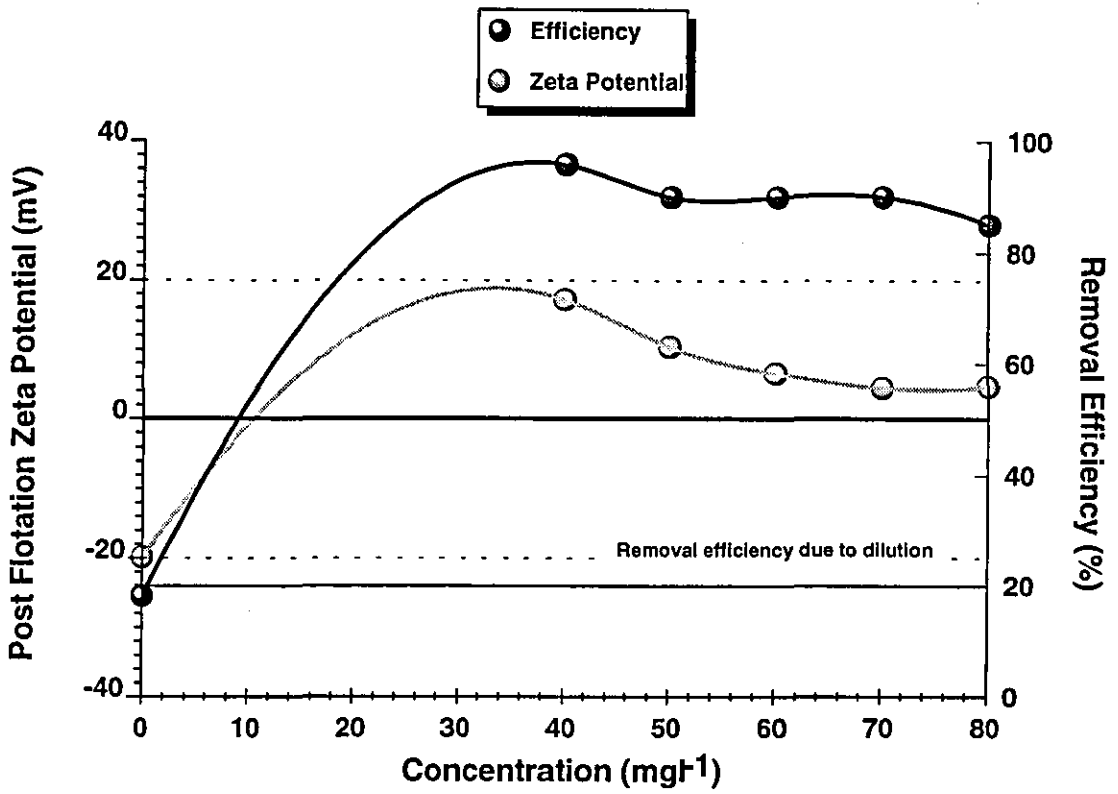


Figure C1: Flotation response of dispersed Wyoming Bentonite particles conditioned with Alum, air injection ratio = 25%

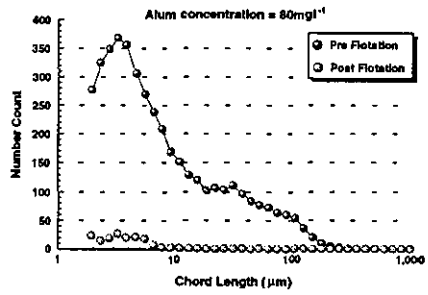
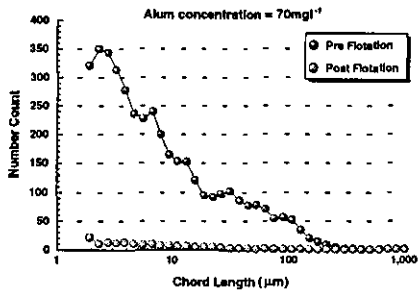
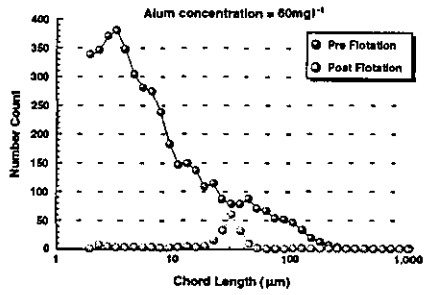
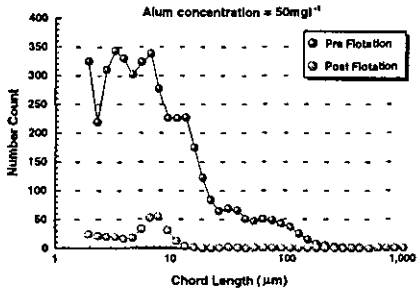
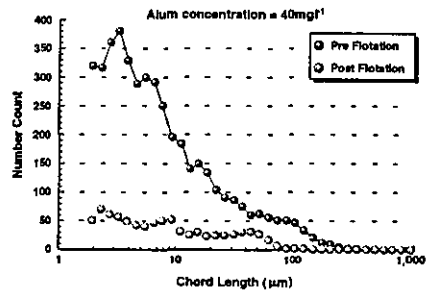
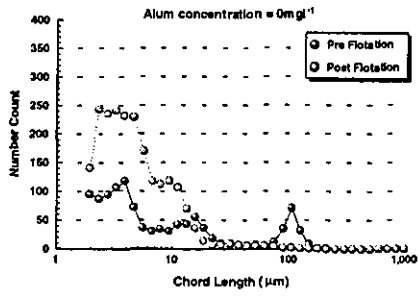


Figure C2: Pre and Post flotation particle size distributions for dispersed Wyoming Bentonite particles conditioned with Alum, air injection ratio = 25%

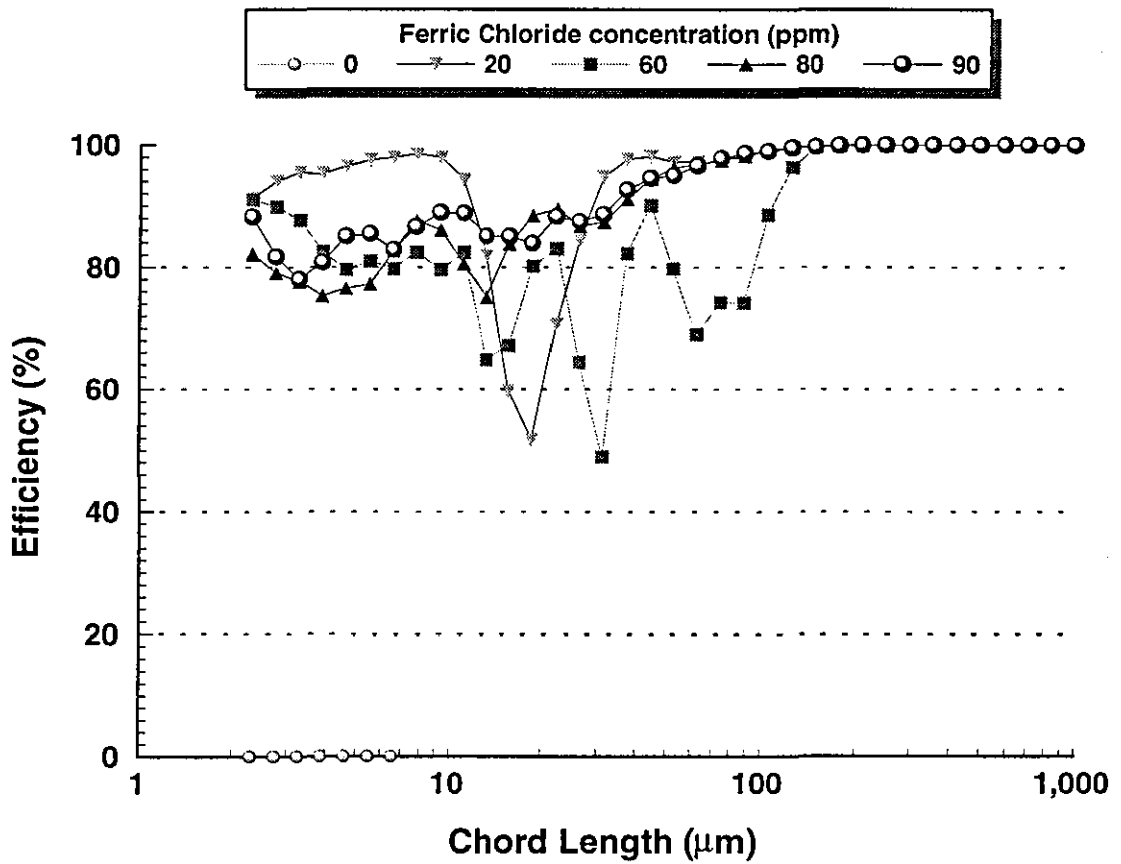
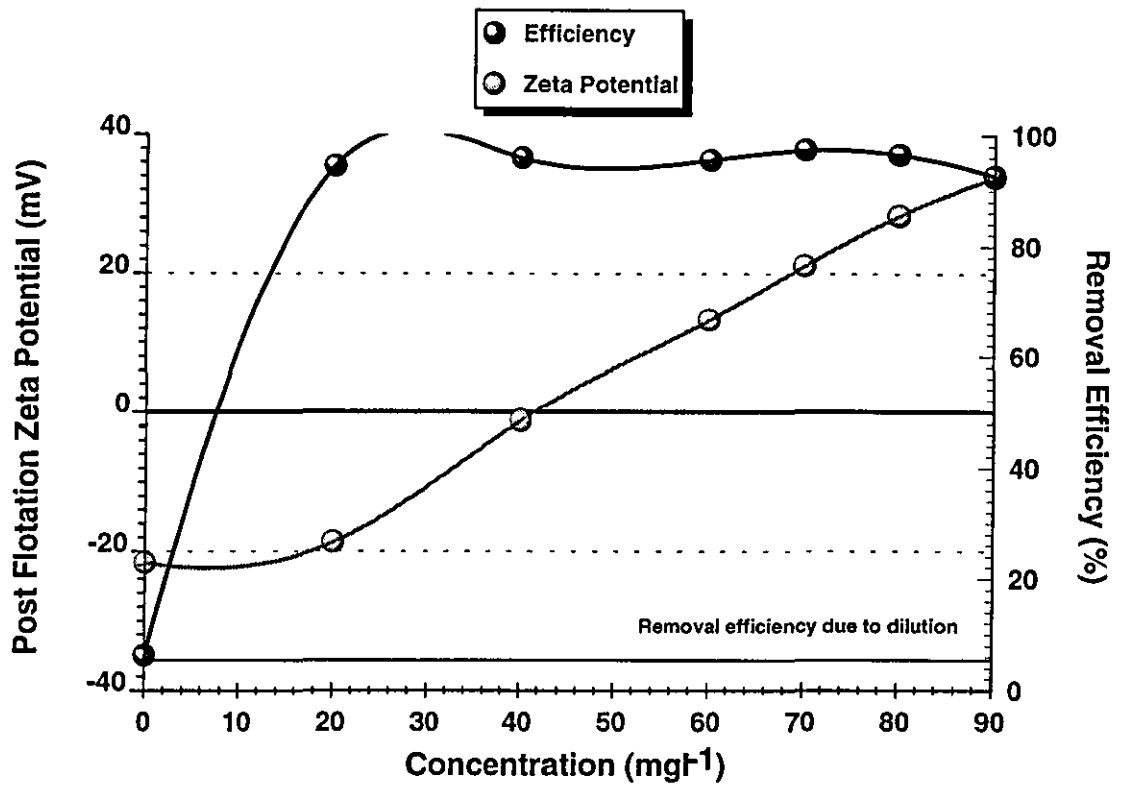


Figure C3: Flotation response of dispersed Wyoming Bentonite particles conditioned with Ferric Chloride, air injection ratio = 5%

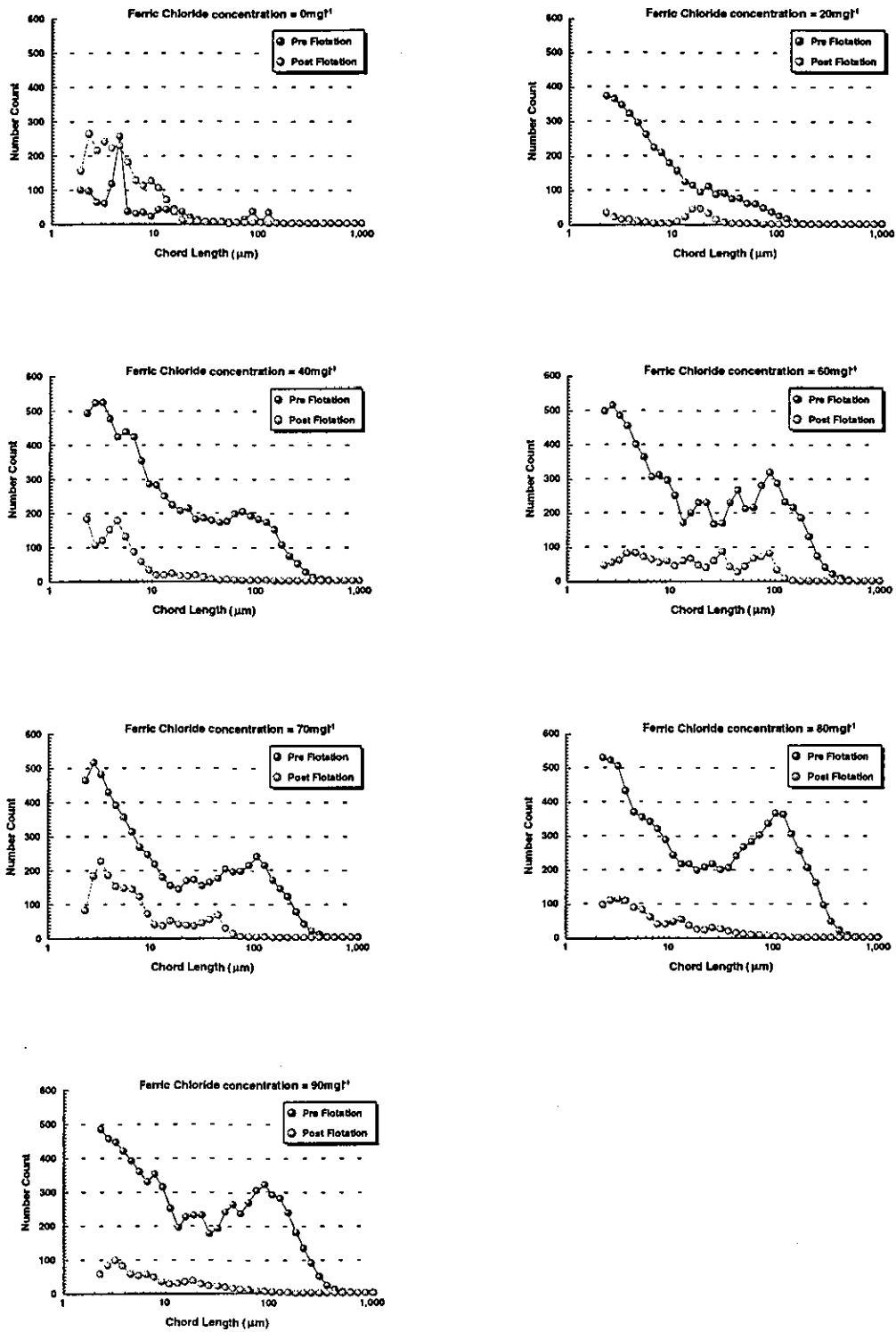


Figure C4: Pre and Post flotation particle size distributions for dispersed Wyoming Bentonite particles conditioned with Ferric Chloride, air injection ratio = 5%

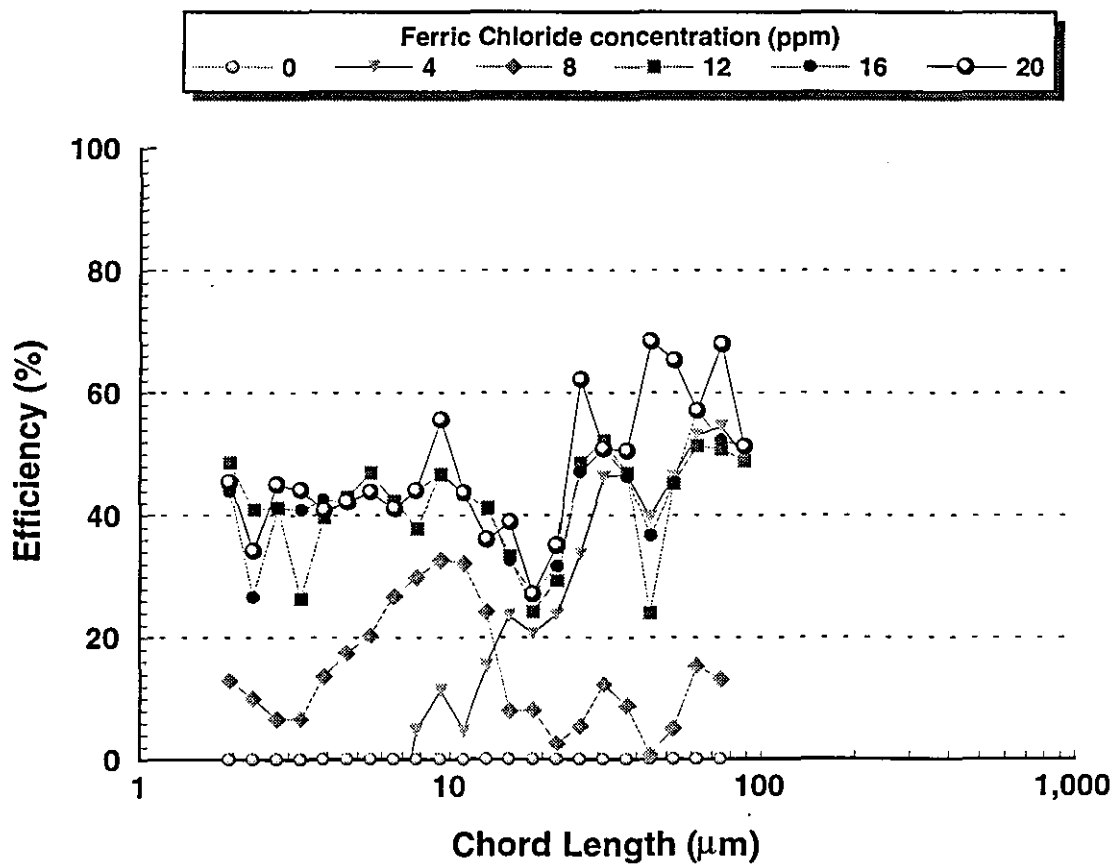
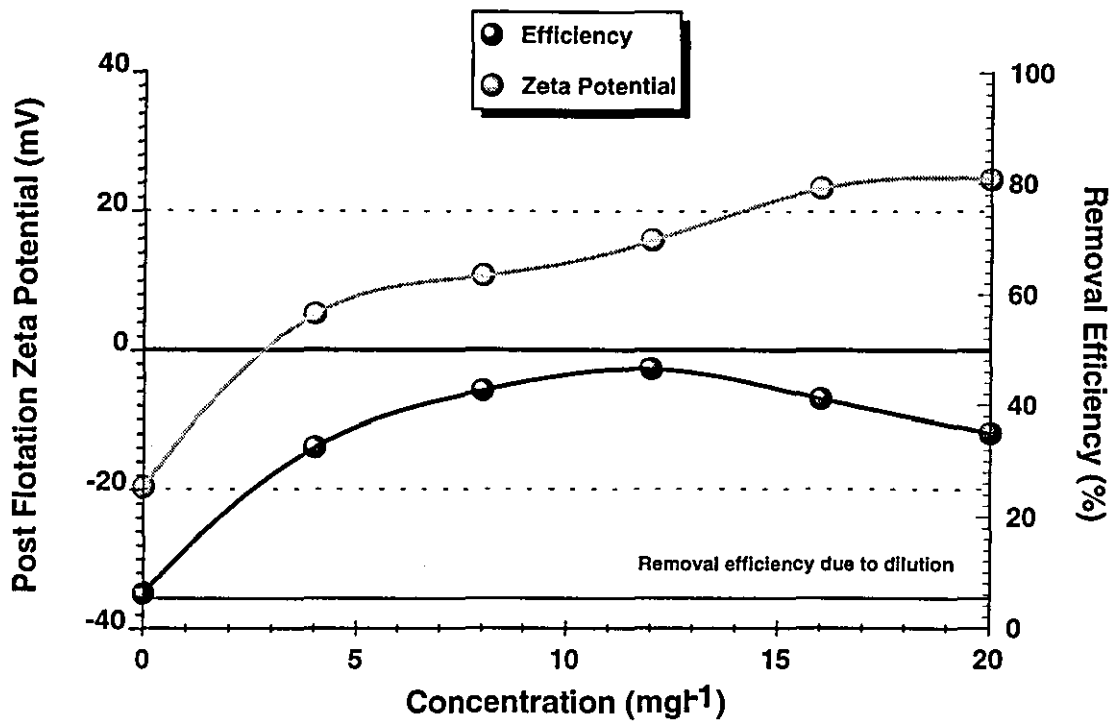


Figure C5: Flotation response of dispersed Kaolin particles conditioned with Ferric Chloride, air injection ratio = 5%

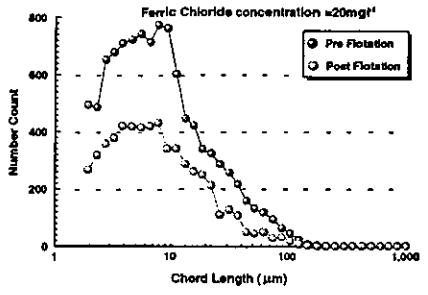
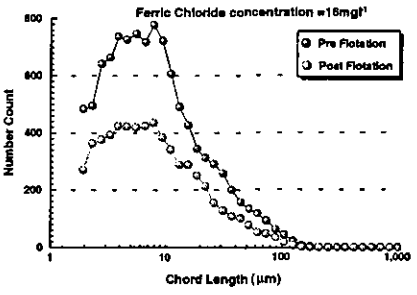
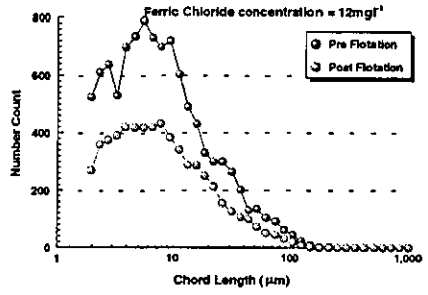
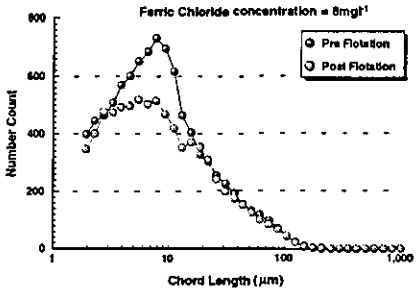
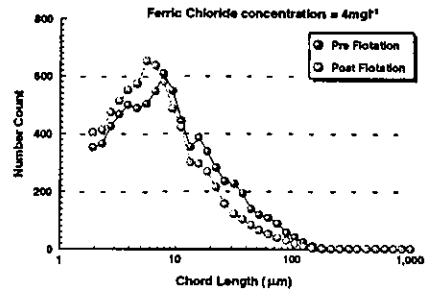
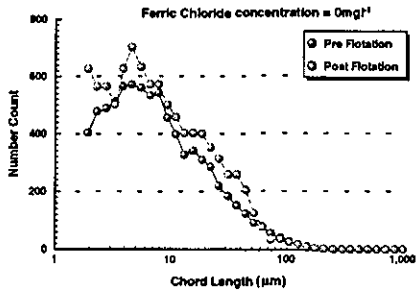


Figure C6: Pre and Post flotation particle size distributions for dispersed Kaolin particles conditioned with Ferric Chloride, air injection ratio = 5%

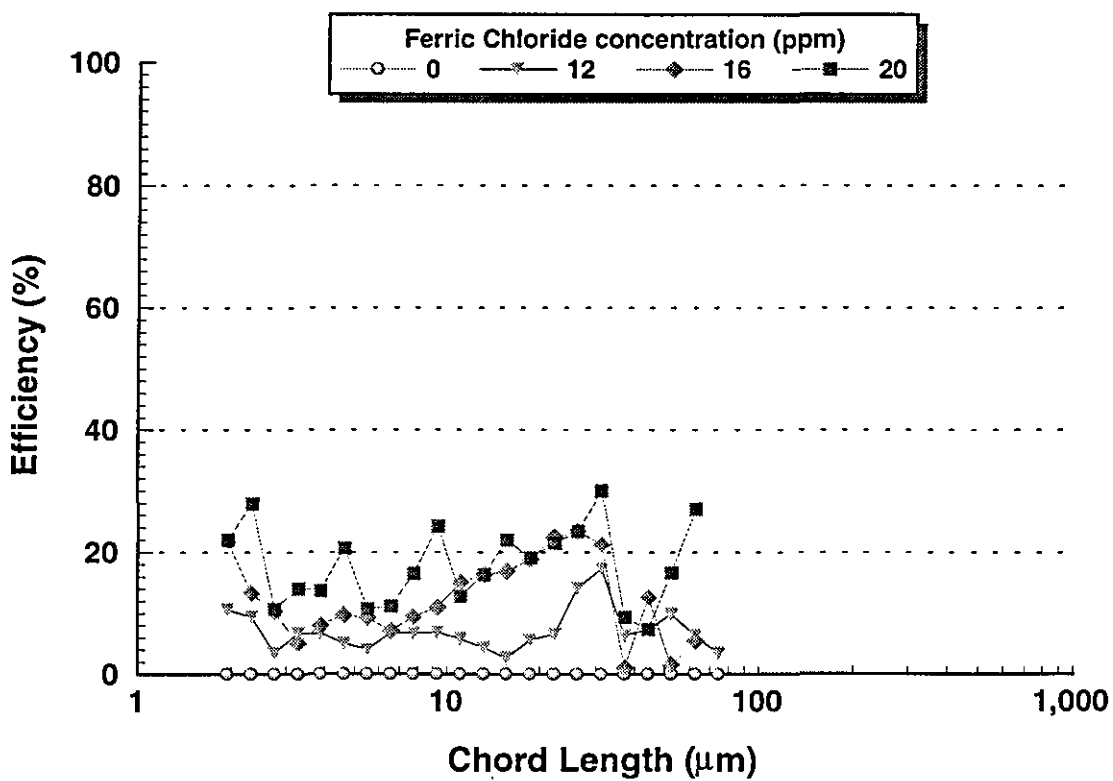
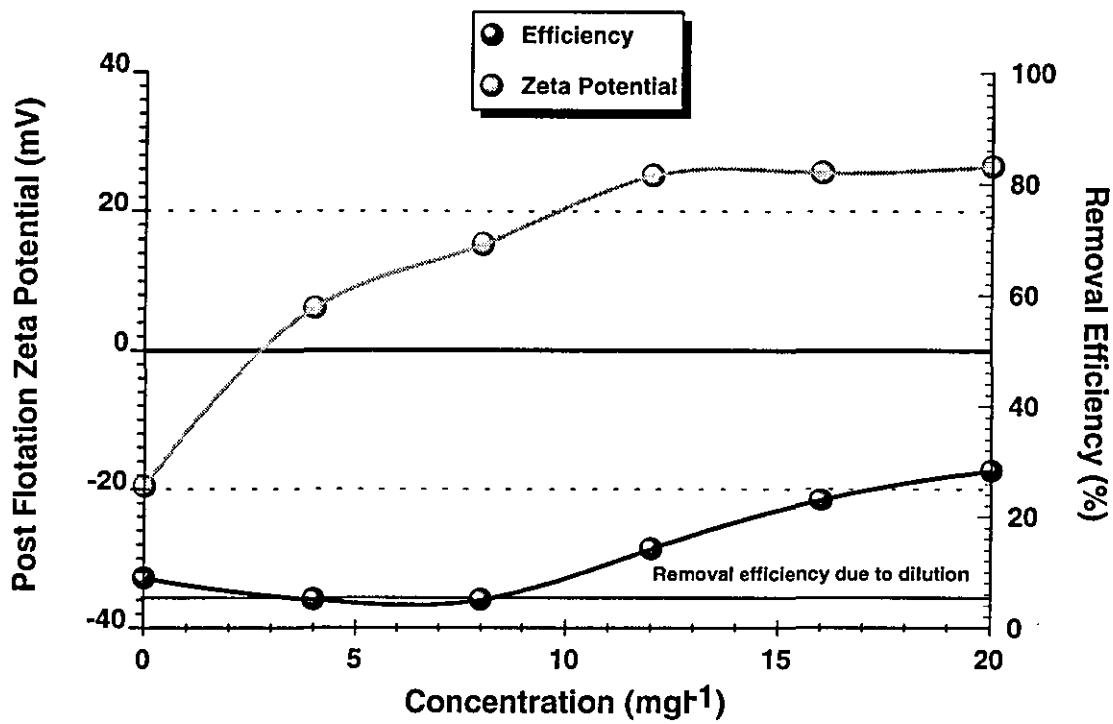


Figure C7: Flotation response of dispersed Kaolin particles conditioned with Alum, air injection ratio = 5%

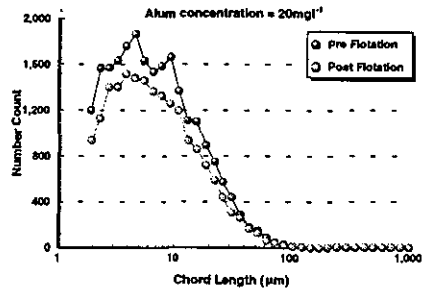
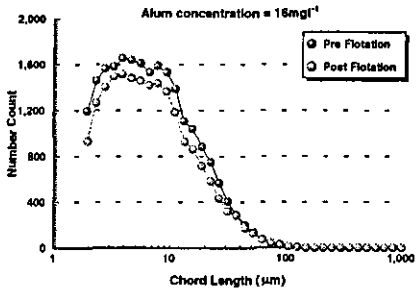
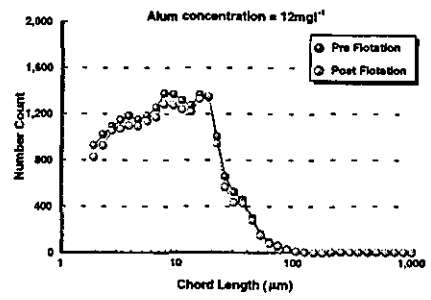
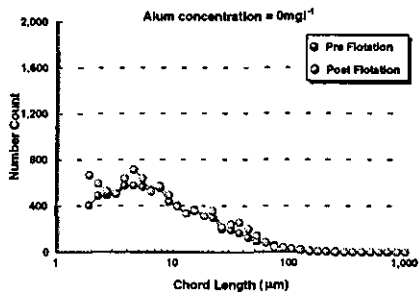


Figure C8: Pre and Post flotation particle size distributions for dispersed Kaolin particles conditioned with Alum, air injection ratio = 5%

APPENDIX D

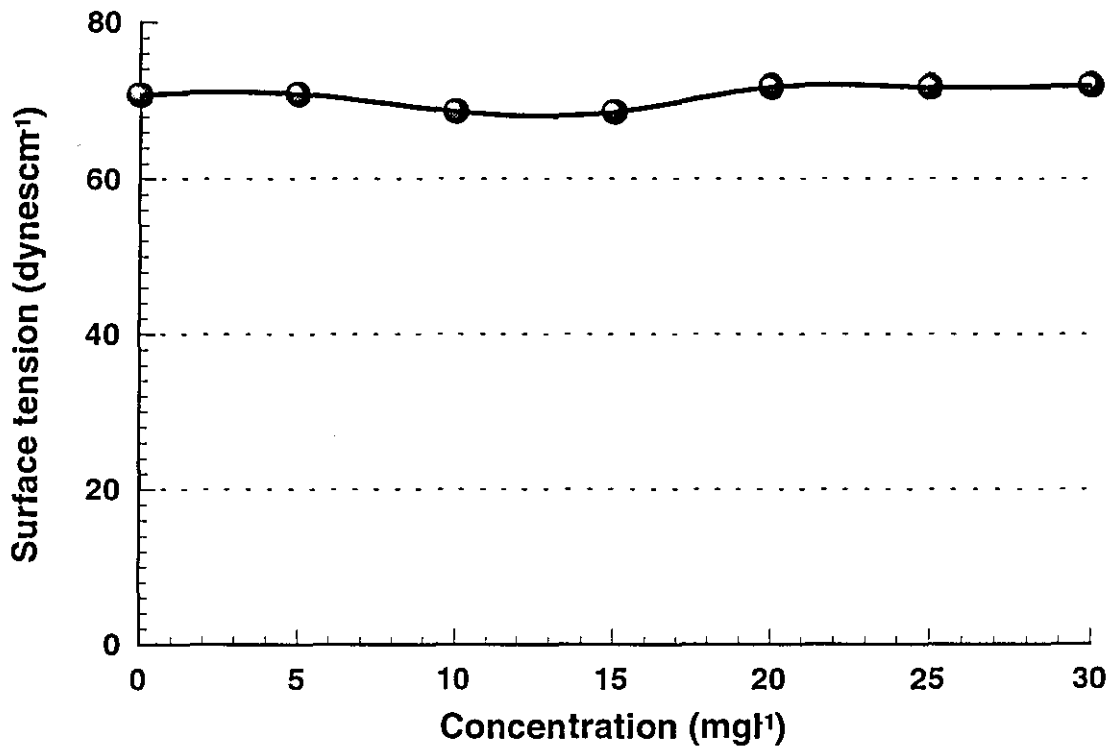
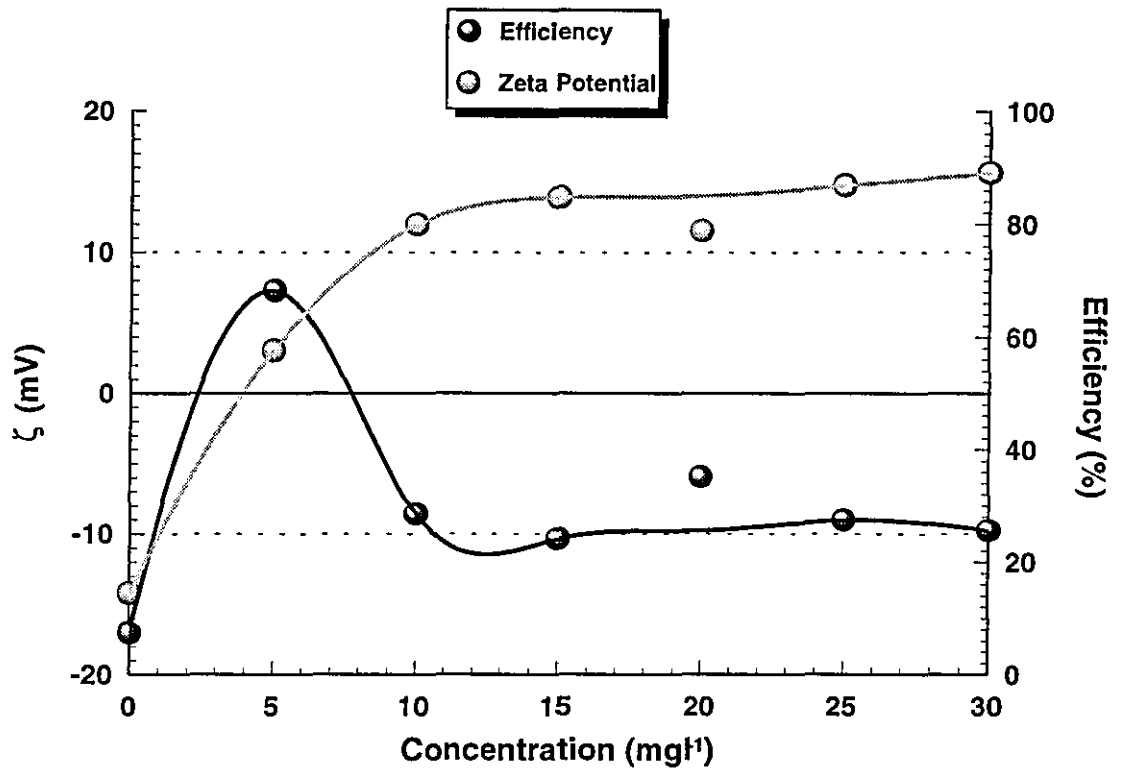


Figure D1: Jar test response of dispersed Kaolin particles vs concentration of Alum

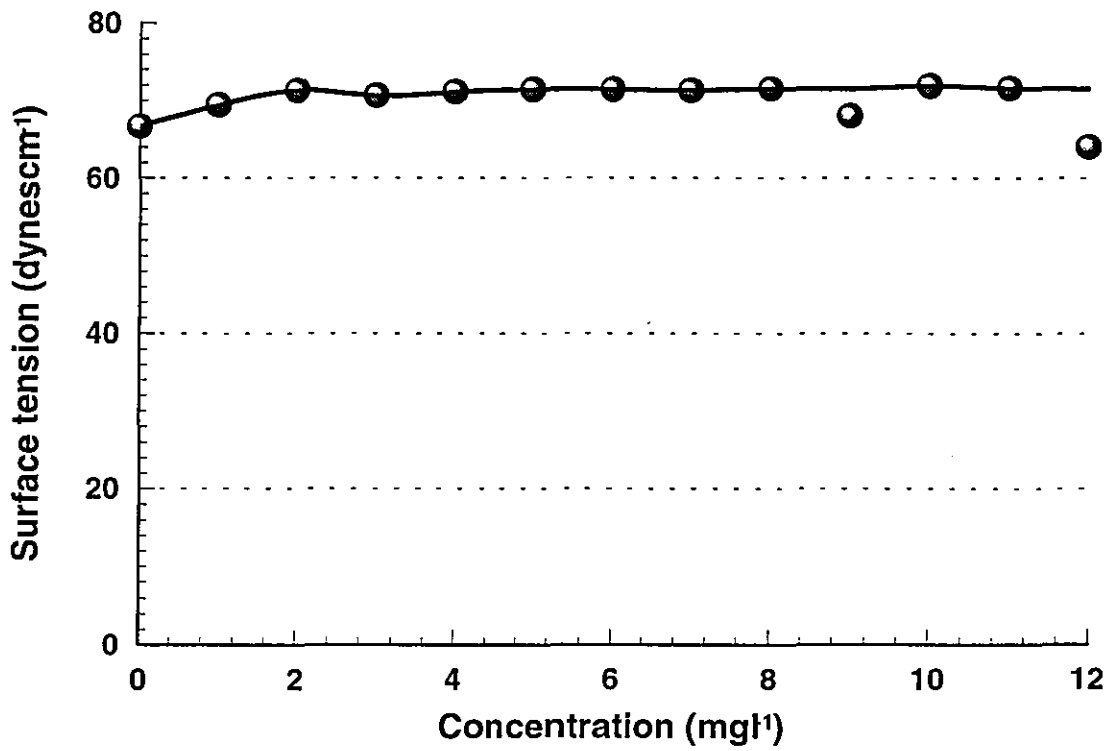
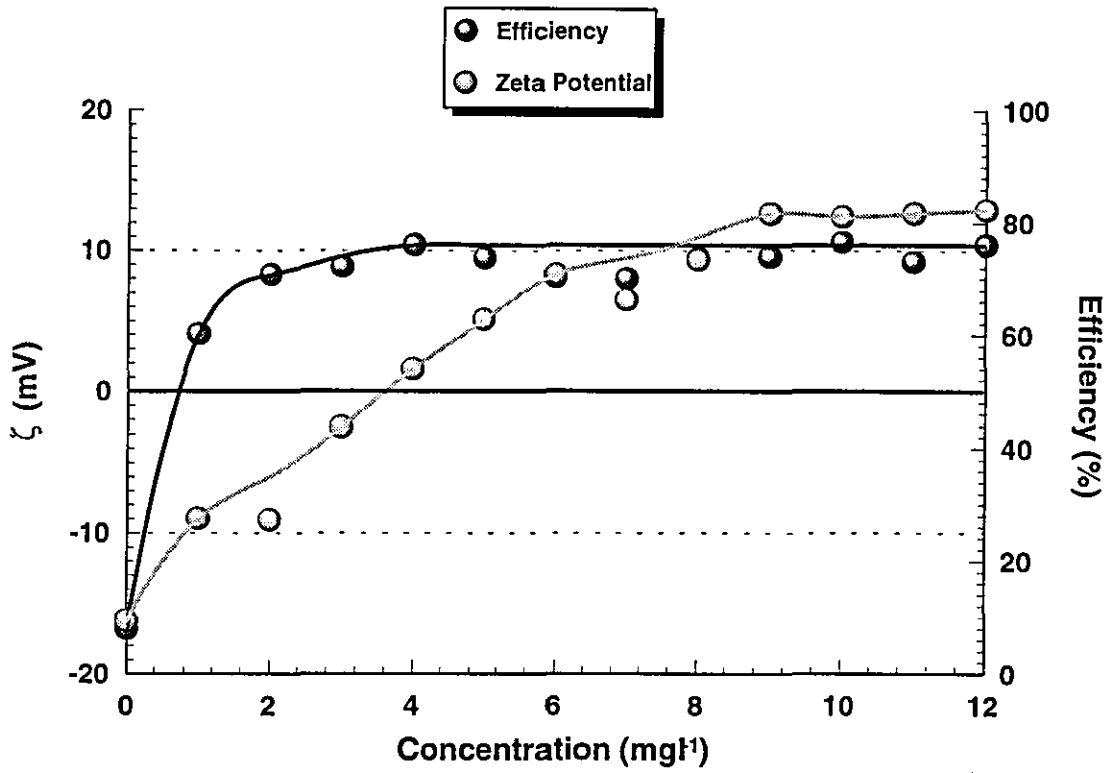


Figure D2: Jar test response of dispersed Kaolin particles vs concentration of Alum

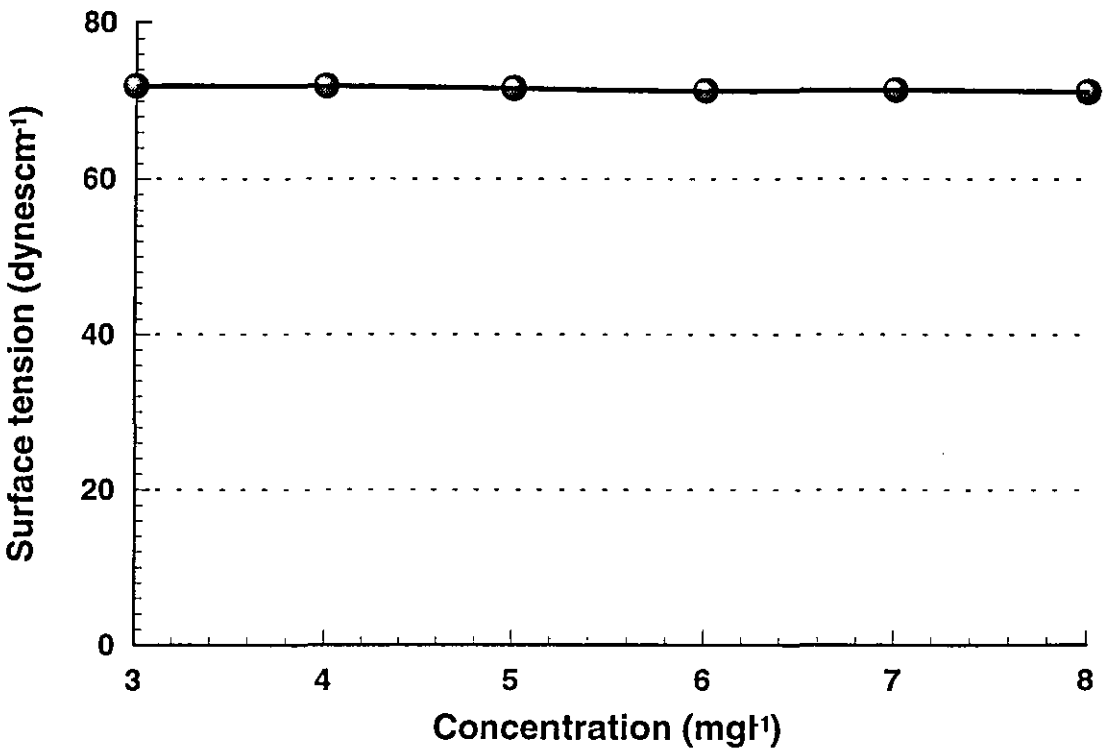
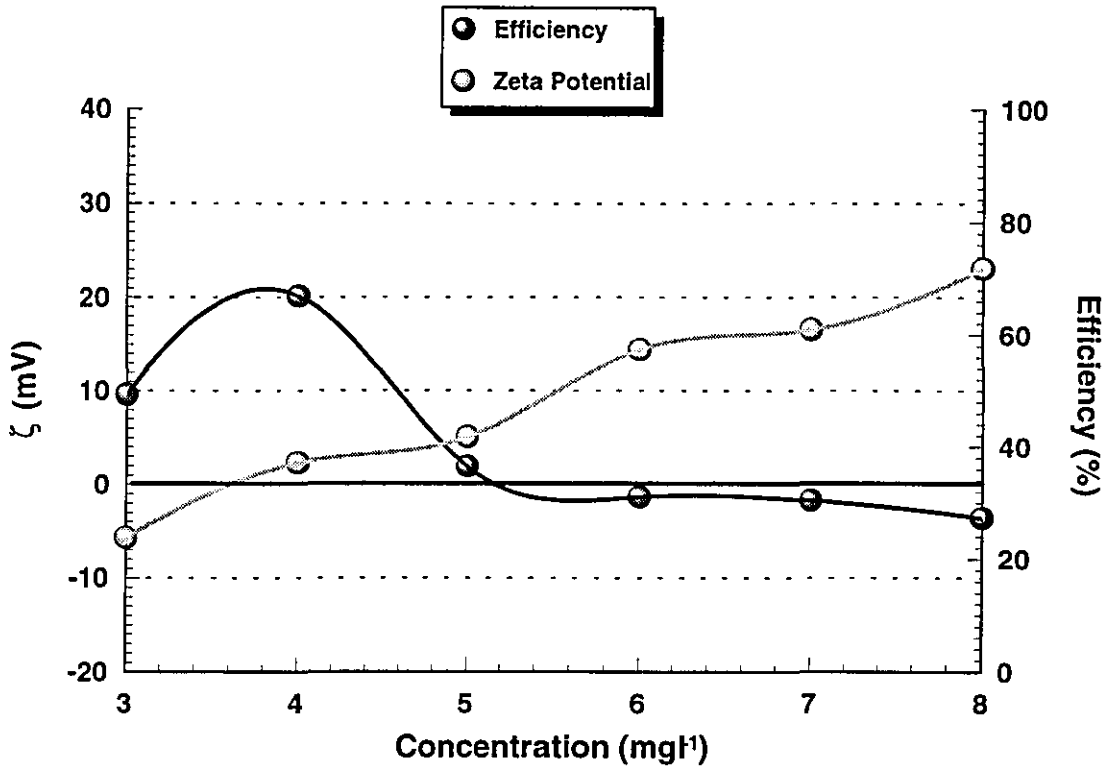


Figure D3: Jar test response of dispersed Kaolin particles vs pH, Alum concentration = 5 ppm

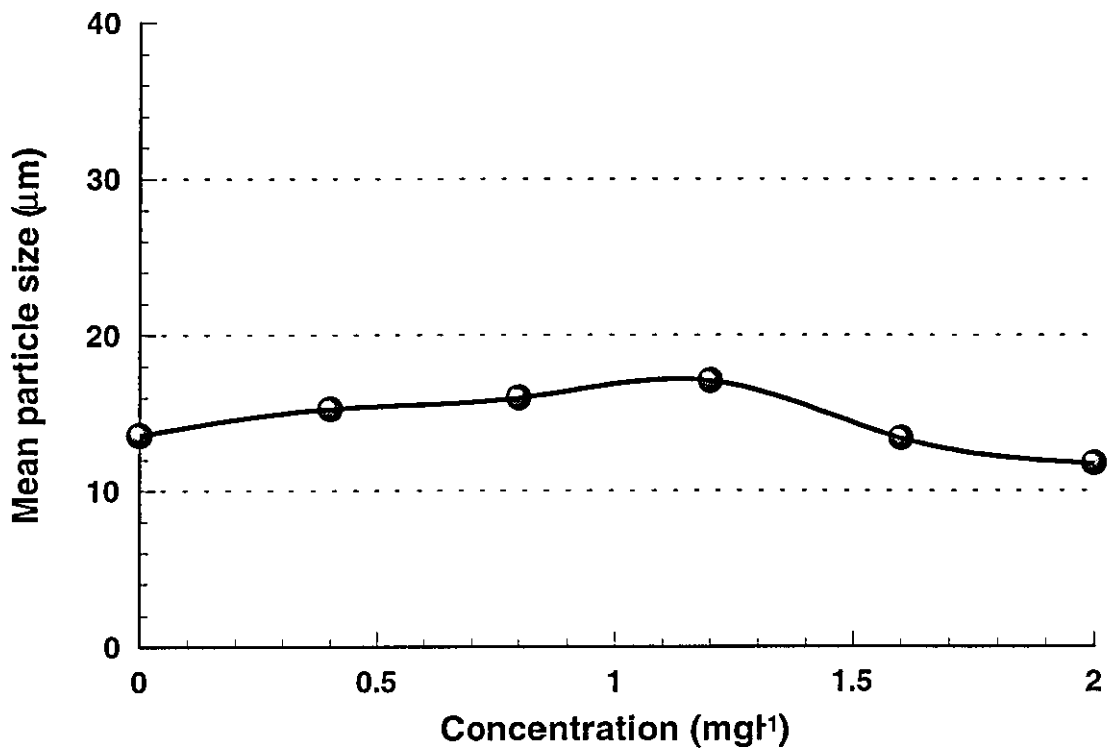
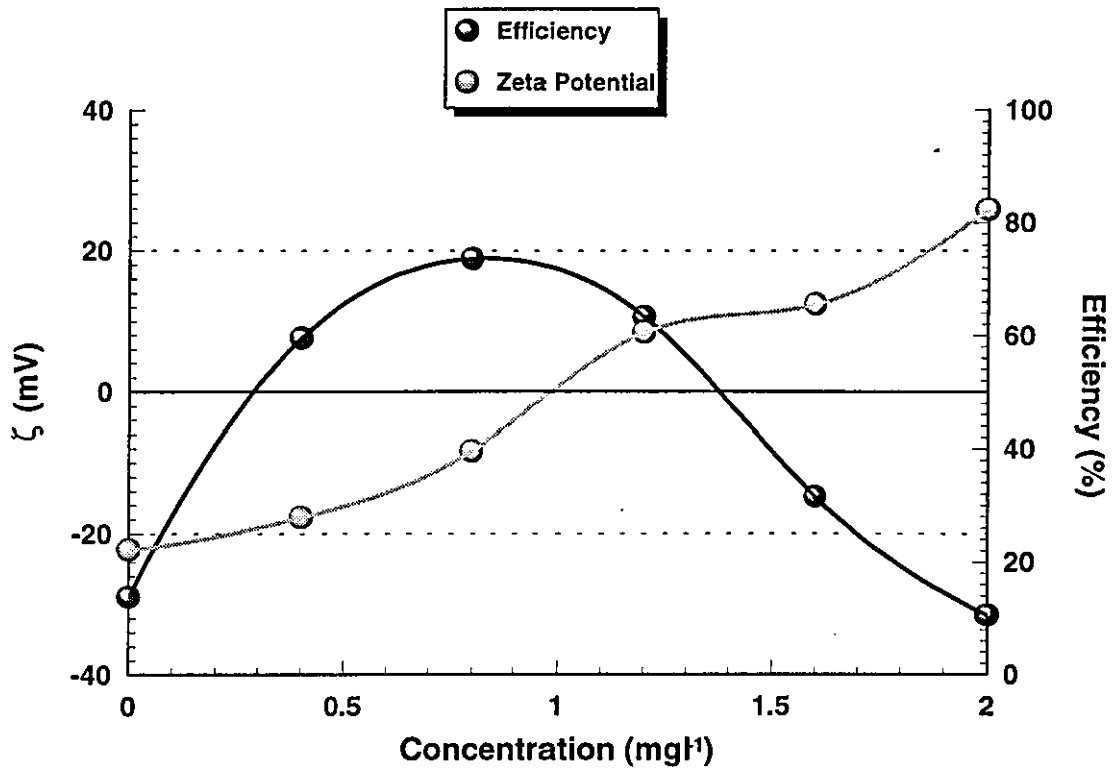


Figure D4: Jar test response of dispersed Kaolin particles vs concentration of Ferric Chloride

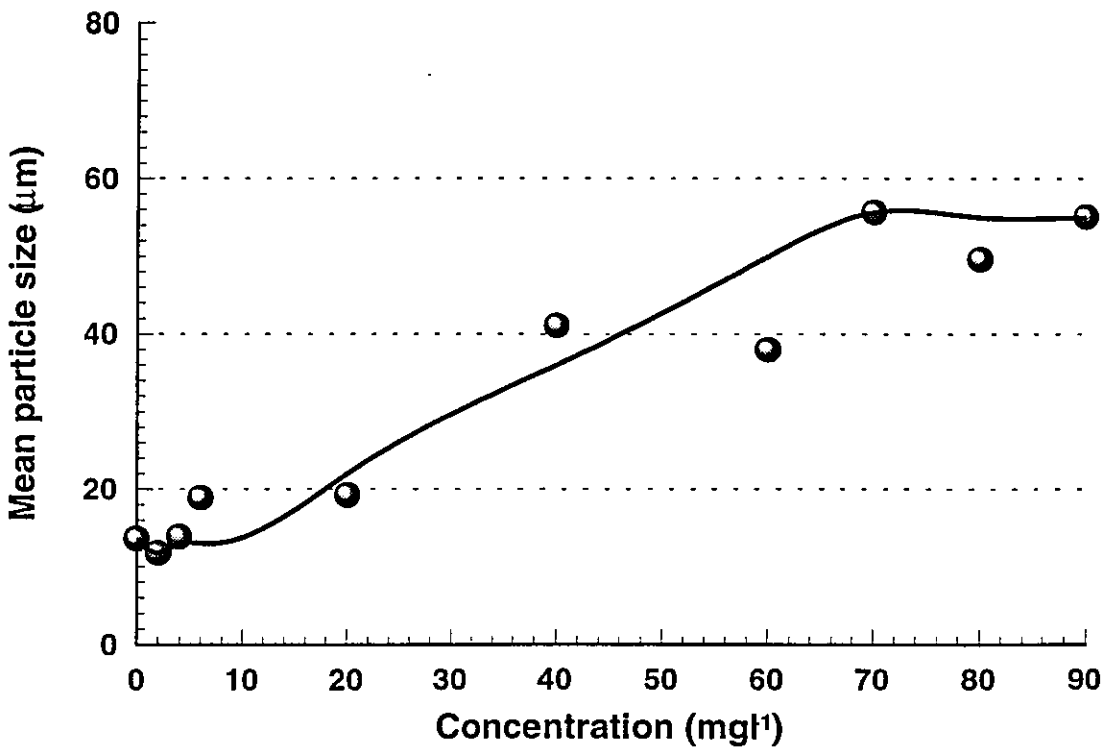
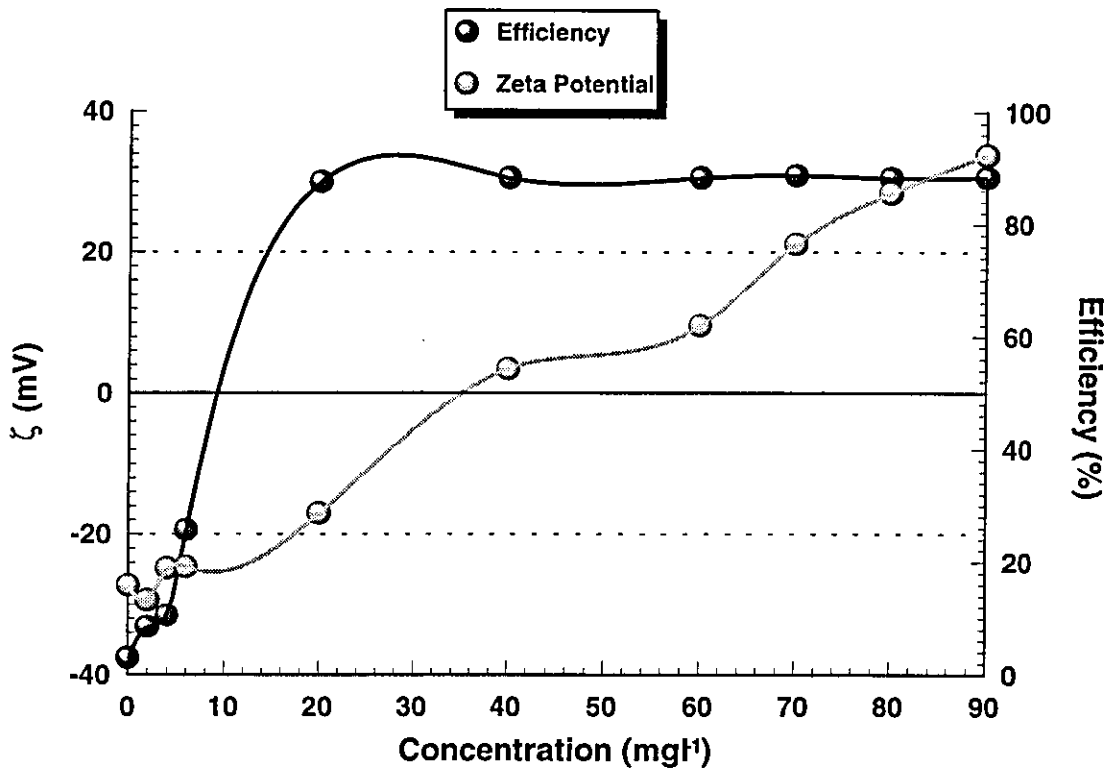


Figure D6: Jar test response of dispersed Wyoming Bentonite particles vs concentration of Ferric Chloride

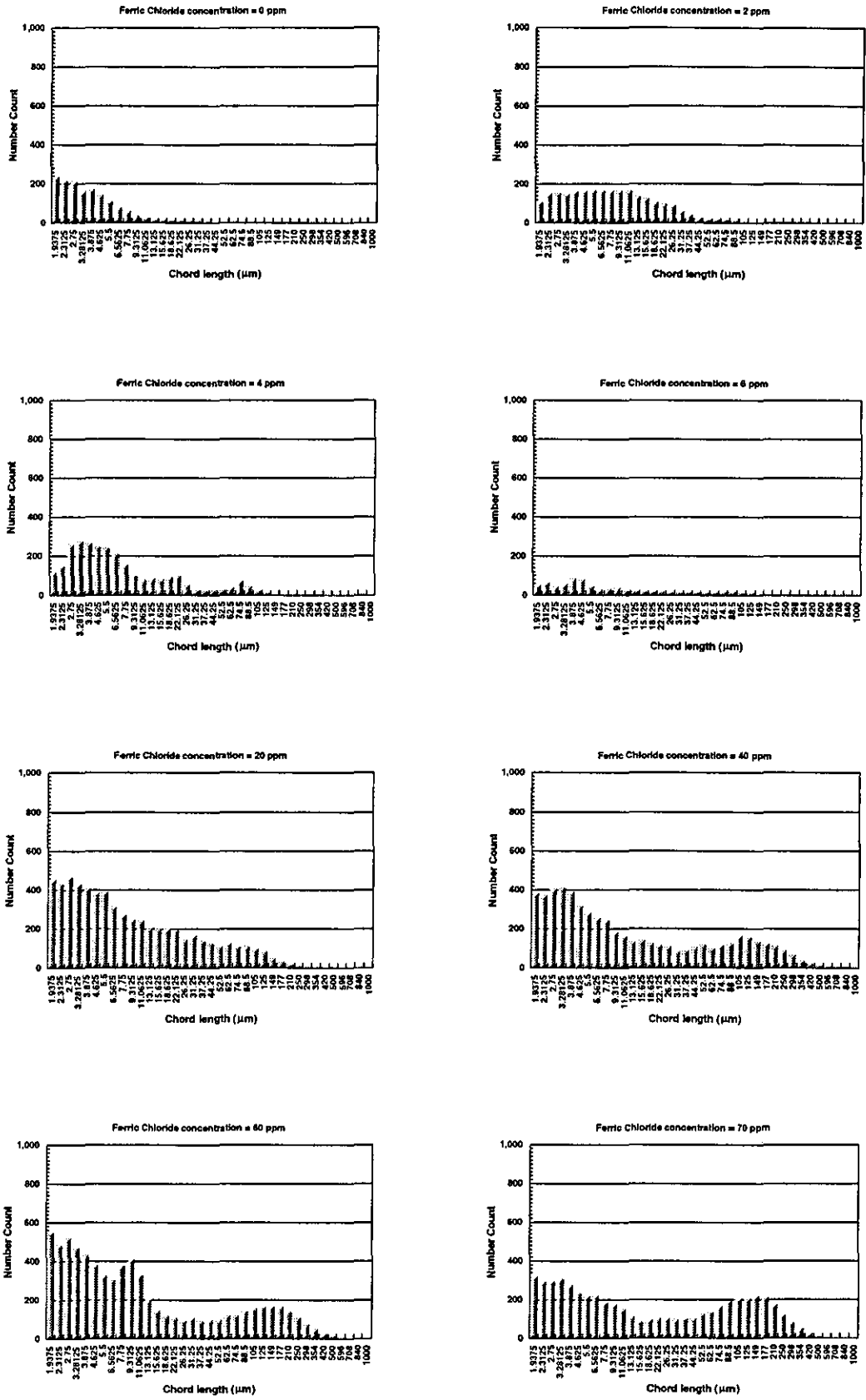
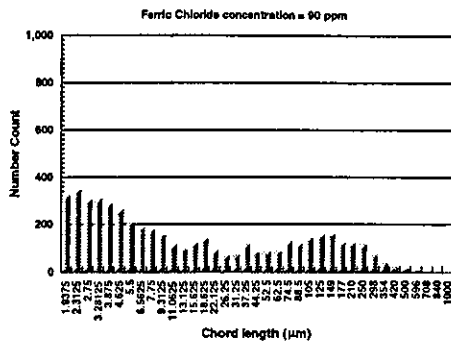
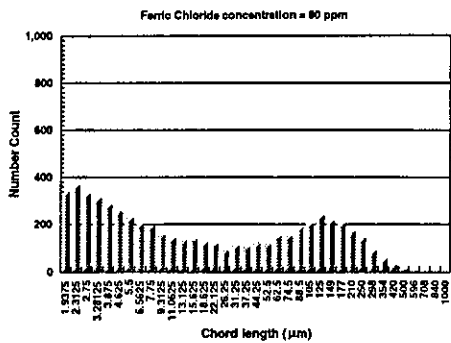


Figure D7: Particle size distributions vs Ferric Chloride concentration for dispersed Wyoming Bentonite particles



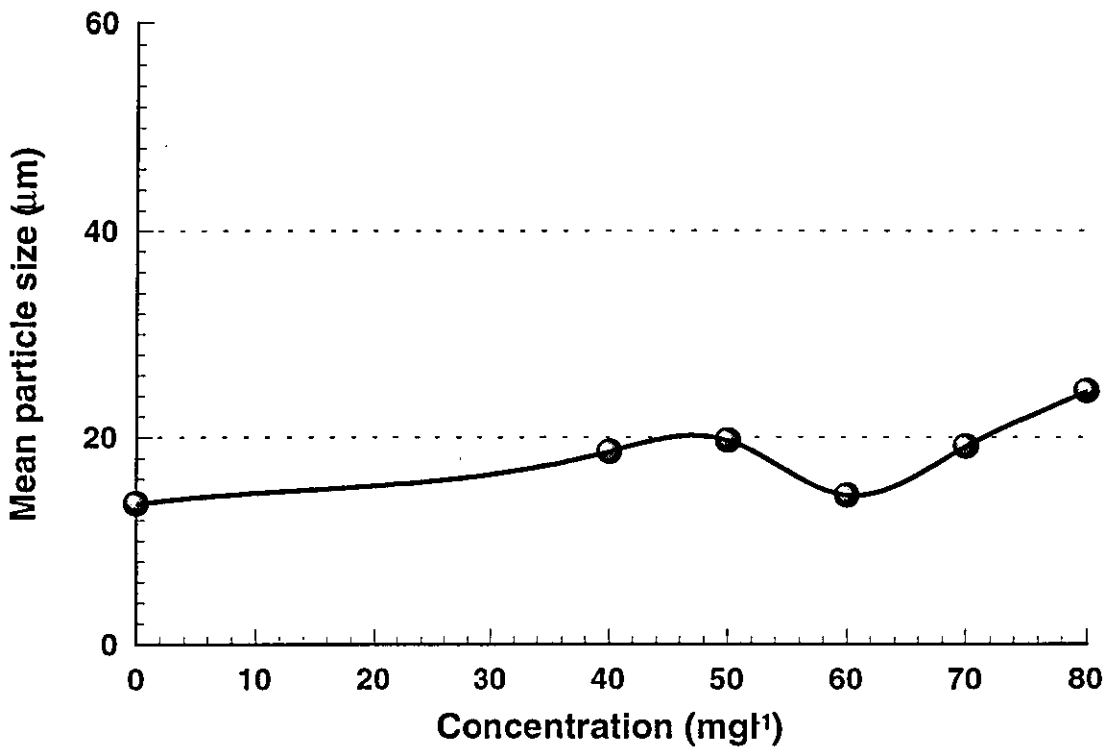
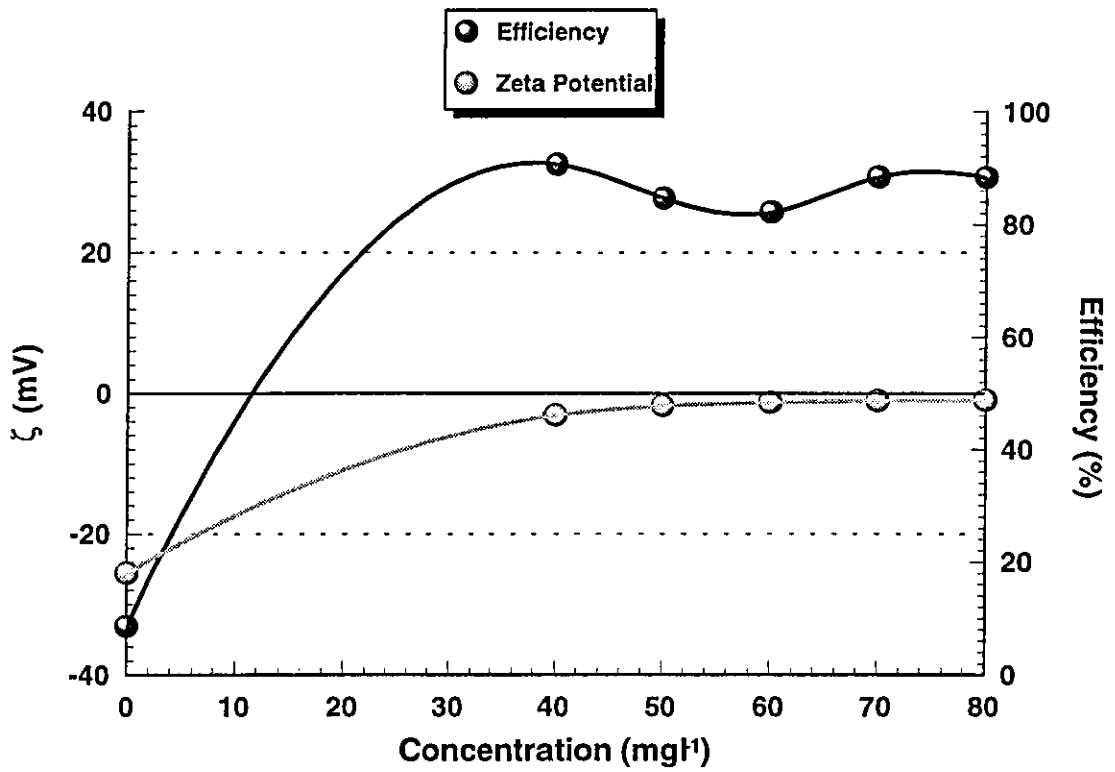


Figure D8: Jar test response of dispersed Wyoming Bentonite particles vs concentration of Alum

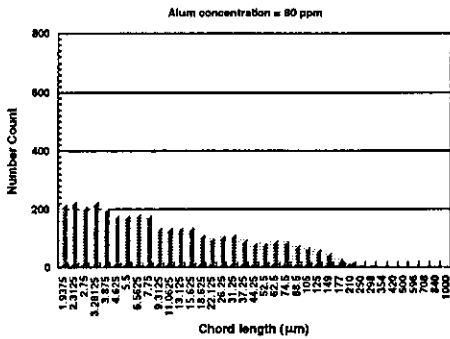
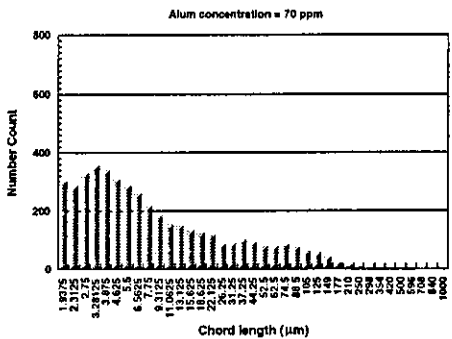
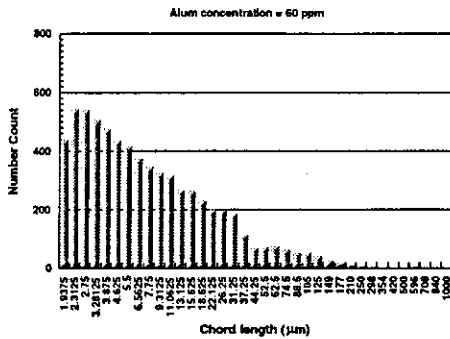
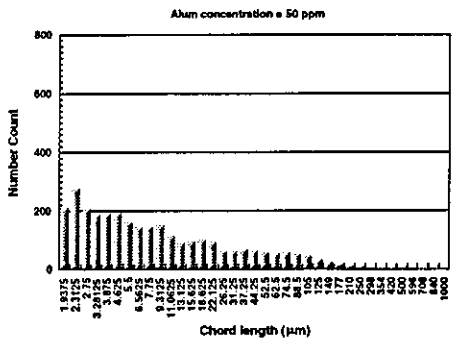
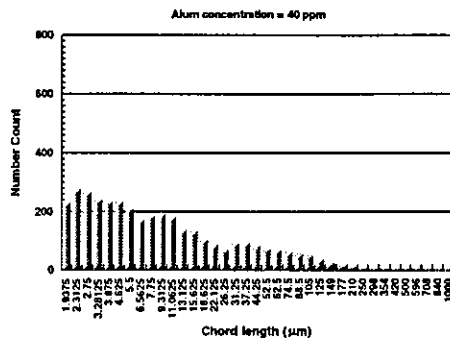
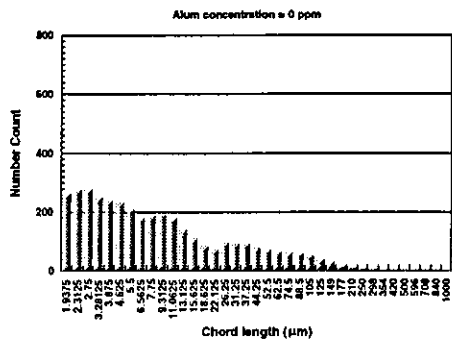


Figure D9: Particle size distributions vs Alum concentration for dispersed Wyoming Bentonite particles

APPENDIX E

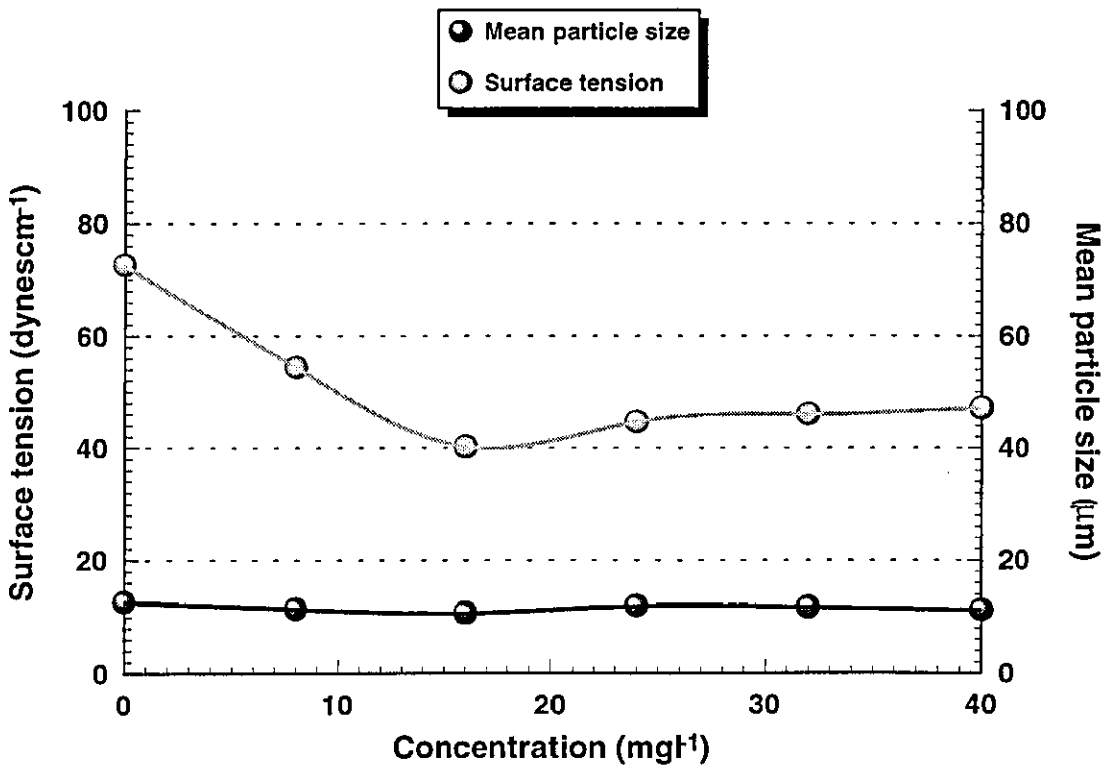
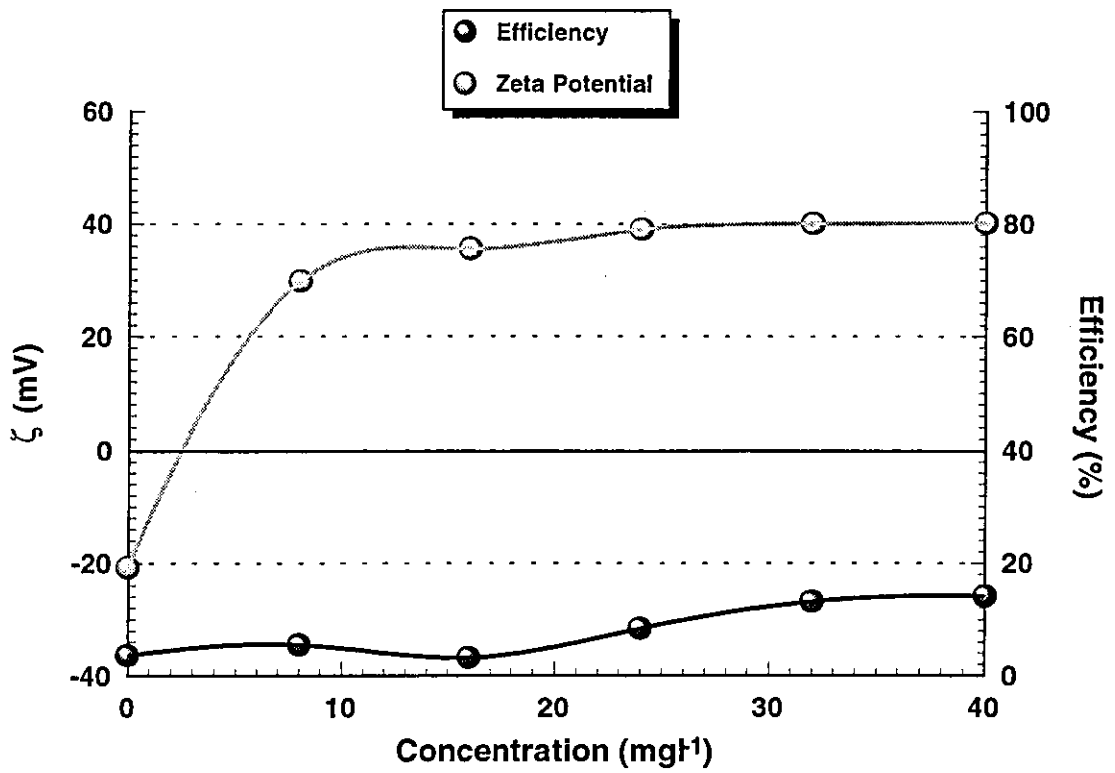


Figure E1: Jar test response of dispersed Kaolin particles vs concentration of Hexadecyltrimethylammoniumbromide

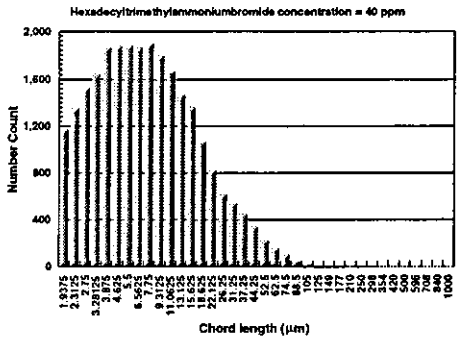
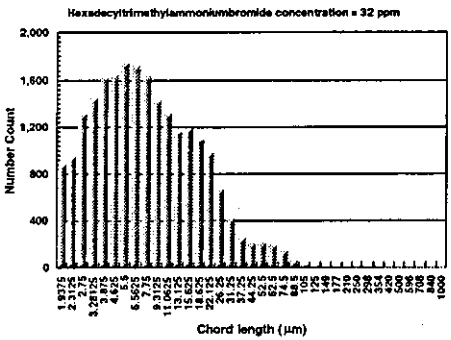
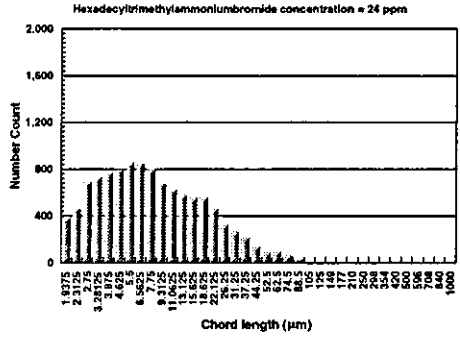
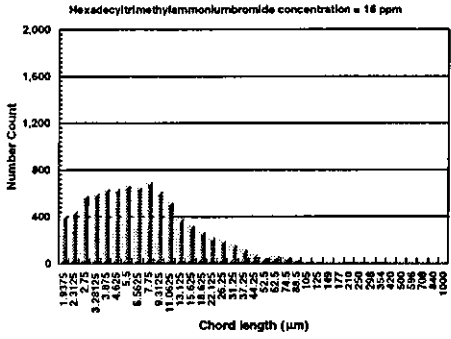
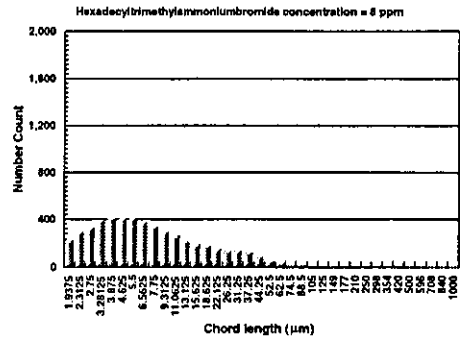
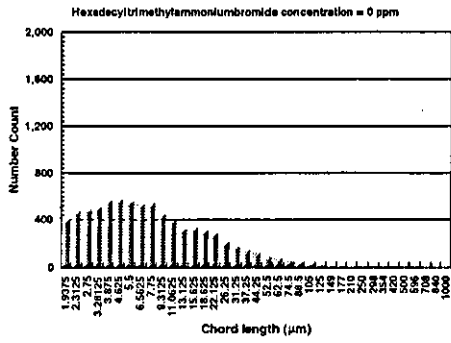


Figure E2: Particle size distributions vs Hexadecyltrimethylammoniumbromide concentration for dispersed Kaolin particles

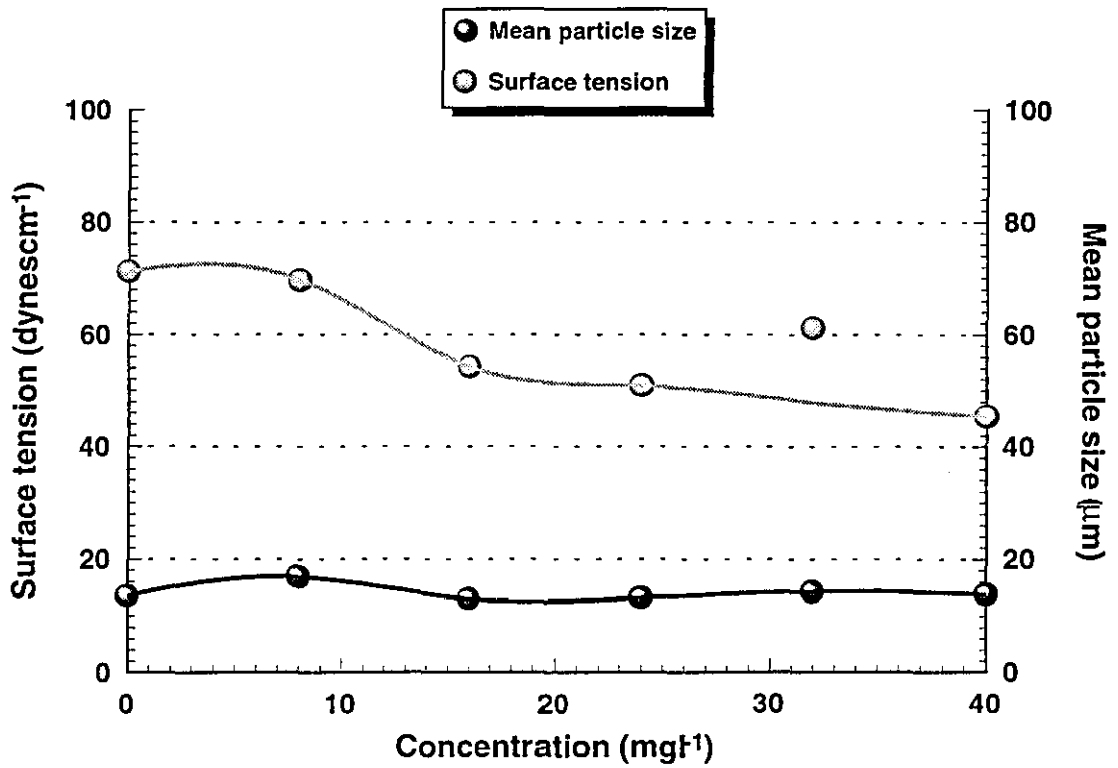
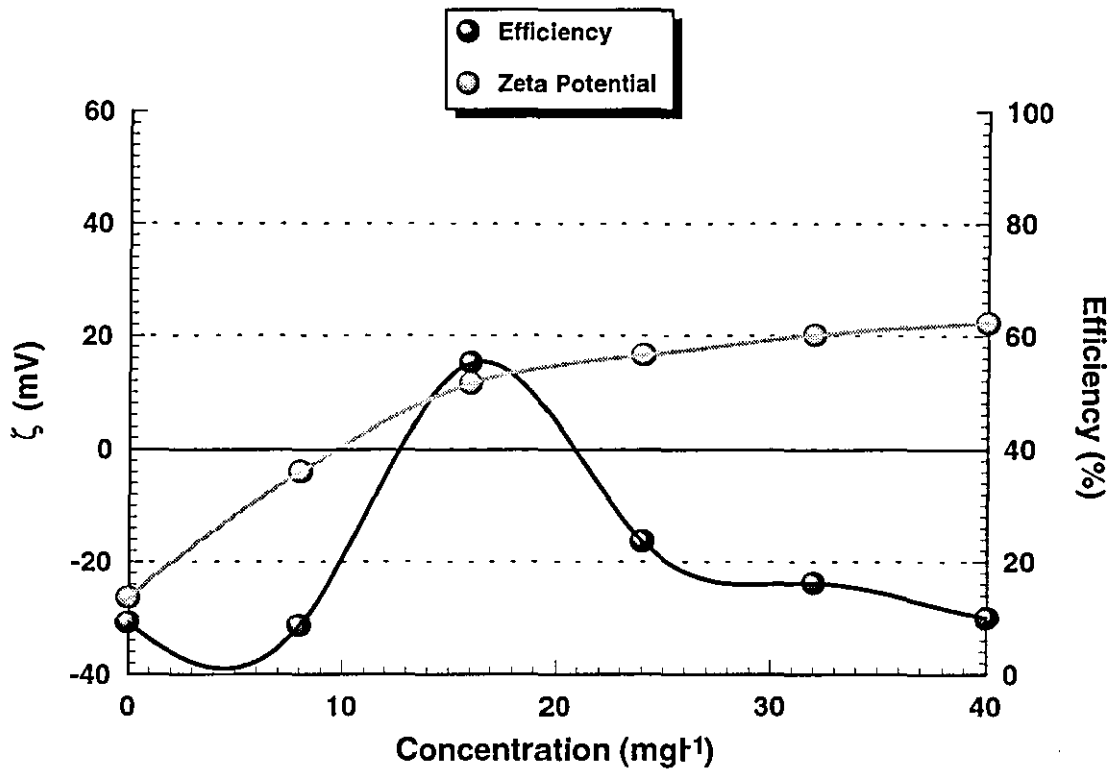


Figure E3: Jar test response of dispersed Kaolin particles vs concentration of Tetradecyltrimethylammoniumbromide

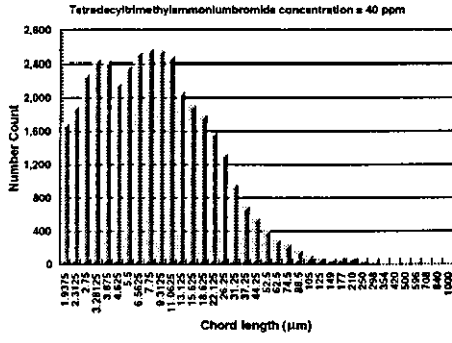
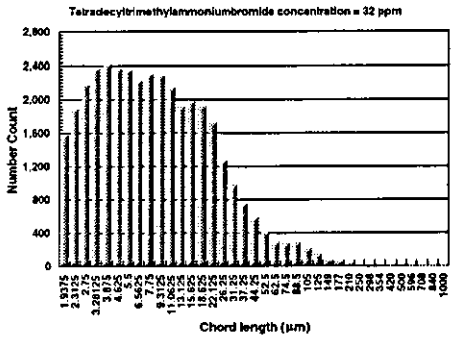
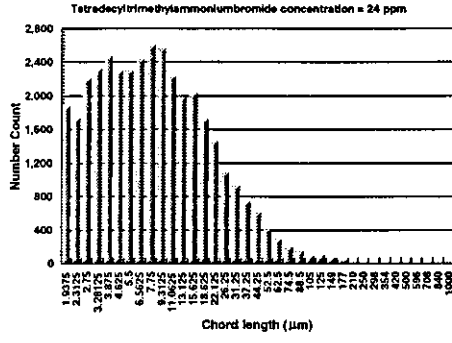
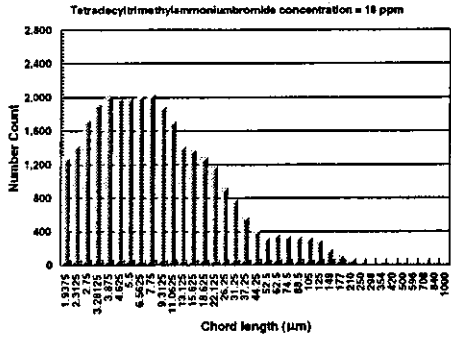
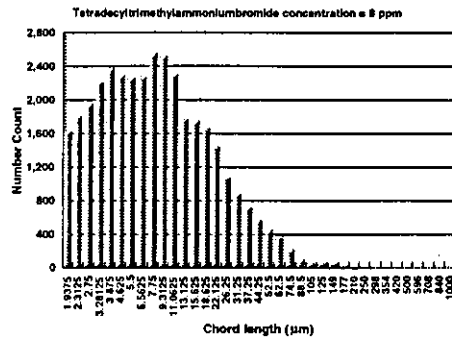
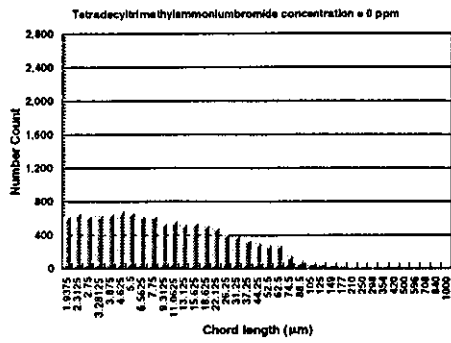


Figure E4: Particle size distributions vs Tetradecyltrimethylammoniumbromide concentration for dispersed Kaolin particles

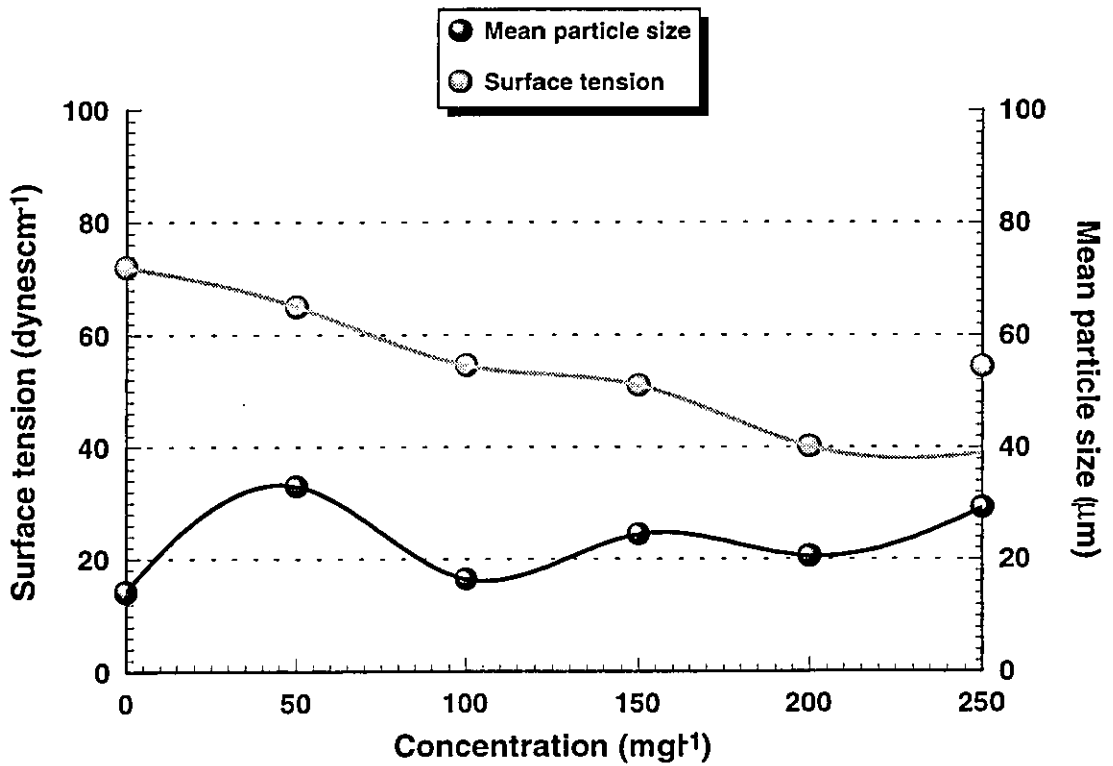
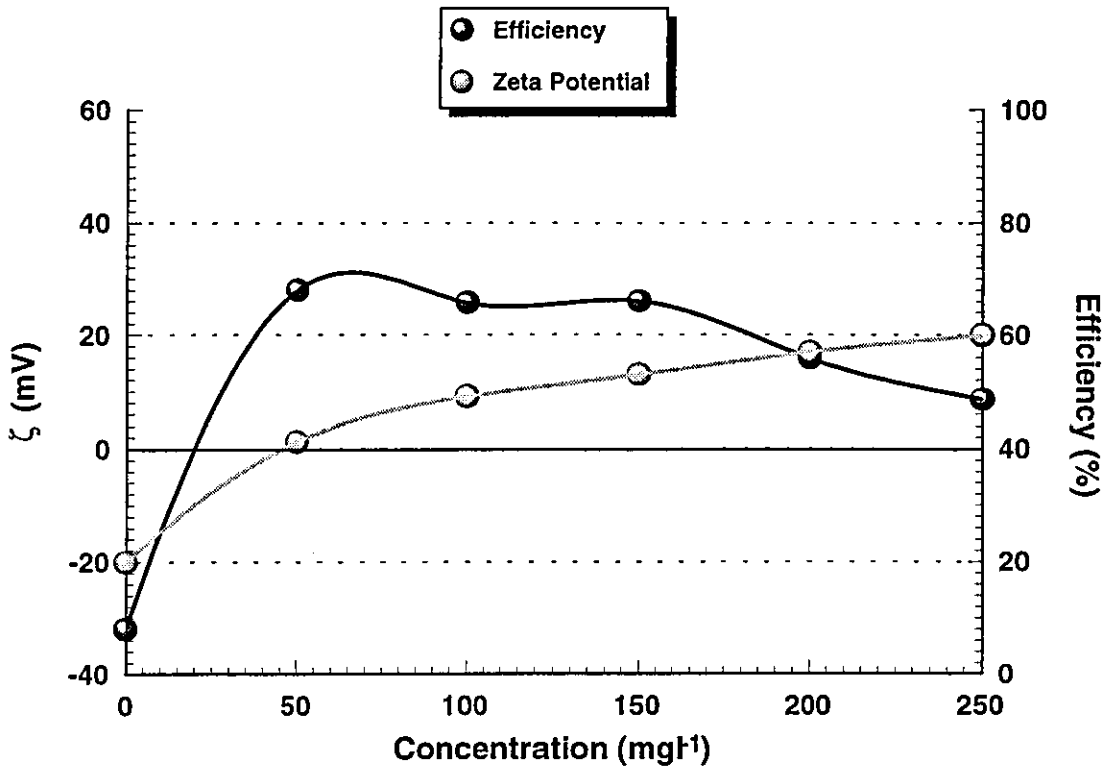


Figure E5: Jar test response of dispersed Kaolin particles vs concentration of Dodecyltrimethylammoniumbromide

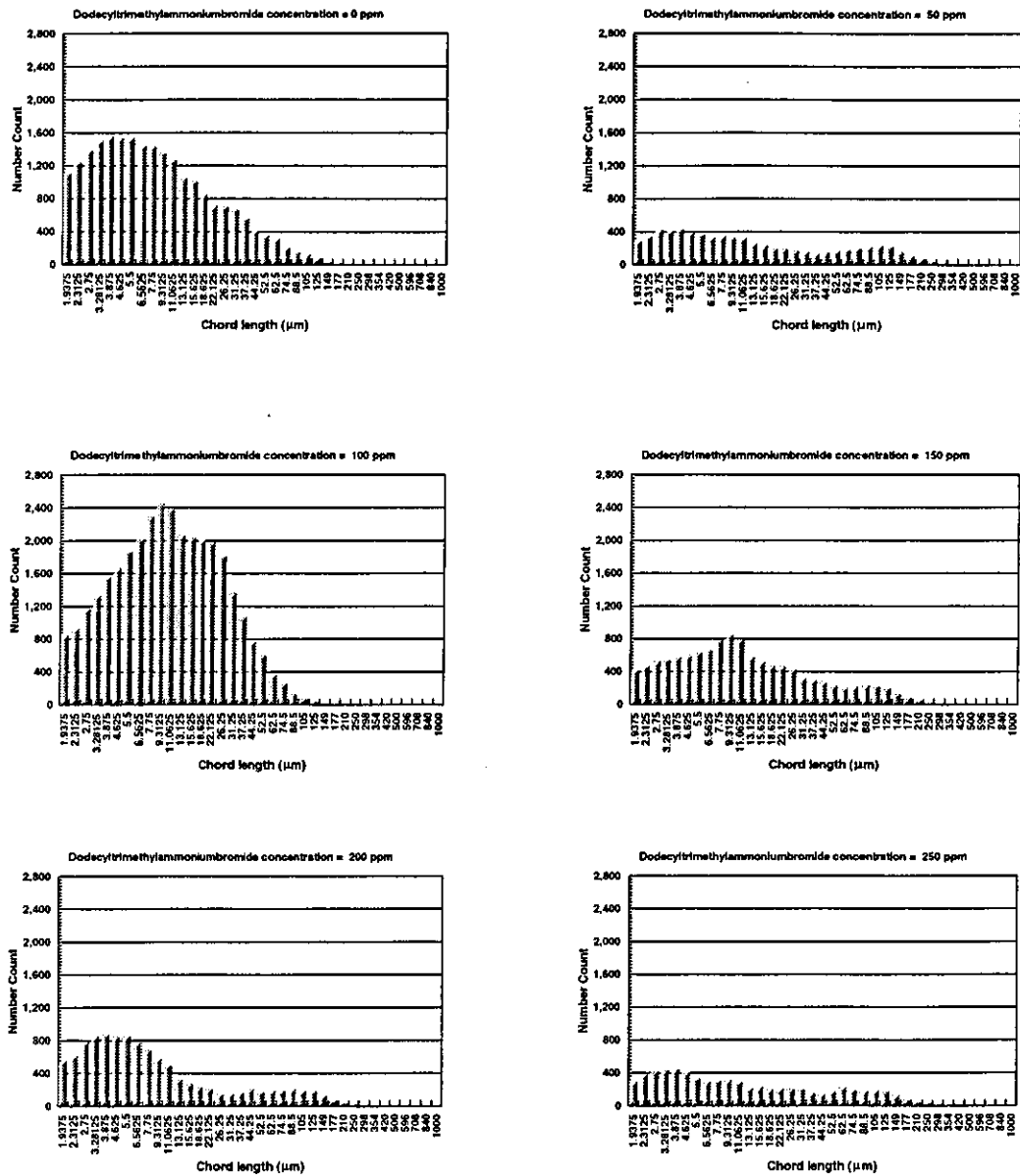


Figure E6: Particle size distributions vs Dodecyltrimethylammoniumbromide concentration for dispersed Kaolin particles

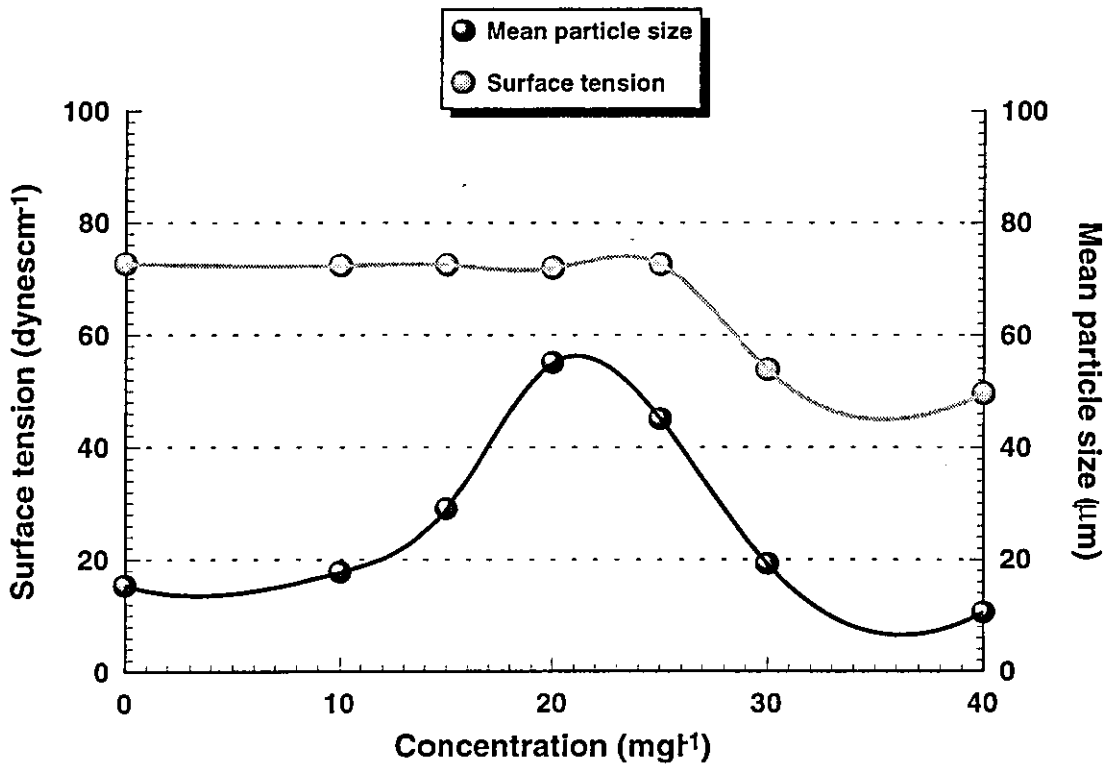
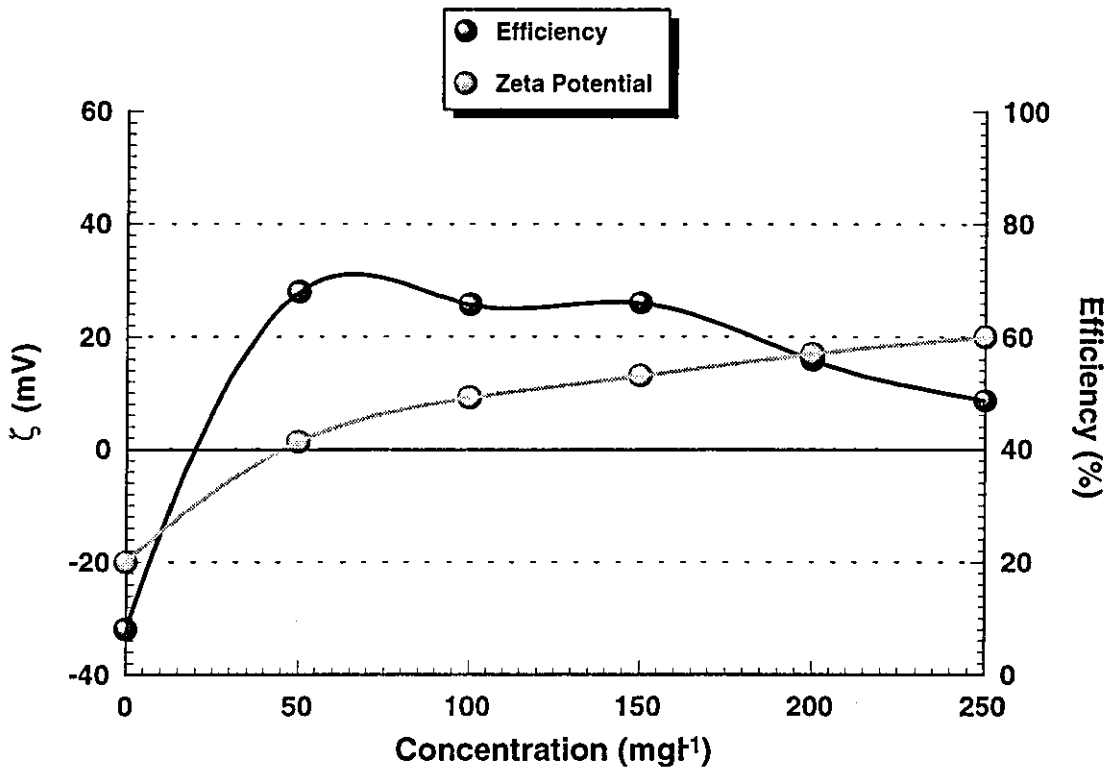


Figure E7: Jar test response of dispersed Wyoming Bentonite particles vs concentration of Hexadecyltrimethylammoniumbromide

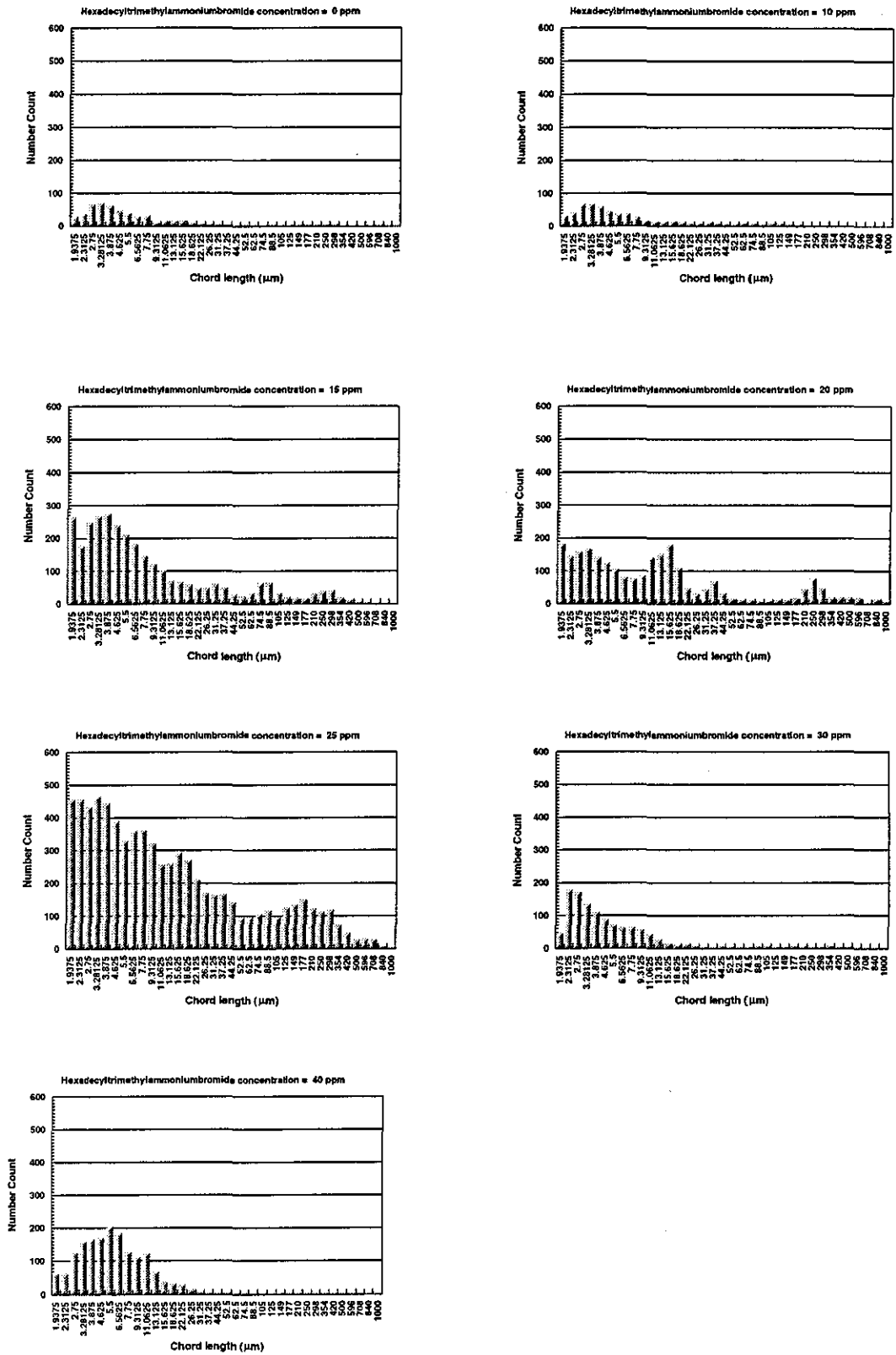


Figure E8: Particle size distributions vs Hexadecyltrimethylammoniumbromide concentration for dispersed Wyoming Bentonite particles

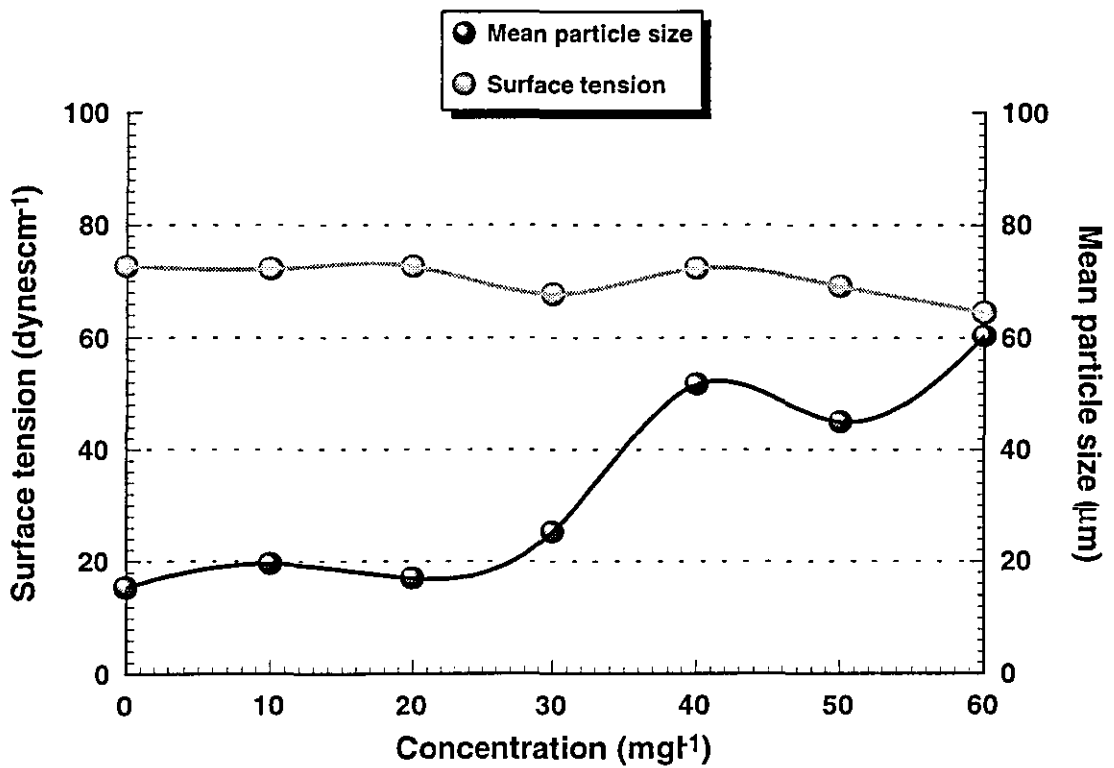
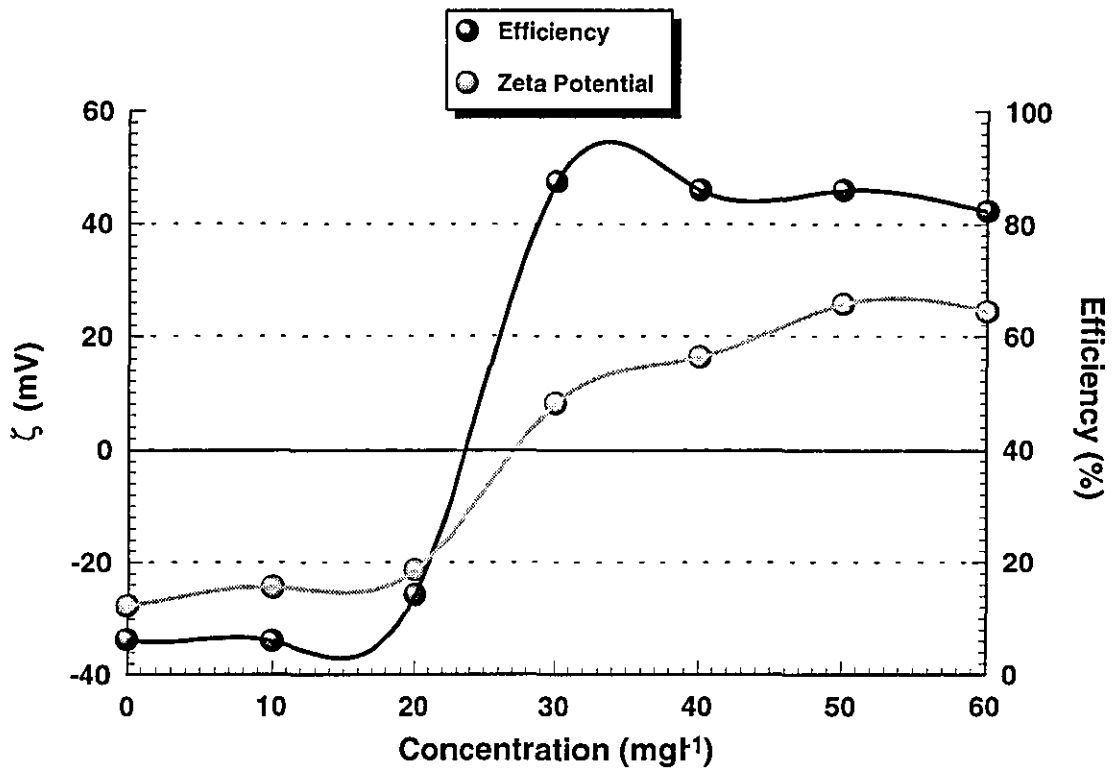


Figure E9: Jar test response of dispersed Wyoming Bentonite particles vs concentration of Tetradecyltrimethylammoniumbromide

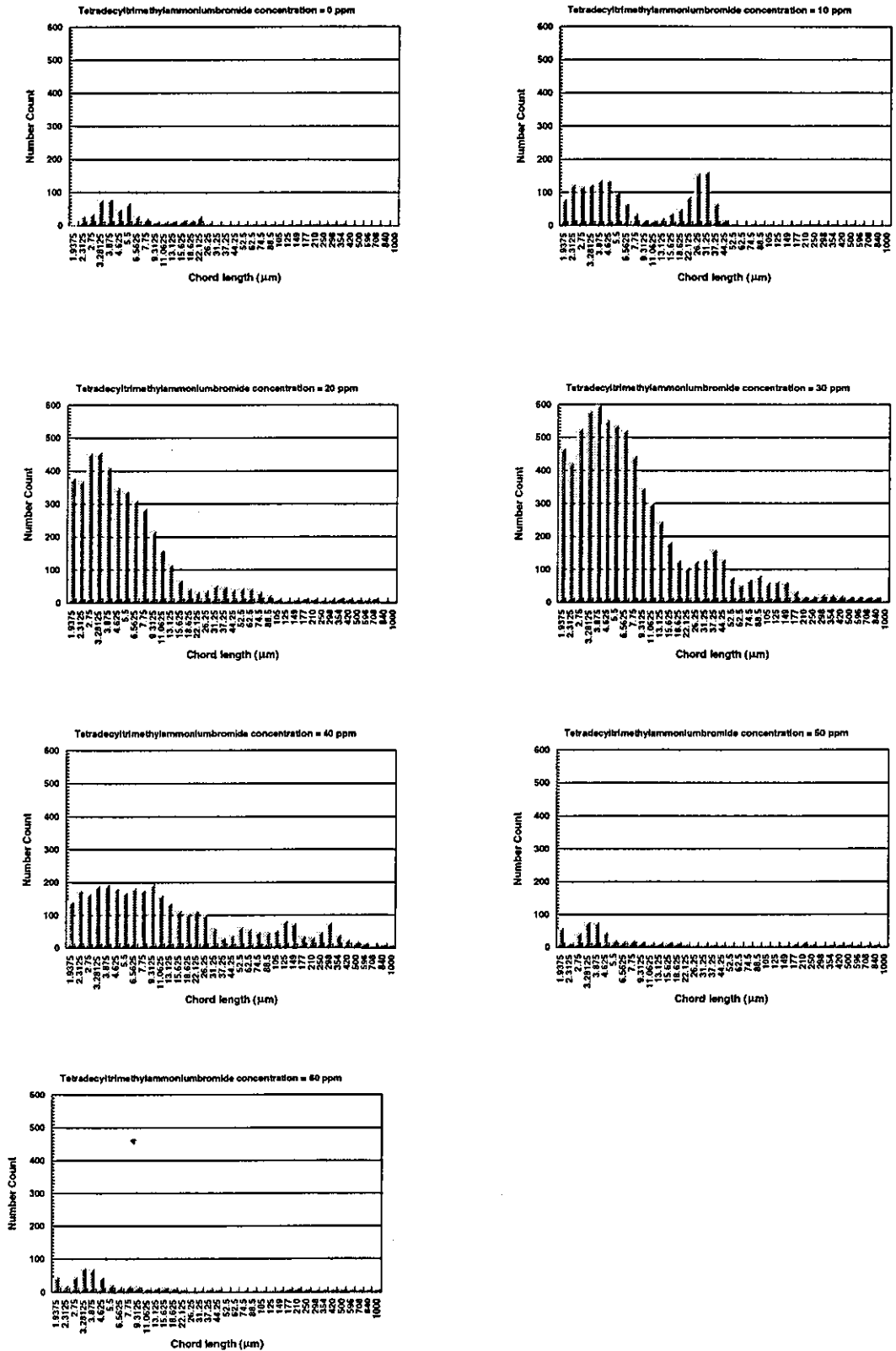


Figure E10: Particle size distributions vs Tetracycltrimethylammoniumbromide concentration for dispersed Wyoming Bentonite particles

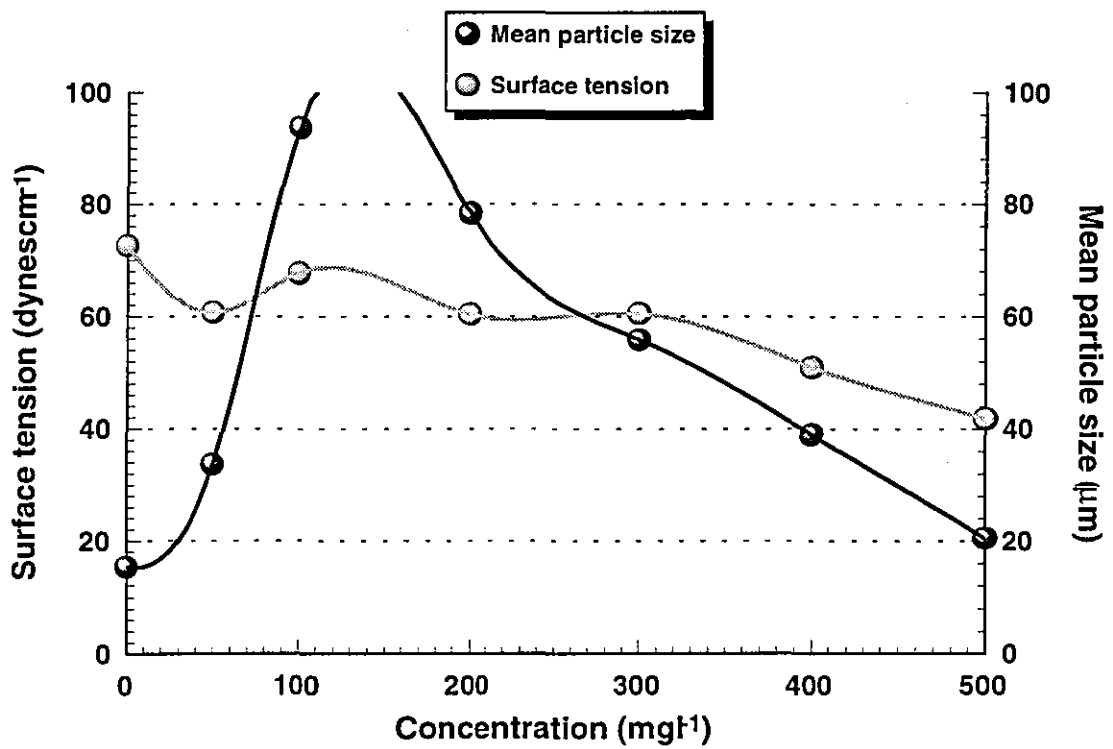
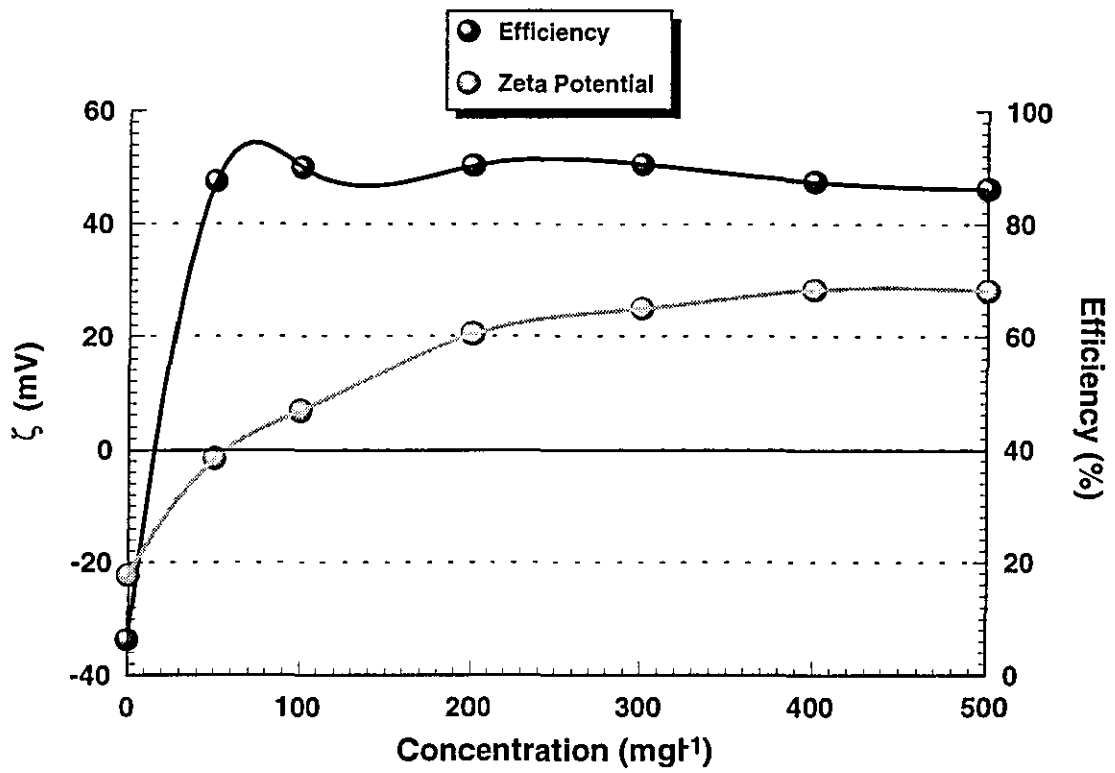


Figure E11: Jar test response of dispersed Wyoming Bentonite particles vs concentration of Dodecyltrimethylammoniumbromide

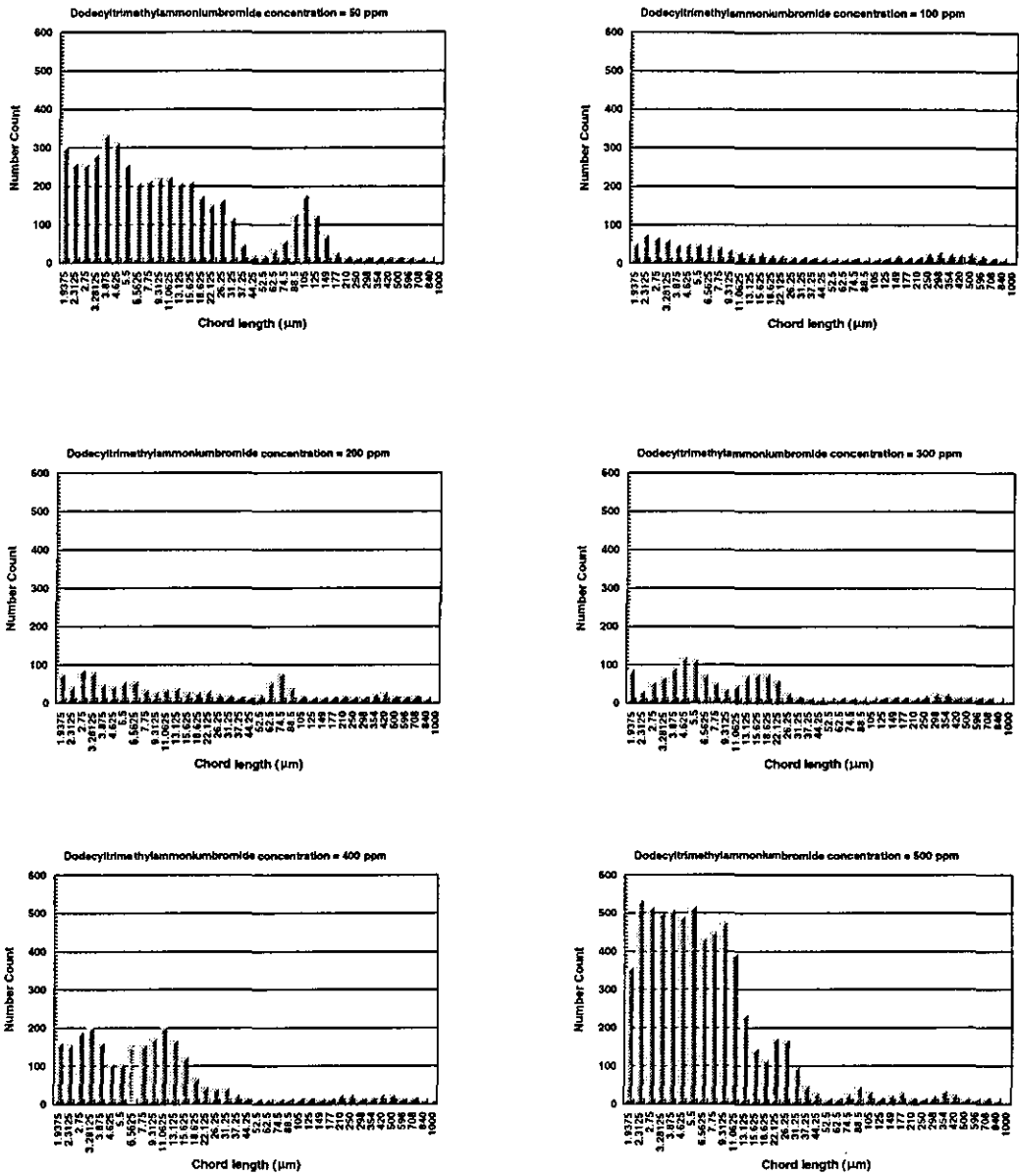


Figure E12: Particle size distributions vs Dodecyltrimethylammoniumbromide concentration for dispersed Wyoming Bentonite particles

APPENDIX F

KEY

| CODE | DESCRIPTION OF FOAM |
|------|---------------------|
| VC | Very Coarse |
| C | Coarse |
| C/F | Coarse/Fine |
| F/C | Fine/Coarse |
| F | Fine |
| VF | Very Fine |

| Test | Concentration (mg l ⁻¹) | Injection Ratio (%) | Foam Height (mm) | Structure | Mobility of Foam | Surface Tension | Temperature (°C) |
|-------------|--|------------------------|---------------------|-----------|---------------------|--------------------|---------------------|
| Kaolin/Hexa | 0 | 5 | 0 | - | Poor | 71.2 | 22 |
| Kaolin/Hexa | 1 | 5 | 0 | - | Poor | 71.1 | 20 |
| Kaolin/Hexa | 2 | 5 | | | | | |
| Kaolin/Hexa | 3 | 5 | 0 | - | Poor | 71.1 | 19.5 |
| Kaolin/Hexa | 4 | 5 | 1 | C | Poor | | 19.5 |
| Kaolin/Hexa | 5 | 5 | 2 | C | Poor | 66 | 20.5 |
| Kaolin/Hexa | 6 | 5 | | | | | |
| Kaolin/Hexa | 8 | 5 | 1 | C | Poor | 62.1 | 21 |
| Kaolin/Hexa | 12 | 5 | 2 | C/F | Poor | 58.8 | 21 |
| Kaolin/Hexa | 16 | 5 | 2 | F | Poor | 56.5 | 21 |
| Kaolin/Hexa | 20 | 5 | 2 | F | Good | 55 | 21.5 |
| Kaolin/Hexa | 30 | 5 | 2 | F | Good | 52.8 | 21.5 |
| Kaolin/Hexa | 40 | 5 | 2 | F | Good | 52 | 21.5 |
| Kaolin/Hexa | 0 | 10 | 0 | - | Poor | 71.2 | 20.5 |
| Kaolin/Hexa | 1 | 10 | 2 | C | Poor | 65.4 | 19 |
| Kaolin/Hexa | 2 | 10 | 3 | C/F | Poor | 64.7 | 20.5 |
| Kaolin/Hexa | 3 | 10 | 2 | C | Poor | 63 | 19.5 |
| Kaolin/Hexa | 4 | 10 | 3 | C/F | Poor | 61 | 21 |
| Kaolin/Hexa | 5 | 10 | 2 | C/F | Poor | 59.6 | 18.5 |
| Kaolin/Hexa | 6 | 10 | 3 | C/F | Poor | | 20.3 |
| Kaolin/Hexa | 8 | 10 | 3 | F/C | Good | 54 | 21 |
| Kaolin/Hexa | 12 | 10 | 3 | F | Good | 51.9 | 21 |
| Kaolin/Hexa | 16 | 10 | 5 | F | Good | 49.1 | 21 |

| | | | | | | | |
|-------------|----|----|-----|-----|------|-------|------|
| Kaolin/Hexa | 20 | 10 | 6 | F | Good | 44.9 | 21 |
| Kaolin/Hexa | 30 | 10 | 6 | VF | Good | 44.3 | 21 |
| Kaolin/Hexa | 40 | 10 | 7 | VF | Good | 39.5 | 18.5 |
| Kaolin/Hexa | 0 | 15 | 0 | - | Poor | 71.2 | 17.5 |
| Kaolin/Hexa | 1 | 15 | 3 | C | Poor | 62.1 | 18 |
| Kaolin/Hexa | 2 | 15 | 5 | C | Poor | 63.3 | 16.5 |
| Kaolin/Hexa | 3 | 15 | 2 | VC | Poor | 60.9 | 18 |
| Kaolin/Hexa | 4 | 15 | 6 | C | Poor | | 17 |
| Kaolin/Hexa | 5 | 15 | 3 | VC | Poor | 59.2 | 18 |
| Kaolin/Hexa | 6 | 15 | 6 | F/C | OK | 51.7 | 17.5 |
| Kaolin/Hexa | 8 | 15 | 6.5 | F/C | Good | 52 | 17.5 |
| Kaolin/Hexa | 12 | 15 | 7 | F | Good | 51.56 | 17 |
| Kaolin/Hexa | 16 | 15 | 7 | VF | Good | 45.54 | 18 |
| Kaolin/Hexa | 20 | 15 | 7 | VF | Good | 51.7 | 17.5 |
| Kaolin/Hexa | 30 | 15 | 7 | VF | Good | 52.2 | 18 |
| Kaolin/Hexa | 40 | 15 | 8 | VF | Good | 53.36 | 17.5 |
| Kaolin/Hexa | 0 | 20 | 0 | - | Poor | 71.2 | 17 |
| Kaolin/Hexa | 1 | 20 | 3 | VC | Poor | 70.6 | 18 |
| Kaolin/Hexa | 2 | 20 | 5 | VC | Poor | 65.5 | 16 |
| Kaolin/Hexa | 3 | 20 | 2 | VC | Poor | 71.5 | 19 |
| Kaolin/Hexa | 4 | 20 | 5 | VC | Poor | 56.8 | 16 |
| Kaolin/Hexa | 5 | 20 | 3 | VC | Poor | 59.5 | 19 |
| Kaolin/Hexa | 6 | 20 | 3 | F/C | OK | 57.5 | 18 |
| Kaolin/Hexa | 8 | 20 | 6 | C | Good | 59.3 | 17.5 |
| Kaolin/Hexa | 12 | 20 | 5 | F | Good | 52.9 | 18.5 |
| Kaolin/Hexa | 16 | 20 | 7 | F | Good | 61.4 | 18.5 |

| | | | | | | | |
|-------------|----|----|---|-----|------|------|------|
| Kaolin/Hexa | 20 | 20 | 7 | VF | Good | 65 | 18.5 |
| Kaolin/Hexa | 30 | 20 | 7 | VF | Good | 53.4 | 18 |
| Kaolin/Hexa | 40 | 20 | 7 | VF | Good | 52.3 | 18 |
| Kaolin/Hexa | 0 | 25 | | | | 71.2 | |
| Kaolin/Hexa | 1 | 25 | 3 | VC | Poor | 69.6 | 19 |
| Kaolin/Hexa | 2 | 25 | | | | 66.7 | |
| Kaolin/Hexa | 3 | 25 | 2 | VC | Poor | 60.5 | 19 |
| Kaolin/Hexa | 4 | 25 | 5 | C | Poor | 55.8 | 18 |
| Kaolin/Hexa | 5 | 25 | 4 | C | Poor | 57.3 | 19 |
| Kaolin/Hexa | 6 | 25 | | | Poor | 56.2 | |
| Kaolin/Hexa | 8 | 25 | 6 | C/F | OK | 58.4 | 18 |
| Kaolin/Hexa | 12 | 25 | 6 | F | Good | 51.5 | 20 |
| Kaolin/Hexa | 16 | 25 | 6 | F | Good | 50.3 | 20.5 |
| Kaolin/Hexa | 20 | 25 | 7 | VF | Good | 50.2 | 20.5 |
| Kaolin/Hexa | 30 | 25 | 7 | VF | Good | 49.7 | 20 |
| Kaolin/Hexa | 40 | 25 | 7 | VF | Good | 48.6 | 20 |

Appendix F1: Foam characterisation table for dispersed Kaolin particles conditioned with Hexadecyltrimethylammoniumbromide

| Test | Concentration (mg/l) | Injection Ratio (%) | Foam Height (mm) | Structure | Mobility of Foam | Surface Tension | Temperature (°C) |
|--------------|----------------------|---------------------|------------------|-----------|------------------|-----------------|------------------|
| Kaolin/Tetra | 0 | 5 | 0 | - | Poor | 71 | 21 |
| Kaolin/Tetra | 8 | 5 | 1 | F | Poor | 70.9 | 21 |
| Kaolin/Tetra | 16 | 5 | 1 | F | Poor | 63 | 21 |
| Kaolin/Tetra | 24 | 5 | 0 | - | Poor | 55 | 21 |
| Kaolin/Tetra | 32 | 5 | 0 | - | Poor | 57 | 22.5 |
| Kaolin/Tetra | 40 | 5 | 0 | - | Poor | 58 | 21.5 |
| Kaolin/Tetra | 0 | 10 | 0 | - | Poor | 71.2 | 22 |
| Kaolin/Tetra | 8 | 10 | 2 | C | Poor | 71 | 22.5 |
| Kaolin/Tetra | 16 | 10 | 3 | C | Poor | 65.1 | 21.5 |
| Kaolin/Tetra | 24 | 10 | 2 | C | Poor | 60.7 | 21 |
| Kaolin/Tetra | 32 | 10 | 2 | C | Poor | 58.2 | 20.5 |
| Kaolin/Tetra | 40 | 10 | 1 | C | Poor | 58 | 21 |
| Kaolin/Tetra | 0 | 15 | 0 | - | Poor | 71.4 | 23 |
| Kaolin/Tetra | 8 | 15 | 4 | C | Poor | 72.1 | 21.5 |
| Kaolin/Tetra | 16 | 15 | 5 | C | Poor | 69.3 | 21 |
| Kaolin/Tetra | 24 | 15 | 4 | C | Poor | 58.7 | 21 |
| Kaolin/Tetra | 32 | 15 | 5 | C/F | Poor | 56.3 | 21 |
| Kaolin/Tetra | 40 | 15 | 3 | VC | Poor | 59.2 | 21 |
| Kaolin/Tetra | 0 | 20 | 0 | - | Poor | 71.2 | 21.5 |
| Kaolin/Tetra | 8 | 20 | 3 | C | Poor | 69.7 | 21.5 |
| Kaolin/Tetra | 16 | 20 | 2 | C | Poor | 68.3 | 22 |
| Kaolin/Tetra | 24 | 20 | 4 | C/F | Poor | 57 | 21.5 |
| Kaolin/Tetra | 32 | 20 | 5 | F | Good | 57.5 | 22 |
| Kaolin/Tetra | 40 | 20 | 4 | F | Good | 58.3 | 22 |

| | | | | | | | |
|--------------|----|----|---|-----|------|------|------|
| Kaolin/Tetra | 0 | 25 | 0 | - | Poor | 71.2 | 23.5 |
| Kaolin/Tetra | 8 | 25 | 5 | C | Poor | 71.2 | 23.5 |
| Kaolin/Tetra | 16 | 25 | 4 | C | Poor | 60.3 | 23 |
| Kaolin/Tetra | 24 | 25 | 5 | C/F | Poor | 57.3 | 23.5 |
| Kaolin/Tetra | 32 | 25 | 5 | C/F | Poor | 58.2 | 25 |
| Kaolin/Tetra | 40 | 25 | 5 | VC | Poor | 57.2 | 21 |

Appendix F2: Foam characterisation table for dispersed Kaolin particles conditioned with Tetradecyltrimethylammoniumbromide

| Test | Concentration (mg l ⁻¹) | Injection Ratio (%) | Foam Height (mm) | Structure | Mobility of Foam | Surface Tension | Temperature (°C) |
|--------------|--|------------------------|---------------------|-----------|---------------------|--------------------|---------------------|
| Kaolin/Dodec | 0 | 5 | 0 | - | Poor | 71 | 24.5 |
| Kaolin/Dodec | 12.5 | 5 | 0 | - | Poor | 69 | 24.5 |
| Kaolin/Dodec | 25 | 5 | 0 | - | Poor | | 24 |
| Kaolin/Dodec | 37.5 | 5 | 1 | C/F | Poor | 43.9 | 24 |
| Kaolin/Dodec | 50 | 5 | 0 | - | Poor | 42.3 | 21 |
| Kaolin/Dodec | 62.5 | 5 | 0.5 | F | Poor | 48.6 | 21 |
| Kaolin/Dodec | 75 | 5 | 0 | - | Poor | 62.2 | 21 |
| Kaolin/Dodec | 100 | 5 | 0 | - | Poor | | 22 |
| Kaolin/Dodec | 125 | 5 | 0 | - | Poor | | 22 |
| Kaolin/Dodec | 150 | 5 | 0 | - | Poor | | 22 |
| Kaolin/Dodec | 200 | 5 | 0 | - | Poor | | 22 |
| Kaolin/Dodec | 0 | 10 | 0 | - | Poor | 71 | 22 |
| Kaolin/Dodec | 12.5 | 10 | 2 | C | Poor | 71 | 22 |
| Kaolin/Dodec | 50 | 10 | 4 | C/F | Poor | 54.6 | 21 |
| Kaolin/Dodec | 75 | 10 | 4 | F/C | Poor | 64.4 | 21 |
| Kaolin/Dodec | 100 | 10 | 3 | F/C | Poor | 51.1 | 21 |
| Kaolin/Dodec | 125 | 10 | 3 | F/C | Poor | 47.1 | 20 |
| Kaolin/Dodec | 150 | 10 | 3 | F/C | Poor | 56.4 | 20 |
| Kaolin/Dodec | 175 | 10 | 3 | F/C | Poor | 46.3 | 20 |
| Kaolin/Dodec | 200 | 10 | 3 | F/C | Poor | 59.1 | 20 |
| Kaolin/Dodec | 250 | 10 | 3 | F/C | Poor | | 20 |
| Kaolin/Dodec | 0 | 15 | 0 | - | Poor | 71 | 22 |
| Kaolin/Dodec | 50 | 15 | 4 | C/F | Poor | 52.3 | 22 |
| Kaolin/Dodec | 100 | 15 | 4 | C/F | Poor | 40.86 | 22 |

| | | | | | | | |
|--------------|-----|----|---|-----|------|-------|------|
| Kaolin/Dodec | 125 | 15 | 5 | C/F | Poor | 33.73 | 22 |
| Kaolin/Dodec | 150 | 15 | 4 | C/F | Poor | 31.86 | 18 |
| Kaolin/Dodec | 175 | 15 | 5 | C/F | Poor | 33.73 | 18 |
| Kaolin/Dodec | 200 | 15 | 3 | C | Poor | 30.97 | 18 |
| Kaolin/Dodec | 250 | 15 | 4 | C | Poor | 33.8 | 18 |
| Kaolin/Dodec | 0 | 20 | 0 | - | Poor | 71 | 20.5 |
| Kaolin/Dodec | 50 | 20 | 4 | C | Poor | 49.3 | 20.5 |
| Kaolin/Dodec | 100 | 20 | 5 | C/F | Poor | 40.3 | 20.5 |
| Kaolin/Dodec | 125 | 20 | 6 | C/F | Poor | 37.1 | 21.5 |
| Kaolin/Dodec | 150 | 20 | 5 | C/F | Poor | 39.1 | 21.5 |
| Kaolin/Dodec | 175 | 20 | 5 | C/F | Poor | 36.1 | 21.5 |
| Kaolin/Dodec | 200 | 20 | 5 | C/F | Poor | 40.3 | 21 |
| Kaolin/Dodec | 250 | 20 | 5 | C/F | Poor | 39.7 | 21 |
| Kaolin/Dodec | 0 | 25 | 0 | - | Poor | 71.2 | 21.5 |
| Kaolin/Dodec | 50 | 25 | 5 | C | Poor | 63.9 | 21.5 |
| Kaolin/Dodec | 100 | 25 | 5 | C | Poor | 63.1 | 23.5 |
| Kaolin/Dodec | 125 | 25 | 5 | C | Poor | 59.9 | 23.5 |
| Kaolin/Dodec | 150 | 25 | 6 | C/F | Poor | 54.6 | 23 |
| Kaolin/Dodec | 175 | 25 | 6 | C/F | Poor | 48.8 | 23 |
| Kaolin/Dodec | 200 | 25 | 6 | F/C | Poor | 44.5 | 23 |
| Kaolin/Dodec | 250 | 25 | 7 | F/C | Poor | 41.3 | 23 |

Appendix F3: Foam characterisation table for dispersed Kaolin particles conditioned with Dodecyltrimethylammoniumbromide

| Test | Concentration (mg ^l ⁻¹) | Injection Ratio (%) | Foam Height (mm) | Structure | Mobility of Foam | Surface Tension | Temperature (°C) |
|----------|--|---------------------|------------------|-----------|------------------|-----------------|------------------|
| WB/Hexa | 0 | 5 | 0 | - | Poor | 72 | 19 |
| WB/Hexa | 10 | 5 | 0 | - | Poor | 61.5 | 19 |
| WB/Hexa | 15 | 5 | 0 | - | Poor | 72.5 | 19 |
| WB/Hexa | 20 | 5 | 3 | F/C | Poor | 72.4 | 19 |
| WB/Hexa | 25 | 5 | 4 | C/F | Poor | 72.4 | 19 |
| WB/Hexa | 30 | 5 | 0 | - | Poor | 72 | 19 |
| WB/Hexa | 40 | 5 | 0 | - | Poor | 51.86 | 19 |
| WB/Hexa | 50 | 5 | 0 | - | Poor | 48.3 | 19 |
| WB/Hexa | 0 | 25 | 0 | - | Poor | 72 | 19 |
| WB/Hexa | 10 | 25 | 6 | C/F | Poor | 71.9 | 19 |
| WB/Hexa | 15 | 25 | 5 | C/F | Poor | 71.5 | 18 |
| WB/Hexa | 20 | 25 | 6 | C | Poor | 73 | 19 |
| WB/Hexa | 25 | 25 | 7 | F | Good | 71.9 | 18 |
| WB/Hexa | 30 | 25 | 3 | C/F | Good | 72 | 19 |
| WB/Hexa | 40 | 25 | 6 | F | Good | 63.8 | 19 |
| WB/Hexa | 50 | 25 | 6 | F | Good | 47.7 | 19 |
| WB/Tetra | 0 | 5 | 0 | - | Poor | 71.5 | 19 |
| WB/Tetra | 10 | 5 | 0 | - | Poor | 70 | 19 |
| WB/Tetra | 20 | 5 | 4 | F/C | Poor | 70.5 | 19.5 |
| WB/Tetra | 30 | 5 | 4 | F/C | Poor | 44.4 | 19 |
| WB/Tetra | 40 | 5 | 4 | F | Good | 47.8 | 19 |
| WB/Tetra | 50 | 5 | 4 | F | Good | 45 | 19 |
| WB/Tetra | 0 | 25 | 0 | - | Poor | 71.5 | 20 |
| WB/Tetra | 10 | 25 | 6 | F | OK | 72 | 20 |

| | | | | | | | |
|----------|-----|----|---|-----|------|-------|------|
| WB/Tetra | 20 | 25 | 4 | F | OK | 70.5 | 20 |
| WB/Tetra | 30 | 25 | 4 | C | Ok | 48.1 | 20 |
| WB/Tetra | 40 | 25 | 8 | F/C | Good | 48 | 19 |
| WB/Tetra | 50 | 25 | 7 | C | Good | 59.33 | 19 |
| WB/Dodec | 0 | 5 | 0 | - | Poor | 70.5 | 25.5 |
| WB/Dodec | 50 | 5 | 5 | C | Poor | 45.4 | 24 |
| WB/Dodec | 100 | 5 | 5 | C | Poor | 46.7 | 224 |
| WB/Dodec | 150 | 5 | 4 | C | Poor | 34.1 | 22 |
| WB/Dodec | 200 | 5 | 4 | C | Poor | 44.86 | 22.5 |
| WB/Dodec | 300 | 5 | 5 | C/F | Good | 50.3 | 25 |
| WB/Dodec | 400 | 5 | 7 | F/C | Good | 42.06 | 24 |
| WB/Dodec | 500 | 5 | 6 | F/C | Good | 48.7 | 24 |

Appendix F4: Foam characterisation table for dispersed Wyoming Bentonite particles conditioned with Akyldcyltrimethylammoniumbromide

| Test | Concentration (mg l ⁻¹) | Injection Ratio (%) | Foam Height (mm) | Structure | Mobility of Foam | Surface Tension | Temperature (°C) |
|---------------|-------------------------------------|---------------------|------------------|-----------|------------------|-----------------|------------------|
| Kaolin/Alum | 0 | 5 | 0 | - | Poor | 60.9 | 20 |
| Kaolin/Alum | 4 | 5 | 0 | - | Poor | 71.7 | 20 |
| Kaolin/Alum | 8 | 5 | 0 | - | Poor | 65.8 | 20 |
| Kaolin/Alum | 12 | 5 | 0 | - | Poor | 71.5 | 21 |
| Kaolin/Alum | 16 | 5 | 0 | - | Poor | 71.6 | 21 |
| Kaolin/Alum | 20 | 5 | 0 | - | Poor | 71.4 | 21 |
| Kaolin/Ferric | 0 | 5 | 0 | - | Poor | | 22 |
| Kaolin/Ferric | 4 | 5 | 2 | C | Poor | | 22 |
| Kaolin/Ferric | 8 | 5 | 2 | C | Poor | | 22 |
| Kaolin/Ferric | 12 | 5 | 4 | C | Poor | | 22 |
| Kaolin/Ferric | 16 | 5 | 5 | C | Poor | | 22 |
| Kaolin/Ferric | 20 | 5 | 4 | C | Poor | | 22 |

Appendix F5: Foam characterisation table for Dispersed kaolin particles conditioned with Coagulant

| Test | Concentration (mg ^l ⁻¹) | Injection Ratio (%) | Foam Height (mm) | Structure | Mobility of Foam | Surface Tension | Temperature (°C) |
|-----------|---|------------------------|---------------------|-----------|---------------------|--------------------|---------------------|
| WB/Alum | 0 | 5 | 0 | - | Poor | | 20 |
| WB/Alum | 40 | 5 | 10 | F | Good | | 20 |
| WB/Alum | 50 | 5 | 10 | F/C | Good | | 20 |
| WB/Alum | 60 | 5 | 10 | F | Good | | 20 |
| WB/Alum | 70 | 5 | 10 | F | Good | | 20 |
| WB/Alum | 80 | 5 | 10 | F | Good | | 20 |
| WB/Ferric | 0 | 5 | 0 | - | Poor | | 22 |
| WB/Ferric | 20 | 5 | 5 | F | Good | | 22 |
| WB/Ferric | 40 | 5 | 8 | F | Good | | 22 |
| WB/Ferric | 60 | 5 | 12 | F | Good | | 22 |
| WB/Ferric | 70 | 5 | 8 | F | Good | | 22 |
| WB/Ferric | 80 | 5 | 8 | F | Good | | 22 |
| WB/Ferric | 90 | 5 | 8 | F | Good | | 22 |

Appendix F6: Foam characterisation table for Dispersed Wyoming Bentonite particles conditioned with Coagulant

APPENDIX G

KEY

| CODE | DESCRIPTION | UNITS |
|------|--|--------------------|
| A | Orifice diameter | mm |
| B | Nozzle diameter | mm |
| C | Nozzle length | mm |
| D | Pressure in saturator | bar |
| E | Cone angle of diverging nozzle | ° |
| F | Distance of impingement plate from nozzle exit | mm |
| G | Surfactant concentration | mg l ⁻¹ |
| H | Electrolyte concentration | mg l ⁻¹ |

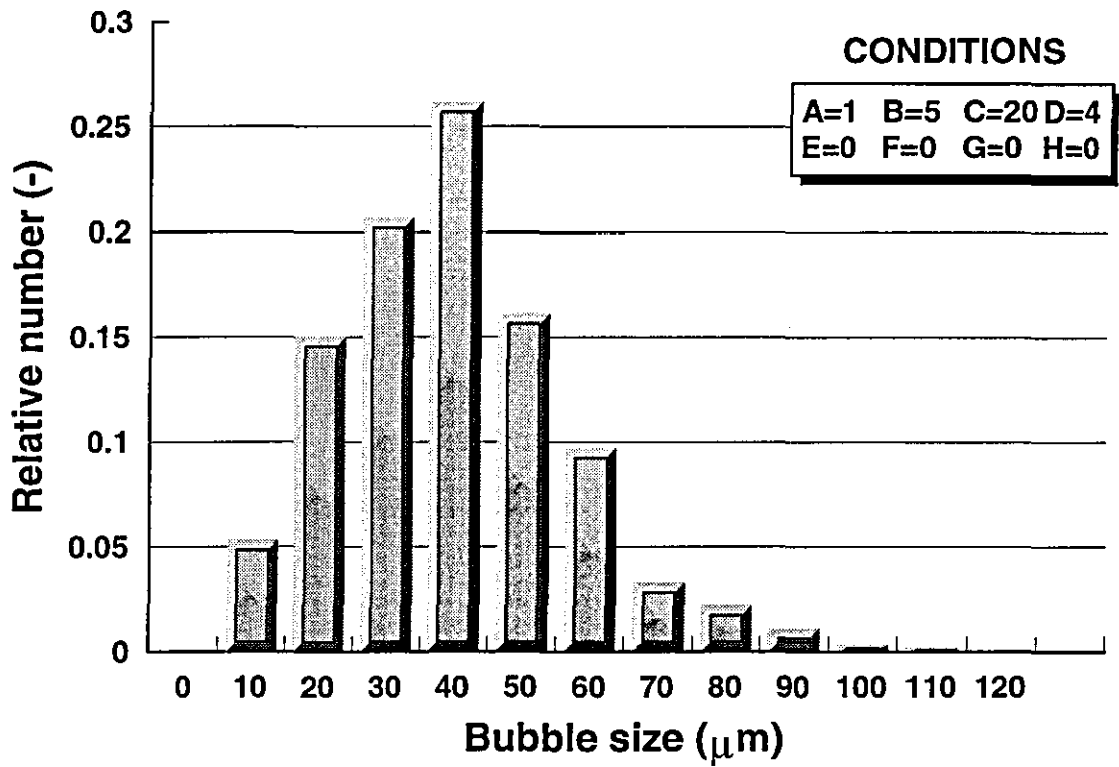


Figure G1 : Bubble size distribution, pressure = 4 bar

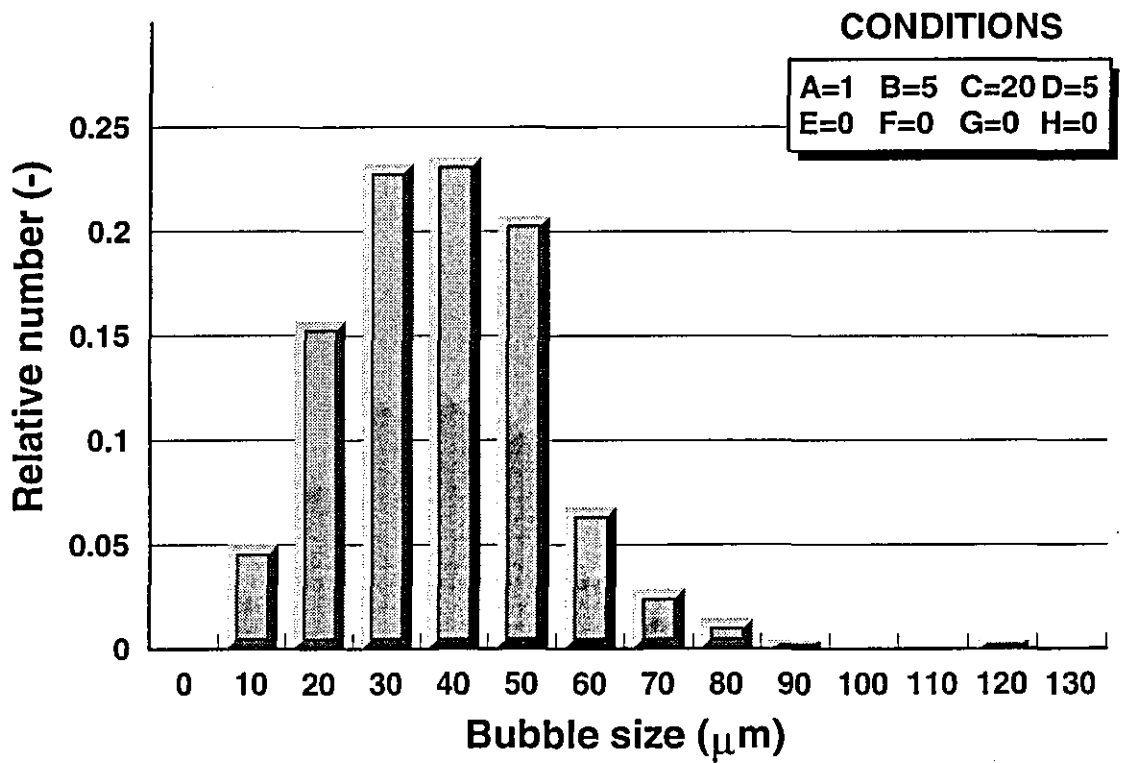


Figure G2 : Bubble size distribution, pressure = 5 bar

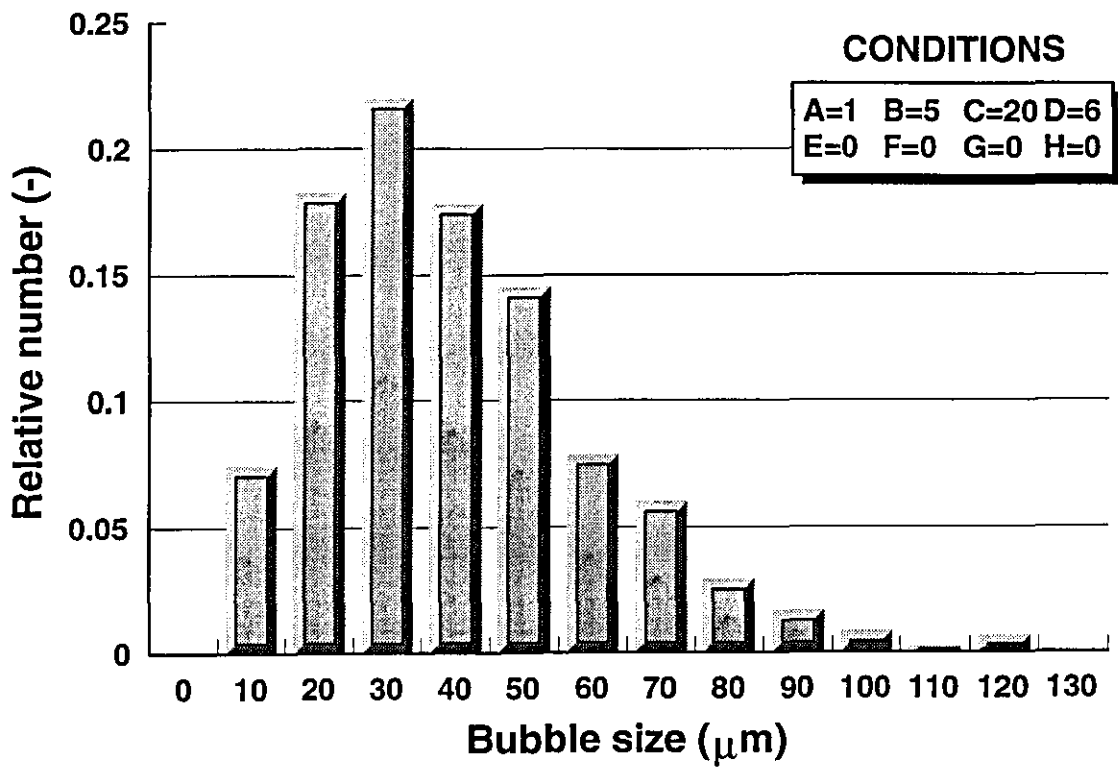


Figure G3 : Bubble size distribution, pressure = 6 bar

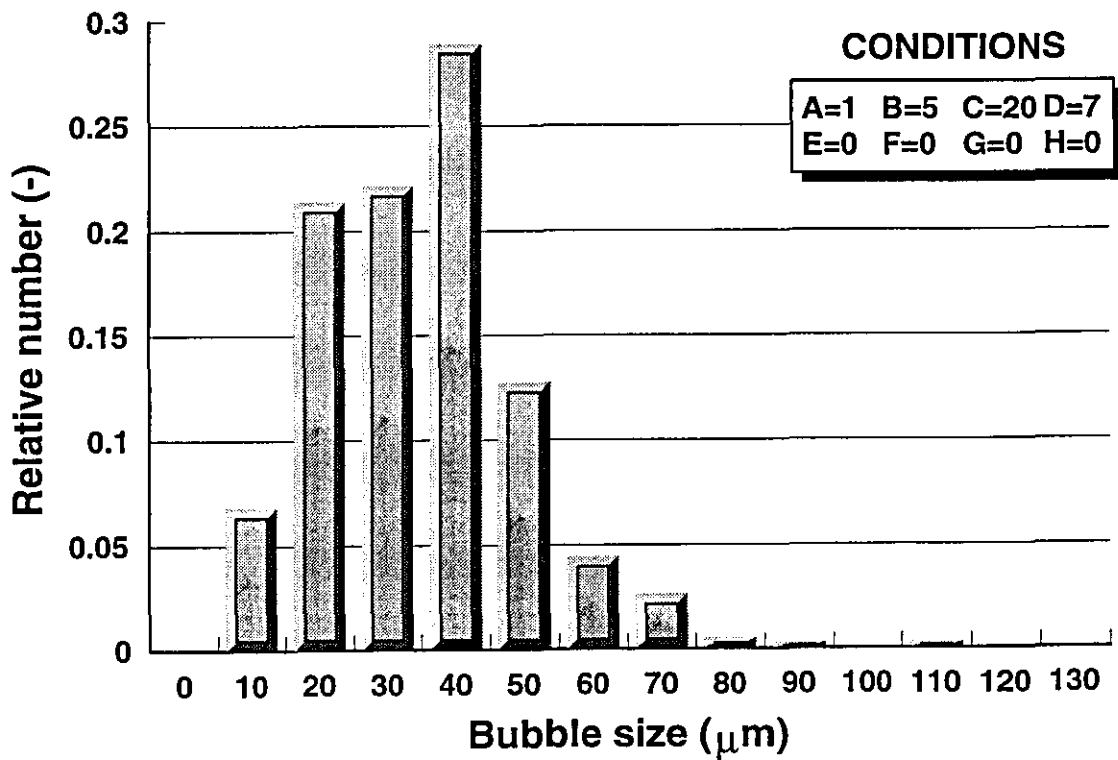


Figure G4 : Bubble size distribution, pressure = 7 bar

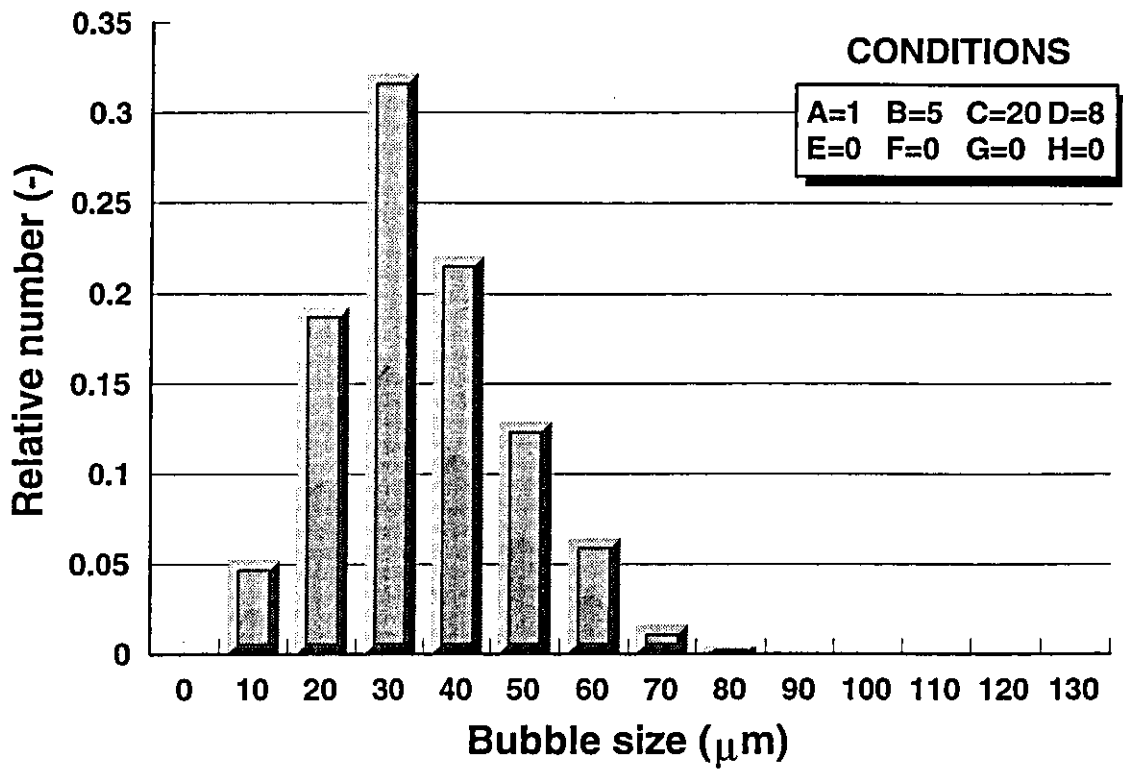


Figure G5 : Bubble size distribution, pressure = 8 bar

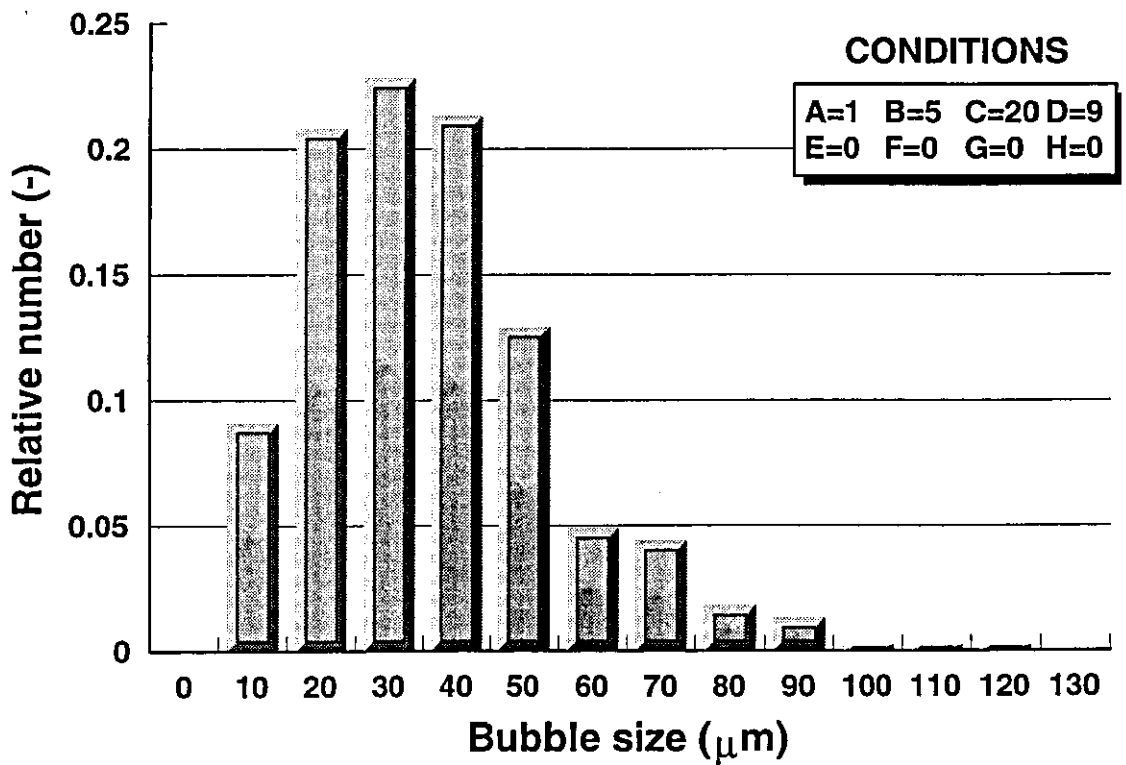


Figure G6 : Bubble size distribution, pressure = 9 bar

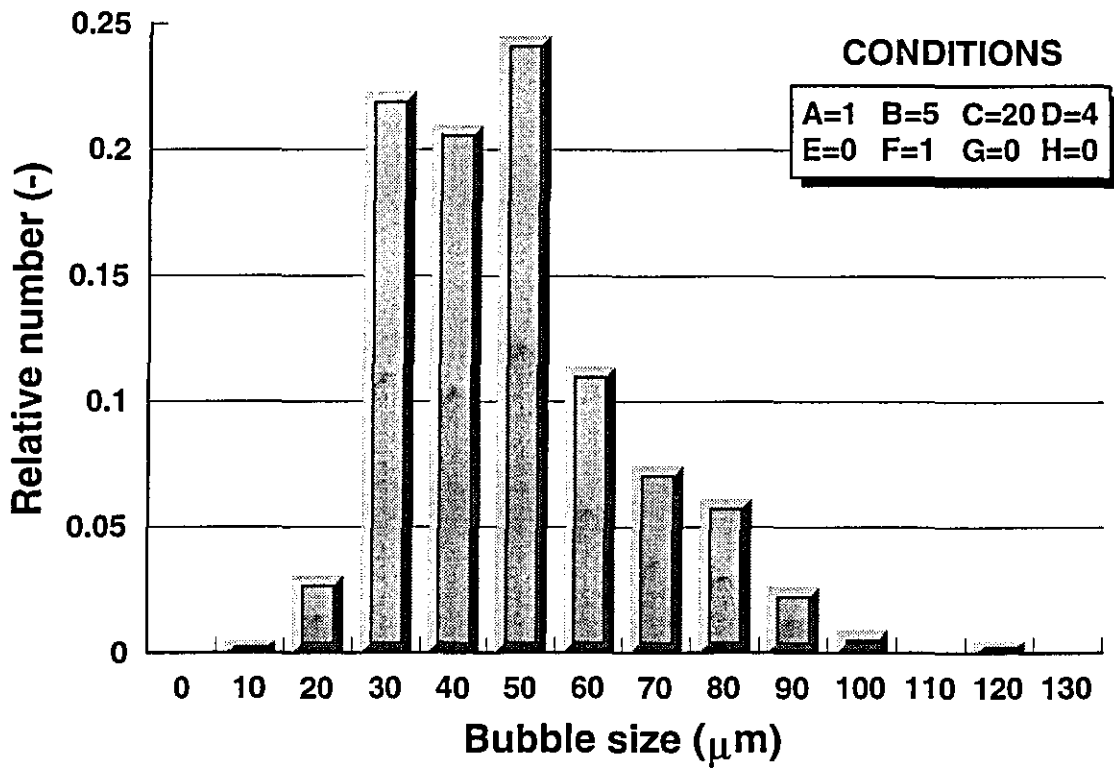


Figure G7 : Bubble size distribution, impingment plate 1mm from nozzle exit

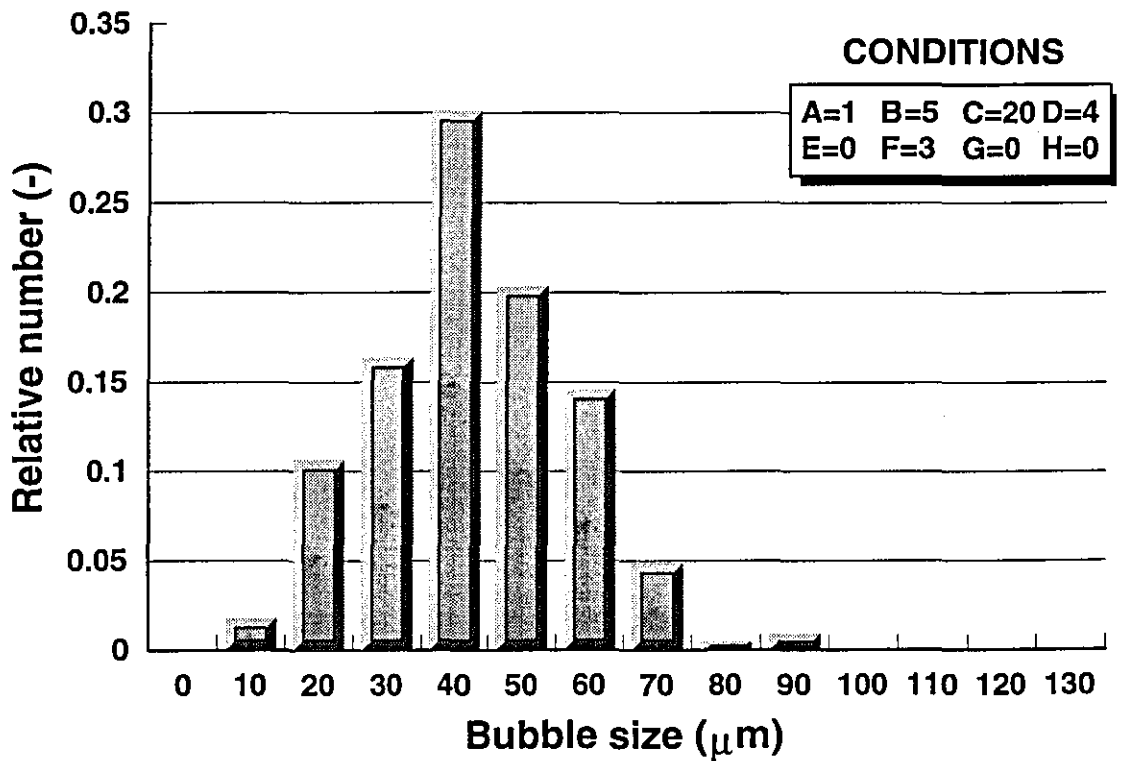


Figure G8 : Bubble size distribution, impingment plate 3mm from nozzle exit

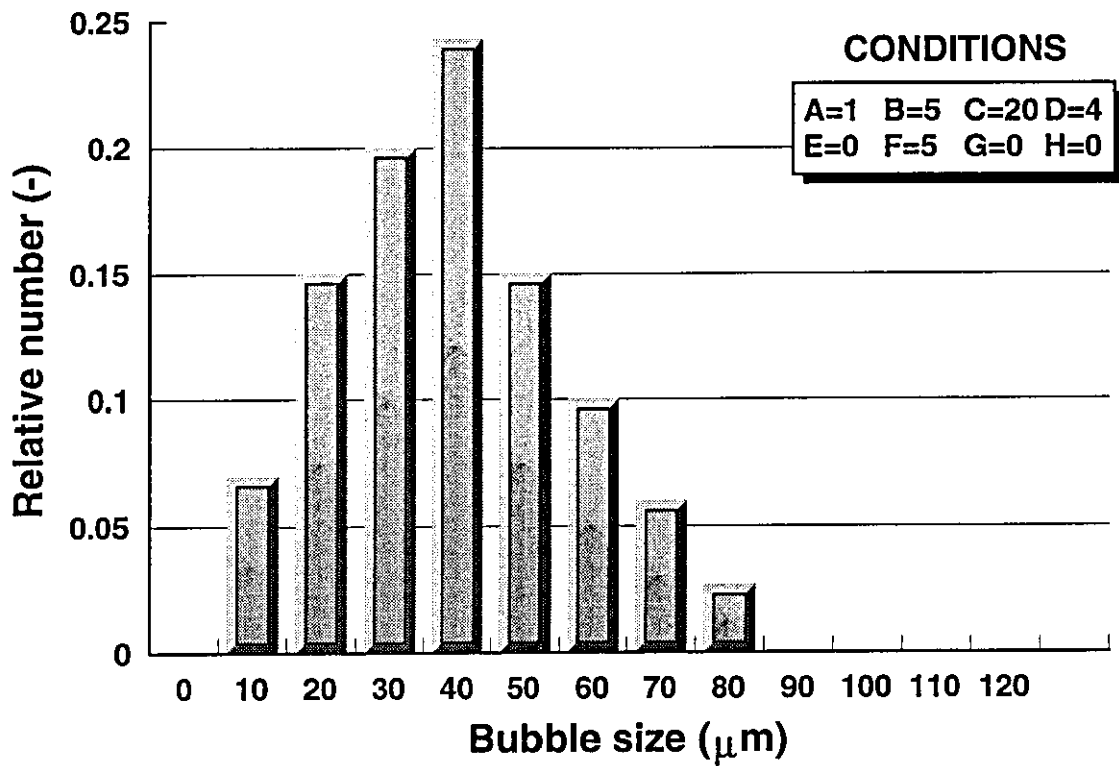


Figure G9 : Bubble size distribution, impingment plate 5mm from nozzle exit

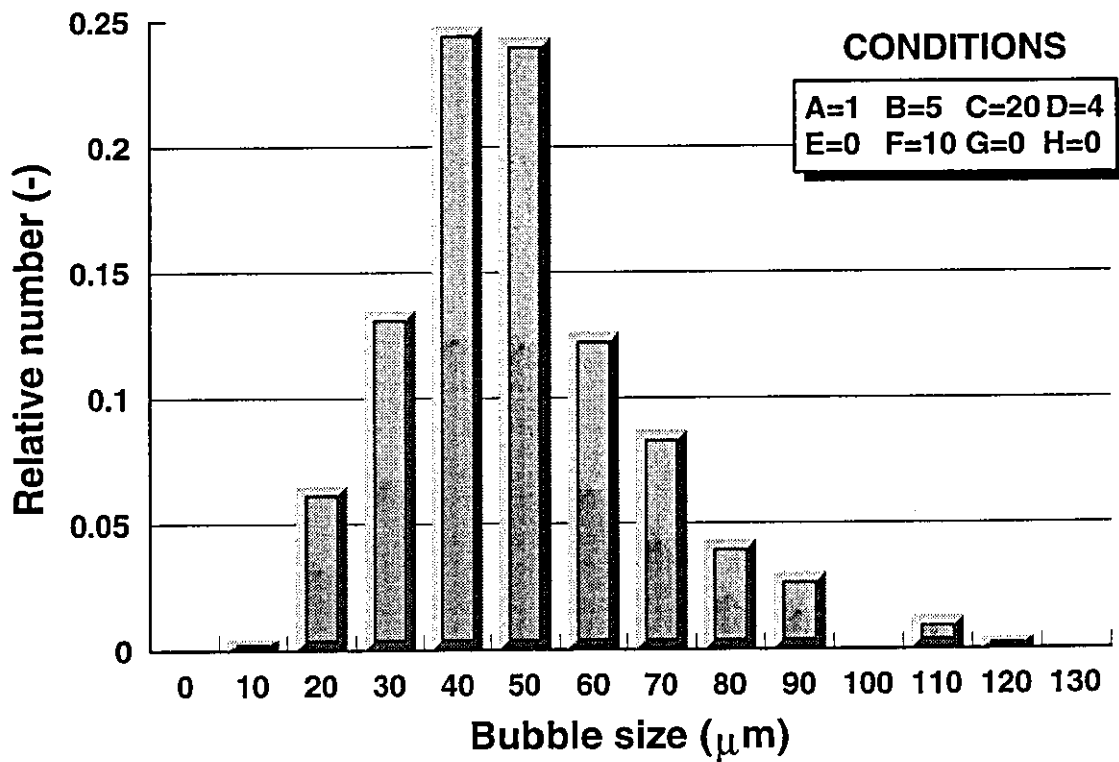


Figure G10 : Bubble size distribution, impingment plate 10mm from nozzle exit

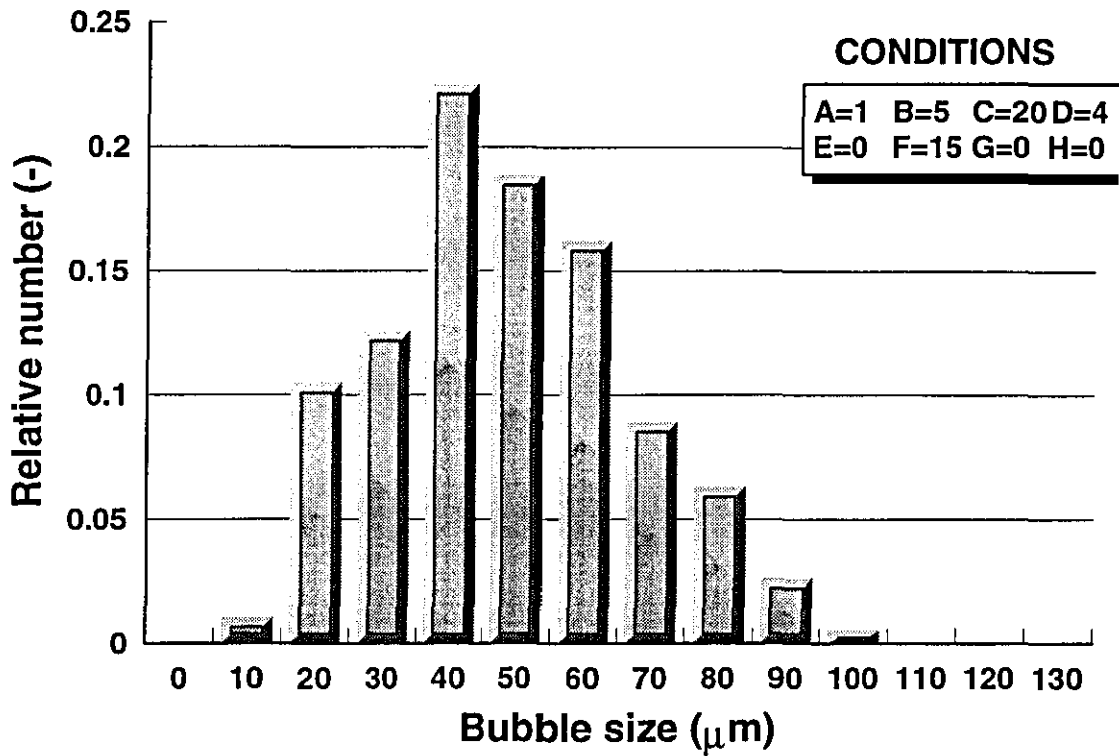


Figure G11 : Bubble size distribution, impingement plate 15mm from nozzle exit

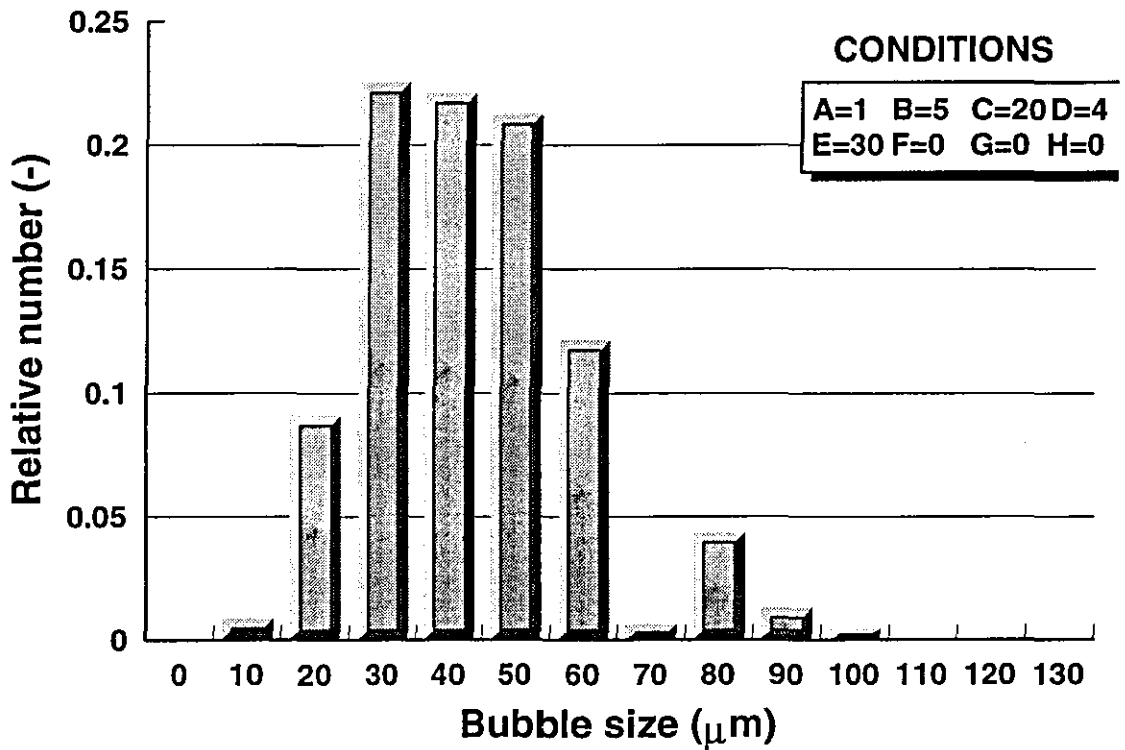


Figure G12 : Bubble size distribution, 30° diverging nozzle cone

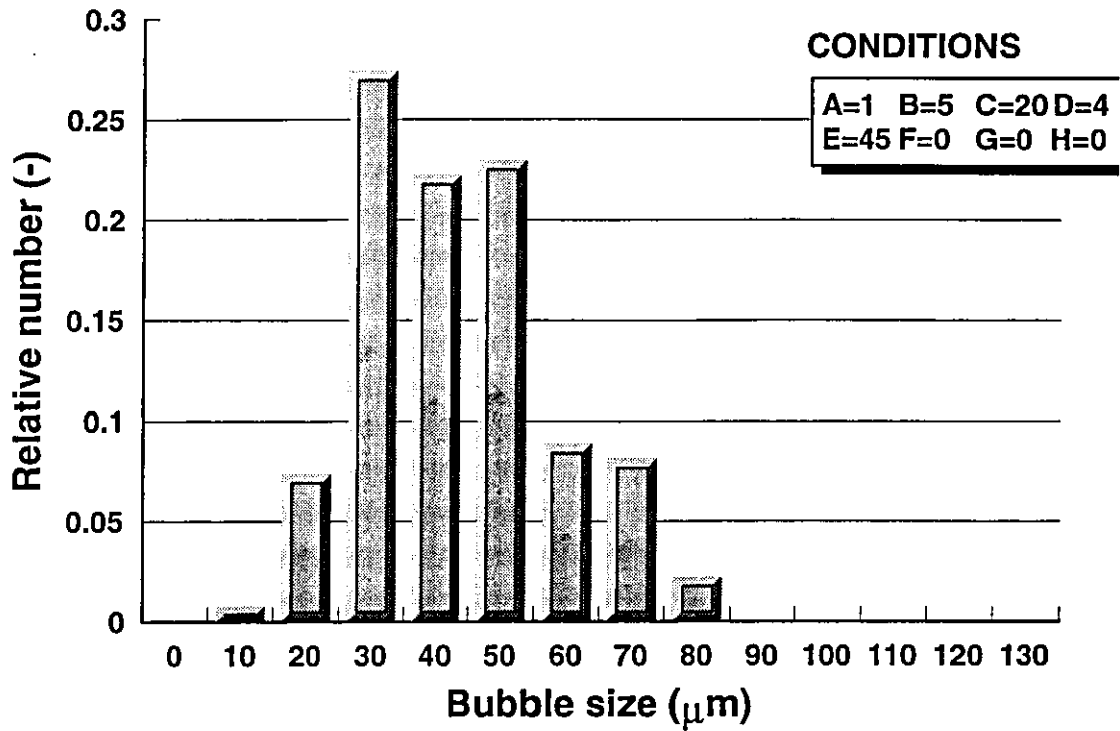


Figure G13 : Bubble size distribution, 45° diverging nozzle cone

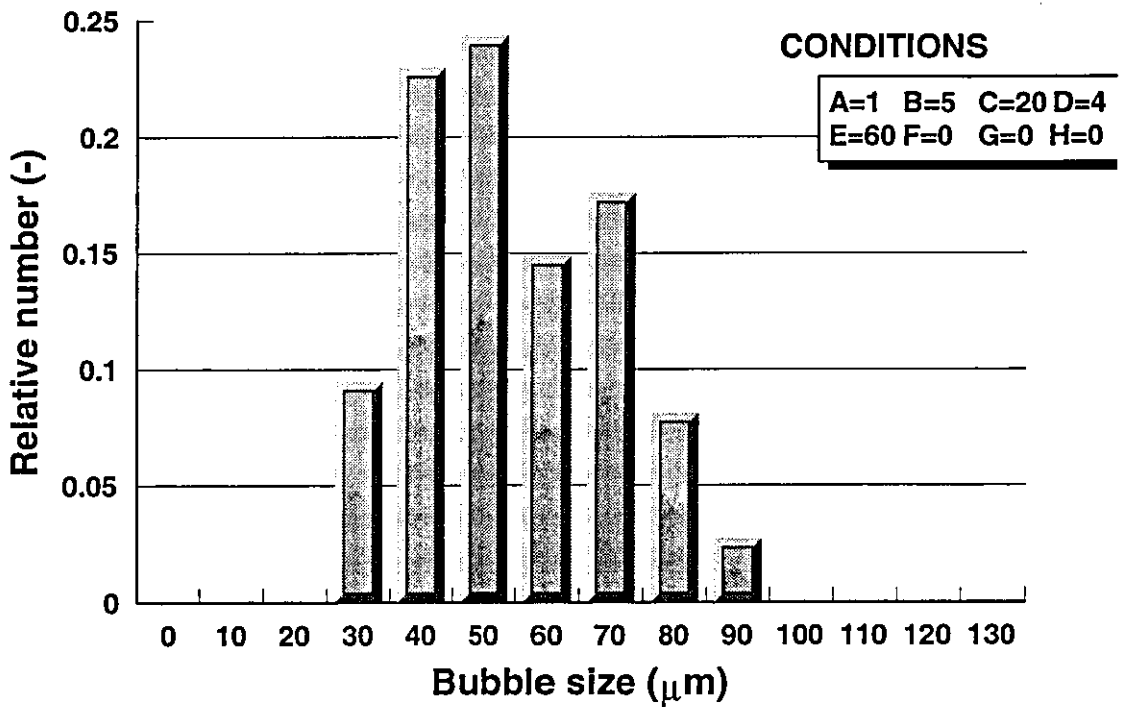


Figure G14 : Bubble size distribution, 60° diverging nozzle cone

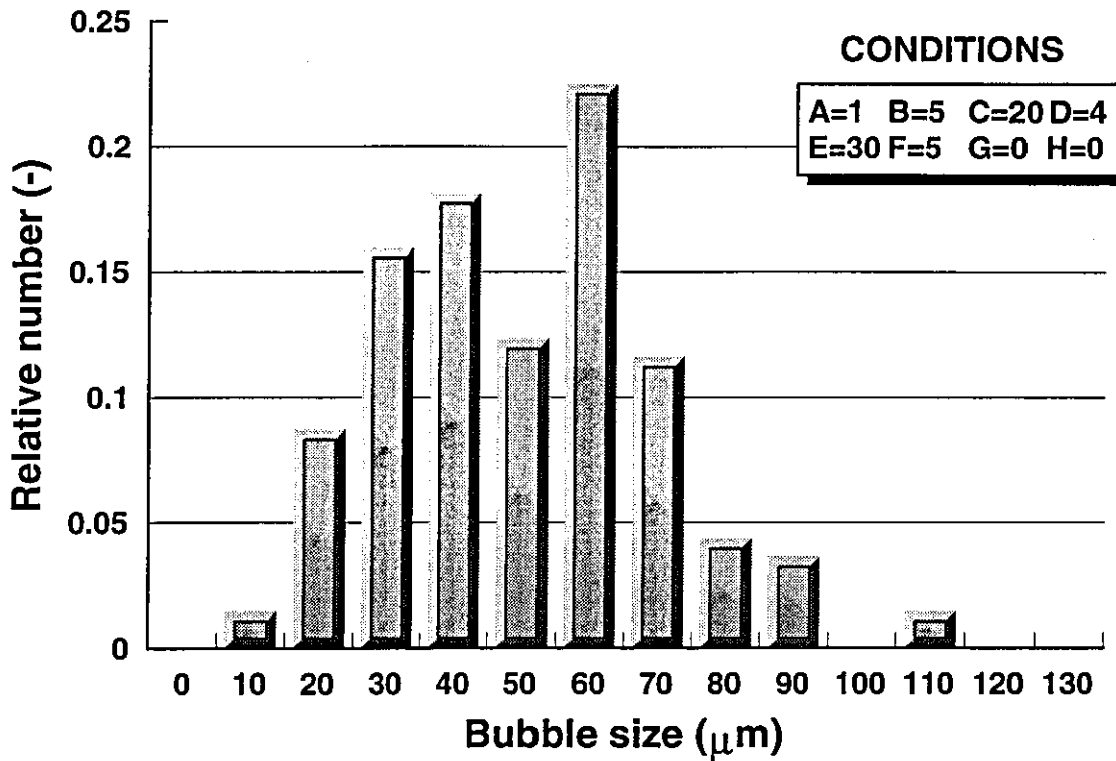


Figure G15 : Bubble size distribution, 30° diverging nozzle cone with an impingement plate 5mm from nozzle exit

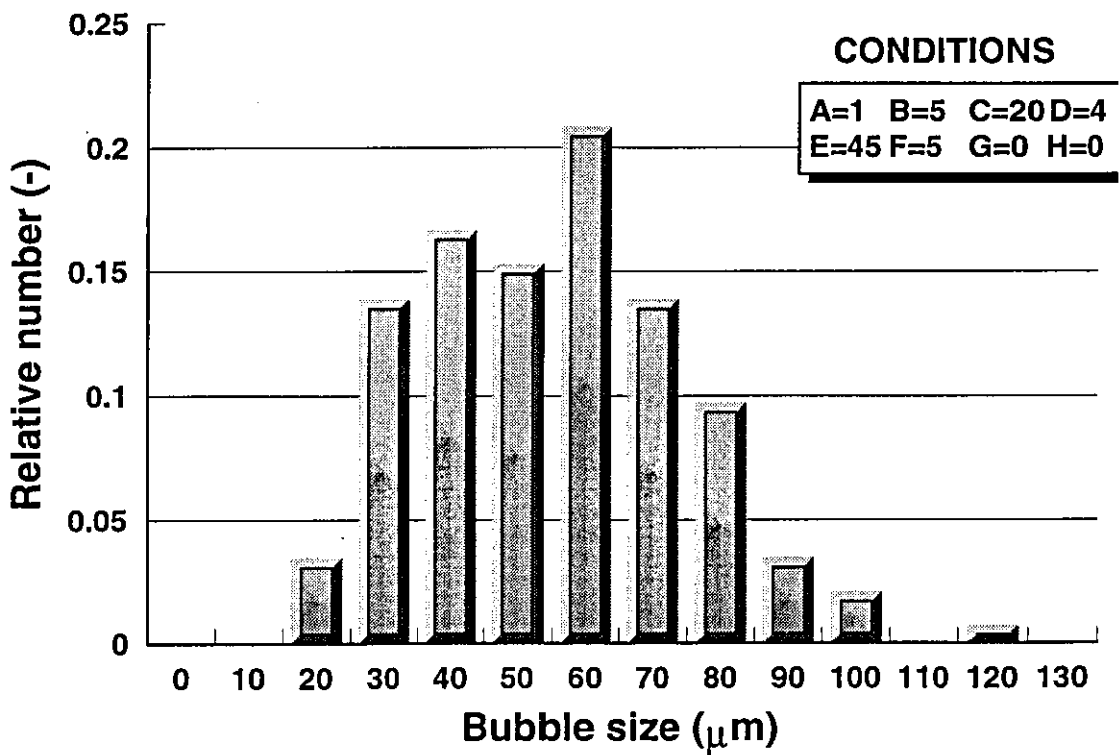


Figure G16 : Bubble size distribution, 45° diverging nozzle cone with an impingement plate 5mm from nozzle exit

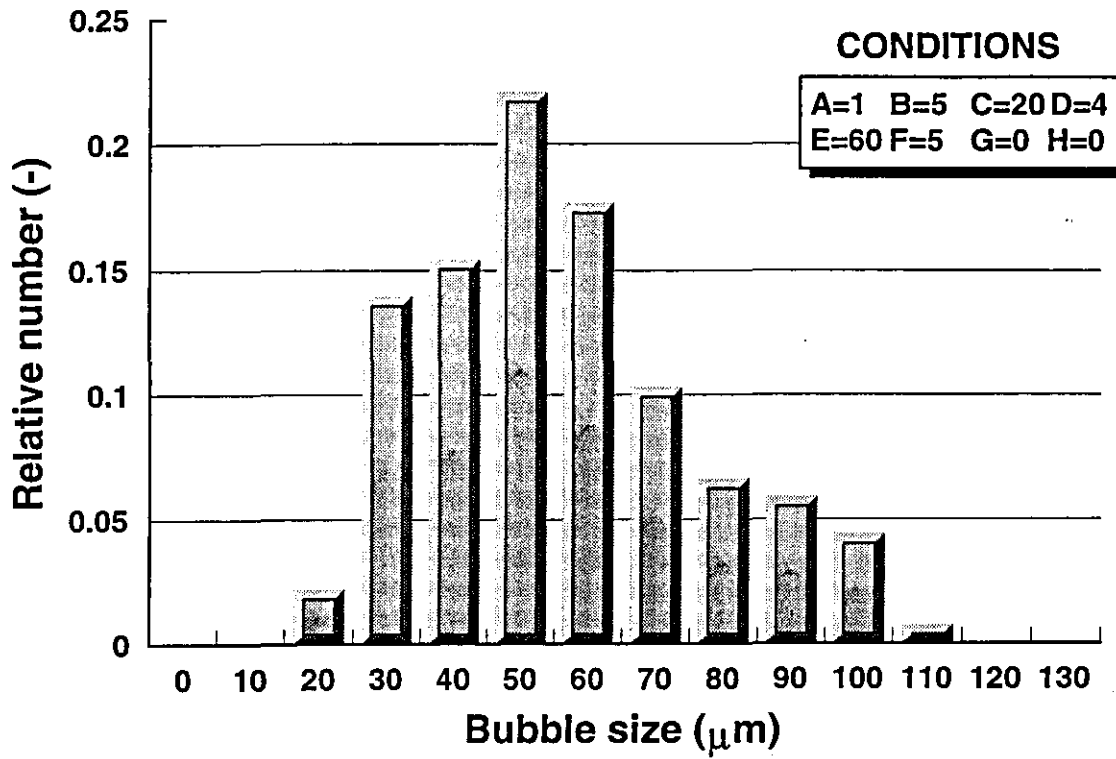


Figure G17 : Bubble size distribution, 60° diverging nozzle cone with an impingement plate 5mm from nozzle exit

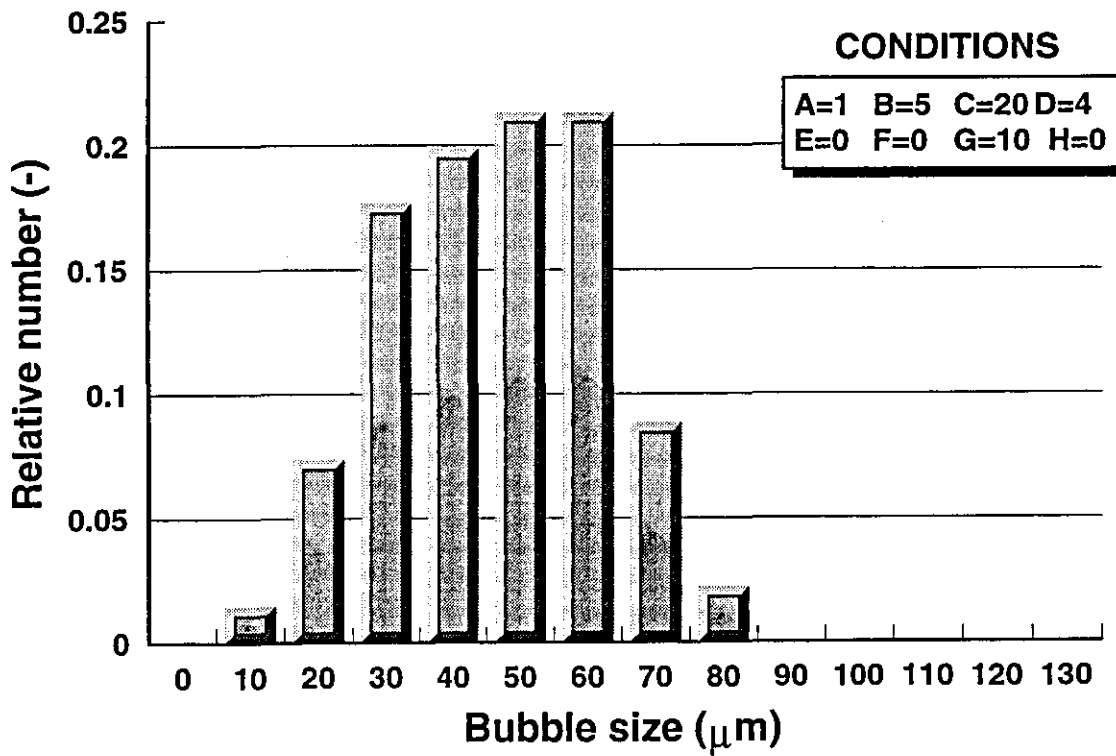


Figure G18 : Bubble size distribution, HTAB concentration = 10 ppm

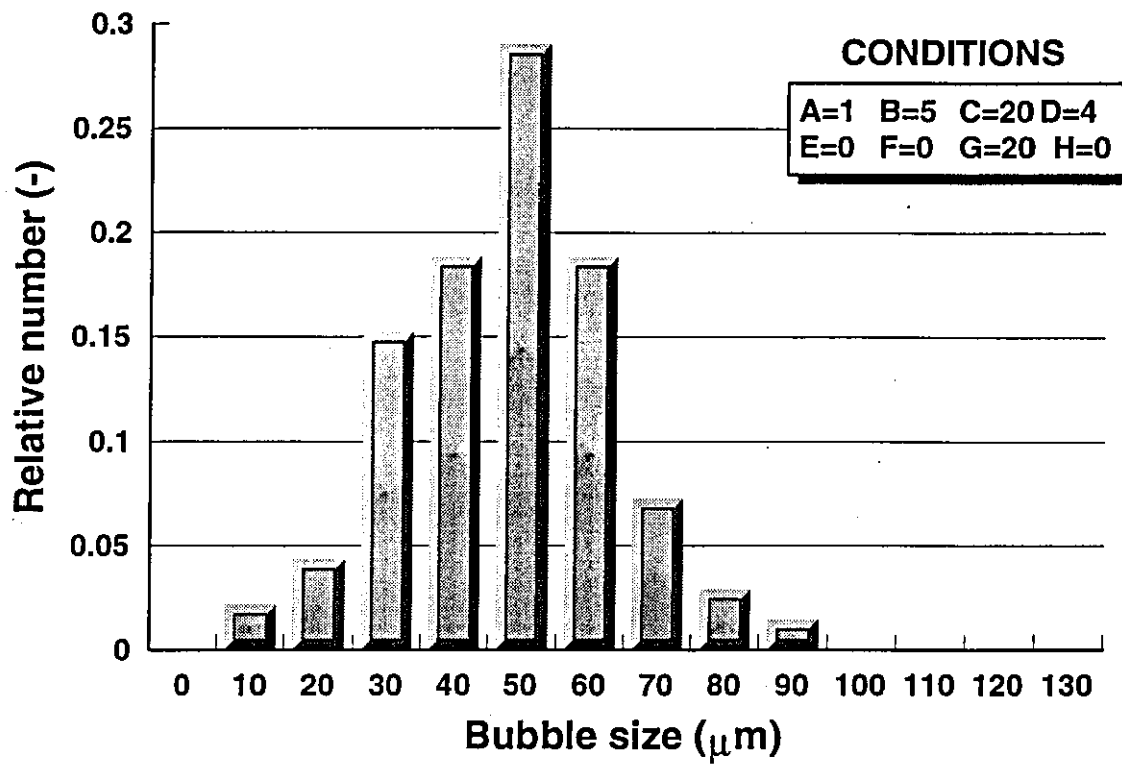


Figure G19 : Bubble size distribution, HTAB concentration = 20 ppm

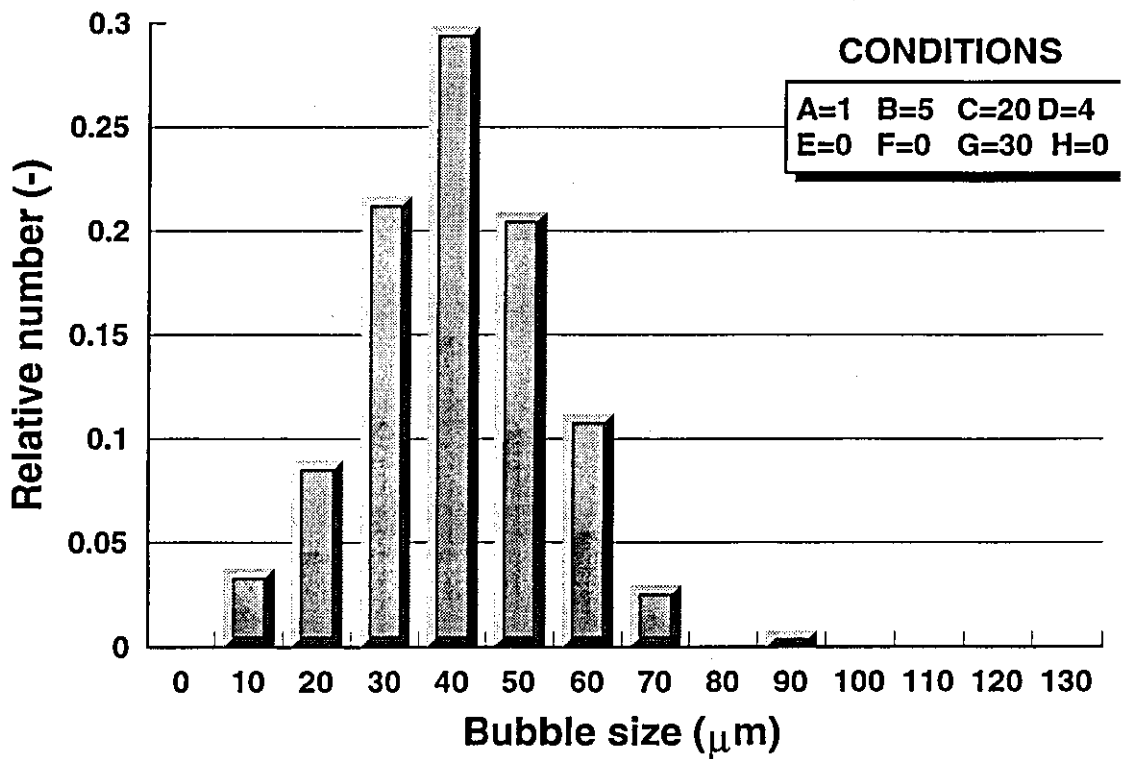


Figure G20 : Bubble size distribution, HTAB concentration = 30 ppm

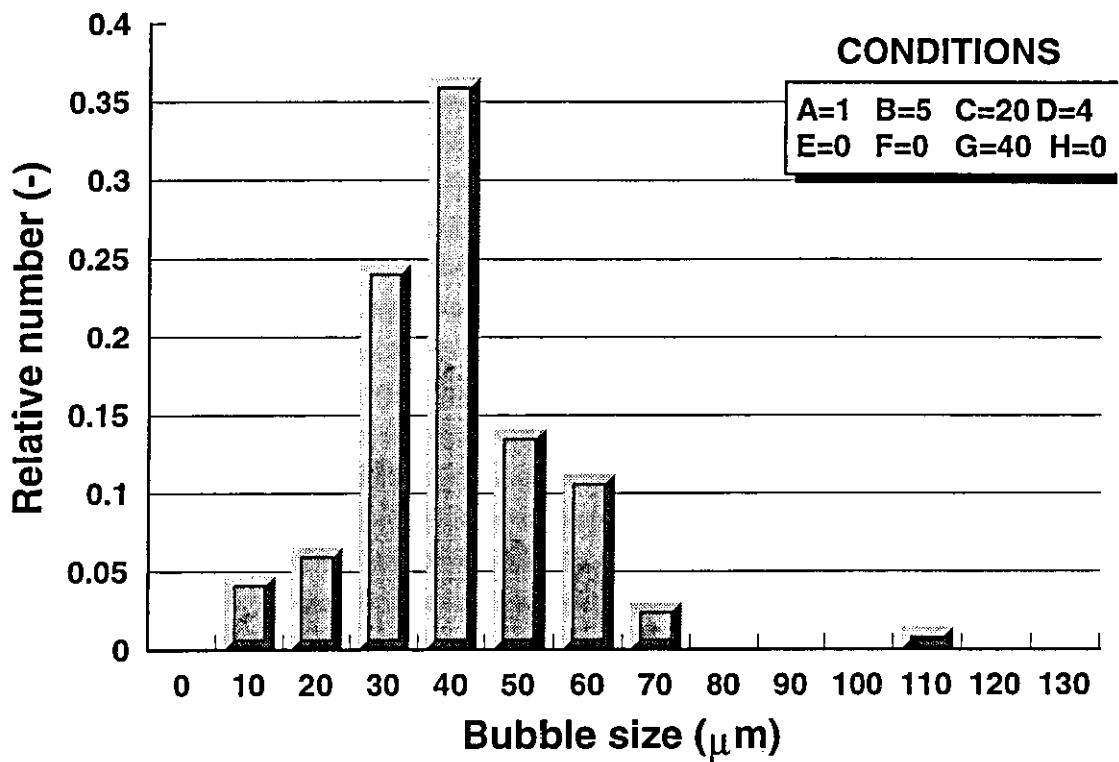


Figure G21 : Bubble size distribution, HTAB concentration = 40 ppm

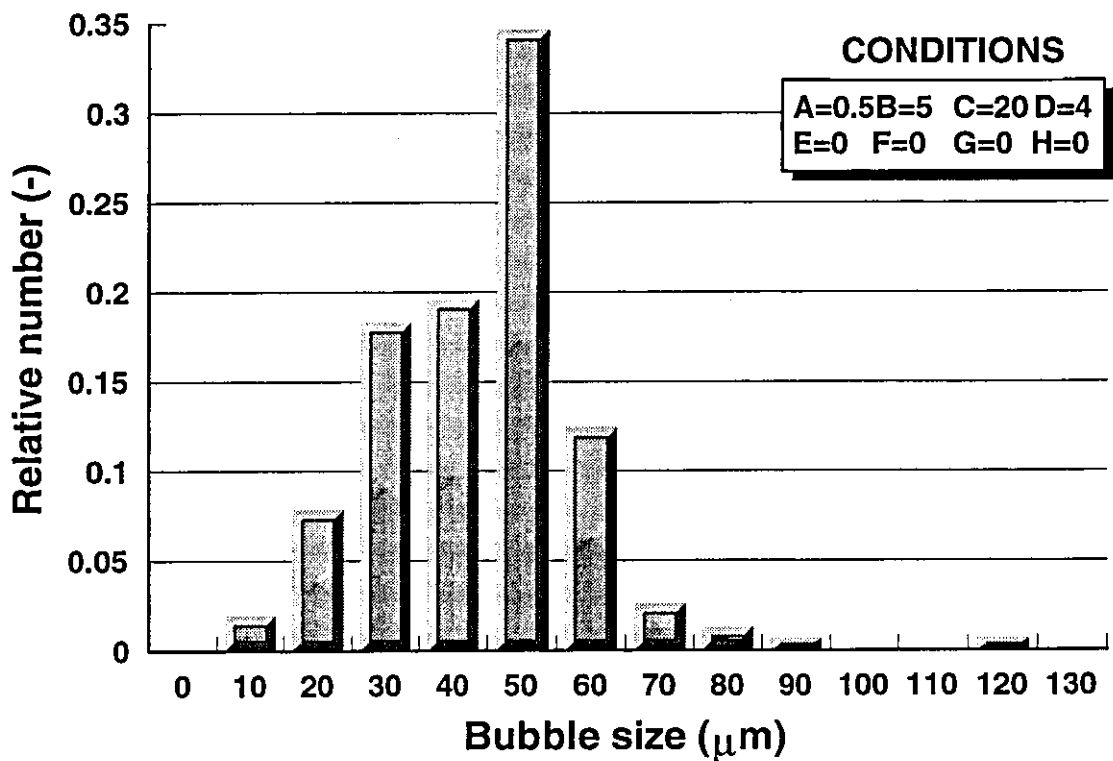


Figure G22 : Bubble size distribution, 0.5 mm orifice plate

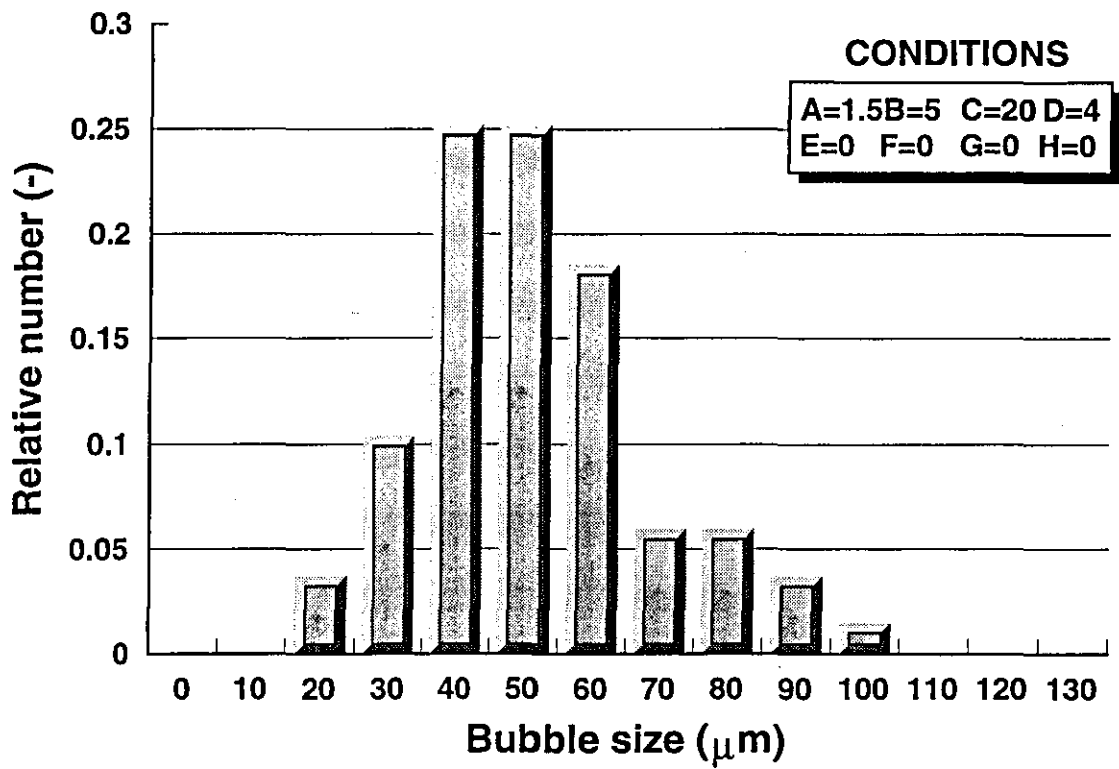


Figure G23 : Bubble size distribution, 1.5 mm orifice plate

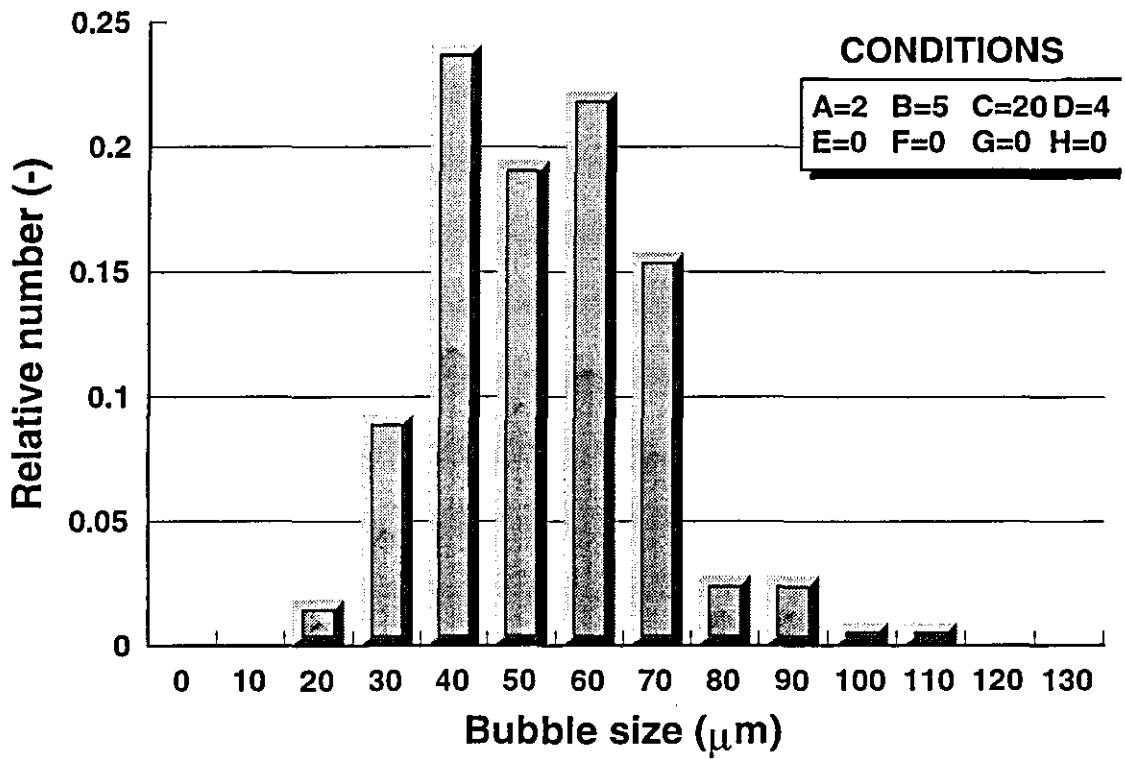


Figure G24 : Bubble size distribution, 2 mm orifice plate

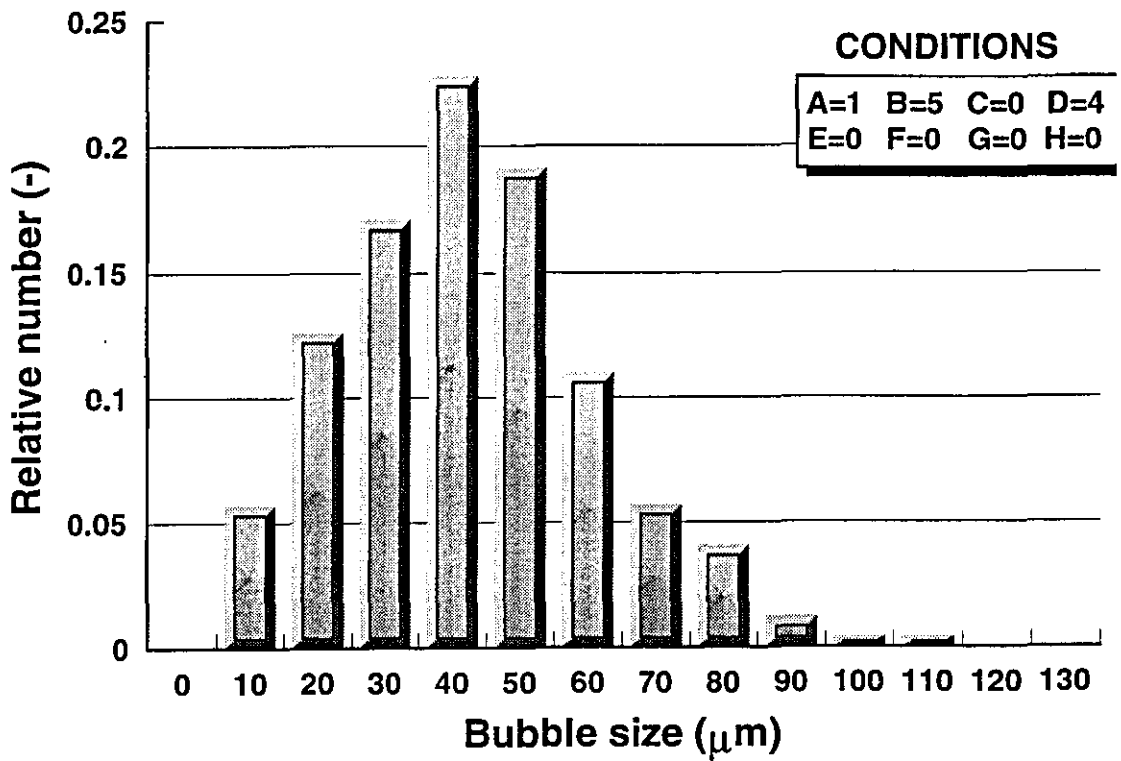


Figure G25 : Bubble size distribution, no nozzle chamber

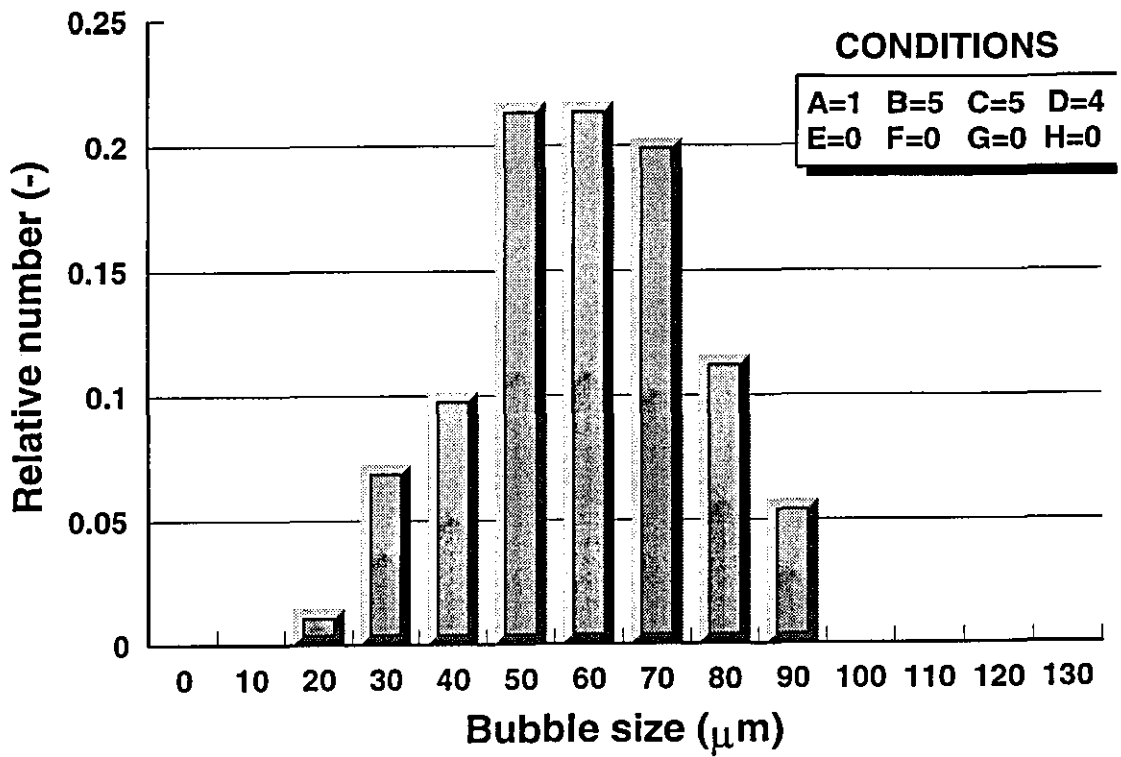


Figure G26 : Bubble size distribution, 5 mm nozzle chamber

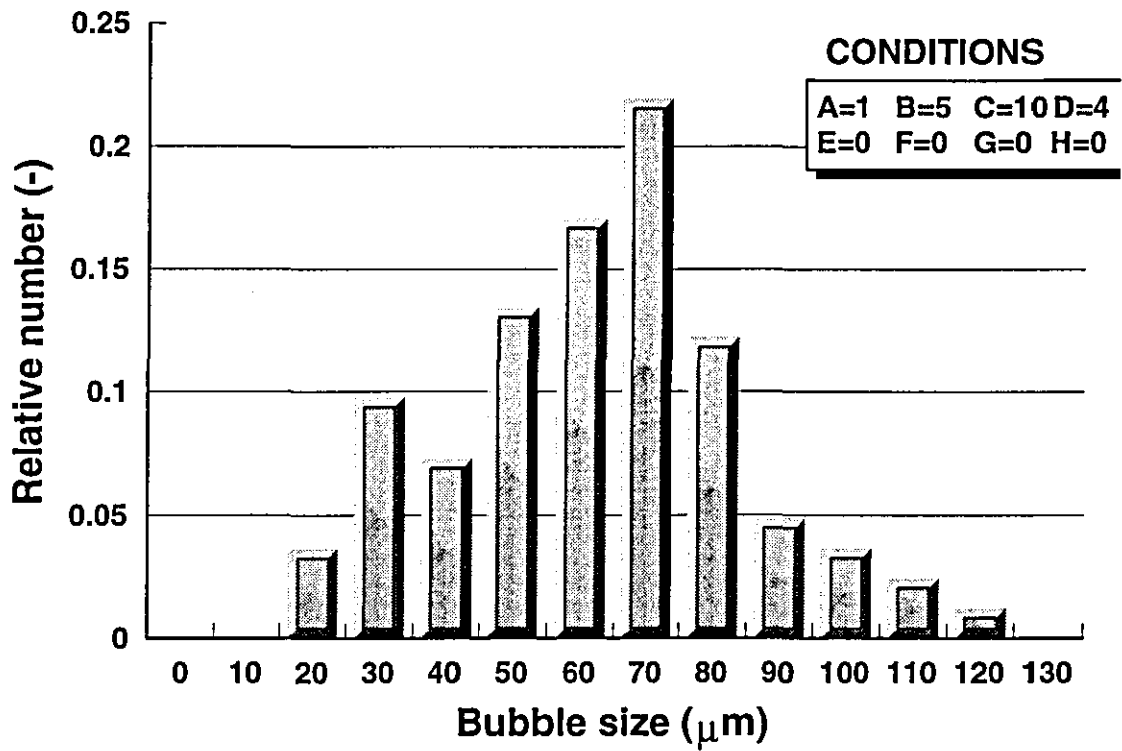


Figure G27: Bubble size distribution, 10 mm nozzle chamber

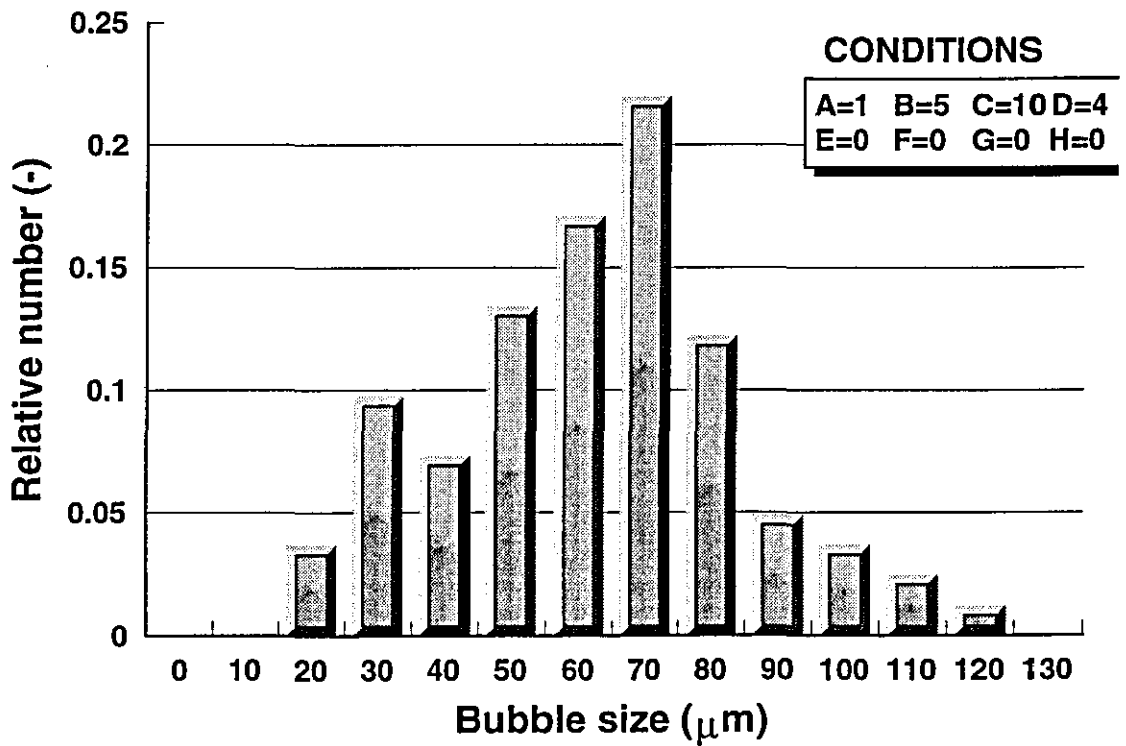


Figure G28: Bubble size distribution, extended cavitation plate

APPENDIX H

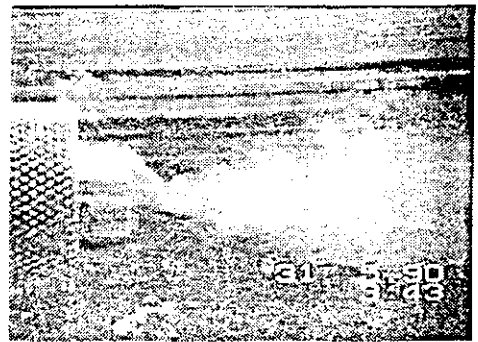
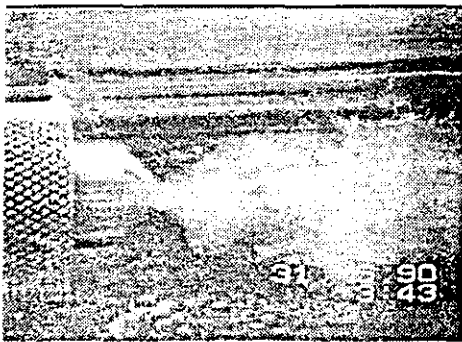
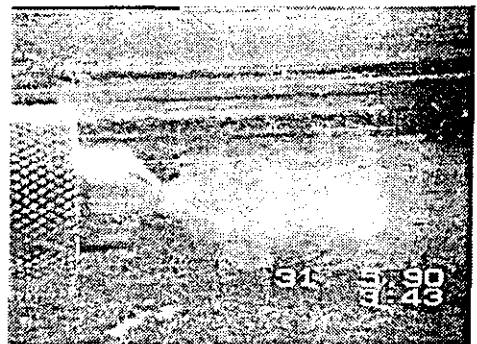
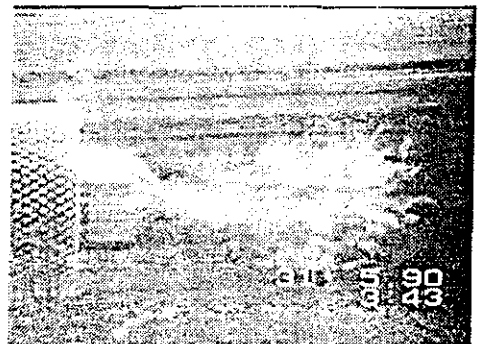
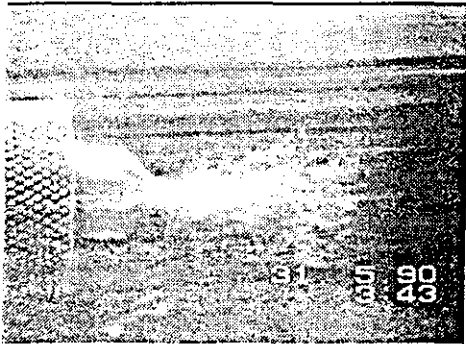
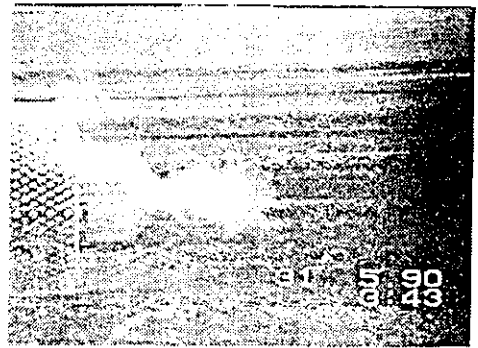
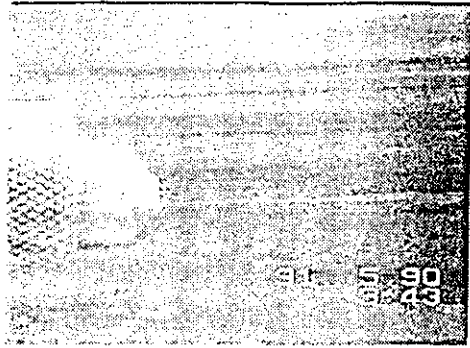


Figure H1: Picture board of bubble formation from a nozzle

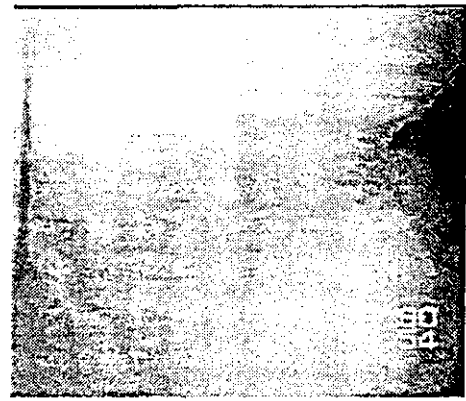
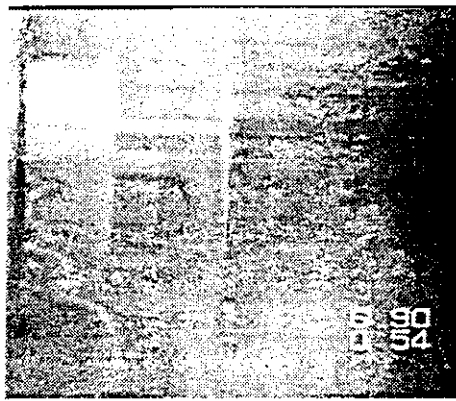
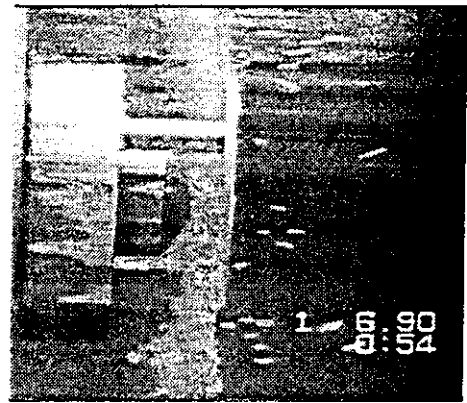
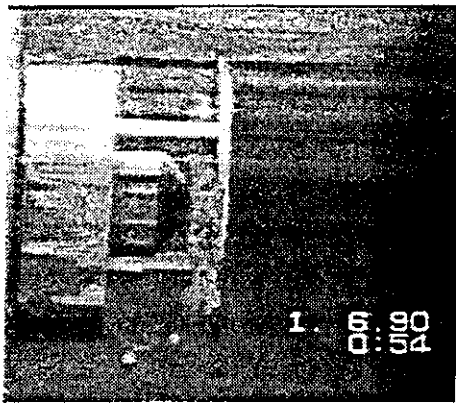
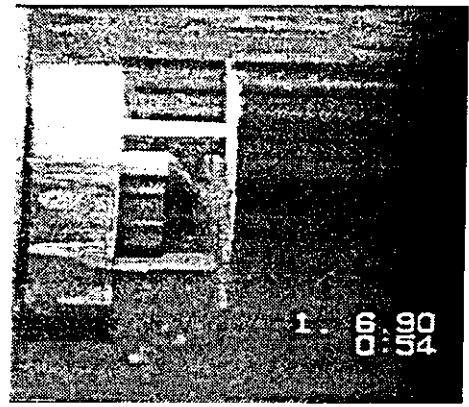
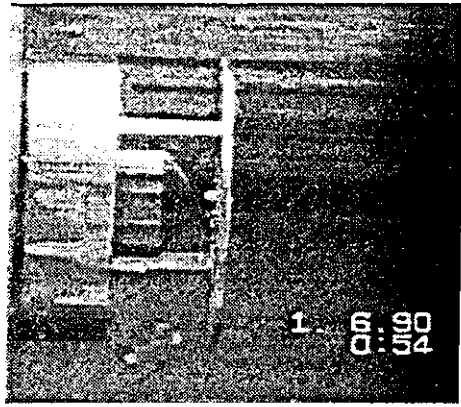


Figure H2: Picture board of bubble formation from a nozzle with an impingent plate

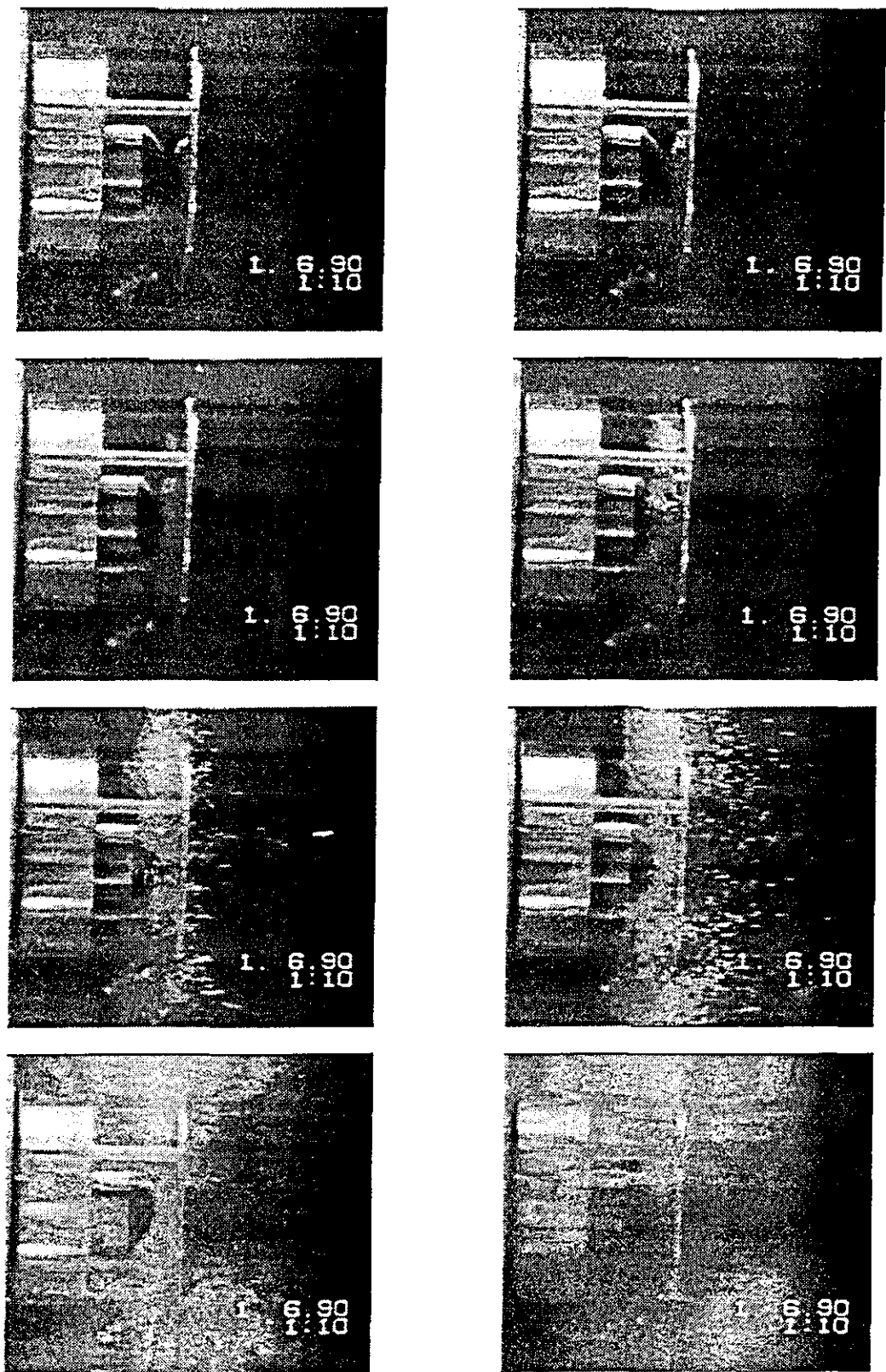


Figure H3: Picture Board of bubble formation from a nozzle with an impingement plate

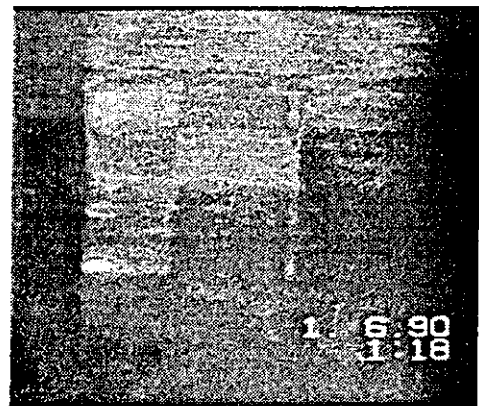
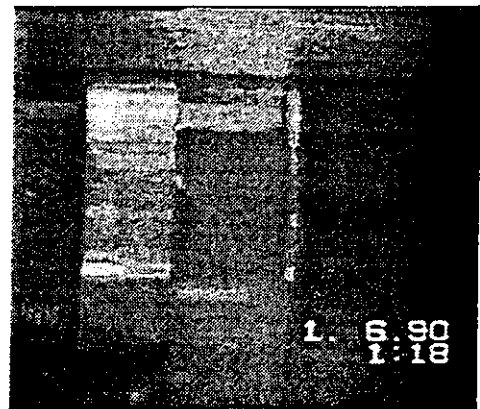
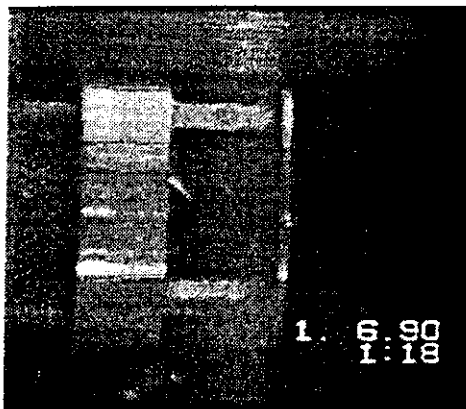
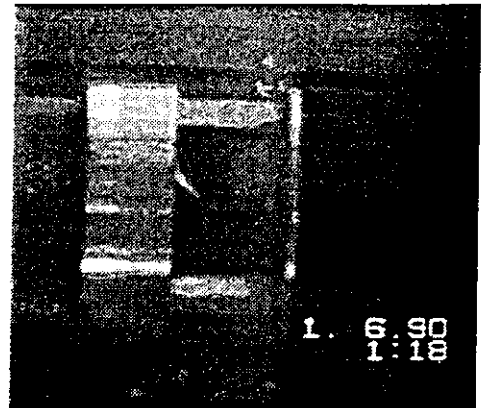
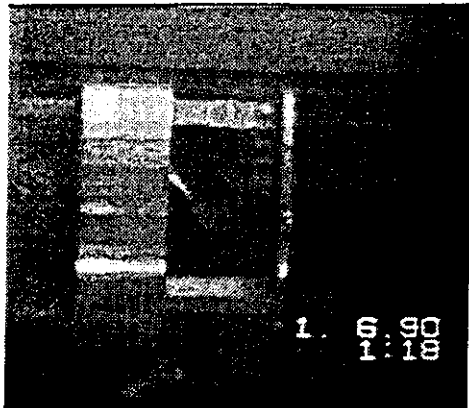
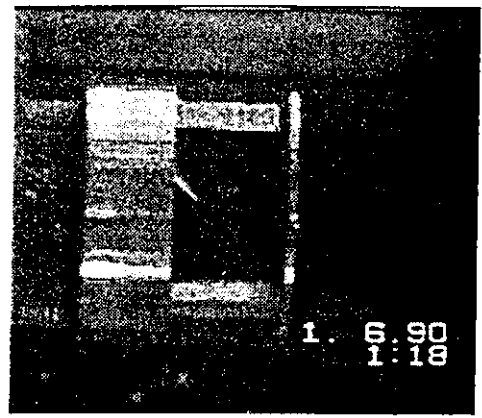
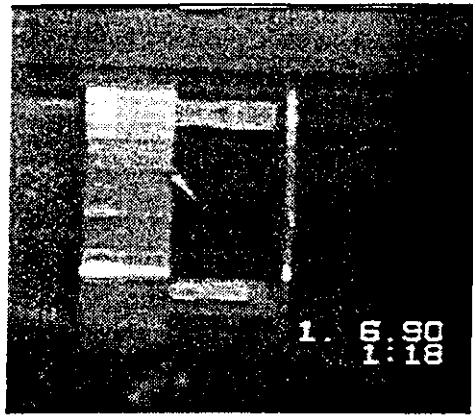


Figure H4: Picture board of bubble formation from a nozzle with an impingement plate.

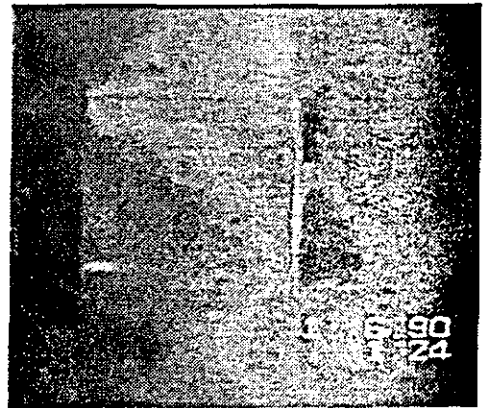
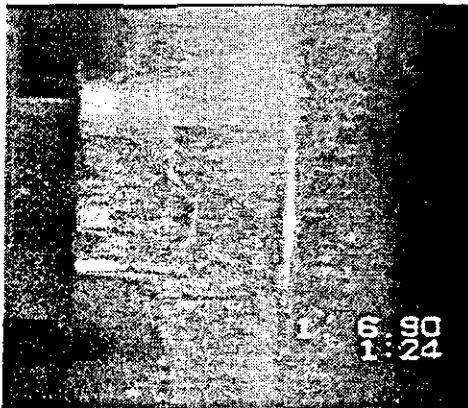
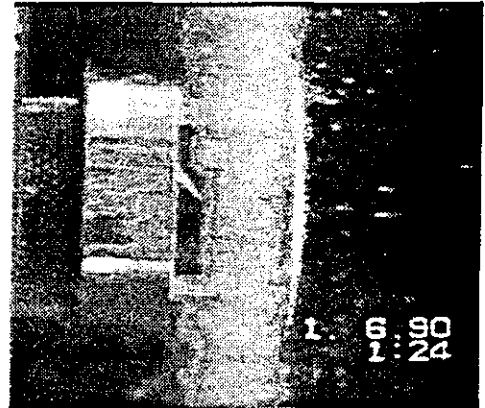
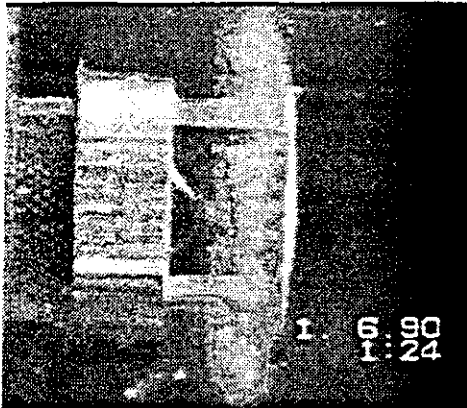
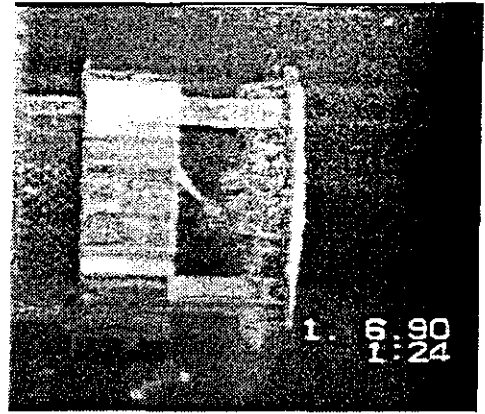
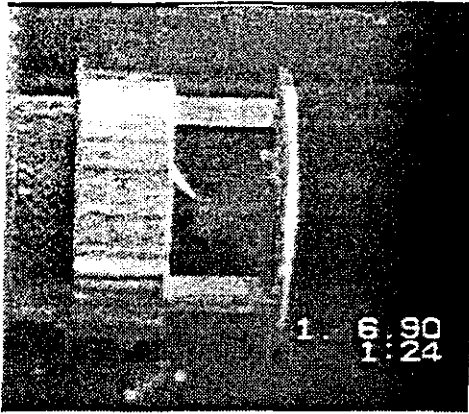
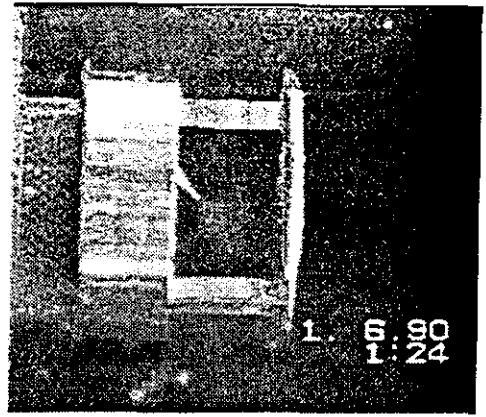
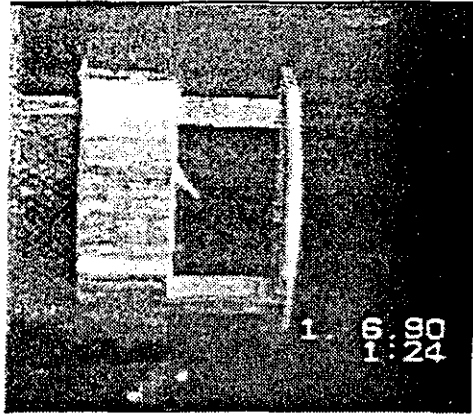


Figure H5: Picture board of bubble formation from a nozzle with an impingment plate

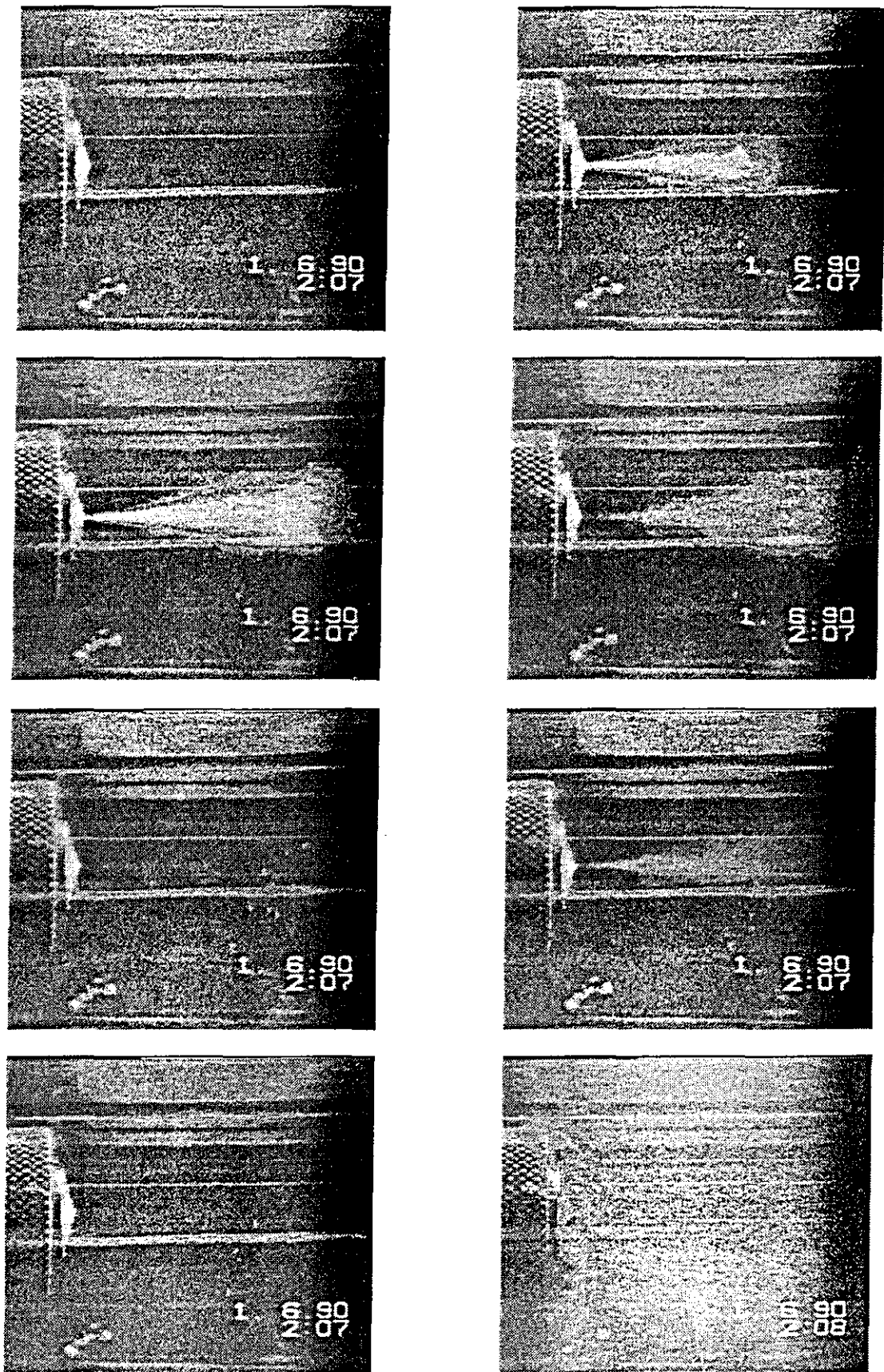


Figure H6: Picture board of bubble formation from a nozzle with an impingement nozzle

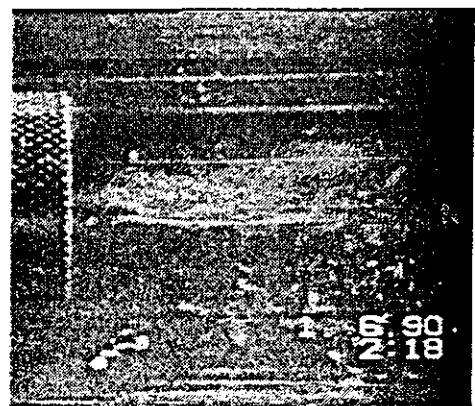
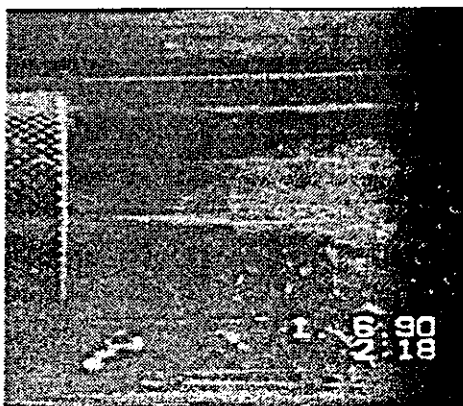
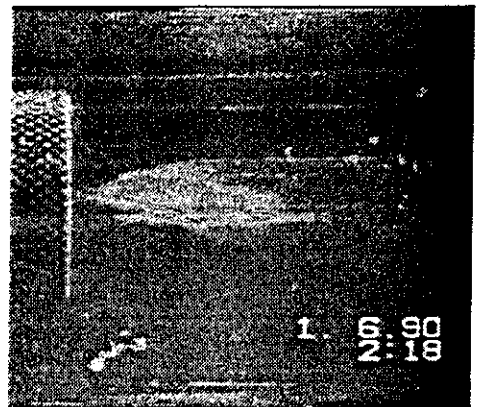
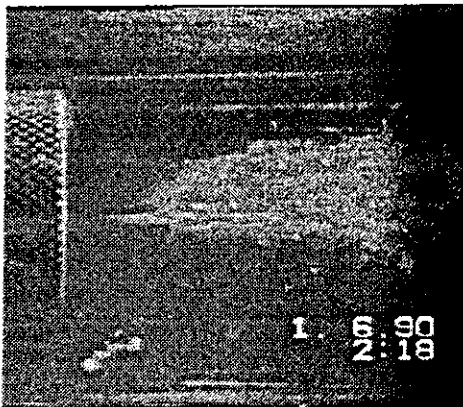
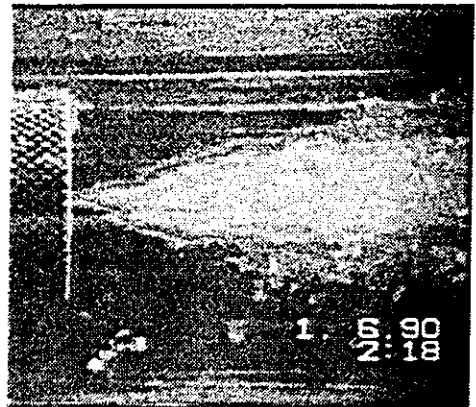
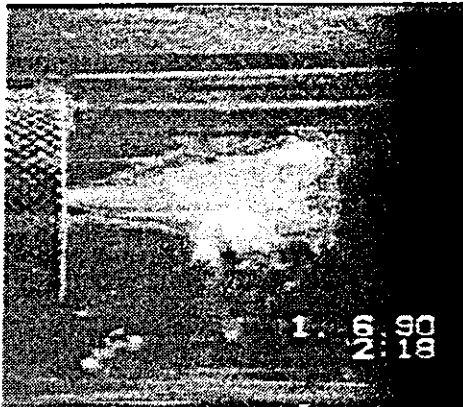
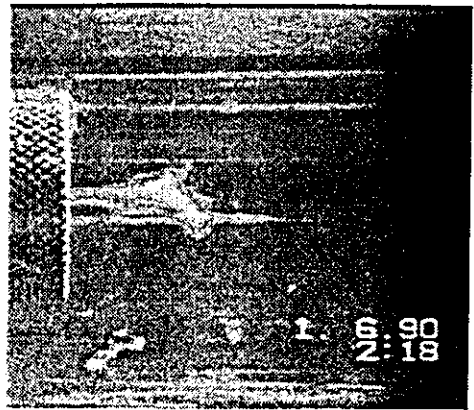
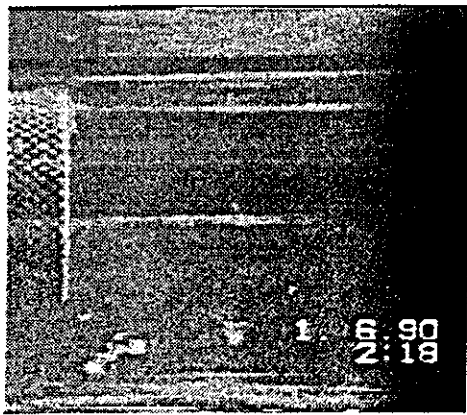


Figure H7: Picture board of bubble formation from a nozzle with no nozzle chamber

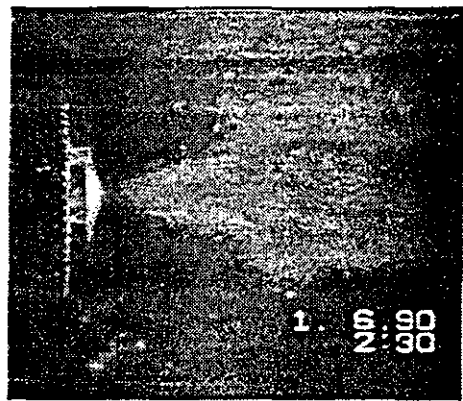
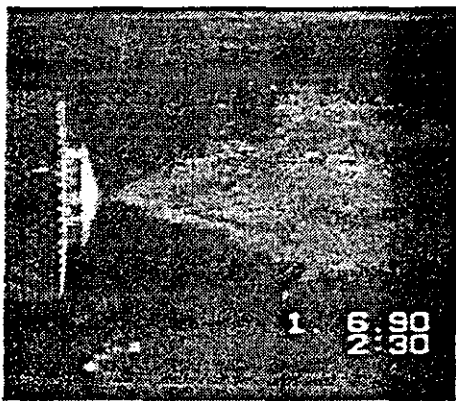
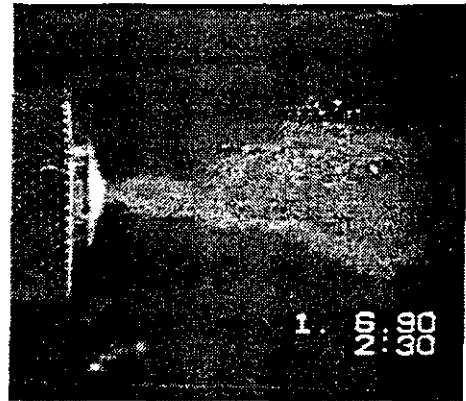
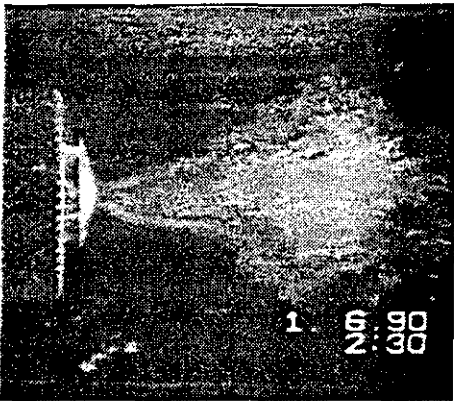
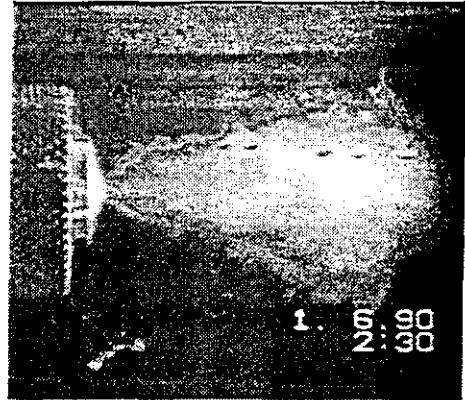
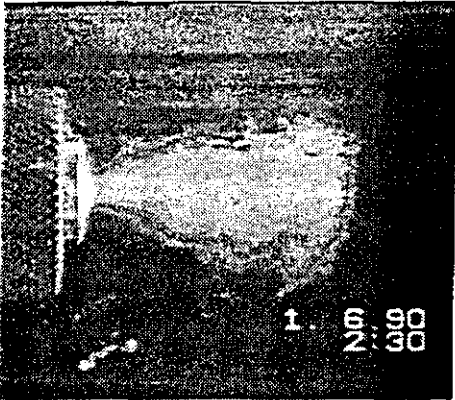
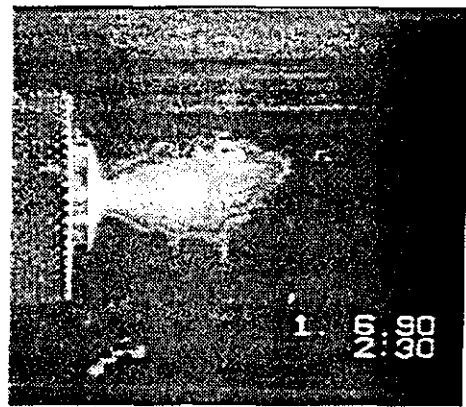
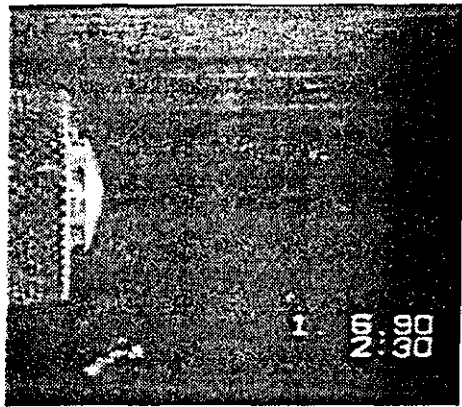


Figure H8: Picture board of bubble formation from a nozzle with a reduced nozzle chamber

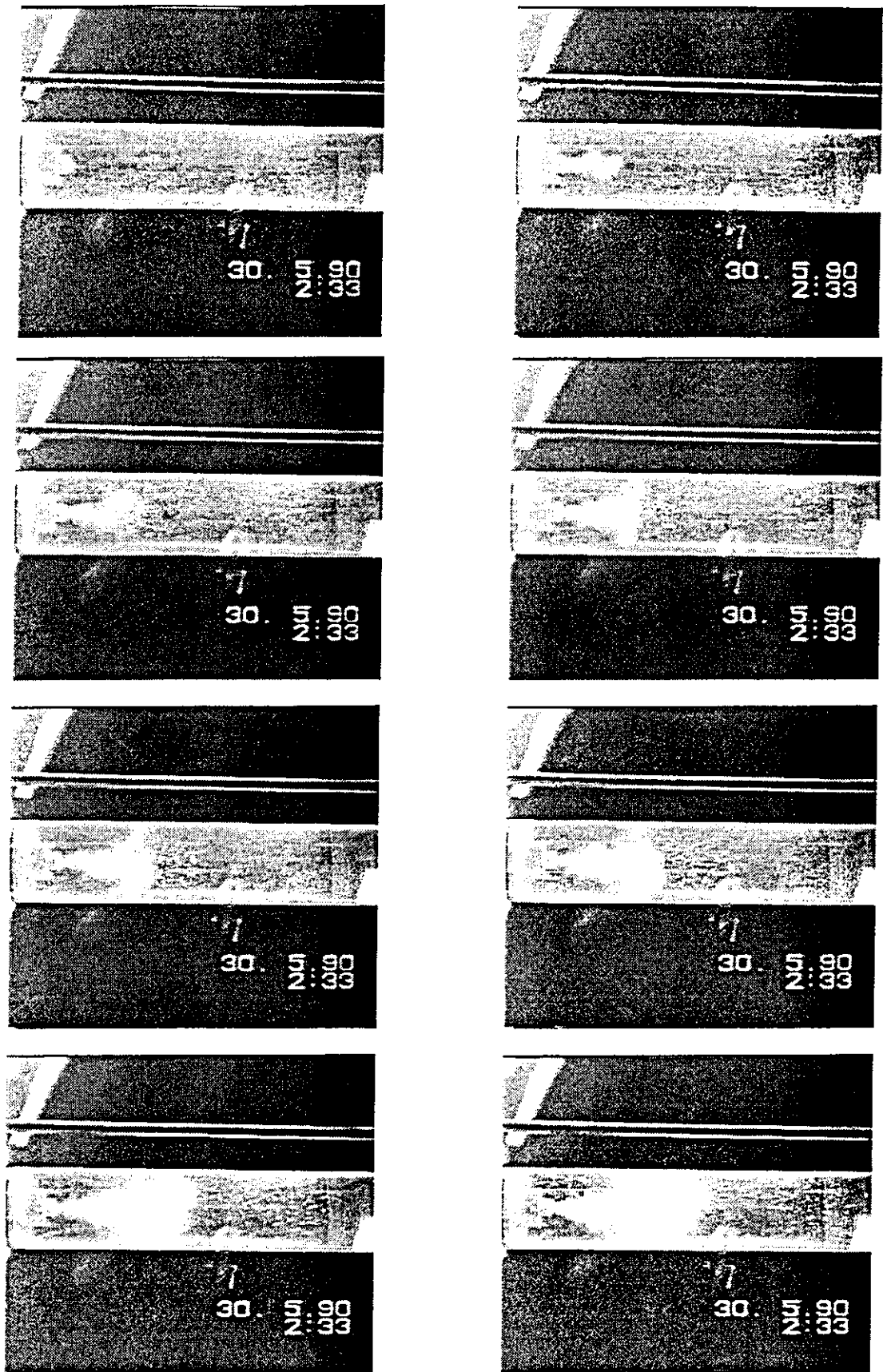


Figure H9: Picture board of bubble formation from a nozzle-global view

APPENDIX I

A Programme listing for trajectory analysis of particle capture

```
DIM crt(40)
for j=1 to 1      'particle size'
dp=j*1E-6
hit=0
miss=0
crt(1)=1
crt(2)=0.000001 ← step
for i=2 to 5

y0#=crt(i)
y1#=y0#
alpha=.10      'density of bubbles'
r1#=(alpha)^(-1/3)
x1#=-sqr(r1#*r1#-y1#*y1#)
dt#=.0001
x0#=x1#-dt#

      'to stop display type "goto 50"

screen 12
window (-3.2,2.4)-(3.2,-2.4)
circle (0,0),1,4

50 count=0
10 x1#=#x1#
GOSUB Datar
20 x1#=#x1#
gosub flow
gosub forces
30 x1#=#x1#
gosub traj

      'to stop display type "goto 60"

pset (x1#,y1#)
60 count=count+1

if count>600000 then 210
if x1#>1 then 210
if hrd#> 0 then 20
if hrd#<0. then 3000
210 miss=miss+1
hit=0
crt(i+1)=(crt(i)+crt(i-miss))/2
goto 3010
3000 hit=hit+1
miss=0
crt(i+1)=(crt(i)+crt(i-hit))/2
```

hit = 1/2 distance out again.

$$y_0 = y_0/2$$

miss: $y_0 = 1$

$$y_{52} = y_{51} - \frac{(y_{50} + y_{51})}{2}$$

↑ starting point.

readjust position
if hit or miss

```

3010 test=sqr((crt(i)-crt(i-1))*(crt(i)-crt(i-1)))
if test<0.001 then 3110

next i
3110 print using "#####.#####" ;(dp*1E+6),crt(i),feldd,fvdwdd
next j
3100 end

```

Datar:

```

epi=78.5*8.85E-12
ka=1.04E+6
zetap=-0.010
zetab=-0.010
visc=.001
A11=2.0E-19
A22=2.0E-19
A33=4.0E-21
A=(sqr(A11)-sqr(A33))*(sqr(A22)-sqr(A33))
A=3E-20
db=40E-6
dp=dp
denp=2600
denf=1000
denb=1.25
u0=9.81*(denp*dp*dp+denb*db*db-2*denf(dp*dp+db*db))/(18*visc)
feldd=2*ka*epi*zetap*zetab/(3*visc*u0)      'electric parameter

fvdwdd=A/(9*3.142*visc*u0*dp*dp)            'Van der Waal parameter

G=(denp-denf)*dp*dp*9.81/(18*visc*u0)      'gravity parameter
stk=(denp-denf)*dp*dp*u0/(18*visc*db)      'Stokes number

RETURN

```

Datar

flow:

```

r#=sqr(x1#*x1#+y1#*y1#)
p=(alpha)^(1/3)

wd=1-5*p/9+p*p*p-.2*p^(6)
A=-(1-0.4*p*p*p)/(4*wd)
B=3/(4*wd)
C=-(1+0.5*p*p*p)/(2*wd)

```

$p \sim \frac{1}{\alpha}$

```

D=0.15*p*p*p/wd
utheta#=-(-A/(r#*r#*r#)+B/r#+2*C+4*D*r#*r#)*y1#/r#
ur#=2*x1#*(A/r#+B*r#+C*r#*r#+D*r#*r#*r#)/(r#*r#*r#)

```

```

4005 ux1#=utheta#*y1#/r#-ur#*x1#/r#
uy1#=-utheta#*x1#/r#-ur#*y1#/r#

```

```

4010 x1#=x1#
RETURN

```

forces:

calculate force
 $rr\# = \sqrt{x1\#^2 + y1\#^2} * db/2$ — *dim. positn.*

$rtr\# = (dp + db)/2$ — *min*

$hr\# = rr\# - rtr\#$ —

$hrd\# = hr\#^2 / dp$

$hrds\# = hrd\# * hrd\#$ — *why*

if $hr\# > 1E-9$ then 5050

$hr\# = 1E-9$

$5050 fdielr = -feldd * \exp(-ka * hr\#) / (1 + \exp(-ka * hr\#))$ — *dep force*

$vx\# = hr\#^2 / (db + dp)$

$nr = dp / db$

If $hrds\# = 0$. THEN 5040

$fvdwr = fvdwdd / hrds\#$

GOTO 5010

5040 $fvdwr = 0$.

5010 $s = hr\#^2 / dp$

$vr\# = ur\# - (ux1\# * x1\# / r\# + uy1\# * y1\# / r\#)$

IF $s < 0$. OR $s > 1$. THEN 5020

$fdihr = -3 * nr * nr * (s + 1) * (s + 1) / ((1 + s * nr + nr) * (1 + s * nr + nr)) * ur\# * (3.23 - 2.91 * s + 1.56 * s * s)$

goto 5030

5020 $fdihr = 0$.

5030 $s = s$

RETURN

$$s = \frac{p}{r_0} \frac{H}{r_0}$$

} Hydrated force

traj:

$fr\# = fdihr + fdielr + fvdwr$

$fx\# = -fr\# * x1\# / r\#$

$fy\# = -fr\# * y1\# / r\#$

7010 $uy1\# = uy1\# + fy\#$

$ux1\# = ux1\# + fx\# + G$

$x2\# = (2 * ux1\# * dt\# + x0\# * (dt\# - 4 * stk) + 8 * x1\# * stk) / (4 * stk + dt\#)$

} calculate position.

```

y2#=(2*uy1#*dt#*dt#+y0#*(dt#-4*stk)+8*y1#*stk)/(4*stk+dt#)
x0#=x1#
x1#=x2#
y0#=y1#
y1#=y2#
RETURN

```

→ next part

B User level listing of visilog routine to select focussed bubbles

```

skell ()
{
    deleteall(
        /* Delete All images in Memory : */ 1
    );
    read(
        /* Input file */ ""
        /* Output image */ , "In"
        /* Type */ , 0
    );
    UpdateLut(NORMAL);
    UpdateLut(NORMALF);
    Threshold(
        /* Input image */ "In"
        /* */ , {
            0
            , 120
        }
        /* Output binary image */ , "Bi"
    );
    UpdateLut(NORMALF);
    border_kill(
        /* Input binary image */ "Bi"
        /* Output binary image */ , "Bord"
    );
    showaoi(
        /* Input image */ "Bord"
    );
    opening(
        /* Input image */ "Bord"
        /* Number of iterations */ , 4
        /* Output image */ , "open"
    );
    UpdateLut(NORMALF);
    skeleton(
        /* Input binary image */ "open"

```

```
/* Output binary image */    ,"skel"  
);  
prune(  
/* Input image */    "skel"  
/* Output image */    ,"prune"  
);  
reconstruct(  
/* Input image 1 */    "Bi"  
/* Input markers image */    ,"prune"  
/* Output image */    ,"rec"  
);  
UpdateLut(NORMALF);  
label(  
/* Input binary image */    "rec"  
/* Output label image */    ,"label"  
);  
}
```


Our ref

Your ref

Date

Direct line

10th January 1996 0171 938 9274

Facsimile 071-938 9268

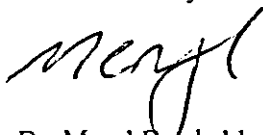
Dr B Jefferson
Department of Chemical Engineering
Loughborough University of Technology
Loughborough
Leicestershire LE11 3TU

Dear Bruce,

I have finally completed the mineralogical and chemical analyses of the two clay samples (A and B) which you sent to the Museum last year. The rapid quantitative X-ray-diffraction method used is outlined in Cressey and Schofield (1995). The method relies on a 120° curved Enraf-Guñi position sensitive detector and associated peak stripping software. Both samples were relatively pure examples of clay minerals however this method can be also used in the quantification of more complex mixed assemblage mudrocks typically used as landfill liners.

I have forwarded a copy of the results and some background information on relevant reference material to Ian at Nottingham University. The invoice for the analyses is to be forwarded next week (our Finance Officer is away); the analysis of each sample will be ~ £115, including tax (unfortunately its the same cost for simple or complex mixtures). Please do not hesitate to contact me if you need more information.

Yours sincerely



Dr. Meryl Batchelder

Ref. JeffAB

Min. Dept.
NHM
London SW7 5BD

Tel: 0171 938 9274

MINERALOGICAL and CHEMICAL ANALYSES of SAMPLES A and B

The X-ray diffraction patterns were collected over $3 - 100 2\theta$ for 10 minutes with Cu K α radiation at 45 kV and 45 mA. The calculated volumes are corrected from the measured volumes to allow for the difference in absorption coefficients and are based on 3 analyses of each sample to ensure random orientation of the powder. Figures 1 and 2 are the 'peak-stripping' profiles for samples A and B respectively; in each case the impurity is removed and the residual pattern is that of the pure mineral (strongest reflections labelled). The measured, and absorption coefficient corrected, mineral proportions are given in Table 1.

| <i>sample</i> | <i>mineral</i> | <i>measured volume (%)</i> | <i>density (gcm⁻³)</i> | <i>absorption coeff. (μ)</i> | <i>calculated volume (%)</i> |
|---------------|-----------------|----------------------------|-----------------------------------|---|------------------------------|
| A (white) | kaolinite | 90 | ~ 2.6 | 139 | 93 |
| | illite | 10 | ~ 2.8 | | 7 |
| B (beige) | montmorillonite | 93 | ~ 2.8 | 121 | 91 |
| | quartz | 6 | 2.65 | 97 | 8 |
| | cristobalite | <1 | 2.33 | 85 | <1 |

Table 1; Mineral proportions (as volume %) in Samples A and B

The chemical compositions of the samples, obtained by lithium metaborate fusions and ICP/AES analyses, are presented in Table 2. The cation exchange capacity of the samples were assessed by the ammonium replacement method described in Thomas, 1982**.

Sample A is typical of naturally occurring white, kaolinitic clays. The narrow peaks on the XRD trace indicate that the kaolinite is well crystalline as with increasing structural disorder the non-basal reflections become broader. In highly disordered kaolinites the closely spaced reflections between 20° and $30^\circ 2\theta$ and the group of reflections around $38^\circ 2\theta$ are not clearly resolved. There is approximately 7 % near-illite, which may be partially interlayered with the kaolinite.

Sample B is a bentonite-type montmorillonite with a small impurity of quartz (~ 8 %) and cristobalite (< 1 %). The clay mineral is highly expandable and, on glycolation, produces a 17.5 Å peak. The XRD patterns of expandable clay minerals vary with exchangeable cation, humidity, temperature and degree of interstratification of illitic layers in the mineral. The degree of crystallinity of the bentonite is low, based on the peak width.

| <i>chemical</i> | <i>SAMPLE A</i> | <i>SAMPLE B</i> |
|--------------------------------------|-----------------|-----------------|
| SiO ₂ | 47.4 | 55.7 |
| TiO ₂ | 0.03 | 0.12 |
| Al ₂ O ₃ | 40.3 | 16.9 |
| Fe ₂ O ₃ (tot) | 0.52 | 5.25 |
| MnO | 0.01 | 0.09 |
| MgO | 0.19 | 2.28 |
| CaO | 0.06 | 2.14 |
| Na ₂ O | 0.10 | 1.77 |
| K ₂ O | 1.42 | 0.60 |
| P ₂ O ₅ | 0.09 | 0.06 |
| H ₂ O | <u>8.3</u> | <u>14.1</u> |
| TOTAL | 98.4 | 99.01 |
| Linear absorption coefficient (μ) | 53.5 | 43.2 |
| Mass absorption coefficient (μ/ρ) | 139 | 121 |
| Density (ρ) gmc ⁻³ | 2.6 | 2.8 |
| CEC (meq/ 100g) | 12.5 | 63.1 |

Table 2; Chemical and physical properties of Samples A and B

* Cressey G and Schofield P F, 1995. Powder Diffraction (December 1995 issue).

** Thomas G W, 1982. Exchangeable cations. In Methods of Soil Analysis, Part 2, Chemical and Microbial Properties, Second Edition, Agronomy, 9, (2), Soil Science Society of America.

FIGURE 1

SAMPLE A; kaolinite with minor illite

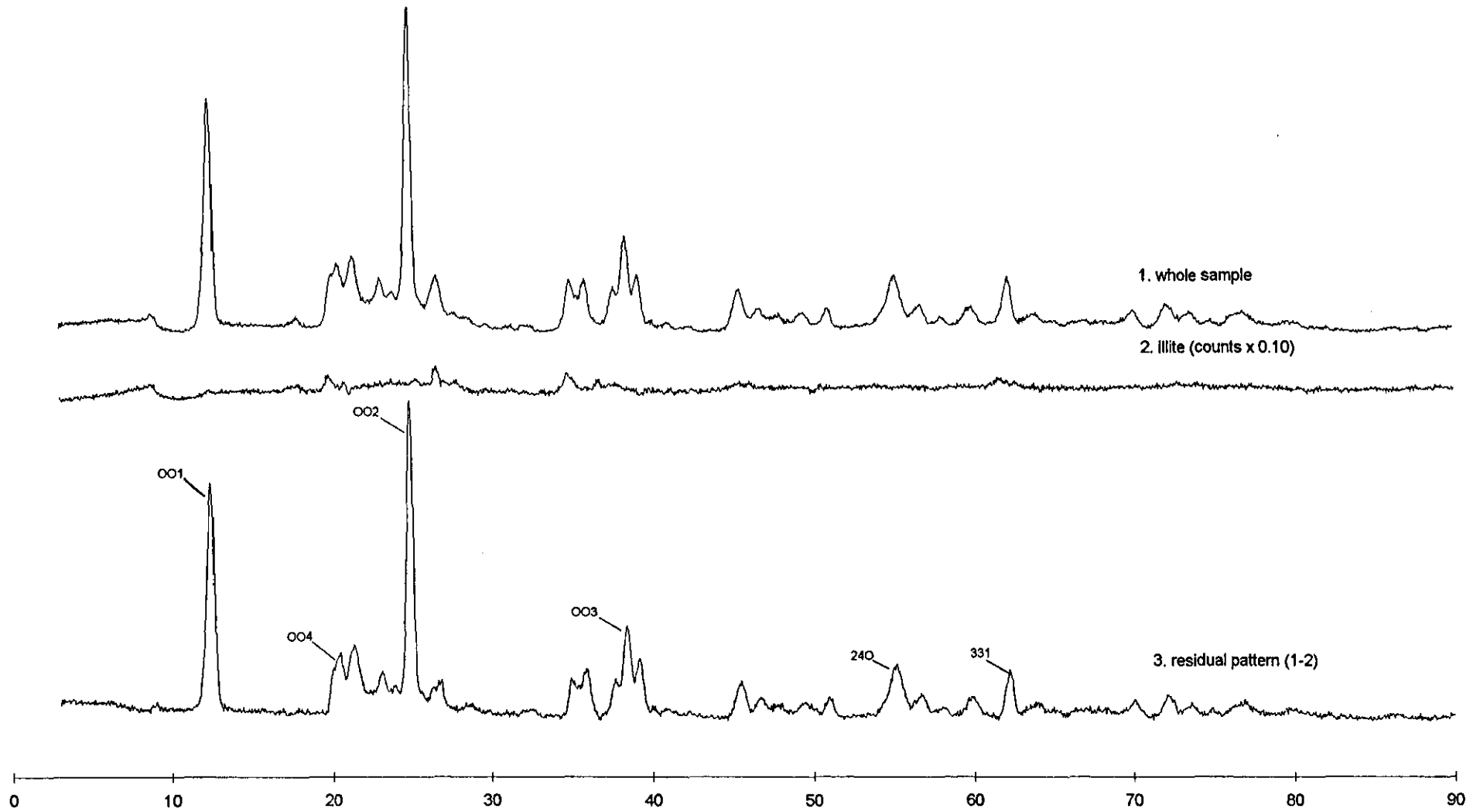
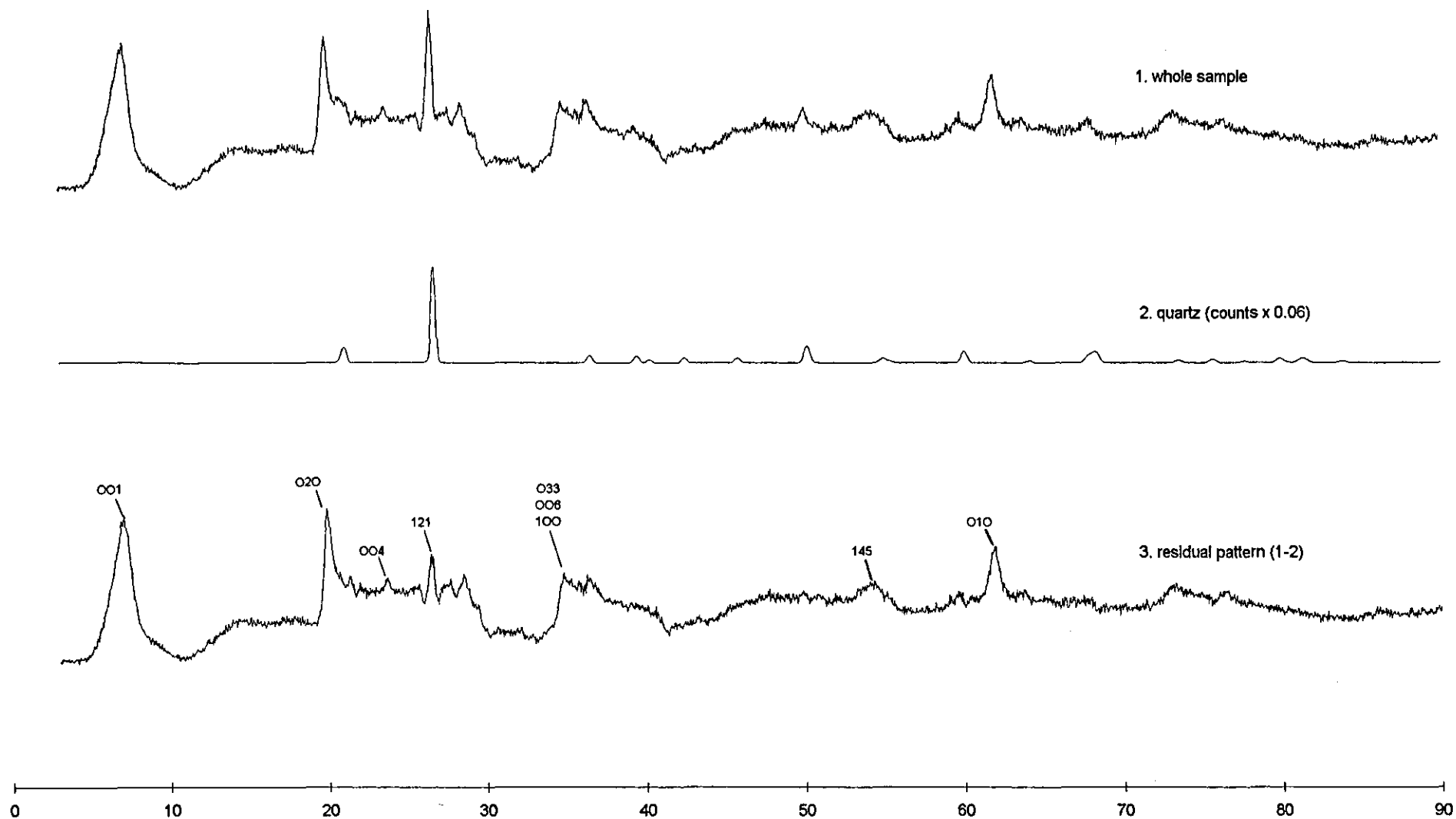
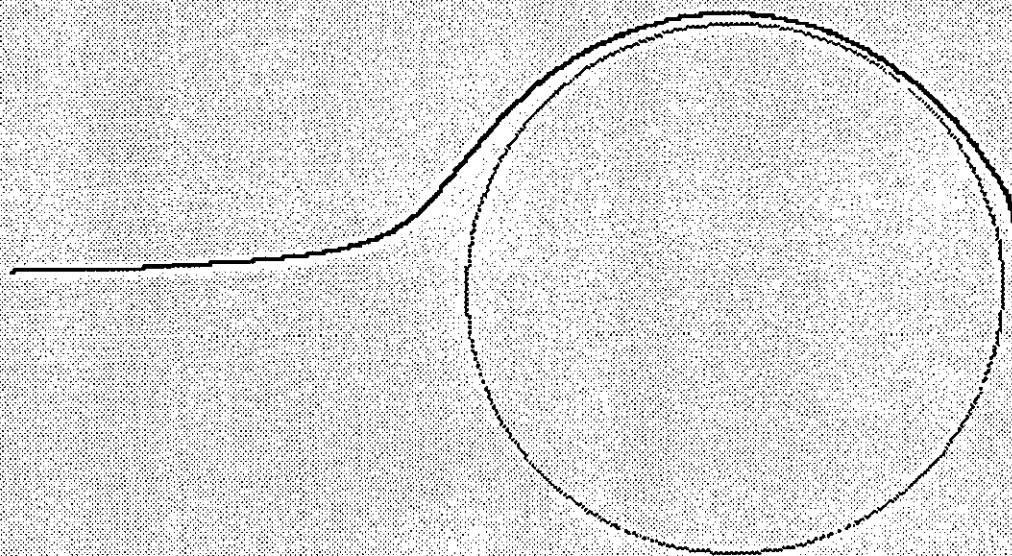


FIGURE 2
SAMPLE B; montmorillonite with minor quartz





Typical Trajectory Plot

Determination of correct density term in particle trajectory analysis

Hinze (1959) describes the equation for the motion of a particle in a fluid by:

$$V\rho_p \dot{\underline{u}}_p = \beta(\underline{u} - \underline{u}_p) + V_p \dot{\underline{u}} + \frac{1}{2}V_p(\dot{\underline{u}} - \dot{\underline{u}}_p) \quad (\text{A.1})$$

The first term on the right hand side is the normal steady state drag -Stokes drags,

The second term is caused by the acceleration of the fluid by the particle which causes a pressure gradient on the particle.

The third term is the force required to accelerate the apparent mass of the particle from the fluid to the particle condition.

$$\therefore (\rho_p + \frac{1}{2}\rho)\dot{\underline{u}}_p - \frac{3}{2}\rho\dot{\underline{u}} = \frac{\beta}{V}(\underline{u} - \underline{u}_p) \quad (\text{A.2})$$

Consider the normal force balance used in a trajectory calculation in which stokes number is applied:

$$\rho_{st} \dot{\underline{u}}_p = \frac{\beta}{V}(\underline{u} - \underline{u}_p) \quad (\text{A.3})$$

Here ρ_{st} is the density term used in the stokes number which is under dispute:

let

$$\dot{\underline{u}}_p = \dot{\underline{u}} + \Delta \quad (\text{A.4})$$

where Δ is the difference between the acceleration of the particle and the fluid

then

$$[(\rho_p - \rho)\dot{u} + (\rho_p + \frac{1}{2}\rho)\Delta] = \frac{\beta}{V}(u - u_p) \quad (A.5)$$

$$= \rho_s \dot{u}_p$$

where ρ_s , density to be used in the stokes number

$$\therefore \rho_s = (\rho_p - \rho) \frac{\dot{u}}{\dot{u}_p} + (\rho_p + \frac{1}{2}\rho) \frac{\Delta}{\dot{u}_p} \quad (A.6)$$

consider two extreme cases:-

case A: Low inertia systems

When a particle moves around an object it does not deviate from the streamline, i.e.

$$\Delta=0$$

substituting $\Delta=0$ into the equation above yields

$$\rho_s = \rho_p - \rho \quad (A.7)$$

case B High inertia systems

When a particle is shot into a stagnant fluid or a fluid moving with a steady linear motion, then it does not stop instantly, then $\dot{u}=0$ and $\dot{u}_p = \Delta$

$$\therefore \rho_s = (\rho_p + \frac{1}{2}\rho) \quad (A.8)$$

Hence before ρ_s can be defined the conditions must first be specified. Generally, ρ_s is given by equation A.7. In the extreme cases of low and high inertia (stokes number) we have:

- (a) high Stk. $\rho_x = (\rho_p + \frac{1}{2}\rho)$
- (b) low Stk. $\rho_x = \rho_p - \rho$

In the present case under consideration, the Stokes number is low or Δ is very small, hence

$$\rho_x = \rho_p - \rho$$

Thus the model put forward by Derjaguin is correct in the present case and not that of Flint and Howarth.

